

# NUCLEAR FUELS

GURINSKY – DIENES

*DR. J. G. BECKERLEY, GENERAL EDITOR*

THE GENEVA SERIES ON THE  
PEACEFUL USES OF ATOMIC  
ENERGY

1956





# NUCLEAR FUELS

# THE GENEVA SERIES ON THE PEACEFUL USES OF ATOMIC ENERGY

---

*Editor of the Series*

JAMES G. BECKERLEY

*Head, Engineering Physics Department,  
Schlumberger Well Surveying Corporation;  
Formerly Director of Classification  
United States Atomic Energy Commission*

---

## NUCLEAR FUELS

*by David H. Gurinsky and G. J. Dienes*

## EXPLORATION FOR NUCLEAR RAW MATERIALS

*by Robert D. Nininger*

## NUCLEAR REACTORS FOR RESEARCH

*by Clifford K. Beck*

## NUCLEAR POWER REACTORS

*by James K. Pickard*

## SAFETY ASPECTS OF NUCLEAR REACTORS

*by C. Rogers McCullough*

## NUCLEAR RADIATION IN FOOD AND AGRICULTURE

*by W. Ralph Singleton*

# NUCLEAR FUELS

---

*Edited by*

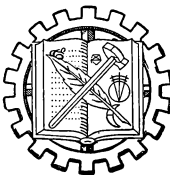
**DAVID H. GURINSKY**

*Head, Metallurgy Division  
Brookhaven National Laboratory*

AND

**G. J. DIENES**

*Senior Physicist  
Brookhaven National Laboratory*



**MACMILLAN AND CO. LIMITED  
ST. MARTIN'S STREET, LONDON**

THIS BOOK IS COPYRIGHT IN ALL COUNTRIES  
WHICH ARE SIGNATORIES TO  
THE BERNE CONVENTION

PRINTED IN THE UNITED STATES OF AMERICA

“. . . the United States pledges before you—and therefore before the world—its determination to help solve the fearful atomic dilemma—to devote its entire heart and mind to find the way by which the miraculous inventiveness of man shall not be dedicated to his death, but consecrated to his life.”

PRESIDENT DWIGHT D. EISENHOWER  
address before the General  
Assembly of the United Nations,  
December 8, 1953.



## FOREWORD

---

---

No matter how the Geneva Conference will be judged by historians of the future, there is one fact which will hardly be forgotten for some time to come: in ten days of August, 1955, an unprecedented volume of technical information on atomic energy was put into the public record. Not all the items of information were of equal value, to be sure, but relatively little was of a trivial nature.

Realizing that a verbatim record of this avalanche of data would be relatively indigestible to a large body of workers in the field, the Publishers requested me to undertake the task of organizing and editing a series of books which would present material of most urgent usefulness. Preprints of many of the conference papers were made available through the courtesy of the United Nations staff.

From a study of these papers it was concluded that six volumes of nominal length would be required. Each would cover a specific subject and include the key papers, suitably edited to eliminate duplication and secondary material, and arranged in a logical manner.

Because of the great interest in finding the raw materials for the growing nuclear appetite, Robert D. Nininger, Deputy Director for Exploration, Division of Raw Materials, United States Atomic Energy Commission, was asked to edit a volume on the geology of and the exploration for uranium and thorium.

All atomic energy projects to date have had research reactors at the base of their technical efforts. Dr. Clifford Beck, Professor of Physics, North Carolina State College, whose foresight and determination put the first research reactor on a university campus, consented to edit a volume on research reactors.

At the center of the stage, particularly for the energy-hungry nations of the world, is the power reactor, a device of many and varied forms. James K. Pickard, now a consultant engineer on atomic energy developments, for many years previously one of the stalwarts of the AEC Reactor Development Division, accepted the task of preparing a nuclear power reactors volume.

Because one of the most difficult and urgent problems in the power reactor program is assessing the hazard and providing safety in reactor operation, it appeared urgent to include a volume devoted exclusively to reactor safety. One of the pioneers in the field, Dr. C. R. McCullough of the Monsanto Chemical Company, has undertaken to edit a volume on the safety aspects of nuclear reactors.

## FOREWORD

The heart of the power reactor is the nuclear fuel, the energy source and the focal point for intense metallurgical and solid state research efforts. Dr. David H. Gurinsky and Dr. G. J. Dienes of Brookhaven National Laboratory, who have made substantial contributions to these efforts, have edited a volume on nuclear fuels.

In addition to the direct heat energy from fission, the ten per cent or so of reactor energy available as radiation is already exerting profound effect on civilization. One who has probed deeply into what might be termed the interaction of nuclear energy and agriculture, Dr. W. Ralph Singleton, Director of the Blandy Experimental Farm, University of Virginia, has edited a volume on nuclear radiations in food and agriculture.

These six volumes are not intended to cover all the technical areas of the Geneva Conference. Subjects such as radiobiology, nuclear physics, reactor physics, chemical processing—to name but a few—were not included (except where they touch on the subjects chosen) for a variety of reasons. A first consideration was that, if all subjects were properly represented, the series would presume an ungainly large number of volumes. Reducing the number of volumes could only be done by limiting coverage either to a few papers on each subject or to a superficial digest of a large number of papers. It seemed a better choice to cover fewer topics more completely. A secondary consideration was an assessment of the state of the literature—where a subject was rather well represented in the public literature, it could be argued that the need for a corresponding volume was less urgent. Certainly, for example, the literature of nuclear physics does not urgently require amplification. Moreover, although the nuclear physics papers published at Geneva were substantial, they did not disclose any striking new information. (In addition, many of the new nuclear data have been adequately disseminated by the United States Government handbooks.)

In any effort of this kind, arbitrary decisions are made in many places. Material is deleted, rearranged, abbreviated, and new material is added. It is hoped that these decisions have been wise and that the six volumes will be a fundamental reference work for the increasing number of scientists and engineers devoted to the peaceful uses of atomic energy.

J. G. BECKERLEY

## PREFACE

---

---

A large body of previously classified information was disclosed for the first time at the International Conference on the Peaceful Uses of Atomic Energy held in Geneva in August of 1955. To meet the needs of this conference, many review papers were presented containing both recently released material and the related information available in the open literature. The editors' purpose in preparing this volume was to present a clear picture of the status of the field of nuclear fuels. To accomplish this end, selected material was assembled from the many excellent papers presented at the International Conference for Peaceful Uses of Atomic Energy.

It was imperative, if continuity of development was to be achieved, that some details of importance to the specialist be deleted. Consequently, this volume should be considered as an introduction, although a rather detailed one, to the field. It is hoped that this volume will also prove useful as an introduction to the specialized papers by providing a proper perspective for further study.

The volume has been subdivided into three parts: I. The metallurgy of uranium and thorium; II. Radiation effects; and III. Solid and fluid fuels. The purpose of this subdivision is (1) to acquaint the reader with the fundamental information necessary for designing a fuel system; (2) to point out the problems specific to reactor systems, i.e., radiation effects; (3) to show how the engineering requirements and the fundamentals are fused to produce specific fuel systems.

As the first topic of this volume the editors have chosen the Ames process for the reduction of uranium salt to metal since this process probably represents the most important development toward industrial scale production of fissionable material. The book does not include material on the prior activities of prospecting, mining and ore concentration. Thorium has been included as a fuel since its relation to the fissionable U-233 is the same as U-238 with respect to Pu-239.

An attempt has been made to provide complete references and to give credit to the sources from which the material was obtained. In order to make this volume available as early as possible, it was necessary to use much of the material as prepared for the Geneva Conference by the various authors. The material has been rearranged to fit a logical pattern and to avoid duplication. Although this may, in some instances, make it difficult to identify at a glance the

## PREFACE

author of each individual paragraph, the editors believe that a valuable integration of important information has been achieved in the process.

Grateful thanks are extended to Florence Gurinsky and Margaret Dienes for their patient and invaluable assistance during the preparation of this book.

D. H. GURINSKY  
G. J. DIENES

## CONTENTS

---

CHAPTER		PAGE
FOREWORD		vii
PREFACE		ix
<b>PART I—THE METALLURGY OF URANIUM AND THORIUM</b>		
I. THE PREPARATION OF URANIUM METAL		3
A. The Reduction of Uranium Tetrafluoride with Magnesium		3
1. The reaction		4
2. The reaction bombs		6
3. Quality of materials		8
4. Operational considerations		13
5. The direct-pour process		16
B. Production of Uranium Metal		18
1. Ore crushing and sampling		18
2. Extraction		18
3. Purification		18
4. Preparation of uranium tetrafluoride		19
5. Reduction to metal		19
6. Recovery stages		20
References for Chapter I		20
II. THE PHYSICAL METALLURGY OF URANIUM		21
A. Physical and Thermal Properties of Uranium		21
B. Plastic Deformation Mechanisms in Alpha Uranium		21
C. Preferred Orientation in Alpha Uranium		28
1. Rod (rolled, swaged or extruded)		28
2. Powder compacts		30
3. Rolled sheet and strip		31
D. Recrystallization and Grain Growth in Uranium		33
1. Effect of method of fabrication on uniformity of recrystallized structures		33
2. Effect of impurities		36
3. Effect of degree of work hardening on recrystallization		41
4. Grain size after recrystallization		44
5. Grain size and structure resulting from transformation		45
6. Preparation of alpha uranium single crystals		48

CHAPTER		PAGE
E.	Thermal Expansion Characteristics of Uranium	49
1.	Thermal expansion coefficients determined from x-ray measurements	49
2.	Thermal expansion coefficients and characteristics determined from dilatometric measurements	50
F.	Mechanical Properties of Uranium	57
	References for Chapter II	67
III.	THE ALLOYS OF URANIUM	69
A.	Alloying of Uranium	69
B.	Transformation Kinetics in Uranium Alloys	76
1.	Uranium-chromium	79
2.	Uranium-molybdenum	80
3.	Uranium-niobium	83
4.	Uranium-zirconium	83
5.	Uranium-zirconium-niobium	84
C.	Mechanical Properties of Uranium Alloys	86
D.	Creep Properties	90
E.	Aqueous Corrosion of Uranium and High Uranium Alloys	91
	References for Chapter III	97
IV.	CASTING AND FABRICATION OF URANIUM AND ITS ALLOYS	99
A.	Uranium	99
1.	The casting process	99
2.	Fabrication	100
B.	Uranium Alloys	103
1.	Uranium-chromium	104
2.	Uranium-zirconium	104
3.	Uranium-molybdenum	106
4.	Uranium-silicon	107
	References for Chapter IV	108
V.	THE PRODUCTION OF THORIUM	109
A.	Occurrence of Thorium and Monazite Processing	109
1.	Occurrence of thorium	109
2.	Processing of monazite sand	110
B.	Thorium Metal Preparation	113
1.	Thorium oxide reductions	113
2.	Thorium chloride reductions	114
3.	Thorium fluoride reductions	115
4.	The iodide process for purifying thorium metal	116
C.	Melting and Casting	118
	References to Chapter V	118

## CONTENTS

xiii

CHAPTER		PAGE
VI. THE METALLURGY OF THORIUM AND ITS ALLOYS		120
A. Physical Metallurgy of Thorium		121
1. Recrystallization		121
2. The effect of alloying elements on hardness		124
3. Preferred orientation in cold worked and recrystallized material		125
B. Mechanical Properties		125
1. Tensile properties		125
2. Impact		126
3. Fatigue		127
4. Creep		127
5. Work hardening		127
C. Forming and Fabrication		128
1. Extrusion		128
2. Forging		129
3. Rolling		129
4. Swaging		130
5. Wire drawing		130
6. Machining		130
D. Powder Metallurgy		130
1. Production of thorium powder by the hydride process		131
2. Properties of thorium powder		132
3. Pressing and sintering		132
E. Corrosion of Thorium and Thorium Alloys		134
1. Corrosion of thorium in water		134
2. Corrosion of thorium in gaseous media		135
3. Corrosion of thorium in other media		136
4. Corrosion of thorium alloys		136
F. Metallography		138
G. Thorium Alloy Systems		139
1. Thorium-carbon		139
2. Thorium-uranium		140
3. Thorium-zinc		141
4. Thorium-zirconium		142
H. Hazards Encountered in Handling Thorium		143
References for Chapter VI		144

## PART II—RADIATION EFFECTS

VII. BASIC CONSIDERATIONS IN RADIATION EFFECTS	149
A. Qualitative Description of Radiation Effects	149
B. Calculation of the Number of Displaced Atoms	151

CHAPTER		PAGE
C.	Comparison of Theory and Experiment	154
	References for Chapter VII	158
VIII.	THE EFFECT OF RADIATION ON STRUCTURAL MATERIALS	160
A.	Metals	160
1.	General	160
2.	Structural metals	162
B.	Non-Metals	167
1.	Diamond	167
2.	Silica	169
3.	Ionic crystals	173
4.	Miscellaneous	175
C.	Graphite	176
D.	Minimization of Radiation Effects	183
1.	Adjustment of bombardment temperature	183
2.	Alloying	184
3.	Dispersion	184
4.	Material selection	184
	References for Chapter VIII	184
IX.	RADIATION EFFECTS IN FISSIONABLE MATERIALS	187
A.	Uranium and Its Alloys	187
1.	Changes in linear dimensions	188
2.	Variables which affect dimensional stability	194
3.	Miscellaneous property changes	207
4.	Thermal cycling effects in uranium	212
B.	Thorium and Its Alloys	223
C.	Dispersion Type Fuel Elements	223
1.	Metallic diluents	223
2.	Ceramic fuels	227
D.	Radiation Effects in Liquids	228
1.	The rate of the radiolysis of water due to the action of fast neutrons and $\gamma$ -radiation under stationary reactor operation	228
2.	The radiolysis of contaminated water at elevated temperatures	233
3.	Effect of radiation on heterogeneous systems of air or nitrogen and water	238
	References for Chapter IX	239
<b>PART III—SOLID AND FLUID FUELS</b>		
X.	THE TECHNOLOGY OF REACTOR FUELS	243
A.	Solid Fuels	243
1.	Fundamentals	243

## CONTENTS

xv

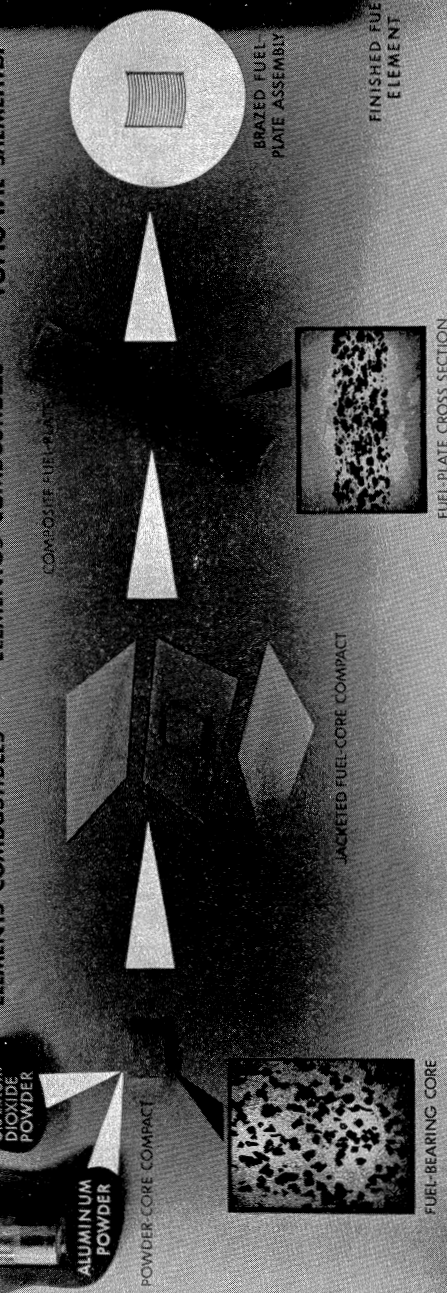
CHAPTER	PAGE
2. Fuel types	247
B. Fluid Fuels	253
1. Fundamentals	254
2. Fuel types	255
References for Chapter X	257
XI. A URANIUM BASE FUEL ELEMENT (Details of the fabrication of the Brookhaven fuel element)	259
A. The Basic Materials	260
B. The Production Operations	262
C. Description of the Operations	265
1. Stripping the anodized film	265
2. Trimming the finned tube	265
3. Welding the butt closure	266
4. Dehydrating the anodized film	267
5. Leak test number 1	267
6. Loading of the welded tube	268
7. Trimming of the loaded tube	269
8. Induction brazing of the helium cap	269
9. Leak test number 2	271
10. Hydrostatic collapsing of the finned tubing	272
11. Flame brazing of the anchor	273
12. Flame brazing of the helium tube to the fuel element	274
13. Continuity and final leak test	274
D. Discussion—Recent Changes	275
References for Chapter XI	277
XII. DISPERSION TYPE FUEL ELEMENTS	278
A. The Dispersion Type Fuel Element	278
1. Design objectives	278
2. Systems flexibility through dispersion techniques	279
3. Fabrication	281
B. The MTR Fuel Element	286
1. Materials choice	288
2. Description of fuel component	288
3. Fabrication of aluminum fuel plates	290
4. Component assembly by brazing	293
5. Reactor performance	295
References for Chapter XII	295
XIII. FLUID FUEL SYSTEMS	296
A. Introduction	296
B. Properties of $\text{UO}_2\text{SO}_4\text{-H}_2\text{O}$ Fuel System	298
1. Chemical properties	298

## CONTENTS

CHAPTER	PAGE
2. Physical properties	305
3. Corrosion behavior and materials of construction	307
C. Properties of the U-Bi Fuel System	307
1. The uranium-graphite reaction	307
2. Stability of the uranium bismuth fuel with respect to materials other than graphite	313
3. Corrosion and mass transfer of Fe and Fe + Cr by liquid bismuth	317
References for Chapter XIII	333
ADDITIONAL CHAPTER REFERENCES	335
GENERAL BIBLIOGRAPHY	337
SOME ABBREVIATIONS USED IN THE TEXT	341
SUBJECT INDEX	343
NAME INDEX	361

# FUEL ELEMENT

ELEMENTS COMBUSTIBLES ELEMENTOS COMBUSTIBLES ГОРЮЧИЕ ЭЛЕМЕНТЫ



Completed Geneva Reactor Fuel Element and Its Components



## *Part I*

---

### THE METALLURGY OF URANIUM AND THORIUM



# *Chapter I*

---

## THE PREPARATION OF URANIUM METAL \*<sup>1</sup>

---

### A. THE REDUCTION OF URANIUM TETRAFLUORIDE WITH MAGNESIUM <sup>2</sup>

A survey of the available literature in 1942 revealed that uranium metal could be prepared by any one of a number of methods. Laboratory tests on some of the more promising of these methods for production were subsequently reproduced. These tests showed, however, that the methods described in the literature either gave poor quality uranium metal or left much to be desired processwise for a large-scale low-cost operation. These results warranted an exploratory effort directed toward the development of new methods for the preparation of uranium metal. A process employing the reduction of uranium tetrafluoride with calcium was the first major step in the desired direction. This process was soon followed by the development of the method for producing uranium metal from uranium tetrafluoride with magnesium.

When the program on atomic energy in the U.S.A. was expanded early in 1942, there were two producers of uranium metal operating on a small scale in America. One producer used calcium hydride for the reduction of uranium oxide. The mixture of  $\text{UO}_2$  and  $\text{CaH}_2$  was placed in a steel cylinder inside a retort which was heated to  $960^\circ\text{C}$ . After the reaction occurred, the charge was allowed to cool under a vacuum to eliminate the hydrogen. The product of the primary reaction was a sintered clinker, which was then crushed to a powder. This powder was subsequently leached with dilute acetic acid, washed, dried, briquetted and sintered to form a fairly dense metal. This uranium was rather impure and contained considerable oxide.

The other producer employed an electrolytic process in which either  $\text{KUF}_5$  or  $\text{UF}_4$  was dissolved in a fused salt mixture of 80 per cent  $\text{CaCl}_2$  and 20 per cent  $\text{NaCl}$  in a graphite crucible. This crucible served as the anode and the

\* This chapter is based on the following Geneva Papers:

Section A: 817—H. A. Wilhelm, "The Preparation of Uranium Metal by the Reduction of Uranium Tetrafluoride with Magnesium."

Section B: 407—L. Grainger, "Production of Uranium Metal."

## 4 THE METALLURGY OF URANIUM AND THORIUM

uranium was electrolyzed out in the form of a granular deposit on a central molybdenum cathode. A temperature of about 900°C was employed for the fused salt electrolyte in order to produce coarser, less pyrophoric metal. The uranium was subsequently leached, dried, briquetted and melted and cast in beryllia crucibles to give good quality metal.

Neither of these two methods met all of the desired requirements as processes for large-scale low-cost production of high purity uranium metal. Production was stepped up, however, by both of these methods beginning early in 1942 and plans for even larger expansion of the electrolytic plant were shaping up when the practicability of the uranium tetrafluoride-calcium process was demonstrated.

Efforts on the  $\text{UF}_4\text{-Ca}$  process were expanded and a few tons of the metal were produced in the chemistry laboratories at Iowa State College during the latter half of 1942 while a separate building on the campus was being remodeled and furnished to serve as a small production plant. Meanwhile, efforts were also directed toward the experimental development of the process employing magnesium in place of calcium; and as a result early in 1943 all uranium metal production was converted from the calcium to the magnesium reduction of the tetrafluoride.

This first uranium metal production plant employing the  $\text{UF}_4\text{-Mg}$  process served not only to supply metal for experiments and for charging atomic piles but also served as a pilot plant. The process proved to be one that could be readily expanded and it gave high purity uranium at a low cost. Over a thousand tons of uranium metal billets were shipped from the production plant on the college campus before industry took over uranium metal production entirely.

**1. The reaction.** There are certain advantages in using magnesium instead of calcium for the reduction of  $\text{UF}_4$ . The purity of the uranium metal product depends largely on the purity of the materials that go into the charge and the materials that the metal contacts before solidification. Commercial-grade magnesium generally has fewer contaminants than commercial distilled calcium with respect to undesirable elements. Furthermore, the weight of calcium required to reduce a pound of uranium is about 1.6 times as great as the weight of magnesium required for the same weight of uranium produced. In addition, the cost per pound of the calcium may be five to ten times the cost per pound of magnesium. These factors, as well as relative availability, favored magnesium and made it desirable to explore the conditions for using magnesium instead of calcium in the reduction of  $\text{UF}_4$ .

Some of the requirements for the magnesium reduction can be introduced by first considering the process of reducing  $\text{UF}_4$  with calcium. If a mixture of  $\text{UF}_4$  and excess Ca metal (at room temperature) is ignited at some point by means of a hot wire or a fuse, the reduction reaction ( $2\text{Ca} + \text{UF}_4 \rightarrow 2\text{CaF}_2 +$

U) is propagated rapidly throughout the entire charge. The heat of the reaction is sufficient to heat both uranium metal and calcium fluoride to a temperature well above their melting points. The liquid products then separate readily because of the difference in their densities.

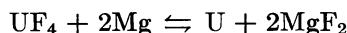
The heat generated by the reaction between  $\text{UF}_4$  and magnesium metal is about 45 kcal less per gram-atom of uranium formed than by the corresponding reaction employing calcium metal. The melting point of the  $\text{MgF}_2$  differs only slightly from that of  $\text{CaF}_2$ . Experimentally, it has been found that the heat generated during the reduction with magnesium is not adequate, by itself, to give the necessary fusion of the products. If heat is added, however, to the charge before or during the reaction, the necessary temperature for fusion and separation of the products may be attained in the magnesium process.

This heat can be added by mixing in the charge an agent which reacts with the magnesium and thus generates excess heat on its own to serve as a thermal booster to the main reaction. If such a charge containing adequate booster at room temperature is ignited by a hot filament, the reactions will proceed spontaneously and give massive metal well separated from the slag. A mixture containing seven (7) mols of  $\text{UF}_4$  to one (1) mol of  $\text{KClO}_3$  and a small excess of magnesium will behave in this manner.

A more convenient method of accomplishing this same objective is to preheat the charge of  $\text{UF}_4$  and Mg to ignition. The heat added to the charge before ignition and the heat of the reduction reaction together is sufficient to yield the products in the desired molten condition.

In the calcium reduction, the charge can be placed in an open vessel and very little calcium metal will be lost by vaporization during the reaction. However, in the magnesium reduction the boiling point of the magnesium metal is well below the melting point of the slag, making it essential that the reaction by this process be carried out in a closed vessel. The vapor pressure of excess magnesium metal at the peak temperature is well above one atmosphere and this pressure tends to drive the chemical reaction in the desired direction.

The reaction between uranium tetrafluoride (green salt) and magnesium metal,



when carried out under proper conditions in a closed vessel generates sufficient heat to reach a temperature at which the products of the reaction are molten. The dense liquid uranium metal collects to form a regulus, with the molten magnesium fluoride slag on top. After allowing the products to cool to near room temperature, the reaction vessel can be opened and the massive metal recovered.

**2. The reaction bombs.** The reaction vessels employed in the very early experiments were made from iron pipe of diameters up to four inches and in lengths of six to twelve inches. However, for the various stages of the work described here, the vessels were made from sections of standard-wall seamless pipes that ranged in sizes from six to thirteen inches inside diameter. The lengths of these pipe sections ranged from about 36 inches to 45 inches, with the greater lengths generally employed with the larger diameters. A companion flange was attached at one end of the pipe section and a welded-in steel plate closed the other end to form a crucible. A blind flange was bolted to the companion flange for closing this crucible, which was then referred to as a bomb.

As experience was gained on small-scale reductions and as more materials became available, the larger sizes of bombs were cautiously tried for the reductions. Only a few experimental reductions were made in 4-inch-diameter bombs. A rather large tonnage of metal was produced by reductions in 6-inch-diameter bombs 36 inches in length. The size of charge was stepped up for a few 8-inch bomb reductions before increasing the bomb size to 10 inches in diameter by 42 inches in length for further tonnage production. The regulus of massive uranium metal produced in a bomb reduction was referred to as a "biscuit." Biscuits were obtained in good yields from charges containing 56 pounds of  $\text{UF}_4$  in the 6-inch bombs, 180 pounds of  $\text{UF}_4$  in the 10-inch bombs and 318 pounds of  $\text{UF}_4$  in the 13-inch inside-diameter bombs. An average of 98.3% yield of biscuit metal was produced in the 13-inch bombs after determining the proper operating conditions. The 6-inch and 10-inch bombs also yielded about 98% of biscuit metal under favorable conditions. Since the plant developed from laboratory tests it was not highly mechanized for handling the larger biscuits and rather limited special production was carried out in bombs larger than 10-inch diameter.

*a. Lining the bomb.* The products of the reduction reaction attain a rather high temperature and it is necessary to prevent interaction between the charge and the steel bomb. A finely ground refractory material is used as a bomb liner to keep the molten mass and the magnesium vapor from attacking the bomb walls. Such attack would cause contamination of the uranium and possible failure of the bomb. The quality of this liner material and the care in the lining operation are very important to the success of the reduction.

The bomb lining operation is started by placing the empty bomb on an air-operated jolting table. Sufficient powdered refractory is placed in the crucible to form a layer about one inch thick on the bottom. After jolting for a few minutes the operation is stopped. A mandril, preferably made from metal tubing and closed on the ends, is inserted and rests on this bottom liner. The mandrils for the larger bombs are an inch less in diameter at the bottom than the inside diameter of the crucibles. The mandrils are tapered slightly,

being a fraction of an inch larger in diameter at the top. The mandril is centered in the crucible and then more refractory liner material is introduced into the annular space between the mandril and the crucible wall. This loose refractory is jolted down and more is added until the entire annular space is filled. The top region of the refractory liner is further rammed by means of a weighted metal cylinder that fits in the annular space at the top.

During the jolting operation it is essential to maintain the mandril in the center of the crucible for uniform wall thickness and also not to allow it to sink and thus produce a thin liner on the bottom. The mandril should be constructed with a small plug that fits flush on the bottom face of the mandril. This plug is attached to a rod which protrudes at the top of the mandril. Removal of this plug allows air to enter at the bottom as the mandril is slowly and carefully removed from the lined crucible. A properly lined crucible will have a lining that is strong and difficult to impress with the fingers.

*b. Charging and closing the bomb.* Proper amounts of finely ground UF<sub>4</sub> and granular magnesium are thoroughly mixed in preparing the charge. This mixed charge is emptied from the mixer into the refractory-lined crucible through a funnel. The charge is rammed down with care so as not to disturb the liner. The amount of the charge is controlled so that it fills the crucible to within 3 inches of the top.

A thick graphite disc (or cake) slightly larger in diameter than the lined cavity above the charge is then forced down on top of the charge. The top section of the liner above the charge is then reworked and packed by hand to cover the graphite disc, or cake, with the liner material. A straight edge is then used to level off the liner top even with the machined surface of the companion flange. The machined face of a blind flange is then bolted in place on the machined surface of the companion flange. No gasket material is used. The charged bomb is then placed in a furnace, or heat soaking pit, to initiate the reaction, or to fire.

*c. The bomb furnace and firing time.* One design of furnace that serves quite well for the uranium reduction process is shown in Fig. 1. It is gas-fired and has its top at floor level. The drawing shows a two-bomb capacity section of such a furnace. Only one bomb is shown in position.

The furnace temperature for best operation will depend on a number of factors such as size of bomb, rate of furnace recovery on introduction of a cold bomb, point at which temperature is measured and other factors associated with the bomb lining and charge. The optimum temperature of operation will generally be within the range of 550°C to 700°C with the thermocouples positioned as in Fig. 1. The time required for the reaction to initiate will usually be longer, the larger the bomb and the lower the furnace temperature. As much as 3½ hours are required for ignition to take place in the 13-inch diameter bombs with the furnace temperature at 565°C while the 10-

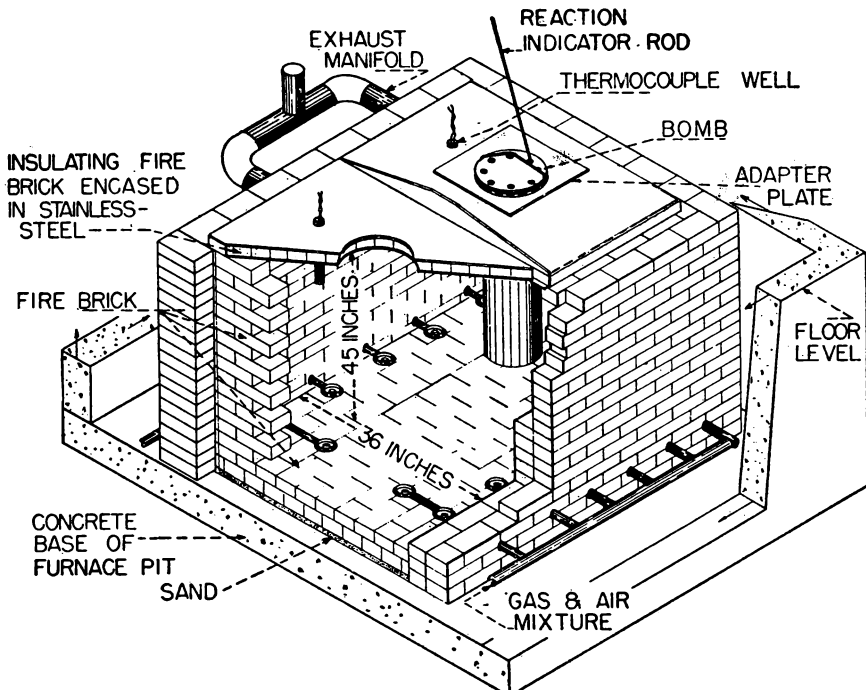


FIG. 1. Gas-fired bomb furnace.

inch bombs require about  $2\frac{1}{2}$  hours and the 6-inch size about  $1\frac{1}{2}$  hours with the furnace operating at the same temperature.

When the reaction takes place, sufficient agitation of the bomb occurs for a contact microphone on the opposite end of the reaction indicator rod (see Fig. 1) to indicate the event. The reaction is essentially complete in a minute and the entire metal phase may remain molten for at least 10 minutes in the larger sizes of bombs.

*d. Unloading the bomb.* After the reaction has subsided the bomb is removed from the furnace and allowed to cool in an upright position in air until its temperature is near that of boiling water. It is then sprayed on the sides with cold water until its contents are near room temperature. The cover plate is then removed and the bomb inverted on a jolting table to remove the metal biscuit, the slag and the liner.

Adhering slag is then broken or chipped loose and the cleaned metal is weighed and delivered to the casting room. The bomb is cleaned and returned to the loading line for another charge.

**3. Quality of materials.** In the calcium reduction of uranium tetrafluoride sufficient heat is evolved by the reaction so that preheating of the charged

bomb is not necessary, and good yields of biscuit metal can be obtained with relatively low-grade liner material and low-grade uranium tetrafluoride. However, in the magnesium reduction, especially by the preheat process, the yield of metal and degree of slag separation are quite sensitive to the quality of materials employed.

The specifications for the uranium tetrafluoride (green salt), the liner material and the magnesium metal are dependent upon the yield and quality of metal that are acceptable. For example, suppose that the green salt that is readily available analyses 96% UF<sub>4</sub>. It is an experimental fact that, other things being equal, a higher percentage of UF<sub>4</sub> gives a better yield of final metal. Whether or not this possible increase in metal yield would warrant the extra treatment necessary in making the better grade of UF<sub>4</sub> will depend on economic factors that exist at the particular location.

Some of the factors to be considered in choosing materials for this process follow.

*a. The green salt.* Uranium tetrafluoride can be produced from UO<sub>2</sub> and other compounds of uranium by a number of processes. Regardless of the process employed in its manufacture, there are a few common features of the green salt that should be considered as bearing upon its behavior and metal yield and quality.

It is obvious that certain elements if present in the green salt would be carried into the biscuit metal and be present as impurities in the final metal. Uranium ore processing and purification by liquid-liquid extraction are sufficiently developed to give high purity UO<sub>2</sub> and other intermediates. Impurities of the type considered here that are carried by UF<sub>4</sub> would most likely come from reagents and equipment employed in the conversion of these intermediates.

High moisture is detrimental in the charge regardless of its source. It may cause side reactions and lower the yield and quality of the product. Furthermore, if a large amount of H<sub>2</sub>O is present when the reaction fires, the resulting gas pressure may be sufficient to cause failure of the bomb.

The oxygen of dry green salt may be present as UO<sub>2</sub>F<sub>2</sub> or UO<sub>2</sub>. The higher the oxygen content, the lower the UF<sub>4</sub> content and, other things being equal, the lower the biscuit metal yield and poorer the slag separation. Green salt analyzing 96% UF<sub>4</sub> can be employed to give fair yields of metal but 98% or higher UF<sub>4</sub> content is preferred.

The packing density of the green salt is a factor that is dependent on the method of preparation and particle size. A dry-process UF<sub>4</sub> may have a packing density of greater than 3.5 grams per cm<sup>3</sup>, while a wet-process UF<sub>4</sub> may have a packing density of only about half this value. The higher the packing density, the greater the amount of charge that can be placed in a certain volume and the greater the amount of heat developed per unit area of con-

## 10 THE METALLURGY OF URANIUM AND THORIUM

tainer wall. The charge with higher packing density generally has better heat conductivity which would result in greater heat penetration into the charge before the surface reached ignition temperature. For good yields a packing density of 3.0 grams per cm<sup>3</sup> or greater is desired for the green salt.

Related to the packing density and a factor to be considered in bomb reductions of UF<sub>4</sub> with magnesium is the fineness of grind, or particle size distribution. The particle size distribution, however, can vary over rather wide limits without major effects on the behavior of the green salt. Green salt that met other qualifications and which came within the following ranges of sieve analyses reduced with good yields:

<i>U.S. Standard</i>	
<i>Sieve No.</i>	<i>Per Cent Passed</i>
60	96 to 99
80	91 to 95
100	85 to 92
200	62 to 75
325	52 to 62

*b. The liner material.* Since a small fraction of the impurities in a refractory liner is picked up by the metal during the vigorous reduction reaction, it is essential that the refractory be produced from good-quality starting materials. Liner materials that were successfully employed in the early production plant included dead-burned high-calcium lime and electrically fused dolomitic oxide, both in a fine state of division. The sources of limestone and dolomite were selected on the basis of purity, and the final refractories contained about 500 ppm iron, 60 ppm manganese and 5 to 10 ppm boron.

The evolution of water or other gases from the liner before or during the main reaction can be detrimental. It is essential then that the finally ground liner material have a low loss of weight on ignition and that it be protected from picking up moisture or gases before use. Rapid evolution of gas in the liner during the reaction may cause large amounts of the liner to become mixed with the reacting charge or cause complete liner failure resulting in a blow-out. Loss of weight on ignition by the two refractory materials mentioned ranged from 0.20% to 0.90% for the dead-burned lime, while for the electrically fused dolomitic oxide the value of 0.24% was a maximum. Although the dead-burned lime cost much less per pound, the large variation in its loss on ignition made it the less desirable refractory of the two.

Evolution of water vapor from the liner during the preheat period can cause side reactions that lower the yield of metal. As a charged bomb heats in the furnace the liner gets hot first. If moisture is released by the liner it can pass into the charge and react with the UF<sub>4</sub> to form UO<sub>2</sub> and HF. The HF can then return to the liner and form a fluoride and more water to hydrolyze more

$\text{UF}_4$ . The net result is a layer of  $\text{UO}_2$  formed next to the liner. When the bomb fires, the magnesium does not effectively reduce this  $\text{UO}_2$ ; therefore, the yield of metal is lowered by the slow evolution of  $\text{H}_2\text{O}$  from the liner. A measure which tends to correct this effect is to add a few per cent of very fine magnesium or calcium metal to the refractory powder before packing the liner. Then, as the water is released in the hot liner, the hot magnesium or calcium present reacts with the water to form hydrogen. This hydrogen diffuses into the charge and may eventually escape between the flanges at the top of the bomb.

Another property which is related somewhat to the quality of liner that a certain refractory will make is the packing density. The greater the sintering or degree of fusion of the oxide, the greater its packing density and the more inert is the material to picking up moisture or carbon dioxide. The dead-burned lime has a packing density of about 1.75 grams per  $\text{cm}^3$ , while the electrically fused dolomitic oxide has a packing density of about 2.0 grams per  $\text{cm}^3$ . Ordinary high-calcium lime and dolomitic lime show packing densities of about 1.45 and about 1.35 grams per  $\text{cm}^3$ , respectively, and they are unsatisfactory as liner materials.

Although many batches of the dead-burned lime performed very satisfactorily, it was entirely replaced by the electrically fused dolomitic oxide which performs consistently well. The distribution of particle size of the liner material can vary over wide limits and still give a hard and strong jolt-packed liner that will stand up well during the reaction. A sieve analysis that represents a number of batches of electrically fused dolomitic oxide is given here.

<i>U.S. Standard</i>	
<i>Sieve No.</i>	<i>Per Cent Passed</i>
45	98
80	78
170	53
325	40

*c. The magnesium.* In the early work, magnesium available from different manufacturers was tested in an attempt to determine the source of the best magnesium for use in the reduction of  $\text{UF}_4$ . A redistilled electrolytic magnesium, a redistilled carbothermic magnesium and a number of other batches of magnesium made at different plants employing the ferrosilicon process were tested.

Considerable variation seemed to exist in the reduction behavior of all batches of magnesium metal. The variations observed in the behavior of batches from the same producer were as great as were observed between batches of magnesium made by different processes. At the time of these tests, the quality of the liner material and the quality of the green salt varied widely.

## 12 THE METALLURGY OF URANIUM AND THORIUM

Much of the scatter of individual values in the data obtained in the magnesium tests was, no doubt, attributable to the other materials.

On the average, better results were obtained, however, with magnesium from a plant employing the ferrosilicon process, so production was standardized on magnesium from this one source. The magnesium from the selected source consistently met all purity requirements as far as the regular chemical analysis was concerned. This was true also of the magnesium made by the other producers. Some differences were observed in the macroforms of the crystals and in the physical shapes of the finely ground particles of magnesium from the various sources. Neither of these characteristics, however, could be related to the performance of the magnesium in the reduction. The possibility existed that the erratic behavior of different batches of magnesium even from the same producer was due to variations in operations connected with the processing at the magnesium metal plant. The temperature of the metal when exposed to air on removal from the magnesium production retort as well as possible air leaks in the vacuum system might have developed conditions that resulted in the variations experienced with different batches of magnesium.

Most of the magnesium from the selected source was supplied in the form of hollow cylinders, or muffs, that consisted essentially of matted and finger-like crystals. The muffs were about 10 inches in diameter. They were formed on the condenser as the crystals grew from the magnesium vapors produced in the ferrosilicon reduction of magnesium oxide. The crystal orientation in the muffs was somewhat radial with little indication of any tendency of the crystals to grow together. The muffs were readily broken into smaller pieces by blows with a sledge hammer. These pieces were then cut to hand-size chunks on a punch press fitted with a cutter blade. These magnesium chunks were passed over a magnetic separator to remove any tramp iron before feeding the chunks to the next machine.

These chunks were reduced to pieces about  $\frac{1}{4}$  inch in size by a cutter-type mill. The cutting in the mill was done by heavy knives mounted in the face of a heavy rotor; the knives passed within a fraction of an inch of heavy metal bars. With the rotor operating at high speed, the chunks of magnesium were readily cut to pass through a screen in the bottom of the mill. This mill was a standard machine of the type that is employed in shredding wood and paper and is often referred to as a "garbage hog." The  $\frac{1}{4}$ -inch size product from this mill was passed over a magnetic separator to protect the more delicate machine used in cutting the magnesium to a finer size.

The next machine was of a type that consisted of a number of long knives mounted on the outer edge of an open framework reel that rotated on an axis. In operation the rotating knives passed within a few thousandths of an inch of a number of stationary knives mounted in the housing of the mill. This machine, except for its screens, was a standard mill used for cutting corn

and other grain to fine particles. This cutting action reduced the magnesium to sizes that would pass through a bottom screen.

The magnesium was then passed over a screen to remove the fines and the dust. Samples were taken for chemical and sieve analyses. The approved ground magnesium was passed over a magnetic separator just prior to weighing for the charge. The particle size distribution of most magnesium cut in the manner described here is represented as follows:

<i>U.S. Standard</i>	
<i>Sieve No.</i>	<i>Per Cent Passed</i>
10	90-99
20	25-55
30	10-35
40	3-15
60	0-1

Since magnesium does react slowly with air, it is advisable to grind the magnesium at such time that the finely divided metal will not remain in storage for long periods.

#### 4. Operational considerations

a. *Excess magnesium.* It has been established experimentally that an excess of magnesium over the stoichiometric amount for reaction with the  $\text{UF}_4$  in the charge is essential to obtain better yields of uranium metal. As the per cent of excess magnesium increases from zero there is a sharp increase in biscuit yield. This increased yield reaches a maximum and rather abruptly levels off on a plateau for higher percentages of excess magnesium. The amount of excess necessary to reach this maximum with good-quality materials varies slightly with production sizes of bombs; the larger bombs require slightly less excess than the smaller bombs. Ten-inch and larger bombs require about 5% excess and a 6-inch bomb requires approximately 7% excess. Small experimental bombs employing only a few pounds of  $\text{UF}_4$  may require 20% to 30% excess magnesium to reach the maximum.

b. *Liner thickness.* The material, the compactness and the thickness of the refractory liner in a bomb are factors that contribute to the success of the reduction operation. The flow of heat to the charge before ignition must take place through this medium which also must serve as an inert heat insulator after the reaction. A liner that is too thin might conduct heat too rapidly and tend to cause firing before sufficient heat enters the major part of the charge. Further, if a charge fires properly with a thin liner the high temperatures may reach the steel bomb wall and lower its strength while pressure exists in the bomb, resulting in a blow-out. Refractories such as magnesium and calcium fluorides require greater thicknesses because of their low melting points. The refractory oxides employed in the development work have high

melting points and can be employed in thicknesses of less than an inch in the production-size bombs mentioned here. Actually  $\frac{1}{2}$ -inch,  $\frac{5}{8}$ -inch and  $\frac{3}{4}$ -inch walls were employed in the biscuit region of the 6-inch, 10-inch and 13-inch bombs, respectively. Since the mandrels were tapered slightly the walls were thinner at the tops. Exact centering of the bottom end of the mandrel was done by means of a ball gage of the proper size. The thickness of the liner on the bottom of the bombs was usually about one inch.

*c. Preparing the charge.* In the hand operations employed in the plant at Ames, the separate ingredients of the charges were merely poured into weighing buckets on over-under weighing scales that carried tare weights for the buckets. The weighed magnesium and green salt were dumped into a batch blender of the double-cone type. A thorough mixing of the charge is essential for best results. Furthermore, the mixed charge should be well packed into the lined crucible in order to increase the charge density and to get better heat conductivity.

*d. Protection walls around furnace.* Due to the fact that the internal pressure of the bomb at its peak inside temperature is well above atmospheric pressure it is essential that the operators be protected from possible bomb failure. Brick walls around the furnace working space have been found adequate for the protection of operators. Ports through these walls permit the necessary operations. Furthermore, operators should not remove any fired bomb from a furnace until the reaction has fully subsided. Hot spots may develop on the bomb at areas where the liner is thin and at areas having partial liner failure. Complete failure of the liner at a point usually results in a blow-out. Although blow-outs were not uncommon in the early development days, as better oxide liner materials became available and lining techniques improved, blow-outs were rare indeed.

*e. Furnace temperature and yield.* The design of the furnace can vary widely. Whether the bombs are heated by gas burners, electrical resistance heaters, radiation heaters or by induction makes little difference so long as the heat gets to the charge with the proper rate and distribution. Generally the higher the temperature of a furnace and the smaller the bomb diameter, the shorter the time of heating to produce ignition. Some data on firing time as related to bomb size and temperature of a furnace, such as that described earlier, are shown in Fig. 2. The higher temperatures that shorten the soaking time may or may not be advantageous from the standpoints of yield of metal and furnace life.

In tests to determine the relationship of yield to any of the numerous variables that bear upon the behavior of the magnesium reduction process, the furnace temperature must be given prime consideration. As an example of the importance of furnace temperature, results from a series of tests on two different magnesiums in two different sizes of bombs at various temperatures

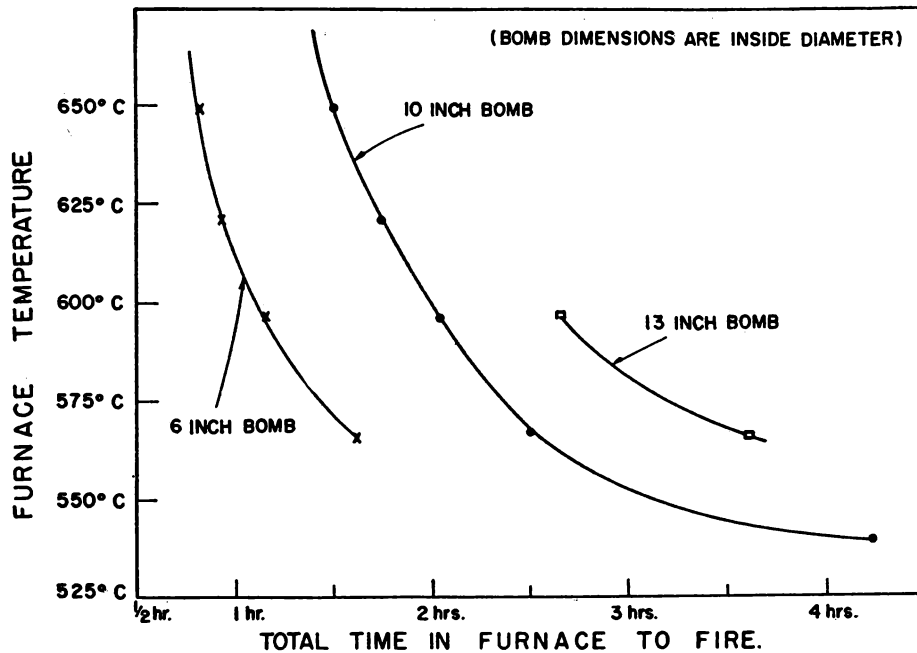


FIG. 2. Variation of firing time with furnace temperature.

are shown graphically in Fig. 3. The green salt and liner materials were essentially the same in all of the reduction tests made in this series. It is to be noted that for all four curves, each of which represents one magnesium in one size of bomb, the biscuit yields exhibit essentially the same maximum with temperature. Furthermore, in these tests the 10-inch bombs gave higher yields than the 6-inch bombs with the same magnesium and at the same furnace temperature. In addition, the yields with one of the magnesia were slightly more sensitive to temperature variations in both sizes of bombs. The essential difference in these two magnesia was that No. 109 magnesium had been ground and then stored for 5 months before the tests, while No. 259 was ground only 5 days before the tests.

The curves shown in Fig. 3 are not to be interpreted as representing the type of behavior to be expected in all such tests on materials. Some tests made on batches of liner material, green salt and magnesium, especially when the quality of each of these materials varied widely, have exhibited very flat curves, curves with two maxima, and curves with maxima shifted to higher or lower temperatures. Changes in furnace design and in position of the thermocouple would also cause shifts in such curves. Figure 3 does show that to be reasonably sure of getting the best yields with the materials and equip-

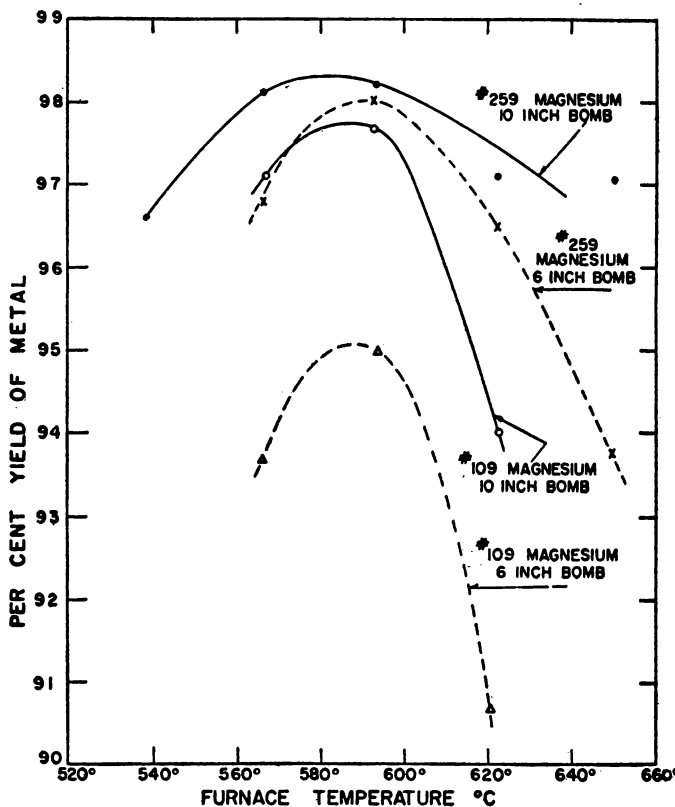


FIG. 3. Variation of yield of metal with furnace temperature.

ment available, tests of the kind described are essential. These tests may also include a standard casting operation and be based not on biscuit yields but on over-all yields of final cast metal.

**5. The direct-pour process.** In the bomb process described above the objective was to produce uranium metal which was allowed to solidify in the bomb and then, by means of remelting and casting, produce the desired shape of ingot. The objective of the process described briefly in this section is to cast the liquid metal, which results from the reduction reaction, directly into the desired shape of ingot.

The bomb, lined with electrically fused dolomitic oxide (E.F.D.) and charged with the usual mixture of  $\text{UF}_4$  and magnesium, is sketched in cross section in Fig. 4. This bomb has a special bottom which accommodates a valve for pouring the molten metal when desired. This valve is inserted by a special adapter on the mandrel used in the lining operation.

The charged bomb is placed in the furnace and, a few minutes after it has

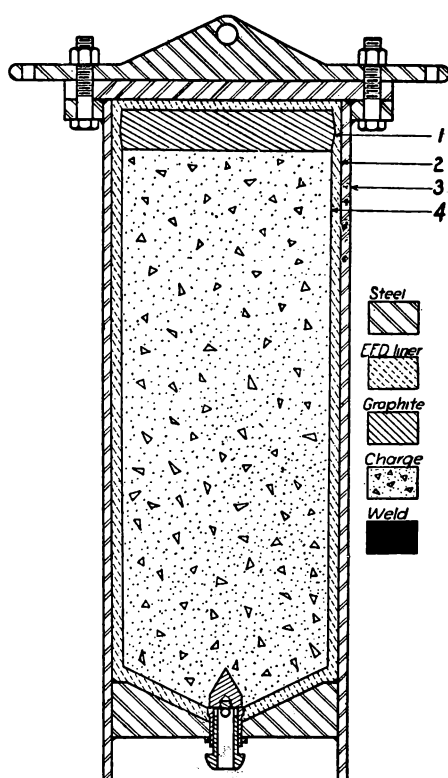


FIG. 4. Charged direct-pour bomb ready for furnace. (1) Graphite cake. (2) Refractory liner. (3) Bomb wall. (4) Charge of  $\text{UF}_4$  and Mg.

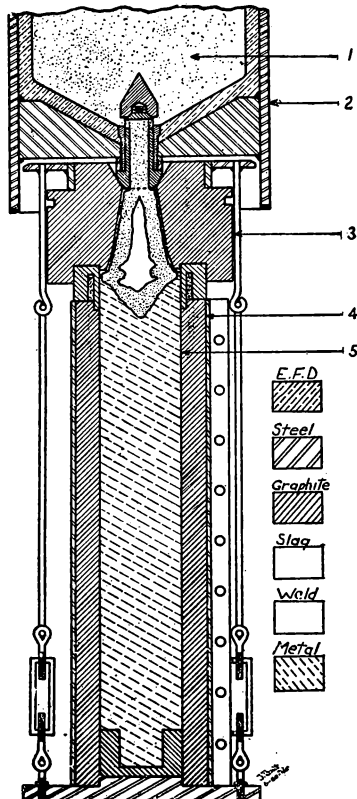


FIG. 5. Solidified ingot and slag. (1)  $\text{MgF}_2$  slag. (2) Lower end of bomb. (3) Mold cover. (4) Mold. (5) Uranium ingot. (Shrinkage of ingot not shown.)

fired, the metal is poured into a graphite mold that is in an assembly held rigidly together by turnbuckles. The ball face of the valve spout fits into a cone in the top face of a graphite cover to the mold. In bringing the top of the mold and the valve of the bomb together sufficient pressure is exerted to force the valve spout up in the valve housing, thus permitting the metal to flow through the spout to the mold. A sketch that represents conditions after the metal has poured and cooled is shown in Fig. 5.

Bomb charges containing 318 pounds of green salt gave about 238 pounds of metal for each casting. The ingots when cropped below the pipe gave billets weighing about 220 pounds. Ingots produced by this process are exceedingly low in carbon content but are higher in magnesium and hydrogen content than metal melted and cast in vacuum.

### B. PRODUCTION OF URANIUM METAL<sup>3</sup>

The outline of the process used in the United Kingdom is included in this volume to place in proper perspective, with respect to the whole process, the reduction step presented in the first part of this chapter. It should be noted that both the British and the French<sup>4</sup> processes use calcium for the reducing agent.

**1. Ore crushing and sampling.** *a.* The ore, consisting of fine powder, granular material, or lumps up to 8 inches in diameter, arrives in drums and contains a certain amount of radium and radon. Any radon released on opening the drum is taken up and discharged from the stack of the ventilation system. The ore is tipped into a hopper and fed to a jaw crusher. The discharge from this passes to a screen, oversize material being fed to a cone crusher and returned to the screen after reduction to about  $\frac{1}{4}$ -inch mesh.

*b.* Sampling of the ore is a matter of great importance because the price paid is based on assay. The sample is taken by feeding the crushed ore to a series of four Vezin samplers which continuously remove a proportion of the feed. The final sample is pulverized in a disc grinder and emerges as 80 B.S. mesh material. It is then coned and quartered to give a number of samples which are distributed between buyers' and sellers' representatives for analysis.

*c.* The whole of the crushing and sampling process is done in a plant which is not approached while it is in operation. Ventilation of the plant is achieved by two powerful fans which draw air from numerous points through cyclone dust separators and discharge through an air scrubber to a high level stack. The air scrubber is sprayed with water circulating in a closed system; dust removed from the ventilation system is recovered from a labyrinth, drummed and returned to store.

**2. Extraction.** *a.* The crushed ore is slurried with water, reduced to about 30 mesh in a ball mill and discharged into a stirred stock tank. The slurry is fed at a controlled rate to the first of three cascade dissolvers, stainless steel tanks fitted with stirrers, to which nitric and sulfuric acids are added continuously according to the uranium content of the slurry. Heating is by live steam and radon and acid fumes are efficiently extracted. The slurry overflows from the first to the second dissolver, which is also heated, and barium nitrate solution is then added to form insoluble barium sulfate and co-precipitate the radium present as sulfate. The mixture then overflows to the third dissolver where it is cooled by a cold water coil, causing further separation of insoluble sulfates. It is then pumped to filter presses which retain all insoluble materials, including the radium and precious metals.

**3. Purification.** *a.* The uranium in the clear liquor from the presses is next precipitated as uranium peroxide by the addition of hydrogen peroxide under

carefully controlled conditions of acidity and temperature and is removed from the solution by filter pressing.

*b.* The crude oxide is redissolved in warm nitric acid to form uranyl nitrate solution. The final free acidity and specific gravity of the solution are carefully adjusted within prescribed limits, and the solution is then evaporated under reduced pressure until it reaches the composition of uranyl nitrate hexahydrate.

*c.* The molten concentrate is then pressure-filtered through fine gauze to take out some of the impurities, and further purified by a single-stage ether extraction. The majority of the uranium is dissolved in the ether,\* while the bulk of the impurities remains in the aqueous layer which falls to the bottom of the extractor and is run off continuously to stock tanks. The ether layer is then washed with a small amount of warm demineralized water to remove most of the remaining impurities, and finally treated with a large volume of cold demineralized water to wash back the uranium into aqueous solution.

**4. Preparation of uranium tetrafluoride.** *a.* The pure uranyl nitrate solution from the ether purification plant is treated with ammonia to precipitate ammonium diuranate. The yellow precipitate is washed with water in the precipitator and dropped on to a Nutsch filter. Vacuum is applied under the cloths, producing a semi-dried cake which is filled into trays for use in the "Dryway" plant.

*b.* It should be noted that at this stage the uranium reaches its highest purity. Up to this point in the process impurities have been progressively removed from it; after this stage it inevitably picks up some impurities from the plant and apparatus with which it makes contact.

*c.* The next stage is the conversion of the ammonium diuranate to uranium tetrafluoride, a series of operations which is carried out in the "Dryway" plant. Trays containing the ammonium diuranate paste are stacked in a cylindrical reactor so that reactant gases which are introduced can pass from tray to tray across the surface of the contained solid. The reactor is lowered into an electric furnace, and the conversion proceeds in three stages. The diuranate is first heated to decompose it to uranium trioxide; during this calcination ammonia and steam are driven off. The trioxide is then reduced to dioxide by hydrogen, and finally the dioxide is treated with anhydrous hydrofluoric acid to convert it to uranium tetrafluoride. All these reactions are carried out in the same reactor which has a series of connections to the hydrogen and hydrofluoric acid supplies and to a caustic scrubber where effluent gases are either absorbed or discharged to atmosphere if harmless.

**5. Reduction to metal.** *a.* The final step is the reduction of the tetrafluoride with metallic calcium. The uranium tetrafluoride is transported in drums to

\* In the French process<sup>4</sup> tri-butyl-phosphate diluted with an inert solvent is used to extract the uranium nitrate.

the reduction plant and calcium chips are added, the operations being carried out in an enclosed cabinet. The contents are mixed under an argon blanket by tumbling the drum and finally charged into the reduction mould. This consists of a mild steel casing resembling an inverted, truncated cone. It is lined with calcium fluoride which has been rammed round a wooden former and carefully dried. The mould is mounted on a bogey running on a light rail track which passes through a long drying oven, through a charging cubicle, into a firing chamber, and out again into a cooling bay.

*b.* The charged mould is moved forward into the firing chamber, and vertical, electrically operated doors lowered into position. The charge is fired by dropping into it an ignited pellet of potassium nitrate and lactose mixture. An elaborate system of interlocking controls ensures that the charge is only fired when full safety precautions have been observed.

*c.* The reaction in the mould is rapid and exothermic. The heat generated melts the uranium formed so that the metal runs down to the bottom of the mould where it forms a solid billet, while the calcium fluoride, which is the other product of the reaction, floats on top as a slag.

*d.* When the reaction is complete, the mould is moved forward by remote control into the cooling bay. After cooling, the mould is hoisted into a break-down cubicle where it is inverted over a grid so that both the uranium billet and the calcium fluoride slag and mould lining fall out of the mould. The billet is finally cleaned and washed.

**6. Recovery stages.** *a.* From all the wet processes effluent liquors arise and pass into a recovery section. To this section are also sent various solid residues from later stages in the process. The recovery of uranium from these effluents and residues forms an essential part of the whole process, and governs the over-all efficiency. The basis of all the recovery processes is to convert the uranium present in the material to uranyl nitrate, if not already present in that form. The uranium is then precipitated as uranium peroxide, and the recovered material rejoins the main stream at the ether purification stage.

#### REFERENCES FOR CHAPTER I

1. See also the following Geneva Papers:  
341—B. Goldschmidt and P. Vertes, "Preparation of Pure Uranium Metal."  
627—A. P. Vinogradov, "Physico-chemical Methods of Uranium Production Control."  
531—B. Kopelman, "Fundamental Considerations in the Reduction Processes of Uranium and Thorium."
2. As described in Geneva Paper No. 817.
3. As described in Geneva Paper No. 407.
4. B. Goldschmidt and P. Vertes, Geneva Paper No. 341.

## *Chapter II*

---

### THE PHYSICAL METALLURGY OF URANIUM \*<sup>1</sup>

---

---

This chapter deals only with the subject commonly described as physical metallurgy. The information on this topic is quite extensive and for the most part not yet available in the open literature. It has not been possible to cover all topics in the general field of physical metallurgy nor to abstract adequately the reports of all investigators in this field. An attempt has been made to include a moderately detailed discussion of certain characteristics of uranium which are of importance in the development of its technology and in the understanding of its behavior during use.

#### A. PHYSICAL AND THERMAL PROPERTIES OF URANIUM

Certain of the properties of a metal are independent or nearly independent of the prior metallurgical history or, within limits, of the exact state of purity of the sample. Many of these properties are listed in Table I, and a few are also presented in summary form in Figs. 1 and 2. These properties will not be further discussed in this chapter, although in some cases they form the basis for the discussion of other properties, such as grain size, recrystallization behavior, and tensile properties, which are markedly dependent upon prior history. Data on the more structure sensitive properties are presented in this chapter.

#### B. PLASTIC DEFORMATION MECHANISMS IN ALPHA URANIUM

Studies of the plastic deformation mechanisms † in alpha uranium at room temperature have been carried out by L. T. Lloyd and H. H. Chiswick.<sup>2</sup> The

\* This chapter is based entirely on the following Geneva Paper: 555—F. G. Foote, "Physical Metallurgy of Uranium."

† See also R. W. Cahn, *Plastic Deformation of Alpha Uranium; Twinning and Slip*, Acta Met. 1:49-70 (1953). Cahn used very coarse grained uranium to determine the slip, twinning and kink band planes, the slip directions and the direction and magnitudes of the twinning shears.

TABLE I. PHYSICAL AND THERMAL PROPERTIES OF URANIUM

Density:			
High purity uranium, directionally solidified (at 25°C)	19.05 ± 0.02 grams/cm <sup>3</sup>		(a)
Calculated from x-ray data on high purity uranium (at 25°C)	19.04 grams/cm <sup>3</sup>		(b)
Wrought material	18.7 to 19.08 grams/cm <sup>3</sup>		(c)
Transformation Points:			
α-β	668°C		
β-γ	774°C		(d)
Melting Point	1132 ± 1°C		(e)
Boiling Point:			
Extrapolated from vapor pressure measurements	3818°C		(f)
Vapor Pressure from 1630 to 1970°K: (see also Fig. 1)	$\log p \text{ (mm)} = \frac{2330 \pm 21}{T} + (8.583 \pm 0.011)$		(f)
Heat of Fusion (estimate):	4.7 kcal/mole		(f)
Heat of Vaporization:	106.7 ± 0.1 kcal/mole		(f)
Heat of Sublimation at 0°K:	116.6 ± 0.1 kcal/mole		(f)
Enthalpy at 25°C:	1521.4 ± 1.6 cal/mole		(g)
Heat Capacity at 25°C:	6.612 ± 0.007 cal/deg-mole		(g)
Entropy at 25°C:	11.99 ± 0.02 cal/deg-mole		(g)
Heats of transformation:			
α-β, ΔH at 668°C	0.674 kcal/mole		(h)
β-γ, ΔH at 774°C	1.131 kcal/mole		(h)
Entropy of Transformation:			
α-β, ΔS at 668°C	0.717 cal/deg-mole		(h)
β-γ, ΔS at 774°C	1.081 cal/deg-mole		(h)
Thermal Conductivity (70°C)	0.071 cal/cm-sec-°C		(i)
Temperature coefficient (100–225°C)	+1.5 × 10 <sup>-3</sup>		
Temperature coefficient (225–450°C)	+0.4 × 10 <sup>-3</sup>		(j)

## Lattice Constants:

I. Alpha Phase, Orthorhombic Space Group—Cmcm 4 atoms per unit cell (k)

Temperature (°C)	Lattice Constants (A)	Volume of Unit Cell (10 <sup>-24</sup> cm <sup>3</sup> )	Volume per Atom (10 <sup>-24</sup> cm <sup>3</sup> )	Calculated Density (gram cm <sup>-3</sup> )
Room (25°C) (b)	$a_0 = 2.8541 \pm 0.0003$ $b_0 = 5.8692 \pm 0.0015$ $c_0 = 4.9563 \pm 0.0004$	83.02	20.75	19.04
200 (l)	$a_0 = 2.8675$ $b_0 = 5.8660$ $c_0 = 4.9775$	83.73	20.93	18.88
400 (l)	$a_0 = 2.886$ $b_0 = 5.861$ $c_0 = 5.005$	84.66	21.17	18.67
650 (l)	$a_0 = 2.920$ $b_0 = 5.834$ $c_0 = 5.064$	86.27	21.57	18.33

Thermal expansions (10<sup>-6</sup> per °C) from x-ray data, parallel to:

	axis	25–125°C	25–325°C	25–650°C
	$a_0$ $b_0$ $c_0$	21.7 -1.5 23.2	26.5 -2.4 23.9	36.7 -9.3 34.2

TABLE I. PHYSICAL AND THERMAL PROPERTIES OF URANIUM (Continued)

## II. Beta Phase, Tetragonal Space Group—P4/mnm 30 atoms per unit cell (m)

Temperature (°C)	Lattice Constants (Å)	Volume of Unit Cell ( $10^{-24}$ cm $^3$ )	Volume per Atom ( $10^{-24}$ cm $^3$ )	Calculated Density (gram cm $^{-3}$ )
720 (n)	$a_0 = 10.759 \pm 0.001$ $c_0 = 5.656 \pm 0.001$	654.7	21.82	18.11

## II-a. Beta Phase (1.4 a/o Cr)

Tucker's (m) sample contained 1.4 a/o Cr and the beta phase was retained to room temperature. Thewlis (n) has also reported lattice constant values for a similar alloy at 720° and 20°C.

720 (n)	$a_0 = 10.763 \pm 0.005$ $c_0 = 5.652 \pm 0.005$	654.7	21.82	18.11
20 (n)	$a_0 = 10.590 \pm 0.001$ $c_0 = 5.634 \pm 0.001$	631.8	21.06	18.77
20 (m)	$a_0 = 10.52$ $c_0 = 5.57$			

Linear coefficients of thermal expansion from 20–720°C.

$$(n) \text{ along } a_0 = 23 \times 10^{-6} \text{ per } ^\circ\text{C}$$

## III. Gamma Phase, Body-centered cubic, 2 atoms per unit cell (o)

(p) 805	$a_0 = 3.525$	43.76	21.88	18.06
(q) 800	$a_0 = 3.49$			
(q) 25	$a_0 = 3.474$	41.93	20.96	18.85

Value at 25°C extrapolated from measurements on U-Mo in which gamma phase can be retained by quenching.

Approximate linear expansion coefficient =  $18 \times 10^{-6}$  per °C.

- (a) B. Blumenthal, Argonne National Laboratory.
- (b) M. H. Mueller, Argonne National Laboratory.
- (c) J. H. Kittel, Argonne National Laboratory.
- (d) Selected values from several sources.
- (e) A. I. Dahl and H. E. Cleaves, *The Freezing Point of Uranium*, J. Research Natl Bur. Standards 43:513 (1949).
- (f) E. G. Rauh, and K. J. Thorn, *Vapor Pressure of Uranium*, J. Chem. Phys. 22:1414 (1954).
- (g) H. E. Flotow and H. R. Lohr, Argonne National Laboratory.
- (h) D. C. Ginnings and R. J. Corruccini, *Heat Capacities at High Temperatures of Uranium, Uranium Trichloride, and Uranium Tetrachloride*, J. Research Natl. Bur. Standards 39:309 (1947).
- (i) J. L. Weeks, *Thermal Conductivity of Uranium and Several Uranium Alloys*, J. Metals 7, AIME Trans. 208: 192 (1955).
- (j) J. Katz and E. Rabinowitch, *The Chemistry of Uranium*: National Nuclear Energy Series, Division VIII, Vol. 5, McGraw-Hill Book Co., New York (1951).
- (k) C. W. Jacob and B. E. Warren, *Crystalline Structure of Uranium*, J. Am. Chem. Soc. 59:2588–2591 (1937).
- (l) C. M. Schwartz and D. A. Vaughan, Battelle Memorial Institute.
- (m) C. W. Tucker, Acta Cryst. 4:425 (1951); see also C. W. Tucker and P. Senio, *The Refined Crystal Structure of Beta Uranium*, KAPL-844 (1952).
- (n) J. Thewlis, *X-ray Power Study of  $\beta$ -Uranium*, Acta Cryst. 5:790 (1952).
- (o) Battelle Memorial Institute.
- (p) J. Thewlis, *Structure of Uranium*, Nature 168:198 (1951).
- (q) A. S. Wilson and R. E. Rundle, *The Structures of Uranium Metal*, Acta Cryst. 2:126–127 (1949).

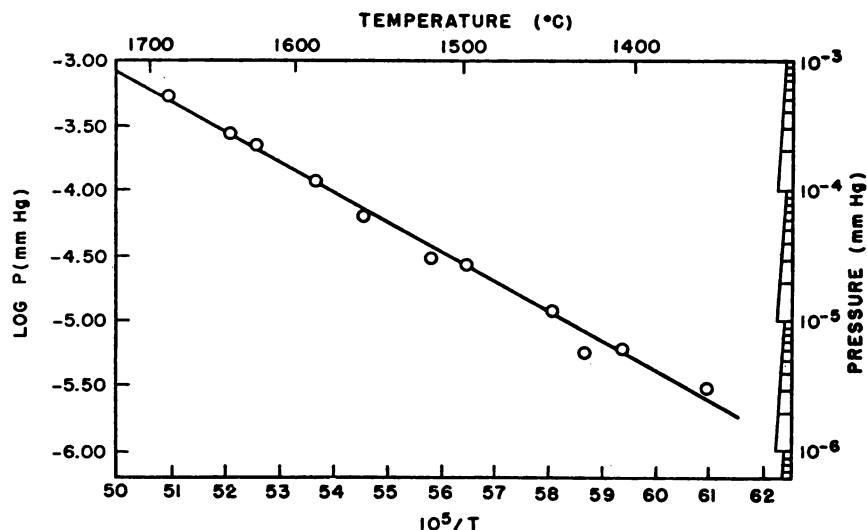


FIG. 1. Vapor pressure of uranium.

$$\log P \text{ (in mm)} = \frac{2330}{T} + 8.583$$

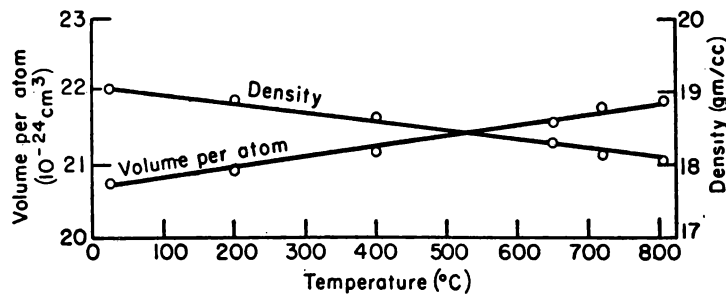


FIG. 2. Some physical constants of uranium metal.

Phase	Temp. (°C.)	No. of Atoms per Unit Cell	Vol. per Atom ( $10^{-24} \text{ cm}^3$ )	Density (gm/cc)
$\alpha$	Room (25°C)	4	20.75	19.04
$\alpha$	200	4	20.93	18.88
$\alpha$	400	4	21.17	18.67
$\alpha$	650	4	21.57	18.33
$\beta$	720	30	21.82	18.11
$\gamma$	805	2	21.88	18.06

operative deformation elements in alpha uranium have been determined as a function of the crystallographic direction of testing. Single crystals, produced by grain coarsening techniques, were tested under compression at room temperature. The location of the compression directions studied are plotted in (001) standard projection in Fig. 3.

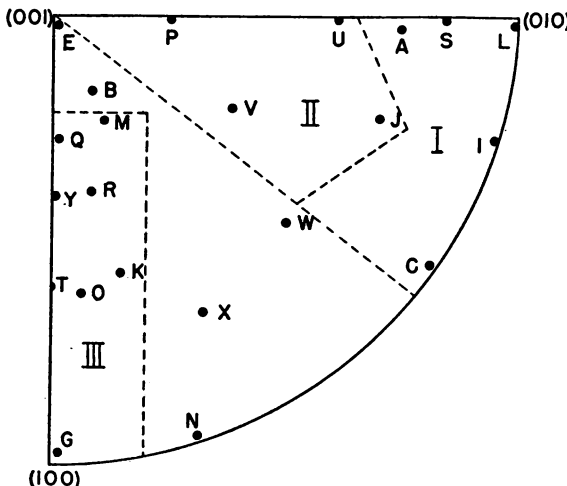


FIG. 3. Compression directions studied. Dotted lines delineate areas of operation of the various deformation mechanisms.

The most frequently observed deformation mechanism was slip on the (010) plane. All crystals except E yielded evidence of (010) plane slip. The slip direction for the (010) system was determined to be the [100] from the following considerations: (1) it is the most densely packed direction in the slip plane; (2) the rotational asterism of Laue spots; and (3) it is in accord with the crystallography of kinking deformation discussed later. The critical shear stress value for this (010)-[100] slip system was determined to be  $0.34 \pm 0.02$  kilogram per square millimeter.

A minor slip plane, of identity {011}, was identified by pole-locus analysis of eight slip traces observed on two crystals. The most probable slip direction for this system would be the [100]—the most densely packed direction in that plane. It must be emphasized that this system was observed in only two crystals compressed in directions unfavorable for slip on the major (010) system; hence, its role as a room temperature deformation mechanism must be viewed as minor.

Several crystals deformed principally by kinking; others showed evidences of cross-slip. Kinking was obtained in crystals which were compressed in a

direction nearly parallel to the [100] slip direction and the (010) slip plane. The operative slip plane in this type of deformation was identified as the (010) by Laue spot asterism. The cross-slip appeared in crystals whose compression directions were also nearly parallel to the (010) slip plane but displaced from the [100] direction. The major slip traces were identified as (010) plane traces. The minor cross-slip traces were found to correspond to (001) planes. In a cross-slip system the slip direction should be common to both cooperating planes, which in this case would be the [100] direction.

The second most frequently observed deformation mechanism and the most frequently observed twinning system were on the {130} composition plane. The occurrence of extensive {130} twinning was always accompanied by (010) slip. This was even true in the case of a crystal which was compressed nearly perpendicular to the (010) slip plane. The occurrence of (010) slip in such a crystal would indicate that extensive {130} twinning is always accompanied by an accommodating slip.

Two additional twin systems of irrational composition planes having indices of approximately {172} and {176} were observed. The more prevalent of these two twins were those occurring on the {172} planes. The various crystallographic elements of the three twinning systems were identified by x-ray and/or goniometric measurements; these are tabulated in Table II.

TABLE II. TWINNING SYSTEMS <sup>a</sup>

$K_1$	$K_2$	$n_1$	$n_2$	$2\phi$	$S$
(130)	(110)	[310]	[110]	81°30'	0.299
~(172)	(112)	[312]	X <sup>b</sup>	83°32'	0.229
~(176)	(111)	[512]	X <sup>b</sup>	83°50'	0.216

<sup>a</sup>  $K_1$  is the first undistorted plane or twin composition plane.

$K_2$  is the second undistorted plane. Its identity and shape are maintained both in the parent and twinned metal.

$n_1$  is the shear direction. The plane containing the shear direction and perpendicular to the twin composition plane is the plane of shear.

$n_2$  is the intersection of the plane of shear with the  $K_2$  plane.

$2\phi$  is the angle between the  $K_1$  and  $K_2$  planes.

$S$  is the magnitude of shear and it is equal to  $2 \cot 2\phi$ .

<sup>b</sup> X indicates the lack of rational direction indices.

The deformation mechanisms that were identified as operative in the various crystals are summarized in Table III. In the case of twinning systems, only those unmistakably identified by a two-surface analysis and/or x-ray Laue determinations are included. Similarly, the slip deformation mechanisms indi-

TABLE III. OPERATIVE DEFORMATION MECHANISMS

Crystal <sup>a</sup>	Operative Twin Systems <sup>b</sup>			Slip Deformation Mechanisms <sup>c</sup>			(011)
	{130}	{172}	{176}	(010)	(010)-(001) Cross-Slip	Kinking	
A	2	—	—	—	—	—	—
B	—	—	—	X	—	—	—
C	1	—	—	X	—	—	—
E	—	—	4	—	—	—	X
G	—	—	—	X	—	X	—
I	2	—	—	X	—	—	—
J	1	1	—	X	—	—	—
K	—	—	—	X	—	X	—
L	2	—	—	X	—	—	—
M	—	—	—	X	X	—	—
N	—	—	—	X	—	—	—
O	—	—	—	X	—	X	—
P	2	2	—	X	—	—	—
Q	—	—	—	X	X	—	—
R	—	—	—	X	X	—	—
S	2	—	—	X	—	—	—
T	—	—	—	X	X	X	—
U	2	2	—	X	—	—	—
V	1	1	—	X	—	—	—
W	—	—	—	X	—	—	—
X	—	—	—	X	—	—	—
Y	—	—	2	X	X	—	X

<sup>a</sup> A pictorial representation of the crystal compression direction may be found in Fig. 3.

<sup>b</sup> Only twin systems identified by two-surface analysis and constituting a principal portion of the deformation observed are indicated. The number refers to the number of operative twin planes.

<sup>c</sup> X indicates that deformation of the indicated type was observed microscopically.

cated are only those that resulted in microscopically visible traces on the polished surfaces. The major and most frequently occurring deformation mechanisms were: (010) slip, {130} twinning, and {172} twinning. Under special cases of stress application, deformation by {176} twinning, {011} slip, kinking and cross-slip were noted. The areas of crystallographic directions for which these deformation mechanisms operate are shown in Fig. 3. The depicted boundaries are not to be considered as exact, but rather as outlines which include the crystals for which the various deformation mechanisms operated. Evidence of slip on the (010) plane was observed in all crystals

except E. Twinning on {130} planes was observed in the crystals within area I and II. {172} twinning occurred for crystals in area II. Twinning on {176} planes and slip on the {011} planes were confined primarily to crystals compressed in the [001] direction. Kinking and cross-slip were observed in crystals within area III.

### C. PREFERRED ORIENTATION IN ALPHA URANIUM

**1. Rod (rolled, swaged or extruded).** The early investigations of the preferred orientation developed in uranium, as a result of rolling or swaging, were carried out using an x-ray photographic technique. Although this method at its best was only qualitative, it did give a good indication of some of the types of textures which were obtained. A. Fischer<sup>2</sup> reported that a rod swaged at 300°C and annealed 2 hours at 575°C showed (002) poles perpendicular to the rolling direction and (010) poles parallel to the rolling direction. In rods rolled at 300°C without an anneal, a duplex texture with the (010) and (110) poles parallel to the rod axis has also been reported.<sup>2</sup>

As a result of this earlier work, it was felt that the texture of swaged or rolled rods and rolled uranium sheet did not change after recrystallization.

Uranium rods which were either slow or fast beta treated after deformation appeared to be very nearly random, as reported by A. Fischer<sup>2</sup> and by J. B. Burnham, Jr., and J. H. Bach.<sup>2</sup>

Practically all of the more recent investigations of the preferred orientation in uranium have been carried out with an x-ray diffractometer using a Geiger tube as a detecting device. Several different types of sample holders have been designed and built for imparting the necessary motion or movement to the sample in order to collect the necessary intensity data from the x-ray diffractometer for the construction of pole figures, pole charts and inverse pole figures.

In a method described by L. K. Jetter and B. S. Borie, Jr.,<sup>3</sup> spheres are machined from rods by a rather unique method to very close tolerances and have an attached stem for support. By providing two independent motions, perpendicular to each other, it is possible to obtain the necessary intensity data for the construction of one-half of a complete pole figure from one specimen.

The modified Schulz reflection technique<sup>4</sup> employing flat samples has been used by A. N. Holden and W. E. Seymour,<sup>2</sup> W. P. Chernock,<sup>2</sup> and M. H. Mueller,<sup>2</sup> for the determination of textures in uranium, with the x-ray diffractometer. The instrumental arrangement used for this technique has been described by A. N. Holden<sup>5</sup> and by Mueller and others.<sup>6</sup> Each particular instrument varied somewhat in detail with respect to sample movements and recording of intensity data. In most cases, however, three samples were cut in

different directions from rods and a number of small flat pieces were assembled together for the determination of sheet textures. The number of sections used for plotting a pole figure for sheet textures varied from the one large cube used by W. P. Chernock, several large cubes used by W. E. Seymour,<sup>7</sup> to seven different assembled sections used by M. H. Mueller and H. W. Knott.<sup>8</sup> In addition, W. E. Seymour and J. Duffey have made use of the Norton technique.<sup>9</sup>

J. H. Bach and J. B. Burnham, Jr.<sup>10</sup> and P. R. Morris have made use of the x-ray diffractometer for evaluating the preferred orientation of rods on an industrial control basis. In this method the ratio or "psi" value is obtained between the intensity for a particular reflection from a sample and a randomly oriented specimen. It has been shown by M. H. Mueller and P. A. Beck<sup>2</sup> that the intensity of various reflections from the sample cannot be compared directly to the (111) intensity. It was once thought that the (111) would serve as an internal standard.

Rods rolled at 300 or 600°C both contained the (010) and (110) components; however, the relative amounts of these two components varied, depending upon temperature of rolling. The (010) component seems to predominate at the lower temperature and (110) at the higher temperature. A similar duplex fiber texture has also been reported by L. K. Jetter<sup>2</sup> for 500°C swaged rods.

Since considerable spread in intensity has been observed, some workers have indicated that some of this intensity might be accounted for by minor texture components such as (451), (021), (131) in rolled rods or [031], [431], [100] directions found in 500°C swaged rods. Some evidence has been found by M. J. Sanderson<sup>2</sup> for the development of a (100) component at high rolling temperature or after beta treatment.

It was found by M. H. Mueller, H. W. Knott and P. A. Beck<sup>2</sup> that if uranium rods are rolled at 300°C to a sufficiently high reduction (70% or greater) the preferred orientation obtained will be practically the same regardless of the prior fabrication history, that is, whether the rods were previously beta treated, 600°C rolled or 300°C rolled and annealed. The texture obtained after 70% reduction may be described by a concentration of the fiber axis between (010) and (041), with considerable scatter in the direction of the (100) including a minor maximum near (120). Below 70% reduction the type of orientation obtained may vary considerably, depending upon the starting material. For example, inverse pole figures prepared according to a modified Harris Method<sup>11</sup> indicated that the beta treated material initially was nearly random and showed a gradual increase of fiber axis concentration near the (010) and (120) poles as the amount of reduction at 300°C increased.

Rods rolled at 600°C after beta treating varied from a nearly random condition, produced by beta treating, to a strong (110) component with consider-

able spread toward and including the (010) pole and some spread towards the (100) pole.

A study was made by M. H. Mueller<sup>2</sup> of the radial symmetry of the (001) planes which lie parallel to the rod axis. It was found that this symmetry was in the form of a "cloverleaf" when rods were rolled with the oval-round or oval edge-oval pass sequence (Fig. 4). Rods rolled with hand round passes showed a more nearly symmetrical intensity distribution.

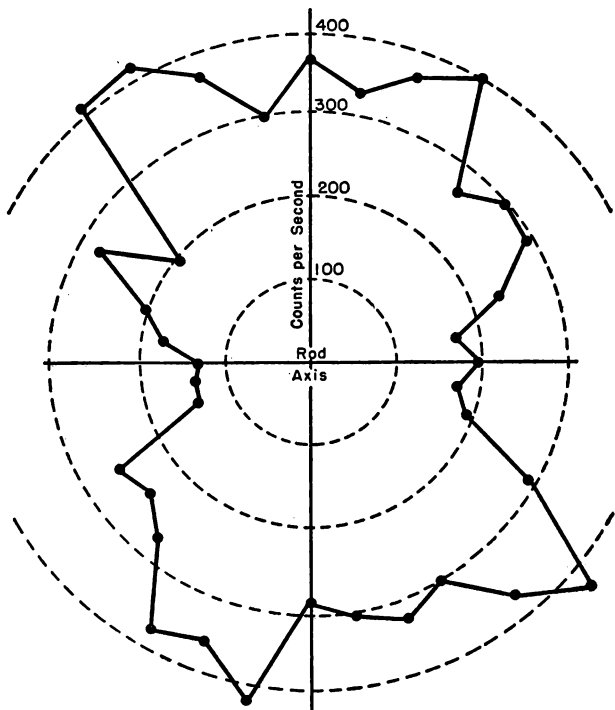


FIG. 4. Radial intensity of the (002) reflection in a uranium rod rolled in an oval edge-oval pass sequence.

The results obtained by L. K. Jetter<sup>2</sup> and W. P. Chernock and P. A. Beck<sup>2</sup> from the x-ray diffractometer indicated that there were definite textural changes occurring upon recrystallization of rolled or swaged rods. Some of the results indicated that the (010) component remained after recrystallization, although it may have decreased in amount, and that the (110) component is replaced by an approximately (140) component with considerable spread which in some cases has been described as a (131) orientation.

**2. Powder compacts.** An x-ray diffractometer study (M. H. Mueller;<sup>2</sup> M. J. Sanderson<sup>2</sup>) of the preferred orientation in hot-pressed uranium com-

pacts indicated that there appeared to be very little orientation and that the samples were essentially random.

**3. Rolled sheet and strip.** The preferred orientations obtained in uranium sheet formed under various conditions have been investigated (W. E. Seymour;<sup>7</sup> W. P. Chernock; <sup>2</sup> M. H. Mueller, H. W. Knott and P. A. Beck<sup>2</sup>).

Since the specimens were fabricated under various conditions it would not be expected that all the pole figures would be the same. However, it was observed in general that there was a high (010) pole concentration in "as rolled" material near the rolling direction as shown in Fig. 5. In sheet rolled

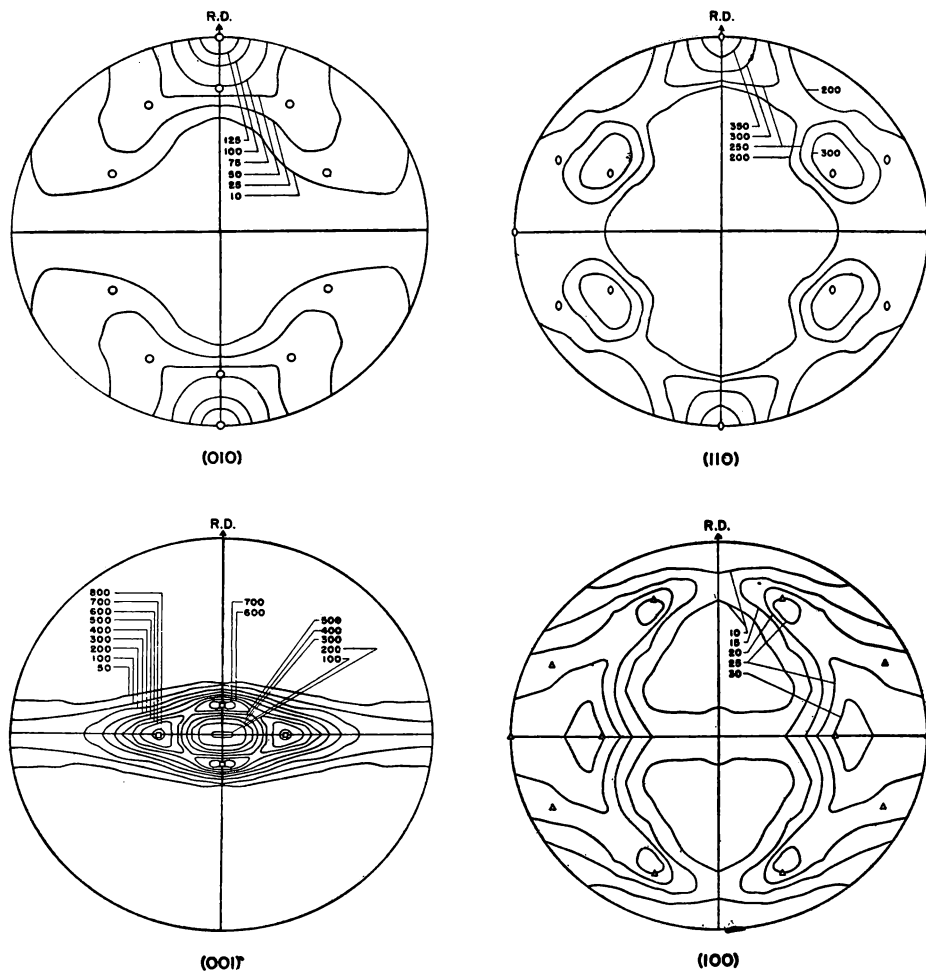


FIG. 5. Pole figures for uranium sheet rolled at 300°C to an 87% reduction.

at the higher temperatures there was also a high (110) pole concentration near the rolling direction. These two observations are very reminiscent of the textures observed in rolled uranium rod. In addition, the (001) pole figures showed a high concentration near the center of the pole figure but displaced towards the transverse direction and in some cases towards the rolling direction.

The pole figures for the 300°C rolled uranium sheet after recrystallization at 525°C are shown in Fig. 6. The (010) pole figure is very similar to that obtained for the as rolled sheet; however, the distribution of the (110) and (100) pole intensity has changed considerably.

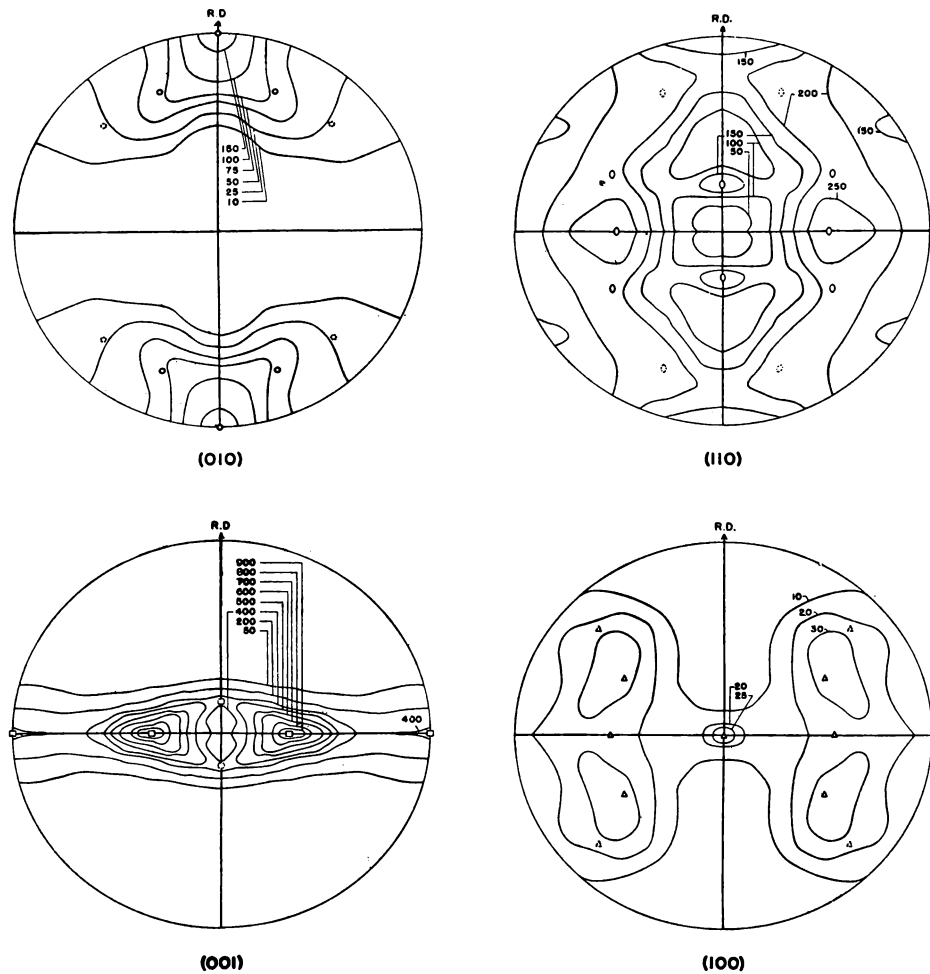


FIG. 6. Pole figures for uranium sheet 300°C rolled and recrystallized.

#### D. RECRYSTALLIZATION AND GRAIN GROWTH IN URANIUM

A study of recrystallization and grain growth in metals involves a large number of variables. A complete study of the effects of all the factors requires considerable time as well as careful experimentation. A review of the literature indicates that grain growth and recrystallization in uranium have been studied to some extent at many different laboratories and production centers. Most of these studies were comparatively brief and were statistical studies of the effects of a few variables under production conditions. Systematic studies under laboratory conditions are relatively scarce.

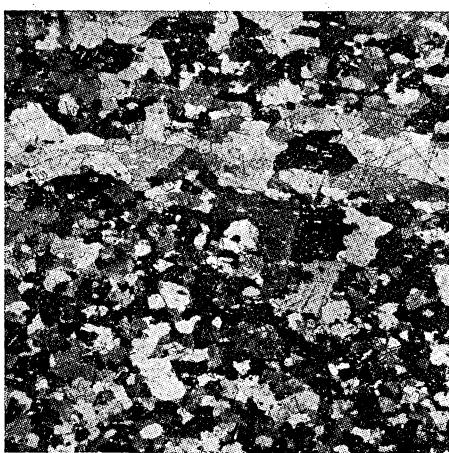
One of the reasons for the absence of more systematic data is understandable. The need for quick information on the properties of uranium appeared simultaneously with the availability of the metal. However, another reason may be the complexity of the problem, as indicated in the conclusions of the reports on statistical studies with a large number of specimens. Inconsistencies appeared to be the rule. In order to explain the inconsistencies it was first necessary to know the sources. Although most of the report writers reasoned that the impurities, the anisotropy of the crystal structure, and the allotrophic transformations were the primary sources of the lack of uniformity in results, the effects of these factors were not easily studied. Some better understanding has resulted from the studies of E. S. Fisher<sup>2</sup> on high purity uranium. This work has shown that impurities have a very pronounced effect on grain growth and recrystallization and that the anisotropic properties of uranium result in nonuniform microstructures.

In this section an attempt is made to summarize the effects of various factors on the recrystallization kinetics, grain growth after recrystallization, and the grain sizes produced by transformation of high temperature phases to alpha uranium. A brief summary of a method used to prepare single crystals and the attempts to do so by strain-anneal and phase transformation is included. The significance of any data depends on how representative it is in terms of structural uniformity and chemical composition. These two important factors are discussed before describing the effects of other variables.

**1. Effect of method of fabrication on uniformity of recrystallized structures.** When uranium metal is rolled to high reductions in area in the case of rods, or in thickness in the case of plate, the recrystallized grains appear to be grouped in longitudinal bands which differ in average grain size and in orientation with respect to the longitudinal plane of examination. Figure 7a shows the appearance of bands in longitudinal sections of a rod reduced 89% in area from a 0.9-inch diameter casting at a temperature between 500 and 600°C; the same rod as recrystallized at 600°C (Fig. 7b); and a rod reduced 87% in area at 300°C and recrystallized at 475°C (Fig. 7c). The bands appear to



a. 89% reduction in area at 600°C.

b. Same as (a) recrystallized 600°C—  
1 hour.

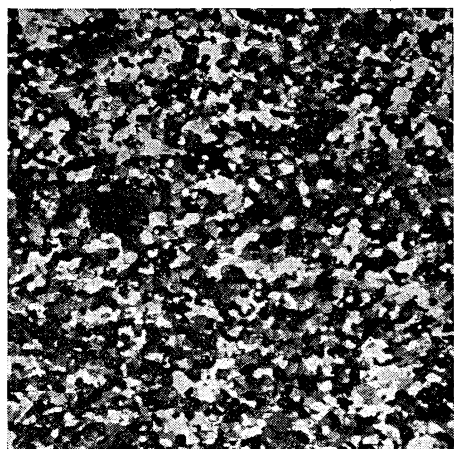
→ Direction of rolling



c. 87% reduction in area at 300°C, annealed 1 hour at 475°C.

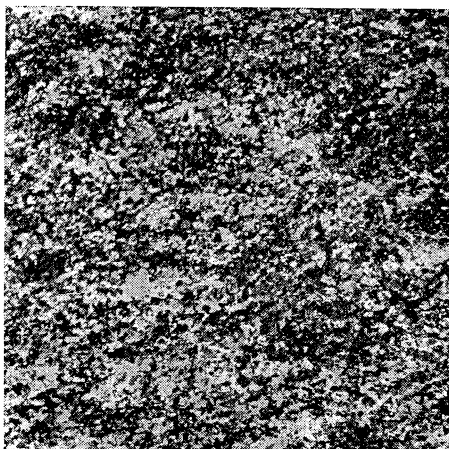
d. High purity rod, 90% reduction in area  
at 300°C, annealed 2 hours at 525°C.

FIG. 7. Banding in rolled and recrystallized uranium rods.



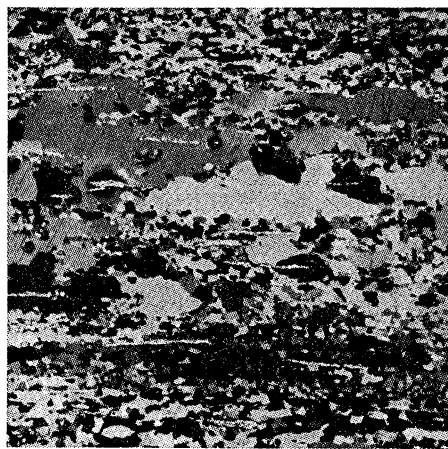
100X

e. 90% total reduction in area at 300°C in 5 steps (15%, 30%, 30%, 48% and 48%) with intermediate recrystallization. Final anneal 1 hour at 475°C.



50X

f. 73% reduction in area at 600°C, heated to 725°C for 3 minutes and water quenched, 47% reduction in area at 300°C and annealed 1 hour at 525°C.



100X

g. Coarse grains within bands after long anneal.

FIG. 7. (Continued)

form as a result of differences in degree and modes of deformation of the grains existing prior to deformation. In Fig. 7a differences in degree of recrystallization during rolling are very obvious. The result of difference in degree of deformation on the uniformity of grain size after recrystallization is apparent in Fig. 7b. Even after heavy deformations below the recrystallization temperature, marked differences in grain size and orientation are evident after recrystallization.

The differences in grain size between such bands are magnified when grain growth is less inhibited, as shown in Fig. 7d. This material was reduced approximately 90% in area from an ingot of relatively high purity and annealed at 525°C for 2 hours. If a quantitative correlation between per cent reduction, annealing treatment, and grain size were attempted from such nonuniform structures the data would be of little significance.

The differences in grain size between bands can be reduced to a minimum if the coarse-grained billets are reduced in small steps with intermediate recrystallization between each reduction step. Figure 7e shows a longitudinal section of a high purity rod which was rolled from a 1-inch diameter ingot by a 5-step schedule with a 48% final reduction in area and annealed one hour at 475°C. Very little variation in grain size was observed, but a careful study of the structure using polarized light revealed that traces of banding were still present.

Both differences in orientation and grain size between bands can be minimized by subjecting the rod to a fast quenching treatment from the beta phase at some intermediate stage of rolling. Figure 7f shows the structure of an impure material which was reduced 73% in area at 550°C from a 1-inch diameter ingot, heated at 700°C for 3 minutes and water quenched, further reduced 47% in area at 300°C and recrystallized at 525°C. Instead of the longitudinal fibrous appearance, small patches of similarly oriented grains are observed.

An interesting effect of banding occurs when heavily reduced rods, even of impure material, are annealed at temperatures between 600 and 650°C. Those bands which recrystallized to very fine grain sizes during the early stages of annealing may contain abnormally large grains after prolonged annealing (Fig. 7g).

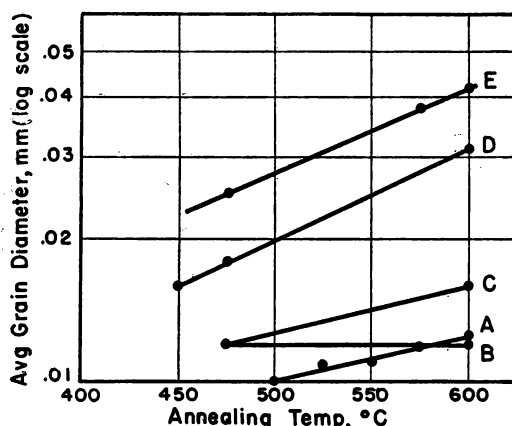
## 2. Effect of impurities

*a. Effect of inclusions on grain growth.* From a lengthy study by E. S. Fisher<sup>2</sup> of grain growth in uranium containing different quantities of impurities it is concluded that most elements are nearly insoluble in alpha uranium, i.e., very small weight per cents can produce a second phase. Consequently, grain growth in uranium is extremely sensitive to differences in purity and to the heat treatments that affect the dispersion of the second

phase. If the inclusions are in finely dispersed form they will have a much greater inhibiting effect on grain boundary movement than the same amount of material in relatively large inclusions. The inhibiting effect of both types of inclusions will increase with their concentration.

It was also concluded that many of the impurities are much more soluble in gamma uranium than in the alpha phase, with the solubility increasing with increasing temperature in the gamma phase. If the metal is quenched to room temperature from some solution temperature in the gamma range, the solute reprecipitates during 300°C rolling and inhibits grain growth after recrystallization to an extent dependent on concentration. However, at temperatures between 600 and 660°C the inhibiting effect of the precipitate is decreased with time because of coalescence of particles or because of slightly higher solubility in the high alpha range, so that the character of grain growth changes to a discontinuous type.

The above conclusions are based on correlations between chemical composition, microscopic observations of inclusions, and grain size. Figure 8 shows grain size versus temperature curves of five different lots of material for one-hour anneals after 300°C rolling. All the rods were reduced by a step reduction process with a 50% final reduction in area. Curve A is for an impure material containing 230 ppm carbon, 40 ppm nitrogen, 30 ppm silicon and 30



All rods similarly fabricated.

Curve A—impure material.

B—impure material plus tantalum.

C—high purity uranium—high concentration of submicroscopic inclusions.

D—high purity uranium—low concentration of submicroscopic inclusions.

E—high purity uranium—very low concentration of submicroscopic inclusions.

FIG. 8. Average grain size after 1-hour anneals at different temperatures for different inclusion dispersions.

ppm iron. The as-etched microstructure showed numerous inclusions. The grain sizes at temperatures up to 600°C were relatively small, as might be expected from the inclusion concentration. The material of Curve B contained 200 ppm carbon, approximately 10 ppm each of nitrogen, silicon and iron, plus 200 ppm of tantalum. The microstructure appeared free of inclusions, but grain growth was strongly inhibited as indicated by very insignificant effect of annealing temperature.

The high purity metals, containing 10–40 ppm carbon and less than 15 ppm of the other impurities, all appeared relatively free of inclusions. Grain growth, however, varied considerably, with no direct correlation between grain growth and chemical composition. Curves C, D and E are examples of the types of grain growth curves one could obtain from some lots of material by proper choice of heat treatment prior to fabrication. In other lots of material the range of inhibition was narrower, i.e., curves such as D and E could be produced but the highly inhibited structures could not.

Discontinuous grain growth, or grain coarsening, at annealing temperatures above 600°C was a further indication of the differences in inhibition between lots. Figure 9 shows grain size versus time of annealing at 650°C for five

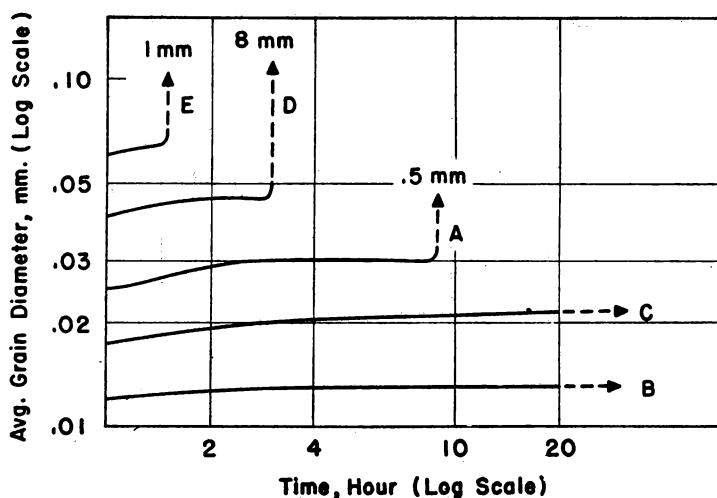


FIG. 9. Average grain size vs time at 650°C for the 5 different materials described in Fig. 8.

different lots of material. The vertical parts of the curves indicate grain coarsening and the relative heights indicate the coarse grain sizes resulting from coarsening after prolonged annealing. Note that the impure material, Curve A, exhibited coarsening, whereas the inclusion-free materials, Curves B

and C, remained fine grained. The coarse grain size in the impure material was, however, limited by the inhibition due to the large inclusions (grain sizes up to 1 mm could be produced in such material). In the high purity material, the coarse grain size and the incubation period for coarsening varied with the concentration of fine particles and with differences in matrix grain sizes before coarsening occurred. Figure 10 is a schematic representation of the effect of

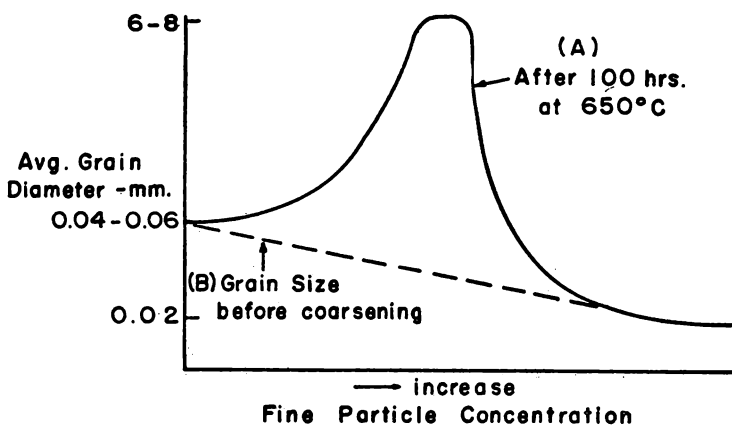


FIG. 10. Postulated curves relating average grain size, after (A) 100 hours at 650°C, and (B) before coarsening, and fine particle concentration.

fine particle concentration on grain size after prolonged anneals at 650°C. For the maximum grain size an optimum concentration exists.

*b. Effect of impurities on recrystallization.* Although it seems probable that the recrystallization temperatures would be affected by inclusion dispersion as is continuous grain growth, this effect has not been extensively investigated. Figure 11 shows the relative recrystallization temperatures after 1-hour anneals for the material represented by Curves A and D, respectively, in Fig. 9, as determined from Vicker's hardness measurements on metallographically polished longitudinal sections. Metallographic observations showed the high purity material to be completely recrystallized at 425°C, whereas the impure material was completely recrystallized at 475°C. In both of these materials the grain sizes were relatively uniform throughout the specimens as a result of step-reduction rolling prior to recrystallization.

From a study of critical strain in various materials it was found that, other conditions being similar, the critical strain, as determined from grain size observations, for 650°C anneals decreased with decreasing concentration of both large and submicroscopic particles. Impure materials (Curve A in Fig. 8) had a critical room temperature tensile strain of approximately 1.2%

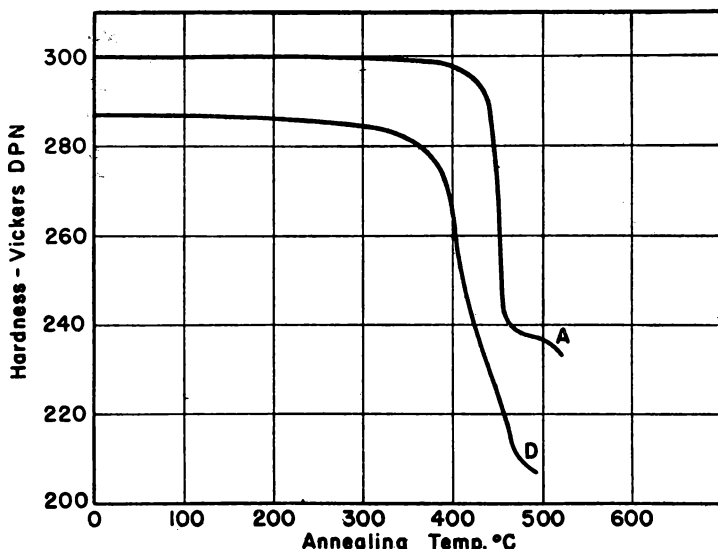


FIG. 11. Vickers hardness versus annealing temperature after 50% final reduction at 300°C for high purity material (D) and low purity material (A). Both curves are for 1-hour anneals.

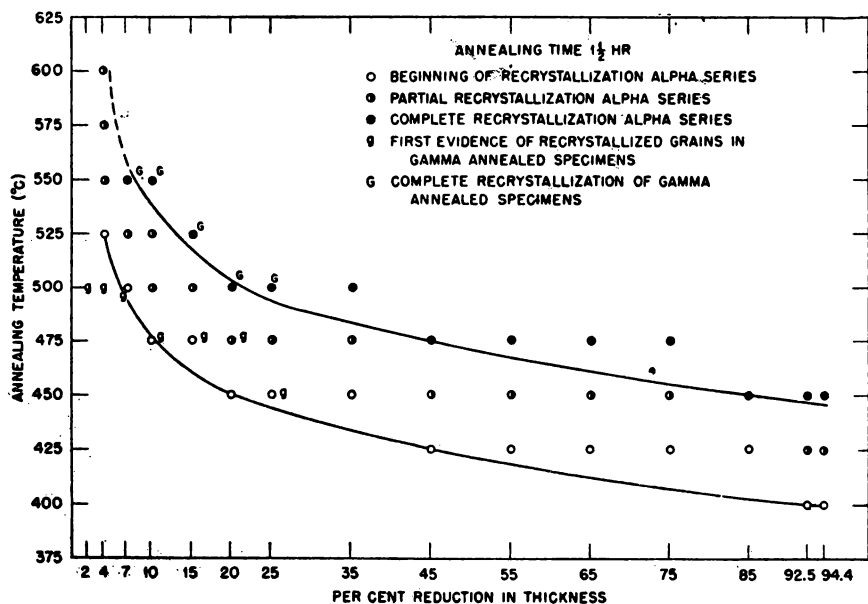


FIG. 12. Recrystallization temperatures as function of per cent reduction of uranium plate at room temperature.

elongation, as did the materials represented by Curve C of Fig. 8. Critical strains of 0.5% were found in lesser inhibited specimens, decreasing to 0% for the high purity material which exhibited grain coarsening.

### 3. Effect of degree of work hardening on recrystallization

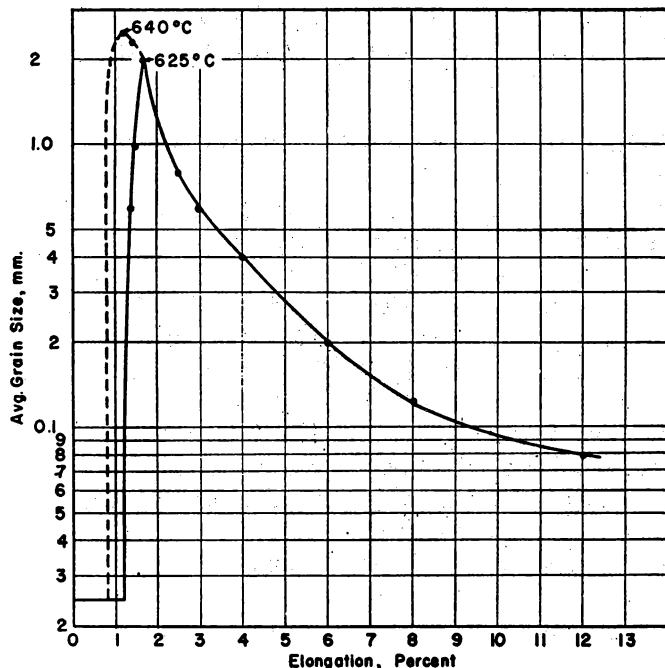
*a. Recrystallization temperature versus room temperature strain in polycrystalline material.* E. E. Hayes<sup>2</sup> has studied recrystallization versus temperature and time for sheet specimens of impure uranium (500 ppm C, 60 ppm Fe) which were reduced 2% to 94% in thickness by room temperature rolling. To prepare the specimens, the casting was extruded at 600°C, rolled at 500°C and machined to  $\frac{3}{16}$ -inch thick slabs; one set was annealed at 600°C (alpha series) and a second set annealed at 843°C (gamma series) prior to final rolling. The specimens were annealed for 1½ hours (at temperatures up to 600°C) after room temperature rolling and subsequently examined metallographically for the degree of recrystallization. The composite results appear in Fig. 12. For 94% reduction, recrystallization began at 425°C and was completed at 450°C. For 4% reduction, recrystallization started at 525°C and was not complete in the 600°C annealed sample. The results for both sets of specimens were not significantly different.

During strain-anneal studies by E. S. Fisher<sup>2</sup> the effect of per cent elongation in tension on recrystallized grain size was determined for various conditions as described in a later section. For a final anneal of 45 hours at 640°C and a starting grain size of approximately 0.012 mm in impure material, a sharp drop occurred in the grain size versus per cent elongation curve at approximately 1.2% (Fig. 13). It can be concluded that recrystallization did not occur in specimens strained less than 1.2%. For the same material and starting grain size the critical strain for 625°C annealing occurred at 1.6% elongation.

Although the material strained less than the critical strains noted above did not show evidence of recrystallization, examination of the microstructures and x-ray diffraction evidence indicated that the relief of strain by gradual grain growth had occurred.

E. E. Hayes<sup>2</sup> studied the appearance of Debye-Scherrer back-reflection rings as a function of per cent reduction by rolling in sheet. After 2% reduction the reflections from the individual grains showed no effect of deformation; after 4% reductions appreciable continuous background between high intensity spots was observed, and after 10% reduction the rings were continuous.

*b. Recrystallization time versus strain at room temperature.* E. E. Hayes<sup>2</sup> studied the effect of time for recrystallization at various temperatures after 85% reduction at room temperature with the same specimens described above. The data are shown in Table IV. After 24 hours at 400°C recrystallization



Increase of grain size with decreasing strain in elongated, tapered tensile bar annealed by heating at 5°C per hour to 625°C (solid line), and subsequently heated at 640°C for 45 hours (dotted line).

FIG. 13. Grain size vs strain in impure uranium.

TABLE IV. EFFECT OF TIME ON RECRYSTALLIZATION RANGE AFTER 85% REDUCTION AT ROOM TEMPERATURE OF IMPURE MATERIAL

Annealing Temperature, °C	Recrystallization Time	
	Beginning	Complete
350	Over 2 weeks	
375	Over 1 week	
400	24 hr	
425	1½ hr	24 hr
450	5 min	1½ hr
475	1 min	5 min
500		1 min

had started. After one minute at 500°C recrystallization was complete. Using these data the activation energy for the start of recrystallization is calculated to be close to 100,000 calories per mol.

*c. Recrystallization after 300°C rolling.* There is no record of a systematic study of recrystallization temperature as a function of strain at 300°C. Scattered data are available, but an accurate compilation is not possible because of differences in other conditions. However, the 475°C recrystallization temperature for a final reduction of 50% in impure material, corresponds to the recrystallization temperature for impure sheet reduced 50% at room temperature as reported by Hayes.<sup>2</sup> The annealing times, 1 hour and 1½ hours, respectively, are close enough to permit comparison. Further data show that for 87% reduction of impure rods at 300°C, the recrystallization temperature after two hours is also 475°C. Hayes' data for 85% cold worked sheet show a 450°C recrystallization temperature.

*d. Effect of grain size prior to strain.* It is quite probable that the grain size prior to deformation can have a marked effect on recrystallization after small strains. Strain-anneal studies by E. S. Fisher<sup>2</sup> show that a 1-mm grain size bar strained 1.3% in elongation did not recrystallize at 650°C, whereas 0.010-mm penultimate grain size showed a critical strain of 1.0%. It is also probable that a large grain size will lead to nonuniform recrystallization after small reductions by rolling. Recrystallization after large reduction in impure material apparently is not affected significantly by grain size difference, as indicated by E. E. Hayes.<sup>2</sup>

*e. Effect of rolling temperature on recrystallization during rolling.* The effect of rolling temperature on the as-rolled microstructure is of interest in the processing of uranium where reproducibility of structure and properties is desired. However, based on inconsistent data gathered from various sources, this temperature is not easily regulated. Although the temperature of the billet before entering the rolls can be controlled by careful operation, the change in temperature during deformation is markedly affected by the type of mill and the reduction per pass. It is also probable that the reduction per pass determines the effect of the actual temperature. A study of the problem by R. M. Mayfield<sup>2</sup> using a single stand mill indicated that rod finishing temperatures less than 600°C did not yield completely recrystallized structures.

A study of a large number of rods by S. P. Rideout<sup>2</sup> which were rolled in a 6-stand commercial mill showed that the rods which finished at temperatures above 500°C were generally completely recrystallized.

*f. Effect of rolling temperature on recrystallization temperature after rolling.* A comparison of the data on room temperature rolled sheet and 300°C rolled rod, both of impure material, indicates that recrystallization temperatures after 50% final reduction are similar. After 85% reduction the room temperature rolled sheet recrystallized at 450°C after 1½ hours, whereas 300°C

rolled rod was not completely recrystallized after two hours at this temperature.

S. P. Rideout<sup>2</sup> reports that rods rolled in a 6-stand mill which finished at 480°C required over 20 minutes of annealing at 500°C for complete recrystallization. This may be compared with 1 minute at 500°C for cold-rolled sheet reduced 85%; however, the degree of reduction at 480°C is not known.

#### 4. Grain size after recrystallization

a. *Effect of time at temperature.* In Sect. 2 titled "Effect of Impurities," the occurrence of discontinuous grain growth at high alpha temperatures was described. The effect of time depends on the inclusion dispersion, the as-recrystallized grain size and on the type of grain growth under consideration, i.e., continuous or discontinuous grain growth. From observations in different materials there appears to be an equilibrium average grain size after reductions above 40% which increases with temperatures up to the range at which coarsening can occur. The rate of approach to equilibrium decreases with increasing inhibition and with increasing time. For example, the grain size in high purity material represented by Curve D in Fig. 8 showed no significant increase in grain size after ½ hour at 450°C, i.e., the equilibrium grain size was rapidly approached. The impure materials (Curve A in Fig. 8) showed a gradual increase in grain size over a 2-hour annealing period at 475°C and very little change in subsequent annealing. The heavily inhibited high purity materials showed an even less effect of time. At 650°C the grain size increased from 0.018 mm to 0.022 mm over a 115-hour period.

The effect of time on grain size in metal which tended to coarsen was, of course, very marked. The final grain size depended on how fast the first coarse grains grew before a general release in inhibition occurred, which was primarily a function of temperature and the degree of inhibition. It was generally noted that structures attained after 20 hours were close to equilibrium, i.e., longer annealing had little effect on the grain size distribution.

b. *Effect of temperature of annealing.* The temperature of annealing determines the character of grain growth after recrystallization as described above. The effect of temperature on grain size from anneals after 50% final reduction for 5 different lots of material has been shown in Fig. 8. It can be concluded from these curves that the effect of temperature on continuous grain growth decreases with increasing quantity of fine inhibitor. The grain size in rods from impure castings increases significantly with temperature, whereas heavily inhibited high purity material was less affected.

Temperature has a significant effect on the coarse grain size. The maximum coarse grain size was attained at the highest annealing temperatures. At the lower coarsening temperatures the rate of coarse grain growth was not suffi-

cient to prevent the formation of additional coarse grains or a gradual increase in matrix grain size.

*c. Effect of matrix grain size on coarse grain growth.* If a high purity specimen was annealed at a low coarsening temperature (600–625°C) and developed a matrix grain size mixture ranging from 0.04 to 1 mm, further anneals at high temperatures had little effect on the structure. Consequently, slow rates of heating to 650°C produced relatively small coarse grains.

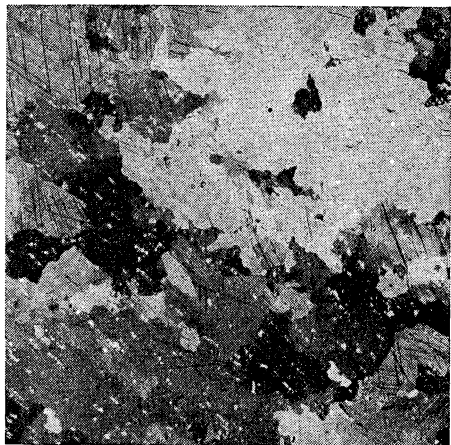
*d. Effect of strain on grain size after recrystallization.* In Fig. 13, grain size after 45 hours at 640°C is plotted against per cent elongation at room temperature. These data are for impure tensile specimens which were machined from rods reduced 90% in area and recrystallized to a fine grain size prior to extension. The curve shows a significant effect of strain differences below 13% elongation, the effect increasing with decreasing strain. Other data indicate that strain differences above 40% reduction in area at 300°C have very little effect on the grain size after recrystallization.

Data by J. H. Bach<sup>2</sup> and S. P. Rideout<sup>2</sup> indicate a marked effect of rolling temperature on grain size after recrystallization. As is to be expected, the grain size increases with temperature of rolling.

## 5. Grain size and structure resulting from transformation

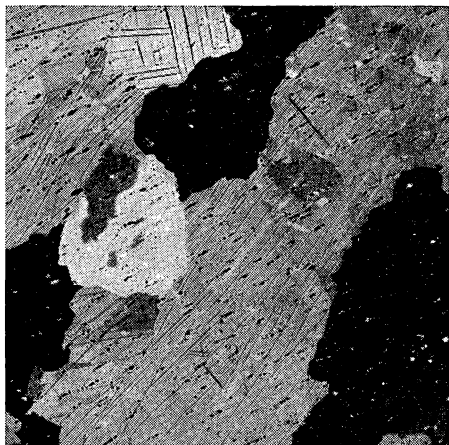
*a. Definitions.* When high purity uranium or impure uranium in which carbon is the predominant impurity is cooled to temperatures below 660°C, grains of the alpha phase form and replace the high temperature phase. Unless the transformation occurs under very special conditions, i.e., extremely slow cooling rates in high purity metal, the grains present at room temperature contain sub-boundaries separating regions of slightly differing orientation. These subgrains can be detected by polarized light examination because of the differences in orientation across boundaries as shown in Fig. 14, and by x-ray diffraction Laue patterns from single grains. The grain size can be defined as the cross-sectional diameter of the volume occupied by a number of subgrains which were formed within the same grain. However, when the difference in orientation between subgrains becomes relatively large this volume will no longer approximate the behavior of a single orientation and the subgrain size may act as the effective grain size. In this section the effect of various factors on the grain size, as defined above, and the degree of orientation difference are summarized.

*b. Factors affecting grain size in uniformly cooled specimens.* When small specimens are uniformly heated into the beta or gamma phase and then transformed to the alpha phase by quenching all of the metal in water or air or by furnace cooling, all parts of the sample transform at about the same time. Data from various sources indicate that the alpha grain size produced under these conditions is primarily dependent on the rate of cooling through the



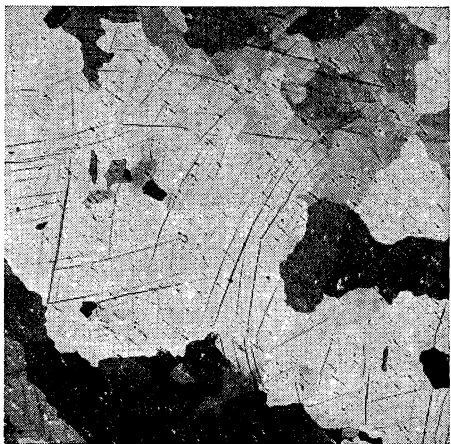
100X

a. Heated 2 hours at 675°C and water quenched.



100X

b. Heated 2 hours at 675°C and furnace cooled.



100X

c. Heated 2 hours at 1000°C, cooled to 800°C, held 1½ hours, water quenched.



100X

d. Same as 14c, furnace cooled.

FIG. 14. Grain sizes in alpha uranium after different transformation heat-treatments.

transformation and, to a lesser degree, on the grain size prior to transformation. The importance of the rate of cooling is demonstrated in numerous data from actual measurements of cooling rates. Figures 14a and 14b (from experiments by L. T. Lloyd<sup>2</sup>) show the alpha grain size in two specimens, both heated in the beta phase under the same conditions, but cooled by quenching in water and furnace cooling, respectively. Water quenching not only produces smaller grains, but the grain boundaries are markedly jagged in comparison to the relatively straight grain boundaries in more slowly cooled specimens. The fast cooling rate apparently prevents appreciable movement of grain boundaries.

The importance of the grain size prior to transformation is indicated by the correlation with temperature and time of heating prior to transformation (Figs. 14a and 14c).

The grain size prior to heating above the transformation temperature and the rate of heating appear to have little effect on the final grain size. Annealing in the alpha phase subsequent to transformation does not affect the grain size significantly, although there is some effect on the shape of the grain boundaries and substructure in high purity metals, as discussed in Sect. 6.

*c. Effect of temperature gradient on grain size.* Uranium specimens which are cooled through the beta to alpha transformation so that a systematic temperature gradient exists contain grains which are generally columnar in shape. These observations were made from experiments by E. S. Fisher<sup>2</sup> on the preparation of single crystals by moving pencil-shaped specimens through a temperature gradient so that the point transformed first. It was observed that the pointed or tapered parts contained a region of equi-axed grains, but the grains above this region were longer in the general direction of the temperature gradient. The number of columnar grains at a section decreased with increasing distance above the point. With impure material a single columnar grain occupying a complete cross section could not be obtained in specimens larger than  $\frac{1}{8}$ -inch diameter. A high purity specimen produced a single crystal slightly less than  $\frac{1}{4}$ -inch diameter. It was concluded that grains tend to grow in a preferred crystallographic direction. If the nuclei were oriented with this direction almost parallel with the specimen axis they grew to long grains; otherwise, the grains would terminate at the cylindrical surface.

The number of grains which existed in the upper part of the specimens did not depend significantly on the rate of movement of the specimen or the starting temperature, but was primarily dependent on the size of the specimen and the purity of the material.

*d. The effect of cooling rate and alpha annealing on subgrains.* The single crystals prepared by the phase change method exhibited a scatter in orientation within a grain of the order of  $10^\circ$  because of accumulation of differences in orientation across sub-boundaries. H. H. Chiswick and L. T. Lloyd<sup>2</sup>

have shown that the number of sub-boundaries formed by the beta to alpha phase change can be considerably reduced, at least in high purity uranium, by extremely slow cooling rates. Small specimens which were heated uniformly to 725°C and cooled to 625°C at 0.5°C per hour contained grains which were similar in perfection to those resulting from recrystallization after deformation. Other specimens which were cooled at 4°C per hour exhibited a significant substructure within the grains.

B. Blumenthal<sup>2</sup> heated high purity specimens which were water quenched from 1000°C at 650°C for 3½ weeks. The grain boundaries appeared relatively straight and no significant substructure was observed within the grain boundaries. It is quite probable that coalescence of subgrains and straightening of pre-existing grain boundaries accounted for this change in structure.

**6. Preparation of alpha uranium single crystals.** Because of the imperfections in single crystals formed by the phase change method it is desirable to prepare single crystals by inducing growth of alpha grains which are more perfect. Attempts to prepare such crystals by strain-anneal techniques have been carried out by a number of laboratories with no success. This lack of success can be attributed to the following causes:

- a. Deformation by twinning causes copious nucleation.
- b. Optimum conditions are difficult to attain (considering inhibition by inclusions, penultimate grain size, degree of strain and temperature of final annealing).

E. S. Fisher<sup>2</sup> has developed a method by which single crystals can be produced from fine, recrystallized alpha grains in high purity uranium. This method makes use of the grain-coarsening phenomenon described in Sect. 2 titled "Effect of Impurities." A concentration gradient of fine inhibitor is produced in rod-shaped specimens by diffusion of small quantities of silicon from the cylindrical surface. The rod is then quenched from the gamma phase and fabricated by a step reduction-annealing schedule so that a fine and close to uniform grain size exists after primary recrystallization. Referring now to Fig. 10, if a close-to-optimum concentration of fine inhibitor exists at the region about the rod axis (as determined by the temperature from which the rod was quenched prior to fabrication) a minimum number of coarse grains will form in this region during prolonged annealing at high temperatures (640–660°C) and grow radially into the fine grained matrix. Under optimum conditions only one coarse grain is produced which grows almost to the cylindrical surface. In most cases a thin layer of fine surface grains remain because of the high silicon concentrations in the outer volume. However, in some cases the grains grow to the surface.

Up to the present no single crystals larger than ¼-inch diameter have been

made by this method. The single crystals exhibited no substructure under polarized light examination. The x-ray diffraction spots from normal Laue techniques show no segmentation.

### E. THERMAL EXPANSION CHARACTERISTICS OF URANIUM

Two of the uranium allotropic modifications are anisotropic in nature, namely, the orthorhombic alpha uranium and the tetragonal beta uranium. Because of these lattice anisotropies, their linear thermal expansion coefficients are dependent upon the specific crystallographic directions under consideration. True measurements of linear thermal expansion coefficients cannot be obtained from polycrystalline samples of these phases; they must be either calculated from x-ray determinations of lattice parameters as a function of temperature, or determined by dilatometric measurements performed on single crystals. On the other hand, true measurements of linear thermal expansion coefficients of the body-centered cubic gamma uranium can be obtained from dilatometric studies of polycrystalline materials.

**1. Thermal expansion coefficients determined from x-ray measurements.** No systematic studies have been made of the beta and gamma uranium lattice parameters as a function of temperature. Values of the alpha uranium lattice parameters over the temperature range 25 to 625°C have been reported by C. M. Schwartz and D. A. Vaughan.<sup>2</sup> These values have been used to calculate the volumetric and linear thermal expansion coefficients for alpha uranium.

Table V records the volumetric thermal expansion coefficients and the linear thermal expansion coefficients for the three principal crystallographic directions of alpha uranium. The values were determined from the mean expansions over the temperature intervals indicated. The equations which give the volume and the lengths in the three principal crystallographic directions at temperature  $T$  (°C) as a function of the original dimensions and the temperature are:

$$V_T = V_{25}(1 + 32.03 \times 10^{-6}T + 32.87 \times 10^{-9}T^2 + 16.25 \times 10^{-12}T^3) \quad (1)$$

$$L_{[100]_T} = L_{[100]_{25}}(1 + 10.64 \times 10^{-6}T + 47.46 \times 10^{-9}T^2 - 16.65 \times 10^{-12}T^3) \quad (2)$$

$$L_{[010]_T} = L_{[010]_{25}}(1 - 1.503 \times 10^{-6}T + 9.09 \times 10^{-9}T^2 - 31.79 \times 10^{-12}T^3) \quad (3)$$

$$L_{[001]_T} = L_{[001]_{25}}(1 + 19.69 \times 10^{-6}T - 7.79 \times 10^{-9}T^2 + 43.26 \times 10^{-12}T^3) \quad (4)$$

TABLE V. MEAN VOLUMETRIC AND LINEAR THERMAL EXPANSION COEFFICIENTS OF ALPHA URANIUM

Tempera-ture, °C	Mean Thermal Expansion Coefficient per °C			
	$a \times 10^6$	$b \times 10^6$	$c \times 10^6$	$v \times 10^6$
25–100	17.74	-0.68	22.6	39.70
25–175	21.02	-0.91	22.3	42.40
25–250	24.92	-1.28	22.96	46.60
25–325	27.33	-2.10	24.01	49.20
25–400	28.79	-3.27	25.61	51.10
25–475	30.75	-4.62	28.03	54.20
25–550	33.24	-6.49	30.36	57.10
25–625	35.16	-8.49	32.62	59.30

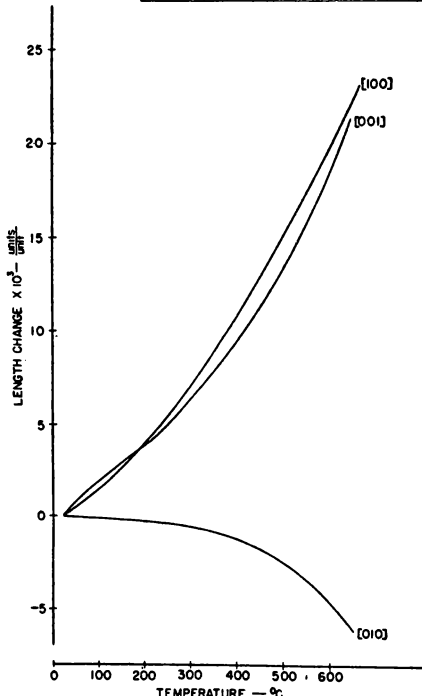


FIG. 15. Length changes of the three alpha uranium principal crystallographic directions as a function of temperature.

Figure 15 shows the curves of the length changes for the three principal crystallographic directions as a function of temperature. The length changes for the [100] and [001] directions are similar, the former being slightly larger. The length change for the [010] direction is negative; the higher the temperature, the smaller the dimension becomes.

**2. Thermal expansion coefficients and characteristics determined from dilatometric measurements.** Dilatometric curves of single crystal expansions have been determined for five alpha uranium samples by L. T. Lloyd.<sup>2</sup> The crystallographic directions of testing for all these crystals were within a few degrees of the [010] axes. The thermal expansion coefficient is slightly positive at low temperatures. As the temperature increases the thermal expansion coefficient decreases, passes through an inversion, and becomes negative. The temperature at which the inversion occurs is dependent upon the angular misorientation of the test-

ing direction from the [010] direction; the greater this misorientation the higher is the temperature of inversion. These experimental determinations prove physically that the linear thermal expansion coefficient in the [010] direction is negative. No attempt has been made to analyze these data for thermal expansion coefficients in the three principal directions of the alpha uranium lattice. The errors in the coefficients for the [100] and [001] directions would be great because these are considerably displaced (nearly 90°) from the direction along which the thermal expansion measurements were made.

The pronounced anisotropy of thermal expansion in alpha uranium is demonstrated by the dependency of the measured values upon the previous fabrication history, thermal history, and direction of testing of polycrystalline samples. Tables VI and VII give representative values of the mean thermal expansion coefficients of uranium rods of various histories between 25° and 100°C. All thermal expansion coefficients were determined parallel to the axis of the rod. The mean thermal expansion coefficient of essentially randomly oriented polycrystalline material ( $\beta$  treated)\* in this temperature range is about  $16 \times 10^{-6}$  units/unit/°C. Increased per cent reduction in area at 300° and 600°C causes the mean thermal expansion coefficient to decrease; the coefficient of the former is reduced more than the latter. For a constant per cent reduction in area, the mean thermal expansion coefficient is reduced with a decrease in rolling temperature. Recrystallization causes the mean thermal expansion coefficient to be decreased over that observed on the material in the as-cold-rolled condition.

These data are consistent with the preferred orientations determined for the same specimens by M. H. Mueller.<sup>2</sup> Increased per cent reduction in area causes an increase in the (010) preferred orientation. The [010] direction in alpha uranium has a negative thermal expansion coefficient. An increase in the (010) preferred orientation should result in a decrease in the mean thermal expansion coefficient; the data are in agreement. At 300°C the increase in (010) preferred orientation is more pronounced than at 600°C; thus, the mean thermal expansion coefficients for material rolled at the former temperature are decreased more rapidly than those for the latter. As the temperature of rolling is increased, for a constant per cent reduction, the (010) preferred orientation is decreased; again, the mean thermal expansion coefficients are in agreement. Recrystallization causes the (110) preferred orientation component to be shifted towards the [010] direction and the (010) preferred orientation is shifted away from the [010] direction; the former component is shifted further towards the [010] than the latter is shifted away from it. Qualitatively, this indicates that the mean thermal expansion coefficient should be reduced by recrystallization. The data indicate this to be true.

\* A specimen heated to 725°C and either slow-cooled or quenched to room temperature.

TABLE VI. MEAN THERMAL EXPANSION COEFFICIENTS OF ALPHA URANIUM RODS FOR VARYING FABRICATION TREATMENTS AND PER CENT REDUCTIONS IN AREA

(R. M. Mayfield)<sup>2</sup>

Treatment Prior to Final Rolling	Nominal Finish Rolling Temperature, °C	Mean Thermal Expansion Coefficients (25°–100°C) × 10 <sup>6</sup> units/unit/°C			
		0% Reduction	10% Reduction	45% Reduction	70% Reduction
600°C rolled—80%	300	13.42	10.16	8.62	8.94
600°C rolled—80% and beta treated	300	15.98	12.8	10.02	9.17
600°C rolled—80% and beta treated	600	15.86	14.9	13.39	12.71

TABLE VII. MEAN THERMAL EXPANSION COEFFICIENTS OF ALPHA URANIUM RODS FOR VARYING TEMPERATURE OF ROLLING AND THERMAL TREATMENT, UNIFORM 75% REDUCTION IN AREA

(R. M. Mayfield)<sup>2</sup>

Nominal Rolling Temperature, °C	Mean Thermal Expansion Coefficients (25°–100°C) × 10 <sup>6</sup> units/unit/°C	
	As Rolled	Recrystallized at Approximately 625°C
300	8.5	6.8
400	9.3	7.9
500	11.4	9.2
600	12.9	—
640	14.1	—

The mean thermal expansion coefficient data given above do not represent the nature of the entire thermal expansion curves for these materials. This is particularly true for rods rolled at 300°C and recrystallized. A series of typical expansion curves obtained by L. T. Lloyd<sup>2</sup> in a direction parallel to the rolling direction for such a specimen is shown in Fig. 16. As the temperature increases, the specimen elongates with a positive thermal expansion coefficient until an inversion point is reached at approximately 180°C; continued

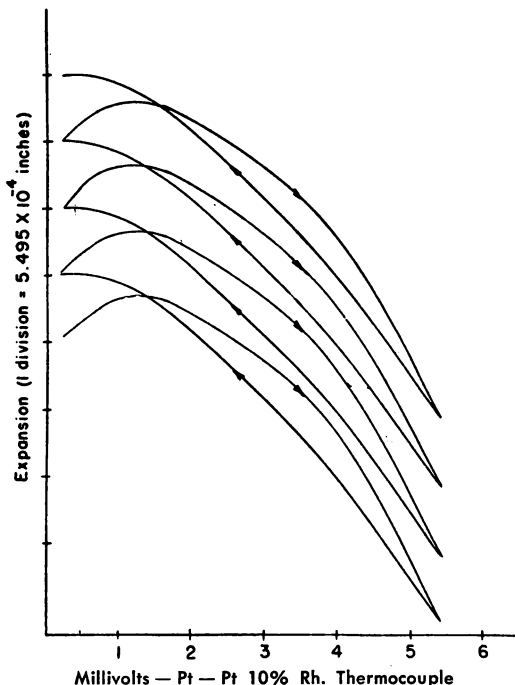


FIG. 16. Thermal expansion curves for a 300°C alpha rolled uranium sample cycled in alpha range (30 to 630°C). The bottom curve represents the first thermal cycle expansion curve, the curve directly above that represents the second thermal expansion curve, etc.

heating causes the specimen to contract. The cooling curve does not follow the heating curve because of the plastic interaction between grains. When the sample again reaches room temperature it is longer than it was prior to the thermal cycle. Additional cycling of the sample further increases its length.

Similar thermal expansion curves for 300°C rolled and alpha annealed uranium rods have been observed by A. D. Schwope.<sup>2</sup> In general, an increase in length as a result of each thermal cycle occurs regardless of the temperature interval of cycling. For a particular sample, depending upon its past fabrication and thermal history, it is possible to select a temperature interval of cycling which results in a zero net length change of the specimen. Uranium rods rolled at 600°C show a similar increase in length as a result of thermal cycling, but to a lesser extent. In these cases the expansion curves do not go through an inversion, but rather the thermal expansion coefficients are positive at all temperatures.

The thermal expansion characteristics of alpha uranium developed by

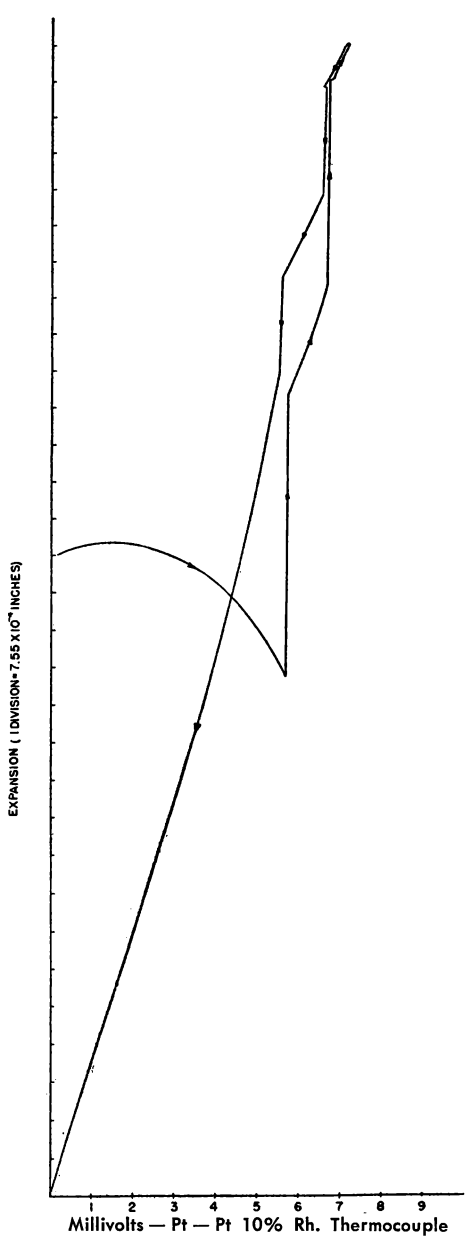


FIG. 17. Typical thermal expansion curve of a 300°C rolled and 575°C annealed uranium sample.

previous fabrication and thermal history may be changed by causing the sample to undergo phase transformation. A typical expansion versus thermocouple millivoltage curve obtained in a direction parallel to the rolling direction for a 300°C rolled and 575°C annealed sample is shown in Fig. 17. The specimen shows an initial elongation at low temperatures followed by a contraction as the temperature is further increased. At the alpha to beta transformation temperature the sample increases in length abruptly. Within the beta phase expansion is at a uniform rate. At the beta to gamma transformation temperature the sample again increases in length abruptly, but to a lesser extent than at the alpha to beta transformation temperature. Expansion in the gamma phase is at a uniform rate. Upon cooling the sample contracts uniformly in the gamma phase and decreases in length as it passes through the gamma to beta transformation temperature. The contraction during this phase transformation is smaller than that observed upon heating. The specimen contracts uniformly within the beta phase, but at a different rate than that observed upon heating. This behavior would be expected because of the lattice anisotropy of the beta phase. Further cooling through the beta to alpha transformation temperature results in a sharp contraction, but of smaller amount than that observed upon heating through the alpha to beta

transformation. Subsequent cooling in the alpha region results in a uniform contraction of the sample. The difference in the heating and cooling curves in the alpha region is brought about by a reorientation of the structure resulting from destruction of the preferred orientation by passage through phase transformations.

The expansion characteristics of the alpha phase, after passage through phase transformation temperatures, are not predictable. In some cases the specimen may show an expansion upon cooling after phase transformation. The curve for a specific sample may and probably would be entirely different from the curve shown here. In general, however, there is a greater tendency for specimens to show cooling curves in the alpha region similar to that of Fig. 17, regardless of the previous fabrication and thermal history.

The thermal expansion curves for rolled uranium sheet materials differ from those obtained from rod specimens. This behavior is that which is expected as a result of the differences in preferred orientation developed in rolled uranium sheet over those developed in rolled uranium rods. Figure 18 (L. T. Lloyd<sup>2</sup>) is a typical series of length change curves obtained from uranium sheet which was given a final reduction of 75% in area at 300°C. The thermal

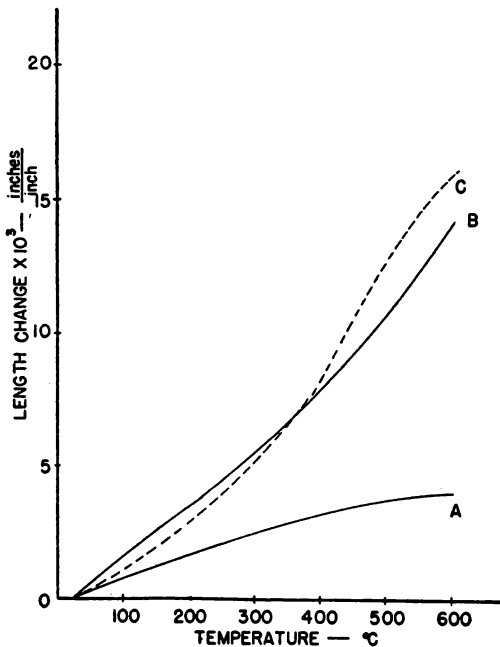


FIG. 18. Thermal expansion curves for uranium sheet given a final reduction of 75% in thickness at 300°C.

expansion curves for three mutually perpendicular directions are shown: curve A is the plane of the sheet parallel to the rolling direction, curve B is in the plane of the sheet perpendicular to the rolling direction, and curve C is perpendicular to the plane of rolling. The latter curve was obtained from the volumetric thermal expansion of alpha uranium, as calculated from x-ray lattice parameter determinations and the data of curves A and B. The thermal expansion curve in the direction parallel to the rolling direction shows a relatively low value of thermal expansion coefficient as compared to those for the other two directions. It does not, however, show a negative thermal expansion coefficient as do the curves obtained from rods reduced in area to a comparable reduction. This agrees with the preferred orientations of the two materials. Qualitatively, the (010) component in the rod orientation is stronger than that in the sheet for comparable reductions in area. The thermal expansion curves in the other two directions of the sheet material are similar despite the fact that there is a difference in the preferred orientations. These preferred orientation differences involve primarily the [100] and [001] directions. The thermal expansion curves for these crystallographic directions do not differ greatly; this accounts for the similarity of curves B and C.

It was stated above that true measurements of the thermal expansion coefficients of beta uranium cannot be obtained from polycrystalline samples because of its lattice anisotropy. No studies of the lattice parameters of pure uranium as a function of temperature are available, nor are thermal expansion curves for single crystals. Dilatometric studies of polycrystalline uranium in the beta phase indicate the mean thermal expansion coefficient over the temperature range 675–750°C to be from 9.6 to  $47.6 \times 10^{-6}$  units/unit/°C (L. T. Lloyd<sup>2</sup>). The beta uranium lattice parameters of a 1.4 weight per cent chromium-uranium alloy have been determined at 20 and 720°C.<sup>10</sup> The beta phase, which is stable at 720°C in an alloy of this chromium content, can be retained in a metastable state at 20°C by quenching. From the lattice parameters determined at these two temperatures, the mean thermal expansion coefficient was calculated to be  $23 \times 10^{-6}$  units/unit/°C for the  $a_0$  axis and  $4.6 \times 10^{-6}$  units/unit/°C for the  $c_0$  axis. The maximum value obtained from the dilatometric studies greatly exceeds that calculated for the  $a_0$  axis. This discrepancy can possibly be attributed to a nonlinear relationship between the  $a_0$  lattice parameter and temperature. The slope of this curve may be greater at higher temperatures and thereby yield a greater value of mean thermal expansion coefficient over a small temperature range at high temperatures.

The mean thermal expansion coefficient data obtained from dilatometric studies of polycrystalline gamma uranium are valid because of the isotropic nature of its crystallographic structure. The average mean thermal expansion coefficient of gamma uranium over the temperature range 775 to 800°C, as

determined from several dilatometric tests by L. T. Lloyd,<sup>2</sup> is  $22.6 \pm 1.0 \times 10^{-6}$  units/unit/ $^{\circ}\text{C}$ . The mean thermal expansion coefficient for gamma uranium over the temperature range room temperature to  $805^{\circ}\text{C}$  can be calculated from lattice parameter data. J. Thewlis<sup>12</sup> has reported the lattice parameter for gamma uranium at  $805^{\circ}\text{C}$ . A. S. Wilson and R. E. Rundle<sup>13</sup> have determined the room temperature lattice parameter of gamma uranium stabilized with molybdenum. These lattice parameters were used to extrapolate to the value at zero per cent molybdenum. The mean thermal expansion coefficient for this temperature range, as calculated from the lattice parameters, is  $18 \times 10^{-6}$  units/unit/ $^{\circ}\text{C}$ . The difference between the value determined from dilatometric studies and that which was calculated is not large if the differences in the temperature ranges are taken into consideration.

#### F. MECHANICAL PROPERTIES OF URANIUM

Since uranium is a highly anisotropic material, the mechanical properties are affected considerably by orientation, a result of fabrication and heat treatment. Uranium has a very low proportional limit; consequently there is very little straight line portion to the stress-strain curve obtained under normal practice. N. Grossman and S. Priceman<sup>14</sup> obtained compressive values of Young's modulus, Poisson's ratio, shear and bulk moduli, modulus of resilience, proportional limit, and yield strength using SR-4 strain gages on two specimens of hot-rolled uranium 2.5 inches long by 0.900 inch in diameter. Stress-strain curves for the low stress regions of the initial loading are illustrated in Fig. 19. A complete stress-strain curve is shown in Fig. 20. The longitudinal and transverse strains are plotted as a function of stress in Fig. 21. The elastic properties obtained are summarized in Table VIII. The authors conclude from their limited results that there is a very low but well-defined proportional limit (3000 psi), Poisson's ratio is not a constant but increases with increasing stress, and that any determination of Young's modulus and an offset yield strength by the standard initial tangent method is of little practical significance. Yield strength values may be obtained by an arbitrary method outlined by Chiswick, Mayfield and Mueller.<sup>2</sup> Load values are chosen so that,

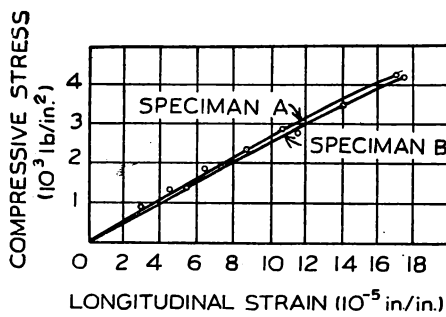


FIG. 19. Compression stress-strain curves of hot-rolled uranium in low stress region. [From N. Grossman and S. Priceman,<sup>14</sup> *Compressive Properties of Uranium*, *Nucleonics* 12: No. 6, pp. 68-69 (June, 1954).]

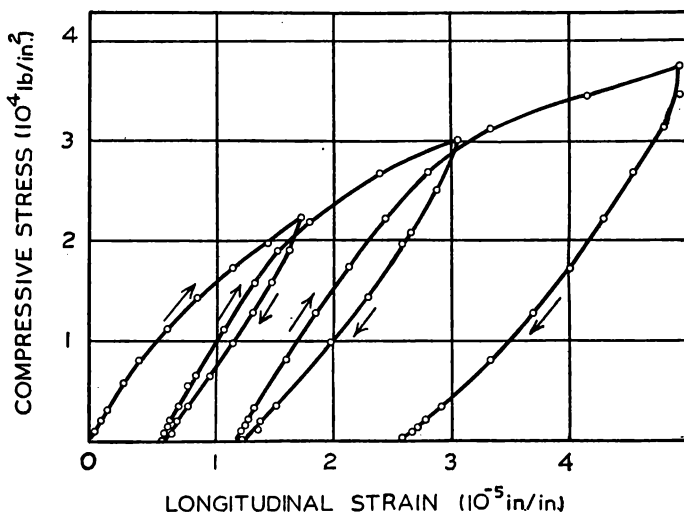


FIG. 20. Complete compressive stress-strain curve for hot-rolled uranium specimen B. [From N. Grossman and S. Priceman,<sup>14</sup> *Compressive Properties of Uranium*, Nucleonics 12: No. 6, pp. 68-69 (June, 1954).]

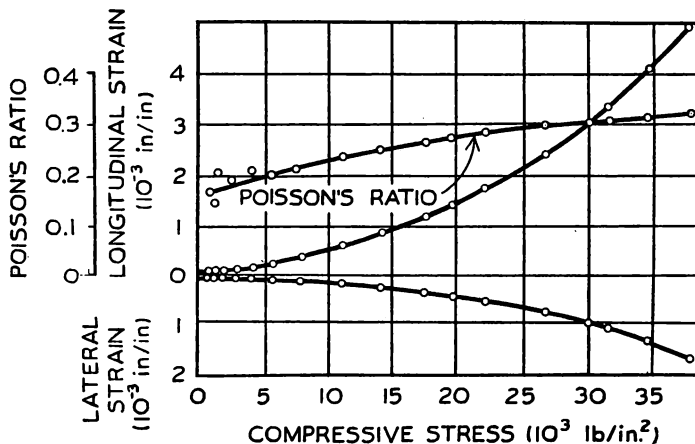


FIG. 21. Longitudinal and transverse stress-strain curves and Poisson's ratio for hot-rolled uranium specimen B. [From N. Grossman and S. Priceman,<sup>14</sup> *Compressive Properties of Uranium*, Nucleonics 12: No. 6, pp. 68-69 (June, 1954).]

TABLE VIII. ELASTIC PROPERTIES OF URANIUM IN COMPRESSION  
(Average Values)

[N. Grossman and S. Priceman,<sup>14</sup> *Compressive Properties of Uranium*, Nucleonics 12: No. 6, pp. 68-69 (June, 1954)]

Modulus of Elasticity, psi	$25.5 \times 10^6$
Poisson's Ratio	
(Limit value at zero stress)	0.20
Shear Modulus, psi	$10.6 \times 10^6$
Bulk Modulus, psi	$14.2 \times 10^6$
Modulus of Resilience in lb/in. <sup>3</sup>	0.176
Proportional Limit, psi	3,000
Yield Strength, (approx.) psi	
0.1% Offset	27,000
0.2% Offset	33,000

upon removal, the resulting permanent set is near the predetermined offset value. Slight corrections may be made by passing a straight line through the required offset value and parallel to a line between the end point and zero stress point of an unloading curve.

As a result of the capricious nature of uranium, numerous attempts have been made to determine the elastic constants by dynamic means based on the measurements of sound velocities. Table IX contains the results of H. L. Laquer, W. E. McGee and M. F. Kilpatrick,<sup>15</sup> M. B. Reynolds,<sup>16</sup> and E. W. Kammer, I. Vigness and L. C. Cardinal.<sup>2</sup> The manner in which some of the elastic constants change with temperature is shown in Fig. 22. Orientation

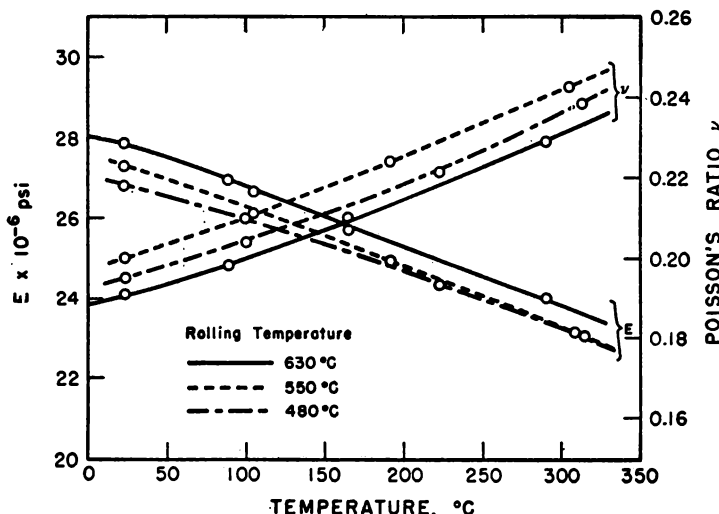
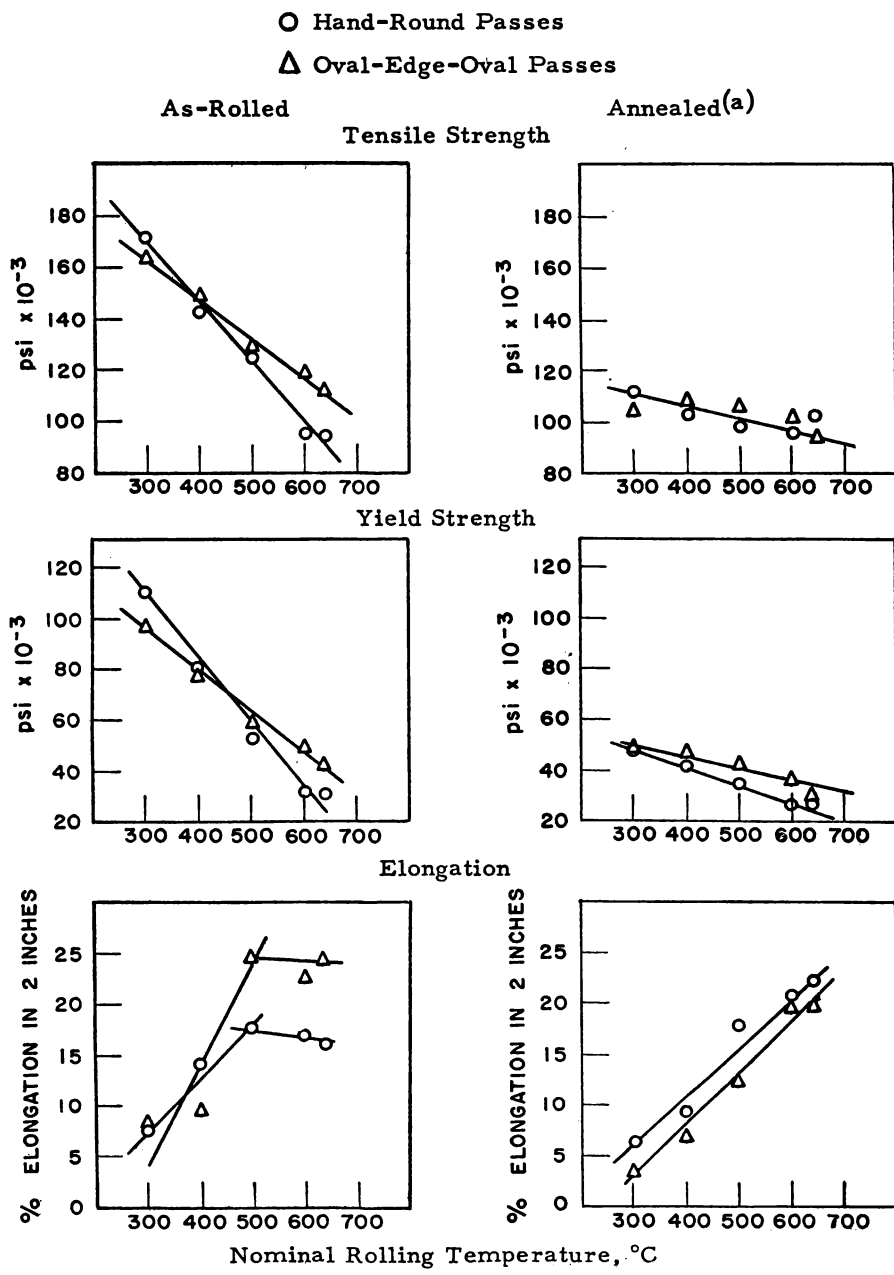


FIG. 22. Young's modulus and Poisson's ratio as a function of rolling temperature.

TABLE IX. SUMMARY OF ELASTIC CONSTANT DATA OBTAINED BY ULTRASONIC TECHNIQUES

Condition	Young's Modulus (psi $\times 10^{-6}$ )	Shear Modulus (psi $\times 10^{-6}$ )		Poisson's Ratio		$\frac{1}{E} \frac{dE}{dT}$ ( $10^{-4}/^{\circ}\text{C}$ )
Laquer, McGee and Kilpatrick <sup>c</sup>						
1 Swaged, annealed	29.1	11.9		0.22		
3 Extruded	29.3	12.0		0.21		
4 Extruded	30.3	12.1		0.25		
7 Cast	29.5	12.1		0.22		
8 Cast	30.0	12.1		0.24		
Reynolds <sup>d</sup> Uranium cubes, alpha-rolled and water-quenched from 740°C	25.5	10.2		0.25		
Kammer, Vigness and Cardinal						
Group A	25°C	300°C	25°C	300°C	25°C	300°C
No History	27.0 25.5 <sup>a</sup> 22.9 <sup>b</sup>	23.3	11.5	9.61	0.18	0.22
Group B						
Alpha-rolled and an- nealed $\frac{1}{2}$ hour at 600°C	26.2 26.4	22.6 22.5	11.0 11.2	9.09 9.14	0.19 0.19	0.24 0.24
Alpha-rolled and $\beta$ - treated 70 seconds at 720°C	28.0 29.1	23.6 24.1	11.9 12.3	9.53 9.76	0.18 0.19	0.23 0.24
Group C						
Rough rolled to $1\frac{1}{2}$ in. diam. at 600°C. Finish rolled to 1 in. diam. at temperature indicated:						
630°C	27.4	23.6	11.4	9.50	0.20	0.23
550°C	26.8	22.9	10.9	9.32	0.20	0.24
480°C	26.4	22.8	11.0	9.19	0.20	0.24

<sup>a</sup> Using method of Laquer, McGee and Kilpatrick.<sup>b</sup> Static test in compression.<sup>c</sup> See Reference 15.<sup>d</sup> See Reference 16.



(a) In argon, at times and temperatures required to produce grain size of 0.025–0.035 mm for 300, 400, and 500°C rolled material.

FIG. 23. Tensile properties of uranium as rolled and annealed.

variations, differences in fabrication and treatment, as well as individual techniques, probably account for the range of values reported. Still, the most accurate elastic constant values are probably obtained in this manner in contrast with a certain amount of guesswork involved in treating ordinary tensile test data.

R. M. Mayfield and H. H. Chiswick<sup>2</sup> have determined the variation of tensile properties with rolling temperature and roll pass design in both the as-rolled and annealed conditions. Rolling temperature was measured using a radiation-type pyrometer and a fast-acting recorder. For the single stand mill used, the actual finish rolling temperature was found to be considerably below the nominal preheat bath temperature for 500, 600, and 640°C rolling, and somewhat higher than the bath temperature for 300 and 400°C rolling. For rods rolled at 500°C and below, the rolling direction texture was predominantly (010-

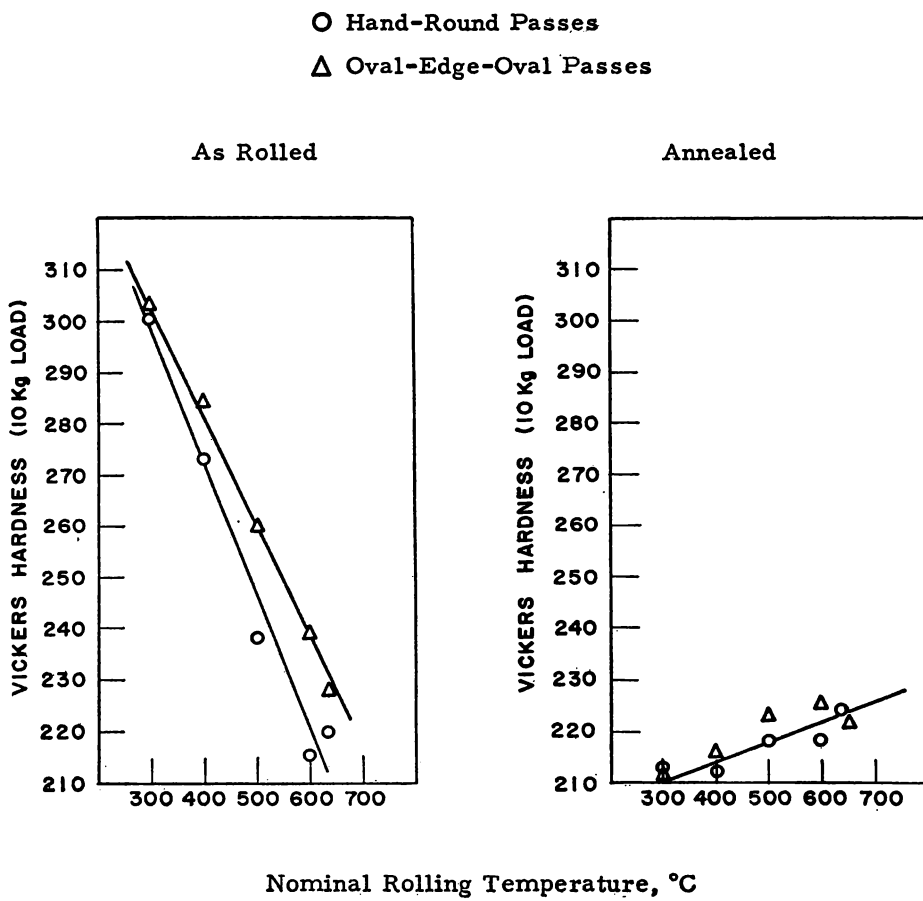


FIG. 24. Hardness of uranium as rolled and annealed.

120), which changed to a (140) upon annealing. [Most of the 600 and 640°C rolled rods were recrystallized in the as rolled condition, and the texture was predominantly (110-010).] The test results are summarized in Figs. 23 and 24. Significant variations of tensile properties in the rolling direction with rolling temperature are apparent. The effect of roll pass design was not pronounced in most cases. Annealing of 300°C rolled uranium in an argon atmosphere was found to lower the ductility, the decrease becoming more pronounced with higher annealing temperatures for longer periods of time. Annealing in vacuum produces no such effect. Typical results are shown in Table X.

TABLE X. VARIATION OF PROPERTIES OF 300°C ROUND ROLLED URANIUM RODS WITH ANNEALING TREATMENT

Annealing Treatment	Grain Size Average Diameter, mm	Ultimate Tensile Strength, psi	Yield Strength 0.2% Set, psi	Reduction of Area, %	Elongation in 2 in., %
575°C, 2 hr (0.05 $\mu$ vacuum)	0.012	124,000	57,000	14	12
575°C, 2 hr (argon)	0.011	120,000	52,000	13	11
635°C, 48 hr (10-20 $\mu$ vacuum)	0.03	126,000	52,000	14	11
635°C, 48 hr (argon)	0.03	125,000	57,000	6	6
630°C, 18 hr (argon)	0.035	113,000	49,000	7	7
655°C, 48 hr (argon)	0.045	107,000	51,000	2	3
As-rolled	—	171,000	109,000	14	7.5

Similar observations have been reported by G. Hanks, J. Taub, and D. Doll,<sup>2</sup> and by J. T. Waber<sup>2</sup> who attributed this behavior to a hydrogen embrittlement effect. The results of Waber indicate that hydrogen contents in the vicinity of 2 ppm will reduce the tensile elongation of uranium, and, further, that most of the deleterious effects of hydrogen can be removed by vacuum annealing. The better the vacuum, the greater the improvement in elongation.

A recent study by L. L. Marsh, C. T. Muehlenkamp and G. K. Manning<sup>2</sup> on the effect of hydrogen and heat treatment on the ductile transition in alpha uranium does not completely confirm these views. A more complex phenomenon is believed to be involved. The transition from ductile to semibrittle behavior in tension was observed in the temperature range 25 to 65°C. Tensile data are summarized in Tables XI and XII. The transition was found sensi-

TABLE XI. TENSILE PROPERTIES AT VARIOUS TEMPERATURES OF URANIUM CONTAINING DIFFERENT AMOUNTS OF HYDROGEN AND WITH VARYING HEAT TREATMENTS

Temperature, °C	Hydrogen Content, ppm	Tensile Strength, psi	Elongation in 2 in., %	Reduction of Area, %
As Hot Rolled <sup>a</sup>				
-56	0.8 ± 0.1	106,000	10.5	9.2
-18	0.8 ± 0.1	118,000	10.0	9.5
+4.5	0.8 ± 0.1	119,000	11.0	9.2
+10	0.8 ± 0.1	120,000	12.5	11.2
+24	0.8 ± 0.1	126,000	32.5	28.0
+24	0.8 ± 0.1	125,500	22.0	21.2
+49	0.8 ± 0.1	111,500	32.5	34.3
+100	0.8 ± 0.1	96,500	39.0	51.0
+177	0.8 ± 0.1	63,800	35.0	53.0
Hydrogenated <sup>b</sup>				
-18	4.7 ± 0.5	76,000	4.5	4.9
+24	4.7 ± 0.5	84,000	8.5	8.6
+24	4.7 ± 0.5	84,000	6.0	10.0
+66	4.7 ± 0.5	86,500	16.5	13.3
+66	4.7 ± 0.5	87,000	22.5	6.6
+100	4.7 ± 0.5	81,500	28.5	20.5
+149	4.7 ± 0.5	68,000	34.5	42.5
Dehydrogenated <sup>c</sup>				
-18	0.3 ± 0.1	74,000	4.5	10.7
+10	0.3 ± 0.1	74,000	7.5	6.8
+24	0.3 ± 0.1	88,000	13.5	12.9
+38	0.3 ± 0.1	98,000	17.5	15.0
+66	0.3 ± 0.1	90,000	28.5	30.5
+100	0.3 ± 0.1	80,500	30.0	41.0
+149	0.3 ± 0.1	68,500	35.5	45.0

<sup>a</sup> Rolled at 550°C, water quenched to room temperature.

<sup>b</sup> Hot rolled, dehydrogenated at 600°C (vacuum), hydrogenated at 600°C (12 atm. hydrogen) and water quenched, aged at 350°C for 1 hour.

<sup>c</sup> Hot rolled, dehydrogenated at 600°C (vacuum) and water quenched, heated at 350°C for 1 hour.

## METALLURGY OF URANIUM

65

TABLE XII. TENSILE PROPERTIES OF URANIUM UNDER VARIOUS CONDITIONS OF HEAT TREATMENT AND STRAIN RATE

Temperature, °C	Hydrogen Content, ppm	Tensile Strength, psi	Elongation in 2 in., %	Reduction of Area, %
As Rolled <sup>a</sup>				
10	0.8	122,000	16	13
24	0.8	122,000	18	16
24	0.8	127,000	20	22
93	0.8	109,000	28	39
Alpha Annealed <sup>b</sup>				
10	0.8	82,100	6.0	7.2
24	0.8	84,200	8.5	11.4
38	0.8	96,100	14.5	15.5
52	0.8	98,000	16	18.2
93	0.8	89,000	31	34.7
Gamma Phase Annealed <sup>c</sup>				
24	—	55,200	6.2	4
52	—	74,000	16.5	24.5
66	—	60,200	11.0	37
93	—	58,500	21.3	48
149	—	49,500	23.5	48
Beta Phase Impregnated <sup>d</sup>				
24	—	71,100	5	6
66	—	78,600	12	11
93	—	74,300	18	21

<sup>a</sup> Hot rolled at 550°C, water quenched; strain rate 75 inches per minute.<sup>b</sup> Alpha annealed 10 hours at 600°C; strain rate 0.0057 inch per minute.<sup>c</sup> 940°C anneal in vacuum; strain rate 0.0057 inch per minute.<sup>d</sup> ½ hour at 700°C (12–15 ppm hydrogen); strain rate 0.0057 inch per minute.

tive to residual strain, strain rate, hydrogen content, and, to a smaller extent, heat treatment. The effect of hydrogen in the composition range 0.3 to 0.47 ppm is observed principally in the values for reduction of area. At 4.7 ppm hydrogen, the reduction of area at fracture is noticeably less than for material that has been dehydrogenated. On the basis of the data available the authors conclude that the transition appears to be similar to transitions observed in other metals not of the face centered cubic type and is not the result of hydrogen embrittlement. The exact role of hydrogen on the tensile properties is not clearly resolved and further work to clarify its behavior will be required. Charpy-notched impact tests were conducted on some of this same material and the results are shown in Fig. 25. A marked transition occurs

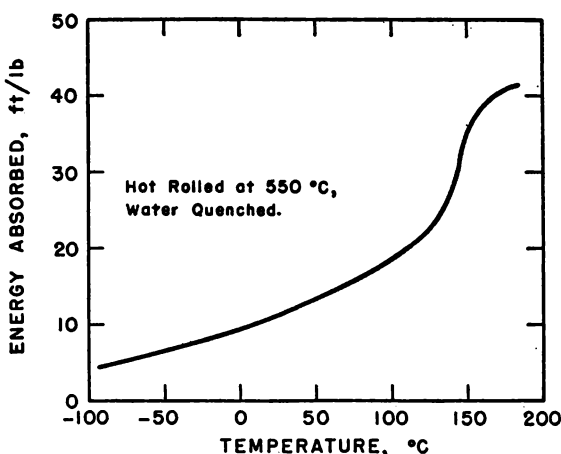


FIG. 25. Impact strength of hot-rolled uranium.

in the 100–150°C temperature range, with a further gradual decrease in energy absorbed with decreasing test temperature.

Uranium rapidly loses strength at elevated temperatures as shown by hot hardness curves (A. B. Holden<sup>2</sup>) and by tensile tests at elevated temperatures (H. A. Saller<sup>2</sup>). Typical tensile properties at elevated temperatures are given in Table XIII.

Other mechanical properties such as hardness, impact strength, creep, etc., have received limited attention and have been reported by many investigators. In view of all the variables which affect the properties of uranium, many reported results are of little significance because the condition of the material is not clearly defined. As an example, many previously reported creep values are questionable, since the small amount of thermal cycling which occurs during normal creep testing has been found sufficient to cause growth in uranium (A. D. Schwope<sup>2</sup>).

TABLE XIII. TENSILE PROPERTIES OF URANIUM AT ELEVATED TEMPERATURES

Specimen <sup>a</sup>	Test Temperature, °C	Ultimate Tensile Strength, psi	Yield Strength 0.2% Set, psi	Elongation, %
<i>300°C Rolled</i>				
Alpha annealed <sup>b</sup>	R.T.	111,000	43,000	6.8
Beta annealed <sup>c</sup>	R.T.	64,000	24,500	8.5
<i>600°C Rolled</i>				
Alpha annealed	R.T.	88,500	26,000	13.5
Beta annealed	R.T.	62,000	25,000	6.0
<i>300°C Rolled</i>				
Alpha annealed	300	35,000	17,500	49.0
<i>600°C Rolled</i>				
Alpha annealed	300	32,000	19,000	43.0
Beta annealed	300	27,000	15,500	33.0
<i>300°C Rolled</i>				
Alpha annealed	500	11,100	5,100	61.0
Beta annealed	500	10,500	7,100	44.0
<i>600°C Rolled</i>				
Alpha annealed	500	10,500	5,500	57.0

<sup>a</sup> All specimens were standard 0.505-inch rounds.

<sup>b</sup> Alpha anneal is 12 hours at 600°C, slow cool.

<sup>c</sup> Beta anneal is 12 hours at 700°C, slow cool.

#### REFERENCES FOR CHAPTER II

1. See also the following Geneva Paper:  
825—J. P. Howe, "The Metallurgy of Reactor Fuels."
2. As described in Geneva Paper No. 555.
3. L. K. Jetter and B. S. Borie, Jr., *A Method for the Quantitative Determination of Preferred Orientation*, J. Appl. Phys. 24:532-535 (1953).
4. L. G. Schulz, *A Direct Method of Determining Preferred Orientation of a Flat Reflection Sample Using a Geiger Counter X-Ray Spectrometer*, J. Appl. Phys. 20:1030 (1949).
5. A. N. Holden, *Spiral Scanning X-ray Reflection Goniometer for the Rapid Determination of Preferred Orientations*, Rev. Sci. Instr. 24:10-12 (1953).
6. W. P. Chernock, M. H. Mueller, H. R. Fish, and P. A. Beck, *An Automatic X-Ray Reflection Specimen Holder for the Quantitative Determination of Preferred Orientation*, Rev. Sci. Instr. 24:925-928 (1953).
7. W. Seymour, *Preferred Orientation of Cold-Rolled Uranium Foil*, J. Metals 6, AIME Trans. 200:999-1003 (1954).
8. M. H. Mueller and H. W. Knott, *Quantitative Pole Figures for Sheet Material by the Reflection Technique*, Rev. Sci. Instr. 25:1115-1118 (1954).
9. J. T. Norton, *A Technique for Quantitative Determination of Texture of Sheet Metals*, J. Appl. Phys. 19:1176 (1948).

10. J. H. Bach and J. B. Burnham, Jr., *Determination of Preferred Orientation*, J. Metals 4:1043 (1952).
11. G. B. Harris, *Quantitative Measurement of Preferred Orientation in Rolled Uranium Bars*, Phil. Mag. (7) 43:113 (1952).
12. J. Thewlis, *Structure of Uranium*, Nature 168:198 (1951).
13. A. S. Wilson and R. E. Rundle, *The Structures of Uranium Metal*, Acta Cryst. 2:126-127 (1949).
14. N. Grossman and S. Priceman, *Compressive Properties of Uranium*, Nucleonics 12, No. 6:68-69 (June, 1954).
15. H. L. Laquer, W. E. McGee, and M. F. Kilpatrick, *The Elastic Constants of Uranium*, Trans. Am. Soc. Met. 42:771 (1950).
16. M. B. Reynolds, *The Determination of the Elastic Constants of Metals by the Ultrasonic Pulse Technique*, Trans. Am. Soc. Met. 45:839 (1953).

## *Chapter III*

---

### THE ALLOYS OF URANIUM \*<sup>1</sup>

---

The study of the alloys of uranium is based on the following considerations. Unalloyed uranium has relatively poor mechanical properties. The metal is chemically reactive. As has already been pointed out in the preceding chapters uranium is anisotropic in its physical properties. Radiation damage (see Part III of this book) is severe in the pure metal largely because of the anisotropy. Alloying can be expected to alleviate many of these difficulties. Finally, the study of alloys has been spurred by the interest in lower melting alloys by the need for dilution of enriched uranium for power reactors.

#### A. ALLOYING OF URANIUM

Before surveying the data that are available on various uranium alloys, it is appropriate to look at the metal uranium and its alloying from a theoretical viewpoint. It has three allotropic modifications. Alpha uranium is stable up to 662°C, beta uranium is stable from 662°C to 769°C, and gamma uranium is stable from 769°C to the melting point at 1129°C.<sup>2-8</sup> In alpha uranium, which is orthorhombic, there are two groups of interatomic distances of about 2.8 and 3.3 Å. The structure may be regarded as being composed of corrugated sheets of atoms parallel to the ac plane in which the atoms are tightly bound as indicated by the characteristic interatomic distance of 2.8 Å. The binding between the corrugated sheets is much weaker and is characterized by interatomic distances of 3.3 Å. The anisotropic nature of the atomic arrangement in alpha uranium suggests appreciable covalent bonding analogous to that occurring in arsenic, antimony, and bismuth.<sup>9</sup>

The metal uranium has six orbital electrons outside an inert core. The electronic configuration of alpha uranium can probably be best represented

\* This chapter is based on the following Geneva Papers:

558—H. A. Saller and F. A. Rough, "The Alloys of Uranium."

555—F. G. Foote, "Physical Metallurgy of Uranium."

by  $7s^26d^25f^2$ , if a single configuration can be considered to be representative, where the  $7s^2$  electrons are inert, and the  $6d^2$  and  $5f^2$  electrons are in hybrid d-f orbitals acting with a valence of about four.<sup>9</sup> As in other transition metals, hybridized electrons do not act as a whole number of electrons, and alpha uranium may be regarded as having a valence of 3.8.

The orthorhombic crystal structure of alpha uranium is unique among metals, and, since it is characterized by some degree of covalent bonding, it is to be expected that the formation of solid solutions will be restricted even though atomic sizes and valence of solute elements are favorable.

Based on the assumption that alpha uranium has a valence of about 4, or 3.8, it might be expected that the quadrivalent elements such as titanium, zirconium, and hafnium would stabilize alpha relative to the beta phase. This effect has been observed experimentally in the systems uranium-titanium and uranium-zirconium, but the solid solubilities of titanium and zirconium in both alpha and beta are limited.<sup>10</sup> The system uranium-hafnium has not been studied. The experimental data which are available on other quadrivalent elements such as silicon and germanium where the size factors, related to the coordination number 12, are within 15%, give no indication of the relative solid solubilities in the two phases.

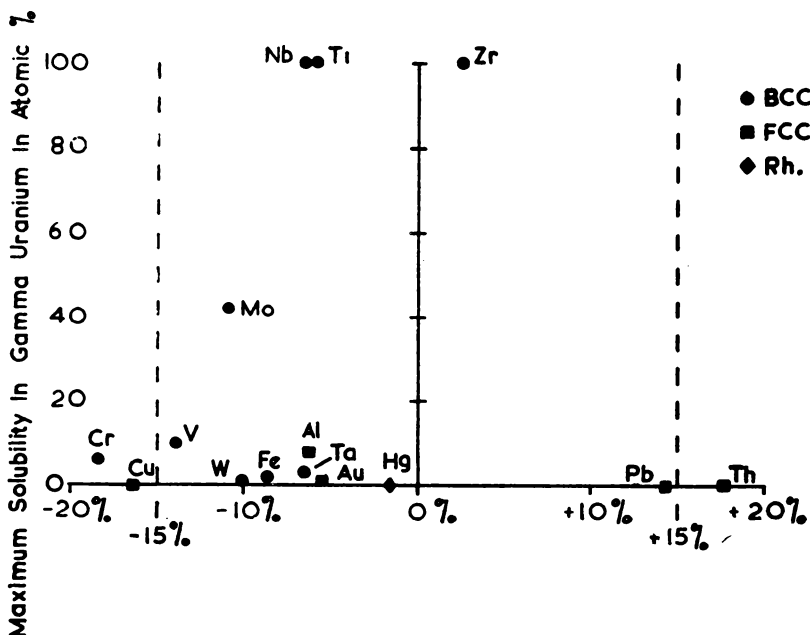


FIG. 1. Size factor with respect to gamma uranium.<sup>11</sup>

In the gamma phase, which is body-centered cubic, uranium is in its most metallic state.<sup>9</sup> It is generally accepted that gamma uranium is characterized by a valence of 6 or perhaps 5.8. The elements which on the basis of size factor, crystal structure, and valence might be expected to form appreciable solid solutions in gamma uranium are the Group IVA elements, titanium, zirconium, and hafnium; the Group VA elements, vanadium, niobium, and tantalum; and the Group VIA elements, chromium, molybdenum, and tungsten. (See Fig. 1.)<sup>11</sup> Of these elements, nothing is known of the uranium-hafnium system, but titanium, zirconium, niobium, and molybdenum form extensive solid solutions. Vanadium and chromium have solubilities in gamma uranium of 12 and 4 atomic per cent, respectively, while tantalum and tungsten are progressively less soluble.<sup>10</sup>

The complex tetragonal structure of beta uranium and its hard nature suggest that it has some degree of nonmetallic bonding, as does alpha uranium. Its intermediate position between alpha and gamma suggests that beta may

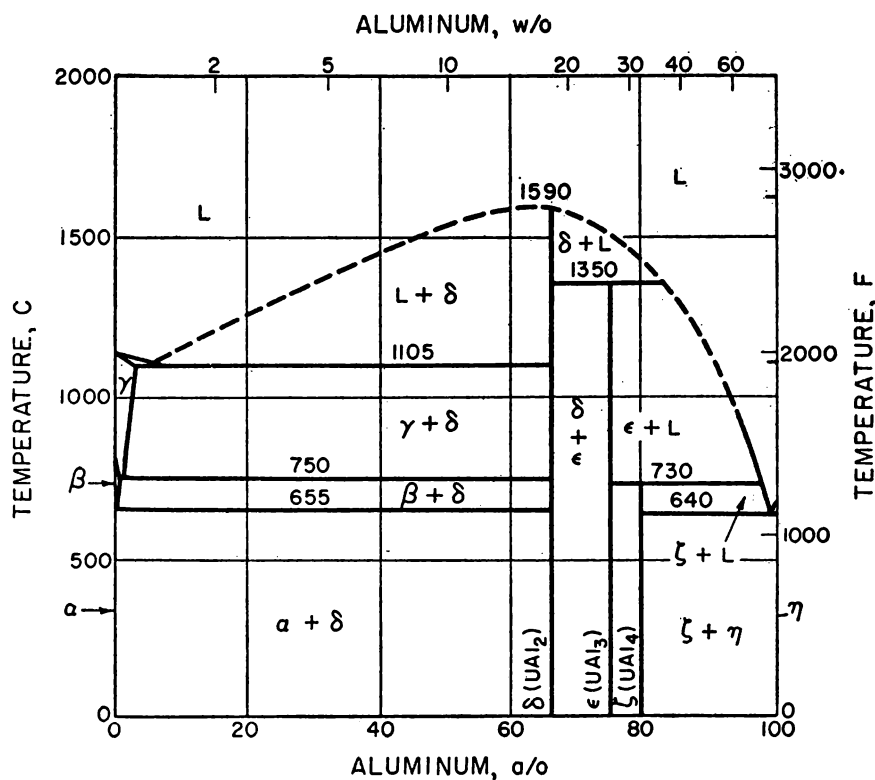


FIG. 2. The system uranium-aluminum.

be characterized by a valence of about 5. Since the structure of beta is unique among elements, only limited solid solubilities are likely.

If the assumption that beta has an effective valence of about 5 electrons per atom is correct, one might expect that beta would be stabilized relative to alpha and gamma by pentavalent elements such as vanadium, niobium, and tantalum. Since the crystal structures are more favorable for solid solution in the gamma, it is not surprising that these elements stabilize beta relative to alpha, but not relative to gamma. Many of the 6-valent gamma-stabilizing elements can also be expected to stabilize beta relative to alpha, although only limited solubilities may exist. As a result, we find that vanadium and niobium of the pentavalent elements and chromium and molybdenum of the hexavalent elements do stabilize beta relative to alpha and are capable of retaining the beta phase during quenching.

Recently, the uranium alloy systems from both the United States and United Kingdom were compiled.<sup>10</sup> As might be expected, the uranium-alloy diagrams fall into a number of standard types. For purposes of discussion, they may be grouped as systems in which intermetallic compounds are found and those in which no true compounds are found. This latter group can be further subdivided into systems showing little and appreciable solid solubility.

Many elements form one or more intermetallic compounds when alloyed with uranium.<sup>10</sup> It is characteristic of these systems that limited solid solubility exists in each of the terminal phases. The uranium-aluminum system shown in Fig. 2, and the uranium-silicon system, Fig. 3, may be considered typical of these compound-forming elements. Other elements in this category which have received intensive study and for which uranium-alloy diagrams have been established are beryllium, bismuth, carbon, cobalt, copper, gallium, gold, hydrogen, iron, lead, manganese, mercury, nickel, and tin. Elements which form compounds with uranium but whose systems are only partially known are antimony, arsenic, boron, germanium, indium, iridium, nitrogen, oxygen, palladium, phosphorus, platinum, selenium, sulfur, tellurium, thallium, and zinc. In addition, some data are available on parts of the ternary systems of uranium with aluminum and silicon, beryllium and carbon, bismuth and lead, cobalt and iron, chromium and iron, and cobalt and nickel.

Several elements when alloyed with uranium do not produce intermetallic compounds or show large solid solubility in the terminal phases.<sup>10</sup> Such systems contain either eutectic, peritectic, or monotectic reactions. Among the elements in this category for which uranium-alloy diagrams are known are chromium, magnesium, silver, tantalum, thorium, tungsten, and vanadium. Other elements which do not form compounds nor appreciable solid solutions, but whose uranium alloy diagrams are partially known, include calcium, cerium, lanthanum, neodymium, praseodymium, and sodium.

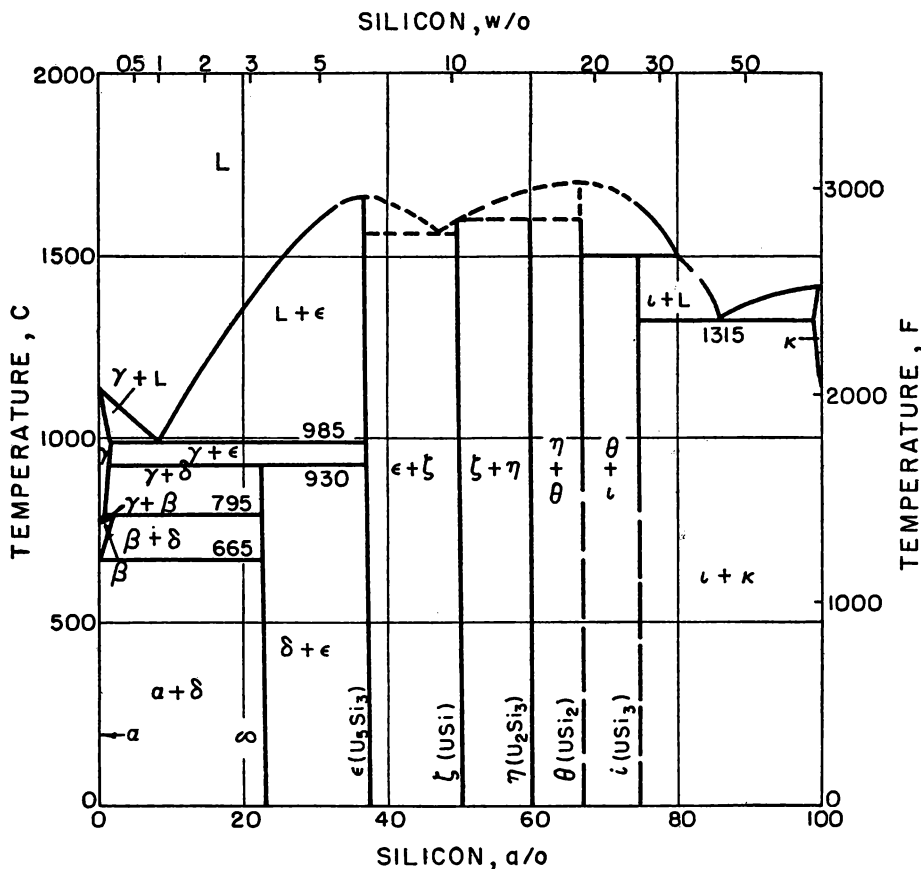


FIG. 3. The system uranium-silicon.

The uranium-vanadium system, shown in Fig. 4, exemplifies the simple eutectic system. The uranium-chromium system is similar, but the eutectic reaction occurs at a somewhat lower temperature. A peritectic characterizes both the uranium-tantalum and uranium-tungsten systems. The latter is shown in Fig. 5. Because the solid solubilities are low, the details of the uranium end are not known, and the isotherms are extended to 100% uranium. A typical monotectic system, that of uranium-magnesium, is shown in Fig. 6. Thorium and silver, and probably cerium, lanthanum, neodymium, and praseodymium, also form monotectic systems with uranium.<sup>10</sup>

Another group of elements when added to uranium produce alloys with extensive solubility at elevated temperatures, but with no true intermetallic compounds. The uranium-molybdenum system shown in Fig. 7 might be considered typical of these systems. The uranium-titanium and uranium zir-

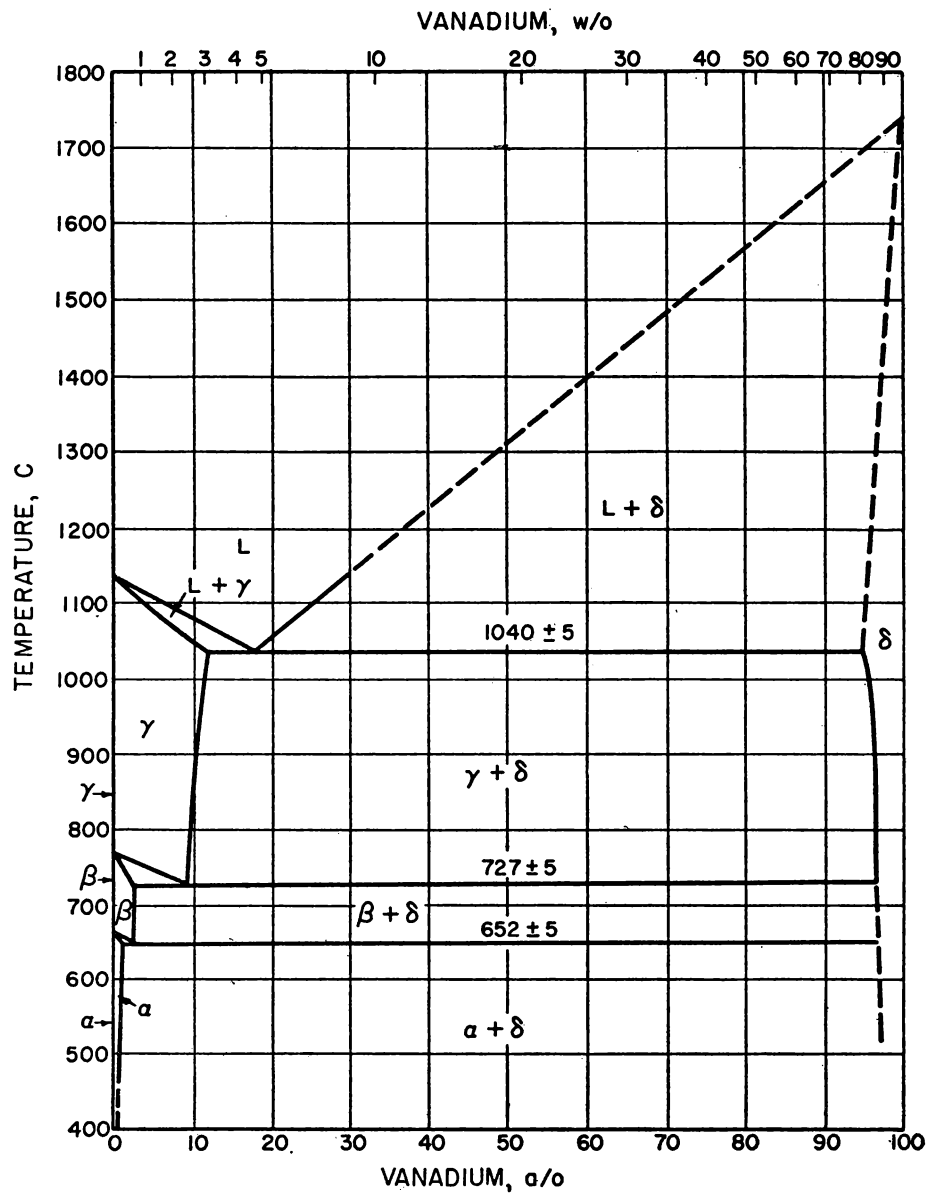


FIG. 4. The system uranium-vanadium.

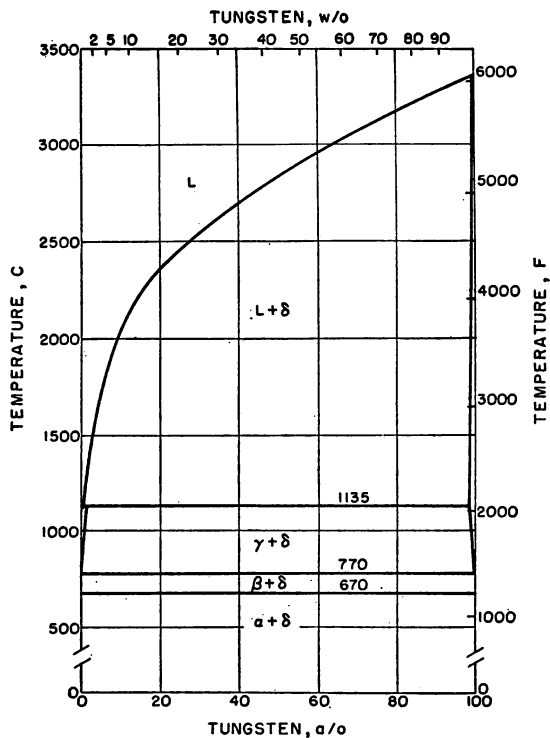


FIG. 5. The system uranium-tungsten.

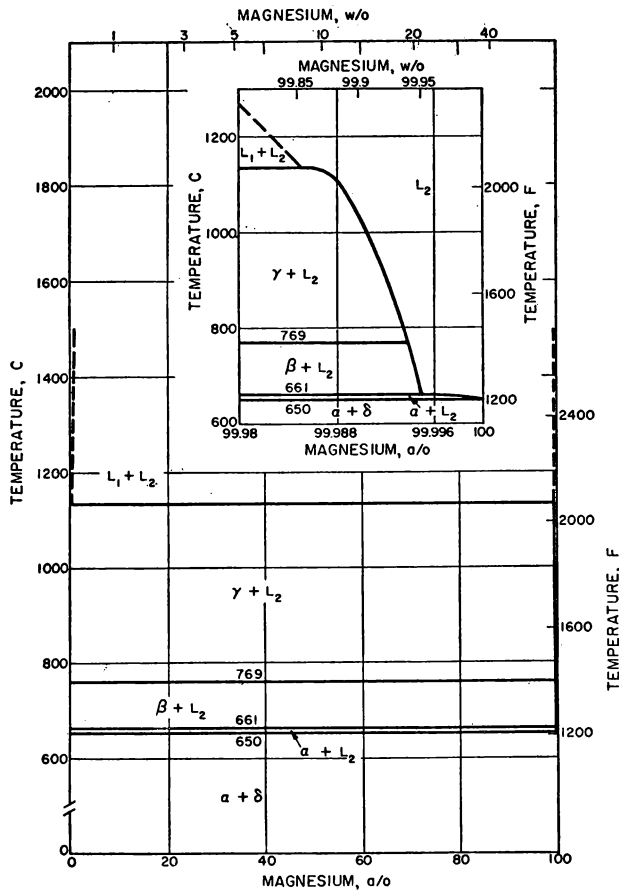


FIG. 6. The system uranium-magnesium.

conium systems (Fig. 8) differ only in that solid solubility is complete at elevated temperatures. The uranium-niobium system has complete solid solubility at elevated temperatures, but does not have an intermediate or delta phase.<sup>10</sup> The intermediate phases found in the uranium-molybdenum, uranium-titanium, and uranium-zirconium systems form from a metastable gamma phase. Because they are metallic in nature, they are not considered as intermetallic compounds.

#### B. TRANSFORMATION KINETICS IN URANIUM ALLOYS

All uranium alloy systems whose transformation kinetics have thus far been studied have a common feature: the alloying component is more soluble

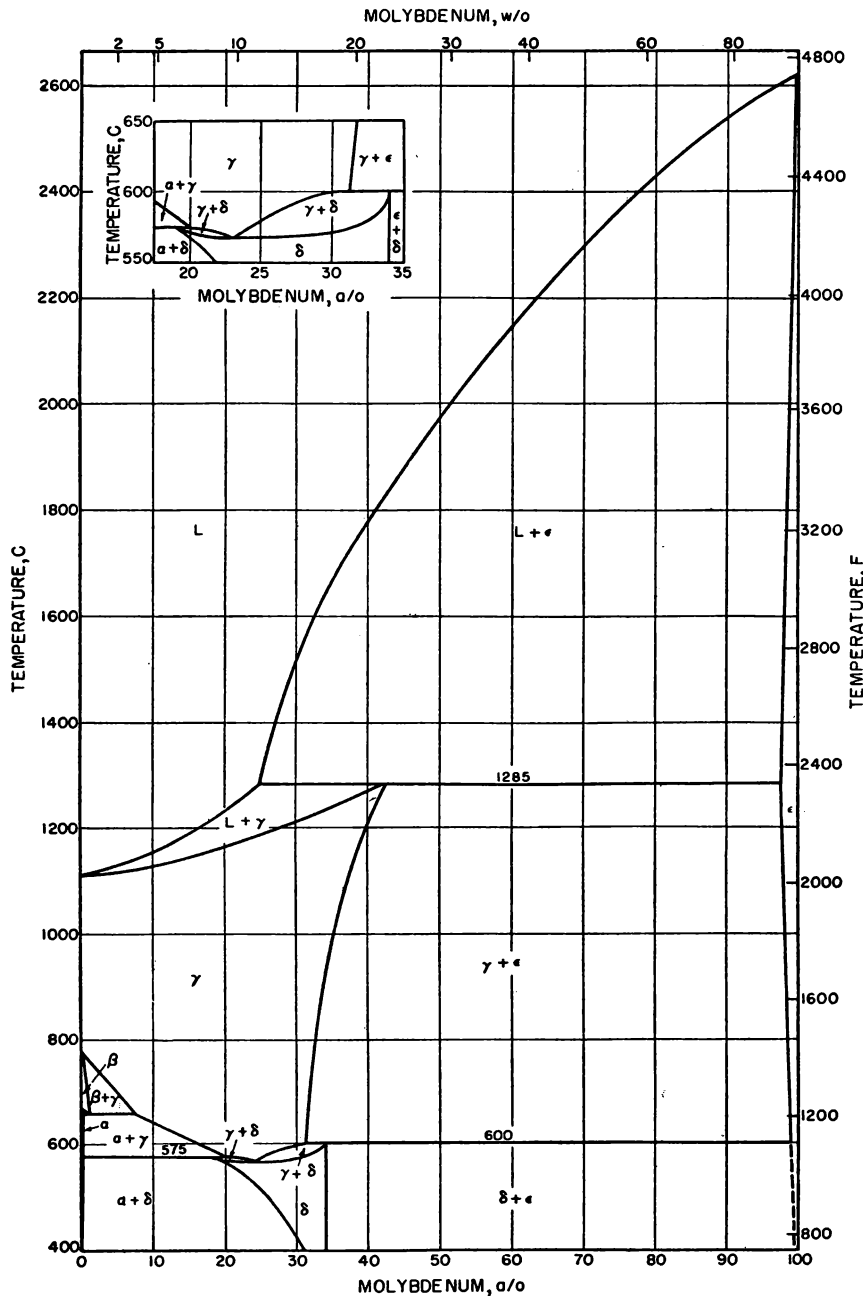


FIG. 7. The system uranium-molybdenum.

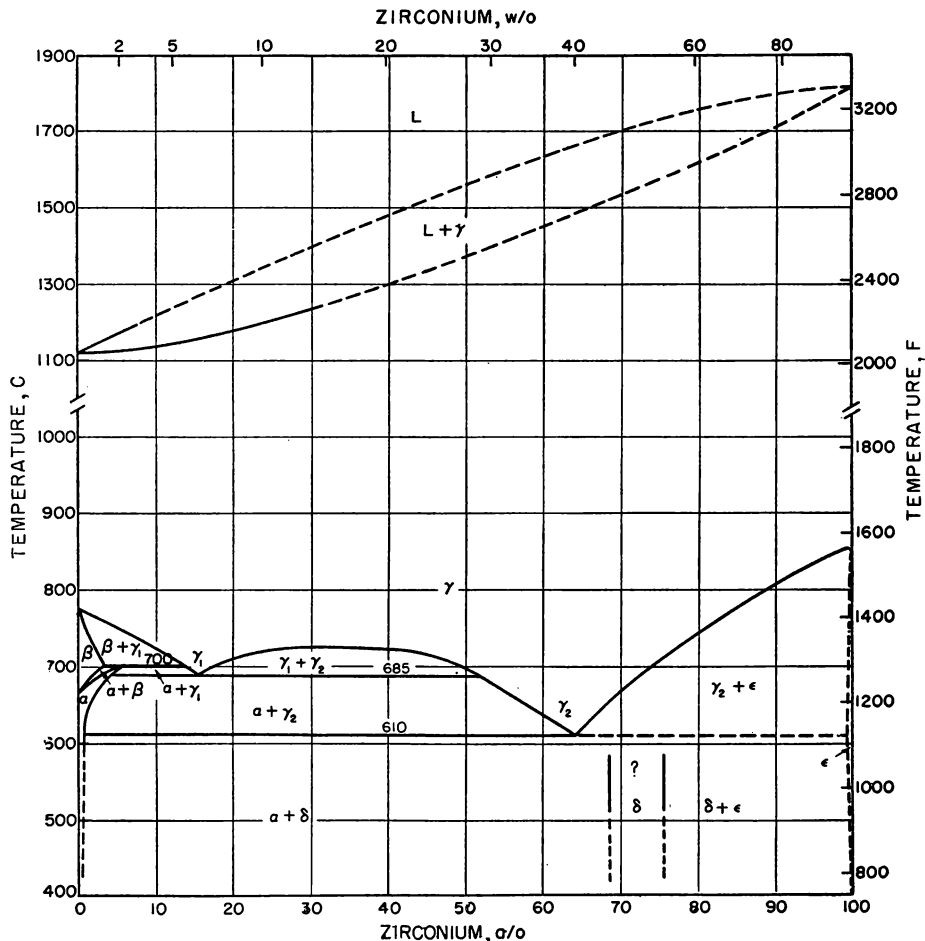


FIG. 8. The system uranium-zirconium.

in the gamma body-centered cubic phase than in the tetragonal beta and orthorhombic alpha phases, and more soluble in the beta phase than in the alpha phase. In general then, when a high temperature phase is rapidly cooled to temperatures below the equilibrium temperature range, a metastable supersaturated solid solution structure results. Transformation kinetics are the time-temperature-composition relationships which describe the transformation of this metastable structure to a structure more closely approximating the equilibrium structure.

Nearly all transformation kinetic studies can be separated into three groups depending upon the type of heat treatment used. These classes are described below and shown diagrammatically in Fig. 9.

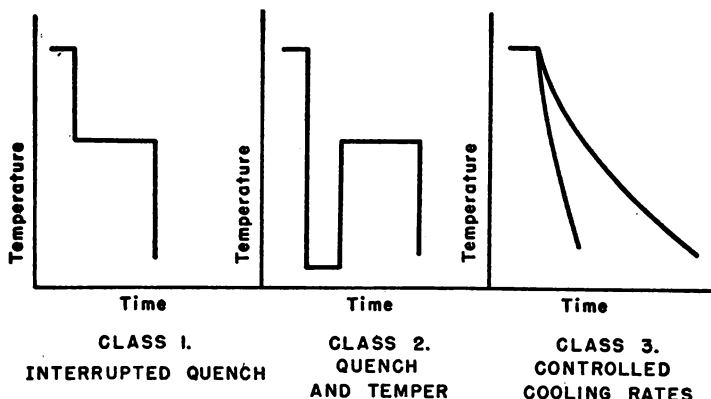


FIG. 9. Heat treatments for study of time-temperature transformations.

(1) *Interrupted quenching* refers to a heat treatment wherein the specimen is held at a temperature in the gamma or beta range long enough to bring about an equilibrium structure, then is rapidly cooled to a lower temperature and held at that temperature for a measured time. The process is comparable to austempering of steel.

(2) *Quench and temper treatments* are those wherein the specimen is heated into the gamma or beta range long enough to bring about an equilibrium structure, then drastically quenched to 100°C or below. The gamma or beta phase may be retained or may undergo a diffusionless transformation during the quench, depending on the nature and amount of the alloying elements. In either case, the structure is metastable and transforms on tempering. The study of quench and temper transformations consists of tempering the quenched specimens at various temperatures for measured times.

(3) *Continuous cooling treatments* are those wherein the specimen is heated into the gamma or beta range long enough to bring about an equilibrium structure, then cooled to room temperature at various cooling rates, without interruption. Included are such treatments as water quenching, air-cooling and furnace-cooling.

The reported data on transformation kinetics can best be analyzed by breaking them down, first into alloy systems, then into the three classes of heat treatment.

**1. Uranium-chromium.** D. W. White, Jr.<sup>12</sup> has reported the transformation kinetics of the uranium-chromium system for chromium contents of 0.3, 0.6, 1.8, and 4 a/o.\* Chromium tends to stabilize the beta-uranium phase and the study was concerned with the subcritical transformation of the beta solid solutions. The interrupted quench method was used and the transformation followed dilatometrically.

\*For "atomic per cent" the abbreviated form "a/o" is used.

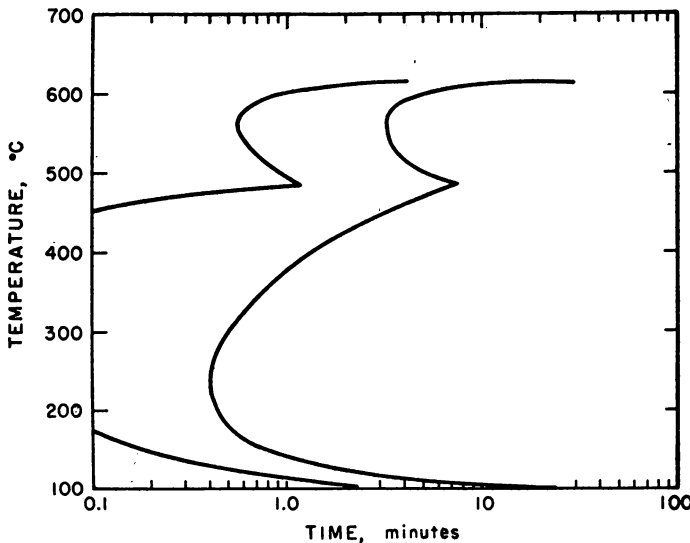


FIG. 10. TTT curve for uranium-0.3 a/o chromium alloy.

The data obtained are presented in Figs. 10 through 13. The existence of two C's in the time-temperature transformation (TTT) diagrams for the lower chromium alloys indicated that there are two transformation mechanisms, one at upper and another at lower temperatures. One may speculate that the higher temperature mechanism is controlled by the rate of diffusion of chromium in beta uranium, while the lower temperature mechanism is diffusionless. The temperature of transition between the two mechanisms of transformation is depressed with increased chromium content. By qualitative extrapolation to zero per cent chromium, one would conclude that pure uranium transforms from beta to alpha entirely by the mechanism of the lower "C," and retarded transformations were observed in uranium of nominal purity. P. Duwez<sup>13</sup> has reported that the beta-alpha transformation temperature can be depressed appreciably only by extremely drastic quenching.

At higher chromium contents, the lower "C" vanished altogether and the beta phase can be retained at room temperature. This feature of the transformation was used by C. W. Tucker<sup>14</sup> to obtain crystals of beta uranium for his structure studies.

**2. Uranium-molybdenum.** The work of T. I. Jones, C. G. Hoffman, J. M. Taub and D. T. Doll<sup>12</sup> illustrates the transformation of uranium-molybdenum alloys containing 0.56, 1.12, 1.67 and 2.18 w/o molybdenum.\* The transformation was of the quench and temper type, class 2. The alloys were prepared by

\* For "weight per cent," the abbreviated form "w/o" is used.

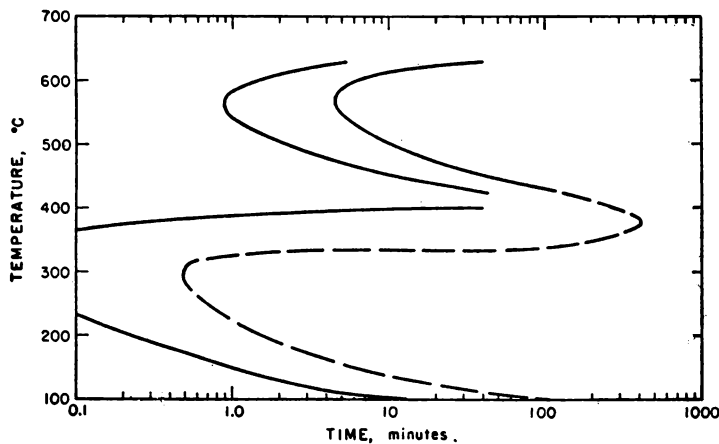


FIG. 11. TTT curve for uranium-0.6 a/o chromium alloy.

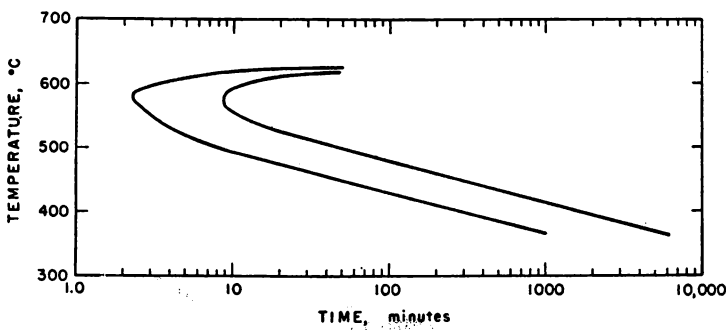


FIG. 12. TTT curve for uranium-1.8 a/o chromium alloy.

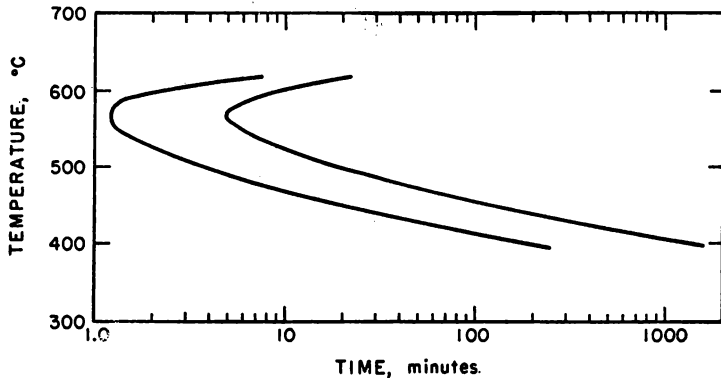


FIG. 13. TTT curve for uranium-4.0 a/o chromium alloy.

vacuum melting and were subsequently forged. The 1.12, 1.67, and 2.18 w/o molybdenum alloys, when quenched from 780°C and above (gamma solid solution phase), appear to undergo a type of transformation resulting in an acicular structure similar to martensite in appearance. These quenched alloys are entirely in the alpha condition. These supersaturated alpha solid solution alloys are relatively soft (DPN 350-380). Tempering markedly increases the hardness, as illustrated in Fig. 14. Overaging occurs rather soon at a tempering temperature of 500°C.

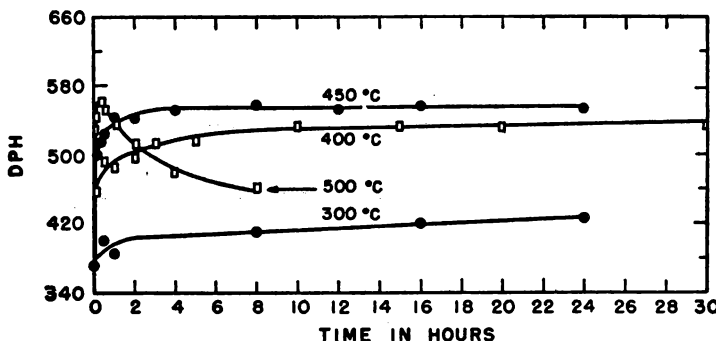


FIG. 14. Precipitation hardening curves for 1.67 w/o molybdenum-uranium alloys.

H. A. Saller, F. A. Rough, and A. A. Bauer<sup>12</sup> have reported on the transformation kinetics of uranium-molybdenum alloys containing 9.8, 12.6 and 14.8 w/o molybdenum. The class 2 heat treatment, quench and temper, was used. In this composition range, the gamma phase could be easily retained by quenching. The phases stable at room temperature are alpha uranium, solid solution, and delta (a tetragonal intermediate) phase, centered at around 16 w/o molybdenum. The transformations were quite sluggish, and the course of transformation was followed by metallographic examination and electrical resistance measurements. Transformation of the 9.8 w/o molybdenum alloy occurs by a nucleation and growth mechanism. The alpha and delta phases are nucleated at the gamma grain boundaries and grow inward to consume the gamma grains. The decomposition products have a lamellar distribution. The transformation curve is given in Fig. 15.

The 12.6 and 14.8 w/o molybdenum alloys transform by an ordering reaction which probably occurs by a nucleation and growth mechanism. Sufficient data are available to indicate that the transformation in the 14.8 w/o alloy has a C-curve-type behavior. During transformation of the alloys, the electrical resistance and hardness first increase and then decrease with time, the peaks in resistance and hardness almost coinciding. Transformation is not observed metallographically until after the resistance and hardness peaks are passed.

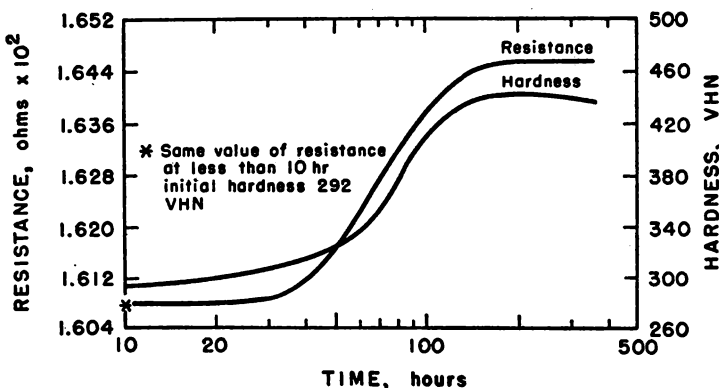


FIG. 15. Resistance and hardness curves of a 9.8 w/o molybdenum sample during annealing at 500°C.

The increased hardness and resistance during aging are attributed to strain developed in the matrix as a result of the formation of coherent nuclei. Precipitation, and loss of coherency, are accompanied by a decrease in resistance and hardness. The induction period, preceding transformation, and attendant C-curve behavior originate in the temperature dependence of the tendency of the alloy to order and of the rate of diffusion.

The transformation of gamma to delta phase is sluggish at all temperatures and the rate decreases rapidly below 440°C. The optimum temperature of transformation, or nose of the C-curve, lies close to 500°C.

**3. Uranium-niobium.** O. N. Carlson<sup>12</sup> has reported data on the transformation kinetics of the uranium-niobium alloys containing 1, 3, 5, and 10 w/o niobium. The transformations were studied by the quench and temper method and changes followed by hardness measurements. The data are reproduced in Fig. 16. The curves show evidence of precipitation hardening followed by overaging.

A. E. Dwight<sup>12</sup> has reported a continuous cooling TTT curve for a uranium-4.9 w/o niobium alloy. Niobium was found to retard the decomposition of the gamma phase sufficiently so that quenching rates of 18°C per second and less will avoid touching the nose of the C curve on continuous cooling. Specimens in which the gamma phase is retained in a metastable condition by quenching have a hardness of 20 Rockwell "C."

**4. Uranium-zirconium.** O. N. Carlson<sup>12</sup> has also studied the transformations in alloys containing 2, 5, 10, and 20 w/o zirconium by the quench and temper method. The data are plotted in Fig. 16 and show a moderate increase in hardness with indications that the maximum hardening occurs at 400°C in the 2, 5, and 10 w/o alloys.

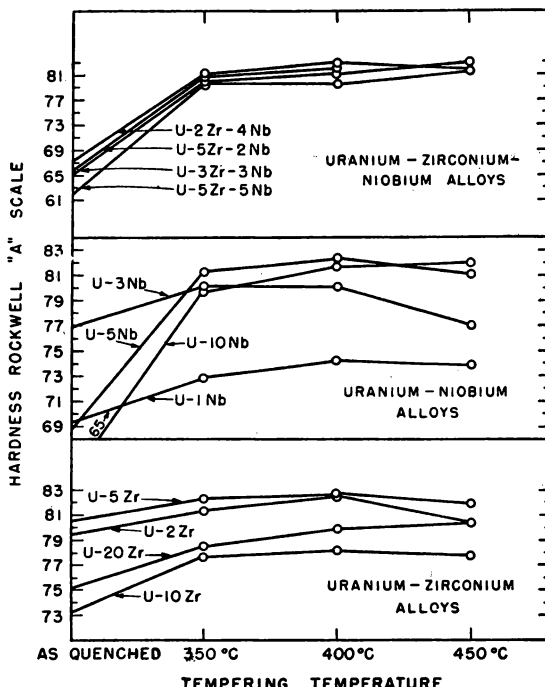


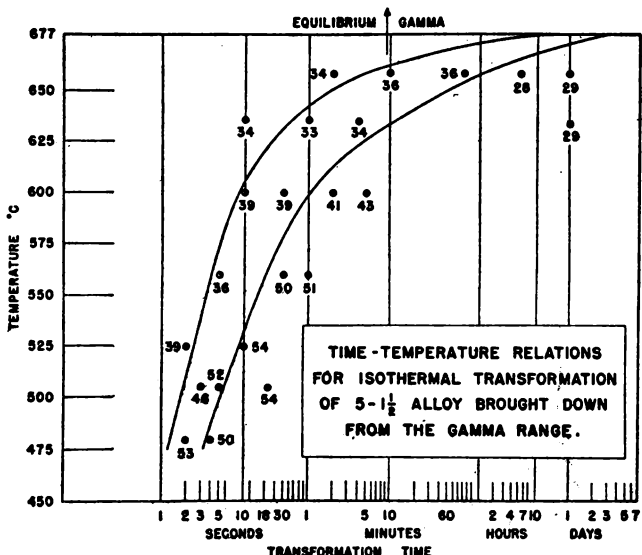
FIG. 16. Effect of tempering temperatures on hardness of uranium alloys. (Annealing time: 48 hours.)

**5. Uranium-zirconium-niobium.** O. N. Carlson<sup>12</sup> has studied a group of ternary alloys containing small amounts of zirconium and niobium by the same methods as those used for the U-Nb and U-Zr binary alloys. His results are also included in Fig. 16 and indicate a marked hardening in all alloys at tempering temperatures up to 450°C.

H. H. Chiswik and A. E. Dwight<sup>12</sup> have studied the heat treatment of a ternary alloy containing 5 w/o zirconium and 1½ w/o niobium by several methods.

The transformation curve obtained by the interrupted quench method is shown in Fig. 17. The lines represent the beginning and end of transformation as determined by metallographic observation. The numbers represent the Rockwell "C" hardness during various stages of the transformation. The hardness after transformation is plotted as a function of transformation temperature in Fig. 18.

For a quench and temper treatment, it was found that tempering the water-quenched structure resulted in appreciable age hardening. In Fig. 19, lines of constant hardness are plotted on time-temperature coordinates. This figure



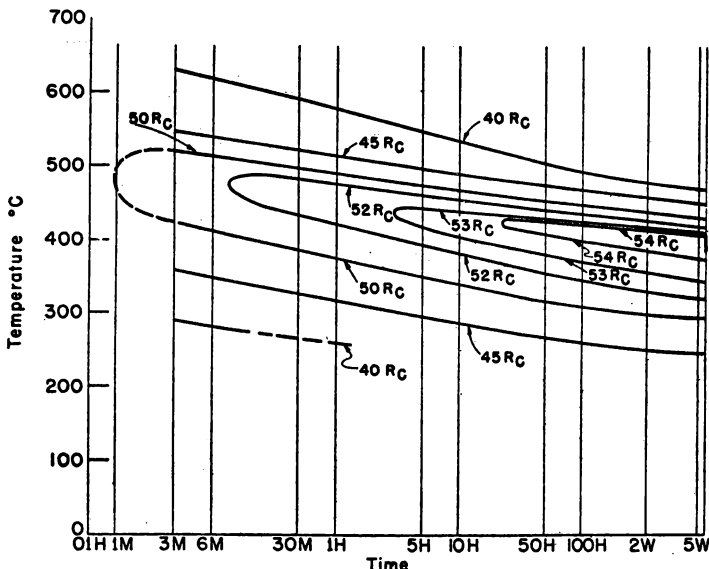


FIG. 19. Effect of time and temperature of tempering on the hardness of water-quenched uranium-5 w/o zirconium-1½ w/o niobium alloy.

exhibits behavior typical of precipitation hardening and overaging. Little change in microstructure was observed until the maximum hardness was reached and had started to drop (overaging).

### C. MECHANICAL PROPERTIES OF URANIUM ALLOYS

A number of elements are effective in improving the high-temperature mechanical properties of uranium when added in small amounts. The tensile properties at 500°C of base uranium and some low-chromium and low-zirconium alloys are given in Table I.<sup>15</sup> It is apparent that a yield strength of three to five times that of uranium can be readily attained at 500°C by these additions.

A number of compound-forming elements, such as aluminum<sup>16</sup> and silicon, are also effective in improving the mechanical properties of uranium when added in small amounts. In larger amounts, these elements form brittle compounds which detract from the fabricability of the alloys.

Very high strengths are possible in high-uranium alloys of the solid-solution-type systems by means of a martensite-type transformation. If, for example, binary alloys of 5 to 10 w/o zirconium are gamma-quenched, a martensitic alpha-like structure (alpha prime) forms in which virtually all of the zirconium is in metastable solid solution.<sup>15</sup> This alpha prime structure is very

TABLE I. TENSILE PROPERTIES OF URANIUM AND URANIUM ALLOYS AT 500°C

Analysis	Grain Size, mm	Ultimate Tensile Strength, psi	0.2% Yield Strength, psi	Elongation in 2 in., %	Reduction of Area, %
Base uranium, <0.01 Carbon	>0.118	11,260 12,460	8,330 7,900	36 29	~78 ~87
0.10 chromium, <0.01 Carbon	0.057	32,050 25,980	23,300 15,300	24.5 25.5	~57 ~85
0.42 chromium, <0.01 Carbon	0.025	38,750 37,100	24,600 23,800	23 23	82 82
1.11 zirconium, <0.01 Carbon	0.033	43,300 61,000	31,400 48,200	11.3 21	61 94
2.21 zirconium, <0.01 Carbon	0.009	46,100 52,400	41,300 45,000	18 24	85 94

hard and strong in the quenched condition. By varying the tempering or annealing of such a structure to control the precipitation of the excess solute from solid solution, a whole range of properties can be obtained. The hardness data in Table II<sup>15</sup> give some indication of the vastly different properties

TABLE II. VICKERS HARDNESS OF URANIUM-5 W/O ZIRCONIUM ALLOY

Heat Treatment	Hardness <sup>a</sup>
1 hr 900°C, water quenched	535
1 hr 900°C, water quenched, 2 hr 200°C, water quenched	520
1 hr 900°C, water quenched, 2 hr 300°C, water quenched	512
1 hr 900°C, water quenched, 2 hr 400°C, water quenched	545
1 hr 900°C, water quenched, 2 hr 500°C, water quenched	475
1 hr 900°C, water quenched, 2 hr 575°C, water quenched	375
1 hr 900°C, water quenched, 2 hr 650°C, water quenched	315

<sup>a</sup> Obtained with 30-kg load.

that can be obtained by treating the uranium-5 w/o zirconium alloy in this manner. Similar properties can also be obtained in the other solid-solution-forming systems. In the system uranium-molybdenum, the greatest strength of the 2 w/o molybdenum alloy is achieved by quenching from the gamma (700°C) and aging 2 hours at 400°C. With these heat treatments 0.2% offset yield strengths as high as 226,000 to 248,000 psi have been obtained in the 2 w/o molybdenum alloy in compression at room temperature.<sup>15</sup> Unfortu-

TABLE III. TENSILE PROPERTIES OF ARC-MELTED URANIUM-ZIRCONIUM ALLOYS AT 370°C

Zirconium Content, w/o	Yield Strength (0.2 Offset), psi	Tensile Strength, psi	Elongation in 2 in., %	Reduction in Area, %
0	21,300	31,400	27.0	57.0
2.4	35,100	48,400	17.0	49.0
5.5	50,500	77,000	10.0	25.0
11.5	100,800	122,800	8.0	29.0
20.5	124,000	135,200	8.0	18.0
31.4	112,000	145,200	7.0	7.0
41.7	97,000	115,300	8.0	13.0
50.5	68,100	96,100	22.0	28.0
60.6	63,800	97,800	22.0	20.0
70.4	64,800	86,400	20.0	27.0
80.0	72,000	77,900	5.0	22.0
89.4	53,200	64,200	7.0 <sup>a</sup>	11.0 <sup>a</sup>
100.0	8,500	17,300	42.0	—

<sup>a</sup> Specimens broke in what appeared to be rolling defects.

TABLE IV. TENSILE PROPERTIES OF URANIUM-12 W/O MOLYBDENUM ALLOY

Heat Treatment	Test Temp., °F	0.5% Offset Yield Strength, psi	Tensile Strength, psi	Per Cent Elongation in 1 in.		Reduction in Area, %
				Uniform	Total	
24 hr 900°C, water quenched	500	102,000	104,000	1.8	6.9	50
	600	107,000	108,000	2.3	3.6	23
	600	104,000	105,000	—	—	—
	700	98,000	102,000	3.0	4.3	33
24 hr 900°C, water quenched, aged 3 hr 500°C	600	103,000	104,000	15	5.8	45
24 hr 900°C, water quenched, aged 40 hr 500°C	600	114,000	118,000	2.1	5.3	32
24 hr 900°C, water quenched, aged 40 hr 500°C	500	114,000	116,000	1.4	5.2	37

nately, the high strength of these alpha prime materials would be lost during extended service at high temperatures by overaging.

Perhaps the greatest improvement in high-temperature mechanical properties is to be achieved in the higher alloys of the solid-solution-type systems such as uranium-molybdenum, uranium-niobium, uranium-titanium, and uranium-zirconium.

The tensile properties at 370°C of a series of uranium-zirconium alloys are shown in Table III.<sup>15</sup> These samples were hot worked and heat treated 24 hours at 575°C and furnace-cooled. In this case, the maximum strength was attained at about 20 w/o zirconium. At higher temperatures, in the gamma phase region, the maximum strength may occur at a higher zirconium composition.

The tensile properties of a 12 w/o molybdenum alloy are shown in Table IV.<sup>15</sup> This alloy has high strength and rather limited ductility. It is not as strong at 370°C as the strongest uranium-zirconium alloy shown in Table III, but it may be stronger at temperatures in the gamma phase region.

TABLE V. CREEP DATA FOR URANIUM-ZIRCONIUM ALLOYS AT 815°C IN VACUUM

Composition, w/o			Condition	Stress, psi	Time for 1% Deforma- tion, hr	Min- imum Creep Rate, %/hr	Test Time, hr <sup>b</sup>	Elonga- tion, %						
Nom- inal Zirco- niuum	Analysis													
	Zirco- nium <sup>a</sup>	Carbon												
5.0	7.1	0.07	Induction melted and cast in graphite, rolled at 1550°F	500	0.8	0.65	6.0	8.1						
11.3 22.4	12.6 25.8	0.08 —	Ditto Arc melted twice; jacketed, forged and rolled at 1450°F	1422	<0.1	43	1.0	93.8						
				500	0.45	1.0	11	14						
46.5 72.3	47.1 72.6	— —	Ditto	500	56	0.013	169	15.1						
			Ditto	500	40	0.021	162.7	12.3						

<sup>a</sup> Zirconium by difference.

<sup>b</sup> Test discontinued before rupture.

## D. CREEP PROPERTIES

Creep data for a series of uranium-zirconium and a series of uranium-titanium alloys are shown in Tables V and VI, respectively.<sup>15</sup> In the zir-

TABLE VI. CREEP DATA FOR URANIUM-TITANIUM ALLOYS AT 815°C IN VACUUM

Alloy	Composition, w/o			Condition	Stress, psi	Time for 1% Deforma- tion, hr	Mini- mum Creep Rate, %/hr	Test Time, hr <sup>b</sup>	Elonga- tion, %						
	Nom- inal Tita- nium	Analysis													
		Tita- nium <sup>a</sup>	Carbon												
48	12.1	4.2	0.38	Induction melted and cast in graphite; rolled at 1800°F	500	0.7	0.14	30.9	6.4						
Ti2-2	6.3	4.3	0.19	Induction melted and cast in copper mold; <sup>c</sup> rolled at 1500°F	500	0.04	28	0.4	11.0						
35	20.0	9.3	0.22	Induction melted and cast in graphite; rolled at 1800°F	500	3.0	0.05	78	4.6						
30	20.0	12.3	0.25	Induction melted and cast in graphite; rolled at 1500°F	500	8.5	0.06	170.4	12.8						
28	32.0	17.0	0.27	Ditto	500	35	0.0034	211	2.6						
63	20.0	20.3	0.45	Induction melted and cast in graphite; rolled at 1800°F	500	23	0.008	149.5	2.9						
57	25.5	25.7	1.00	Ditto	500	163	0.003	238.6	1.4						
64	30.0	32.6	0.80	Induction melted and cast in graphite; rolled at 1800°F <sup>c</sup>	500	40	0.0045	167.7	2.2						
36	32.0	37.2	0.32	Ditto	500	44	0.0032	197	2.1						
66	50.0	47.4	1.64	Ditto	500	9.5	0.06	111.8	7.4						
Ti54	55.0	55.4	0.19	Arc melted; remelted in BeO; forged and rolled at 1700°F	500	12.5	0.007	193	3.7						
Ti62	65.0	62.2	0.95	Ditto	500	10.5	0.017	116	3.7						
Ti75	75.0	75.6	0.49	Ditto	500	<0.1	12.0	1.1	12.2						
Ti90	90.0	90.6	0.28	Ditto	500	1.7	0.4	44.7	9.4						

<sup>a</sup> Ti by difference except for Ti2-2 and Ti2-4 which were analyzed directly for Ti.

<sup>b</sup> Test discontinued before rupture except for Ti2-4 which was ruptured during test.

<sup>c</sup> Melted twice; inverted for second melting.

conium system, the best results were obtained with an alloy of 47.1 w/o zirconium which is in the gamma solid solution near the composition of the gamma eutectoid. In the titanium alloys, near maximum results were achieved over a range of composition from 17.0 to 55.4 w/o titanium. This range of composition is on the titanium side of the intermediate or delta phase and

brackets the titanium-rich gamma eutectoid, which occurs at about 34 w/o titanium.

Creep data at 815°C for a series of molybdenum alloys are shown in Table VII. The best results in these alloys were obtained with a 13.3 w/o molybdenum alloy which is in the gamma solid solution at 815°C.

TABLE VII. CREEP DATA FOR URANIUM-MOLYBDENUM ALLOYS AT 815°C IN VACUUM

Composition, w/o			Condition	Stress, psi	Time for 1% Deforma- tion, hr	Minimum Creep Rate, %/hr	Test Time, hr <sup>b</sup>	Elonga- tion, %						
Nom- inal Molyb- denum	Analysis													
	Molyb- denum <sup>a</sup>	Carbon												
4.3	4.8	0.50	Induction melted and cast in graphite; rolled at 1650°F	500	1	2.16	6.9	15.1						
10.0	7.5	0.13	Ditto	500	7	0.034	160	4.5						
10.0	7.8	0.13	Ditto	500	2	0.052	166	7.5						
29.0	12.3	0.24	Induction melted and cast in graphite; canned and rolled at 2200°F	500	29	0.014	172	3.6						
12.0	13.3	0.10	Induction melted and cast in graphite; canned and rolled at 2000°F	500	>330 <sup>c</sup>	0.00008 <sup>c</sup>	337 <sup>c</sup>	0.1 <sup>c</sup>						
12.0	13.3	0.27	Ditto	500	150	0.0023	191	1.1						

<sup>a</sup> Molybdenum by difference except for first three alloys in which molybdenum was analyzed directly.

<sup>b</sup> All tests were discontinued before rupture.

<sup>c</sup> Stress subsequently raised in successive steps above 500 psi.

### E. AQUEOUS CORROSION OF URANIUM AND HIGH URANIUM ALLOYS

Uranium reacts with water to form the stable oxide  $\text{UO}_2$  and with hydrogen to form  $\text{UH}_3$ . The reaction rate between uranium and hydrogen is at all temperatures considerably higher than that between uranium and water (R. P. Straetz and J. E. Draley; <sup>12</sup> W. M. Albrecht and M. W. Mallett <sup>12</sup>). Two types of corrosion of uranium occur in water, depending on whether a protective film of  $\text{UO}_2$  is formed and retained on the metal surface. In air-saturated distilled water protective films are formed, as shown in Fig. 20.<sup>12</sup> The curves for 50, 60 and 70°C show low corrosion rates for significant periods of time, followed by increased rates of reaction. At the time when the reaction rates increased it was observed that the thin protective oxide films broke down to form areas where the corrosion product was porous and black. These areas then spread, eventually enveloping the entire sample. At the time this had occurred the corrosion rate was apparently about the same as that observed

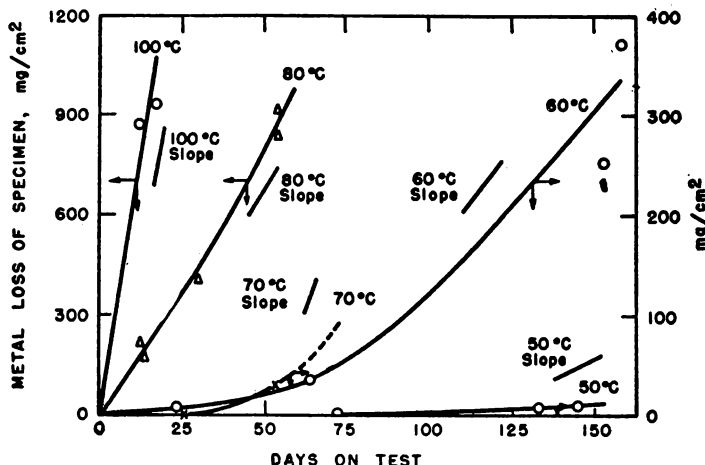


FIG. 20. Corrosion of standard uranium in aerated distilled water.

for uranium in hydrogen-saturated water, as indicated by comparison to the short lines drawn to show the slopes of the corrosion curves obtained in hydrogen-saturated water. It is observed that as the temperature is increased (and the amount of dissolved oxygen decreases) the time during which protection occurs decreases until, at 80°C and above, no apparent protection is afforded by a thin film of corrosion product.

It is believed that these experiments indicate that when thin films are formed, atomic hydrogen migrates through the oxide films and produces uranium hydride between the metal and the oxide. Such a hydride layer spoils the adherence of the oxide to the metal and its protectiveness disappears. Subsequently corrosion rates are determined by relatively rapid diffusion processes through the powdered oxide corrosion product.

In hydrogen-saturated water or degassed water corrosion is linear with respect to time, at least for significantly long periods at moderate temperatures. Corrosion rates so obtained are shown as a function of temperature in Fig. 21.<sup>12</sup>

J. A. Ayres and R. Dillon<sup>12</sup> have recently examined the short-time corrosion of uranium at 350°C. They report that the rate of reaction fits the extrapolated curve shown. In steam and, to a lesser extent, in water, the presence of hydride has been discovered beneath the oxide coating on samples corroded at 150 to 180°C (M. Bensen, R. P. Straetz and J. E. Draley;<sup>12</sup> L. R. Kelman<sup>12</sup>). At about the time the hydride was believed to form in significant quantities the corrosion rates were observed to increase. It has generally been considered that the hydride reaction plays a significant role in increasing the total corrosion rate when the oxide corrosion product shields the metal surface from access to water. At this time the hydrogen produced in the corrosion

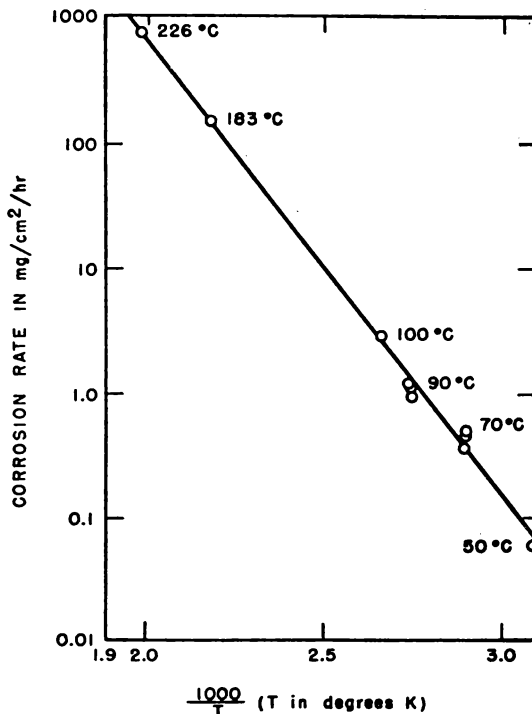


FIG. 21. Corrosion rate of standard uranium in hydrogen-saturated water.

reaction diffuses through the corrosion product (more permeable to hydrogen than to water), allowing rapid reaction of the hydrogen with uranium. When water reaches this uranium hydride, reaction occurs to form the more stable  $\text{UO}_2$ , and the hydrogen produced is free to diffuse ahead of the water again, thus providing an ample supply of the gas to react with the uranium.

The same mechanism is believed to describe the formation of uranium hydride in defectively jacketed pieces of uranium. When the jacket is not bonded to the uranium piece, water enters through the defect and reacts with the uranium to liberate hydrogen; the hydrogen is believed to diffuse along the surface of contact between jacket and uranium and may start reacting with the uranium at a considerable distance away from the jacket perforation. This distance is determined by such things as the temperature and the "induction period" which has been observed prior to initial reaction between hydrogen and uranium (R. P. Straetz and J. E. Draley;<sup>12</sup> W. M. Albrecht and M. W. Mallett<sup>12</sup>). If the reactions are allowed to proceed in unbonded jacketed pieces in water, eventually water reaches the site where uranium hydride exists and converts it to uranium oxide. Thus, if such pieces are examined when a local

swelling is first observed the product is  $\text{UH}_3$ ; after longer exposure the larger swellings are composed of  $\text{UO}_2$ .

The corrosion behavior of uranium of usual purity is influenced by heat treatment. In boiling distilled water, where protective films do not form, corrosion rates were reduced by heating alpha-annealed material into the beta or gamma region and cooling. The lowest rates, reduced by a factor of two compared to the alpha-annealed metal, were obtained by furnace cooling after one hour in vacuo at 1000°C. High purity metal had essentially the same corrosion rate as the typical uranium after heat treatment, and it did not show the heat treatment effect (J. E. Draley and J. W. McWhirter<sup>12</sup>). Dissolution and redistribution of impurities in the typical metal may account for these results. Similar reduction in boiling water corrosion rate had been observed in heat-treated samples of rather miscellaneous histories.

Alloying can be effective in stabilizing the protective oxide film on uranium metal surfaces. A uranium-5 w/o zirconium alloy, for example, required a very much smaller concentration of oxygen in the water to provide the highly corrosion-resistant surface film. Thus, in actively boiling distilled water in contact with air, this alloy developed the typical thin film showing interference colors and a very low corrosion rate. Eventually these films seem to break down in much the same way as does the film formed on uranium in air-saturated water at lower temperatures. However, when oxygen-free gas is bubbled through the boiling distilled water, the corrosion rate of the uranium-5 w/o zirconium alloy was nearly the same as that of unalloyed uranium and the thin protective film was not observed (J. E. Draley, J. W. McWhirter, F. Field and J. Guon<sup>12</sup>).

There are three general classes of alloys which appear to be able to form and to retain the protective oxide films, even in oxygen-free water, at temperatures as high as 350°C. These are:

- (1) Certain metastable gamma-phase alloys.
- (2) Certain supersaturated alpha-phase alloys.
- (3) Certain intermetallic compounds.

Typical of alloys of the first class are those containing more than about 7 weight per cent molybdenum or niobium. Of the corrosion-resistant alloys which have received serious study these appear to provide the lowest corrosion rates at elevated temperatures (see Fig. 22). In these alloys the alloying constituent dissolves in the uranium gamma phase which, upon moderate to rapid cooling, is retained as metastable gamma solid solution, since the transformations are sluggish. Low corrosion rates are exhibited by these materials so long as the gamma phase is retained and no transformations to other phases occur (B. Lustman and D. E. Thomas<sup>12</sup>).

There is a characteristic improvement in corrosion resistance of these alloys

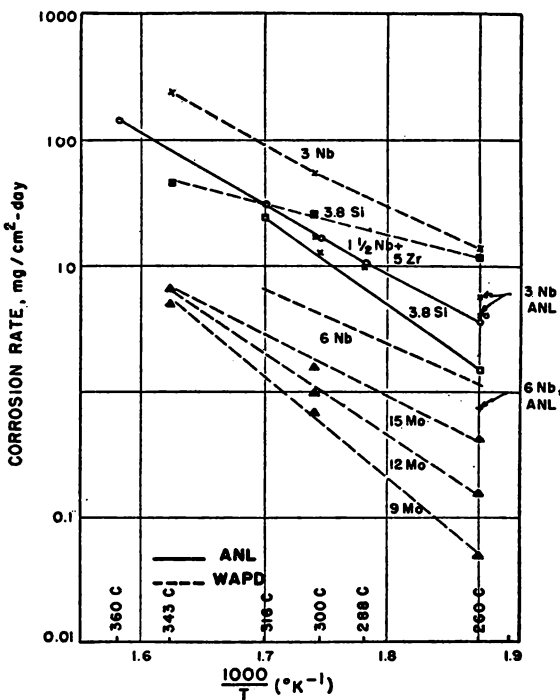


FIG. 22. Corrosion of uranium base alloys in distilled water.

if, after their initial rapid cooling from a gamma phase, they are given a mild heat treatment. The nature of the change in the material during this treatment is not understood, but definite reductions in corrosion rates are observed.

All of these alloys are susceptible to failure induced similarly to that of uranium in air-saturated water at low temperatures. The nature of the failure is entirely different, but it apparently occurs due to the solution of hydrogen in the metal. The hydrogen apparently diffuses into the alloy structure. The nature of the damage caused is not completely understood, but it is apparently true that a small amount of uranium hydride phase is formed within the structure of the metal. The lattice expansion in forming this hydride results in very high local stresses and in cracking. Such cracking results in breaking of samples into smaller pieces or in crumbling.

A uranium-3 w/o niobium binary alloy is typical of supersaturated alpha-phase alloys. This alloy shows moderate corrosion rates (see Fig. 22). Supersaturated alpha alloys undergo a martensitic transformation from the gamma phase, in which the alloying constituent is dissolved, to the alpha phase. If the cooling is done too slowly, a normal alpha phase is formed (not martensite) with the alloying constituents precipitated, usually as compound. These alloys

are corrosion resistant only so long as the martensitic alpha phase is retained. A slight aging treatment characteristically reduces the corrosion rate of these materials in much the same way that the rate of the gamma-phase alloys is reduced. Further aging causes grain boundary precipitation and reversion to the normal alpha-uranium structure. In this condition the alloy has poor corrosion resistance.

The temperature required to cause this over-aging can be increased, and hence the usefulness of the alloys can be improved, by adding zirconium to the niobium alloy. A typical example of this type of alloy contains 1.5 w/o niobium + 5 w/o zirconium. Its corrosion rate is approximately the same as the 3 w/o niobium alloy as shown in Fig. 22. Another modification contains approximately 0.7 w/o tin added to the 3 w/o niobium alloy. This alloy is in some respects quite similar in behavior to the uranium-5 w/o zirconium-1.5 w/o niobium alloy, but it appears to be more susceptible, during initial heat treatment, to effects such as cracking during quenching, and required the mild thermal aging treatment to avoid early corrosion cracking.

This type of alloy is susceptible to "failure" in the same fashion as the gamma-phase alloys. Failure is again by cracking or crumbling caused by the penetration of hydrogen into the metal structure. It has not been determined whether a hydride phase forms prior to the initiation of cracking.

The third type of corrosion-resistant alloy is typified by the stable delta \* phase ( $U_3Si$ ) in the U-Si system. Corrosion rates (see Tables VIII and IX) are similar to those for the supersaturated alpha alloys (Fig. 22). The compound must be nearly pure to possess adequate corrosion resistance. There is only slight solubility in it of uranium and of compounds richer in silicon. Formation of the delta phase requires maintenance at a temperature near

TABLE VIII. CORROSION OF HEAT-TREATED  $U_3Si$  SAMPLES IN DISTILLED WATER AT 100 AND  $178^{\circ}\text{C}$ <sup>15</sup>

Composition, w/o	Temper- ature, $^{\circ}\text{C}$	mg/cm <sup>2</sup>			52.3 days	Corrosion Rate, mg/cm <sup>2</sup> /hr
		4 days	16 days	32 days		
2.58 Silicon	100	5.0		16.4		0.014
3.07 Silicon	100	1.8		9.7		0.008
3.63 Silicon	100	1.4		4.3		0.003
3.82 Silicon	100	0.5 at 2 days		11.1		Insufficient data
2.58 Silicon	178					Cracked in 1 day
3.07 Silicon	178					Cracked in 2-3 days
3.63 Silicon	178	2.98	10		10.9	—

\* In the earlier phase diagrams this phase was called epsilon.

TABLE IX. CORROSION OF HEAT-TREATED U<sub>3</sub>-Si SAMPLES IN WATER AT 260 AND 316°C<sup>15</sup>

Composition	Heat Treatment	Corrosion Rate, mg/cm <sup>2</sup> /mo	
		260°C	316°C
3.70 Silicon, 0.08 Carbon	3 days 800°C	50	1400
3.75 Silicon, 0.05 Carbon	6 days 800°C	60	1400
3.82 Silicon, 0.05 Carbon	3 days 800°C	30	1250

the maximum at which the phase is stable (850°C) for a significant period. Although formation of the delta phase appears to occur within the first few hours, longer times at this elevated temperature seem to provide material with a somewhat improved corrosion resistance (A. Kaufmann, T. T. Magel, D. Kneppel<sup>12</sup>). This alloy has the advantage that the phase which is corrosion resistant is stable at temperatures where the metastable gammia phase and the supersaturated alpha-phase alloys are over-aged and have entirely lost their corrosion-resistant characteristics.

It is not known whether this alloy is susceptible to the type of failure exhibited by the other two types of corrosion-resistant alloys.

#### REFERENCES FOR CHAPTER III

1. See also the following Geneva Papers:  
 416—P. C. L. Pfeil, "Alloys of Uranium and Thorium."  
 786—R. Kiessling, "The Solid State Reaction between Uranium and Aluminum."  
 352—M. Englander, "Etude des Alliages Uranium-Aluminum."
2. J. E. Baumrucker and H. H. Chiswick, Unpublished work (see Geneva Paper No. 558).
3. C. W. Jacob and B. E. Warren, *The Crystalline Structure of Uranium*, J. Am. Chem. Soc. 59:2588 (1937).
4. J. S. Lukesh, *Note on the Structure of Uranium*, Acta Cryst. 2:420 (1949).
5. C. W. Tucker, Jr. and P. Senic, *An Improved Determination of the Crystal Structure of Beta Uranium*, Acta Cryst. 6:753 (1953).
6. A. S. Wilson and R. E. Rundle, *The Structure of Uranium Metal*, Acta Cryst. 2: 126 (1949).
7. J. Thewlis, *Structures of Uranium*, Nature 168:198 (1951).
8. J. Thewlis, *X-Ray Powder Study of Beta Uranium*, Acta Cryst. 5:790 (1952).
9. C. W. Tucker, Jr., *The Crystal Structures of Metallic Uranium*, Trans. ASM 42: 762 (1950).
10. A compilation of United States and United Kingdom Uranium and Thorium Constitutional Diagrams, compiled for the USAEC by Battelle Memorial Institute, H. A. Saller, F. A. Rough, Editors (June 1955), BMI-1000.

11. As given by P. C. L. Pfeil in Geneva Paper No. 416.
12. As described in Geneva Paper No. 555.
13. P. Duwez, *The Effect of Cooling on the Allotropic Transformation Temperature of Uranium*, J. Appl. Phys. 24:152 (1953).
14. C. W. Tucker, Jr., *The Crystal Structure of the Beta Phase of Uranium*, Acta Cryst. 4:425 (1951).
15. As described in Geneva Paper No. 558.
16. See also Geneva Paper No. 352.

## *Chapter IV*

---

### CASTING AND FABRICATION OF URANIUM AND ITS ALLOYS \*<sup>1</sup>

---

#### A. URANIUM

**1. The casting process.** In early 1942 small castings of uranium metal were made by vacuum self-induction heating of uranium powder compacts supported in beryllia crucibles. On heating to high temperatures the liquid uranium metal would break through its tough oxide skin and flow through a grill and into a beryllia mold. Experimental work at Ames soon demonstrated that graphite crucibles could be employed for vacuum induction melting of uranium. The melting point of uranium was found to be about 1130°C and, at pouring temperatures of up to 1300°C and even higher, the solubility of carbon in the uranium was not greater than a few hundred parts per million. In the early production plant, uranium was melted in a graphite crucible having a grill for the bottom to catch oxide skins as the metal flowed into a heated graphite mold below.

In certain phases of uranium metallurgy there may develop concentrations of materials that present chemical and radiological health problems. The vacuum melting and casting operation does give some concentration of such materials, especially in the flue dust and in the dross from graphite melting crucibles.

The uncertainty of pouring temperature and rate of flow in the grill-type casting set-up made it necessary to work out designs for melting and casting units that would give better control of the operation for larger sizes of ingots. The designs for these larger casting units were modified from time to time as sizes and shapes of castings were changed.

One design that can be used for vacuum casting a single uranium ingot is

\* This chapter is based mainly on the following Geneva Papers:

827—A. R. Kaufman, "Fabrication of Uranium Alloys."

817—H. A. Wilhelm, "The Preparation of Uranium Metal by the Reduction of Uranium Tetrafluoride with Magnesium."

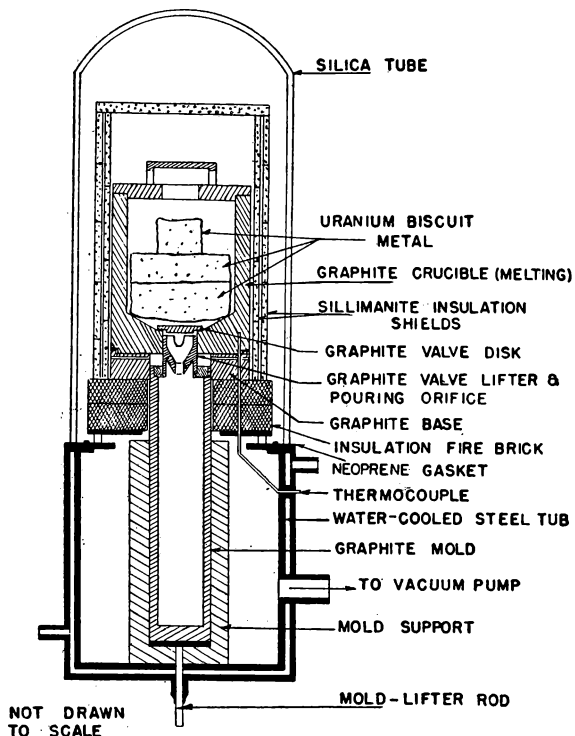


FIG. 1. Uranium casting unit.

shown in Fig. 1. The heating is effected by a hoist-type induction coil (not shown) which is lowered to its operating position around the silica tube. Heat is generated in the graphite crucible and its temperature is followed by means of the thermocouple. When the metal is at casting temperature it is poured into the mold by opening the valve in the crucible by means of an upward thrust on the mold-lifter rod. The valve lifter is mounted in the top of the mold. This thrust lifts the mold and the valve lifter which in turn lifts the valve disk. The valve disk is forced far enough from its seat to float to the top of the melt as the uranium liquid flows through the orifice and into the mold. Ventilation of the mold cavity takes place through ports (not shown) in the valve lifter below the orifice.

The ingot obtained by this process is cropped to remove the pipe and the resulting billet is an intermediate form for further fabrication into shapes.

**2. Fabrication.<sup>2</sup>** The three allotropic forms of pure uranium dominate the problem of working it. In the alpha phase (up to 660°C) uranium work hardens when deformed at temperatures up to about 450°C. The minimum recrystallization temperature for heavily cold-worked metal is about 425°C.

From about 450 to 660°C true hot working can be carried out with the metal becoming softer as the temperature is raised. In the beta phase (660 to 770°C) the force required to hot work the metal is 2 to 3 times as great as at 650°C and the ductility is substantially less. In the gamma phase (above 770°C) uranium is so soft and plastic that difficulty is sometimes encountered in having it flow well and retain its shape. This difficulty is accentuated by certain impurities such as iron which may lead to hot shortness in the gamma phase.

a. *Extrusion.*<sup>2\*</sup> The work on extrusion indicated it could be done in either the alpha or the gamma phase; the pressures required in the alpha phase are high. For gamma extrusion, the uranium slugs are heated to 1700°F in a reducing atmosphere and extruded by the direct method. Extrusion liners and dies wore rapidly, but use of refractory alloys of the "Stoodite" type overcame this trouble. For alpha extrusion the uranium can be either copper plated or handled bare. A soft steel cone is placed in front of the uranium and graphite cut-off cylinders are charged after the uranium. The laboratory studies of extrusion have been extended principally by A. R. Kaufmann, S. U. Arnold and R. M. Treco.<sup>3</sup> The last two workers have summarized their work on the temperature range 199°C (390°F) to 593°C (1100°F) in Fig. 2. The studies of extrusion of uranium in the temperature range of stability of the gamma allotrope 770°C (1418°F) to 1135°C (2057°F) (the gamma range) have not been similarly systematized.

Impact extrusion in the gamma phase (1920°F) has been used successfully to form a number of shapes, and it appears feasible to form any number of complicated shapes by this process. Extruded shapes have much better physical properties than similar cast shapes.

b. *Drawing.* Uranium wire and tubing have been cold drawn with considerable success. For any drawing, the lubricant is the most critical factor. Tubing was drawn by the Superior Tubing Company using one of their proprietary lubricants. Rods and wire have been drawn using the following lubricant developed primarily for thorium: 100 cm<sup>3</sup> of Duco black lacquer (No. 246-2048 thinned 3 to 1 with lacquer thinner), mixed with 30 grams of Molykote (molybdenum disulfide), and 10 grams of fumed lead-zinc oxide. The lubricant is sprayed or brushed on and allowed to dry before drawing. It may be necessary to recoat the wire after two or three drawing passes. Reductions of 20% per pass are feasible with this lubricant.

Wire has been drawn down to 0.003 inch in diameter by silver plating the wire prior to drawing. Some success has been achieved with copper plated wire.

c. *Rolling.* While uranium can be rolled in the beta and gamma phase with some difficulty, most of it is processed in the alpha. Rolling is done in the

\* A study of the malleability of uranium in the three phases and of the extrusion variables has been made by Stohr and Chevigny.<sup>4</sup>

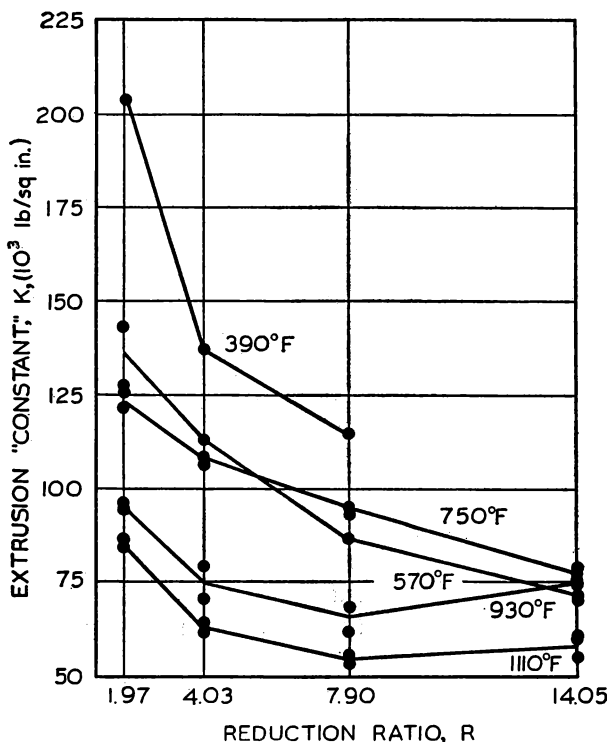


FIG. 2. The extrusion constant for alpha-uranium vs reduction ratio.

$$P = K \ln \frac{A_1}{A_2}$$

The pressure required for extrusion may be conveniently expressed by the relation where  $P$  is pressure on the ram in psi,  $K$  is a constant which varies with temperature, and  $A_1$  and  $A_2$  are the cross-sectional areas of the billet and the extruded rod respectively.  $K$  varies somewhat with the lubrication and for a given set of extrusion conditions it does not become constant until the reductions in area are greater than about 5 times.  $K$  has lower values the larger the diameter of the extrusion billet.

range from room temperature to 1110°F. Uranium has been rolled using rolls of many shapes including diamonds, squares, guide rounds, hand rounds, ovals, and gothics. Uranium rolls easily and large reductions per pass may be taken.

A number of methods have been employed to heat uranium for rolling. These include inert-atmosphere furnaces, oil baths, lead baths, and salt baths.

Thin uranium foil of very good quality down to 0.0005 inch thick has been produced by cold rolling. In one method, starting stock 0.020 inch thick is produced by hot rolling. This is then cold rolled on a "four-high" mill with

1-inch work rolls. A large number of passes and about two anneals are required during the rolling. Recently, 2-mil foil has been rolled directly from 20-mil stock with no anneals by using a Sendzimer Mill.

*d. Forging.* Uranium has been forged successfully at 930 to 1200°F using standard forging techniques. The metal must be protected from the atmosphere during heating but is forged bare. Heating methods described for rolling can be used.

*e. Pressing.* Uranium can be formed by pressing in the gamma range (1470 to 1830°F). The metal is very soft and plastic and deforms under comparatively light loads. The major problem in high-temperature pressing is in finding die materials to withstand the temperature.

It is possible to deep draw uranium to form cups and cylinders. The sheet should be hot rolled at 1110°F, cold rolled to size at 525°F, and then annealed at 1065°F. Dies are designed using the same criteria as those applicable to the drawing of copper. Dies and blanks should be heated to about 345°F. A good lubricant is "liqui-moly" \* or Acheson "Dag" dispersion #41.

*f. Swaging.* Uranium can be swaged either cold or at temperatures around 930 to 1110°F, and reductions of 10 to 15% per pass can be taken. In cold swaging, it may be necessary to anneal after three or four passes.

*g. Straightening.* Uranium can be straightened by any of several methods including (1) hand hammering, (2) Medart Rotary, (3) Torrington-12 roll straightener, or (4) stretching.

## B. URANIUM ALLOYS

The preparation and fabrication of uranium alloys present a number of practical problems which are often troublesome. In this section these difficulties will be discussed in a general way to show that they can be solved if the investigator has a proper understanding of uranium itself and in addition has available the phase diagram of the alloy system involved.

The fabrication of uranium rich alloys differs from that of the pure metal only insofar as the alloying element modifies the three allotropic forms of uranium. Since no elements of appreciable solid solubility in alpha uranium have been found, fabrication of the alloys in the alpha existence range is governed by the degree of hardening caused by the second phase. If this second phase is a brittle intermetallic compound, the uranium alloy rapidly decreases in ductility with alloy addition, and working in the alpha phase may become impractical. There are some cases, however, where the intermediate phase is not brittle and thus does not alter the uranium radically. Solid solubilities in the beta phase are also rather restricted and as far as is known there are no alloy additions which make it more feasible to fabricate in the beta phase. Presumably, alloys containing second phases are even more difficult to work

\* Oil suspension of MoS<sub>2</sub>.

in the beta phase than pure uranium. Since there are a number of elements such as Mo, Zr, Nb, V, and Ti which have extensive solubility in the gamma phase, the feasibility of working above 770°C is increased since the gamma uranium is stiffened and has more high temperature ductility. In those instances in which the beta to gamma transformation is lowered by the alloy addition it then becomes possible to fabricate in the body-centered cubic phase below 770°C. With some alloys such as 6 to 15% molybdenum it is possible to retain the gamma phase in a metastable state at room temperature and cold working of the body-centered cubic phase then can be carried out. It is possible to retain the beta phase by quenching a 1 to 2 a/o chromium alloy, but this has no significance as far as fabrication is concerned since the beta structure apparently transforms during cold deformation.

The production and fabrication of some typical alloys are described below.

**1. Uranium-chromium.** In most respects the alloys with chromium constitute a simple situation since there are no intermetallic compounds. This is then a case of processing a mixture of two somewhat ductile metals.

*a. Melting.* Melting can be satisfactorily accomplished in graphite crucibles for compositions up to the eutectic at about 5.2 w/o. There is no great difficulty with regard to carbide formation or segregation.

It is interesting to note that the eutectic alloy, which melts at about 860°C, has a particularly high fluidity. When poured from about 1000°C into heated molds, it will fill very small openings. For example, plates 0.040" × 3" × 24" can be cast without difficulty and various intricate structures are readily produced.

*b. Fabrication.* Chromium alloys up to the eutectic composition can be extruded in the gamma phase at about 800°C or the alpha phase at about 600°C. Typical values for extrusion constants for several compositions are shown in Table I. It is clear that chromium is stiffer than uranium and hence should make the alloys more difficult to work. The extrusion constant has been defined in the caption to Fig. 2.

It is possible to forge the eutectic composition at about 800°C by a pressing operation using pressures of about 2000 psi. Alloys with less chromium deform still more easily at that temperature.

Rolling can be carried out readily at 600°C, but cold rolling becomes increasingly difficult as the chromium content is increased. It is to be noted that chromium itself does not possess much ductility.

Hot swaging of alloys containing up to 2 a/o chromium can be carried out at 275°C, and up to 4 a/o chromium at 550°C.<sup>3</sup> Annealing at 550°C removes the effects of cold work.

**2. Uranium-zirconium.** This system represents a case of complete solid solubility in the high temperature body-centered cubic region with no appreci-

TABLE I. EXTRUSION CONSTANTS FOR SOME URANIUM ALLOYS \*

Material, w/o	Temperature, °C	K, psi	Remarks
Uranium	590	40,000	
	870	6,500	
98U 2Zr	590	50,000	
	650	45,000	
	700	28,000	
	735	16,000	
50U 50Zr	610	50,000	
	650	42,000	
	732	32,000	
	760	29,000	
	815	28,000	
20U 80Zr	650	41,000	
	760	27,000	
	850	16,000	
	910	15,000	
8U 92Zr	760	40,000	
	815	31,000	
	870	32,000	
	927	30,000	
93.5U 5Zr 1.5Nb	620	40,000	
	650	35,000	
	677	30,000	
	705	26,000	
	732	23,000	
	760	20,000	
	788	17,000	
99.9U 0.1Cr	635	48,000	
97.5U 2.5Cr	600	63,000	
	800	29,000	
95U 5Cr	600	68,000	
	765	44,000	
	850	31,000	
96U 4Mo	600	>94,000	Failed to extrude
	900	35,000	
92U 8Mo	600	71,000	
	900	58,000	
88U 12Mo	600	>94,000	Failed to extrude
	900	63,000	
99.9U 0.1Si	635	45,000	
97.5U 2.5Si	600	86,000	As cast
	800	34,000	
96.2U 3.8Si	850	55,000	Heat treated to form delta

\* Billets used were 2 to 3 inches in diameter.

able solid solubility in the low temperature phases and the occurrence of one intermetallic phase.

a. *Melting.* Zirconium is even more reactive than uranium at high temperatures and therefore the choice of melting crucibles must be made carefully. Beryllium oxide and probably zirconia are satisfactory for compositions up to about 3 w/o zirconium. Graphite may be used for all compositions if the molten metal is not overheated and is poured soon after melting. Without these precautions large amounts of zirconium carbide will form, especially in the range from 5 to 95 w/o zirconium. Arc melting in a water-cooled copper crucible must be used to produce alloys of the highest purity.

b. *Fabrication.* Zirconium is a ductile metal and its body-centered cubic alloys with uranium are easy to hot work. Zirconium is much stiffer than uranium in this phase and therefore the extrusion constants at a given temperature increase with zirconium content as shown in Table I. It is noteworthy that a 2 w/o zirconium alloy can be extruded in the temperature range where the uranium beta phase is normally encountered. According to the phase diagram the alpha phase persists up to about 700°C at this composition. The relatively low  $K$  for the extrusion at 735°C is presumably due to large amounts of gamma phase mixed with beta phase. The existence range of the gamma phase may be further lowered by certain ternary alloys. As an example, an alloy containing 5 w/o zirconium and 1½ w/o niobium has stable gamma phase down to about 620°C. The data in Table I show that there are no discontinuities in  $K$  for this alloy in the normal beta phase existence range. The results for the 50 w/o zirconium alloy illustrate another case of working the body-centered cubic phase at temperatures as low as 610°C.

In general it appears that the intermediate phase, delta, is reasonably ductile. Extrusion data below 600°C for alloys in this range have not been obtained. It may be said, however, that alloys containing delta may be cold rolled and cold swaged with reasonable reductions before annealing becomes necessary.

**3. Uranium-molybdenum.** Molybdenum has extensive solubility in gamma uranium, as discussed in Chapter III, and forms an intermediate phase at about 15 w/o molybdenum. The exact location of the boundaries of this delta phase is somewhat uncertain, but there is no doubt of its existence. For alloys above about 5 w/o molybdenum the transformation of gamma to alpha becomes increasingly sluggish. Above about 10 w/o molybdenum the gamma phase is retained even without quenching.

a. *Melting.* Induction melting of alloys up to 15 w/o molybdenum is readily carried out in crucibles suitable for melting uranium. Graphite crucibles with a zirconia wash are quite satisfactory. Arc melting is not particularly satisfactory for making these alloys since there is a possibility that the molybdenum additions may not melt completely.

*b. Fabrication.* Alloys containing up to about 3 w/o molybdenum may be extruded or rolled in the high alpha region. For larger amounts of molybdenum it is necessary to fabricate in the gamma phase since the alloy becomes increasingly stiff. The extrusion constants shown in Table I show that at 12 w/o molybdenum the alloy is almost too stiff to extrude at 900°C<sup>6</sup> with an appreciable reduction in area. The table shows that the 4 and 12 w/o molybdenum failed to extrude at a *K* value of 94,000 at 600°C, whereas the 8 w/o alloy did extrude. The reasons for this are not known. One possible explanation is that the 4 w/o alloy was in the alpha phase, whereas the 8 and 12 w/o alloys were in the gamma phase at 600°C. All the molybdenum alloys up to 12 w/o may be cold worked to some extent by swaging. In the case of the 12 w/o alloy, it is desirable to take a heavy reduction in each pass through the machine since there is then less trouble with cracking. Cold working of the 12 w/o alloy does not appear to transform appreciable amounts of the retained gamma phase.

**4. Uranium-silicon.** There are a number of intermetallic compounds in this system, and all of them are quite brittle except for the delta\* phase at about 23 a/o (3.6 w/o) silicon. It is not feasible to fabricate the alloys above about 30 a/o silicon by conventional means and the discussion will therefore be confined to the uranium-rich alloys. The delta phase forms rather sluggishly and hence alloys as-cast consist essentially of mixtures of uranium and U<sub>5</sub>Si<sub>3</sub>. A heat treatment of 4 to 24 hours' duration at 800°C is required to convert most of the U<sub>5</sub>Si<sub>3</sub> to delta, although it is likely that for alloys below the eutectic composition (8 a/o) the peritectoid reaction may occur more readily.

*a. Melting.* The uranium-rich alloys may be melted in any type of crucible suitable for melting uranium itself. Above about 20 a/o silicon it is desirable to heat to at least 1600°C in order to make sure that all the high melting compounds are in solution. It has been found that a graphite crucible which has been given a zirconia wash is suitable for this operation. An alloy of about 25 a/o silicon will contain only about 0.06 w/o carbon if made in this way. It is desirable to chill-cast alloys above the eutectic composition in order that the primary U<sub>5</sub>Si<sub>3</sub> particles be as small as possible. The small particle size is desirable in order that the peritectoid reaction to form delta can go to completion readily.

*b. Fabrication.* It is possible to extrude all compositions up to about 28 a/o silicon in the as-cast condition where the alloy consists of uranium and U<sub>5</sub>Si<sub>3</sub>. At the higher silicon content it becomes necessary to use a temperature of about 900°C. Obviously part of the U<sub>5</sub>Si<sub>3</sub> will convert to delta during this operation. It is also possible to convert first the U<sub>5</sub>Si<sub>3</sub> to delta and then

\* In the older compilation of phase diagrams this phase was referred to as epsilon.

extrude. If the composition is such that substantial amounts of free uranium remain after the heat treatment, it is necessary to use an extrusion temperature which avoids the uranium beta phase region. Low silicon contents can be extruded at about 600°C in the uranium alpha phase. Above about 10 a/o silicon it is more practical to use an extrusion temperature of about 850°C which is high enough to avoid the beta phase and yet low enough to avoid decomposing the delta. Some typical extrusion constants are shown in Table I.

Hot rolling can be carried out at 600°C for compositions up to about 10 a/o silicon. It is not known whether or not rolling of higher compositions at 850°C is feasible. A limited amount of cold rolling is possible on the lower silicon compositions. An alloy consisting of essentially all delta has only a small amount of ductility. It can be cold swaged with 20 to 30% reduction in area, but it is doubtful that rolling or drawing can be done.

In summary, uranium-rich alloys can exist in a number of states having widely different degrees of ductility and crystal form. In alloys containing free uranium it is difficult to fabricate in the beta phase range. Alloys containing small amounts of intermetallic compound can be hot worked either in the high alpha range or in the gamma phase region. A limited amount of cold working is also possible if the amount of compound is sufficiently small. If the amount of compound is 50 to 75 volume per cent of the alloy it is necessary to work in the gamma region, preferably by extrusion. The silicon delta alloy is an exception to this. Elements having extensive solid solubility in the gamma phase may be fabricated conveniently in the gamma region. In some cases this can be done at lower temperatures than the beta to gamma transformation for pure uranium. With molybdenum alloys above about 10 w/o it is possible to retain the gamma phase at room temperature and cold work does not cause the alloy to transform.

#### REFERENCES FOR CHAPTER IV

1. See also the following Geneva Papers:  
825—J. P. Howe, "The Metallurgy of Reactor Fuels."  
351—J. A. Stohr and R. Chevigny, "Extrusion of Uranium in the Gamma Phase."
2. Part of this section is based on "The Reactor Handbook," Vol. 3, Section 1, AECD—3647 (1955).
3. As described in Geneva Paper No. 825.
4. As described in Geneva Paper No. 351.
5. A compilation of United States and United Kingdom Uranium and Thorium Constitutional Diagrams, compiled for the USAEC by Battelle Memorial Institute, H. A. Saller, F. A. Rough, Editors (September 1954), BMI-1000.
6. See Geneva Paper No. 827.

## *Chapter V*

---

### THE PRODUCTION OF THORIUM \*<sup>1</sup>

---

---

The use of thorium in the atomic energy program has accelerated the rate of production of this element in the past few years. The nucleus of the thorium atom (Th-232) can undergo reaction with a neutron to form Th-233 which is relatively short-lived. Subsequent radioactive disintegrations of this isotope produce a relatively long-lived U-233 which can be caused to fission and serve as an atomic fuel in a manner similar to U-235 and Pu-239.

Although the transformation process from Th-232 to U-233 is independent of the chemical state of the thorium, the high concentration of thorium atoms in thorium metal and other properties of the metallic state are advantageous in certain reactor designs.

The material presented in this and the following chapters has been selected from a large amount of data obtained by many workers and represents the present knowledge of the metallurgy of thorium and its alloys.

#### A. OCCURRENCE OF THORIUM AND MONAZITE PROCESSING

**1. Occurrence of thorium.** Thorium is widely distributed in nature, but rich deposits are scarce. It has been estimated that the thorium content of the earth's crust is between 0.0003 and 0.001% or about two to five times that of uranium. Traces of thorium have been found in more than 100 minerals, a few of which contain more than 1% thorium. Monazite sand, however, is the only commercially feasible source of thorium.

Monazite sand occurs as a primary mineral in granites, gneisses and pegmatites. As a result of erosion, the sand is concentrated sufficiently along the courses of rivers or on beaches to be of commercial interest. The largest and richest deposits of monazite are in Brazil and India. Sizable deposits are

\*This chapter is based mainly on the following Geneva Paper: 556—O. N. Carlson, P. Chiotti, G. Murphy, D. Peterson, B. A. Rogers, J. F. Smith, M. Smutz, M. Voss, and H. A. Wilhelm, "The Metallurgy of Thorium and Its Alloys."

## 110 THE METALLURGY OF URANIUM AND THORIUM

present in the Netherlands East Indies, South Africa, and the United States.<sup>2</sup>

In 1893, Welsbach patented the use of a mixture containing 98 to 99% thoria for gas mantles and the industry grew rapidly thereafter. In the years preceding World War I, over 300 million gas mantles were consumed annually. Brazil dominated the world market from 1895 to 1914. The wide adoption of electricity for home lighting just prior to World War I caused a sharp decline in the demand for gas mantles and for thorium. Brazil produced less monazite from 1914 to 1941 than in the single year 1909. The advent of the atomic energy program has caused a renewed interest in thorium and thus in monazite.

Monazite sands are essentially the orthophosphates of rare earths, thorium and uranium. The chemical composition is shown in Table I. The sands are yellow to reddish-brown in color and are hard and brittle.

TABLE I. CHEMICAL COMPOSITION OF MONAZITE SANDS

	Indian Monazite, %	Brazilian Monazite, %	Idaho Monazite, %
Total Oxides	69.2	68.1	68.9
ThO <sub>2</sub>	9.4	6.5	3.95
CeO <sub>2</sub>	28.5	—	29.2
U <sub>3</sub> O <sub>8</sub>	0.37	0.18	0.15
P <sub>2</sub> O <sub>5</sub>	25.9	26.0	28.5

**2. Processing of monazite sand.** The first step in processing monazite is to destroy the chemical structure of the sand. Sulfuric acid digest has been used for more than a half century to produce a water-soluble product. An alternate process starting with a caustic digestion of the sand has also been developed.<sup>3</sup> Both of these processes will be described briefly.

a. *Sulfuric acid process.* Monazite sand is added to concentrated sulfuric acid heated to about 200°C. The time of digestion depends primarily upon the particle size of the sand. If the sands are finely ground the reaction is complete in about 1 hour. If the sands are quite coarse, 4 to 6 hours are required. As the reaction proceeds the digested mass becomes more and more viscous. When the reaction is nearly complete, a pasty mass results. The minimum acid-to-digested sand weight ratio, based on the stoichiometry of the reaction, is about 0.60. The actual minimum acid-to-digested sand weight ratio is limited by the solubility of the thorium phosphate in the resulting monazite sulfate solution. Shaw et al.<sup>4</sup> found the actual minimum ratio to be 1.6 for both Indian and Idaho monazite.

Dissolution of the digest mass is accomplished by adding about 10 pounds

of water per pound of digested sand. Cold water is preferable because the rare earth sulfates are more soluble at lower temperatures than at higher temperatures. The resulting solution is stable and is very close to saturation with respect to rare earths and thorium. This solution is called monazite sulfate solution.

The monazite sulfate solution can be decanted immediately from the heavy undigested sand. Upon standing, the fine suspended solids will settle out of the monazite sulfate solution. These solids are primarily silica but contain a very large fraction of the radioactive daughter products of thorium and uranium. The monazite sulfate solution can be decanted from this sludge.

The separation of the desired components from the monazite sulfate solution can be accomplished in several ways. Fractional crystallization methods have been used in the past. Many attempts are being made to extract the thorium and uranium directly from the monazite sulfate solution using a selective solvent.

Shaw et al.<sup>4</sup> developed a process for separating thorium, rare earths and uranium from the monazite sulfate solution. A thorium concentrate was produced by diluting the monazite sulfate solution and adjusting the pH to 1.0 by using dilute ammonium hydroxide. At this pH, about 99% of the thorium and 5% of the rare earths precipitated. Since the rare earths are originally present in much larger amounts than the thorium, the resulting precipitate was about half thorium phosphate and half occluded rare earth sulfates. The solids were allowed to settle, the clear solution was decanted, and the remaining mixture was filtered. The thorium concentrate was dissolved in nitric acid and fed to a multistage extractor using tributyl phosphate as a solvent. A thorium product containing only a few parts per million of rare earth contaminants was obtained as an extract product. A wide variety of inert diluents can be used to enhance phase separations.<sup>7</sup>

The filtrate and decantate from the thorium precipitation were then neutralized with ammonium hydroxide to a pH of 2.3. At this pH most of the rare earths were precipitated. The precipitate was allowed to settle and the clear solution was decanted from the solids. The concentrated precipitate was then filtered. These solids were sent to a rare earth recovery unit. The individual rare earths can be separated by ion exchange<sup>5</sup> or solvent extraction processes.

The filtrate and decantate from the rare earth precipitation step were then neutralized to a pH of 6.0. At this pH the remainder of the rare earths and the uranium were precipitated. The filtrate and decantate were discarded, and the uranium concentrate, containing about 1% uranium, was obtained. The uranium concentrate was dissolved in nitric acid and extracted in a multi-stage extractor using tributyl phosphate as a solvent. A uranium product was obtained containing only a few parts per million of rare earth contaminants.

Processes starting with a sulfuric acid digestion of the monazite cause the presence of sulfate ions in the solution to be extracted. Sulfate ions decrease the distribution coefficients for thorium and uranium markedly. The addition of nitric acid helps to overcome the effect of sulfate ion. Since the phosphate and sulfate ions are not extracted into tributyl phosphate, the scrub sections of the extractors are not influenced by the presence of these ions in the feed, and separations can be carried out to any desired purity.

*b. Caustic digestion process.*.. The caustic digestion process developed by Bearse et al.<sup>3</sup> consists of the following five operations:

- (1) Reaction of the sand with a hot concentrated sodium hydroxide solution. This converts the metal phosphates of the sand to hydrous metal oxides and trisodium phosphate.
- (2) Separation of the hydrous metal oxides from the dissolved sodium phosphate and excess sodium hydroxide.
- (3) Dissolution of the hydrous metal oxides in hydrochloric acid.
- (4) Precipitation of a thorium product by partial neutralization of the acid solution.
- (5) Precipitation of a rare earth hydroxide product by further neutralization of the chloride solution.

The effect of the sodium hydroxide-to-sand ratio was studied and a weight ratio of 1.5 was found satisfactory. The recommended reaction time was 3 hours at 140°C if the sand were ground to 96.5% less than 325 mesh, and the initial concentration of sodium hydroxide was about 45%.

In pilot plant runs the mixture was heated to 140°C and maintained at that temperature with moderate agitation for 3 hours. The mixture was then diluted with a wash solution from a later step. The slurry was digested for 1 hour to facilitate filtration and was then filtered to remove the hydrous oxides from the trisodium phosphate and excess caustic soda. The filtration was carried out at 80°C and 60 psig. The clear filtrate was sent to an evaporator for concentration and removal of trisodium phosphate. The cake was blown dry and sent to the acid dissolution vessel.

The hydrous oxide cake was added to 37% hydrochloric acid and heated for 1 hour at 80°C. The solution was then diluted and partially neutralized with sodium hydroxide solution to a pH of 5.8. At this pH, all of the thorium and uranium precipitated, accompanied by about 3% of the rare earths. The slurry was allowed to stand and then the solution was decanted and filtered from the solids. The thorium and uranium were recovered from the cake by dissolving it in nitric acid and extracting with tributyl phosphate. The thorium and uranium were selectively stripped from the solvent. The absence of phosphate and sulfate ions permitted high concentrations and high separation factors in the extraction and scrub sections of the column.

The filtrate and washings from the filtration of the hydrous oxide cake were neutralized with sodium hydroxide to precipitate the rare earths as hydroxides. The slurry was filtered giving a rare earth cake containing very small quantities of uranium and thorium.

c. *Cost estimates.* The sulfuric acid and caustic digestion processes have been compared on a cost basis assuming the same rate of production and the same source of monazite sand. There is apparently little economic advantage of one process over the other, although pilot plant work on both processes was not extensive enough to arrive at accurate costs. The actual cost of the thorium depends principally on the value credited to the by-product rare earths and on the scale of production.

### B. THORIUM METAL PREPARATION

Thorium metal, because of its reactivity (especially at elevated temperatures) and its relatively high melting point, presents a number of special problems in its preparation from the readily available compounds. However, a number of methods for producing thorium metal have been described in the literature since its first preparation by Berzelius<sup>6</sup> who reduced thorium tetrachloride with potassium metal and obtained an impure thorium metal powder. Most of the methods described yield the metal as a powder or granular product which can be fabricated by powder metallurgical techniques to give solid metal shapes.

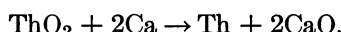
In general, thorium metal can be prepared from thorium halides by reduction with reactive metals such as sodium, calcium and magnesium or by electrolysis of the halide in a fused salt bath. The thermal decomposition of the iodide to give thorium metal has been used only as a means for purifying metal prepared by other processes employing more stable thorium compounds. Thorium metal can be prepared also by the reduction of thorium oxide with calcium metal and a number of processes have been developed with this reaction as their basis. The processes for virgin metal described in some detail below are selected from among those that have been demonstrated to be capable of giving good quality metal in quantity.

1. **Thorium oxide reductions.** The original process developed by Marden and Rentschler<sup>7</sup> employed calcium chloride mixed in the charge with thorium oxide and a large excess of calcium metal. The charge was heated in a closed steel bomb for 1 hour at 950°C. After cooling, the reacted mass was leached with dilute (1:10) nitric acid, then with water followed by a wash with alcohol and a final wash with ether. The metal powder was then dried in vacuo, compacted and then sintered at about 1300°C to give solid ductile thorium metal having a purity of at least 99.7%.

Rentschler et al.<sup>8</sup> describe in detail the production of good-quality thorium

metal by the calcium reduction of thoria under an inert atmosphere and without additives such as calcium chloride. A variation of the process employing this reduction reaction is carried out in a refractory-lined steel crucible in an inert gas atmosphere. The liner material may be made of thin sheets of a metal such as molybdenum. The liner is to prevent reaction between the charge or products and the iron crucible at the high temperature employed in the processing.

The crucible is charged with alternate layers of calcium metal (granular) and finely divided thorium oxide with a layer of the calcium on the top. About 100% excess of calcium is employed over that calculated for the reaction:



The charged crucible is then placed in a larger steel vessel having a lid fitted with a pipe for admitting an inert gas. The lid is bolted on, the air is replaced with argon and the assembly is then introduced into a furnace which can be heated to 1200°C.

The reaction occurs as the charge heats. The temperature of the charge is raised to 1000°C or higher in order to obtain better yields of good-quality thorium powder. The crucible and its contents are then allowed to cool under the inert gas to near room temperature. The product is then leached from the crucible by dumping the crucible and its contents into just sufficient dilute (10%) acetic acid to react with all of the calcium metal and oxide.

The first leaching solution is removed, leaving the product as an impure mud. This mud is further leached by agitation with more dilute acetic acid. The product is allowed to settle and the leach solution poured off. The product is similarly washed a number of times with pure water. The water is removed and the product is then washed with alcohol and then with ether. The last traces of ether are removed by vacuum drying.

The dry product is a free-flowing powder which can be formed into solid thorium metal bars by pressing and sintering. Cold pressing at about 10 tons per square inch followed by vacuum sintering at temperatures up to 1450°C for 30 minutes results in a thorium metal that is of almost theoretical density.

**2. Thorium chloride reductions.** Calcium, magnesium, or sodium can be used to produce thorium metal by the reduction of thorium tetrachloride. In most cases, the processes employing the tetrachloride yield the metal in a finely divided state and powder metallurgical processes are then employed to prepare shapes. One problem that is common to a number of these methods is that  $\text{ThO}_2$  or  $\text{ThOCl}_2$  in the tetrachloride may give high oxygen values in the final metal. These oxygen-containing compounds and carbon are reduced considerably by sublimation of the tetrachloride in a vacuum.

The oxide-containing compounds are of little concern if calcium is employed as the reducing agent. A process described by Lilliendahl<sup>9</sup> employs a charge made up of 30 parts of granular calcium with 70 parts  $\text{ThCl}_4$  and 30 parts  $\text{ThOCl}_2$ . The conditions for the reaction and subsequent processing are closely related to those described above for thorium by the reduction of  $\text{ThO}_2$  with calcium, and the process yields a high-purity product.

The magnesium reduction of the tetrachloride offers certain advantages over the use of calcium for large-scale operations since it requires less magnesium per pound of product and magnesium is obtainable usually in higher purity and at a lower cost per pound than calcium. However, experiments have shown that a high quality of thorium tetrachloride is required for good-quality final metal by the magnesium reduction. Properly sublimed thorium tetrachloride meets this requirement. Since magnesium and thorium form a low melting alloy it is possible to obtain thorium sponge instead of thorium powder with magnesium reduction of the tetrachloride.

Thorium metal of reportedly good quality has been prepared in batches of several pounds each by electrolysis of thorium tetrachloride in a fused salt bath. Since the electrode products are essentially thorium metal and chlorine gas, the process has possibilities of being operated on a somewhat continuous basis by adding make-up salts.

**3. Thorium fluoride reductions.** The successful preparation of thorium powder by the electrolysis of  $\text{ThF}_4 \cdot \text{KF}$  in a fused salt bath containing sodium and potassium chlorides has been described by Driggs and Lilliendahl.<sup>10</sup> This process was employed in production at Westinghouse Electric Corporation but has been replaced by a process similar to that described above for the calcium reduction of thorium dioxide.

According to Kaplan<sup>11</sup> the electrolysis of fused thorium fluoride mixture with potassium and sodium chlorides using a solid cathode is practiced on a large scale in the U.S.S.R. The electrolysis reduces the rare earth impurities and results in considerable purification of the product thorium. With a current density of about 20 amps/cm<sup>2</sup> a stable metal yield is obtained at a current efficiency of 70–80%. The effect of temperature was studied and it was determined that the optimum particle size for powder metallurgy at a 70–80% current efficiency was obtained at 800°C. Baths with thorium contents in excess of 11% operate for long periods of time.

The production of thorium metal by the calcium reduction of  $\text{ThF}_4$  has been operated on a tonnage scale by the U.S. Atomic Energy Commission. Metal referred to later as "Ames" metal was prepared by this process at Iowa State College, Ames, Iowa, U.S.A., where the process was developed and was operated for a number of years. The  $\text{ThF}_4$  was obtained by precipitation of thorium oxalate from a solution of purified thorium nitrate, followed by calci-

nation of the oxalate to oxide and then hydrofluorination of the oxide to ThF<sub>4</sub>.

In addition to the ThF<sub>4</sub> and the calcium metal, the charge for the Ames process for thorium contains anhydrous zinc chloride. The mixed charge which reacts spontaneously after ignition gives thorium metal, calcium fluoride, zinc metal and calcium chloride as the primary reaction products. The addition of the anhydrous zinc chloride to the charge serves three purposes in promoting the thorium separation from the slag: (1) the zinc alloys with the thorium to give a low melting metal phase; (2) the calcium chloride fluxes the calcium fluoride slag; (3) the heat of the auxiliary reaction between ZnCl<sub>2</sub> and calcium serves as a thermal booster and raises the temperature reached by the reaction mixture.

As a result of these three contributions by the addition of zinc chloride to the charge, the products of the reaction reach a temperature at which they are molten and the metal and slag phases readily separate and subsequently solidify in position on cooling. Because of the high vapor pressure of zinc metal at temperatures reached by the reaction it is necessary to carry out the reaction in a closed pressure vessel. This vessel is lined with a refractory material such as calcium oxide or dolomitic oxide. After the charge is introduced and covered a lid is placed on the vessel, or bomb, and the assembly then placed in a furnace until it fires.

After the products are cool the bomb is opened and the massive metal piece, referred to as a "biscuit," is cleaned of adhering slag. The biscuit is placed in a vacuum and heated to remove the zinc, leaving thorium metal sponge. A charge containing about 275 pounds of sponge and croppings is then vacuum-melted by induction in a beryllia crucible and bottom-poured into a graphite mold of the proper shape for the ingot.

**4. The iodide process for purifying thorium metal.** Veigel et al.<sup>12</sup> have described the preparation of massive thorium metal of high purity, in lots of several hundred grams each, by the van Arkel-deBoer (iodide) process.

The deposition vessel used in this work was made from Pyrex glass tubing and was about 10 cm in diameter and 75 cm in length. This tube, in an upright position, was closed at the bottom while the top was sealed only after the vessel had been charged. The seal cap for the top was made of Pyrex glass and contained a connection for the vacuum line, a side arm for about 10 grams of iodine and current lead-in wires from which the starting filament for the deposition was suspended.

The vessel accommodated a perforated molybdenum cylinder, the feed retainer, of such size as to leave an annular space sufficient to hold about 4 kilograms of thorium chips between the cylinder and the walls of the vessel. The starting filament was made of thorium wire 0.64 mm in diameter and about 115 cm in over-all length. The two ends of this filament wire were

attached to 6.35 mm diameter tungsten electrodes in the cap by means of molybdenum tie-wires. A quartz spacer ring was attached to the bottom end of the filament loop by means of tungsten wires. This ring served to hold the filament straight and keep it well spaced from the molybdenum feed retainer.

The filament assembly was inserted in the charged deposition vessel and the top cap sealed in place. The vessel was then vacuum outgassed at 510°C for a period of 24 hours. The iodine in the side arm was kept under refrigeration during the outgassing. The vacuum system was sealed off and the vessel and its contents cooled to 260°C. The iodine was then vaporized into the vessel to form the thorium tetraiodide.

It was found that deposition of thorium on the filament took place most readily when the externally measured temperature of the unit was in the range of 455 to 485°C. The deposition furnace was equipped with sectional heating elements and copper cooling coils to maintain the temperature in the desired range as the deposit built up and more and more heat was generated in the filament.

Since it was difficult to determine the temperature of the filament, correct operating conditions were arrived at by current and voltage control. The voltage applied to the filament from a sixty-cycle a-c power supply was increased in steps until onset of deposition was indicated by an increase in current while the voltage was held at a particular value. Deposition was then controlled by adjusting the voltage and current at intervals to satisfy the equation,

$$I^{1/4}E = K$$

within a range of values for  $K$ , where  $I$  is the current in amperes and  $E$  is the applied voltage. Deposition usually began when  $E$  and  $I$  were such that  $K = 0.43$  per cm of filament length and burnout of the filament rarely occurred if  $K$  were equal to or less than 0.63 per cm. In building up a deposit,  $E$  and  $I$  were initially adjusted for a value of  $K = 0.43$  per cm and then voltage maintained constant until a value of  $K = 0.63$  was reached. Subsequently the voltage was reduced and  $K$  maintained within the operating range. Runs were terminated when the current reached values of the order of 100 amperes which produced excessive heating of the vessel.

After completion of a run the electrode cap seal was cracked and the product removed from the deposition vessel. A representative deposit was about 0.62 cm in diameter for the entire length of the filament. Approximately 200 to 250 grams of "crystal bar" thorium metal was prepared per run. A sample of this iodide process metal contained 0.02% carbon and less than 0.01% each of oxygen and nitrogen.

### C. MELTING AND CASTING

The high temperature required for melting thorium and the reactivity of the metal toward crucible materials present problems in melting operations. Consequently, a variety of container materials have been investigated.

Among the oxides that have been tried, aluminum oxide, magnesium oxide and calcium oxide are attacked rapidly by molten thorium. Thorium oxide is relatively resistant but does cause contamination of the melt with oxide. Furthermore, it is undesirably susceptible to thermal shock. Stabilized zirconia has been used for laboratory melts, but the attack on it becomes increasingly severe as the crucible temperature exceeds the melting point of thorium; consequently an induction cylinder outside the crucible should not be used. Direct inductive heating of the charge is advisable. However, the power input must be controlled carefully so that excessive temperatures do not develop. Beryllia has been the most satisfactory oxide so far tested for melting thorium. It is resistant to thermal shock and has adequate strength at high temperature. In addition, it is resistant to attack by molten thorium at 1800°C and may be used up to 1950°C.

No other container materials have been found that serve satisfactorily as melting crucibles. Graphite may be used, but it contaminates the charge. For example, a melt held for 20 minutes at 1800°C picked up approximately 0.30 w/o carbon. Metallic tantalum can contain molten thorium at just above the melting point of thorium for a short time but the melt is contaminated even during the short exposure. For laboratory melting, the tungsten-arc, water-cooled copper-crucible furnace operating under helium or argon is satisfactory. With purified gas and careful handling of the arc, contamination may be held to a minimum.

### REFERENCES TO CHAPTER V

1. See also the following Geneva Papers:  
636—G. E. Kaplan, "Metallurgy of Thorium."  
531—B. Kopelman, "Fundamental Considerations in the Reduction Processes of Uranium and Thorium."
2. W. C. Lilliendahl, *Rare Metals Handbook*, Thorium, Chapter 23, edited by C. A. Hampel, Reinhold Publishing Corp., New York (1954).
3. A. E. Bearse, G. D. Calkins, J. W. Clegg, and R. B. Filbert, *Thorium and Rare Earths from Monazite*, Chem. Eng. Prog. 50, No. 5, 235 (1954).
4. M. Smutz, G. L. Bridger, K. G. Shaw, and M. E. Whatley, *The Ames Process for Separation of Monazite*, Chem. Eng. Prog. Symposium Series No. 11, Nuclear Engineering—Part II (1954).
5. F. H. Spedding, E. I. Fulmer, T. A. Butler, E. M. Gladrow, M. Gobush, P. E. Porter, J. E. Powell, and J. M. Wright, *The Separation of Rare Earths by Ion Exchange, III. Pilot Plant Scale Separations*, J. Am. Chem. Soc. 69:2812 (1947).

6. J. J. Berzelius, *Untersuchung eines neuen Minerals und einer darin enthaltenen zuvor unbekannten Erde*, Ann. Physik 16:385 (1929).
7. J. W. Marden and H. C. Rentschler, *Metallic Thorium*, Ind. Eng. Chem. 19:97 (1927).
8. H. C. Rentschler, W. C. Lilliendahl, and J. Gray, *Thorium*, U.S. Patent 2,446,062 (1948).
9. W. C. Lilliendahl, *Thorium*, U.S. Patent 2,537,067 (1951).
10. F. H. Driggs and W. C. Lilliendahl, *Preparation of Metal Powders by Electrolysis of Fused Salts*, Ind. Eng. Chem. 22:1302 (1930).
11. G. E. Kaplan, *Metallurgy of Thorium*, Geneva Paper No. 636.
12. N. D. Veigel, E. M. Sherwood, and I. E. Campbell, *The Preparation of High Purity Thorium by the Iodide Process*, AECD-3586 (1953), as described in Geneva Paper No. 556.

## *Chapter VI*

### THE METALLURGY OF THORIUM AND ITS ALLOYS \*<sup>1</sup>

Although the metal thorium has not been studied as intensively as uranium, a great deal of information has been obtained which has not been previously available in the open literature. These data will be summarized in this chapter.

Table I is a compilation of some of the thermal, physical and thermodynamic data on thorium metal. Since some of these properties are dependent on the history of the specimens the type of material has been listed whenever possible.

TABLE I. PROPERTIES OF THORIUM

<i>Lattice constants</i> <sup>2,18-23</sup>	500°C: 0.102 cal sec <sup>-1</sup> cm <sup>-1</sup> deg <sup>-1</sup>
F.C.C. $a_0$ (25°C): 5.086 ± 0.0005 Å	<i>Thermal expansion</i>
B.C.C. $a_0$ (1450°C): 4.11 ± 0.01 Å	0–200°C: $11.0 \times 10^{-6}$ per °C
<i>Transformation temperature</i> <sup>2,18-23</sup>	0–1000°C: $12.5 \times 10^{-6}$ per °C
F.C.C. to B.C.C.: 1400 ± 25°C	<i>Density</i> <sup>2</sup>
<i>Melting point</i> <sup>2,29-34</sup>	X-ray: 11.72 gram/cm <sup>3</sup>
1750°C	Bomb reduced (as cast): 11.5–11.6 gram/cm <sup>3</sup>
<i>Boiling point</i> <sup>35-37</sup>	Arc melted (iodide): 11.66 gram/cm <sup>3</sup>
3300–4500°K	<i>Elastic constants</i> <sup>2,24</sup>
<i>Heat of vaporization</i>	Young's modulus: $10.5 \times 10^6$ psi
130–177 Kcal/mol	Shear modulus: $4.0 \times 10^6$ psi
<i>Heat capacity</i>	Poisson's ratio: 0.27
27°C: 6.54 cal mol <sup>-1</sup> deg <sup>-1</sup>	Compressibility: 16.4 cm <sup>2</sup> /dyne
<i>Enthalpy</i>	<i>Work function</i>
27°C: 12.80 cal/mol	3.39 ev
<i>Heat of fusion</i>	<i>Electrical resistivity</i> <sup>25-28</sup>
4.6 Kcal/mol	Bomb reduced ~18 micro-ohm cm
<i>Thermal conductivity</i> <sup>2</sup>	Estimate pure ~13–14 micro-ohm cm
100°C: 0.09 cal sec <sup>-1</sup> cm <sup>-1</sup> deg <sup>-1</sup>	<i>Superconductance transition</i> <sup>38</sup> <i>temperature</i>
200°C: 0.093 cal sec <sup>-1</sup> cm <sup>-1</sup> deg <sup>-1</sup>	1.3–1.4°K

\* This chapter is based mainly on a portion of the following Geneva Paper: 556—O. N. Carlson, P. Chiotti, G. Murphy, D. Peterson, B. A. Rogers, J. F. Smith, M. Smutz, M. Voss, and H. A. Wilhelm, "The Metallurgy of Thorium and Its Alloys."

## A. PHYSICAL METALLURGY OF THORIUM

**1. Recrystallization.** The softening of severely cold worked, unalloyed thorium by short-time annealing treatments becomes evident at a temperature of 500°C or slightly lower, according to work by Eckert and Boyle.<sup>2</sup> At 600°C, softening is almost complete after 20 or 30 minutes. The relation between hardness and time at a series of temperatures is shown for iodide thorium in Fig. 1 and for Ames thorium in Fig. 2. Both kinds of thorium had been severely cold worked to about 80% reduction in area. The compositions of the metals used in these tests are specified in Table II.

TABLE II. CHEMICAL ANALYSES OF THORIUM

Material	Composition, ppm							
	C	O <sub>2</sub>	N <sub>2</sub>	Al	Si	Fe	Be	Other Elements
Ames thorium billet	370	120	150	90	90	140	30	Faint traces
Iodide thorium	200	110	10		Trace	Trace		Faint traces
Thorium-carbon alloy	1350	500	600		Trace	Trace		Faint traces
Thorium-carbon alloy	1010	400	70		Trace	Trace		Faint traces
Thorium-carbon alloy	850	200	40		Trace	Trace		Faint traces
Thorium-carbon alloy	490	100	10		Trace	Trace		Faint traces

As with most metals, the temperature at which softening of thorium sets in decreases as the degree of previous cold work increases. This effect is pronounced in iodide thorium, as may be seen from Fig. 3, but is less evident in Ames thorium for which the results are presented graphically in Fig. 4. In all cases, the specimens were at temperature for 1 hour.

Eckert and Boyle<sup>2</sup> also found that the addition of small amounts of carbon to iodide thorium has little effect on the temperature of recrystallization although the softening curves have a different shape (Fig. 5). A feature of these curves is the rise in hardness as the temperature of annealing increases beyond 650°C.

In the preparation of these thorium-carbon alloys, Eckert and Boyle added the carbon as a master thorium-carbon alloy to iodide thorium. The melting was conducted in a tungsten-electrode arc furnace under an inert gas. Ingots were cold reduced about 35% and homogenized 12 hours at 1275°C before being subjected to reduction and the subsequent annealing treatments of Fig. 5.

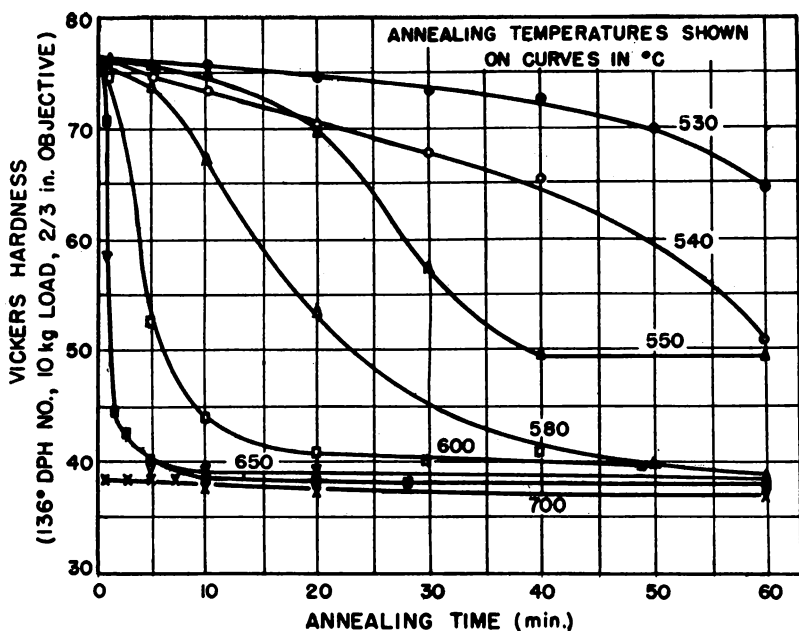


FIG. 1. Isothermal recrystallization curves for iodide thorium.

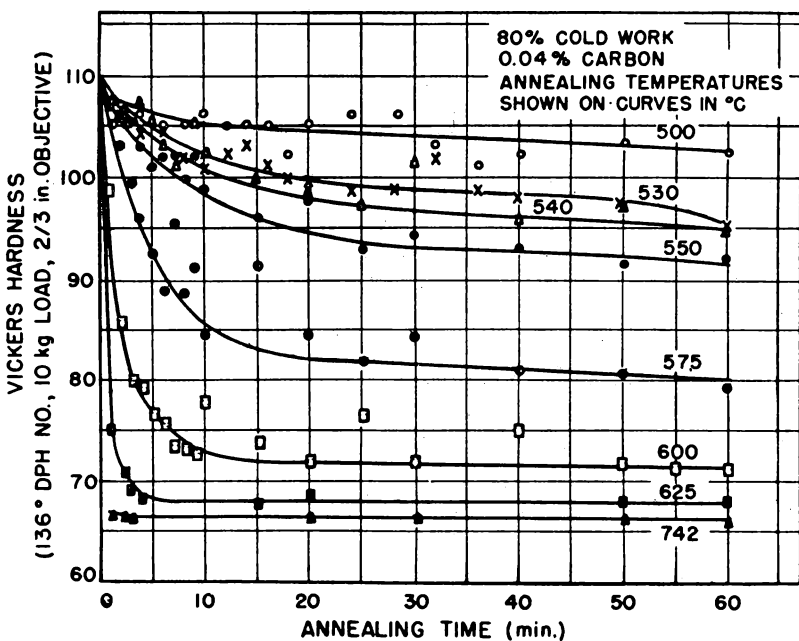


FIG. 2. Recrystallization curves for Ames thorium.

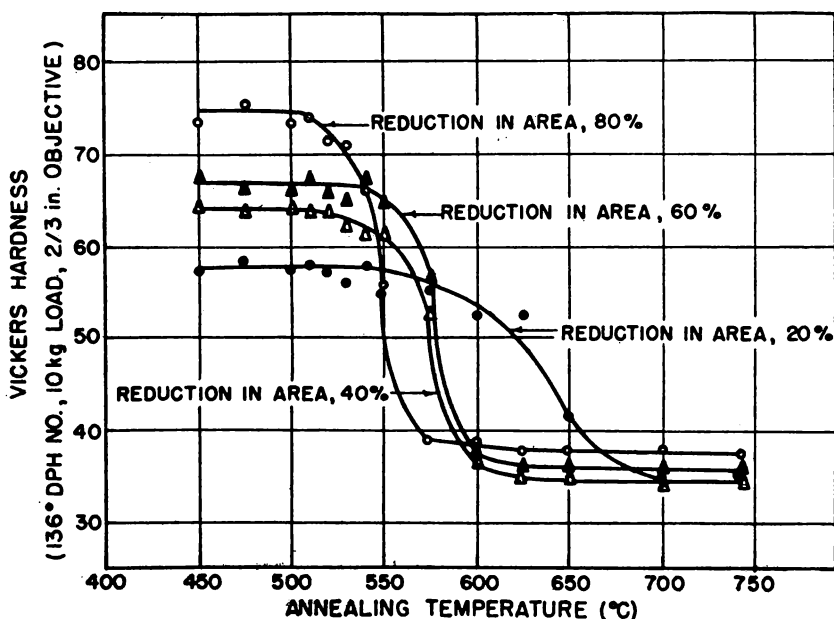


FIG. 3. Effect of cold work on recrystallization of iodide thorium. (Samples annealed one hour at each temperature indicated.)

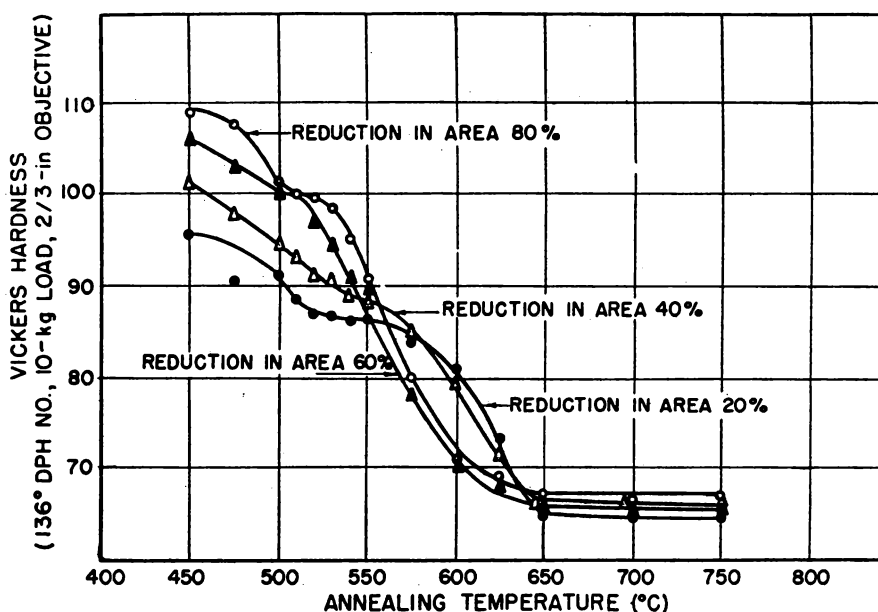


FIG. 4. Effect of cold work on recrystallization of Ames thorium. (Samples annealed one hour at each temperature indicated.)

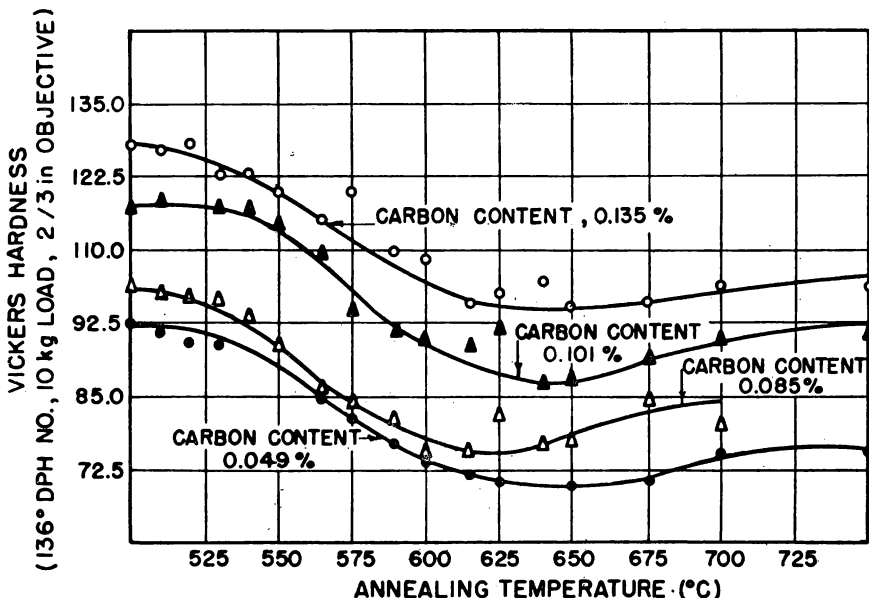


FIG. 5. Effect of carbon on recrystallization of iodide thorium. (Samples annealed one hour at each temperature indicated.)

As would be deduced from a study of the above figures, recrystallization begins to develop in the cold-worked material within the range 500 to 700°C. Eckert and Boyle observed that formation of new grains begins to take place in iodide thorium as soon as the hardness decreases, whereas no change in metallographic structure occurs in Ames thorium until the metal has decreased in hardness to about 100 on the Vickers hardness scale.

**2. The effect of alloying elements on hardness.** Hamby et al.<sup>2</sup> have studied the effects of larger percentages of carbon on homogenized and also on quenched specimens. Specimens homogenized 24 hours at 950°C showed a progressive rise in hardness from 22 to 66 on the Rockwell A scale as the carbon increased from 0.07% to 1.42%. At first, the rise was rapid but the increase in hardness per point of carbon added decreased gradually, and an increase from 1.42% to 2.40% carbon produced little effect on hardness of these specimens.

In general, additions of other elements to thorium have not given rise to important heat treatable alloys. Addition of low percentages of niobium, tantalum, titanium and a few other metals actually lower the hardness of Ames thorium, possibly because these elements form compounds with the carbon and remove it from its role as hardener in the thorium.

Oxygen has a less pronounced effect in hardening iodide thorium than car-

bon does; possibly the lessened effect is due to the relatively low solubility of oxygen in thorium and the form of the oxide inclusions. An increase in oxygen content from 0.006% to 2.0% produced an increase in hardness from RH 45 to RH 95 in specimens that had been homogenized at 950°C for 24 hours.

**3. Preferred orientation in cold worked and recrystallized material.** Orientation has been observed in cold rolled thorium and also in the extruded product. After being rolled,<sup>2</sup> sheet is predominantly of two textures which can be described in the usual manner as (100) [001] and (011) [211]. Recrystallization removes much of the orientation effect of rolling. However, the crystals are not in a completely random arrangement, but have a slight preference for (100) [110] positions and a tendency for (111) planes to lie in the plane of the sheet.

According to Hamby et al.<sup>2</sup> speed of extrusion affects the resulting texture of the metal. If the extrusion rate is low, the texture has [111] as a major direction and [100] as a minor direction. On the other hand, high speed extrusion results in recrystallization with a single [114] texture. Metal extruded at 1 ft/min is about twice as strong as the same material extruded at 600 ft/min.

## B. MECHANICAL PROPERTIES

**1. Tensile properties.** The tensile strength of Ames thorium has been obtained from tests on ASTM standard specimens at temperatures up to 700°C. The ultimate strength varies from about 22,000 psi to 40,000 psi at room temperature, depending on the method of forming and on the impurities present.

A set of typical stress-strain diagrams is given in Fig. 6. There is some indication that the material very nearly exhibits a yield point, and in fact definite yield points have been observed in some tests. The yield strength (0.002 offset) at room temperature is consistently 10,000 psi below the ultimate strength. The yield strength and the tensile strength at room temperature correlate well with the Rockwell Hardness as measured on the E scale.

At elevated temperatures the yield strength is decreased, dropping to the 2000 to 5000 psi range at 700°C, with the lower value corresponding to cast metal. Tests on cold rolled thorium and metal forged at 600°C indicate a yield strength of approximately 800 psi at 700°C. The modulus of elasticity drops from about  $10.5 \times 10^6$  psi at room temperature to about  $6 \times 10^6$  psi at 700°C. Typical data obtained from specimens machined from one cast billet are shown in Fig. 7.

Small amounts of impurities, particularly carbon, may have a marked effect in increasing the tensile strength and reducing the ductility of thorium. For example, the yield strength is approximately doubled when the carbon content is increased from 200 ppm to 800 ppm. Nitrogen and oxygen have

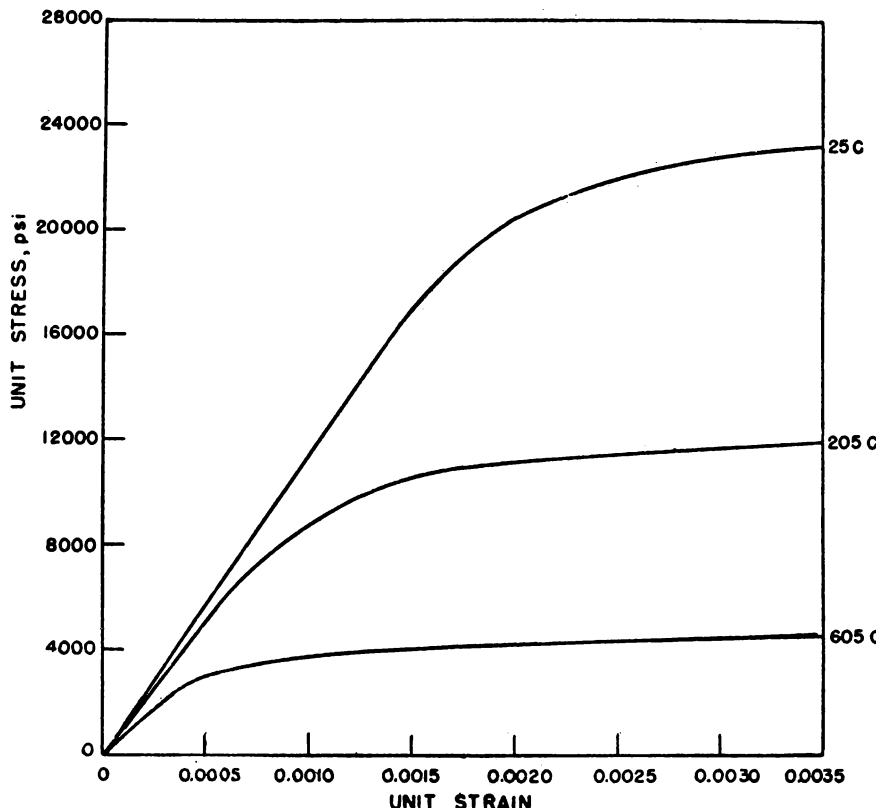


FIG. 6. Typical stress-strain diagrams for cast thorium in tension.

similar effects, but not to as great an extent. Indium is effective in raising the yield strength. The strength properties are sensitive to the rate of straining, with an increase in the strain rate resulting in higher apparent strengths. For example, increasing the strain rate from  $0.003 \text{ min}^{-1}$  to  $0.016 \text{ min}^{-1}$  increases the yield strength approximately 32%.

The compressive properties are about the same as the corresponding properties in tension.

**2. Impact.** An extensive series of impact tests on standard keyhole Charpy specimens showed a marked increase in the impact strength as the temperature was increased from 200 to 500°C. Typical data from specimens machined from two cast billets are shown in Fig. 8. In general the impact strength decreases as the carbon content of the metal increases. This is attributed to the embrittling influence of the carbon, as it has been found that increased impact strength is accompanied by an increase in the angle through which the impact specimen bends before fracturing.

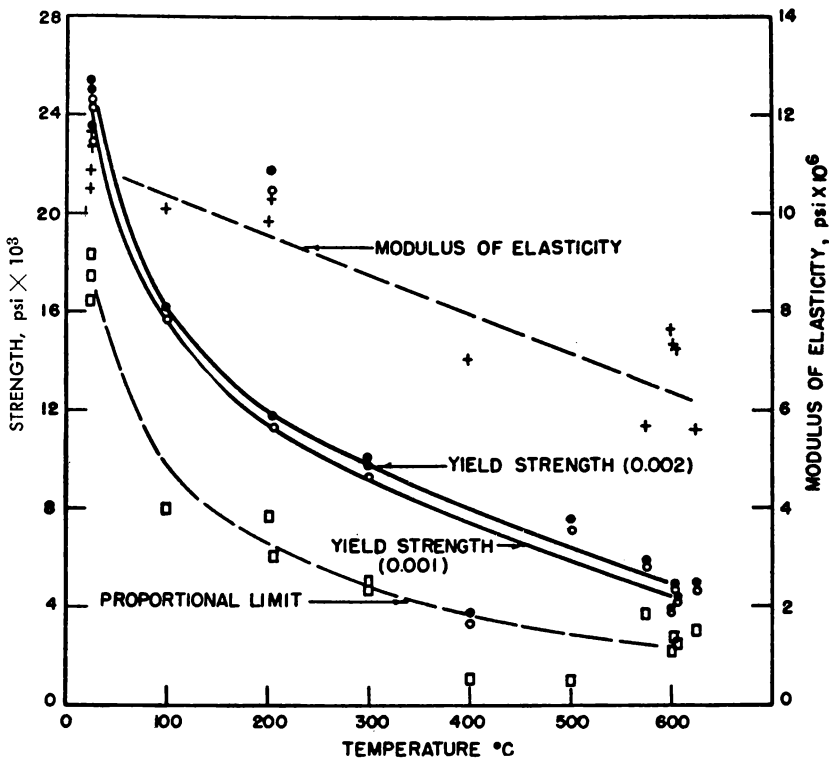


FIG. 7. Tensile properties of cast thorium.

**3. Fatigue.** The endurance limit of cast thorium at room temperature lies between 12,000 and 12,500 psi for rotating beam specimens. A value of approximately 15,000 psi is obtained for the endurance limit of cold rolled material. Specimens machined from stock material forged at 600°C indicated an endurance limit of approximately 13,000 psi at room temperature. A limited number of tests on hot rolled and annealed sheet specimens gave an endurance limit of 22,000 psi in repeated bending.

**4. Creep.** Relatively little work has been reported on the creep of thorium. However, it has been noted that specimens at room temperature loaded to a stress of 80% of the ultimate strength may exhibit a high rate of creep initially, but the creep rate decreases with time stabilizing at small values. At smaller stress levels the creep rate may become zero.

**5. Work hardening.** The strength of thorium is increased by cold rolling. A reduction in area of 25% increases the tensile strength by 30 to 40% and increases the yield strength by 100%. However, reduction in area above 25% has little additional effect on the strength.

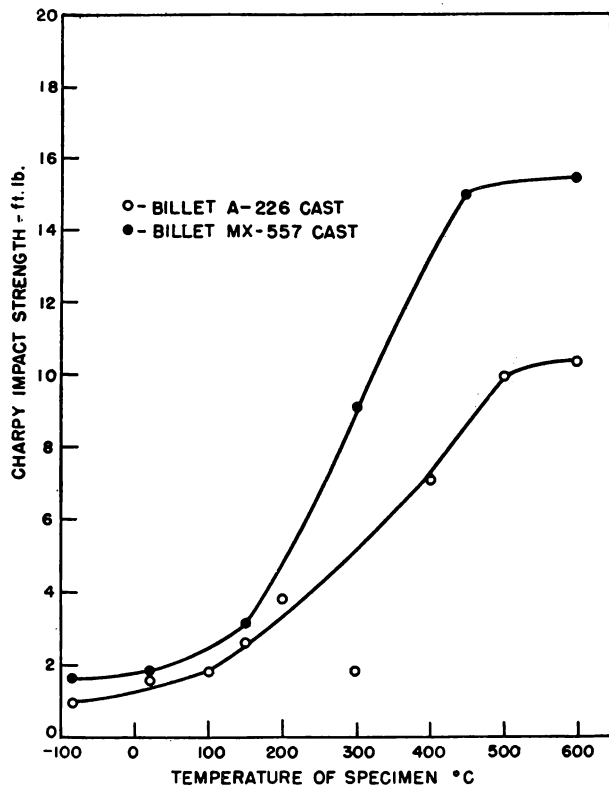


FIG. 8. Effect of temperature on Charpy impact strength of thorium.

### C. FORMING AND FABRICATION<sup>3</sup>

The mechanical working characteristics of bomb-reduced thorium are generally good. The metal is soft and ductile when hot and can be worked by most of the standard metalworking procedures with only a few special precautions. An inert atmosphere or protective jacket is necessary when the metal is heated for hot working. There is no brittle temperature range, although castings have a tendency to crack when cold worked. After the cast structure has been broken up, the metal can be fabricated at room temperature. The various metalworking processes are discussed in the following sections.

**1. Extrusion.** Thorium can be extruded at reasonable pressures at temperatures in the range 900 to 1830°F. The metal generally is jacketed with copper or iron to protect the surface and to lubricate the die, but it also can be extruded bare. Higher pressures are required to extrude unjacketed metal, and some die erosion occurs at the higher extrusion temperatures. Good surface

quality can be obtained in either case under proper conditions.

Thorium and copper react to form a pyrophoric compound at temperatures of 1650°F and above, and some reaction occurs at temperatures as low as 1470°F. This reaction can be prevented by plating the interior of the copper can with chromium or by applying a BeO wash to the thorium prior to canning.

**2. Forging.** Thorium forges readily at temperatures of 1380 to 1470°F. The metal is notch sensitive, and defects in the ends of billets tend to produce cracks during the forging operation.

**3. Rolling.** After the cast structure has been broken up, thorium can be rolled over a wide range of temperatures. Standard open-pass rolls, designed for rolling steel rods, produce satisfactory thorium rods.

Aluminum in the metal makes it hot short, but nitrogen in amounts up to approximately 1000 ppm does not affect the hot-working characteristics. A billet containing 3500 ppm of aluminum could not be rolled, but a heat containing 235 ppm of aluminum and 885 ppm of nitrogen rolled at 1560°F without difficulty. A hot-rolled  $\frac{3}{4}$ -in. diameter rod of this heat was subsequently cold rolled to 0.47-in. diameter in hand-rounding rolls without cracking.

The "as-cast" metal can be cold rolled but develops edge cracks after reductions of approximately 10%. Hot working greatly improves the cold-rolling properties of the metal. Reductions of 80 to 90% can be made on previously hot-rolled sheet without serious edge cracking, and one-mil foil can be rolled from 0.020-in. thick hot-rolled sheet without intermediate anneals. Hot-rolled bar stock can be rolled from 0.875-in. diameter to 0.427-in. diameter in hand-rounding rolls without evidence of cracking.

An indication of the hot- and cold-working characteristics of a large number of alloys has been obtained by forging and rolling small (approximately 38-gram) arc-melted buttons of various alloys. Binary alloys containing 1 and 5 a/o additions of most of the elements were made. Of these, the 5 a/o alloys of aluminum, silver, gold, bismuth, beryllium, cobalt, iron, gallium, germanium, nickel, oxygen, lead, platinum, palladium, antimony, tin, and thallium could not be hot worked at 1290°F. Alloys containing cobalt, palladium, platinum, and antimony could not be hot worked at the 2.5 a/o level. All of the alloys which could be hot rolled also could be cold rolled to 50% reduction.

Induction-melted alloys containing up to 6 w/o of titanium, zirconium, and niobium are ductile, and the castings can be cold rolled to 75% reduction without cracking. All of these elements reduce the as-cast hardness markedly.

The effects of oxygen and carbon on the general fabricating characteristics have not been specifically investigated. However, powder process metal which contains 0.15 to 0.17% oxygen is readily fabricated both hot and cold, and remelted bomb-reduced metal, containing 0.21% carbon, is forged and rolled without difficulty.

**4. Swaging.** The swaging of small-diameter rod and wire is feasible in dies designed for mild steel. Rod  $\frac{3}{8}$  in. in diameter has been swaged to 0.062-in. wire without intermediate anneals. Large-diameter rods,  $\frac{3}{4}$ - to 1-in. diameter, tend to seize in the swaging dies, and special lubrication is required in this size range.

**5. Wire drawing.** The tendency of the metal to seize to steel and Carboloy dies is particularly evident in wire drawing. None of the commercially available lubricants prevent seizure, and early attempts to draw wire were unsuccessful.

A lubricant consisting of 100 cm<sup>3</sup> of thinned (3:1) Duco lacquer (No. 246-2048), 30 grams of Molykote (molybdenum disulfide), and 10 grams of fumed lead and zinc oxides prevents seizure of the thorium, and wire down to 0.045 in. is drawn from a  $\frac{1}{4}$ -in. hot rolled rod without intermediate anneals. Pointing is accomplished by swaging, and reductions of one B-and-S gage number per pass are made. The wire is recoated with lubricant after every second pass.

Thorium wire down to 0.003 in. is made from arc-melted iodide metal by jacketing a  $\frac{1}{4}$ -in. rod in a copper tube and drawing the composite. This wire is pointed by swaging and, in the smaller sizes, by pickling in nitric acid. The copper acts as a lubricant and is stripped from the wire in nitric acid when the desired size is reached. Thorium wire 0.008 in. in diameter is also made from bomb-reduced metal by this technique.

**6. Machining.** The machining characteristics of thorium are comparable to those of mild steel. The metal can be turned with high-speed tools at lathe speeds of 150 to 175 ft/min. Coolants are desirable, but dry turning is practical.

The scale resulting from hot working is hard and dulls the cutting edge of tools much more rapidly than the clean metal. The surface of castings may be pyrophoric and must be machined slowly to avoid combustion of the chips.

Surface grinding produces a smooth, highly reflecting surface, which darkens on standing in air. The grinding wheels, however, tend to become loaded with metal. Shaping and milling operations are also practical.

#### D. POWDER METALLURGY

A number of the processes for producing thorium yield the metal in powder form. In other processes such as the bomb reduction of thorium fluoride the metal in an intermediate stage may be a sponge which can be cast into massive metal. Thorium in the form of sponge, massive metal, chips or lathe turnings can be converted to metal powder by the formation and decomposition of the hydride. In the following discussion, only the preparation of thorium metal powder by the hydride process will be treated in detail, but in addition, the

nature of the powders obtained by some reduction processes will be discussed here for comparison. Thorium powder and the hydride described below present potential explosion, fire and health hazards.

**1. Production of thorium powder by the hydride process.** The hydride process involves, as its first stage, the treatment of metallic thorium, in pieces of any convenient size, with hydrogen. During this stage, the charged pieces disintegrate into a coarse powder as the hydrogenation progresses to completion. Decomposition of the hydrided material in a reversed process yields metallic thorium of the same particle size as the hydride.

Studies of the reaction of thorium with hydrogen have shown that two compounds are formed—one with the formula  $\text{ThH}_2$  and one with the formula  $\text{Th}_4\text{H}_{15}$ . The dihydride has a body-centered tetragonal crystal structure with  $a_0 = 4.10 \text{ \AA}$  and  $c_0 = 5.03 \text{ \AA}$  and a density<sup>4</sup> of 9.20 grams/cm<sup>3</sup>. The higher hydride is cubic with four molecules ( $\text{Th}_4\text{H}_{15}$ ) per unit cell,  $a_0 = 9.11 \text{ \AA}$ , and space group  $I\bar{4}3d$ .<sup>5</sup> The density of the higher hydride is given by Nottorf<sup>6</sup> as 8.33 grams/cm<sup>3</sup>.

Chiotti and Rogers<sup>7</sup> and Wilhelm and Chiotti<sup>8</sup> have described in some detail a procedure for preparing thorium powder from massive metal by means of the reaction between the metal and hydrogen. This procedure can be broken down into the following steps:

- (1) Formation of the dihydride,  $\text{ThH}_2$ , at 600 to 650°C at one atmosphere hydrogen pressure. During this step the charge swells but does not break up to form a powder.
- (2) Formation of the higher hydride at temperatures not above 320°C. The optimum temperature for this step is about 250°C. The charge exfoliates and breaks up into a coarse powder during this operation.
- (3) Decomposition of the higher hydride to the lower hydride by heating to 500°C under a pressure of one atmosphere of hydrogen.
- (4) Decomposition of the lower hydride at 700°C at low pressure. At this temperature the dissociation pressure of  $\text{ThH}_{0.025}$  is approximately 1.0 mm Hg.

For small lots of powder the preparation can be carried out in a fused silica tube. However, if 10 pounds or more of powder are to be produced, a steel (preferably stainless) reaction chamber is more suitable. The remainder of the equipment consists of a mechanical vacuum pump, a diffusion pump, a suitable vacuum gage for measuring low pressure and a manometer for measuring pressures near one atmosphere. It is possible to check the reaction rate by temporarily closing off the hydrogen supply and observing the rate of pressure drop. A purification train for the hydrogen and a liquid nitrogen trap to prevent diffusion of oil vapors from the vacuum pumps to the charge should be included.

**2. Properties of thorium powder.** The plasticity of the particles obtained by the hydride process depends to a considerable degree upon the purity of the original metal and the residual hydrogen content. If the system is pumped to a pressure below 0.5 mm Hg at 700°C, the powder produced from Ames cast metal is soft and plastic.

Chuk-Ching Ma<sup>9</sup> has studied some of the factors influencing the particle size of metal powders produced by fused salt electrolysis. He points out that the primary variables which affect the number of nuclei formed and their subsequent growth are the temperature, current density and bath composition. The crystal size of the deposit is decreased as the current density is increased and also as the impurity content of the bath is increased. These characteristics are believed to be due to the formation of alkali metal films on the cathode surface and to polarization effects. Polarization is more pronounced at low temperatures. He determined the particle size distribution obtained on electrolysis of a salt bath consisting of 1 part KThF<sub>5</sub>, 0.5 part NaCl and 0.5 part KCl at 850°C and at 780°C. During each run the composition, temperature and current density (60 amperes per square decimeter) were held constant. It appears from Chuk-Ching Ma's curves that the thorium powder obtained at 850°C was practically all less than 250 microns, 91% less than 86 microns, and 71% less than 44 microns. At 780°C practically all the powder was less than 250 microns, 93% less than 86 microns, and 78% less than 44 microns.

The reduction of thorium oxide with calcium and reduction of the chloride with magnesium give powders that are usually less than 150 microns, but presumably can be made coarser or finer than this, depending on the final reaction temperature and other conditions.

The major impurities in the metal powder are usually oxygen, nitrogen, hydrogen, and carbon. Some recent work on the vacuum-fusion analysis of thorium powder for oxygen, nitrogen and hydrogen has been reported by Sloman et al.<sup>10</sup> Analyses of metal powder produced by the reduction of thorium halides with magnesium or calcium gave the following analyses: oxygen 0.2 to 1.3 w/o, nitrogen 0.1 to 0.2 w/o, and hydrogen 0.05 to 0.15 w/o. Similar powder, compacted and melted in thoria crucibles under high vacuum, analyzed: oxygen 0.07 to 0.08 w/o, nitrogen 0.02 to 0.03 w/o, hydrogen 0.0010 to 0.0015 w/o. The decrease in oxygen content is believed to be due to the separation of the oxide from the melt by virtue of its lower density and its low solubility at the freezing temperature. The reduction of the hydrogen content is not surprising in view of the dissociation pressures reported for thorium hydride<sup>6</sup> and the work of Wagener<sup>11</sup> on the reversible sorption of hydrogen by thorium. The decrease in nitrogen content might be due to separation of the nitride in a manner analogous to the separation of the oxide.

**3. Pressing and sintering.** Recently Meerson<sup>12</sup> has reported on the effect of compacting pressures for two different source powders. The results obtained

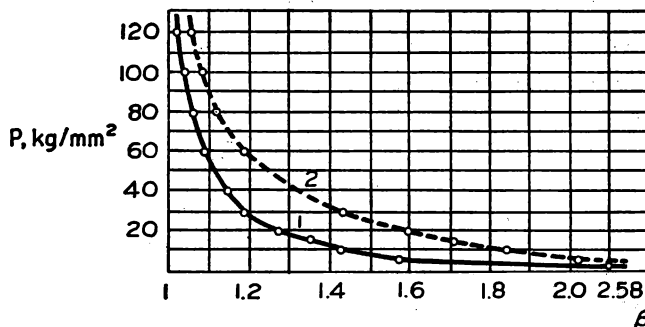


FIG. 9. Influence of compacting pressure ( $P$ ) on the change in relative volume of pressed compacts ( $\beta$ ) made of electrolytic (1) and calcium reduced (2) thorium powders.

are shown in Fig. 9. He arrives at the conclusion that the compressibility of calcium reduced thorium powders is lower than that of the electrolytically produced material. He further concludes that:

- (1) Thorium powder has a high plasticity and good pressibility.
- (2) The pressibility of thorium powder is affected by the production method (the calcium reduced powder is harder than the electrolytic one), as well as by the degree of purity.
- (3) The pressure required to get briquettes with a density of 10.5–11.0 grams/cm<sup>3</sup> and an  $h:d$  ratio ( $h$  = height,  $d$  = diam.) of  $\sim 0.5$  with one direction pressure or  $\sim 1.0$  with two direction, is 8–12 tons per cm<sup>2</sup> for the calcium reduced powder and 6–9 tons per cm<sup>2</sup> for the electrolytic one.
- (4) The high plasticity of thorium powder permits the use of high compacting pressures without causing slipping in the briquettes.

Meerson<sup>12</sup> has also studied the following variables on electrolytic and calcium compacts:

- (1) The effect of sintering temperature and sintering time on the mechanical properties and density.
- (2) The effect of post-sintering coining and annealing.

For electrolytic compacts (starting density 11 grams/cm<sup>3</sup>) the maximum tensile strength (13–15 kg/mm<sup>2</sup>) is attained at temperatures between 1100–1300°C. The effect of longer sintering time (0.5–4 hours) is to increase the tensile elongation 15.3–21.6% at 1100°C and 22.5–29% at 1300°C. There is little change in density.

For calcium reduced powders, because of the swelling of the dense compacts

on heating due to the evolution of residual calcium, the studies were made on green compacts of density 9 grams/cm<sup>3</sup>. Meerson concludes that:

- (1) Unlike the briquettes of the electrolytic powder of high initial density which hardly change on sintering, the porous briquettes of the calcium reduced powder are characterized by considerable shrinkage. Hence, the changes in the tensile properties of the calcium reduced metal with the sintering temperature depend to a great extent on the value of residual porosity.
- (2) The hardness, strength and plasticity of the metal are increased with the rise of the sintering temperature and an increase in density of sintered bodies. The tensile strength is increased from 10 kg/mm<sup>2</sup> at 900°C to 22.5 kg/mm<sup>2</sup> at 1400°C, and hardness from 43 kg/mm to 75 kg/mm, respectively. The plastic properties of the specimens are low at all sintering temperatures, the elongation after sintering at 1400°C does not exceed 5%.
- (3) Thus, despite some residual porosity in the sintered calcium reduced metal, its strength and hardness are higher than those of the electrolytic metal. At the same time the sintered calcium reduced metal is less ductile than the electrolytic one.

The effect of coining and annealing is to increase the density and tensile elongation of both types of sintered products permitting lower sintering temperatures.

#### E. CORROSION OF THORIUM AND THORIUM ALLOYS

**1. Corrosion of thorium in water.** If exposed to boiling distilled water, thorium becomes covered with an oxide scale and usually gains weight. Considerable variation in corrosion rates has been reported for such tests; rates of gain of 0.03 mg cm<sup>-2</sup> hr<sup>-1</sup> to rates of loss of 0.02 mg cm<sup>-2</sup> hr<sup>-1</sup> have appeared in the literature.

Corrosion in 100°C water as a function of time is shown by Draley's<sup>2</sup> results reproduced in Fig. 10 for metal prepared by different methods. The samples were cleaned by grinding before being tested and the resulting corrosion scale was removed chemically or electrochemically after completion of the test, but before weighing. Water quality was maintained by continuous replenishment. For this material, hot rolling was observed to have caused relatively little change in corrosion behavior. Thorium obtained from the reduction of the oxide (Westinghouse sintered) and also the metal produced by reduction of the fluoride (Ames metal) had an initial high rate after which the corrosion proceeded at a slower rate. The estimated rate for Westinghouse sintered metal is about 2½ times that for Ames metal. When Westinghouse metal was re-

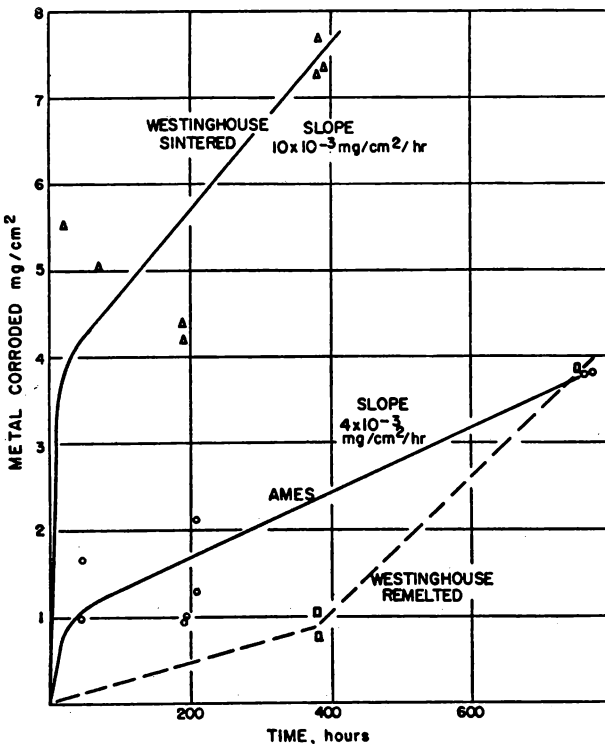


FIG. 10. Graph of corrosion vs time for thorium metal in boiling water.

melted, its rate of corrosion in boiling distilled water roughly approximated that of the Ames metal. Results obtained on samples tested in 178°C water showed that the corrosion rate was relatively low for a few days and then accelerated markedly, approaching a rate of  $0.7 \text{ mg cm}^{-2} \text{ hr}^{-1}$  after 15 to 20 days. In distilled water at 315°C attack was extremely rapid.

**2. Corrosion of thorium in gaseous media.** Levesque and Cubicciotti<sup>13</sup> have studied the reaction of thorium with oxygen in the range from 250 to 700°C. Above 450°C, the temperature of the sample rose considerably above the temperature of the furnace. Below 450°C, the oxidation proceeded almost isothermally. From 350 to 450°C the oxidation curves were linear with time and the energy of activation was calculated to be 22 Kcal/mol. From 250 to 350°C, the oxidation proceeded according to the parabolic law and the energy of activation for the reaction was calculated to be 31 Kcal/mol.

One-half hour scaling tests on thorium samples exposed in flowing air, nitrogen and argon at atmospheric pressure have been reported by Russell, Nelson and Grenell.<sup>2</sup> Their data, which are shown in Table III, indicate that air is the most corrosive of these gases at 800°C. The table does not take

TABLE III. THE CORROSION OF THORIUM IN VARIOUS FLOWING GASES AT 800°C

Atmosphere	Time, hr	Weight Gain, gram/cm <sup>2</sup>
Air	½	6.0
Tank N <sub>2</sub>	½	4.4
Purified N <sub>2</sub>	½	2.0
Tank A	½	1.0
Purified A	½	0.75

gas velocity into account, but the investigators stated that change in rate of flow had very little effect on the rate of corrosion.

Hydrogen reacts with and corrodes thorium extensively at relatively low temperatures. Brugmann and Draley<sup>2</sup> determined the corrosion rates for thorium in hydrogen at atmospheric pressures at temperatures from 400 to 505°C. On the assumption that the formula for the hydride was ThH<sub>4</sub>, they calculated that the loss of thorium at 400°C was 80 mg cm<sup>-2</sup> hr<sup>-1</sup> and that it was 129 mg cm<sup>-2</sup> hr<sup>-1</sup> at 505°C. Upon continued exposure to hydrogen, the specimens turned black, started to swell and eventually disintegrated into a coarse black powder. Although the formula for the hydride has since been determined to be Th<sub>4</sub>H<sub>15</sub>, Brugmann and Draley's data may still be considered to give approximate results.

**3. Corrosion of thorium in other media.** Limited tests have been made on the corrosion of thorium in several molten metals, in bromine-ethyl acetate and in hydrofluoric acid. The results obtained at several laboratories are summarized in Table IV. As indicated in the table, thorium is not significantly attacked by lithium at 600 or at 1000°C, although the specimens were decarburized to a depth of 2 mils during the test. The presence of an adherent protective film of nitride on the thorium is believed to be responsible for the lack of interaction with lithium at 600 and 1000°C.

At 600°C, thorium reacts with any oxygen present in sodium-potassium alloys to form heavy oxide layers which spall off during the test. However, in deoxidized Na-K, thorium takes on a thin oxide film but is otherwise unaffected.

The resistance to attack by hydrofluoric acid may be due to the formation of a protective fluoride film. The addition of thorium nitrate (0.3 M) or nitric acid (0.5 to 15.4 M) causes partial disintegration of pure thorium samples.

**4. Corrosion of thorium alloys.** The effect of alloying upon the corrosion resistance of thorium has been investigated. Most elements, when added to thorium, exert a deleterious effect or at best impart only slight improvement

TABLE IV. BEHAVIOR OF THORIUM IN SEVERAL MEDIA

Corroding Medium	Temp., °C	Time, hr	Results
Bismuth	1000	4	Thorium completely dissolved
Bromine-ethyl acetate	50-60	1	50% of 0.5 gram Th sample dissolved
Gallium	600	48	Reacts extensively
Lead	1000	40	Completely dissolved
Lead-2 w/o uranium	1000	4	Substantially attacked
Lithium	600	6	Not significantly attacked
	1000	40	No attack
Sodium	500	56	No significant attack
Na-K alloy	600	—	No alloying
65% HF acid	15	—	Slight weight gain, specimen covered with gray film

to the resistance of thorium to corrosion by high temperature water. Thorium-zirconium alloys, however, exhibit good corrosion resistance to 100°C water.

Alloys containing 1 to 10 w/o zirconium were prepared by arc melting and cold rolling into thin sheets and were then tested in boiling distilled water. Corrosion tests showed slight but not pronounced improvement with increasing zirconium content for alloys in this composition range.

Alloys containing more than 10 w/o zirconium, however, possess good corrosion resistance in boiling water, the resistance improving as the zirconium content is increased. The results of tests in 100°C and 200°C water on a series of alloys are summarized in Table V. All of the alloys listed in the

TABLE V. THE CORROSION OF THORIUM-ZIRCONIUM ALLOYS IN 100°C AND 200°C WATER

Zirconium, w/o	Temp., °C	Time, hr	Weight Gain, mg cm <sup>-2</sup> mo <sup>-1</sup>
10	100	662	0.07
20	100	662	0.07
25	100	662	0.08
30	100	662	0.04
40	200	100	260
50	200	100	170
60	200	100	100
70	200	100	45
80	200	100	6
90	200	100	0

table were prepared by arc-melting. They were hot rolled, vacuum annealed at 825°C for 20 hours and cooled slowly to room temperature prior to corrosion testing. Some tests performed at higher temperatures, 315°C and 345°C, indicate that the alloys become less satisfactory.

#### F. METALLOGRAPHY

The preparation of specimens of thorium for microscopic examination requires special care. As the metal is soft and ductile, its surface is easily deformed, or worked, during grinding operations. A number of procedures have been used with good results. Grinding can be done on grit papers, either dry or with kerosene or water lubricant on sizes down through 500 or 600 grit. The polishing should be done carefully to avoid leaving hard inclusions in relief. A coarse diamond paste, Linde A abrasive and silicon carbide have been used successfully. The final polishing can be done with Linde B abrasive, with fine diamond paste or with a number of other abrasive powders. A 10% oxalic acid solution has been used as the suspension medium in the final polishing step.

Electropolishing techniques have been developed for thorium, but they have not proven to be entirely satisfactory. Unfortunately, the electropolishing solution that probably is most nearly satisfactory for unalloyed thorium is one that contains perchloric acid and an organic compound and is therefore potentially explosive. This solution, which consists of 1 part perchloric acid and 10 parts glacial acetic acid, has been used by Roth,<sup>2</sup> Dickerson<sup>2</sup> and Pohl.<sup>2</sup> The bath should be maintained at a temperature of about 15°C. The electropolishing operation is conducted at 12 to 40 volts and usually lasts from 3 to 30 seconds. This electropolishing technique produces a clean surface and removes scratches left from mechanical polishing. However, it destroys the inclusions in the metal and produces serious pitting. Gray<sup>2</sup> has reported using a bath of 1 part perchloric acid and 15 parts ethyl alcohol. This bath is also cooled. It produces a polished sample in 15 to 45 seconds at 35 to 40 volts but leaves a thin film that can be removed if the sample is dipped in a fresh bath. The final result is a clean surface free from scratches, but again the inclusions are destroyed and the surface is pitted.

No completely satisfactory chemical or electrochemical etching reagent has been found for thorium. A solution of 3 N HNO<sub>3</sub> to which has been added 1% KF has been used for thorium alloys but does not give sharp outlines and has not worked out well for unalloyed thorium. Inclusions probably are more evident after mechanical polishing than after the surface has been etched. Grain boundaries of unalloyed thorium are partially revealed by electropolishing procedures. Carlson et al.<sup>2</sup> have reported good results on thorium by

cathodic etching but the method has not been investigated sufficiently to establish its utility.

The identification of inclusions in thorium metal has not received sufficient study. Thorium oxide is the most common inclusion in the usual grades of thorium. The form in which the oxide occurs depends on the method of preparing the sample. Thorium which has been melted in a crucible and poured into a mold usually contains rather large globular particles of oxide randomly distributed in the metal. The oxide in arc-melted thorium usually occurs as smaller particles, often in a dendritic array. Thorium oxide is quite easily identified under the microscope by its dark gray color in as-polished samples. Thorium nitride has not been well-characterized but has been reported to appear as golden yellow-colored inclusions.

#### G. THORIUM ALLOY SYSTEMS

The thorium constitutional diagrams have been compiled by Saller and Rough.<sup>14</sup>

Thorium metal transforms from a face-centered cubic to a body-centered cubic lattice on heating at about 1400°C. Its atomic diameter for the face-centered cubic form is 3.59 Å and 3.56 Å in the high temperature form. Only a few metals have atomic diameters which differ from that of thorium by less than 14–15% and which, therefore, might be expected to form extensive solid solutions with it. These include magnesium, zirconium, hafnium, cerium, lanthanum, lead, thallium, bismuth and antimony.

The electronegativity of thorium is 1.3 on Pauling's scale and this highly electropositive value suggests the likelihood of intermetallic compound formation with many of the more noble metals. Because of these considerations only a limited degree of mutual solid solubility of thorium with other elements can be expected. However, actual knowledge of these alloys depends largely upon experimental determinations. A few typical phase diagrams are shown in Figs. 11–13 because of their practical importance.

**1. Thorium-carbon.** The diagram shown in Fig. 11 is taken from work on this system reported in 1950.<sup>15</sup> More recent studies have shown, however, that a small amount of carbon raises the transformation temperature and lowers the melting point. The details of these reactions are not fully understood but a proposed diagram of the low carbon region based on these later data are shown in the inset of Fig. 11. The boundaries of the alpha-beta field are based upon electrical resistivity measurements and have been confirmed by high temperature x-ray studies. The solidus has been determined from melting point observations. From an extrapolation of these data, the melting point of carbon-free thorium appears to be about 1750°C and the transformation temperature approximately 1360°C.

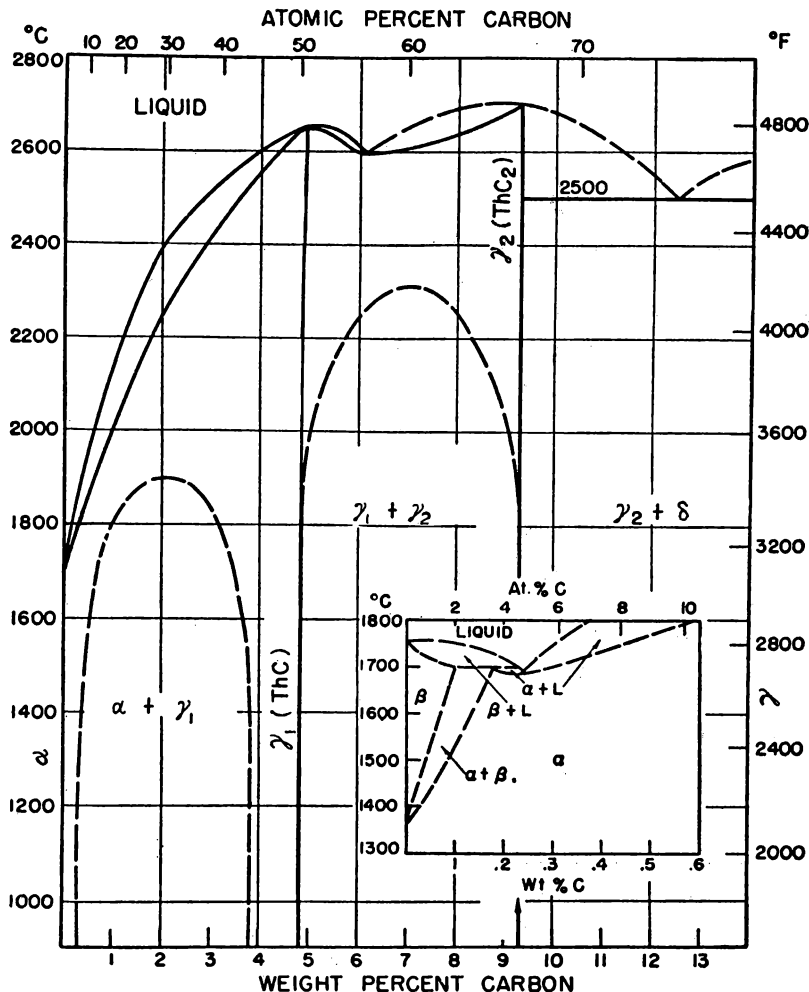


FIG. 11. Thorium-carbon system.

The monocarbide phase, ThC, has considerable solid solubility for thorium. It has the sodium chloride structure with the lattice constant varying from 5.29 Å at 3.9 w/o carbon to 5.34 Å at 4.92 w/o carbon. Rundle et al.<sup>16</sup> have determined the structure of the dicarbide, ThC<sub>2</sub>, by use of x-ray and neutron diffraction studies. They have shown the phase to be C-centered monoclinic with  $a = 6.53$ ,  $b = 4.24$ ,  $c = 6.56$  Å and  $\beta = 104^\circ$ .

**2. Thorium-uranium.** The phase diagram shown in Fig. 12 is based upon work of Carlson.<sup>2</sup> Recent precision x-ray data of thorium-rich alloys which have been annealed at 650°C and furnace-cooled showed very little change

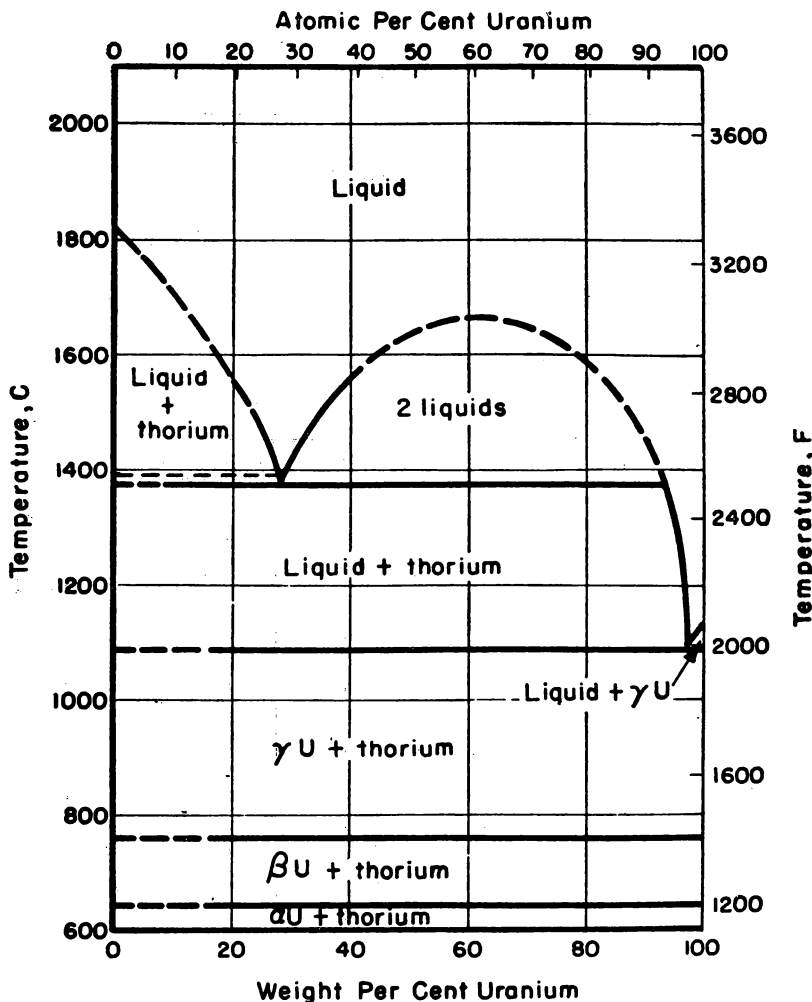


FIG. 12. Thorium-uranium system.

in the thorium lattice constant by the addition of uranium. This would indicate very little solid solubility at this temperature. Tentative data reported by Saller and Rough<sup>14</sup> indicate that the solid solubility at 800°C is approximately 5 w/o uranium while at 600°C it is less than 1 w/o uranium.

**3. Thorium-zinc.** Work done at the Ames Laboratory indicates that an intermetallic compound,  $\text{Th}_2\text{Zn}$ , is formed in this system at 12 w/o zinc. This compound decomposes at 1040°C to give thorium and zinc. The compound is body-centered tetragonal with  $a = 7.95 \text{ \AA}$  and  $c = 5.64 \text{ \AA}$ . The calculated density is 10.6 grams/cm<sup>3</sup> which is in good agreement with observed values.

The melting point of a 6 w/o zinc alloy under pressure is about 1200°C. Under vacuum, the zinc vaporizes readily at temperatures above 1040°C.

Nowotny<sup>17</sup> has investigated the zinc-rich end of this system from 0 to 47 w/o thorium. He noted the existence of two compounds. One was identified as ThZn<sub>9</sub> with a hexagonal structure. A compound that contained more thorium was not identified. No solubility of thorium in zinc was found.

**4. Thorium-zirconium.** The proposed diagram shown in Fig. 13 is based upon the early work of Carlson<sup>2</sup> plus later work at the Ames Laboratory and also work reported by Saller and Rough.<sup>14</sup> The limits of the narrow portion of the alpha plus beta region have been established from microstructures of quenched alloys and confirmed by high temperature x-ray data. The latest

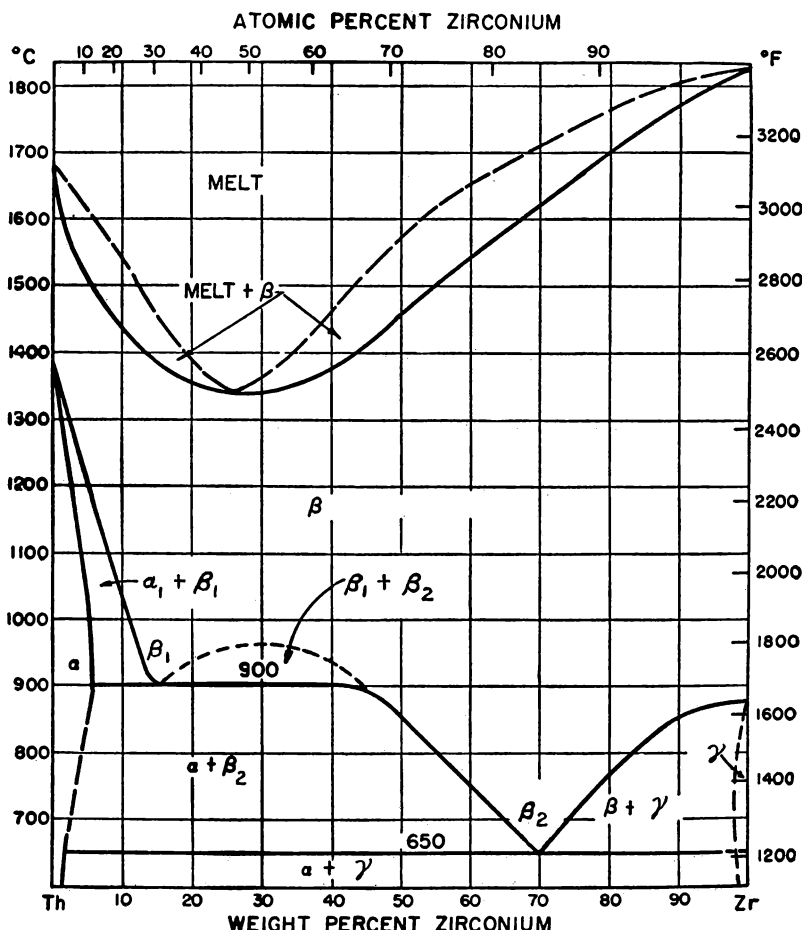


FIG. 13. Thorium-zirconium system.

estimates of the solid solubility limit of zirconium in alpha thorium at 600°C is 1.5 w/o zirconium. This value is based upon measurements of lattice constant versus composition. Because of the flattened portion of the solvus curve at 900°C a monotectoid reaction at 13 w/o zirconium has been proposed with a two-phase  $\beta_1$ , plus  $\beta_2$  region above 900°C. However, since no evidence for such a region has been found either from microscopic or high temperature x-ray studies, this portion of the system has been constructed as shown.

#### H. HAZARDS ENCOUNTERED IN HANDLING THORIUM<sup>3</sup>

Thorium has properties that make it a hazard to health in some metallurgical operations unless particular care is taken in handling it. Little damage has actually been done but the potential for such damage exists and should be taken into account, especially if the scale of operation is relatively large.

The radioactive hazard is present in some degree in all stages of the production of thorium or thorium-containing objects. Usually the first contact that the physical metallurgist has with thorium is in melting operations or preparation for melting operations. Thorium has an extensive chain of decay, or "daughter" products, some of which are relatively volatile and highly radioactive. During melting, which customarily is done in a vacuum furnace, some of these products escape from the charge and contaminate the vacuum line and the interior walls of the melting chamber. Care should be taken against breathing in the material from these deposits or otherwise getting them into the body during cleaning operations. Long external exposure to their radiation may also be hazardous.

Other opportunities for inhaling or ingesting thorium exist in the forging, rolling or extrusion of thorium at elevated temperature. During these operations, brittle scale may be detached and broken into fine particles. Machining and grinding also may be the cause of chips and particles of various sizes getting into the clothing or into places in which they will be readily taken into the body. One simple precaution is to wear leather faced gloves for more than brief manual contact with thorium. All walls and other surfaces in working areas should be kept clean. Even in storage rooms containing thorium products, the gaseous daughter thoron and its decay products may collect in sufficient quantity to be hazardous unless proper ventilation is provided.

The possibility of radiation effects from sources outside the body must also be taken into account. Thorium-bearing materials may have sufficient beta and gamma activity to constitute a hazard. Monitoring with radiation detecting devices should be performed faithfully to make certain that such radiation does not exceed acceptable limits.

A peculiarity of thorium is that its total radioactivity builds up fairly rapidly

to approximately equilibrium value after removal of some of the radioactive decay products by some procedure such as melting.

Like many other metals, thorium in the finely divided state is explosive. Hartmann, Nagy and Jacobson<sup>3</sup> have demonstrated the ease with which clouds of thorium dust (and thorium hydride dust) can be ignited. Freshly prepared thorium powder that has had its surface freed of adsorbed gases may ignite spontaneously when suddenly exposed to air.

#### REFERENCES FOR CHAPTER VI

1. See also the following Geneva Papers:  
635—G. A. Meyerson, "Powder Metallurgy of Thorium."  
636—G. E. Kaplan, "Metallurgy of Thorium."
2. As described in Geneva Paper No. 556.
3. This section is based on "The Reactor Handbook," Vol. 3, Section 1, AECD-3647 (1955).
4. R. E. Rundle, C. G. Shull, and E. O. Woolan, *The Crystal Structure of Thorium and Zirconium Dihydride by X-ray and Neutron Diffraction*, Acta Cryst. 5:22-26 (1952).
5. W. H. Zachariasen, *Crystal Chemical Studies of the 5f Series of Elements. The Crystal Structure of the Higher Hydride of Thorium*, Acta Cryst. 6:393-395 (1953).
6. R. W. Nottorf, *Some Problems in the Chemistry of Uranium and Thorium of Interest to the Development of Atomic Power*, Iowa State College, J. Sci. 26:255-257 (1952).
7. P. Chiotti and B. A. Rogers, *Production of Powdered Uranium and Thorium*, Metal Progress 60: No. 3, 60-65 (1951).
8. H. A. Wilhelm and P. Chiotti, *Powdered Thorium* (To U.S.A. as represented by the Atomic Energy Commission), U.S. Patent 2,635,956, April 21, 1953.
9. Chuk-Ching Ma, *Crystal Size Distribution in Electrolytic Metal Powders from Fused Electrolyte Baths*, Ind. Eng. Chem. 44:342-346 (1952).
10. H. A. Sloman, C. A. Harvey, and D. Kubaschewski, *Fundamental Reactions in the Vacuum-Fusion Method and Its Applications to the Determination of O<sub>2</sub>, N<sub>2</sub>, and H<sub>2</sub> in Mo, Th, Ti, U, V and Zr*, J. Inst. Metals 80:391-407 (1952).
11. S. Wagener, *Sorption of Gases at Very Low Pressures*, Proc. Physical Soc. 66B:400-413 (1953).
12. As described in Geneva Paper No. 635.
13. P. Levesque and D. Cubicciotti, *The Reactions between Oxygen and Thorium*, J. Am. Chem. Soc. 73:2028 (1951).
14. A compilation of United States and United Kingdom Uranium and Thorium Constitutional Diagrams, compiled for the USAEC by Battelle Memorial Institute, H. A. Saller, F. A. Rough, Editors (June 1955), BMI-1000.
15. H. A. Wilhelm and P. Chiotti, *Thorium-Carbon System*, Trans. Am. Soc. Met. 42:1295 (1950).
16. J. V. Florio, N. C. Baenziger, and R. E. Rundle, *Compounds of Thorium with Transition Metals. II. Systems with Iron, Cobalt and Nickel*, submitted to Acta Cryst. (1955).

17. H. Nowotny, *Die Kristallstrukturen von Zn<sub>9</sub>Th, Cd<sub>2</sub>Ca und (Ag,Mg)<sub>2</sub>Ca*, Z. Metallkunde 37:31–34 (1946).
18. H. Bohlin, *Anordnung für röntgenkristallographische Untersuchungen von Kristallpulver*, Ann. Physik 61:(4)421–439 (1920).
19. W. G. Burgers and J. A. M. van Liempt, *Zum Verhalten des Thoroxyds in Wolframglühdrähten*, Z. anorg. u. allgem. Chem. 193:144–160 (1930).
20. M. C. Neuburger, *Gitterkonstanten für das Jahr 1936*, Z. Krist. 93:1–36 (1936).
21. J. O. McCaldin and P. Duwez, *Allotropic Transformations at High Temperature*, J. Metals 6:619–620 (1954).
22. P. Chiotti, *High Temperature Crystal Structure of Thorium*, J. Electrochem. Soc. 101:547 (1954).
23. P. W. Bridgman, *Effects of High Shearing Stress Combined with High Hydrostatic Pressure*, Phys. Rev. 48:(2)825–847 (1935).
24. P. W. Bridgman, *The Compressibility and Pressure Coefficient of Resistance of Ten Elements*, Proc. Am. Acad. Arts, Sciences 62:207–226 (1927).
25. J. W. Marden and H. C. Rentschler, *Metallic Thorium*, Ind. Eng. Chem. 19:97 (1927).
26. W. Meissner and B. Voigt, *Messungen mit Hilfe von flüssigem Helium XI. Widerstand der reinen Metalle*, Ann. Physik 7:892 (1930).
27. D. Bender, *Über die elektrischen Eigenschaften des Thoriums*, Z. Metallkunde 40: 257 (1949).
28. J. H. de Boer, quoted by A. E. van Arkel in *Reine Metalle*, J. Springer, Berlin, 217 (1939).
29. H. A. Wilhelm and P. Chiotti, *Thorium-Carbon System*, Trans. Am. Soc. Met. 42: 1295 (1950).
30. M. Pirani and H. Alterthum, *Über eine Methode zur Schmelzpunkt bestimmung an Hochschmelzenden Metallen*, Z. Electrochem. 29:5–8 (1923).
31. W. von Bolton, *Über das Thorium*, Z. Electrochem. 14:768–770 (1908).
32. H. von Wartenberg, *Über Thorium*, Z. Electrochem. 15:866–872 (1909).
33. K. Honda, *Die thermomagnetischen Eigenschaften der Elemente*, Ann. Physik 32:(4)1027–1063 (1910).
34. J. G. Thompson, *Some Physical Properties of Commercial Thorium, Metals and Alloys* 4:114–118 (1933).
35. M. R. Andrews, *The Evaporation of Thorium from Tungsten*, Phys. Rev. 33:(2)454–458 (1929).
36. C. Zwikker, *Samenvatting van de huidige Gegevens over Dampdrukken bij hooge Temperaturen*, Physica 8:240–250 (1928).
37. L. Brewer, *Chemistry and Metallurgy of Miscellaneous Materials: Thermodynamics*, National Nuclear Energy Series IV-19B, McGraw-Hill Co., New York: Paper 3 (1950).
38. W. Meissner, *Supraleitfähigkeit von Thorium*, Naturwissenschaften 17:390–391 (1929).



## *Part II*

---

### RADIATION EFFECTS



## *Chapter VII*

---

### BASIC CONSIDERATIONS IN RADIATION EFFECTS \*<sup>1</sup>

---

#### A. QUALITATIVE DESCRIPTION OF RADIATION EFFECTS

The impetus for present-day interest in radiation effects is the result of an observation by E. P. Wigner during wartime research on nuclear reactor development. Wigner realized that the energetic neutrons, born in the fission process, would have the ability to displace atoms from equilibrium positions in the crystal lattices of solids that might be far removed from the fuel, and as a consequence would have deleterious effects on many properties of engineering interest in reactor construction. This observation plus the obvious realization that considerable damage to the fuel from fission fragments would result during fissioning prompted an immediate program of theoretical and experimental study of the magnitude of the effects to be expected. A brief account of some of these early studies has been given by Milton Burton<sup>2</sup> and E. P. Wigner.<sup>3</sup>

Radiation damage of a solid in a reactor may arise in three ways: First, through the interaction of the fission fragments with atoms of the parent fuel lattice. This type of damage is usually confined to the fuel bearing material because the range of the fission fragments is only of the order of microns even in the most transparent solids (in graphite, the range is less than 20 microns). The second way in which radiation damage is created is through the elastic collision of a neutron with atoms of a lattice. This type of damage may occur at relatively great distances from the source of the neutron since the probability of capture of a fast neutron is very low at high neutron energies. This means that parts of a reactor other than the fuel will be affected, and hence

\* This chapter is based mainly on the following Geneva papers:

749—F. Seitz and J. S. Koehler, "The Theory of Lattice Displacements Produced During Irradiation."

750—G. J. Dienes, "Theoretical Aspects of Radiation Damage in Metals."

744—D. S. Billington, "Radiation Damage in Reactor Materials."

the moderator, shield, or structural components of the reactor can be damaged. The third manner of introducing radiation damage is by ionization effects. These effects arise through ionization caused by fission fragments traversing the material or by ionization caused by the neutron "knocked-on" atoms or by beta- and gamma-rays. Ionization effects are only of consequence in solids of auxiliary value to a reactor.

The physical consequences of the above interactions are that several types of defects are introduced which affect the properties of a solid. These defects are: vacant lattice sites, interstitial atoms, thermal spikes, ionization effects, impurity atoms (fission fragments and impurities created by neutron capture), displacement spikes and replacement collisions.

**1. Vacancies.** Vacant lattice sites may be created either by collisions of fission fragments or energetic neutrons with the atoms in a solid lattice. The energy transferred in these collisions is usually sufficient to permit the recoiling atom to create further vacant lattice sites by subsequent collisions. Thus for each primary collision, a cascade of collisions resulting in vacancies is initiated.

**2. Interstitial atoms.** The atoms that are displaced from their equilibrium positions in the lattice in general will stop in an interstitial or nonequilibrium position, provided they do not immediately recombine with a near-by vacancy.

**3. Thermal spikes.** This concept in its modern form originated with F. Seitz,<sup>4</sup> who took into account the lattice oscillations that would be set up in the wake of either a fission fragment or a charged knocked-on atom of the lattice. Calculations by H. Brooks<sup>5</sup> and others<sup>6</sup> indicated that the possible duration of a high temperature region of approximately 1000°K involving some 5000 atoms might be  $10^{-10}$  to  $10^{-11}$  second.

**4. Impurity atoms.** The fission process, which introduces foreign fission products, and the capture of the neutron by a nucleus which results in a different atomic species are the means of introducing impurity atoms. The fission fragment effect is most pronounced, though both mechanisms are often insignificant compared to the other effects.

**5. Ionization effects.** The passage of charged particles through a lattice may cause extensive ionization and electronic excitation, which in turn leads to bond rupture, free radicals, etc., in many types of solids. These effects are most important in plastics, elastomers, ionic crystals, etc.

**6. Displacement spikes.** Brinkman<sup>7</sup> has recently extended these ideas by suggesting that displacement spikes are produced at the end of the range of a fast-moving atom. His calculations indicate that, when the energy of the fast-moving atom falls below a transition value (which depends on the atomic number) the mean free path between displacement collisions becomes of the order of the atomic spacing. Thus, each collision results in a displaced atom and the end of the trail is believed to be a region containing of the order of one to ten thousand atoms in which local melting and turbulent flow have

occurred during a very short interval. Brinkman suggests that vacancies and interstitials will anneal more or less completely in this region and that the damage is left in the form of dislocation loops and small misoriented regions. The calculations indicate that this mechanism, if it exists, is only important in heavy metals.

The thermal spike and displacement spike processes are evidently rather complex and it is difficult to carry out reliable calculations. They have been invoked to explain the unexpectedly efficient disordering of ordered alloys by irradiation. Seitz<sup>8</sup> has indicated recently that the simple picture of heating and quenching is inadequate to explain the disordering. He suggests that the irreversible plastic strain which originates in thermal stresses about displacement spikes is the source of the disorder.

**7. Replacement collisions.** Theoretical considerations of radiation damage mechanisms have led Kinchin and Pease<sup>9</sup> to the introduction of the concept of replacement collisions. If a collision between a moving interstitial atom and a stationary atom results in ejection of the stationary atom leaving the interstitial with insufficient kinetic energy for it to escape from the vacancy it has been responsible for creating, then this atom will fall into the vacancy dissipating its kinetic energy through lattice vibrations as heat. Kinchin and Pease show that for a reasonable choice of energy parameters the number of replacement collisions far exceeds the number of displacement collisions, and they obtain satisfactory agreement with the experimentally determined disordering rate of MnNi<sub>3</sub> found by Aronin.<sup>10</sup> The essential importance of this mechanism lies in the concept that by such a process of replacement collisions more displaced atoms are likely to fall into vacant lattice sites of the wrong kind than would be the case if all the atoms were displaced far from vacancies during bombardment and then migrated at random to vacant lattice sites.

In most cases, on raising the temperature of a specimen after irradiation, the physical properties revert to their initial values, i.e., the damage can be annealed out. Annealing also takes place during irradiation at all but the lowest temperatures. Annealing is evidently related to the mobility of the crystalline defects, but a clear understanding of the kinetics of annealing is not yet at hand. This phenomenon is of considerable practical importance since radiation damage may be minimized by appropriate heat treatment or by raising the temperature of exposure. There is some evidence that during irradiation the effects are not purely thermal, but that the radiation itself facilitates annealing. This latter phenomenon is termed radiation annealing.<sup>11</sup>

#### B. CALCULATION OF THE NUMBER OF DISPLACED ATOMS

E. P. Wigner<sup>2</sup> made the first quantitative estimates of the number of displaced atoms produced by high energy particles. The theory was developed

## RADIATION EFFECTS

in detail by Seitz,<sup>4</sup> based on earlier work by Bohr and his coworkers. Seitz calculated the fraction of energy lost in elastic collisions using the Born approximation. These are the collisions which are effective in displacing atoms. Recent advances in the theory are due to Snyder and Neufeld<sup>12</sup> and Harrison and Seitz<sup>13</sup> who have pointed out that the problem is better treated on the basis of classical scattering. A complete account of the present status of the theory is given in Geneva Paper No. 749 by Seitz and Koehler. A brief discussion is given here without going into the details of the mathematical treatment.

The basic equation for the number of displaced atoms is

$$N_d = \bar{v} n \varphi \quad (1)$$

where  $\bar{v}$  is the number of displaced atoms produced for each primary displacement,  $n$  is the number of primary displacements per incident particle and  $\varphi$  is the total number of incident particles. It will be assumed that  $\varphi$  is determinable from knowledge of the experimental arrangements, so that  $\bar{v}$  and  $n$  are the quantities of principal theoretical discussion.

$\bar{v}$  is calculated from the following equations:

$$\bar{v} = 0.885 + 0.561 \log \frac{x_m + 1}{4} \quad x_m \geq 3 \quad (2)$$

in which  $x_m$  is

$$x_m = \frac{4M_1 M_2}{(M_1 + M_2)^2} \frac{E}{E_d} \quad (3)$$

Here  $M_1$  and  $E$  are the mass and energy of the incident particle and  $M_2$  is the mass of the atoms of the lattice. We may note that  $\bar{v}$  varies slowly with  $x_m$  and is relatively insensitive to the quantities which enter into Eq. (3). In the case of copper bombarded by 12 Mev deuterons,  $x_m$  is  $5.64 \times 10^4$  if  $E_d$  is taken as 25 ev.  $E_d$  is the energy required to displace an atom permanently from a stable site in a well-bound solid. The corresponding value of  $\bar{v}$  for copper is 6.23.

For charged nucleon irradiation  $n$  in Eq. (1) is calculated as follows: The number of primary atoms displaced by an incident particle of charge  $Z_1$  and mass  $M_1$ , having the energy  $E$ , in traversing a distance  $dR$  through a solid is

$$dn = n_0 \sigma_d dR \quad (4)$$

Here  $n_0$  is the number of atoms per unit volume and  $\sigma_d$ , which is the cross section for displacement, is given in the form

$$\sigma_d = \frac{\eta}{E} \quad (5)$$

in the non-relativistic case where

$$\eta = 4\pi a_h^2 \frac{M_1}{M_2} \frac{Z_1^2 Z_2^2 R_h^2}{E_d} \quad (6)$$

Here  $Z_2$  and  $M_2$  are the charge and mass of the stationary atom,  $R_h$  is the Rydberg energy and  $a_h$  is the Bohr radius. Thus the total number of atoms displaced when the incident particle traverses a distance  $\Delta R$ , so that its total range drops from  $R_1$  to  $R_1 - \Delta R$  is

$$n = n_0 \eta \int_{R_1 - \Delta R}^{R_1} \frac{dR}{E} \quad (7)$$

For fast neutrons \* the collisions of the neutrons are of the simple hard sphere type and, therefore, the recoil energy spectrum of the struck atom is given by

$$N(E)dE = dE/E_{\max} \quad (0 \leq E \leq E_{\max})$$

where

$$E_{\max} = E^4 M_1 M_2 / (M_1 + M_2)^2$$

Only a very small fraction,  $E_d/E_{\max}$ , of the struck atoms are not displaced and, therefore, the cross section for producing a primary knock-on is the total neutron cross section. For the heavy elements  $E_{\max}$  does not usually exceed the ionization limit,  $L_c$ ;  $L_c$  represents the energy limit below which ionization losses may be neglected. In this case, the total number of displaced atoms per fast neutron collision is given by

$$N_d = E_{\max}/4E_d \quad (8)$$

For lighter elements  $E_{\max}$  generally exceeds  $L_c$ . In most cases the primary knock-ons effectively lose all the excess energy in ionization and in this case

$$N_d = (2 - L_c/E_{\max})L_c/4E_d \quad (9)$$

For details of estimating  $L_c$  the reader is referred to the Kinchin and Pease<sup>1</sup> review.

A few words should be said about the important energy parameter,  $E_d$ , which enters into the theory. This energy has been measured for germanium<sup>14</sup> (30 ev) and copper<sup>15</sup> (25 ev). Two attempts have been made recently to calculate  $E_d$  theoretically. Huntington<sup>16</sup> has considered low energy collisions in copper, a typical close packed metal. He has assumed that the principal interaction between the colliding atoms is the repulsion of closed shells which he approximated by a Born-Mayer type function

$$V(r) = A \exp \left[ -\frac{(r - r_0)}{r_0} \rho \right] \quad (10)$$

Since this force law is short range, a billiard ball model was used for the collision calculations. For copper the value of  $\rho$  can be bracketed between 13

\* We follow here the treatment outlined by Kinchin and Pease.<sup>1</sup>

and 17. For  $\rho = 13$  an energy of 18.5 ev is required to move an atom to an interstitial position in the (111) direction through the triangle formed by its three nearest neighbors. 17.5 ev is required for displacement creation in the (100) direction. In this case the original fast atom moves to another lattice site displacing its nearest neighbor into an interstitial position. For  $\rho = 17$  the corresponding energies were found to be 43 and 34 ev. The experimental value lies well inside these rather wide theoretical limits. Because of this rough agreement one is tempted to conclude, at least tentatively, that in a close-packed metallic lattice the displacement energy is determined primarily by the closed shell repulsive interactions.

Kohn<sup>17</sup> has carried out similar calculations for germanium and found that some of the nearest interstitial positions can be reached by atoms with substantially smaller energies (of the order of 10 ev) than the experimentally determined value of 30 ev. The main reason for the much lower theoretical value is the open structure of the germanium lattice in contrast to the close-packed face-centered cubic structure of copper. Kohn concludes that in germanium the most easily accessible interstitial positions are either unstable or, if stable, do not give rise to acceptor levels and hence would not have been observed in the threshold energy determination which was based on electrical resistivity measurements.

### C. COMPARISON OF THEORY AND EXPERIMENT

A test of the general theory of displacement production is difficult mainly because most physical properties depend in a complicated, and theoretically poorly understood, way on the number of vacancies and interstitials. In this section the results of two basic studies will be described briefly.

Cooper, Koehler and Marx<sup>11</sup> have irradiated 5 mil (0.13 mm) copper wires with 12 Mev deuterons near 10°K and measured the resistivity change as a function of flux. A calculation based upon the equations given in the previous section gave for the fraction of atoms displaced,  $f$ ,

$$f = 4.3 \times 10^{-3}$$

for a flux  $\varphi = 10^{17}$  particles per  $\text{cm}^2$  (using  $E_d = 25$  ev and  $\bar{v} = 6.2$ ). The increment of resistivity to be expected from this fraction of displaced atoms is

$$\Delta\rho = 0.43 \times 2.7 = 1.16 \text{ micro-ohm cm} \quad (11)$$

if one uses the theoretical calculations of Jongenburger<sup>18</sup> and Blatt<sup>19</sup> for the change in resistivity per 1% vacancies and interstitials.

The resistivity change  $\Delta\rho$  obtained after a designated amount of irradiation near 10°K is stable at the bombardment temperature. We shall assume that the initial slope of the  $\Delta\rho$  versus  $\varphi$  curve is to be used in comparing the results

of the experiment with the theoretical value, Eq. (11). When the initial slope is extrapolated to  $\varphi = 10^{17}$  per cm<sup>2</sup>, we find

$$\Delta\rho = 0.23 \text{ micro-ohm cm} \quad (12)$$

which is 5.0 times smaller than Eq. (11).

The discrepancy between observed and calculated values could originate in several factors. The most obvious would be an error in the theoretical estimate of the resistivity contributed by a vacancy and an interstitial atom. Evidently it would be necessary to reduce the resistivity for 1% of displaced atoms from 2.7 micro-ohm cm to a value nearer 0.5 micro-ohm cm. The calculation of the scattering cross section for conduction electrons by defects is a difficult one and the theoretical values may well be too high, although probably not by as much as a factor of 5.

Antal, Weiss and Dienes<sup>20</sup> employed the scattering of long wavelength neutrons for the determination of the number of interstitials and vacancies. Neutrons of sufficiently long wavelength are scattered isotropically by isolated point defects and the scattering can be measured when crystalline effects (Bragg scattering) are absent. Babinet's principle may be applied under such conditions and, therefore, vacancies and interstitials scatter in exactly the same manner. The cross section for this nuclear type of scattering is accurately known from other measurements. Thus, if the scattering from the defects is measurable an absolute method is at hand for determining their concentration.

In the absence of defects and past the last Bragg cut-off ( $\lambda > 2d_{\max}$ ), the transmitted intensity of long wavelength neutrons,  $I_s$ , is given by

$$I_s = I_0 \exp [-NX(\sigma_a + \sigma_i + \sigma_{\text{dis}})] \quad (13)$$

where  $I_0$  = incident intensity

$N$  = number of nuclei per cm<sup>3</sup>

$X$  = path length traversed through the sample

$\sigma_a$  = cross section for absorption

$\sigma_i$  = cross section for inelastic scattering

$\sigma_{\text{dis}}$  = cross section for disorder scattering other than defects (isotopic spin, etc.)

If  $m$  defects are present the transmitted intensity,  $I_d$ , is

$$I_d = I_0 \exp [-NX(\sigma_a + \sigma_i + \sigma_{\text{dis}} + \sigma_b f)] \quad (14)$$

A direct comparison of a crystal containing a fraction,  $f$ , of defects to a control crystal gives

$$\frac{I_d}{I_s} = e^{-NX\sigma_b f} \quad (15)$$

Measurement of the ratio  $I_d/I_s$  immediately gives then a value for  $f$ .

Graphite was chosen for study because of inherent interest in this material and because it fulfilled very well the theoretical and experimental requirements. Samples available were expected to contain of the order of a few per cent defects on the basis of Seitz's theory. This concentration should be easily measurable. For graphite

$$\sigma_b = 4.7 \text{ barns}$$

$$\sigma_a + \sigma_i = 0.9 \text{ barn at } 8 \text{ Å}$$

$$\sigma_{\text{spin}} = 0; \text{ zero spin}$$

$$\sigma_{\text{isotope}} = 0$$

$\sigma_{\text{isotope}}$  is negligibly small because of the combination of a low abundance (1.1%) of C<sup>13</sup> relative to C<sup>12</sup> and a similarity in cross sections, 4.5 barns and 5.5 barns. The graphite specimen served also as a neutron filter, which resulted in a most economical use of the very low intensity available in a long wavelength neutron beam.

In order to avoid spurious effects due to the increase in the *c*-axis of graphite upon pile irradiation a plot of transmitted intensity vs wavelength was obtained using a crystal spectrometer. Any irrelevant change in intensity could then be disregarded.

Several spectra were obtained from the spectrometer for the irradiated and standard (unirradiated) specimen run alternatively and averaged. The areas under each curve give

$$\frac{I_d}{I_s} = 0.607$$

The estimated accuracy of this figure is about  $\pm 10\%$ . By Eq. (15)  $f = 0.0526$ . The fraction of displaced atoms is  $f/2 = 0.0263$ .

The  $f$  value obtained by the above method may now be compared to the number of displaced atoms expected on the basis of Seitz's theory.<sup>4</sup>  $f$  was calculated from the equations

$$\frac{f}{2} = (nvt) \times \sigma_s \sqrt{\frac{\Delta E}{E_0}} \quad (16)$$

$$\Delta \bar{E} = \frac{2mM}{(M+m)^2} E$$

where  $m$  = mass of neutron

$M$  = mass of carbon atom

$\Delta \bar{E}$  = average energy loss per collision

$E_0$  = energy required to displace a carbon atom which will be taken as 25 ev

$E$  = average energy of fast neutron causing displacement, which will be taken as 1 Mev

$\sigma_s$  = collision cross section for carbon atom =  $2.5 \times 10^{-24}$  cm<sup>2</sup>

(nvt) = effective total integrated flux of fast neutrons causing displacement  
( $n$  is the flux of neutrons per cm<sup>2</sup> per second and  $t$  is the irradiation time)

The number to be used for (nvt) is the most uncertain quantity in these equations since the fast flux and its energy distribution are not known with any accuracy. The best estimate of the effective (nvt) for the graphite sample used in these experiments is  $1.1 \times 10^{20}$  neutrons/cm<sup>2</sup>.

$\Delta\bar{E}$  is 0.142 Mev and with  $1.1 \times 10^{20}$  neutrons/cm<sup>2</sup> for nvt Eq. (16) give for the number of displaced atoms

$$f/2 = 0.021$$

The uncertainty in this number due to inaccuracy in (nvt) is of the order of 50%. There may be a further error because of possible annealing of the specimen, although its temperature during irradiation probably has not been above 50°C. The use of Eq. (16) overestimates  $f$  since the pile spectrum has been replaced by neutrons of average energy of 1 Mev. On the other hand, recent refinements in the theory<sup>12,13</sup> discussed earlier indicate that the number calculated by Eq. (16) should be raised by about a factor of two. These two effects will largely cancel each other. Because of the uncertainty in (nvt) a more detailed calculation was not carried out.

The experimentally determined value of  $f$  is known, therefore, with greater accuracy than any theoretically derived value, largely because of uncertainties in the value of (nvt). Consequently, the theory itself cannot be judged too critically. The fraction of displaced atoms determined experimentally by this method is in excellent agreement with the theory within the limitations mentioned above.

Essentially the same conclusion is reached by Hennig and Hove<sup>21</sup> from a careful analysis of the changes in the electronic properties of graphite after irradiation. They derive the concentration of electron traps rather than directly the number of displaced atoms and find agreement with theory within a factor of two.

In summary one is perhaps justified in concluding, on the basis of this limited experience, that theory and experiment for the number of displaced atoms produced by irradiation are in essential agreement. A factor of two to three is not a serious discrepancy for such an intricate process.

## REFERENCES FOR CHAPTER VII

1. For reviews of the topic of radiation damage see:  
 J. C. Slater, *The Effects of Radiation on Materials*, J. Appl. Phys. 22:237-256 (1951).  
 G. J. Dienes, *Radiation Effects in Solids*, Annual Reviews of Nuclear Science, II, 187-220 (1953).  
 G. J. Dienes, *Effects of Nuclear Radiations on the Mechanical Properties of Solids*, J. Appl. Phys. 24:666-674 (1953).  
 F. Seitz, *Radiation Effects in Solids*, Physics Today 5:6, 6-9 (1952).  
 S. Siegel, *Radiation Damage as a Metallurgical Research Technique*, Chapter in *Modern Research Techniques in Physical Metallurgy*, American Society for Metals (1953), pp. 312-324.  
 J. W. Glen, *A Survey of Radiation Effects in Metals*, U.K. unclassified report AERE M/TN 27 (1954) (Harwell, England); Phil. Mag. Suppl. 4:381 (1955).  
 G. R. Sutton and D. O. Leeser, *How Radiation Affects Structural Materials*, Iron Age 174:97 (1954).  
 G. H. Kinchin and R. S. Pease, *The Displacement of Atoms in Solids by Radiation*, Rep. Prog. Phys. 18:1 (1955).
2. Milton Burton, *Radiation Chemistry*, Phys. Colloid Chem. 51:611 (1947).
3. E. P. Wigner, *Theoretical Physics in the Metallurgical Laboratory of Chicago*, J. Appl. Phys. 17:857 (1946).
4. Frederick Seitz, *On the Disordering of Solids by Action of Fast Massive Particles*, Discussions of the Faraday Soc. 5:271 (1949).
5. H. Brooks, Unpublished work.
6. H. M. James, Unpublished work.
7. J. A. Brinkman, *On the Nature of Radiation Damage in Metals*, J. Appl. Phys. 25:961-970 (1954).
8. F. Seitz, *Source of Disordering of Alloys during Irradiation*, Bull. Am. Phys. Soc. 30, No. 2, 17 (1955) (A).
9. G. H. Kinchin and R. S. Pease, *The Mechanism of the Irradiation Disordering of Alloys*, J. Nuc. Energy 1:200-202 (1955).
10. L. R. Aronin, *Radiation Damage Effects on Order-Disorder in Nickel-Manganese Alloys*, J. Appl. Phys. 25:344-349 (1954).
11. See for example: H. G. Cooper, J. S. Koehler, and J. W. Marx, *Irradiation Effects in Cu, Ag and Au near 10°K*, Phys. Rev. 97:599 (1955).
12. W. S. Snyder and J. Neufeld, *Disordering of Solids by Neutron Radiation*, Phys. Rev. 97:1636-1646 (1955).
13. W. A. Harrison and F. Seitz, *On the Theory of Radiation Damage*, Bull. Am. Phys. Soc. 30, No. 2, 7 (1955) (A).
14. K. Lark-Horovitz, *Nucleon Bombarded Semiconductors*, Reading Conference on *Semiconducting Materials*, Butterworth's Scientific Publications, London, England, 1951, pp. 47-78.
15. D. T. Eggen and M. J. Laubenstein, *Displacement Energy of Radiation Damage in Copper*, Phys. Rev. 91:238 (1953) (A).
16. H. B. Huntington, *Creation of Displacements in Radiation Damage*, Phys. Rev. 93:1414 (1954).
17. W. Kohn, *Bombardment Damage of Ge Crystals by Fast Electrons*, Phys. Rev. 94:1409 (1954) (A).

18. P. Jongenburger, *The Extra Resistivity due to Vacancies in Copper, Silver and Gold*, Appl. Sci. Res. B3:237-248 (1953).
19. F. J. Blatt, *Effect of Point Imperfections on the Electrical Properties of Copper I. Conductivity*, Phys. Rev. 99:1708 (1955).
20. J. J. Antal, R. J. Weiss, and G. J. Dienes, *Long Wavelength Neutron Transmission as an Absolute Method for Determining the Concentration of Lattice Defects in Crystals*, Phys. Rev. 99:1081 (1955); see also Geneva Paper No. 750.
21. G. R. Hennig and J. E. Hove, Geneva Paper No. 751, *Interpretation of Radiation Damage to Graphite*.

## *Chapter VIII*

---

### THE EFFECT OF RADIATION ON STRUCTURAL MATERIALS \*<sup>1</sup>

---

In this chapter the behavior of various types of solids under reactor irradiation is discussed. The important changes in physical properties are described as a function of irradiation and temperature. The special problems arising in the case of fissionable materials and application to actual fuel elements will be covered in Chapter IX.

#### A. METALS

**1. General.** Before discussing some of the experiments on reactor materials it is appropriate to review briefly some of the experiments of a more general nature that have been done in order to provide some insight into the interpretation of data on more complex materials. In order to avoid any uncertainty in interpretation, only that work which has been done using neutron bombardment will be considered here. In addition to such work, however, bombardment experiments using cyclotron particles have, in a number of cases, also yielded interesting and similar results.

First it has been shown by a number of investigators <sup>2-5</sup> that most metals and alloys become harder and stronger as a result of bombardment, particularly if the temperature of bombardment is sufficiently low.

The most striking effect on mechanical properties is the increase in critical

\* This material is based mainly on the following Geneva Papers:

- 744—D. S. Billington, "Radiation Damage in Reactor Materials."
- 747—F. E. Faris, "The Effect of Irradiation on Structural Materials."
- 680—S. T. Konobeevsky, N. F. Pravdyuk and V. I. Kutaitev, "The Effect of Irradiation on the Structure and Properties of Structural Materials."
- 444—J. H. O. Varley, "Radiation Damage in Non-Fissile Materials."
- 753—J. H. Crawford, Jr. and M. C. Wittels, "A Review of Investigations of Radiation Effects in Covalent and Ionic Crystals."
- 746—W. K. Woods, L. P. Bupp and J. F. Fletcher, "Irradiation Damage to Artificial Graphite."

shear stress of copper single crystals observed by Blewitt and Coltman.<sup>3</sup> The critical shear stress was observed to rise from an unirradiated value of 0.2 kg/mm<sup>2</sup> to 7.5 kg/mm<sup>2</sup>. However, it was also seen that once the sample began to flow plastically its behavior began to resemble that of an alloy rather than a cold worked material, suggesting that alloying with interstitial atoms was taking place, even though the values of the critical shear stress obtained far exceeded those obtainable by alloying. Making a number of assumptions concerning the stability of the defects involved, Blewitt estimated that one interstitial atom was forty times as effective as a zinc atom in raising the critical shear stress. A. N. Holden and F. Kunz<sup>4</sup> performed similar studies on iron and zinc single crystals and were able to obtain similar increases in the critical shear stress. McReynolds<sup>5</sup> studied copper and aluminum after bombardment at 80°K and found that the effects in aluminum annealed out before reaching room temperature while temperatures of 300°C were required to anneal out the increase in the flow stress of copper in agreement with Blewitt and Coltman's observations.

Makin<sup>11</sup> has shown that there is a marked temperature dependence of critical shear stress at temperatures well below those at which any annealing of radiation damage occurs; this effect is reversible. In keeping with other studies on the effects of radiation damage on physical and mechanical properties it is found that the effects are not completely removed in a given material until annealing is carried out in that temperature range where the rate of creation and movement of vacancies is rapid. Thus in copper the activation energy associated with such a process is about 2.1 ev corresponding to annealing in a temperature range around 300°C. This again suggests that the final defects to be removed may be cluster defects, either of vacancies or interstitials, inasmuch as vacancies will be created at the surfaces of vacancy clusters and diffuse into the crystal so dispersing the clusters, or alternatively vacancies will be produced at dislocations in the crystal and diffuse to interstitial aggregates so annihilating them.

Besides the plastic behavior, the effect of neutron bombardment on a number of other properties of copper has been studied. The elastic constants of copper have been measured by D. O. Thompson<sup>17</sup> who found rapid increases in the apparent elastic constants and a sharp reduction in internal damping. This has been attributed by Eshelby<sup>17</sup> to the pinning down of dislocation loops. These measurements would appear to indicate that dislocations are not introduced as a result of neutron bombardment. Slight increases in the electrical resistivity of irradiated copper have been observed at room temperature with substantial increases at low temperature.<sup>3,5</sup> The large resistance increase found in copper at 80°K by McReynolds confirmed earlier observations by Blewitt and Coltman, who have since performed irradiations at approximately 20°K. They report even larger increases by a factor of 2-4 in copper. Only very slight

density decreases are reported. There seems to be no broadening of x-ray diffraction lines and no observable dimensional changes. The thermal conductivity is relatively unaffected at room temperature.

Studies of a variety of metals indicate strongly that there is a relationship between activation energy for self-diffusion and the temperature stability or radiation effects in pure metals, radiation effects being greater the lower the rates of self-diffusion at a given temperature. The above experiments tend to show that interstitial atoms play an important role in radiation effects. Furthermore, the creation of dislocations seems unlikely, and the temperature stability of radiation effects is a function of the diffusional characteristics of the solid.

Another series of observations has been made by several investigators which shows the influence of the excess vacancies introduced by bombardment. The ability of reactor radiation to order rapidly a sample of disordered Cu<sub>3</sub>Au<sup>6</sup> at temperatures where in the absence of radiation the rate is negligible is attributed to enhanced diffusion on a micro-scale resulting from excess vacancies.

Neutron bombardment has been shown to accelerate precipitation<sup>7</sup> in unstable supersaturated solid solutions. The effect of the irradiation is roughly equivalent to raising the temperature 50–150°C. Neutron bombardments performed at liquid nitrogen temperatures show that the radiation effect in copper beryllium is influenced by a thermally activated process.<sup>8</sup> The rate of disordering of Cu<sub>3</sub>Au was substantially altered for the same reasons.

Taylor and Murray<sup>7</sup> have shown that nucleation of a new phase can be initiated by neutron bombardment. A phase transformation in black phosphorus has been observed by B. E. Warren et al.<sup>9</sup> Fleeman and Dienes<sup>10</sup> have investigated the effect of low-temperature (liquid nitrogen) reactor irradiation on the white-to-grey tin transformation. It was found that, compared to an unirradiated pure sample, the transformation, measured by dilatometry, is drastically accelerated by prior irradiation. The irradiation apparently eliminates the normally very long induction period. The kinetic behavior of reactor irradiated samples and of samples seeded with grey tin were found to be qualitatively similar. These results indicate that the defects introduced into white tin by reactor irradiation serve as nuclei, or at least embryos of nucleation, for the subsequent phase transformation.

**2. Structural metals.** The moderator in a reactor often serves as the main structural component, but in cases where this is not possible one is required to make use of certain of the conventional structural metals to make up this deficit. Consequently, these metals may be in high fast-neutron flux regions. The thermal neutron absorption cross section of metals such as the carbon steels, while not ideal, may still be sufficiently low to warrant consideration in reactor design.

An increasing amount of attention is being paid to these materials in regard

to their resistance to radiation damage, particularly in regard to strength and ductility characteristics. Most of the conventional alloys become harder and stronger. Recently Sutton and Leeser<sup>12</sup> described radiation effects in a wide variety of alloys. One important observation on carbon steels revealed that the impact strength was reduced appreciably. In addition, the temperature of transition from brittle to ductile fracture was raised 50–100°C after a bombardment of approximately  $10^{19}$  neutrons/cm<sup>2</sup>. Bombardments at 300°C for the same exposure gave only a 25°C increase in transition temperature. These observations become of importance when it is realized that the carbon steels they examined were pressure vessel type. These carbon steels as well as stainless steels, nickel and cobalt base alloys showed higher yield strengths and a reduction in ductility. Electrical resistivity and density changes were slight for all alloys examined. Several of the stainless steels showed an increase in magnetic susceptibility. A careful study by M. B. Reynolds, J. R. Low and L. O. Sullivan<sup>13</sup> indicates that the amount of ferrite precipitated is probably insufficient to cause concern in regard to the stainless character of these alloys. However, additional attention to this effect is warranted in view of its possible importance.

A typical stress-strain curve for nickel, taken from the work of Bruch, McHugh and Hockenbury,<sup>14</sup> is shown in Fig. 1 to illustrate the significant changes often observed upon irradiation.

In the case of those metals which exhibit a brittle behavior below a certain temperature and a ductile behavior above the same temperature, the effect of irradiation is to increase the brittle-ductile transition temperature. In addition it is often found that irradiation decreases the energy required to fracture the material in the ductile region. Evidence to date indicates that irradiation

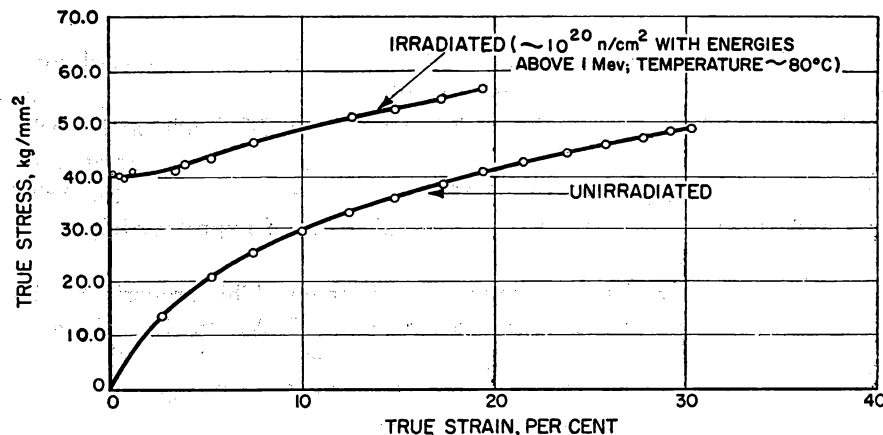


FIG. 1. The effect of reactor exposure on the stress-strain curve of nickel.

will not induce brittle behavior in metals which exhibit no such behavior in the unirradiated state.

SA-70 pressure-vessel steel and molybdenum are examples of body-centered-cubic systems which suffer significant changes in their impact properties as a result of irradiation. The curves of Berggren and Kernohan<sup>14</sup> in Fig. 2 illus-

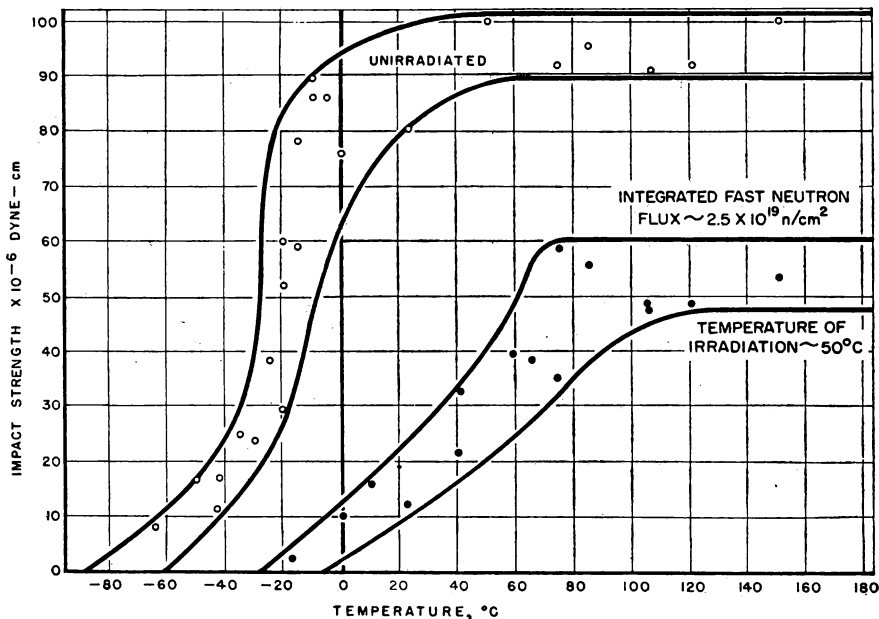


FIG. 2. The effect of reactor irradiation on the impact strength of SA-70 pressure vessel steel.

trate the changes produced in the impact properties of SA-70 steel by exposure. Similar effects are observed to result from the deuteron bombardment of mild steel.<sup>15</sup> In the case of molybdenum Bruch, McHugh, and Hockenbury<sup>16</sup> find that exposure of molybdenum at  $\sim 80^\circ\text{C}$  to an integrated fast-neutron flux (energy  $> 1$  Mev) of  $10^{20}$  neutrons/cm $^2$  increases the brittle-ductile transition temperature from an initial value of approximately  $-30^\circ\text{C}$  to a final value of approximately  $70^\circ\text{C}$ .

A metallic property of engineering interest is creep. This property has been studied as a function of neutron bombardment. J. C. Wilson, J. C. Zukas and W. W. Davis<sup>17</sup> have seen a decrease in the creep rate of nickel and Inconel at low temperature in agreement with observations by L. Coffin on stainless steel and by Witzig<sup>17</sup> on zirconium and aluminum by J. G. Morgan.<sup>17</sup> However, if the temperature is raised high enough, a slight increase in the creep rate has

been observed by J. C. Wilson et al. The temperature at which the increase occurs appears to be a function of the stress level.

Solid solution alloys of copper with aluminum, zinc, gallium, germanium, arsenic and manganese have been shown by R. H. Kernohan and D. S. Billington<sup>17</sup> to yield an anomalous decrease in electrical resistivity of 1-3%. An adequate explanation is not presently available. The hardness and strength in these alloys increase upon irradiation. Rosenblatt, Smoluchowski and Dienes<sup>18</sup> have studied the alpha-brass system in detail. The alloys were irradiated in a reactor at +50°C and at 80°K. It appears that the results can be best interpreted in terms of the formation of lattice defects upon low temperature exposure and increase of short-range order upon irradiation at +50°C. The change of residual resistivity is negative while the change of resistivity due to thermal scattering is positive for the samples irradiated at +50°C. The former depends upon irradiation flux and upon annealing time in a different manner from the latter. Short-range order appears to be produced also by proper heat treatment.

Konobeevsky and coworkers<sup>19</sup> describe radiation damage studies at higher temperatures than have been discussed so far. In addition to changes in mechanical properties they report interesting changes in microstructure. Their experiments are described below.

Annealed copper, nickel, iron-armco and aluminum were studied. Copper and iron were annealed at 700°C, nickel at 800°C and aluminum at 400°C. In all cases the annealing exposure was one hour. These metals were irradiated at temperatures from 250 to 300°C. The integrated neutron flux was 1.1 to  $1.4 \times 10^{20} nvt$ .

In spite of the high temperature at which radiation took place, all the materials studied were hardened (with the exception of aluminum). This is displayed in:

- (a) an increase in ultimate strength,
- (b) a decrease in relative elongation and in a reduction in area,
- (c) a decrease in impact strength, and
- (d) an increase in microhardness.

The most pronounced change was observed in iron (its elongation was decreased threefold and the impact strength tenfold); the least change of the three hardened metals was displayed by copper. This may be explained by the fact that copper has a lower temperature of recovery and recrystallization than iron or nickel. This also accounts for slight changes observed in the properties of aluminum, for which the radiation temperature of 250 to 300°C is above its recrystallization temperature.

The changes in mechanical properties of copper, nickel and iron are somewhat similar to those in the hardening of metals by plastic deformation. The

cause in both instances can be considered to lie in the appearance of defects. One can show, however, that radiation hardening differs from mechanical hardening. This is apparent, for example, from the change of the microhardness of irradiated metals vs the degree of prior deformation.

The course of the change in microhardness with the degree of deformation differs for irradiated and unirradiated materials and there is no evident convergence of the two curves until 40% of deformation. Such a convergence should be observed if the nature of irradiation hardening were similar to that produced by deformation.

A second difference can be seen from the microstructure of irradiated materials. Micrographs of the irradiated metals, copper, nickel and iron, have a slight difference over those of metals in the original annealed condition. No changes inherent to cold worked metals (such as slip lines, twins, etc.) are evident in this case. The grain size is increased in copper and nickel. Thus, prior to irradiation copper grains were  $32 \mu$  average diam. and after irradiation  $43 \mu$ , the average diam. of nickel being  $68 \mu$  and  $103 \mu$ , respectively. The average grain size of iron did not change.

Thus, grain growth (*recrystallization in situ*) is observed in copper and nickel when subjected to radiation at temperatures of 250 to  $300^{\circ}\text{C}$ . This recrystallization leads to increasing grain size without appreciable formation of new crystals. Such grain growth is not met in the metals under consideration in an annealed state under ordinary conditions. It shows that their ability to recrystallize is greatly increased due to irradiation.

Of interest is the fact that, contrary to the ordinary behavior of a metal which softens when recrystallized, in this case recrystallization is accompanied by an increase in hardness. The increase in tensile properties of iron, where recrystallization of this sort is not observed, is still larger.

Curves for the annealing of irradiated materials are different from those of cold worked and hardened metals. Stress relaxation occurs at a lower temperature and extends over a larger temperature range.

Zirconium was also studied. It was exposed to an integrated flux of  $2 \times 10^{20} nvt$  at a temperature ranging from 180 to  $240^{\circ}\text{C}$ . Microhardness of zirconium (annealed for one hour at  $900^{\circ}\text{C}$  prior to exposure) is raised from 120 to  $146 \text{ kg/mm}^2$ . Specific electrical resistivity changes from 0.446 to 0.456 ohm-mm $^2$ /m, and its temperature coefficient of electrical resistivity is decreased from 3.88 to  $3.78 \times 10^{-3}$ . Its density practically undergoes no changes.

Of interest are the changes in microstructure. Simultaneous processes of inner distortions accompanied the appearance of deformation. Processes of recrystallization also took place in zirconium under the influence of radiation. Recrystallization of zirconium during irradiation, at a temperature not ex-

ceeding 250°C, apparently is possible owing to crystal lattice distortions caused by a neutron effect.

Their studies of magnetic changes in stainless steel indicate high sensitivity to plastic deformation. Magnetic measurements were made on several samples of type X18H9T \* stainless steel. The object of these measurements was to ascertain whether austenite decomposes to form a ferritic constituent during irradiation, the latter phenomenon accompanying plastic deformation of this type stainless steels. The specimens were placed in a nonuniform magnetic field and the tare measured on a microbalance. If certain measures were taken to prevent plastic deformation ferromagnetism was not observed to appear.

### B. NON-METALS

Radiation effects in non-metallic crystals may be divided roughly into two categories: (1) the effect of fast neutron bombardment on crystal structure and (2) effects of both corpuscular and electromagnetic radiation on certain properties which are markedly dependent on lattice imperfections. The first category has the greatest practical interest since it is directly related to the dimensional stability and strength of irradiated non-metals. Consequently, much study has been devoted to this group of effects. The second category includes studies of optical absorption, magnetic susceptibility, paramagnetic resonance and electrical conductivity on various ionic and covalent crystals after exposure to a variety of energetic radiations. Studies of these properties lead to a better understanding of the nature of bombardment induced defects. There is a great deal of literature on the effects of purely ionizing radiation.<sup>20</sup> Separation of displacement effects and ionization effects is often difficult, particularly in ionic crystals. A clear-cut separation of the two effects has been reported by Levy and Dienes<sup>21</sup> for aluminum oxide. In this section we shall be concerned primarily with fast neutron bombardment. Some representative studies will be described.

**1. Diamond.** Lattice expansion of diamond induced by fast neutron bombardment was first observed by Primak and coworkers.<sup>22</sup> Extensive data have been reported by Crawford and Wittels<sup>23</sup> and this section is based on their presentation.

Figure 3 shows the density decrease in diamond as a function of irradiation and indicates that this change is approaching saturation near 4%. It is evident that a large number of atomic displacements are produced in diamond and examination of the diamond lattice reveals the  $(\frac{1}{2} \frac{1}{2} \frac{1}{2})$  and  $(\frac{3}{4} \frac{3}{4} \frac{3}{4})$  positions in the unit cell (cubic indexing) to be the most probable trapping sites for interstitial atoms. Random checks on the x-ray density measurements

\* 18% Cr, 9% Ni, 0.6% Ti and 0.1% C.

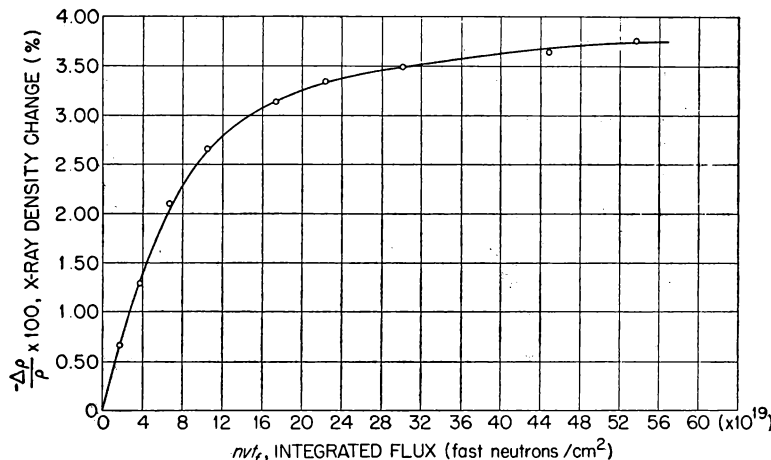


FIG. 3. Effect of neutron irradiation on the density of diamond.

made with conventional density methods were found to agree within experimental error ( $\pm 0.05\%$ ). This is the result to be expected for uniformly distributed Frenkel defects.<sup>24-26</sup>

A high degree of long-range order is maintained in irradiated diamonds. Single crystal x-ray studies of irradiated crystals reveal no appreciable line broadening and preliminary measurements indicate that there is an increase in the integrated intensity of some of the coherent reflections which would follow if Frenkel defects were produced.

Preliminary theoretical calculations by H. C. Schweinler<sup>23</sup> have led to the search for the so-called "forbidden" reflections in irradiated diamond and it can be reported that the (200) reflection is observed in neutron irradiated diamond following bombardments as small as  $5.0 \times 10^{19}$  neutrons/cm<sup>2</sup>. At the same time an increase in integrated intensity is observed for the anomalous (222) reflection. In addition to these observations of coherent x-ray scattering in neutron irradiated diamond, the bombardment induced diffuse scattering, which is seen at small angles in the forward region, is currently being investigated.

Annealing phenomena in the damaged diamond structure are indeed complex. It should be mentioned that clear crystals become an opaque black color after an approximate bombardment of  $10^{17}$  neutrons/cm<sup>2</sup>, and remain so upon continued irradiation. One crystal bombarded by  $2 \times 10^{20}$  neutrons/cm<sup>2</sup> failed to lose this opacity after annealing at 1600°C for two hours. The same crystal recovered approximately 70% of its density change during this anneal. From Krishnan's work<sup>27</sup> on the thermal expansion of the diamond lattice, the expansion at 2000°C would not even remotely approach the expansion result-

ing from neutron bombardment. These results indicate that some of the defects in irradiated diamonds have an extremely high thermal stability.

**2. Silica.** Optical absorption bands introduced into both crystalline quartz and silica glass by energetic radiations have been the subject of numerous investigations. Besides coloration with ionizing radiation,<sup>28-30</sup> recent studies of effects produced<sup>31-34</sup> by reactor exposure have been reported. On irradiation both quartz and glass develop a number of absorption bands in the visible and near ultraviolet. Regardless of the source of material, both forms of silica develop a band in the region of 2100 to 2200 Å, whereas the visible coloration is apparently markedly sensitive to either impurities or lack of stoichiometry. In both materials prolonged exposure to fast neutrons tends to bleach the visible bands while further enhancing the near ultraviolet band.

C. M. Nelson<sup>23</sup> has investigated silica from three sources: (1) natural quartz crystals, (2) impure fused silica (Vitrosil), and (3) "purified" Corning silica glass. Spectra for quartz and Vitrosil are in agreement with those previously reported. The Corning glass, however, possesses almost no visible absorption, but rather shows a narrow absorption band centered at 2150 Å, as reported by P. W. Levy.<sup>34</sup> In the following each of these materials will be considered.

For fast neutron exposures up to  $10^{18}$  neutrons/cm<sup>2</sup>, studies of optical absorption in natural quartz crystals are in essential agreement with the results reported by Mitchell and Paige.<sup>32</sup> For greater exposures, the visible coloration is rapidly bleached and, after  $\sim 2 \times 10^{19} nvt$ , the crystals were nearly colorless in the visible, possessing only pink to magenta coloration. Absorption measurements indicate that this is caused predominantly by the long wavelength tail of the intense ultraviolet band at  $\sim 2200$  Å.

It has been observed that irradiated quartz has a paramagnetic component.<sup>35,36</sup> If it is assumed that the paramagnetism is associated entirely with unpaired electrons which, in turn, are responsible for the ultraviolet absorption band, the concentration of absorbing centers can be obtained directly from magnetic susceptibility measurements. D. K. Stevens<sup>23</sup> has measured the susceptibility of a series of irradiated quartz specimens. The curve for the unirradiated specimen is temperature independent, possessing no paramagnetic component, whereas all irradiated specimens show a decreasing diamagnetism toward low temperature. The paramagnetic component is obtained by subtracting the curves from that for the unirradiated specimen. As a function of temperature Curie's law is obeyed and the slopes are proportional to the concentration of centers. The dependence of unpaired electron concentration on fast neutron exposure is shown in Fig. 4. It is noted that the concentration is not a monotonic function of exposure but rather reaches a maximum at  $\sim 6 \times 10^{19} nvt$ . It is interesting that this is the exposure at which the rate of density change of quartz becomes large.<sup>37,38</sup> The saturation paramagnetic center con-

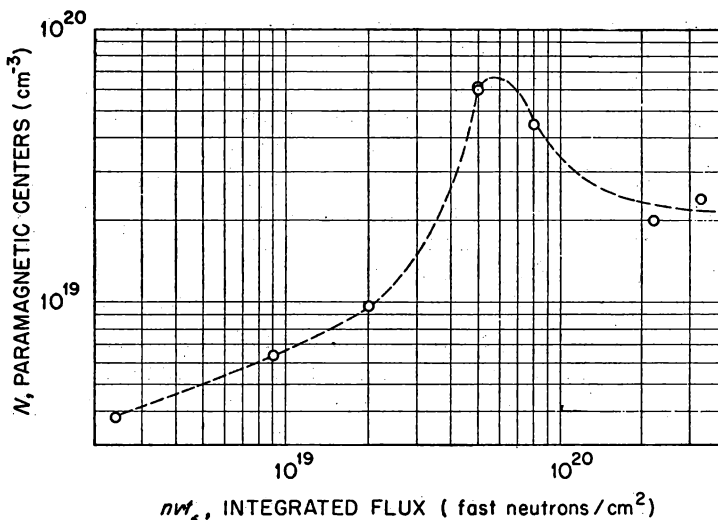


FIG. 4. Bombardment introduced paramagnetic centers in quartz vs irradiation.

centration is estimated from Fig. 4 to be  $\sim 2 \times 10^{19}$  for an exposure temperature of 100°C. If these are associated only with the 2200 Å absorption band, it is possible to obtain the oscillator strength of the absorbers directly. Such a determination for Corning fused silica will be discussed below.

A number of specimens of Vitrosil glass have been exposed to fast neutrons, high energy electrons (0.2 to 2 Mev), 250 kv x-rays, and gamma rays from a Co<sup>60</sup> source. The variety of radiations was used in an attempt to detect possible differences in effects arising from the nature of the radiation. The optical absorption spectra obtained for each type of source were essentially the same. Although not nearly so pronounced as with fast neutrons, prolonged x-ray exposure was also observed to bleach the visible absorption band while further enhancing the ultraviolet band. The visible bands could be optically bleached to some extent by exposure to light with a range of wavelengths corresponding to that of the band in question. Much more effective bleaching of the entire spectrum could be accomplished by exposing to wavelengths in the ultraviolet band.

Corning fused silica is extremely resistant to coloration by ionizing radiation.<sup>30,34</sup> Consequently, the material is a valuable one, aside from its practical importance, in which to study the ultraviolet absorption bands without the complication of the visible, impurity-sensitive coloration. Optical studies have been carried out on this material with the same variety of high energy radiations used in studies of Vitrosil. The absorption spectrum was qualitatively the same for each type of radiation, but the efficiency in producing the

ultraviolet band differed widely from one type to another. The form of the absorption band obtained after a fast neutron exposure of  $5 \times 10^{17}$  neutrons/cm<sup>2</sup> is shown in Curve I of Fig. 5, from which it is evident that the band is a composite of at least two overlapping bands. It was found that the shorter wavelength band, which is apparently the most intense of the two, was bleached much more rapidly with ultraviolet light. Curve II was obtained after prolonged exposure to a mercury-vapor lamp in which most of the emission was concentrated in the 2537 Å line. The difference between Curves I and II, indicated by the dashed line, may be used as a basis for resolving the com-

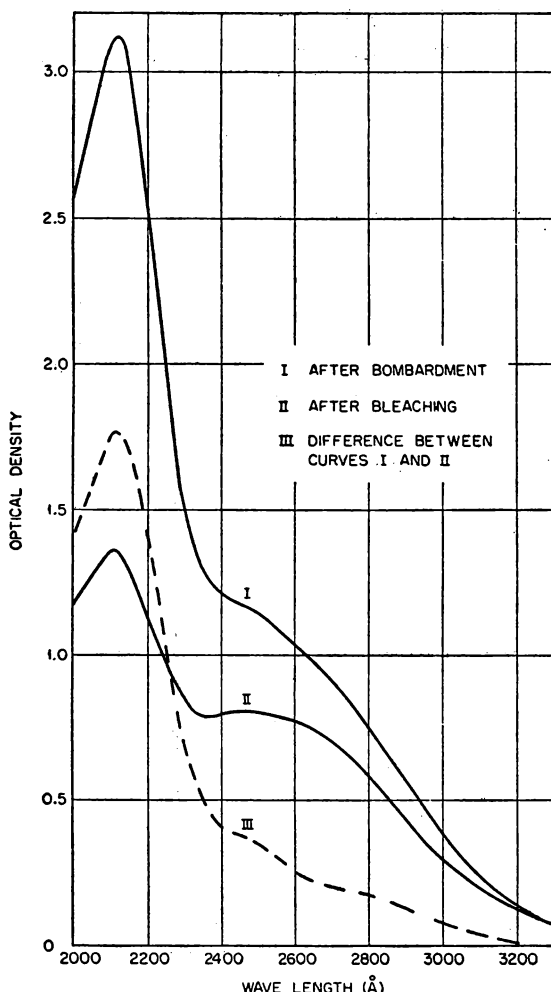


FIG. 5. Optical density vs wavelength for fast-neutron bombarded Corning silica glass.

## RADIATION EFFECTS

posite band into two approximately symmetrical bands, one centered at 2120 Å and the other at 2570 Å. The origin of these two absorption bands is not yet understood.

The efficiency of the various radiations in producing the composite ultraviolet band varies widely. 250-kv x-radiation is four times as effective as the Co<sup>60</sup> gamma rays and, in addition, produces a greater saturation absorption. At saturation the absorption coefficient is 11.5 cm<sup>-1</sup> for the x-rays as compared to 8.7 cm<sup>-1</sup> for gamma rays. High energy electrons are also effective in producing the ultraviolet bands with both the rate of growth and saturation absorption depending on electron energy. The saturation absorption coefficient for 2 Mev electrons is  $\sim 20$  cm<sup>-1</sup>.

Of all types of radiation investigated, fast neutrons are the most efficient

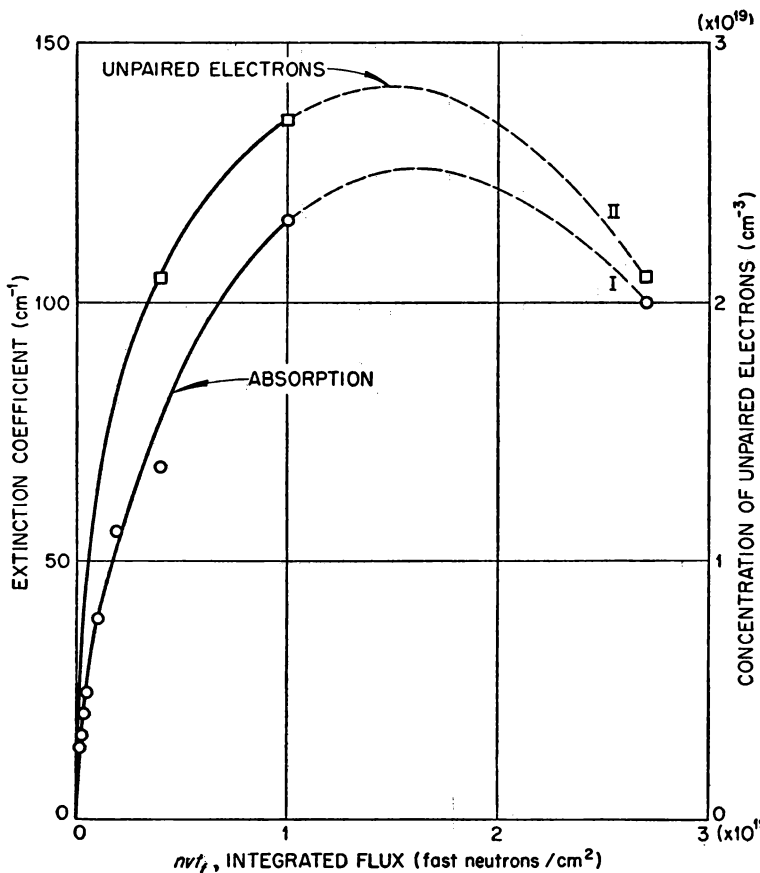


FIG. 6. Absorption and unpaired electron concentration in irradiated Corning silica glass.

in developing the ultraviolet band.<sup>34</sup> This presumably results from the fact that fast neutron bombardment introduces additional lattice defects. The growth of the composite band is shown in Fig. 6. Although the absorption at 2150 Å apparently reaches a maximum of  $270 \text{ cm}^{-1}$  at  $\sim 1.5 \times 10^{19}$  neutrons/cm<sup>2</sup>, the point at  $2.7 \times 10^{19}$  neutrons/cm<sup>2</sup> is somewhat in doubt as indicated by the dashed line. The longest exposure was obtained in a position where the temperature was not controlled and, hence, it is possible that appreciable thermal bleaching could have taken place. Also shown in Fig. 6 is the concentration of paramagnetic centers as determined by magnetic susceptibility measurement. It is interesting to note that the concentration of paramagnetic centers, presumably unpaired electrons, is approximately proportional to the absorption coefficient at the maximum of the composite absorption band.

Using the concentration of unpaired electrons determined magnetically it should be possible to calculate the oscillator strength of the absorbers in Corning silica. Unfortunately, the situation is complicated by the presence of two absorption bands. However, for all exposures used the absorption in the 2570 Å band was less than 20% of that in the 2120 Å band. Hence, if it is assumed that the oscillator strengths are comparable for the two bands, and that there are no absorption bands at shorter wavelengths, it should be possible to obtain an approximate value by means of Smakula's formula. Calculations for three specimens give oscillator strengths of 0.14, 0.18 and 0.22 for exposures of  $4 \times 10^{18}$ ,  $1 \times 10^{19}$  and  $2.7 \times 10^{19}$  neutrons/cm<sup>2</sup>. If the assumptions indicated above are valid, it appears that the oscillator strength for the 2120 Å line is  $\sim 0.2$ .

Preliminary thermal bleaching experiments have been performed for all three forms of silica. The results seem to indicate that the fast neutron induced optical absorption is removed long before any appreciable annealing of structural changes has occurred. It therefore seems reasonable to conclude that the color centers may be identified with trapped electrons.

**3. Ionic crystals.** Ionic conductivity and optical absorption are two properties of ionic crystals which are convenient indices of lattice imperfections resulting from high energy irradiation. Ionic conduction is dependent on diffusion rate and hence on the concentration of mobile, charged defects. Optical absorption, on the other hand, is electronic in origin and depends on the concentration of electrons and holes trapped in the vicinity of lattice defects. Potassium chloride was chosen for investigation because it is quite representative of the ionic type crystal and has been extensively studied. Furthermore, it is not rendered excessively radioactive by exposure to neutrons.

The ionic conductivity of a number of specimens was measured as a function of temperature both before and after exposure. A direct-current method was used employing a vibrating-reed electrometer for current measurements.

Early experiments<sup>39</sup> revealed that exposure to Co<sup>60</sup> gamma radiation and short reactor irradiations decreased the ionic conductivity by as much as an order of magnitude, whereas prolonged reactor exposure to both gamma rays and fast neutrons increased the conductivity by about the same factor. This behavior has been interpreted as follows: the ionizing radiation is expected to produce hole-electron pairs which are trapped at lattice vacancies, thus rendering them electrically neutral. This effect would tend to decrease the concentration of charged positive-ion vacancies (the mobile defect), hence decreasing the conductivity. Fast neutrons, on the other hand, increase appreciably the concentration of both vacancies and interstitial atoms and, even though an appreciable fraction of these defects may be neutralized by trapped charge, the net effect is to increase the conductivity. Similar effects to those of gamma irradiation have been observed in x-irradiated crystals.

Attempts have been made by C. M. Nelson<sup>23</sup> to identify the radiation produced defects by studying the annealing kinetics of the property change. Unfortunately, the annealing behavior is exceedingly complex, both increases and decreases of conductivity occurring with time at various annealing temperatures. At certain temperatures a conductivity decrease is successively followed by an increase during a single isothermal anneal. These results indicate that the annealing of the conductivity change produced by both fast neutrons and gamma rays proceeds by multiple processes. Attempts to separate and to identify the various steps have not yet been successful. The results reported here are in qualitative accord with observations on alkali halides bombarded with 400 Mev protons as discussed by Smoluchowski.<sup>40</sup>

Varley<sup>41-43</sup> has suggested a new mechanism whereby ions can be displaced from their normal sites to interstitial sites in a heteropolar lattice by the indirect process of utilizing that portion of the energy of a fast charged particle which is given up initially to ionization losses. Some of the ionization processes will result in more than one electron being removed from a negative ion in the lattice. If this multiple ionization leads to the removal of, say, four or five electrons from one negative ion, then, provided the ion does not recover electrons in a time short compared with its vibrational period, this ion may be ejected from its lattice site by the lattice vibrations. Ejection of such a negative ion, stripped of several electrons, is probable because the ion is temporarily a positive ion at a lattice site normally occupied by a negative ion. Thermal activation may then remove the ion from such an unstable position into some interstitial position which to a first approximation is electrically neutral. Alternatively, the multiple-ionized negative ion may displace one of the neighboring positive ions into an interstitial site, itself temporarily occupying the positive ion lattice site. Considerations of the magnitudes of the ionization potentials of negative ions such as chlorine suggest that the anions so displaced into interstitial sites will regain enough electrons to become elec-

trically neutral, the remaining electrons being trapped at negative ion vacancies. The cations displaced interstitially will probably remain positively charged.

The subsequent fate of these interstitial anions and cations is that they migrate either to normal lattice sites of the right kind so tending to restore the crystal towards equilibrium, or they may be trapped at vacant sites of the wrong kind. Thus a neutral anion may occupy a positive ion vacancy, while an interstitial cation may combine with an electron trapped at a negative ion vacancy, so occupying such a vacancy as a neutral atom. An attempt has been made<sup>43</sup> to interpret radiation induced changes in such physical properties as optical absorption in alkali halides on the basis of these considerations.

This concept of the displacement of ions in solids by the indirect process of multiple ionization is a logical development of the mechanisms for the production of free radicals already described from studies in radiation chemistry. Furthermore, McLennan's work<sup>44</sup> on bombardment of alkali halide crystals with 50 Kev electrons led him to suggest that single ionization of a halogen ion, leaving it temporarily uncharged, might result in the formation of some interstitial neutral anions. Such a process is, however, unlikely, and it is only if multiple ionization of a single anion occurs that the displacement probability will be relatively large. Platzman<sup>45</sup> (private communication) has suggested that the multiple ionization mechanism may arise from Auger cascades following the ejection of a single inner electron.

One important aspect of this multiple ionization displacement process is that such relatively low energy radiation as x-rays can give rise to atomic displacements in ionic lattices. Thus x-rays will produce photoelectrons which in turn may multiply-ionize anions and hence indirectly produce displacements. The cross section,  $\sigma$ , for multiple ionization is large; thus  $\sigma \sim 10^{-16} \text{ cm}^2$  for the removal of one electron, decreasing by approximately  $(n - 1)$  orders of magnitude for the removal of  $n$  electrons.

**4. Miscellaneous.** Although they are not reactor components in the strictest sense of the word, electrical and electronic accessories are quite important in reactor-control and monitoring systems. Moreover, in the case of research reactors, electronic instrumentation is quite often an integral part of experimental equipment for in-pile measurements. Consequently, information regarding the radiation stability of various electrical materials and components is valuable to both reactor engineers and scientists.

In recent years considerable emphasis in circuit development has been given to semiconductor devices, both diodes and transistors. The chief advantage of these units is their very small space and power requirements. The very marked sensitivity, however, of the electrical properties of germanium and silicon as well as other diamond-lattice semiconductors to fast neutron bombardment<sup>46, 47</sup> precludes the use of these miniature components inside nuclear reactors.

Germanium point-contact and junction diodes become ohmic after an exposure of  $10^{15}$  fast neutrons  $\text{cm}^{-2}$  and transistor action in p-n-p junction transistors is essentially destroyed by  $10^{12}$  fast neutrons  $\text{cm}^{-2}$ . Consequently, when using these units in electronic equipment near a reactor, careful account of their radiation sensitivity should be taken. Although the rate of deterioration is somewhat slower than in the case of germanium diodes, other semiconductor rectifiers (silicon, copper-cuprous oxide and selenium) also tend to become ohmic when exposed to fast neutrons.

In addition to components, considerable attention has been given an even more important electrical material, namely, lead-wire insulation. The commercially available wire insulations include both inorganic and organic materials. These cover a wide range of radiation stability. Some deterioration, both chemical and electrical in nature, is observed with all insulations studied. In evaluating the effects on the usefulness of a given insulation, it is necessary to take into account the overall impedance of the electrical circuit in which it is to be used. Low impedance networks require a much lower insulation stability than those with high impedances. Besides simple resistance changes, variation of dielectric constant and loss-tangent have been observed in the dielectric materials employed in high-frequency transmission cable (coaxial cable).

A comprehensive study of elastomers and plastomers has been carried on by O. Sisman and C. D. Bopp<sup>48</sup> for several years. They have been able to correlate radiation stability with chemical structure. Other studies of interest have been made by A. Charlesby,<sup>49</sup> K. Little<sup>50</sup> and Ross,<sup>51</sup> Ballentine and coworkers<sup>52</sup> and Mesrobian and coworkers.<sup>53</sup>

A number of insulation materials, available commercially, have been studied. It was found that there is a large difference in insulation resistance, depending whether the reactor is operating (dynamic condition) or not (static condition). In many instances, the dynamic resistance measurements indicate a value lower by two orders of magnitude than pile-off values.

### C. GRAPHITE<sup>54</sup>

The properties of artificially manufactured graphite make it a very suitable material for use in a nuclear reactor, both as a moderator and as a structural component. Of particular advantage are its mechanical strength, moderating properties, low neutron absorption cross section, refractory and heat conducting properties, and availability in large quantities at low cost. However, irradiation in a reactor produces basic changes in the crystalline structure of graphite which result in large changes in its physical properties.

There exists a vast quantity of experimental data, largely empirical, on irradiation damage effects in graphite. The results obtained from irradiation

of a given sample are in many instances dependent upon the fabrication history of the graphite and are very sensitive to the temperature at which the sample is irradiated; reproducible results are obtained only if these factors are kept under close control.

The bulk of the data has been obtained from irradiation of graphite samples in the production reactors at Hanford. In addition to limited amounts of data from other reactors with lower neutron flux intensities, the data have recently been augmented by irradiations in the high flux of the Materials Testing Reactor at the National Reactor Testing Station. In this section the experimental observations of primary interest in reactor technology shall be given.

Damage to the crystallite structure of graphite is incurred during irradiation in a reactor, causing significant and often severe changes in the overall physical properties of the graphite. The mechanical properties are improved—the hardness and strength of the graphite are increased. Other physical properties are detrimentally affected. Thermal and electrical conductivities decrease; graphite shapes exhibit changes in their gross dimensions; and several other effects, such as the storing of potential energy, are encountered. All effects are decreased in magnitude when the temperature of the graphite during irradiation is increased.

**1. Mechanical properties.** The effects of irradiation upon the mechanical properties of graphite are to produce a stronger, harder, and more brittle material. Consequently, irradiation effects on the mechanical properties of graphite have been of little immediate concern in the operation of graphite-moderated reactors, and the amount of reliable data obtained under controlled conditions is limited. Irradiation of graphite produces a tougher, harder graphite which is more difficult to machine.

**2. Thermal conductivity.** Brief irradiations produce large decreases in the thermal conductivity of graphite, or large increases in the thermal resistivity. The conductivity continues to decrease, though less rapidly, with prolonged irradiation. In some instances conductivities have been reduced by factors greater than 50 by irradiation.

**3. Electrical resistivity.** The electrical resistivity of graphite is not of importance in the evaluation of graphite as a reactor component. The measurement of electrical resistivity, however, is useful as an index of radiation damage and is important in theoretical studies of damage. In addition, the simplicity and high accuracy of electrical resistance measurements make them attractive for theoretical irradiation damage studies. The electrical resistivity of graphite changes rapidly during the early stages of irradiation. The resistivity rises quickly to a maximum at about  $2 \times 10^{20}$  neutrons/cm<sup>2</sup>, decreases slightly, and begins a slow increase at exposures above about  $10 \times 10^{20}$  neutrons/cm<sup>2</sup>.

**4. Crystallite properties.** The major effects of radiation upon the crystallite structure of graphite are distortion of the crystal lattice and eventual breakup and disorder of the crystal structure with a trend toward amorphous form. The distortion of the lattice takes the form of an expansion in the  $c_0$ , or interplanar, dimension and a shrinkage or warping of the  $a_0$  dimension along crystal planes.

These distortions are caused primarily by collisions between atoms of carbon in the graphite lattice and impinging energetic particles, particularly fast neutrons. These collisions result in the displacement of carbon atoms from normal positions within the lattice and the production of lattice vacancies. In addition the displaced atoms, in losing kinetic energy, may produce further lattice distortions.

The crystallite changes induced in graphite by irradiation have been studied extensively by x-ray diffraction techniques. Low exposures cause a decrease in the crystalline peak intensity and a shift in the angle of diffraction, but the peak shape remains essentially constant. At exposures above  $4 \times 10^{20}$  to  $6 \times 10^{20}$  neutrons/cm<sup>2</sup> the peak is broadened progressively at its base until at high exposures the peak becomes very diffuse.

The  $c_0$  spacing of graphite samples is the most readily obtained of the crystallite parameters and is useful as an index of radiation damage. Figure

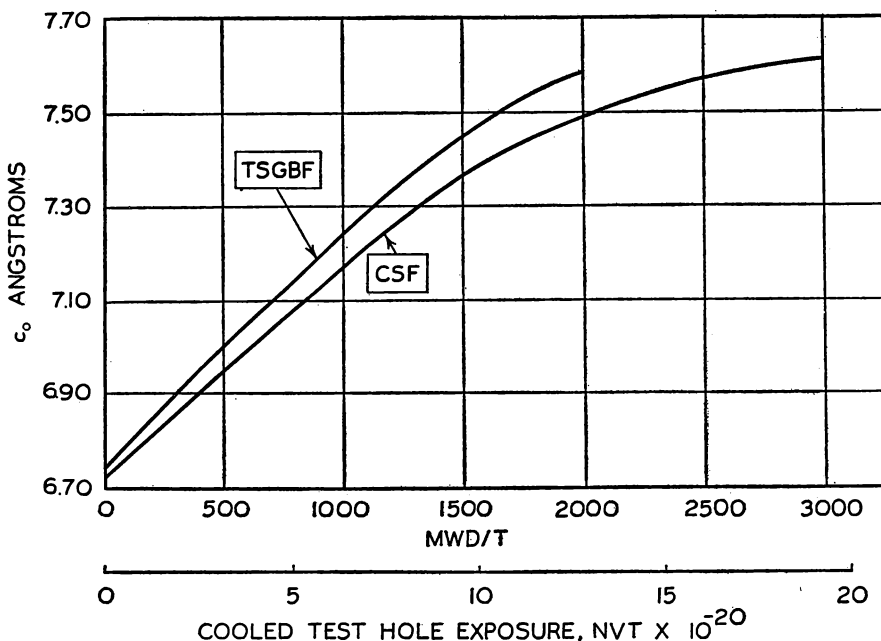


Fig. 7.  $C_0$  displacement in irradiated graphite.

7 shows the variation of  $c_0$  spacing with exposure for two typical grades of graphite. The  $c_0$  values as reported are uncorrected for small angle scattering and other minor effects. The highest uncorrected  $c_0$  spacing observed to date as a result of irradiation damage is around 8.0. This was obtained after irradiation to  $20 \times 10^{20}$  neutrons/cm<sup>2</sup> in the Materials Testing Reactor. The effect of exposure on the  $c_0$  spacing of graphite crystallites is decreased markedly at higher exposure temperatures. Figure 8 shows the effect of exposure

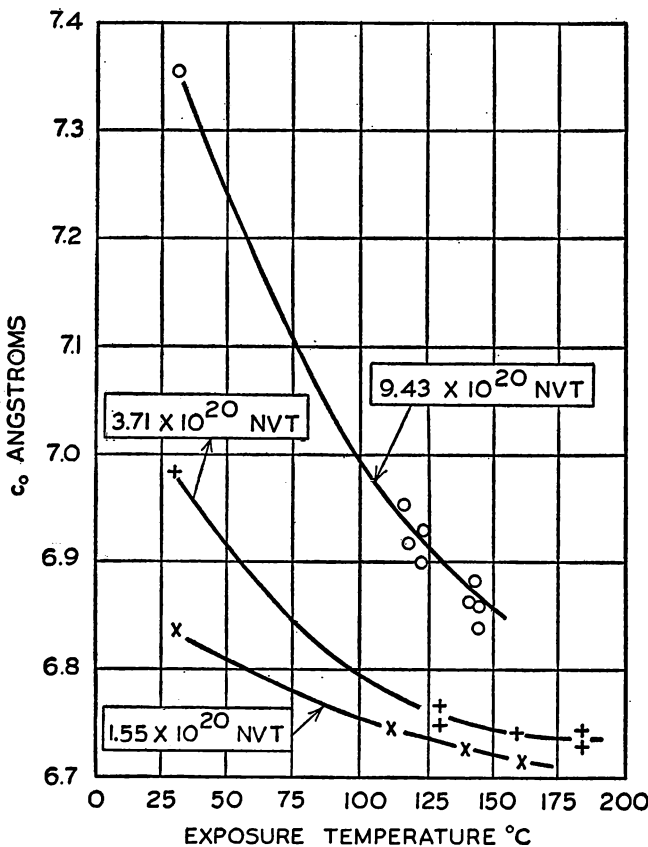


FIG. 8. Variations in  $c_0$  displacement of CSF graphite with exposure temperature.

temperature on the change in  $c_0$  spacing. The  $a_0$  spacing of irradiated graphite samples has not been studied extensively, both because the experimental data are more difficult to obtain and because the irradiation-induced changes in the  $a_0$  spacing are an order of magnitude smaller than those in the  $c_0$  spacing. The meager data which are available indicate that the  $a_0$  spacing decreases as a result of irradiation. The increase in  $c_0$  spacing is believed to be caused

by the retention of displaced carbon atoms in interstitial positions within the lattice.

**5. Dimensional stability.** The dimensional stability of graphite under irradiation is a property of major interest in the design and operation of a graphite-containing reactor. In general, graphite tends to expand along planes transverse to the preferred axis of crystal orientation and to contract along planes parallel to this axis. The behavior varies widely, however, with the degree of orientation attained in the graphite. The overall dimensional changes are only qualitatively related to the crystallite changes. Some of the variation in performance can be accounted for, but other factors remain unknown.

Figure 9 shows the changes in dimensions of several grades of graphite after irradiation. In Fig. 9 note the rather abrupt change in the rate of linear distortion at about  $6 \times 10^{20}$  neutrons/cm<sup>2</sup>; it is believed that this may be associated with the broadening of the x-ray diffraction line peak shapes above this exposure. The values shown in Fig. 9 are the averages of a large number of samples; considerable scatter exists in the data.

In striking contrast to the data shown in Fig. 9, a transverse cut sample of graphite made from large natural flake graphite instead of petroleum coke expanded 24% during an irradiation to  $25 \times 10^{20}$  neutrons/cm<sup>2</sup>. This rate is an order of magnitude greater than that observed in artificial graphites.

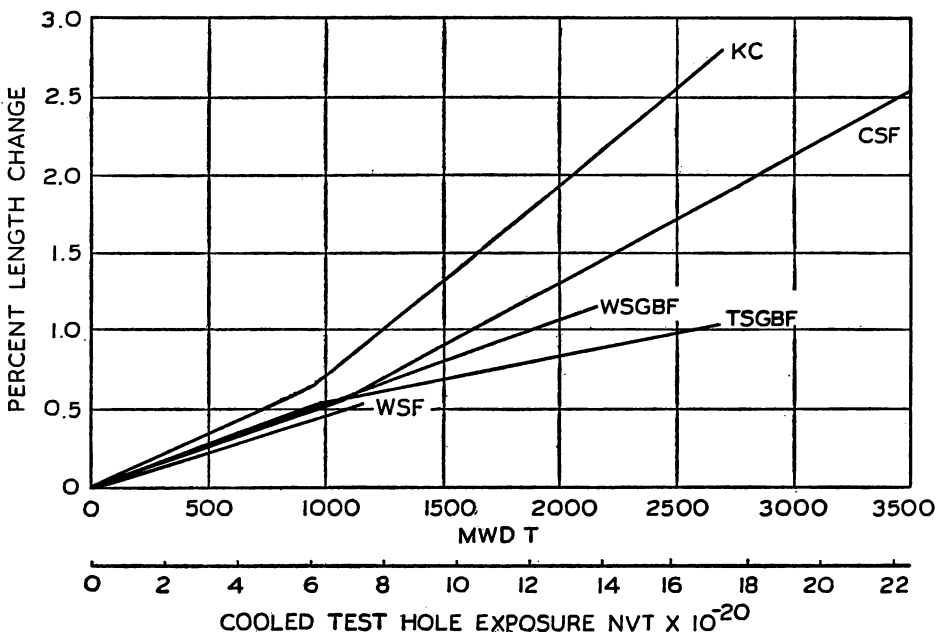


FIG. 9. Physical expansion of transverse cut graphites with irradiation.

The physical distortion of irradiated graphite is dependent on the temperature of exposure. Representative data are shown in Fig. 10.

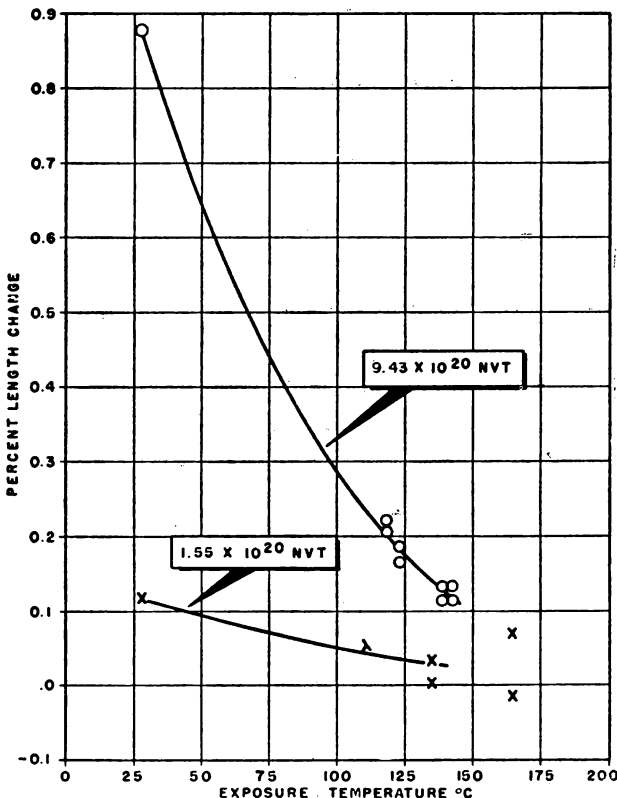


FIG. 10. Effects of temperature on physical expansion transverse cut CSF.

**6. Thermal expansion.** Although conflicting information exists in the literature, most recent data indicate that irradiation has a negligible effect on the temperature coefficient of thermal expansion of reactor grade graphite. In this connection it is sometimes necessary to distinguish the irreversible effects caused by annealing of the radiation induced distortion from the reversible effects normally considered as thermal expansion.

**7. Specific heat.** Irradiation induces a small increase in the specific heat of graphite when measured at temperatures below the temperature of irradiation. Specific heat determinations were made on one sample of graphite before and after irradiation. Although the exposure history of the sample is not known, its total stored energy value (475 cal/gram) indicates an exposure equivalent to about  $15 \times 10^{20}$  neutrons/cm<sup>2</sup> in a cooled test hole. The specific heat at

room temperature was increased about 0.006 cal/gram/ $^{\circ}\text{C}$  (about 3%) as a result of irradiation.

**8. Thermoelectric and magnetic properties.** Considerable work has been done on the determination of the thermoelectric and magnetic properties of irradiated graphite. Although these properties are not important in the engineering consideration of the merits of graphite for nuclear reactor use, they are extremely useful in the theoretical studies directed toward determining a mechanism of irradiation damage.

**9. Stored energy.** Irradiation of graphite in a reactor increases the energy content of the crystal lattice. This increase in energy is referred to as "stored energy." The total stored energy in a graphite sample represents an increase in enthalpy and is observed as an increase in the heat of combustion of the material. Numerous such measurements have been made by the National

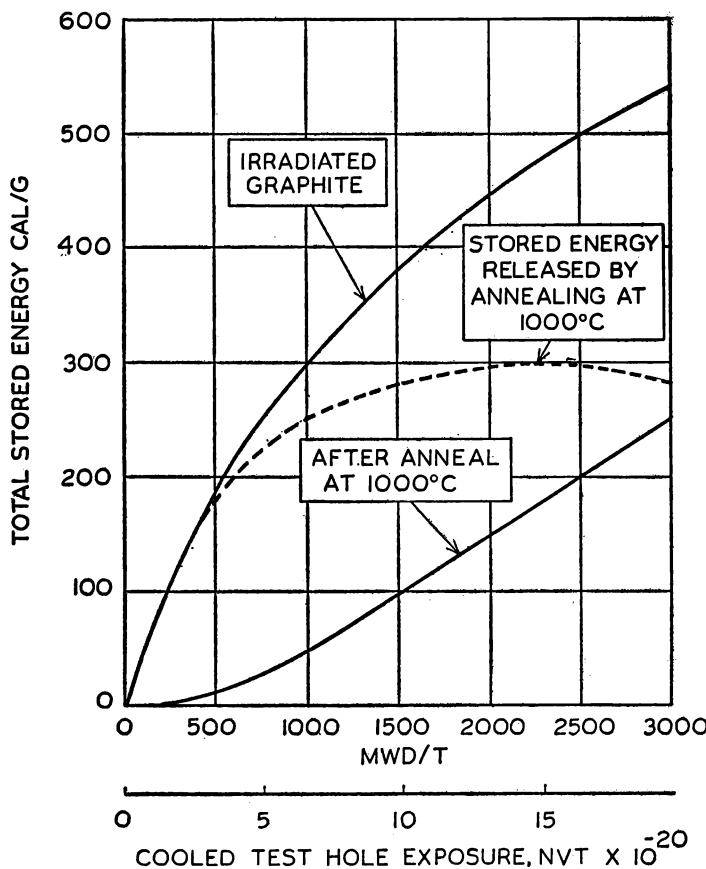


FIG. 11. Build-up of total stored energy in irradiated graphite.

Bureau of Standards. Of greater interest than the total stored energy, however, is the nature of the release of stored energy during annealing. Figure 11 shows the total stored energy in irradiated graphite and the stored energy which remains after prolonged annealing at 1000°C. By difference one obtains the amount of stored energy which was released during the annealing—shown as a dotted line on Fig. 11. The first thing to notice is that these stored energy effects are large; 500 cal/gram of stored energy represents the energy required to raise the temperature of a gram of graphite more than 1200°C. The second observation is that all of the stored energy accumulated during brief irradiations can be released by annealing at a temperature of 1000°C, but essentially none of the incremental amounts of stored energy accumulated after exposures greater than  $13 \times 10^{20}$  neutrons/cm<sup>2</sup> can be released by annealing at a temperature of 1000°C.

**10. Annealing of physical property damage.** Physical property damage to graphite is removed to a greater or lesser degree upon heating the graphite. The rate of annealing and the ultimate degree to which the damage may be removed depend on the annealing temperature and the amount of damage; quantitative recovery of changes in physical properties may be attained as graphitization temperatures are approached. In addition, some of the irradiation damage previously incurred by irradiation at low temperature will be annealed if the temperature of irradiation is increased during the course of the irradiation. This is called nuclear, or radiation, annealing. Nuclear annealing can effect recovery of damage to many physical properties at temperatures substantially lower than those required to obtain equivalent recovery by thermal annealing. Irradiation at 150°C effects an order-of-magnitude reduction in the changes of most physical properties compared with those incurred by irradiating at 30°C.

#### D. MINIMIZATION OF RADIATION EFFECTS

On the basis of the results discussed so far some suggestions can be presented as to how radiation effects may be minimized. Some of the items given below apply specifically to uranium and will be discussed in more detail in the next chapter.

**1. Adjustment of bombardment temperature.** (1) In cases where excessive changes in physical properties occur an increase in bombardment temperature would certainly reduce the magnitude of the effect. This is well illustrated by annealing in metals and by the much-reduced radiation damage in graphite at elevated temperatures.

(2) Where diffusional effects play an important role in radiation damage, for example in metastable solid solutions, then a decrease in bombardment

temperature would prove beneficial by decreasing the mobility of the irradiation generated defects.

Adjustment of bombardment temperature is probably the most important single variable for effecting a reduction in damage.

**2. Alloying.** (1) It appears reasonable to consider alloying to reduce phase instability and anisotropic effects in uranium. The superior performance of an aluminum-uranium alloy has been demonstrated in practice.

(2) Care should be taken to avoid alloys or other solids that transmute to new atomic species, particularly under conditions of extremely long bombardments. The transmutation of manganese to iron is a case in point. Deleterious property changes could easily develop through this mechanism.

**3. Dispersion.** Adjustment of the particle size of fissionable material appears to be an effective means of controlling the damage rate in a uranium mixture by confining most of the fission fragment damage to the volume of the particle.

**4. Material selection.** Metallic bonding appears best for radiation resistance, ionic bonding next for most applications, then covalent and finally molecular bonding. It appears desirable to avoid materials which possess unstable phases at or near the bombarding temperature. Studies reveal that close-packed structures have the highest radiation stability, and in general, simple structures of high symmetry have better radiation characteristics than anisotropic structures.

#### REFERENCES FOR CHAPTER VIII

1. Further details will be found in the following Geneva Papers:  
748—R. Smoluchowski, "Effect of Nuclear Irradiation on Ionic Crystals."  
751—G. R. Hennig and J. E. Hove, "Interpretation of Radiation Damage to Graphite."  
362—G. Mayer, P. Perio, J. Gueron, and M. Tournaire, "Modification de Materiaux Non Metalliques sous L'Influence des Rayonnements et Retrogradation Thermique de ces Modifications."  
442—G. H. Kinchin, "The Effect of Irradiation on Graphite."
2. D. S. Billington and S. Siegel, *Effect of Nuclear Radiation on Metals*, Metal Progress 58:847 (1950); G. R. Sutton and D. O. Leeser, *How Radiation Affects Structural Materials*, Iron Age 174:97 (1954).
3. T. H. Blewitt and R. R. Coltman, *The Effect of Pile Irradiation on the Stress Strain Curve of Copper*, Phys. Rev. 82:769 (1951).
4. F. W. Kunz and A. N. Holden, *The Effect of Short-time Moderate Flux Neutron Irradiations on the Mechanical Properties of Some Metals*, Acta Metallurgica 2:816 (1954).
5. A. W. McReynolds, W. Augustiniak, Marilyn McKeown, and D. B. Rosenblatt, *Neutron Irradiation Effects in Cu and Al at 80°K*, Phys. Rev. 98:418 (1955).
6. T. H. Blewitt and R. R. Coltman, *The Effect of Neutron Irradiation of Metallic Diffusion*, Phys. Rev. 85:384 (1952); T. H. Blewitt and R. R. Coltman, *Radiation Ordering in Cu<sub>3</sub>Au*, Acta Metallurgica 2:549 (1954).

7. G. T. Murray and W. E. Taylor, *Effect of Neutron Irradiation on a Supersaturated Solid Solution of Beryllium in Copper*, Acta Metallurgica 2:52 (1954).
8. J. W. Cleland, D. S. Billington, and J. H. Crawford, *Low Temperature Fast Neutron Bombardment of Copper-Beryllium Alloy*, Phys. Rev. 91:238 (1953).
9. D. L. Chipman, B. E. Warren, and G. J. Dienes, *X-ray Measurements of Radiation Damage in Black Phosphorus*, J. Appl. Phys. 24:1251 (1953).
10. J. Fleeman and G. J. Dienes, *Effect of Reactor Irradiation on the White-to-Grey Tin Transformation*, J. Appl. Phys. 26:652 (1955).
11. M. J. Makin, Unpublished work (see Geneva Paper No. 444).
12. C. R. Sutton and D. O. Leeser, *How Radiation Affects Metals*, Iron Age 174:97-100, 128-131 (1954).
13. M. B. Reynolds, J. R. Low, and L. O. Sullivan, *Study of the Radiation Stability of Austenitic Type 347 Stainless Steel*, Jour. Metals 7:555 (1955).
14. As reported in Geneva Paper No. 747.
15. Robert A. Meyer, *Influence of Deuteron Bombardment and Strain Hardening on Notch Sensitivity of Mild Steel*, J. Appl. Phys. 25:1369 (1954).
16. C. A. Bruch, W. E. McHugh, and R. W. Hockenbury, *Embrittlement of Molybdenum by Neutron Radiation*, Trans. AIME 203:281 (1955).
17. As reported in Geneva Paper No. 744.
18. D. B. Rosenblatt, R. Smoluchowski, and G. J. Dienes, *Radiation Induced Changes in the Electrical Resistivity of Alpha-Brass*, J. Appl. Phys. 26:1044 (1955).
19. Geneva Paper No. 680.
20. See, for example, the review article: F. Seitz, Rev. Mod. Phys. 26:7 (1954).
21. P. W. Levy and G. J. Dienes, *Color Centers Induced in  $Al_2O_3$  by Reactor and Gamma-Ray Irradiation*, "Defects in Crystalline Solids," The Physical Society, London, 1955, pp. 256-260.
22. W. Primak, L. H. Fuchs, and P. Day, *Radiation Damage in Insulators*, Phys. Rev. 92:1064 (1953).
23. As reported in Geneva Paper No. 753.
24. P. H. Miller and B. R. Russell, *Effect of Internal Strains on Linear Expansion, X-Ray Lattice Constant, and Density of Crystals*, J. Appl. Phys. 23:1163 (1952).
25. P. H. Miller and B. R. Russell, *Effect of Distribution of Lattice Defects on Linear Expansion and X-Ray Lattice Constant*, J. Appl. Phys. 24:1248 (1953).
26. J. D. Eshelby, *Geometrical and Apparent X-Ray Expansions of a Crystal Containing Lattice Defects*, J. Appl. Phys. 24:1249 (1953).
27. R. S. Krishnan, *Thermal Expansion of Diamond*, Proc. Ind. Acad. Sci. A24:33 (1946).
28. A. J. Cohen, *Regularity of the F-Center Maxima in Fused Silica and Quartz*, J. Chem. Phys. 22:570 (1954).
29. G. W. Arnold, *Color Centers in Synthetic Quartz*, J. Chem. Phys. 22:1259 (1954).
30. A. J. Cohen, *Impurity Induced Color Centers in Fused Silica*, J. Chem. Phys. 23:765 (1955).
31. G. Mayer and J. Gueron, *Cinetique de la Decoloration de Verres Colores par Irradiation dans la Pile de Chatillon*, J. Chim. Phys. 49:204 (1952).
32. E. W. J. Mitchell and E. G. S. Paige, *On the Formation of Color Centers in Quartz*, Proc. Phys. Soc. B67:262 (1954).
33. M. Levy and J. H. O. Varley, *Radiation Induced Color Centers in Fused Quartz*, Proc. Phys. Soc. B68:223 (1955).
34. P. W. Levy, *Reactor and Gamma-Ray Induced Coloring in Crystalline Quartz and Corning Fused Silica*, J. Chem. Phys. 23:764 (1955).

## RADIATION EFFECTS

35. J. D. McClelland and J. J. Donoghue, *The Effect of Neutron Bombardment upon the Magnetic Susceptibility of Several Pure Oxides*, J. Appl. Phys. 24:963 (1953).
36. J. H. E. Griffiths, J. Owen, and I. M. Ward, *Paramagnetic Resonance in Neutron-Irradiated Diamond and Smoky Quartz*, Nature 173:439 (1954).
37. M. Wittels, *Lattice Expansion of Quartz Due to Fast Neutron Bombardment*, Phys. Rev. 89:656 (1953).
38. M. Wittels and F. A. Sherrill, *Radiation Damage in SiO<sub>2</sub> Structures*, Phys. Rev. 93:1117 (1954).
39. C. M. Nelson, R. L. Sproull, and R. S. Caswell, Phys. Rev. 90:364 (1953).
40. Geneva Paper No. 748.
41. Geneva Paper No. 444.
42. J. H. O. Varley, *A Mechanism for the Displacement of Ions in an Ionic Lattice*, Nature 174:886-887 (1954).
43. J. H. O. Varley, *A New Interpretation of Irradiation-Induced Phenomena in Alkali Halides*, J. Nuc. Energy 1:130-143 (1954).
44. D. E. McLennan, *Study of Ionic Crystal under Electron Bombardment*, Canadian Journal of Phys. 29:122-128 (1951).
45. R. L. Platzman, *On the Primary Processes in Radiation Chemistry and Biology*, Symposium on Radiobiology, John Wiley and Sons, 1952.
46. For a thorough review of radiation effects in semi-conductors see: K. Lark-Horovitz, *Nucleon Bombarded Semi-Conductors*, Reading Conference on Semi-Conducting Materials 47-78 (Butterworths Scientific Publications, London, England, 281 pp., 1951).
47. J. W. Cleland, J. H. Crawford, K. Lark-Horovitz, J. C. Pigg, and F. W. Young, *The Effect of Fast Neutron Bombardment on the Electrical Properties of Germanium*, Phys. Rev. 83:312 (1951); J. W. Cleland and J. H. Crawford, *Neutron Irradiated Indium Antimonide*, Phys. Rev. 95:1177 (1954).
48. Unclassified U.S.A.E.C. reports ORNL-928 and ORNL-1373; Nucleonics 13:28, 51 (1955).
49. A. Charlesby, *How Radiation Affects Long Chain Polymers*, Nucleonics 12:18 (1954); A. Charlesby, *The Crosslinking of Rubber by Pile Irradiation*, Atomics 5:12, 27 (1954).
50. K. Little, *Some Effects of Irradiation on Nylon and Polyethylene Terephthalate*, Nature 173:680 (1954).
51. M. Ross, *Changes in Some Physical Properties of Polyethylene by Pile Irradiation at 80°C*, AERE-M/R-1401 (1954).
52. D. S. Ballantine, G. J. Dienes, B. Manowitz, P. Ander, and R. B. Mesrobian, *Evaluation of Polyethylene Cross-Linked by Ionizing Radiation*, J. Poly. Sci. 13:410 (1954).
53. R. B. Mesrobian, P. Ander, D. S. Ballantine, and G. J. Dienes, *Gamma-Ray Polymerization of Acrylamide in the Solid State*, J. Chem. Phys. 22:565 (1954).
54. This section is based mostly on Geneva Paper No. 746 by Woods, Bupp, and Fletcher. For further details and particularly for atomic interpretations of the experimental observations the reader is referred to Geneva Papers 751, 362 and 442 listed under reference 1. For a summary of the work on graphite in the U.S.S.R. see: V. I. Klimenkov and Y. N. Aleksenko, Proceedings of the Moscow Conference on the Peaceful Uses of Atomic Energy (July 1-5, 1955).

## *Chapter IX*

---

### RADIATION EFFECTS IN FISSIONABLE MATERIALS \*<sup>1</sup>

---

In the two previous chapters we have discussed radiation damage in a rather general way. In this chapter we shall discuss application of these results to fissionable materials, research on and special problems arising in connection with radiation damage in such materials. A fuel material is subjected to both fast neutron and fission fragment damage. Thus, the damage observed is often unusually severe.

#### A. URANIUM AND ITS ALLOYS

Stability of the fuel configuration is perhaps the most important practical problem in the engineering and operation of a heterogeneous reactor. Any general dimensional changes have an important bearing on the nuclear behavior of the reactor and its efficiency as a power producer, and any localized changes may cause local overheating with attendant serious consequences. The fuel materials, therefore, must be fabricated and heat removal must be managed in such a manner as to conserve the lattice arrangement and, in particular, to minimize as much as possible the occurrence of nonreversible changes in the spacings and dimensions of the fuel elements.

Uranium is the only fissionable reactor fuel readily obtainable, and it is,

\* This chapter is based mainly on the following Geneva Papers:

745—S. H. Paine and J. H. Kittel, "Irradiation Effects in Uranium and Its Alloys."

443—S. F. Pugh, "Damage Occurring in Uranium during Burn-up."

681—S. T. Konobeevsky, N. F. Pravyuk, and V. I. Kutaitsev, "Effect of Irradiation on Structure and Properties of Fissionable Materials."

557—H. H. Chiswik and L. R. Kelman, "Thermal Cycling Effects in Uranium."

561—C. E. Weber and H. H. Hirsch, "Dispersion Type Fuel Elements."

679—P. I. Dolin and B. W. Ershler, "Radiolysis of Water in the Presence of H<sub>2</sub> and O<sub>2</sub> due to Reactor Radiation, Fission Fragments and X-Radiation."

quite unfortunately, anisotropic in its properties. Its erratic behavior under thermal cycling and neutron irradiation has made it the object of much study. Of primary interest are the dimensional changes, following discussion of which some data are given on miscellaneous properties changes, such as strength, hardness, thermal conductivity, solid diffusion and corrosion resistance.

**1. Changes in linear dimensions.** A most spectacular effect of irradiation upon uranium metal is manifested by radical changes in dimensions of test specimens. The magnitude of the effect is found to have a close relationship to variables in fabrication technology. Before discussing these, however, it would be well to review briefly what has been learned concerning fundamental behavior, and the theories which appear pertinent to its explanation.

*a. The phenomenon of radiation growth in uranium.* It has been possible to study the basic anisotropy of deformation by irradiating true single crystals of alpha uranium, produced by E. S. Fisher<sup>2</sup> and observing the dimensional changes in the three lattice directions. Figure 1 shows a series of photographs

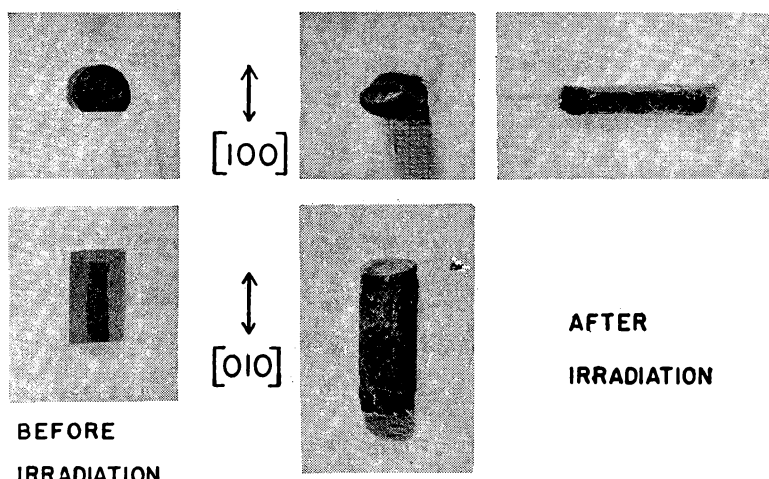


FIG. 1. Aspects of a cylindrical single crystal of alpha uranium before and after irradiation in a reactor (0.1% atom burn-up).

of such a crystal originally nearly a right circular cylinder 0.125 inch (0.32 cm) in diameter. It will be seen that considerable lengthening has occurred and that the circular cross section has become elliptical. Careful measurements after irradiation give the three lattice growth coefficients shown in Table I. The dimensionless unit,  $G_i$ , expressed in microunits of growth per unit length for one fission per million total atoms, has been found convenient to use. Its

TABLE I. COMPARISON BETWEEN THE IRRADIATION GROWTH COEFFICIENTS OF A TRUE CRYSTAL OF URANIUM AND THE THERMAL EXPANSION COEFFICIENT ALONG THE MAJOR CRYSTALLOGRAPHIC AXES IN THE URANIUM LATTICE

Direction Pole	Irradiation Growth Coefficient ( $G_i$ ) <sup>a</sup> ( $10^{-6}$ per part per million burn-up)	Thermal Expansion Coefficient ( $10^{-6}$ per $^{\circ}\text{C}$ ) <sup>b</sup>		
		25-125 $^{\circ}\text{C}$	25-325 $^{\circ}\text{C}$	25-650 $^{\circ}\text{C}$
(100)	$-420 \pm 20$	21.7	26.5	36.7
(010)	$+420 \pm 20$	-1.5	-2.4	-9.3
(001)	$0 \pm 20$	23.2	23.9	34.2

<sup>a</sup> Argonne National Laboratory. Specimen irradiated to 0.1% burn-up at approximately 100  $^{\circ}\text{C}$ .

<sup>b</sup> Battelle Memorial Institute. Computed from x-ray lattice expansion data.

exact value is based upon the well-known exponential relationship between initial and final measurements,  $L_0$  and  $L$ ,

$$G_i = \frac{\log_e (L/L_0)}{\text{Ratio of fissions to total atoms}} \quad (1)$$

For small elongations the following approximation may be used:

$$G_i = \frac{\text{Per cent growth}}{\text{Per cent burn-up}} \quad (2)$$

Imperfect lineage crystals, made by gradient transformation from the beta to the alpha phase, have the same relative behavior under irradiation. They elongate in the [010], shorten in the [100], and remain approximately unchanged in the [001] directions. However, the magnitude of elongation is always greater and the geometric regularity of the distorted specimens is distinctly less than observed in true single crystals.

Cylindrical polycrystalline specimens in which the grains are not randomly oriented also deform under irradiation. They retain their circular cross section, however, if the longitudinal axis coincides with the rolling direction. As will be seen from evidence presented later, the magnitude and character of deformation, including surface distortions, depend upon structural factors. Longitudinal growth rates more than double those measured in single crystals have been observed in highly oriented polycrystalline specimens irradiated at the same temperature. Appreciable shrinkages have also been observed.

*b. Comparison with thermal cycling growth.* Uranium also exhibits marked deformation as the result of thermal cycling. The visual appearance resulting from cycling has a strong resemblance to that of irradiated material, suggesting that the two effects may depend, at least in a measure, on the same basic mechanisms.

Thermal cycling growth has been studied extensively and will be discussed later. Therefore, it will suffice to present only a brief tabulation outlining the respects in which growth by irradiation and by thermal cycling seem to be similar to each other, and also the important respects in which they are known to differ.

Similarities:

1. Irradiation and thermal cycling both induce progressive alterations in the dimensions of polycrystalline uranium specimens. Elongation is the most common manifestation of these phenomena, but shrinkage has also been observed.
2. The characteristic surface distortions—roughening, bumping, etc.—are qualitatively the same for both phenomena.

Differences:

1. Although the direction and magnitudes of the growth phenomena often have a loose correlation, it is by no means consistent. Specimens which elongate in thermal cycling sometimes shrink in irradiation.
2. Irradiation deforms single crystals and lineage crystals as well as polycrystalline uranium, whereas thermal cycling deforms the latter only.

Many ideas have been advanced to explain the basic mechanism of thermal cycling growth, and because of the similarities mentioned above an effort has been made to link this type of deformation to that which occurs during irradiation. It seems advisable to include here comparative data emphasizing some of the similarities observed. The differences in behavior are definitive enough, however, to show that there must be a basic difference in the causative mechanisms.

*c. Fundamental considerations.* In any basic thinking concerning irradiation growth, some primary or predisposing anisotropy of properties must be called upon to permit differential strains, some driving force must be postulated to activate such properties, and there must be cooperating mechanisms which make the strains in some measure irreversible.

*The Role of Thermal Expansion:* In line with this analysis, an obvious choice for consideration as a predisposing anisotropy is the known difference between coefficients of thermal expansion in the three lattice directions (see Table I). Most of the growth theories are based on this property in some

way and postulate as the driving force the high temperature spikes resulting from fission events.

The main differences in thinking relate to the matter of cooperating mechanisms. Thus, J. E. Burke, J. P. Howe and C. E. Lacy,<sup>2</sup> proposed, before the radiation growth of single crystals had been demonstrated, that the fission thermal spikes at grain boundaries activate the same "ratchet" mechanisms which give rise to thermal cycling growth. This model is not disproved by the single crystal results, although inadequate to explain them. It is possible that the accentuated growth of polycrystalline material is due in part to a real effect of this type.

Max Bettman<sup>2</sup> proposed a model which makes elongation of single crystals the result of residual compression stresses in the [010] direction and tension stresses in the (010) plane after the thermal spike cools down. His development does not explain the elliptical deformation noted in the (010) plane of single crystals, although it does account fairly well for their elongation.

A somewhat similar but more extended model has been proposed by J. E. Burke and A. M. Turkalo<sup>2</sup> based on a localized slip mechanism previously discussed by G. A. Last and D. McLachlan.<sup>2</sup> They suggest that the thermal spike volume change buckles the structure perpendicular to the (010) [100] major slip direction in a manner analogous to distortions resulting from ball indentations normal to the basal slip planes of zinc crystals.<sup>3</sup> It is assumed that the [010] expansion would be balanced by [100] and [110] slip and that the deformation would be nonreversing in some measure.

This model makes provision for elliptical deformation of single crystals in the (010) plane, and Bettman's model provides a satisfactory argument for nonreversibility in deformation. Putting these complementary ideas together we have a reasonable growth mechanism based on anisotropy of thermal expansion. It does not depend upon the presence of grain boundaries, and is independent of grain size. However, experimental verification will be exceedingly difficult, and the elementary concepts need further quantitative elaboration.

*The Role of Diffusion:* L. L. Seigle and A. J. Opinsky<sup>2</sup> have proposed a mechanism of dimensional instability which is based upon anisotropic diffusion of displaced atoms and vacancies created in the crystal lattice by fission recoils. The idea that a crystal can suffer alteration of shape due to preferential diffusion was first discussed by Nabarro<sup>4</sup> and later used by Herring<sup>5,6</sup> to explain experimental sintering results obtained by Alexander and Baluffi.<sup>7</sup> Buttner and others<sup>8</sup> have produced additional experimental confirmation.

The theoretical treatment of the alpha uranium lattice by Seigle and Opinsky arrives at the conclusion that interstitial uranium atoms would migrate with some preference for the [010] direction, while vacancies would migrate entirely in the [100] and [001] directions in the computed ratio 5:4.

In fitting this result to the observed behavior of single crystals, the assumption is made that the diffusion of interstitials and of vacancies in the [001] direction is almost exactly balanced; this leaves a net shrinkage in the [100] direction. The theory predicts that the rate of growth in the [010] direction will vary directly with the  $\frac{3}{4}$  power of the neutron flux and the square root of the diffusion coefficient for interstitial atoms. A temperature dependence, of course, should be found. A grain size effect is also expected because of the role of grain boundaries as vacancy sinks; however, it is pointed out that random dislocations and other lattice imperfections are also available as internal sinks.

The anisotropic diffusion model is partly supported by the work of F. W. Kunz and A. N. Holden<sup>2</sup> who showed that the deformation rate of cold rolled uranium foil is greatly reduced when irradiation is done in a liquid air cryostat. Other predictions are capable of experimental check, and will doubtless be subjected to careful test.

*The Role of Grain Boundaries:* Grain boundaries are classically considered as restraints upon deformation mechanisms, hindering the free propagation of strains in polycrystalline structures. In irradiation growth, however, it is apparent that they provide a medium whereby the distortions produced in single crystals may be sharply accentuated. It may be pointed out that this effect is to be expected if the diffusion mechanism discussed above is operative, and it is doubtless true that grain boundary restraints multiply the population of sinks for vacancies and interstitials both at the grain boundaries and within the bodies of the grains. However, in thermal cycling growth the presence of grain boundaries is required in order that the deformation may proceed; moreover, it is evident that the mechanism does not depend upon the anisotropic disposal of large numbers of interstitials and vacancies by diffusion.

Therefore, the inference may be valid that irradiation growth is not entirely a diffusion phenomenon, but may be induced by more than one combination of stress activations with mechanisms of anisotropic strain relief. Thus, the cooperative role of grain boundaries in both irradiation and thermal cycling growth may be identical although the respective driving stresses are dissimilar.

*Twining Mechanism:*<sup>9</sup> Before the results of any single crystal experiments were known a mechanism was developed theoretically at A.E.R.E. Harwell whereby uranium might grow under irradiation.<sup>10</sup> Growth was ascribed to a combination of the effects of fission spikes which cause local expansion of the uranium lattice, and the anisotropic plastic properties of alpha uranium deduced by Cahn<sup>11</sup> from the observed slip and twin systems. This mechanism was used to predict that single crystals of alpha uranium would grow, that the increase in length would be in the [010] direction and that growth would not occur above about 500°C. These predictions have since been confirmed by experiment.<sup>12</sup>

The proposed mechanism is as follows: around the site of fission in a single crystal of alpha uranium there is a region of uniform compressive stress which causes local plastic yielding by twinning, preferentially in the longitudinal [010] direction. When the site of fission cools, the outer region is subjected to a uniform tensile stress and therefore yields plastically, this time in the [100] and [001] directions by twinning. The net result is a local increase in length in the [010] direction of the outer region. In a more recent extension of the mechanism<sup>13</sup> it was suggested that the local extension in the [010] direction throws a stress on the surrounding matrix, which is relieved by equal amounts of slip on both the {110} planes in the appropriate  $\langle 1\bar{1}0 \rangle$  directions to cause extension in the [010] direction. Since tension in the [010] direction produces no resolved shear stress on the (010) plane, slip on this plane does not occur although it is usually the major slip mode. The macro-deformation of the crystal being now by {110}  $\langle 1\bar{1}0 \rangle$  shears the resulting deformation agrees with that found by experiment, in that extension occurs in the [010] direction, contraction in the [100] direction and the [001] direction remains unchanged in length. The direction of the contraction was not specified in the original model except to say that it lay somewhere on the zone passing through the (100) and (001) poles. It has also been realized that the very fine twins lying in the region round the site of fission are unstable, so that when a hot spot due to fission occurs in a finely twinned region the twins anneal back onto the parent lattice. Since annealing takes place by individual atomic migration no change in shape occurs although the crystal is restored to its original twin-free condition. The above model imposes no limit on the extent of growth.

Slip being a reversible process in the geometrical sense, could not be the basis of a ratchet mechanism. It was therefore predicted that growth rates would diminish above 350°C and be practically zero at 600°C because at the higher temperature slip would occur rather than twinning and slip. On the other hand, below 200°C growth diminishes with diminishing temperature due to a corresponding increase in yield strength. Observations on variations of growth rates with temperature<sup>12</sup> are in agreement with these predictions.

Arguments against the twinning mechanism of growth can be based on the supposition that fission spikes are too small or too short in duration to cause plastic deformation. The two recoiling fission fragments will dissipate the energy of fission along a line  $10^{-4}$ - $10^{-3}$  cm long. Calculation indicates that at distances greater than 500 atoms from this line the yield stress will not be exceeded, assuming a yield strength of 4 tons per square inch. According to Cottrell a radius of about 1000 atoms is usually necessary to cause operation of a Frank Read source. The radius of the spike might be increased effectively by two fission spikes sometimes occurring sufficiently close for their stress fields to overlap. For the latter effect to occur a significant number of times the lifetime of the fission spike must be about  $10^{-4}$  second. The heat pulse

## RADIATION EFFECTS

associated with the fission spike is probably dissipated initially at the speed of sound and this part of the energy release is unlikely to cause plastic deformation. A part of the energy release, however, is temporarily stored as interstitials and vacancies which also cause a local expansion and the rate at which these recombine diminishes exponentially with diminishing temperature. A rough estimation indicates that at 600°C recombination is almost as fast as the rate at which the thermal energy is dissipated, but below 500°C, namely in the temperature range in which the growth occurs, the fission spike remains expanded by interstitials and vacancies. In a fission spike about  $10^4$  atoms in length and 500 atoms in radius there are  $10^{10}$  atoms. Since only  $10^5$  interstitials and vacancies are produced per fission, the strain due to the latter at a radius of 500 atoms is only  $10^{-5}$  and is therefore too small to cause plastic flow. If flow occurs, therefore, it must occur very rapidly unless there is some other delaying mechanism, but these objections are not sufficient to allow any definite decision on the validity of the twinning mechanism.

**2. Variables which affect dimensional stability.** We will now consider in greater detail the variables which are found to have an influence upon irradiation growth in uranium. A practical understanding of these is needed in order to predict the over-all behavior of fuel configurations in reactors. It has been found that structure of the metal, its fabrication history and its composition are sensitive variables, as well as the environmental conditions under which irradiation proceeds.

*a. Structural variables.* Early in the investigation of the thermal cycling behavior of uranium it was found that the rolling texture of the material and its grain size had an important bearing upon the character and magnitude

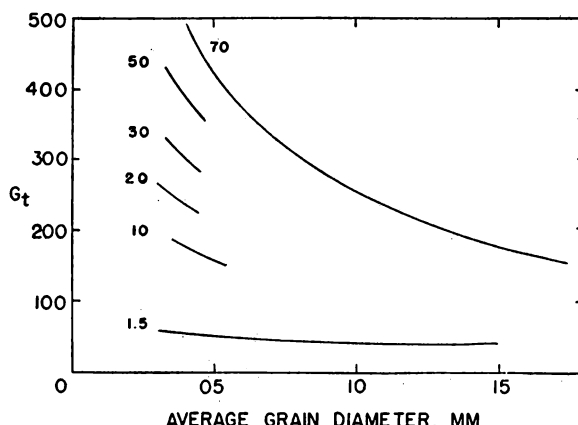


Fig. 2. Combined effect of grain size and cold work upon growth rate ( $G_t$ ) of uranium under thermal cycling. (Curve numbers denote per cent reduction in area by rolling after which the specimens were recrystallized at 575°C,  $G_t$  = micro-in./in./cycle.)

of the effects observed. The relationship between growth and these variables in the case of cold worked (300°C) alpha recrystallized (575°C) material is shown in Fig. 2. The greatest growth for each degree of cold work occurs at the smallest grain size, and the greatest growth for each grain size occurs in the material with greatest preferred orientation. Decrease of growth rate with increase in grain size is quite pronounced, coarse-grained 70% cold worked material being about equivalent in growth to fine-grained 10% cold worked material.

Some of the specimen materials from this study were available for a comparative irradiation growth test. The results are shown in Fig. 3. Scatter

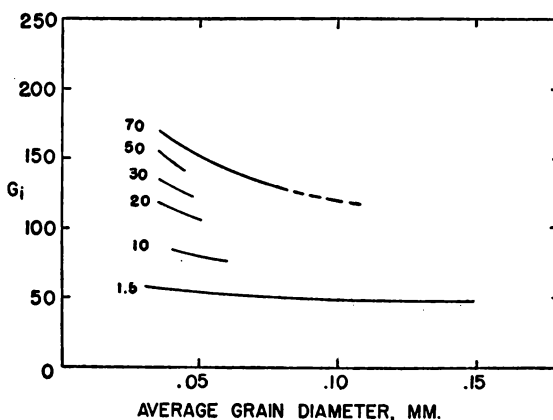


FIG. 3. Combined effect of grain size and cold work upon growth rate ( $G_i$ ) of uranium under irradiation. (Curve numbers denote per cent reduction in area by rolling after which the specimens were recrystallized at 575°C.  $G_i$  = micro-in./in./ppm burn-up.)

of data makes the comparison somewhat uncertain for the coarser grain sizes, but the curve has been drawn to favor the minimum growth numbers. The deduction, therefore, appears valid that as the grain size of 70% cold worked metal is increased, the irradiation growth rate does not decline as rapidly as is the case in thermal cycling. A further comparison is given in Fig. 4, where irradiation growth and thermal cycling growth of fine grain material are shown as functions of cold work. The ordinates have been arbitrarily normalized so that the two effects coincide at 70% reduction in area. Here again it is seen that the phenomena do not exactly correspond. The difference might be described as an inequality in saturation tendencies. It is also observed that changes in degree of cold work are more sharply effective in altering irradiation growth than are changes in grain size.

It should be pointed out that in the figures the ordinates for thermal cycling and irradiation growth are given in  $G_t$  and  $G_i$  units. These are empirical scales

## RADIATION EFFECTS

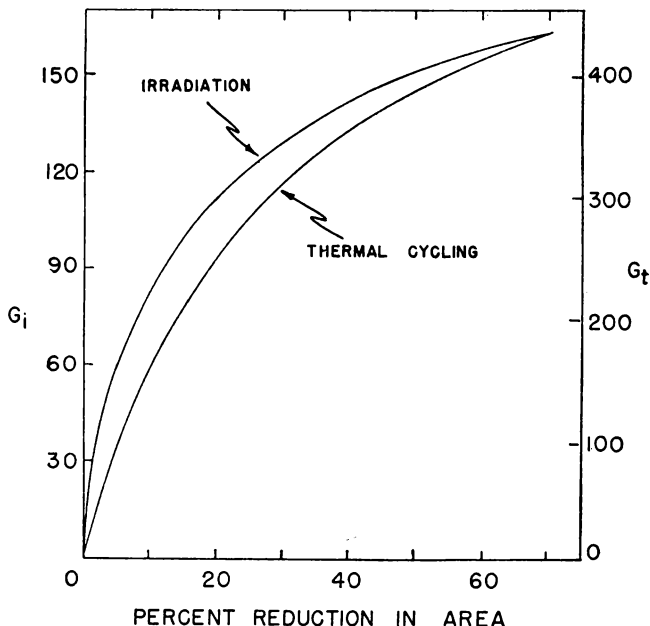


FIG. 4. Effect of cold work upon the irradiation growth rate ( $G_i$ ) and thermal cycling growth rate ( $G_t$ ) of uranium. (Specimens were recrystallized at 575°C before testing.  
 $G_i$  = micro-in./in./ppm burn-up;  $G_t$  = micro-in./in./cycle.)

which have no more than an arbitrary correspondence.  $G_i$  has already been defined in terms of burn-up (Eq. 1), whereas  $G_t$  is given in microunits of elongation per unit length resulting from an arbitrary heating and cooling cycle.

At one time it had been hoped that a direct ratio between the magnitudes of the thermal cycling and irradiation effects might be found so that the effect of burn-up, for example, could be expressed in terms of equivalent thermal cycles. Apparently no simple relationship between the two different units exists, either for variable grain size at constant texture, or for variable texture at constant grain size. The grain size result is not unexpected when it is recalled that thermal cycling growth is entirely dependent upon the presence of grain boundaries, whereas irradiation growth can proceed without them. The texture result is doubtless also a reflection of basic differences in the overall mechanisms of growth.

*b. Fabrication variables.* The magnitude of linear distortion in irradiated uranium is quite sensitive to previous mechanical fabrication procedure and thermal treatment. In general, the effect of these metallurgical factors may be understood in terms of resultant grain size and type and degree of preferred

orientation, structural variables which have been discussed in the preceding section.

Alpha rolling of uranium is successfully accomplished in the range from 300°C (cold work) to 640°C (hot work). The irradiation growth reaction in cold worked and recrystallized material has already been seen in Fig. 4. The starting stock in this experiment had been heated into the beta region and water quenched to produce a moderately fine-grained, random structure so that textures produced by previous fabrication would be erased. This is an important consideration, because the effects of rolling the same material successively at different temperatures are roughly additive. Figure 5 illustrates

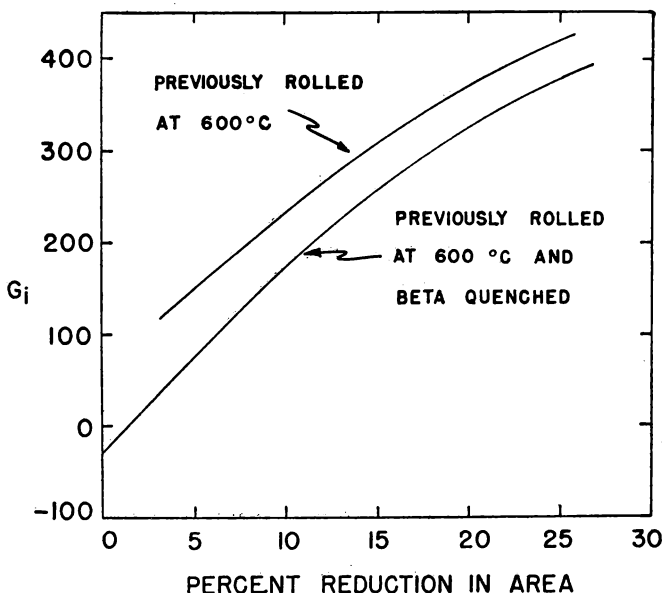
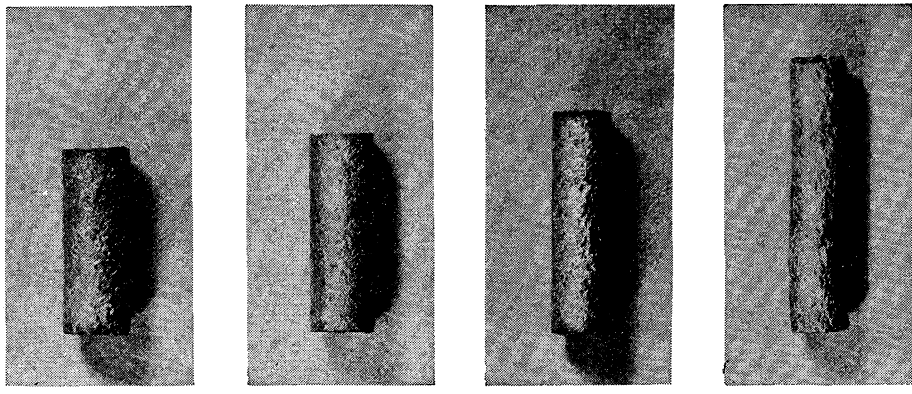


FIG. 5. Effect of additional cold work (at 300°C) on the irradiation growth rate of uranium (previously rolled at 600°C).

the point by comparing the growth resulting from superposing cold work upon previous hot work with that resulting from cold working identical material randomized by beta quenching. Figure 6 shows the beta quenched and cold worked specimens from this test as they appeared after 0.1% burn-up of total atoms.

Before proceeding with a description of the effect of rolling temperature upon growth rate, a comment should be made concerning the rolling technique itself as affected by the behavior just described. It is impossible to conduct a rolling operation strictly at constant temperature. The thermal fluctuations



No cold work.      5% red. at 300°C.      10% red. at 300°C.      25% red. at 300°C.

FIG. 6. Effect of 0.1% atom burn-up on 600°C rolled and beta quenched uranium after further cold work at 300°C.

normally are dependent on degree of reduction per pass, speed of rolling, surface oxidation rate and radiative losses, and may be quite large. As far as irradiation growth is concerned, therefore, each bar may be considered as having been partially rolled at a number of different temperatures, all of these contributing to its final texture and irradiation behavior. Thus, the rolling procedure itself is a variable which has a definite effect upon the reaction of uranium to irradiation.

Cold rolling produces essentially a (010) texture in uranium bar. As the rolling temperature is raised above the recrystallization threshold ( $\sim 400^\circ\text{C}$ ), however, a strong (110) component becomes activated and at higher temperatures even the (100) fiber is brought into play. The original (010) component meanwhile becomes progressively weaker. This means that irradiation growth is greatly attenuated in material rolled at the higher temperatures, and may even become negative. Figure 7 shows this behavior graphically. Irradiation growth coefficients are listed in Table II, together with thermal cycling results for comparison. The bars used in this experiment were carefully soaked at the indicated temperatures before each pass through the rolls, in order to standardize the results as much as possible.

When the roll pass design is changed there is a further variation of irradiation behavior, illustrated by comparing Figs. 7 and 8. The rolling technique was held constant in rolling two identical lots of test bars, but one went through round passes and the other through oval passes. The latter apparently work the material more drastically at higher temperatures than do the former.

The effect of heat treatment has already been mentioned briefly. Beta or gamma recrystallization of alpha rolled material almost completely removes

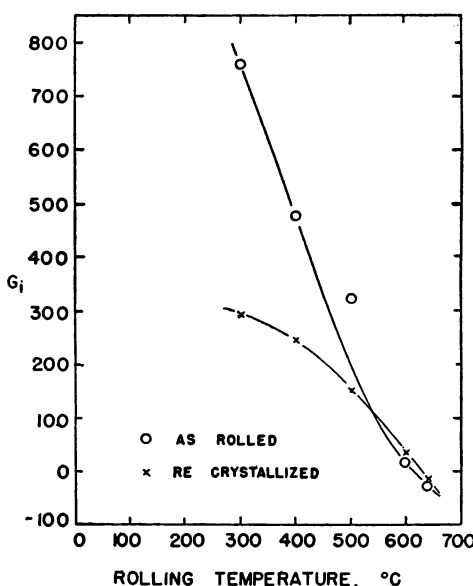


FIG. 7. Effect of rolling temperature on the irradiation growth rate of round-rolled uranium.

TABLE II. GROWTH COEFFICIENTS OF POLYCRYSTALLINE URANIUM ROUND ROLLED TO 75% REDUCTION IN AREA AT THE INDICATED TEMPERATURES

(Compiled from data by R. M. Mayfield, J. H. Kittel and M. H. Mueller)<sup>2</sup>

Rolling Temperature, °C	Subsequent Heat Treatment	Growth Coefficients	
		Irradiation ( $G_i$ )	Thermal Cycling ( $G_t$ )
300	As rolled	—	540
	2 hours at 630°C	294	358
400	As rolled	475	577
	2 hours at 600°C	204	467
500	As rolled	321	519
	2 hours at 600°C	163	446
600	As rolled	4	278
	2 hours at 575°C	6	296
640	As rolled	-22	224
	2 hours at 575°C	-55	183

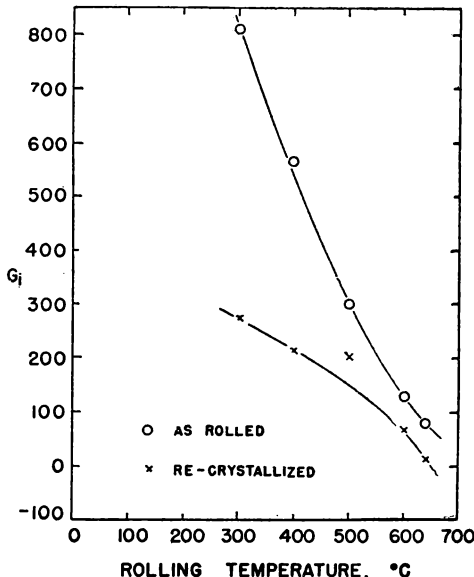


FIG. 8. Effect of rolling temperature on the irradiation growth rate of oval-rolled uranium.

the preferred orientation and reduces the growth rate to  $G_i = 15-20$ . Recrystallization in the high alpha range does not radically modify the texture. The growth rates, however, are appreciably reduced, as shown in Figs. 7 and 8 and Table II. The small shift in texture, coupled with grain coarsening, is probably responsible.

c. *Variations in composition.* It is common metallurgical knowledge that the properties of base metals may be altered and improved by the addition of alloying elements. Uranium is no exception to this principle, and a study of the binary constitution diagrams reveals several ways of inducing such changes.

(1) A composition may be selected which is so low in uranium that the irradiation characteristics of the diluent control the behavior of the alloy. For example, aluminum, beryllium and zirconium are dimensionally stable under irradiation, and continue to be relatively stable in alloys containing uranium as a minor constituent.

(2) In the high uranium alloys, combinations of additives may be sought which by proper heat treatment will refine and stabilize the grain and thereby bring about desirable improvements in the properties of the base metal. For example, one- or two-tenths of a per cent of chromium in uranium permits refinement of the grain so that randomly oriented material has excellent stability under irradiation. Other elements such as molybdenum, niobium

and zirconium, and combinations of two, are equally effective, but the quantities required are somewhat higher. The homogenized compound,  $\text{U}_3\text{Si}$ , is also stable.

(3) In the uranium alloy systems which have large ranges of solid solubility in the gamma phase, compositions may be sought which retain the body centered cubic lattice at room temperatures. The most notable systems of this type are the binaries of molybdenum, niobium and zirconium. Titanium and vanadium in combination with uranium also have large gamma regions. The gamma phase in these systems is not in stable equilibrium at room temperature; therefore, the alloy content must be great enough to inhibit transformation after initial solution heat treatment. For example, approximately 10% of molybdenum in uranium gives excellent dimensional stability when the alloy is irradiated in the gamma condition.

Further details on uranium alloys to illustrate the use of this metallurgical technique for minimizing radiation damage are now given.

*Aluminum-uranium:* One of the first alloy systems to be studied was that of uranium and aluminum containing up to 30% uranium by weight. The microstructure of these alloys is such that at all uranium concentration the aluminum furnishes the continuous matrix and therefore the uranium can be considered as dispersed in the aluminum. There is a eutectic reaction occurring at approximately 13% uranium so that for uranium concentrations near this figure the uranium shows the highest degree of uniform dispersion.

Alloys of aluminum containing 5.7, 15 and 17.2% uranium in the form of strips 9 cm  $\times$  1 cm  $\times$  0.1 cm were irradiated and a series of measurements made after irradiation by S. Siegel and D. S. Billington.<sup>14</sup> No changes as great as 1% were observed in the original dimensions. The changes in electrical resistivity, thermal conductivity and hardness are shown in Figs. 9, 10, 11.

The effect on thermal conductivity and hardness appears to be a function only of the total exposure while the electrical resistivity appears to be influenced by the microstructure. That is, the 5.7% uranium sample microstructure does not permit uniform irradiation of the aluminum matrix by the fission fragments. The increase in hardness and electrical resistivity annealed at approximately the same temperatures is shown in Fig. 12.

The retention of fission gases was measured by collecting the radioactive krypton (10-year half life) as a function of annealing temperature. At temperatures up to 550°C only 0.2% of the krypton present was released and most of this in the first two hours of a 20-hour anneal at each temperature. Complete melting was required to remove all krypton present.

Mechanical property measurements by J. C. Wilson,<sup>14</sup> on the 5.7, 15 and samples previously mentioned show interesting changes. These are as follows: Tensile tests were made on samples of the 5 and 15% alloys. Sharp increases in yield strength (0.2% offset) and in ultimate strength were found with an

## RADIATION EFFECTS

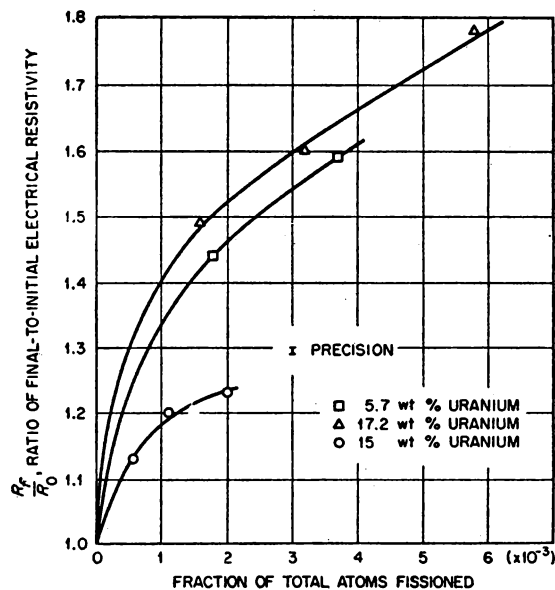


FIG. 9. Effect of fission in aluminum-uranium alloys upon ratio of final-to-initial electrical resistivity.

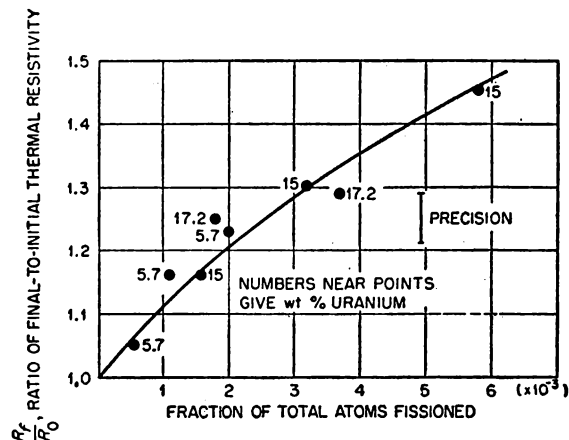


FIG. 10. Effect of fission in aluminum-uranium alloys upon ratio of final-to-initial thermal resistivity.

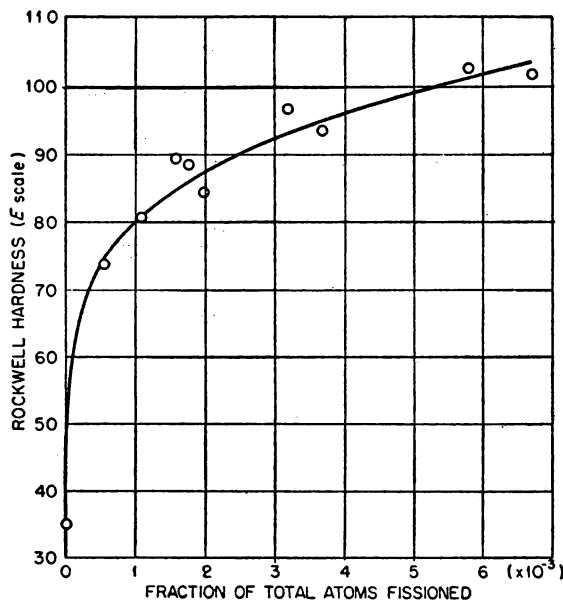


FIG. 11. Effect of fission in aluminum-uranium alloys upon hardness.

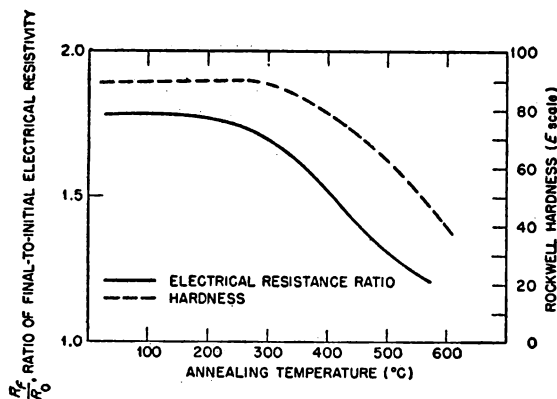


FIG. 12. Annealing of radiation-produced changes of aluminum-uranium alloys.

## RADIATION EFFECTS

attendant loss in ductility. The data are presented in Figs. 13 and 14. It should be observed that in this alloy no serious changes occurred even after

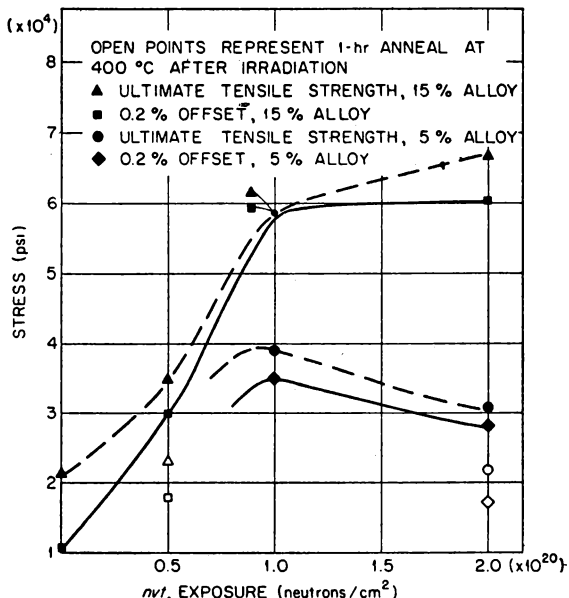


FIG. 13. Effect of fission in aluminum-uranium alloys upon the tensile strength at 30°C.

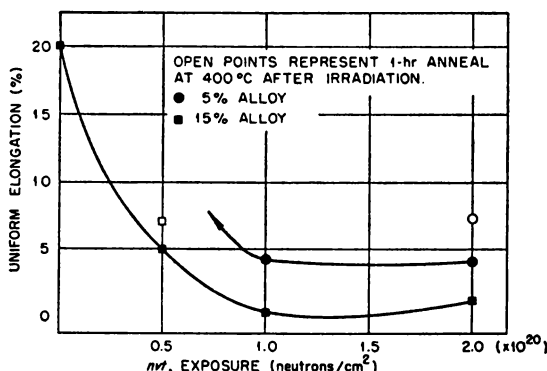


FIG. 14. Effect of fission in aluminum-uranium alloys upon elongation at 30°C.

1 atom in  $10^3$  had fissioned, while in uranium metal severe damage is observed after 1 atom in  $10^4$  has fissioned. This better behavior can be attributed to the dispersion of the uranium in a metal well suited to absorb the damage from the fast neutrons and the fissioning process.

*Beryllium-uranium:* Alloys of beryllium containing 0.5, 1.0 and 3% uranium after 0.06% burn-up of total atoms show an electrical resistivity increase of 1½ to 9%, depending upon the uranium concentration. The changes in dimensions and in density were trivial according to L. S. Castleman, R. T. Jones and W. M. Jones.<sup>14</sup>

*Zirconium-uranium:* Alloys of zirconium-uranium have been studied extensively. There appears to be little change in hardness and in thermal conductivity and the dimensional stability appears good. There does appear to be a density decrease of the order of 1% according to W. E. Johnson, L. S. Castleman and others.<sup>14</sup>

*Chromium-uranium:* C. W. Tucker, Jr. and P. Senio<sup>14</sup> studied the effect of fission on a 2 a/o chromium-uranium alloy and showed that the thermal spike mechanism would not transform the beta quenched phase to the alpha phase nor in the reverse direction for alpha to beta, the time duration of a thermal spike being too short to permit nuclei to grow.

*Uranium-molybdenum:* This alloy has been studied in considerable detail by Konobeevsky, Pravdyuk, and Kutaitshev.<sup>15</sup> A description of their experiments follows. It is pointed out that in some respects the irradiation of uranium is analogous to thermal treatment. This is confirmed by the behavior of an uranium 9% molybdenum alloy. As is known an alloy containing 9% of molybdenum may be in two states. The alloy heated above 600°C and not too slowly cooled is found to be in a homogeneous state of a solid solution of molybdenum in  $\gamma$ -uranium.

Annealing at a temperature below 600°C (for instance, 100 hours at 500°C) brings about its transition into a heterogeneous state eutectoid in the form of a fine mixture of  $\alpha$ -uranium with the intermetallic  $\gamma$  compound.

It was found that, while the specimens of a homogeneous alloy preserve their phase state under irradiation, the specimens of a heterogeneous alloy have become partly or completely homogeneous after irradiation. This is apparent from the following experiment. Wires 60 mm long and 2 mm diameter of an uranium (enriched 5% in U<sup>235</sup>) alloy with 9% of molybdenum were pressed in lead blocks and exposed at the outer temperature of about 50°C to a neutron flux of the order of  $10^{19} nvt$ . The alteration of their properties after irradiation is shown in Table III. It lists changes in density, microstructure, electrical resistivity and temperature coefficient. On the basis of the property measurements and the examination of microstructure the conclusion may be drawn that after irradiation the alloy in wire No. 2 (Table III) has transformed from a heterogeneous to a homogeneous state.

In Table III data are also given on a foil irradiated under conditions completely eliminating any heating above 50°C. In this case a partial transformation to a homogeneous state has occurred. The x-ray diffraction pattern

TABLE III. PROPERTIES AND MICROSTRUCTURE OF URANIUM ALLOYS UNDER IRRADIATION<sup>15</sup>

No.	Heat Treatment	Specific Weight		Specific Electrical Resistivity, ohm mm <sup>2</sup> m <sup>-1</sup>		Thermal Coefficient of Electrical Resistivity × 10 <sup>3</sup>		Microstructure	
		Before	After	Before	After	Before	After	Before	After
1	Quenching (homogeneous state)	17.26	17.23	0.686	0.682	0.01	0.01	Homo-geneous	Homo-geneous
2	Quenching, annealing at 500°C for 100 hr (heterogeneous state)	17.35	17.20	0.531	0.682	1.5	0.01	Hetero-geneous	Homo-geneous
3	The same (as in 2 foil)	—	—	0.523	0.603	1.14	0.39	—	—

(Fig. 15) obtained from a homogeneous specimen of a cold worked foil shows the result of irradiation. It is displayed in a decrease of the width of a line (from 36 mm to 24 mm) and a slight displacement (about 4'-5') corresponding to the relaxation of the first kind of elastic stresses present in a rolled foil.

*d. Irradiation variables.* In general, the growth of uranium specimens under irradiation is found to be an exponential function of the burn-up, which depends upon total integrated flux (see Eq. 1). However, total flux is the prod-

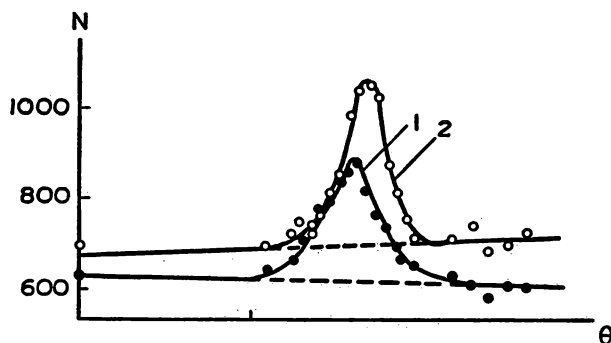


FIG. 15. Lines (112) of x-ray diffraction pattern obtained from uranium alloy with 9% Mo in homogeneous state. (1) Before irradiation. (2) After irradiation.

uct of time and instantaneous flux, which chiefly determines the temperature at which the irradiation proceeds. The higher is the instantaneous flux, the higher also is the burn-up rate and temperature, if other conditions remain constant.

Some of the growth rate data obtained from identical specimens irradiated under different flux conditions when plotted against burn-up have enough scatter to suggest strongly a secondary dependence upon irradiation temperature. The degree of scatter is considerably reduced when a semilogarithmic plot of growth rate against inverse temperature is made (see Fig. 16), although

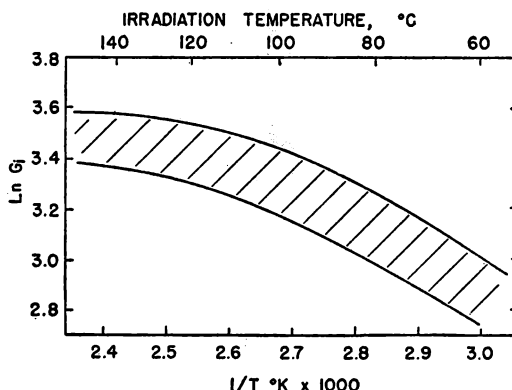


FIG. 16. Effect of irradiation temperature on growth rate ( $G_i$ ) of 300°C-rolled and beta quenched uranium.

a straight-line relationship does not result from this treatment. It is not unlikely that the activation energy required for the growth phenomenon should vary with temperature, as the mechanisms resulting in growth are doubtless in competition with other temperature sensitive healing mechanisms such as recombination of vacancies and interstitials.

There is a great scarcity of accurate data whereby the complete relationship between the irradiation variables and property damage in fuel metals may be deduced, but the effect of temperature will probably prove to be a fruitful field of investigation.

**3. Miscellaneous property changes.** Thus far the discussion has been devoted to the striking changes in dimensions induced in uranium under irradiation. It is understandable that this phenomenon is of primary interest from the engineering viewpoint. Other interesting irradiation effects shall be considered which have been observed, most of them dealing with properties of the metal which have an important bearing on its performance as fuel in a reactor. In general, available information is quite limited and much work

needs yet to be done to complete the understanding of the effect of irradiation upon these properties.

*a. Surface and volume effects.* A second order, but none the less characteristic, result of the dimensional instability of uranium is the distortion of the surface. The roughening becomes progressively worse as burn-up increases, but its distinctive appearance is a function of the grain size and degree of preferred orientation. Figure 17 shows the extremes of this behavior.

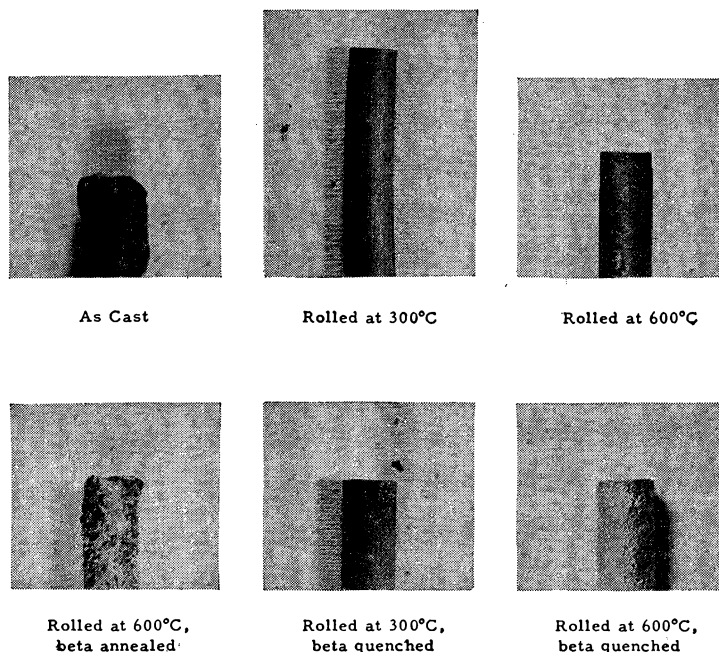


FIG. 17. Relative appearance of various uranium specimens after irradiation to 0.1% atom burn-up.

In large-grain random material, such as gamma recrystallized or as-cast uranium, the surface is distorted by an "orange-peel" effect which is so gross that the contours of the specimen are rapidly destroyed. Fine-grain random material, such as uranium which has had a fast beta cycle and quenching after alpha rolling, roughens with a fine surface irregularity which does not radically change the specimen shape. The effect is intermediate in coarseness for intermediate grain sizes which result from beta annealing or from beta quenching hot rolled uranium.

In alpha worked or alpha worked and recrystallized material the effect is quite different. Although the same dependence upon grain size is shown, the

surface remains much smoother than for comparable random-grained specimens. Roughening is not uniform, but develops as longitudinal striations and ridges into a characteristic woody appearance.

In spite of radical changes in dimensions and shape during irradiation, the volume of uranium specimens experiences only a very nominal shift. This change is remarkably independent of differences in metallurgical history and composition, and is equal in per cent to about twice the burn-up which has occurred. Only half of this change can be accounted for by the creation of fission products. Figure 18 shows the change in immersion density as a func-

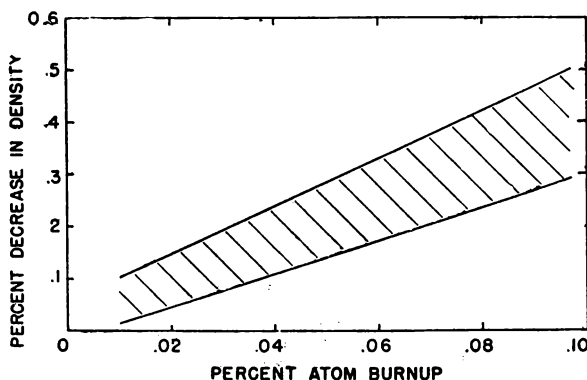


FIG. 18. Decrease in density in uranium and uranium-rich alloys as a function of atom burn-up.

tion of burn-up, and indicates the degree of scatter which has been observed in testing many different specimens.

*b. Metallographic and x-ray behavior.* The metallographic appearance of polycrystalline uranium is altered by irradiation. Whereas the preirradiation structure is fully recrystallized and the grains sharply outlined by polarized light, the structure after irradiation appears to be badly distorted as if by cold work and almost unable to give any distinctive rotation to polarized light.<sup>2</sup> The "cold work" is the result of internal adjustment of the structure by the interference of randomly oriented grains which have been restrained from growing about 50% longer in the [010] direction.

As should be expected, the x-ray structure of equiaxed polycrystalline uranium is also affected by irradiation. C. W. Tucker and P. Senio<sup>2</sup> were the first to identify line-broadening in the x-ray diffraction spectrum, using very lightly irradiated material as the subject of their study. Cummings and Hurst<sup>2</sup> later used a special shielded double crystal spectrometer to examine more heavily irradiated material which had suffered a burn-up of 0.1% of total atoms. Working on cross sections of rolled and alpha recrystallized bar

## RADIATION EFFECTS

they obtained pre- and post-irradiation comparisons from four lines. The degree of broadening is similar to what might be expected from moderate cold working of the structure.

*c. Tensile properties and hardness.* The tensile properties of uranium are strongly affected by moderate irradiation. R. E. Hueschen and J. J. Cadwell<sup>2</sup> report that 0.035% atom burn-up at 120°C is sufficient to decrease the ultimate strength by one-fourth, to double the yield strength, and practically to destroy the ductility of the metal. Data reported by these investigators are presented in Table IV. The ductility is not significantly restored by long-term anneal-

TABLE IV. EFFECT OF IRRADIATION ON THE STRENGTH PROPERTIES OF STANDARD 0.250" DIAMETER URANIUM TENSILE BARS

(Tabulated from data by R. E. Hueschen and J. J. Cadwell<sup>2</sup>)

Description of Specimen	Ultimate Strength		Yield Strength		% Elongation		Young's Modulus, $10^6$ psi
	1000 psi	% Change	1000 psi	% Change	1" Gauge	% Change	
<i>Control specimen</i>	104	—	33	—	17	—	25
<i>Irradiated</i> at 120°C to 0.035% atom burn-up	76	-27	71.5	117	0.36	-97.9	28
<i>Irradiated, annealed</i> 15 hours at 400°C in vacuo	65	-38	52	58	0.54	-96.8	—
<i>Irradiated, hot tensile</i> at 285°C	71	-32	70	112	0.7	-95.9	12

ing at the alpha recrystallization threshold ( $\sim 400^\circ\text{C}$ ), although ultimate strength is attenuated still further by this treatment. These results are believed to indicate that damage to the strength and ductility of uranium by irradiation is in the main due to the presence of fission product atoms as impurities rather than to the disordering of the uranium lattice by thermal spikes.

Appreciable hardness changes occur during the irradiation of uranium. The behavior of rolled and alpha recrystallized metal is a good illustration of this effect. In a large group of tests the average pre-irradiation hardness Vickers Hardness Number  $214 \pm 12$  increases to averages of  $275 \pm 10$  at 0.01% burn-up and  $315 \pm 20$  at 0.10% burn-up. The individual tests in this group were made on the Rockwell A hardness scale and converted to Vickers by use

of a series of uranium test blocks. Hardness changes in as-rolled material are of the same order of magnitude, but with a trend to much greater scatter.

*d. Thermal conductivity.* Of special importance to reactor engineering is a knowledge of the thermal conductivities of fuel materials. This is a difficult property to measure directly with accuracy, and the normal difficulties are greatly aggravated by irradiation of the subject material. For this reason, electrical conductivity measurements are usually taken and considered as an analog from which may be gained a rough idea concerning thermal conductivity changes.

A recent thermal measurement has been made on irradiated material by two teams of investigators: H. W. Deem, G. D. Calkins et al,<sup>2</sup> and S. H. Paine and S. Rothman,<sup>2</sup> using a heat wave method and an equilibrium method, respectively. The results are in good agreement and indicate that a low zirconium alloy of uranium suffers a loss of approximately 5% in thermal conductivity at a burn-up of 0.1% of total atoms. This preliminary result may be taken to indicate the order of magnitude of irradiation-induced change which may be expected in uranium and high-uranium alloys.

*e. Diffusion couples.* Contact of fuel uranium and its alloys with structural metals in the fuel configuration of a reactor is essential. If no barriers exist, such as oxide films, interdiffusion may occur at the proper temperature levels. The possibility that the presence of energetic neutrons and fission product atoms will enhance solid-solid diffusion has been investigated.

Results obtained thus far indicate that the dynamics of uranium-structural metal systems are probably not appreciably affected by irradiation. For example, interdiffusion of uranium-235 with stainless steel at temperatures approaching the eutectic has been shown by R. Weil<sup>2</sup> to be indifferent to the presence of fluxes of the order of  $10^{12}$  neutrons/cm<sup>2</sup>-sec. There are indications that the uranium-aluminum system is equally insensitive. Interdiffusion at elevated temperatures may itself be a serious problem in engineering of the reactor core, but the present data permit the reasonable conclusion that the problem is not aggravated by a radical irradiation effect.

*f. Aqueous corrosion resistance.* The incompatibility of uranium with water is well known. Therefore, much interest has been attached to a search for uranium alloy systems which will resist aqueous corrosion at the reactor temperatures necessary for efficient power production.

The addition of at least 3% niobium or 5% zirconium and proper heat treating is necessary in order to achieve a significant lowering of the corrosion rate. The fully homogenized epsilon U<sub>3</sub>Si compound is also known to have good properties when tested outside of a reactor. However, when such materials are tested after irradiation or while irradiation is proceeding, the corrosion resistant properties are found to be adversely affected at temperatures below 300°C. Gamma-quenched U-Zr(5%)-Nb(1.5%) alloy specimens

## RADIATION EFFECTS

have somewhat better properties in unirradiated tests, but they also are damaged by irradiation so that the corrosion rates are considerably increased. Some comparative data are given in Table V.

TABLE V. EXAMPLES OF PRE- AND POST-IRRADIATION CORROSION RESISTANCE IN URANIUM ALLOYS<sup>2</sup>

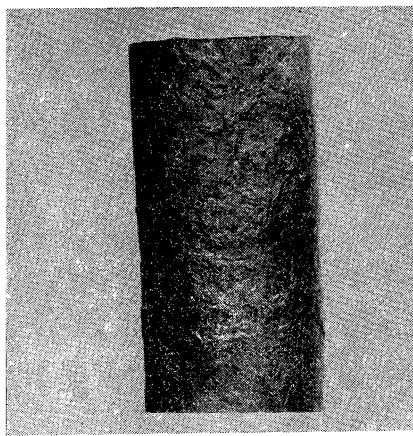
Composition	% Atom Burn-up	Corrosion Resistance (Cracking and Weight Loss)
3% Nb, gamma quenched	None	No failure after 2000 hours at 260°C. Avg. weight loss rate, 4.3 mg/cm <sup>2</sup> -day.
	0.1	Disintegrated after 1 hour at 260°C.
5% Zr-1.5% Nb, gamma quenched	None	No failure after 360 days at 265°C. Avg. weight loss rate, 2.7 mg/cm <sup>2</sup> -day.
	0.04	Cracking after 63 hours at 260°C. Avg. weight loss rate 23 mg/cm <sup>2</sup> -day.

Alloys of uranium containing 9% molybdenum or more have greatly improved temporary corrosion resistant properties. The resistance during test, however, finally ends and sudden failure occurs. After irradiation the behavior is qualitatively quite similar, but the period of time during which the corrosion rates are low is appreciably shortened and the final failure occurs sooner.

It may be concluded that the ability of uranium alloys to resist corrosion is impaired by irradiation. Martensitic zirconium, niobium and zirconium-niobium alloys and the homogenized U<sub>3</sub>Si compound are more adversely affected than molybdenum alloys in which the gamma phase has been stabilized.

**4. Thermal cycling effects in uranium.<sup>16</sup>** In addition to radiation stability, the thermal stability of uranium is of considerable importance in fuel element technology. In this section some of the pertinent experiments will be described.

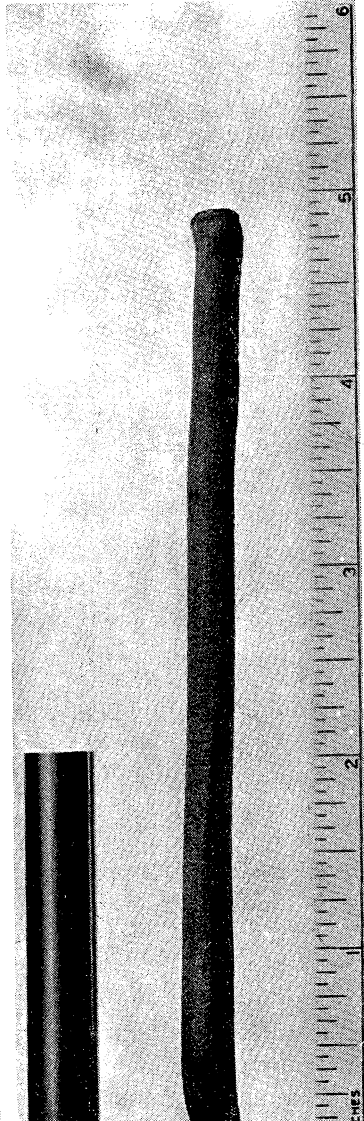
It has been pointed out already that polycrystalline uranium metal undergoes substantial dimensional and structural changes when subjected to repeated heating and cooling in the alpha phase temperature range (room temperature to 660°C). In cast metal the dimensional changes manifest themselves in the form of surface roughening; in wrought metal, such as rolled rod, wire, or plate fabricated in the alpha phase temperature range, the dimensional changes take the form of substantial elongations, generally in directions coincident with the direction of working of the metal. The phenomenon may also be described as "growth." Examples of this behavior are illustrated in Fig. 19, which shows the surface roughening of a smooth cast cylindrical speci-



2X

a. Cast Rod.

300 cycles between 50 and 500°C.



1X

e. 300°C-Rolled Rod.

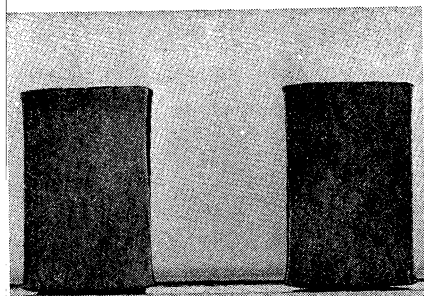
1300 cycles.

3000 cycles.

700 cycles between 100 and 550°C.

Specimens were square before cycling.

Before and after 1300 and 3000 cycles between 50 and 550°C.



1X

b. Rolled Plate:

1/2X

3000 cycles.

Fig. 19. Deformation of uranium specimens on thermal cycling.

men, the growth of some plate specimens, and the growth of a 300°C-rolled specimen to nearly six times its original length when subjected to 3000 thermal cycles between 50°C and 550°C. Accompanying these macro deformations there are also microstructural changes taking place, the chief features of which are a break-up of the grain structure and a development of porosity with a corresponding decrease in density.

The extent of these deformations and structural changes is a function of the number of cycles to which the material is subjected and is dependent upon a number of variables which may be divided into two main categories: (a) material variables, and (b) cycling variables. Among the material variables, the most important are preferred orientation, grain size; and chemical composition; the cycling variables include such considerations as the temperature limits of the cycle, the cycling range, the rate of heating and cooling, and the time of holding at each temperature limit.

*a. Effects of preferred orientation.* That preferred orientation plays a significant role in the process can be demonstrated by a simple experiment as follows: If an alpha-rolled uranium rod which has a well-developed texture and grows considerably is beta-heat treated, the growth rate on thermal cycling is considerably reduced ("beta" heat treatment is defined as heating into the beta phase temperature range followed by cooling to room temperature). By way of example, an alpha-rolled uranium rod may grow at a rate of 500 to 600 microinches/inch/cycle, whereas after beta treatment the growth rate is reduced to about 20 to 30 microinches/inch/cycle. The major effect of the beta treatment is to remove substantially the preferred grain orientations present in the rolled rods. Another example of the effect of preferred orientation on the extent of growth is the experimental observation that 300°C-rolled rods grow at higher rates than 600°C-rolled rods; the reason for this is the development of different textures when rolled at different temperatures. These experimental observations indicate that preferred orientation is a necessary condition for uni-directional elongation to occur and that the extent of the growth depends upon the type of texture present. In randomly oriented material, microscopic plastic deformation of the individual grains also occurs, but it does not result in preferential growth in any given direction.

In addition to the "type" of texture present, the growth rate also depends upon the "degree of perfection" of the texture. In attempting to correlate degree of preferred orientation with growth, however, one is handicapped by the lack of a quantitative number to describe the degree of preferred orientation. In metallurgical research textures are usually described by pole figures, which, at best, are descriptive evaluations of the statistical distributions of the grain orientations. As an alternative, however, one can use the per cent reduction of area following the randomizing beta treatment as a measure of the degree of perfection of preferred orientation. This is illustrated with reference

to a series of specimens that had been rolled to various reductions of area ranging from 3 to 74% following beta treatment, as described in Fig. 20. In

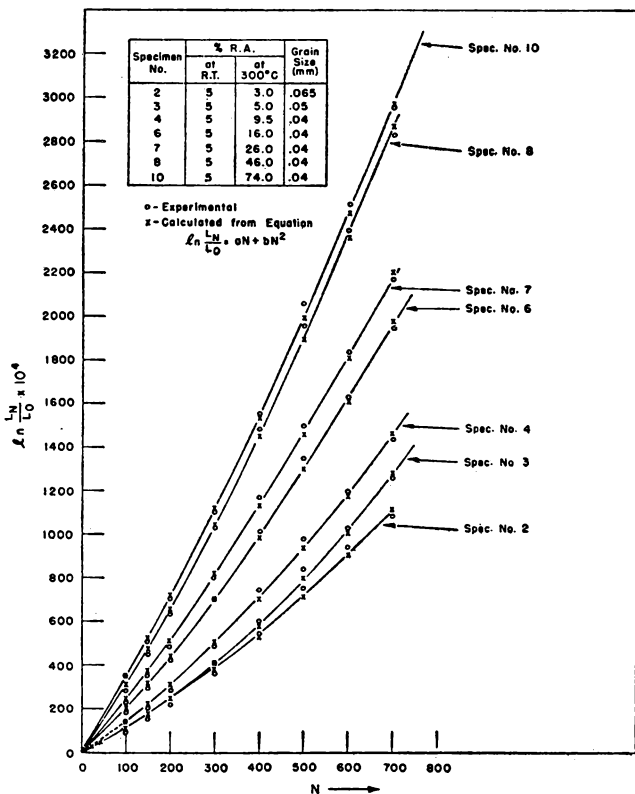


FIG. 20. Plot of  $\ln L_N/L_0$  vs  $N$  for specimens with constant grain size and variable degrees of preferred orientation.

the preparation of such a series of specimens with varying degrees of preferred orientation, care was exercised in heat treatment to maintain the grain size constant.

The specimens were in the form of cylinders, about  $\frac{3}{8}$  in. in diameter and approximately 1 in. long, and were cycled between  $50^\circ\text{C}$  and  $550^\circ\text{C}$  under the following conditions: 5 minutes in the cold temperature zone, 10 minutes in the hot temperature zone, and 5 seconds transfer times between these temperature limits. The growth rates are shown graphically in Fig. 20 by plotting the natural logarithm of the growth ratio  $L_N/L_0$  as a function of  $N$ , where  $L_0$  is the initial length of the specimen,  $N$  is the number of cycles, and  $L_N$  is the length after  $N$  cycles. The "instantaneous growth rate" may be expressed

in terms of the growth coefficient  $G_t$ , which is the slope of the plot  $\ln L_N/L_0$  versus  $N$  ( $G_t = 1/L_N \times dL_N/dN$ ).

The effects of increasing the degree of preferred orientation by increasing the reductions in area are clearly evident in Fig. 20; the growth increased systematically with increasing reductions of area. Specimen #2, which had been rolled to a 3% reduction of area following beta treatment, increased in length 7.8% after 500 cycles, as compared with a growth of 22.9% for specimen #10, which had been rolled to a 74% reduction of area. It cannot be overemphasized that these specific growth rates are valid only for the cycling conditions given above.

X-ray orientation studies of these specimens led to the following observations:

- (1) After slight reductions following beta treatment, the texture was nearly random with only a slight degree of preferredness in orientation.
- (2) As the amount of reduction increased the texture sharpened gradually, with an increase in the concentration of grains having (010) and (131) poles lying in the rolling direction.
- (3) The texture of the specimens with the highest reduction of area (74%) may be described as a fiber texture in which the majority of the grains have (131) poles, or poles close to the (131), lying in the rolling direction, with the remainder of the grains having poles between the (131) and (010) lying parallel to the rolling direction. These x-ray orientation results were in good agreement with measurements of the mean thermal expansion coefficients in the temperature range 25–100°C in the rolling direction and in two mutually perpendicular radial directions. As the reduction of area following beta treatment increased, the expansion coefficients in the rolling direction decreased, with a simultaneous increase in the cross directions; this is what one would expect from a gradual alignment of the (010) poles in the rolling direction, since the [010] crystal direction has a negative expansion coefficient. It should be noted, however, that even at reductions as high as 74% the expansion coefficient in the rolling direction is still substantially positive; this is undoubtedly due to the fact that the texture centers about the (131) pole rather than the (010) pole.

The surface appearance of such a series of specimens with constant grain size and varying preferred orientations after 500 cycles is shown in Fig. 21. Note that the surface roughening decreased as the total elongation of a specimen increased, even though the grain size was the same. It would appear, therefore, that as the tendency toward uni-directional elongation increased, the tendency for surface roughening decreased.

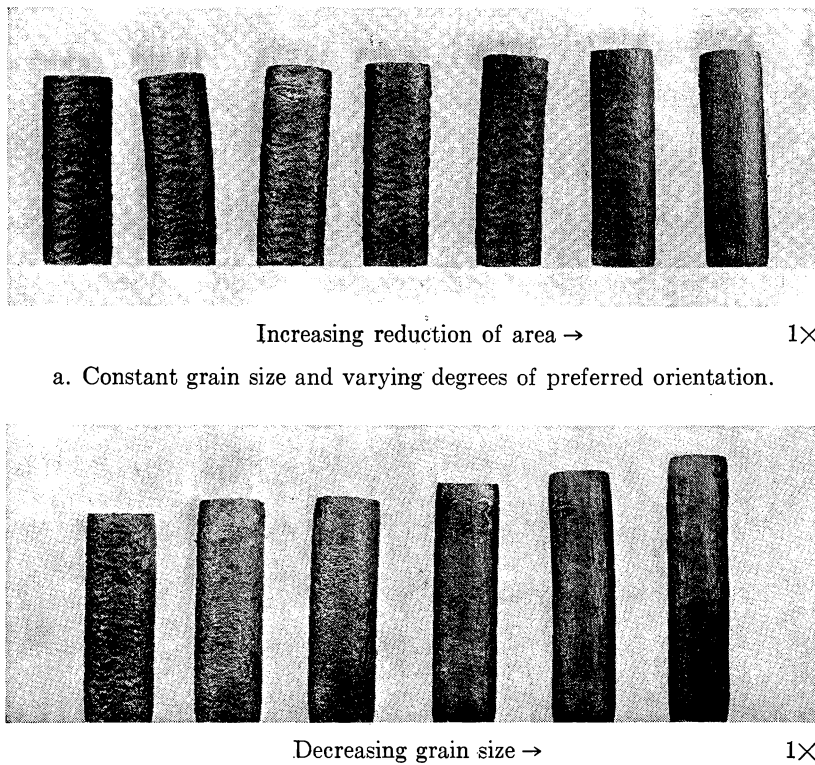


FIG. 21. Macrophotographs illustrating effects of preferred orientation and grain size on growth in 500 cycles. Original lengths all 1 inch.

To exhibit the effect of a change in the "type" of texture present Fig. 22 illustrates the relative growth rates of 300°C-rolled material with a (131)-(010) texture versus a 600°C-rolled material with a (110)-(010) texture. The growth rate of material with the latter texture is considerably lower, although much of this reduction must be attributed to an increased grain size which usually results from higher temperature rolling.

Figure 22 also shows the growth rate of a specimen which has been beta treated, indicating the substantial reduction in the growth rate following such treatment. It will be noted that the growth is not eliminated entirely, even though x-ray studies indicate substantial randomization of the texture. Owing to the large grain size present after beta treatment, however, the experimental conditions for determining textures by x ray do not permit a conclusive evaluation as to the completeness of this randomization. From a macro property point of view, the material after beta treatment becomes essentially isotropic,

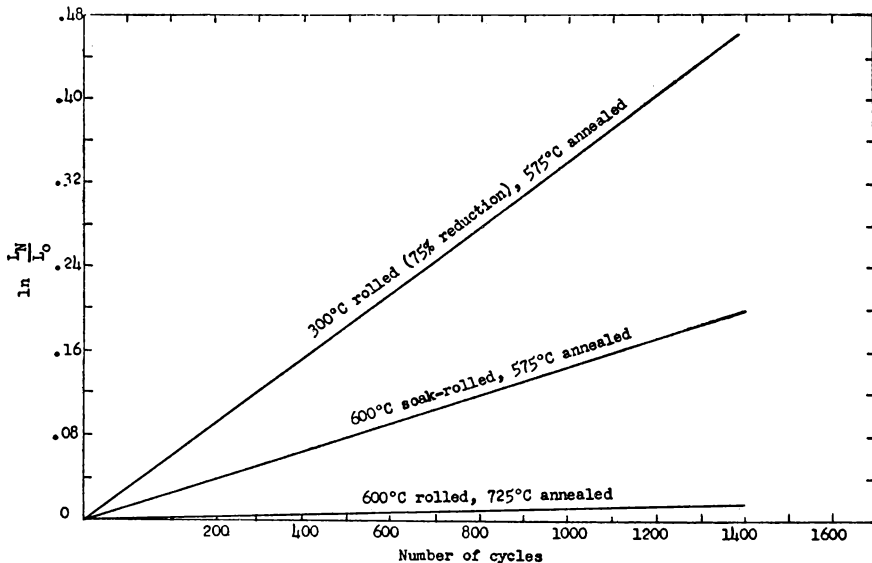


FIG. 22. Elongation of 300°C rolled, 600°C rolled, and beta treated uranium rods due to thermal cycling between 100°C and 550°C.

as evidenced by the fact that the thermal expansion coefficients in all directions are about equal. In view of these considerations, the slight growth of beta-treated uranium may be ascribed to a remnant texture effect inherited from prior fabrication processes which is not completely eliminated in beta treatment.

*b. Effects of grain size.* The influence of grain size on the growth rate may be illustrated with reference to a series of specimens fabricated and heat treated in such a manner as to keep the preferred orientation constant and to vary the grain size. This can be done readily by heavily cold rolling material which had been beta treated, recrystallizing it, then superimposing critical strains ranging from 1½ to 10% at room temperature, and again recrystallizing for various times in the high temperature range of the alpha phase. The growth rates of such a series of specimens of a constant preferred orientation equivalent to a 74% reduction of area and with a grain size variation from 0.01 to 0.18-mm average diameter are shown in Fig. 23. The total growth in 700 cycles increased systematically with decreasing grain size.

It is apparent from Fig. 23 that the growth coefficient increased as cycling progressed, particularly in specimens of large grain size; the variation of  $G_t$  with  $N$  is less apparent when the initial grain size is small. This dependence of the variation of  $G_t$  with  $N$  on the initial grain size may be interpreted qualitatively in terms of the marked structural changes which occur during, and as a direct result of, thermal cycling. A process of subgraining akin to polygonization takes place during cycling, with each grain breaking up into a

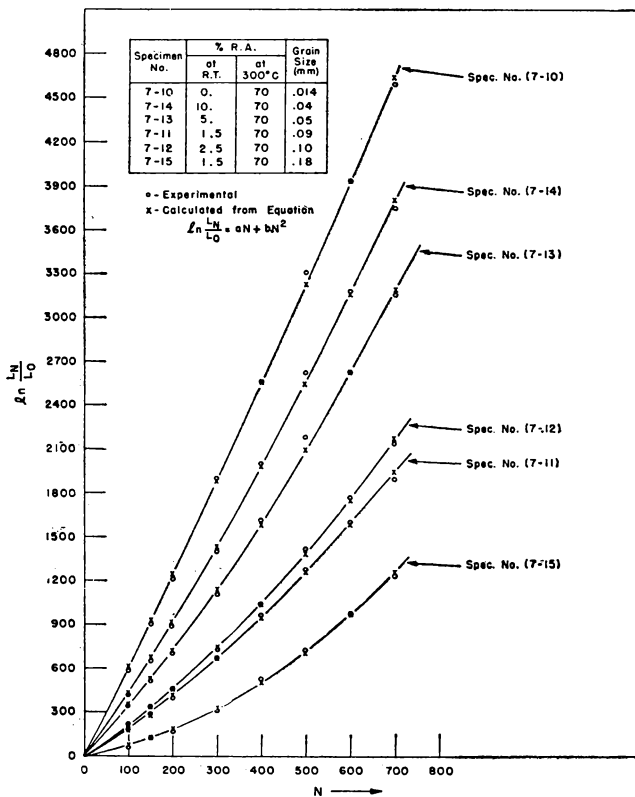


FIG. 23. Plot of  $\ln L_N/L_0$  vs  $N$  for specimens with constant high reduction of area and variable grain sizes.

number of smaller grains differing from each other in orientation by only a few degrees. The process is most pronounced and most readily detectable microscopically in material of initially large grain size. Under conditions of a continuously changing grain size during cycling one would expect an increasing growth rate with increasing cycling level, particularly in initially large-grained material.

c. *Effect of chemical composition.* Additions in low concentrations of alloying elements, such as molybdenum, silicon, aluminum, titanium, zirconium, chromium and vanadium, were found ineffective in appreciably reducing the growth rate of alpha-fabricated uranium. In some cases additions of alloying elements increased the growth rate of alpha-fabricated uranium, but the increase may be interpreted as due to a smaller grain size. Carbon in concentrations up to 500–700 ppm was also found to have no effect; some experimental evidence by Seymour,<sup>16</sup> however, does indicate that higher concentrations of carbon, up to 0.2 w/o, may reduce the growth. The alloy additions

do decrease the surface roughness after a randomizing beta or gamma treatment because they promote grain refinement. To eliminate surface roughness completely, higher concentrations are often required, in some cases as high as 2 w/o.

As shown by experiments on the effect of cycling on the microstructure of uranium, the porosity that develops during thermal cycling appears to be associated with the presence of inclusions. High purity uranium showed no evidence of porosity after cycling, even though its rate of deformation under similar cycling conditions is equal to that of impure metal which developed extensive porosity.

*d. Cycling variables.* The dimensional changes that result from thermal cycling of uranium in the alpha temperature range vary widely with the following cycling variables: (a) rates of heating and cooling, (b) temperature level, (c) temperature range, and (d) time at temperature.

The greatest growth rates per thermal cycle are obtained when slow heating and fast cooling are combined with a large temperature range of cycling. Fast heating and slow cooling result in minimum growth rates, and equal heating and cooling rates, over a wide range of values, yield intermediate growth rates.

With increasing upper cycling temperature, above about 350°C, and constant lower temperature, the growth rate increases. For upper cycling temperatures above about 350°C, the greater the cycling temperature range, the greater the growth. Also, for any given temperature range the higher the temperature level, the greater the resulting growth. Although the growth rate decreases with decreasing temperature range of cycling, appreciable growths can be obtained as a result of exposing highly oriented uranium to many small thermal fluctuations in the high alpha temperature range.

The growth rate is also dependent upon the holding time at the upper cycling temperature. With increasing holding time above about 350°C the growth rate increases rapidly at first and then more slowly until it approaches a constant value. The higher the temperature, the shorter the time required for the growth rate to level off.

*e. Effect of cycling on microstructure and properties.* Accompanying the macro deformations discussed above, thermal cycling results in microstructural changes, the most important of which are: polygonization or subgraining; the development of porosity with an accompanying decrease in apparent density; crystallographic slip; roughening of grain boundaries; and grain boundary migration.

The formation of a subgrain structure is most pronounced and therefore easiest to follow in coarse-grained material. Subgraining develops near grain boundaries in coarse-grained high purity uranium that has undergone relatively few thermal cycles.

In addition to subgraining, crystallographic slip, grain boundary migration, grain boundary roughening, and surface roughening have been observed on a microscopic scale as consequences of the internal stresses developed on thermal cycling. The amount of internal deformation is dependent upon the relative orientations of adjoining grains. Where [010] directions are almost parallel, the deformation is at a minimum and increases with increasing spread between these directions.

It is interesting to note that single crystals of uranium undergo no dimensional changes and show no evidence of internal deformation as a result of thermal cycling in the alpha temperature range.

Another structural change which has been observed on thermal cycling is the formation of voids with a corresponding lower apparent density. The voids are not confined exclusively to grain boundaries; microstructurally, they appear to be associated more closely with inclusions than grain boundaries. This has been demonstrated clearly in a study wherein high purity uranium (10–20 ppm carbon) and uranium containing a relatively large number of inclusions (500 ppm carbon) were cycled 3000 times under similar conditions. Metallographic examinations at various stages of cycling revealed an abundant formation of voids in the impure uranium as compared with practically no detectable voids in the pure uranium, even though both specimens grew extensively.

As regards changes in other properties on thermal cycling the following is pertinent: the thermal expansion coefficient in the range 25–100°C of 300°C-rolled and annealed rods is not altered by 500 thermal cycles between 50 and 550°C, indicating that the degree of preferred orientation is not changed appreciably on cycling. This has been corroborated by x-ray diffraction orientation studies.

*f. Proposed mechanisms.* Several mechanisms have been proposed to account for the phenomenon of growth in uranium. Some of these are based on the fact that the coefficients of expansion of uranium are anisotropic, thus causing a stress to develop across grain boundaries of neighboring grains of different orientations. This circumstance has been proposed by Boas and Honeycombe<sup>17</sup> to account for the plastic deformations they noted in other anisotropic metals. In uranium, however, mechanisms proposed by Boas and Honeycombe are not sufficient, since one has to account for a continuous macro growth in one direction which was not the case in their experiments.

To account for this uni-directional continuous growth Burke, Howe, and Lacy,<sup>18</sup> proposed a so-called "thermal ratcheting" mechanism which makes the deformation irreversible. These authors picture polycrystalline textured uranium to consist of grain couples of different orientations, with stress developed across their boundary. The ratcheting or non-reversibility of the process they picture as resulting from the fact that the stress is relaxed by

slip in the grain that is weaker because of its crystallographic orientation at the low temperatures, whereas at the high temperatures the stress is relaxed by grain boundary flow. In support of such a mechanism they point to the fact that experimentally one can observe grain boundary slip in thermally cycled material like zinc.<sup>18</sup> In essence, therefore, the mechanism pictures one of the grains to be deformed by slip or twinning at the lower temperatures and the stress to be relaxed by grain boundary flow at the higher temperatures, but no slip across the grain boundary taking place at the low temperature. Under such conditions the stronger grain of the couple never suffers plastic distortion in the direction being considered.

Bettman, Brown, and Frankel,<sup>16</sup> have proposed that continued elongation on thermal cycling may occur as a result of creep in the stronger grain of a similar couple at the high temperature part of the thermal cycle, whereas the weaker grain may be deformed plastically in the low temperature part of the cycle. In this model, no flow is assumed to occur at the grain boundary. The amount of creep in the strong grain will be small because the stress in the soft grain will be equally high. Thus, the greater part of the relaxation will occur at the high temperature by creep in the softer grain.

A model has been proposed by Fisher,<sup>16</sup> which attributes the growth to anisotropic diffusion of interstitial atoms and lattice vacancies under thermal cycling.

Mechanisms proposed to account for changes taking place in uranium on thermal cycling do not completely coincide with experimental observations. The anisotropic diffusion mechanism requires that single crystals of uranium show growth which is contrary to experimental fact. The stress-relaxation mechanisms must be able to account for the following: there is no evidence of preferential elongation of grains in the direction of growth as the result of even a large number of cycles; voids that develop as a consequence of thermal cycling are not confined exclusively to grain boundaries, and, in fact, appear to be associated with inclusions; cycling of high purity metal produces no voids; grain boundary slip appears to be a minor effect. Also Bettman, Brown, and Frankel have criticized the Burke, Howe, and Lacy mechanism as being intuitively unsatisfactory for polycrystalline metals because the proposed differential dimensional changes of adjacent grains should be prevented by the surrounding matrix of interlocking grains. The objections to some of the proposed mechanisms might be minimized by resorting to the observed sub-graining as a means of reorientation at grain boundaries in order to accommodate the necessary dimensional changes. This, coupled with diffusion, could account for lack of void formation at grain boundaries.

It is fortunate that some of the methods used to minimize radiation damage and to alleviate thermal effects are the same. Reduction of preferred orientation and increasing the grain size will minimize both effects. Recrystallization

of alpha rolled material in the beta and gamma region reduces radiation damage but has a much smaller effect on thermal growth. Alloying appears to be more effective in reducing radiation damage than thermal growth, at least at low concentrations.

### B. THORIUM AND ITS ALLOYS<sup>14</sup>

There is very little information on thorium and its alloys. Because of its potential use, the available information is described in this section.

The superior isotropic nature of thorium as contrasted with uranium would lead one to expect less radiation damage in thorium. In general, the effects that have been observed thus far do indicate the excellent radiation stability of thorium.

R. H. Kernohan<sup>14</sup> reports no growth and only slight hardness increases after a neutron exposure of  $10^{19}$  neutrons/cm<sup>2</sup>. S. H. Paine and W. F. Murphy<sup>14</sup> confirm the lack of growth and report a hardness increase from 40.5 unirradiated to 67 after irradiation (Rockwell 30T scale) after extensive bombardment. An increase in the yield strength of a factor of two has been reported by J. C. Wilson, R. G. Berggren, and R. E. Adams.<sup>14</sup> However, they report a decrease in impact strength, surprising in a face-centered cubic metal.

Thorium alloys containing 1-5% uranium have been studied by S. H. Paine and W. F. Murphy<sup>14</sup> and by R. M. Carroll.<sup>14</sup> They report only slight changes in dimensions and density with small hardness increases being noted.

### C. DISPERSION TYPE FUEL ELEMENTS

Small compact reactors are now operating at high specific power levels, utilizing enriched uranium as a nuclear fuel. As the specific power of such reactors is increased, the fuel element designer is asked to provide fuel elements capable of withstanding more and more damage due to generation of fission product atoms in the fuel matrix in order to keep the fuel recharging frequency low when the fuel burn-up rate is high. In addition, specific reactor designs call for operation in different coolant media at different ambient temperatures, limiting the choice of fuel media.

**1. Metallic diluents.**<sup>19</sup> Since with highly enriched uranium the U<sup>235</sup> cannot be diluted with U<sup>238</sup> as in natural uranium fuel elements, other diluents must be used. Dispersion type fuel elements are defined as elements in which the fuel is heterogeneous, consisting of a fissile phase dispersed in a continuous matrix of non-fissile material. To minimize radiation damage and provide metallic properties, the diluent must predominate in volume and exist as a continuous matrix surrounding the fissile phase. The matrix metal in effect acts as the structural material in the fuel element.

*a. Radiation damage in a dispersion system.* Data have already been given on the effect of radiation and fast particle bombardment on metals and ionic or molecular compounds. Since fissile phases may consist of metallic, intermetallic, ionic, or molecular compounds, damage may arise through either ionization or displacement of atoms through elastic collision with the fast particles. However, in both cases the major effect will be primarily due to the high energy recoiling fission products. Collision with fast neutrons will be only of secondary importance except in the fission fragment-free regions of the matrix where only the less damaging fast neutrons are available. Therefore, the major damaging effect of fast particle bombardment will be attributed primarily to the motion of fission fragments and will be ascribed to their "dynamic" properties. In fissile material, another significant metallurgical effect will be introduced by the "static" properties of fission fragments as they come to rest in the lattice atoms of the fuel. The total damage is a combination of both the "static" and "dynamic" effects, and it is clear that as higher concentrations of fission products are approached the static effect will predominate. The size and metallic (or non-metallic) properties of the fission product atoms is such that at higher concentrations considerable strain will be introduced in the lattice. The object then in a dispersion type element is to concentrate the damage in the dispersed phase and in a highly localized region

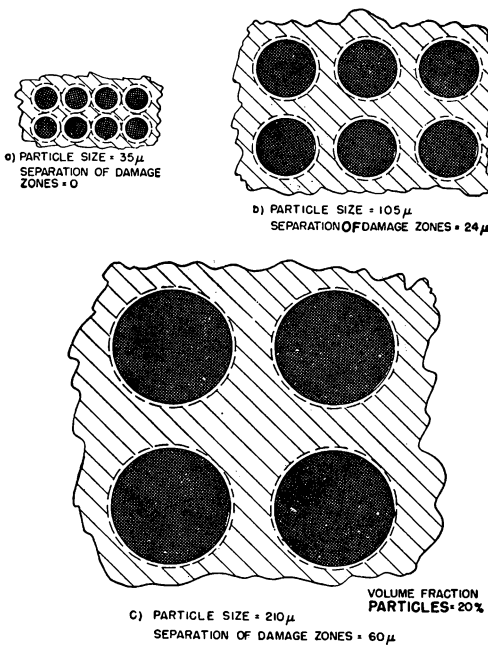


FIG. 24. Damaged matrix regions for a constant volume fraction dispersant.

surrounding the dispersed fissile particle, leaving a fission product-free region of matrix metal around the zone of damage. This objective cannot be achieved in a homogeneous fissile metal or in two-phase alloy systems where both phases may contain fissile atoms.

Schematic cross sections of idealized dispersant systems having a constant volume fraction of fissile dispersant (fixed at 20 volume per cent) are shown in Fig. 24. The dispersed particles are assumed to be spheres in a cubically close-packed array.

Three particle sizes are shown. A spherical zone of damaged matrix metal is shown surrounding each particle. The thickness of the zone is taken as  $\lambda$ , where  $\lambda$ , the range of the fission products in the matrix metal, determines the maximum distance that a fission fragment, leaving normal from the particle surface, can travel into the matrix metal.

For this simplified analysis, the difference in range of the light and heavy fission fragments has been neglected. For convenience, the range of fission fragments in typical materials is given in Table VI.

TABLE VI. RANGE OF FISSION FRAGMENTS IN FUEL MATERIALS

Material	Average Range, mg/cm <sup>2</sup>	Average Range, microns	Average Range, inches
U	12.6	6.8	$2.7 \times 10^{-4}$
UO <sub>2</sub>	10.0	9.4	$3.7 \times 10^{-4}$
Zr	5.8	9.1	$3.6 \times 10^{-4}$
Fe	5.2	6.7	$2.6 \times 10^{-4}$
Al	3.7	13.7	$5.4 \times 10^{-4}$

Referring to Fig. 24, note that while the volume fraction of the dispersed particles is constant, the amount of damaged matrix metal can be varied significantly as the particle size is varied. The damage zones touch for spherical particles 37 microns in diameter and would overlap for smaller particles. For spheres 210 microns in diameter, a significant volume of undamaged matrix metal exists.

It is explicit in the previous discussion of dispersions that thermal diffusion of fission products into the undamaged matrix region does not occur during operation. Certainly at high temperatures, diffusion will occur and may markedly change the properties of both homogeneous and dispersion type fuel media.

An additional advantage of large particles is that a significant fraction of the fission fragments will stop in the particle, whereas with small particles practically all of the fission products will recoil into the matrix metal. The fraction  $P_{(a)}$  of fission products which recoil from a sphere is given by

## RADIATION EFFECTS

$$P_{(a)} = \frac{3}{4} \lambda/a - \frac{1}{16} (\lambda/a)^3 \quad (3)$$

where  $a$  is the sphere radius and  $\lambda$  is the fission fragment range in the dispersed phase. This equation applies for values of  $\lambda/a$  equal to or less than two. With spherical UO<sub>2</sub> particles, the fraction recoiling from particles of different diameters is given in Table VII.

TABLE VII. FRACTION OF FISSION FRAGMENTS RECOILING FROM UO<sub>2</sub> SPHERES

<i>Particle Diameter, microns</i>	$P_{(a)}$
9.4	1.0
19.0	0.69
37.0	0.37
105.0	0.068
210.0	0.034

Through use of large-diameter particles, the damage can be primarily retained in the dispersed particle which in itself need not contribute to the composite strength of the fuel system.

Summarizing these analytical considerations, the design objectives to be achieved in an ideal dispersion system are:

- (1) Dispersed particle size large compared to the fission product range.
- (2) Uniform dispersion of particles in a metal matrix.
- (3) A continuous phase of matrix metal of maximum possible volume fraction.
- (4) High uranium density fissile phase.

Uniform dispersion of a particle of constant diameter cannot be attained in practice, but these idealized considerations can be approximated and serve to indicate the path for progress.

Some experimental results are available, showing that with dispersion fuels the core media is embrittled and hardened at room temperature, as is known to be the case with homogeneous fuels. Typical data on hardening of one of the systems studied, a UO<sub>2</sub>-stainless steel system, are given in Table VIII.

TABLE VIII. HARDENING OF A UO<sub>2</sub>-STEEL MEDIA ON IRRADIATION

<i>Particle Size, microns</i>	<i>Hardness before Irradiation</i>	<i>Hardness after Irradiation</i>
3	225-250 DPH	475-500 DPH
15-44	175-260 DPH	330-440 DPH

The volume fraction of dispersed  $\text{UO}_2$  was 24%. The difference in hardening is small for the two particle sizes studied, since all of the matrix metal is damaged in both cases. Annealing at high temperatures caused little change in post-irradiation hardness, confirming that the "static" effect of the fission products predominated. Data on larger particle sizes are not available at the present time.

**2. Ceramic fuels.<sup>14</sup>** Several studies have been undertaken on mixtures of uranium oxide and a moderator such as graphite or  $\text{BeO}$ .

*a. Uranium-graphite.* L. P. Hunter<sup>14</sup> studied graphite-uranium mixtures that had been prepared in two ways: (1) impregnation of the graphite with an aqueous solution of uranyl nitrate, followed by drying and high temperature firing which converted the uranium to  $\text{U}_3\text{O}_8$  and (2) molded coke pitch and  $\text{U}_3\text{O}_8$  mixture which was baked and fired at high temperature. The latter technique resulted in large particle sizes of  $\text{U}_3\text{O}_8$ .

In-pile thermal conductivity measurements of the two types of samples made at 630–775°C revealed that the thermal conductivity of the impregnated sample was reduced by orders of magnitude while the molded graphite dropped by only one-third. This difference was attributed to a particle size effect. The  $\text{U}_3\text{O}_8$  in the impregnated sample was so finely dispersed that fission recoils were able to damage all portions of the graphite matrix while in the molded sample most of the fission fragments were retained in the  $\text{U}_3\text{O}_8$  particles due to their larger size.

R. H. Kernohan<sup>14</sup> investigated this particle size effect in more detail using samples of molded and baked graphite- $\text{UO}_2$  ranging in particle size from 586 microns to less than 40 microns. After less than 0.01% total atom burn-up he showed that an abrupt decrease in thermal conductivity resulted in the 44 micron particle size samples. An abrupt increase in elastic modulus and electrical resistivity was also observed at this particle size. The results indicated the importance of avoiding complete damage to the matrix material. A suitable size appears to be of the order of 100 microns. Post-irradiation annealing studies up to 750°C showed recovery of most of the neutron damage to the graphite but no recovery of fission damage. Fission damage in the graphite was found to be inversely proportional to the diameter of the imbedded  $\text{UO}_2$  particle.

The work by Gilbreath, Wohlberg, and Simpson<sup>14</sup> on impregnated graphite as a function of total dose showed pronounced changes in dimensions and electrical resistivity. Resistivity changes saturated with continued exposure while dimensional changes did not. Post-irradiation annealing at 1250°C gave recovery of length changes but no recovery of resistivity.

Kierstead and Negy<sup>14</sup> studied elastic modulus as a function of uranium concentration and dosage. They found a 4.7% increase in modulus per milligram of  $\text{U}^{235}$  per gram of graphite for low concentrations. For 16 milligrams

of  $\text{U}^{235}$  per gram of graphite the change saturated at approximately 150% of the original value.

The results on the graphite-uranium mixtures in general reveal serious damage to a number of properties. This appears to result from the undesirable anisotropic nature of the graphite and is to be contrasted to the effects observed in a uranium-aluminum alloy where the properties of the aluminum are well suited for resisting radiation damage.

*b. Beryllium oxide-uranium oxide.* An excellent comprehensive study of the  $\text{UO}_2$ :  $\text{BeO}$  combination was made by J. R. Gilbreath and O. C. Simpson.<sup>14</sup> They studied samples containing 2% and 10%  $\text{UO}_2$ . The largest changes were found in the thermal conductivity which did not saturate after a drop by a factor of six. The linear dimensions increased by 1% while the compressive strength and elastic modulus decreased by 30%.

All these changes occurring after only  $5 \times 10^{-6}$  of the total atoms had fissioned. The difference in uranium content did not result in pronounced differences in the two types of samples. This is regarded as being due to the higher irradiation temperature of the 10%  $\text{UO}_2$  samples. Consequently, some annealing during irradiation may have occurred.

*c. Uranium oxide.* X-ray diffraction studies of irradiated  $\text{U}_3\text{O}_8$  and  $\text{UO}_2$  by Tucker and Senio<sup>14</sup> show pronounced line broadening for burn-up of the order of  $3 \times 10^{-6}\%$ . At a burn-up of  $3 \times 10^{-4}$  the lines in  $\text{U}_3\text{O}_8$  are removed completely according to Chalk River investigators. Presumably the rate of change in  $\text{UO}_2$  is less than in  $\text{U}_3\text{O}_8$ . Other property measurements have not been made on this material. It would appear worthwhile to study them in some detail.

#### D. RADIATION EFFECTS IN LIQUIDS

Radiation effects in liquids properly belong to the field of radiation chemistry.<sup>20</sup> Radiation effects in aqueous systems are, however, of such importance that a brief discussion is in order. Heavy water and light water are both used extensively in reactors as moderators and coolants and it is essential to avoid excessive water decomposition and corrosion of metals in the circuit. There is a great deal of interest in solutions of enriched uranyl salts in water for homogeneous fueled reactors. Liquid metal fuels are also under intensive development. Information on these latter systems is not extensive. In this section some representative studies on the radiolysis of water in a reactor based mainly on the work of Dolin and Ershler<sup>21</sup> will be described.

**1. The rate of the radiolysis of water due to the action of fast neutrons and  $\gamma$  radiation under stationary reactor operation.** The detonating mixture which is generated in a reactor as a result of radiolysis requires a gas circuit to ensure its removal from the liquid. This complicates the design of the reactor. The size of this circuit depends on the rate of radiolysis.

In the first approximation the rate of radiolysis should be proportional to the amount of radiation absorbed by the water and consequently proportional to the reactor power. It may easily be seen, however, that the coefficient of proportionality  $K$ , which may be called the specific rate of radiolysis, is itself a function of power and, in addition, depends on the design of the reactor.

Indeed, as is well known, the specific rate of the radiolysis of water diminishes with concentration of dissolved  $H_2$  and  $O_2$ , and at certain concentrations becomes zero.<sup>22, 23</sup> Therefore, in the absence of impurities, the rate of radiolysis for the water circulating in the reactor must depend upon the concentration of  $H_2$  and  $O_2$  in the water, and must diminish with the concentration. Such a steady-state concentration depends on the rate of degasification of water, i.e., upon the type of equipment; in addition, it will obviously vary with the power and  $K$  will thus become dependent on power.

The character of this dependence may be predicted qualitatively. Indeed, the rate of transfer of a detonating mixture from the liquid to the gas phase, all other conditions being equal (i.e., given the same speed for the circulation of the liquid and of the inert gas), is proportional to the concentration of  $H_2 + \frac{1}{2}O_2$  in the liquid. On the other hand, the total rate of formation of  $H_2 + \frac{1}{2}O_2$  should rise with the power. Since in a stationary state both of these rates must be equal, the steady-state concentration of  $H_2 + \frac{1}{2}O_2$  in the circulating water should also rise with the power. From this it follows that the specific rate of radiolysis of an operating water reactor should fall with increasing power. Data given below confirm this important conclusion.

The experiments were performed on the heavy water reactor of the Academy of Sciences of the U.S.S.R. In it, degasification of the liquid results from circulation through a closed liquid circuit which includes the heat exchanger. During circulation, the liquid comes in contact with a flow of helium. The latter circulates through a gas circuit which has a chamber for the catalytic burning of the detonating mixture. Circulation of the gas may also be achieved when the recombiner is not operating.

The liquid and gas in the reactor were first carefully freed of  $O_2$  and  $D_2$  with the aid of water and helium circulation when the recombiner was working. Simultaneously the content of  $D_2 + \frac{1}{2}O_2$  in the liquid was determined. When the latter fell sufficiently, the reactor was started up and after a definite power was established, the water was periodically analyzed for  $D_2 + \frac{1}{2}O_2$ . Typical curves of gas accumulation in the liquid as a function of operating time are given in Fig. 25. Here the Y-axis is the content of detonating mixture in the liquid, and the X-axis the time from the beginning of the experiment. The initial horizontal sections of these curves give the detonating mixture content in the liquid prior to the beginning of operation of the reactor. The curve rises the moment the power is turned on. The curves show that gas

## RADIATION EFFECTS

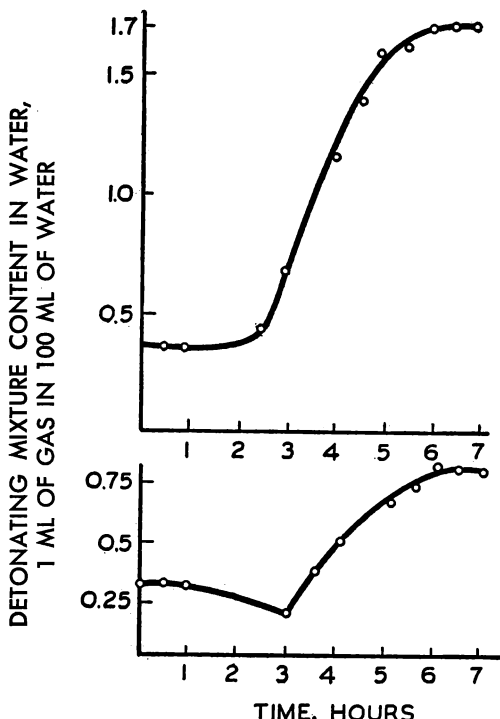


FIG. 25. Variation of detonating mixture concentration in liquid with time at a power of 50 kw (lower curve) and 100 kw (upper curve).

accumulation in the liquid is at first linear with time, and then it slows down and the gas concentration tends to a definite limit, the value of which rises with power.

Table IX gives data on the values of saturation concentrations of a detonating mixture, which were measured at various power levels.

As may be seen from Table IX, the process of radiolysis (depending upon the power and given established operating conditions) takes place in the presence of varied quantities of the dissolved detonating mixture. In evaluating the influence of this factor on the specific rate of radiolysis, the curves of accumulation of the detonating mixture in the liquid and gas phases of the reactor should be considered simultaneously. Such a curve, obtained at 105 kw (when the recombiner was not working), is given in Fig. 26.

From the lower curves it may be seen that accumulation of the detonating mixture in the gas at first proceeds slowly, after which the rate of accumulation increases, and after a period becomes constant. By the time this constant rate has been established, accumulation of the detonating mixture in the

TABLE IX. THE SATURATION OF A DETONATING MIXTURE IN THE LIQUID UNDER VARIOUS OPERATING CONDITIONS

Power, kw	Temperature of Liquid, °C	Content of Detonating Mixture in Liquid, ml of gas per 100 ml of water
38	36	0.85
50	36	1.10
50	60	0.78
100	40	1.69
450	*	3.1

\* The temperature varied considerably during the experiment.

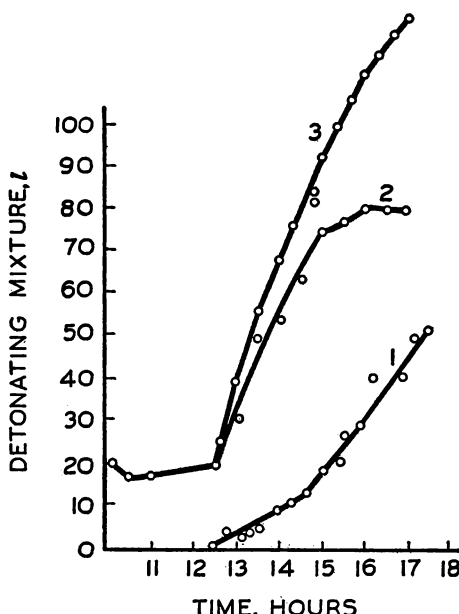


FIG. 26. Accumulation of detonating mixture in liquid and gas at 105 kw. Curve 1: accumulation in gas; 2: in liquid; 3: total accumulation.

## RADIATION EFFECTS

liquid virtually ceases. It is this state that corresponds to a stable operating condition.\*

Table X gives the coefficients  $K$  found from such curves, i.e., the quantity of detonating mixture forming per kwh in the reactor under stationary conditions at various powers. As may be seen from the table  $K$  diminishes sharply with power.

TABLE X. THE DEPENDENCE OF THE SPECIFIC RATE OF RADIOLYSIS  $K$  (THE RATE OF DETONATING-MIXTURE FORMATION IN THE REACTOR IN LITERS/KWH) ON THE POWER

Power in kw	20	50	100	200	400
$K$ (formation rate of $D_2 + \frac{1}{2}O_2$ in liters per kwh)	0.070	0.052	0.048	0.029	0.016

From the initial slopes of the upper curves in Fig. 26 calculations may be also made of  $K$  for a reasonably degassed liquid. The results of such calculations are given in Table XI.

TABLE XI. THE RATE OF DETONATING-MIXTURE FORMATION IN LITERS/KWH IN  
DEGASSED LIQUID

Temper- ature, °C	Power, kw	Accumulation Rate of $D_2 + \frac{1}{2}O_2$ , liters/hour	$K$ Specific Accumulation Rate of $D_2 + \frac{1}{2}O_2$ , liters/kwh
35	50	22	0.44
55	42	17.5	0.42
40	105	36.5	0.35

The values of  $K$  given in the last column of this table depend slightly on the power, as was to be expected. These values are the maximum possible values since they are measured in degassed water. The mean value of this specific rate, 0.4 liters/kwh, should correspond to "initial yields" of gas during radiolysis, which yields are determined in ordinary laboratory experiments with degassed water.<sup>22</sup> Already at 20 kw, the actual specific rate of formation of the detonating mixture in the reactor investigated was considerably below this value. At 20 kw, it is 0.18 of the maximum, and at 400 kw it is only 0.04 of the maximum (see Table X).

\* The steady-state values of concentrations of detonating mixture in the liquid depend, of course, on the efficiency of the system used to remove the gas from the liquid, i.e., on the design of the degassing equipment. The figures given in Table IX refer only to the design studied.

**2. The radiolysis of contaminated water at elevated temperatures.** Since power reactors operate at elevated temperatures and since their construction material is stainless steel, the problem of the radiolysis of water in such conditions is a matter of interest. The literature does not contain any relevant data with the exception of the important work of Hochanadel<sup>24,20</sup> which showed that back-reactions of radiolysis of pure water are accelerated by a temperature rise from 30 to 65°C. In the present work, a qualitative study was made of the influence of temperature on the saturation pressures of the detonating mixture. These pressures arise under the action of reactor radiation and fission fragments in water contaminated with certain impurities.

Since radiolysis of water in the reactor takes place chiefly through the energy of fast neutrons, use was made in these experiments of a neutron converter which increased the portion of fast neutrons in the ampoules undergoing irradiation. The converter was a section of a thick-walled cylindrical uranium pipe 120 mm in length with an inside diameter of 32 mm and an outside diameter of 72 mm. The converter was lowered into the experimental hole of the reactor. The specific rate of the radiolysis of water in the converter, as a number of measurements showed, was of an order of magnitude above the average for the reactor.

The degassed solutions were put into small ampoules which were sealed in a vacuum. In the ampoule, a noticeable gas space (about  $\frac{1}{5}$  of the total volume) was left. The ampoule was then placed in a small aluminum test tube of diameter 12 mm and 100 mm in length. A spiral that could be heated by an electric current was wound around the test tube, which was then placed in the above-mentioned converter. The temperature in the test tube could be raised to 300°C and was measured by a thermocouple. After exposure, the ampoule was cooled, and the pressure of the accumulated detonating mixture was measured by the method of A. O. Allen and co-workers.<sup>25</sup>

Figure 27 gives the results of experiments conducted with 0.001 *M*, 0.01 *M*, and 0.1 *M* HCl at a temperature of 40–50°C. Here, and henceforward, the value of the pressure in the ampoule in atmospheres is plotted as a function of exposure time in hours. The power during these experiments was constant (200 kw) and, therefore, the exposure gives the dose value (in conventional units) directly. The curves show the usual inhibiting influence of impurities on back-reactions, which influence is seen in the rise with impurity concentration of the saturation pressure. In 0.1 *M* HCl, a steady state was not attained at 50°C, even when the pressure of the detonating mixture reached 19 atmospheres.

Figure 28 shows the influence of temperature on the formation of a detonating mixture in 0.01 *M* HCl. The initial section of the curve corresponds to irradiation at 50°C; here the usual linear growth of pressure is found. Section "b" shows that in passing to a temperature of 200°C the pressure begins to

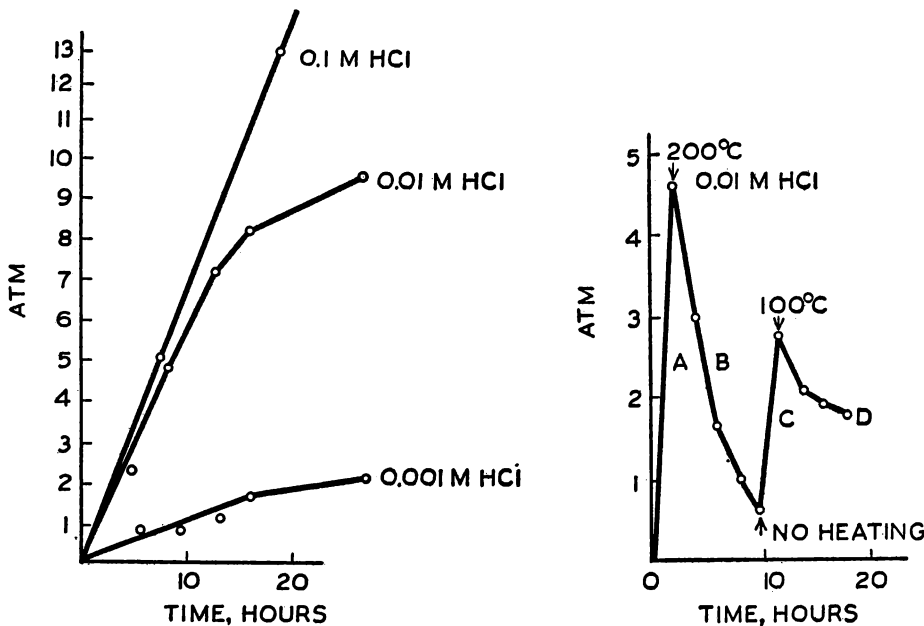


FIG. 27. (Left) Pressure growth during irradiation in solutions of hydrochloric acid.  
FIG. 28. (Right) Influence of temperature on radiolysis of hydrochloric acid solution.

diminish with exposure. In section "c" the temperature is again 50°C and the pressure rises; and finally in section "d" the temperature goes up to 100°C and the pressure again diminishes. Such inhibition of the radiolysis of contaminated water produced by an increase in temperature was observed in the case of all the impurities studied.

Technically, the most important impurities are those of iron, manganese, chromium, and uranium which may get into the water. Figure 29 gives data for solutions of 0.01 M iron sulfate to which 0.1 and 0.5 N sulfuric acid is added to eliminate hydrolysis. In the first case, the pressure reached 3.5 atmospheres, but fell off noticeably at 100°C; as the temperature rose to 200°C it fell to 0.3 atmosphere; in this case, the iron hydroxide is already precipitated. In a more acid solution, the temperature might be raised to 200°C without hydrolysis; in this case also the pressure in the ampoule fell.

Figure 30 gives curve 1 for 0.1 M solution of uranyl sulfate. At 40°C there is a growth in pressure, and at 180°C it falls sharply. The same may be observed in the case of 0.1 M solutions of boric acid (the dotted line).

Curves of pressure increase, obtained for 0.1 M solution of uranyl sulfate, are also of interest when irradiation was conducted without the converter, i.e., directly in the experimental hole. In these conditions heating up to 200°C did not even slow down the pressure rise of the mixture  $H_2 + \frac{1}{2}O_2$  in the

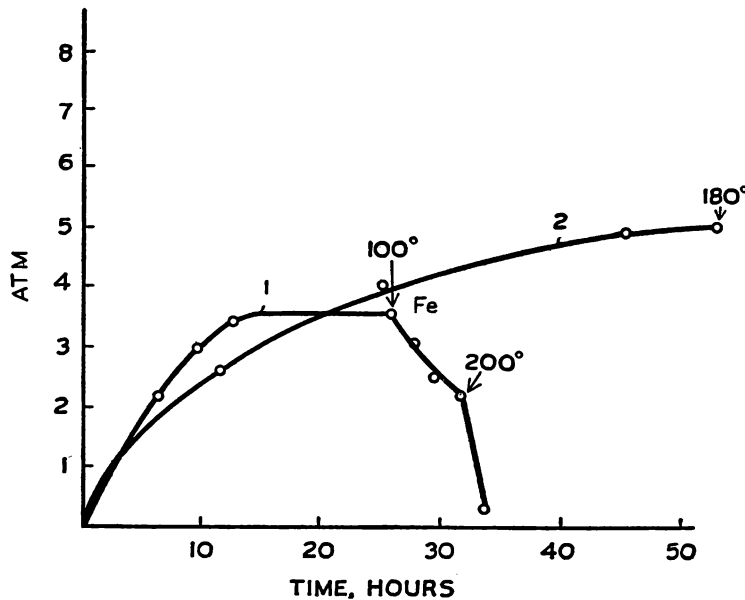


FIG. 29. Influence of temperature or radiolysis of water in the presence of ions of iron. Curve 1: 0.01 M  $\text{FeSO}_4$  + 0.1 N  $\text{H}_2\text{SO}_4$ ; Curve 2: 2 0.01 M  $\text{FeSO}_4$  + 0.5 N  $\text{H}_2\text{SO}_4$ .

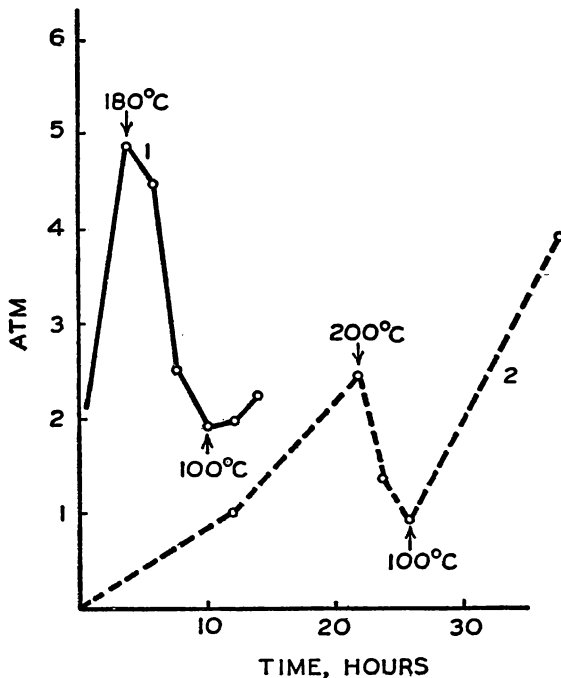


FIG. 30. Influence of temperature on the radiolysis of water in the presence of boric acid and uranyl-ion in the converter. Curve 1: 0.1 uranyl sulfate; 2: 0.1 M boric acid.

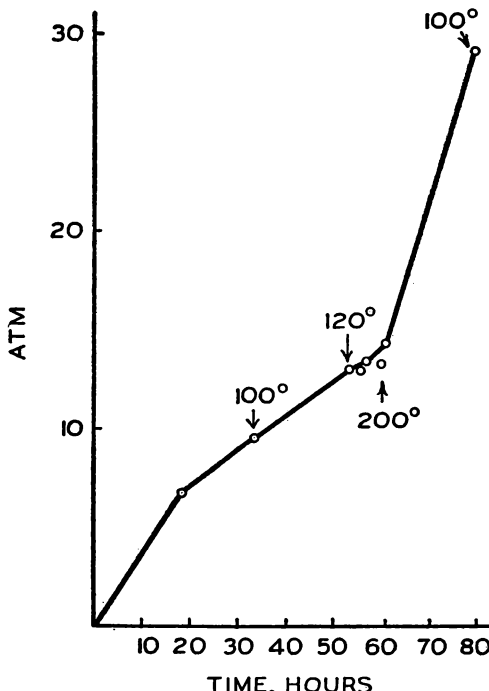


FIG. 31. Radiolysis of 0.1 *M* solution of uranyl sulfate in the experimental hole (outside the converter).

ampoule, although it attained 30 atmospheres (Fig. 31). It should be noted that in these conditions the radiolysis of water in the ampoule is due, to a great extent, to the energy of fission fragments.

The difference in the radiolysis of solutions containing uranium, when they are irradiated in the converter and without it, is due to the fact that the uranyl-ion produces a double action in radiolysis. On the one hand, it inhibits back-reactions as any mixture; on the other hand, it accelerates radiolysis through fission. This latter process increases the saturation pressures. Judging from the behavior of such solutions during irradiation in a converter, when the fission process is relatively slow, the inhibiting action of the uranyl-ion on the back-reactions of radiolysis of water is light. This is confirmed also by experiments at low temperature in the irradiation of ampoules with a solution of uranyl fluoride, containing  $H_2$  and  $O_2$  at a large pressure. These ampoules were wrapped in cadmium foil so that the fission process in them was virtually excluded. The initial pressure of  $H_2$  in these experiments was 5 atmospheres, and of  $O_2$ , 2 atmospheres. As may be seen from Fig. 32, the pressure even in 1 *M* solution of uranyl fluoride during irradiation at 50°C

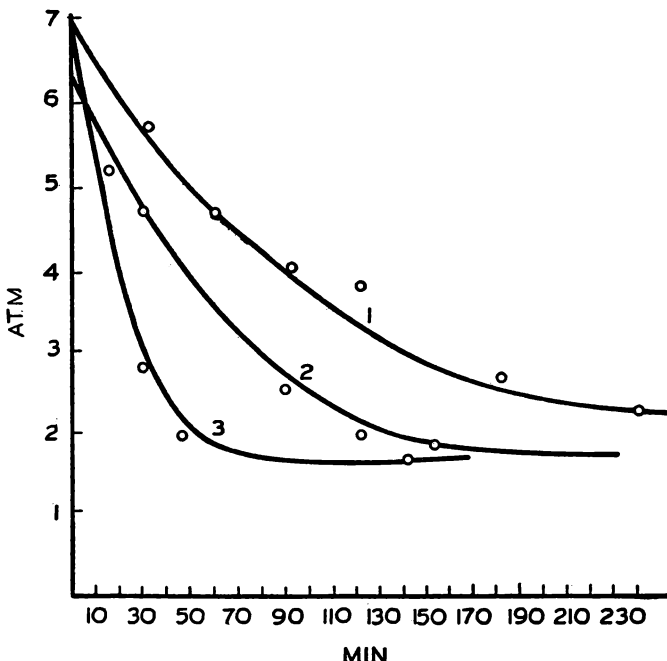


FIG. 32. Recombination of detonating mixture during irradiation of ampoules with solutions of uranyl fluoride wrapped in cadmium foil. Curve 1: 1 M uranyl fluoride; 2: 0.01 M uranyl fluoride; 3: water.

falls, though slowly, to a value close to that attained under these conditions in an ampoule with pure water.

The experiments described above are not quantitative. However, they showed very convincingly that when the water is contaminated with iron, manganese, and chromium (to a content of 100 mg per liter) the saturation pressures of  $H_2 + \frac{1}{2}O_2$  in the liquid at temperatures above 200°C will be of the order of one atmosphere. Since such extreme contamination of water is excluded in actual operation, the saturation pressures of the detonating mixture will be extremely small in heterogeneous power reactors with a temperature above 200°C. The radiolysis scheme in solutions contaminated with uranium is more complicated, since in such solutions it is partly due to the energy of gamma rays and fast neutrons, and partly to fission fragments.

It was also shown that a detonating mixture of a stoichiometric composition does not inhibit reactions of radiolysis due to fragments even at a pressure of 30 atmospheres and a temperature of 200°C. The results of the irradiation of concentrated solutions of uranyl fluoride in ampoules wrapped in cadmium foil show that the uranyl-ion is but a relatively slightly effective impurity

with respect to its inhibitory influence on back-reactions of radiolysis proceeding under the action of fast neutrons.

**3. Effect of radiation on heterogeneous systems of air or nitrogen and water.<sup>26</sup>** Another radiation effect of practical importance has been investigated by Wright and coworkers.<sup>26</sup> Air may leak into a reactor system, and its complete exclusion during periods of maintenance and of fuel rod changing often presents practical engineering difficulties. It is clearly important, therefore, to find out whether acid is produced by the effect of reactor radiation on the heterogeneous system of air and water. Further, in some cases it may be possible to replace the expensive helium normally used in the gas space of low temperature water reactors by nitrogen.

Nitrogen and water, and air and water samples have been irradiated in the Harwell pile, B.E.P.O. Samples were prepared from specially purified water which had been distilled first from alkaline potassium permanganate solution and then from acid potassium dichromate solution to remove organic impurities, and finally distilled from a silica flask and stored before use in silica vessels. Nitrogen was freed from small amounts of oxygen by passage through a column of kieselguhr impregnated with activated copper and maintained at 160°C, resulting in an oxygen content less than 1 part per million. Air was washed successively with concentrated sulfuric acid, concentrated alkali, and purified water, before admission to the irradiation vessels.

In all this work, the irradiation vessels were sealed silica tubes of 2.0 cm diameter and approximately 50 ml volume. These tubes, containing a known quantity of air or nitrogen and a known volume of water, were irradiated for various times in one of the vertical experimental holes of the Harwell pile. The thermal neutron dose to which the tube was exposed was determined from the activity of an accompanying cobalt foil which was measured against a standard cobalt foil of known activity.

Chemical changes resulting from irradiation were determined by analysis of solutions as soon as possible after removal from B.E.P.O. This minimum time was dictated by the radioactivity of the aluminum containers in which the tubes were held, but determinations of the more labile species, such as hydrogen peroxide, were usually completed within 3 hours of the end of irradiation.

For doses up to  $10^{18}$  thermal neutrons/cm<sup>2</sup>, the only products found in solution after irradiation of systems containing water and air or nitrogen were nitric acid and hydrogen peroxide. The hydrogen ion concentration calculated from the measured pH agreed, within experimental error, with that corresponding to the observed nitrate ion concentration. At higher doses, ammonium ion was formed in the nitrogen-water case but not in the air-water systems. Nitrite, hydrazine, and hydroxylamine were not found in concentrations greater than about 2 micromolar under any conditions so far studied.

The concentration of nitrate was found to depend markedly on the ratio of gas volume to liquid volume. The nitrate concentration vs gas-to-liquid volume ratio curves extrapolate to zero concentration at low gas-to-liquid volume ratios, indicating that there is no appreciable reaction in the complete absence of a gas phase. At the lower doses the nitrate concentration is a linear function of the ratio of gas volume to liquid volume to a first approximation, and this suggests that the yield of the radiation chemical reaction is constant if the calculation is based on the energy deposition in the gas phase only while the much greater energy deposition in the liquid phase is ignored. In the air-water system this linear relation persists to higher doses, but linearity breaks down in the nitrogen-water system at the point where ammonium ion production becomes appreciable.

Wright and coworkers conclude that nitric acid production in water reactors to which nitrogen has access may be considerable, and could in certain cases control the size of ion exchange unit required. It is possible to reduce the rate of acid formation by restricting the volume of gas in the radiation field, since reaction occurs only as a result of energy deposited in the gas phase. If the gas space is restricted in this way, it is possible to use nitrogen itself as "blanket" gas in place of the more expensive helium.

#### REFERENCES FOR CHAPTER IX

1. See also portions of the following Geneva Papers:  
744—D. S. Billington, "Radiation Damage in Reactor Materials."  
900—R. Hurst and J. Wright, "Chemical Problems of Power Reactors."  
445—J. Wright, J. K. Linacre, W. R. Marsh, and T. H. Bates, "Effect of Radiation on Heterogeneous Systems of Air or Nitrogen and Water."
2. As described in Geneva Paper No. 745.
3. D. C. Jillson, *An Experimental Survey of Deformation and Annealing Processes in Zinc*, Trans. AIME 188:1009 (1950).
4. F. R. N. Nabarro, *Deformation of Crystals by the Motion of Single Ions*, Rep. Conf. Strength of Solids, Phys. Soc., London (1948), 75.
5. C. Herring, *Surface Tension as a Motivation for Sintering*, Physics of Powder Metallurgy (W. E. Kingston, Editor), p. 143 (McGraw-Hill Book Co., N.Y.C., 1951).
6. C. Herring, *Diffusional Viscosity of a Polycrystalline Solid*, J. Appl. Phys., 21:437 (1950).
7. B. H. Alexander and R. W. Baluffi, *Experiments in the Mechanism of Sintering*, Trans. AIME 188:1219 (1950).
8. F. H. Buttner, E. R. Funk, and H. Udin, *Viscous Creep of Gold Wires Near the Melting Point*, Trans. AIME 194:401 (1952).
9. As described in Geneva Paper No. 443.
10. S. F. Pugh, *The Growth of Alpha-uranium on Irradiation*, unpublished; see Geneva Paper No. 443.
11. R. W. Cahn, *Plastic Deformation of Alpha-uranium; Twinning and Slip*, Acta Met. 1:1, 49-70 (1953).

12. O. S. Plail, *Some Experimental Irradiation Tests on Natural Uranium*, unpublished; see Geneva Paper No. 443.
13. S. F. Pugh, *The Growth, Wrinkling and Fission Product Damage of Uranium and Its Alloys during Irradiation*, unpublished; see Geneva Paper 443.
14. As described in Geneva Paper No. 744.
15. As described in Geneva Paper No. 681.
16. Based mainly on Geneva Paper No. 557 by H. H. Chiswick and L. R. Kelman.
17. W. Boas and R. W. K. Honeycombe, *The Plastic Deformation of Non-Cubic Metals by Heating and Cooling*, Proc. Roy. Soc. London A186:57-71 (1946).  
W. Boas and R. W. K. Honeycombe, *The Deformation of Tin-Base Bearing Alloys by Heating and Cooling*, J. Inst. Metals 73:433-444 (1946-1947).  
W. Boas and R. W. K. Honeycombe, *The Anisotropy of Thermal Expansion as a Cause of Deformation in Metals and Alloys*, Proc. Roy. Soc. London A188:427-439 (1947).
18. J. E. Burke and A. M. Turkalo, *Deformation of Zinc Bicrystals by Thermal Ratcheting*, Trans. A.I.M.E. 194:651-656 (1952).
19. Based on Geneva Paper No. 561 by C. E. Weber and H. H. Hirsch.
20. For some representative papers given at Geneva in this field see:  
738—A. O. Allen, "A Survey of Recent American Research in the Radiation Chemistry of Aqueous Solutions."  
739—C. J. Hochanadel, "The Radiation Induced Reaction of Hydrogen and Oxygen in Water at 25°C to 250°C."  
363—L. Bouby, A. Chapiro, M. Magat, E. Migirdicyan, A. Prevot-Bernas, L. Reinisch, and J. Sebban, "Reactions Chimiques Provoquées par les Rayonnements Ionisants dans Diverses Substances Organiques."  
683—N. A. Bach, "Radiolytic Oxidation of Organic Compounds."  
679—P. I. Dolin and B. V. Ershler, "Radiolysis of Water in the Presence of H<sub>2</sub> and O<sub>2</sub> Due to Reactor Radiation, Fission Fragments and X-Radiation."  
445—J. Wright, J. K. Linacre, W. R. Marsh, and T. H. Bates, "Effect of Radiation on Heterogeneous Systems of Air or Nitrogen and Water."  
900—R. Hurst and J. Wright, "Chemical Problems of Power Reactors."
21. As described in Geneva Paper No. 679.
22. A. O. Allen, J. Phys. Coll. Chem. 52:479 (1948).
23. F. S. Dainton, J. Phys. Coll. Chem. 52:490 (1948).
24. C. J. Hochanadel, J. Phys. Coll. Chem. 56:587 (1952).
25. A. O. Allen, C. J. Hochanadel, J. A. Ghormly, and T. W. Davis, J. Phys. Coll. Chem. 56:575 (1952).
26. As described in Geneva Paper No. 445.

## *Part III*

---

SOLID AND FLUID FUELS



# *Chapter X*

---

## THE TECHNOLOGY OF REACTOR FUELS \*

---

---

Nuclear reactors employed for research and for power production have used at least nine different fuel elements or systems. As many more systems have received detailed study and evaluation. The number of systems under study is still increasing. To make these fuel systems, materials and processes have been devised and improved. Further, a number of important physical, chemical and metallurgical phenomena, some new, have been studied in connection with the production and use of fuels. This chapter will attempt to view this rapidly growing field from the above three aspects and thus discuss the following: (1) The distinct types of fuels; (2) their applications; (3) the requirements on them and their limitations.

### A. SOLID FUELS

The properties and performance of fuel systems are determined in large measure by the bulk material. This obvious assertion serves as the basis for a classification of fuel elements and systems from the point of view of the technology of materials. Solid and fluid systems form two distinct classes, each of which may be subdivided into several families, and so on. Perhaps the central problem in the technology of power reactor fuel systems is to maximize specific power and life, subject to a large number of conditions arising from the type of reactor, the use for the power, and the methods of reprocessing.

**1. Fundamentals.** The anatomy of a solid element is illustrated in Fig. 1. The important phenomena which, in turn, establish the conditions prevailing in the element are as follows: (1) The kinetic energy of the fission recoils is dissipated to the crystal lattice producing effects generally called radiation damage in the manner described by several authors.<sup>1</sup> (2) The fission product

\* This chapter is based entirely on the following Geneva Paper: 825—J. P. Howe, "The Metallurgy of Reactor Fuels."

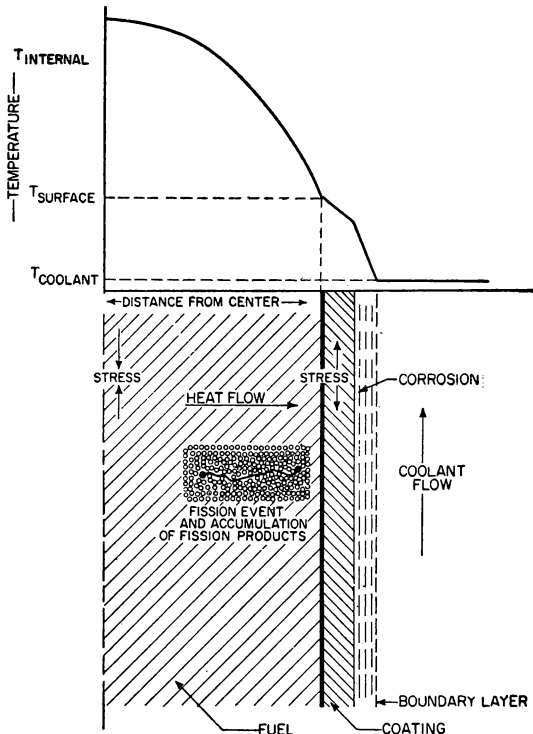


FIG. 1. Diagram of fuel element heat flow, schematic.

atoms either take up positions close to the end of their recoil range in the material or diffuse to the most stable configuration depending on the temperature and the energy of activation for diffusion in the surroundings. Since the atomic volume of the fission product atoms is greater than that of the uranium atom, a corresponding increase in the system volume must be expected at the very minimum. If the temperature is high enough to permit movement of the inert gas fission products, nucleation and growth of gas pockets must be expected at some amount of burn-up. (3) All but a very small fraction of the fission energy appears as heat in the bulk material and flows to the lower temperature coolant. (4) The steady-state temperatures and gradients set up determine: (a) stresses and strains, (b) reactions between jacket and coolant, (c) interdiffusion between bulk material and coating, (d) diffusion of fission products and (e) generally the set of properties of the given systems.

The specific power of an element, defined as the heat rate per unit mass of

fissile materials, e.g. watts per gram, may be limited by one or more of the following:

*a. The nature of the coolant*

(1) Under some practical conditions of gas cooling the heat flux may be determined by surface temperatures. The protective coating may set a limit on this temperature.

(2) Under practical conditions of liquid cooling, boiling of the coolant may limit the heat flux.

For this sort of limitation, the specific power of the element is given by the expression

$$P_s = \frac{2w}{r_0 \rho p} \quad (1)$$

where  $P_s$  = specific power, watts/gram of contained fissile material

$w$  = limiting heat flux, watts/cm<sup>2</sup>

$r_0$  = radius of cylindrical element or thickness of fuel core for a plate element

$\rho$  = density of fuel bearing material

$p$  = weight fraction of fissile material

*b. The temperature gradient*

(1) If the surface temperatures are fixed in a given range by the coolant, then the specific power may be controlled by the maximum permissible central temperature, e.g. the requirement that the central metal temperature not exceed the transformation temperature. In this case

$$P_s = \frac{4K\Delta T}{r_0^2 \rho p} \quad (2)$$

where  $K$  = thermal conductivity of the fuel bearing material, e.g. watts/cm °C

$\Delta T$  = temperature difference center to surface

(2) The stresses set up in the fuel element due to temperature gradients may limit the specific power. The following expression relates these conditions approximately

$$P_s = \frac{8KS_0}{r_0^2 \alpha E \rho p} \quad (3)$$

where  $S_0$  = fracture stress for fuel bearing material

$\alpha$  = thermal coefficient of expansion

$E$  = Young's modulus

(3) Similarly, stresses in jacketing material may limit heat flow. For this case

$$P_s = \frac{2K_j S_j}{r_0 \alpha_j E_j p p r_0} \quad (4)$$

where the subscript  $j$  identifies the quantities defined above with the jacket or coating material and  $r_j$  is the thickness of the jacket.

If a comparison of the specific power of various power systems is desired the average specific power in the core should be used and it is necessary to consider all the fuel in process as well as that in the element.

The last two cases do not define limiting conditions for substances such as metals and ceramics at elevated temperature which yield plastically. If flow occurs the stresses may be relaxed to very low values. However, if the reactor is shut down, the stresses may be set up in reverse. Brittle behavior at low temperatures may then lead to fracture. Even with adequate plasticity and strength for a single cycle, thermal fatiguing is possible after a number of cycles.

The useful life of a solid fuel element may be limited by changes in reactivity of the reactor in which it is used due to burn-up of fissile material and to accumulation of fission products of appreciable cross section or physical changes

TABLE I. METALLIC URANIUM-

Element	Length	Length U Cylinder	Diameter	Coating or Jacket		
				Metal	Thickness	Nature of Fuel-Coating Interface
1. Unbonded Al canned natural U Slug	4.06 in. (10.3 cm)	4 in. (10.2 cm)	1.1 in. (2.8 cm)	Al	0.02 in. (0.05 cm)	No bond drawn fit
2. Ibid.	4.07 in. (10.3 cm)	4 in. (10.2 cm)	1.1 in. (2.8 cm)	Al	0.035 in. (0.09 cm)	Ibid.
3. Ibid.	5 ft-6 in. (168 cm)	5 ft-6 in. (168 cm)	0.85 in. (2.2 cm)	Al	0.059 in. (0.15 cm)	Ibid.
4. Unbonded Al canned finned natural U slug	11 ft (330 cm)	4 in. (10.2 cm)	1.1 in. (2.8 cm)	Al	0.03 in. (0.076 cm)	No bond hydraulic compressed
5. Bonded Al clad natural U slug	4.07 in. (10.3 cm)	4 in. (10.2 cm)	1.36 in. (3.45 cm)	Al	0.035 in. (0.09 cm)	Al-Si bonding material
6. NaK bonded rods	7.5 in. (19.1 cm)	1.9 in. (4.8 cm)	0.364 in. (0.92 cm)	SS	0.022 in. (0.56 cm)	Slugs spaced in stainless steel tube; liquid NaK fills space between fuel and stainless steel cladding
7. NaK bonded rods	266 in. (675 cm)	6 in. (15.3 cm)	0.75 in. (1.9 cm)	SS	0.010 in. (0.025 cm)	Ibid.

in the element due to radiation damage, the accumulation of fission products or any of the conditions described above.

## 2. Fuel types

*a. Metallic uranium base elements.* The several different types of fuel elements in which metallic uranium has been used and the essential features of each are given in Table I. Uranium cylinders protected by aluminum cans produced the first significant amounts of nuclear heat in November, 1943, in the air-cooled graphite-moderated research reactor<sup>2</sup> at the X-10 site of the Plutonium Project, Oak Ridge, Tennessee. These elements, called unbonded aluminum canned slugs, may be made in any convenient size.

The second reactor to produce a reasonably large neutron flux was the heavy water moderated and cooled CP-3<sup>3</sup> set in operation in June, 1944, at the Argonne Site of the Plutonium Project near Chicago, Illinois. It used long uranium rods clad in aluminum tubes fitted by drawing of the cladding onto the uranium. A cross section is pictured in Fig. 2a.

An improved version of the long element, consisting of short slugs closely spaced in a finned aluminum tube filled with slightly pressurized helium to provide for leak detection, is used in the air-cooled graphite-moderated research reactor<sup>4</sup> at the Brookhaven National Laboratory (BNL).

### BASE FUEL ELEMENTS

Final Closure	Reactor	Temperature		Heat Flux, Maximum	Specific Power, Maximum
		Surface	Center		
Seam weld, crimped end	ORNL Air Cooled Graphite	473°F 245°C	660°F 349°C	7300 BTU/hr/ft <sup>2</sup> 2.3 watts/cm <sup>2</sup>	38,400 BTU/hr/lb U-235 24.8 w/g U-235
Shielded arc	Ibid.				
Ibid.	ANL Heavy Water Reactor (CP-3)	110°F 43°C	120°F 49°C	13,300 BTU/hr/ft <sup>2</sup> 4.2 watts/cm <sup>2</sup>	260,000 BTU/hr/lb U-235 168 w/g U-235
Shielded arc and Al-Si brazed	BNL Air Cooled Graphite	660°F 350°C		49,360 BTU/hr/ft <sup>2</sup> 15.5 watt/cm <sup>2</sup>	259,600 BTU/hr/lb U-235 167 w/g U-235
Shielded arc	ORNL Air Cooled Graphite (X-10)	473°F 245°C	660°F 349°C	7300 BTU/hr/ft <sup>2</sup> 2.3 watts/cm <sup>2</sup>	38,400 BTU/hr/lb U-235 24.8 w/g U-235
Ibid.	Experimental Breeder Reactor (EBR)	635°F 335°C	735°F 391°C	756,000 BTU/hr/ft <sup>2</sup> 240 watts/cm <sup>2</sup>	60,000 BTU/hr/lb U-235 38.8 w/g U-235
Ibid.	Sodium Reactor Experiment (SRE)	1000°F 538°C	1200°F 649°C	340,000 BTU/hr/ft <sup>2</sup> 107 watts/cm <sup>2</sup>	643,000 BTU/hr/lb U-235 415 w/g U-235

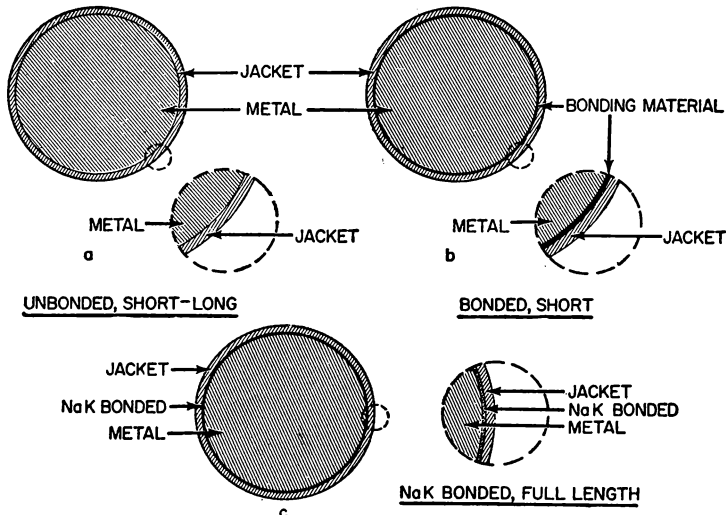


FIG. 2. Schematic cross sections of bonded and unbonded cylindrical type fuel elements.

Bonded uranium cylinders enclosed in aluminum are used in the ORNL Graphite Reactor at the present time.<sup>5</sup> The protective aluminum jackets are brazed to the uranium by means of an aluminum-silicon eutectic alloy. Such elements are called bonded aluminum canned slugs. A cross section is shown in Fig. 2b.

The family of aluminum-clad uranium elements may be used at surface temperatures at which aluminum gives suitable service. In air this is slightly in excess of 300°C. In water conditions of corrosion limit the temperature to near 100°C unless precautions are taken. Recently Draley<sup>6</sup> has found how to achieve tolerable corrosion rates at temperatures approaching 300°C. If the temperature of a clean uranium-aluminum interface exceeds 300°C interdiffusion becomes rapid compared to the life of unbonded fuel elements. In the case of the Oak Ridge unbonded aluminum canned slugs, this interaction occurred at random sites producing bumps which in some cases leaked air permitting destruction of the slug. The aluminum-silicon bonding procedure served to provide a uniform interaction layer which does not thicken significantly with time in the neighborhood of 300°C. Moreover, any leak in the aluminum can provides corroding conditions only in a very localized spot, in contrast to the case of a leak in an unbonded element. The solution of the problem of the aluminum-uranium interaction found at Brookhaven was the interposition of an anodic coating on the inside of the aluminum tube. The detection of leaks through the jacket is assured by a helium pressure monitoring system connected to each element. The maximum temperature of surface and

center and the maximum heat flux in the respective research reactors are given in Table I.

At a given velocity of cooling air, the flux of heat depends on surface temperature of the element. Reasonable air velocities and the accompanying practical pumping power for research reactors, together with the limiting surface temperature tend to limit heat flux to the range noted in Table I; depending, of course, on the expense found acceptable for the cooling system. Thus the air-cooled reactor provides an example of limitation of performance by the nature of the coolant since the surface temperatures are controlling due to oxidation of aluminum in air.

Liquid metal bonded uranium cylinders in steel or other material of reasonable high-temperature strength have been developed and used in a sodium-cooled reactor. The experimental fast breeder<sup>7</sup> reactor built and operated at the National Reactor Testing Station, Arco, Idaho, by the Argonne National Laboratory employed 1-cm diameter highly enriched uranium slugs in stainless steel tubes filled with a sodium-potassium alloy usually called NaK. The sodium-cooled graphite-moderated experimental power reactor<sup>12</sup> under construction near Los Angeles, California, uses  $\frac{3}{4}$ -inch slugs (1.9 cm) of slightly enriched uranium similarly contained. A schematic cross section of such an element is given in Fig. 2c.

The sodium or the sodium-potassium alloy used to cool the above-mentioned elements can provide heat transfer at least at the rate of 500 watts/cm<sup>2</sup> ( $1.59 \times 10^6$  BTU/ft<sup>2</sup> hr) and with corrosion rates less than 0.0001 inch (0.00025 cm)/year at 500°C. Therefore, limitations arise from internal properties of the element.

The chief use of these elements is for power production which favors coolant temperatures near 500°C to obtain high steam plant efficiencies. If the temperatures of the alpha-beta transformation, 660°C, is taken as a limiting central temperature because of the severe distortion which can occur if uranium is repeatedly heated and cooled through the transformation, then an example of limitation under case b (1) above, is provided. The use of uranium alloys may remove this limit.

With steel jackets the limiting surface temperature is lower than the iron-uranium eutectic temperature, 725°C, since near this temperature rapid interaction of jacket with slug would occur at points of contact. The use of zirconium as a jacket or as a barrier layer will obviate this difficulty.

Bonded uranium rods enclosed in zirconium would appear to offer an attractive family of elements for reactor use. The bond between these metals is strong and interdiffusion is acceptably low below 800°C. Such elements have been studied experimentally, for use in the power system, the Pressurized Water Power Reactor.<sup>8</sup>

The use of uranium base elements in a commercial power reactor will require

## SOLID AND FLUID FUELS

as long a life as can be practically obtained in order to reduce reprocessing costs. In thermal neutron power systems neutron reactivity changes limit burn-up to between 1 and 2%. In the case of breeder reactors much higher burn-up is permitted by this consideration. The goal of the materials technologist is therefore set to achieve fuel elements stable to 2% burn-up as a minimum and more if possible. It should also be clear that to increase specific power as much as possible the smallest diameters that can be economically made and handled will be used.

*b. Dispersions of fissile materials in well-behaved metallic matrices.* Aluminum-uranium alloys and the fabrication of fuel elements from them were developed by ORNL and BMI starting in the year 1946. These elements were expressly for use in a high flux reactor for testing reactor materials. The design of this reactor<sup>9</sup> started under E. P. Wigner's direction during the year 1946 and led, after preliminary study, to the proposed use of aluminum fuel elements containing slightly less than 2 a/o U-235 as highly enriched uranium, cooled and moderated with water. Aluminum-uranium alloys of this composition after working and recrystallization have a structure in which a dispersed phase, dominantly  $\text{UAl}_4$ ,<sup>10</sup> is in equilibrium with an aluminum phase containing a very small amount of dissolved uranium.

Details concerning these elements are listed in Table II. Besides serving very effectively in the MTR, this type element is being used in the several swimming pool research reactors now coming into use. The specific power of such elements is limited by the permissible heat flux to the cooling water and is as

TABLE II. DISPERSION OF FISSILE

Matrix	Dispersed Material	Shape	Thickness	Coating Thickness	Width	Length	No. of Plates
Al	$\text{UAl}_4$	Curved plate	0.060 in. 0.14 cm	0.020 in. 0.046 cm	3 in. 6.9 cm	24 in. 55.5 cm	414
Al	$\text{UAl}_4$	Flat plate	0.060 in. 0.14 cm	0.020 in. 0.046 cm	3 in. 6.9 cm	24 in. 55.5 cm	
Al	$\text{UO}_2$						
Stainless Steel (SS)	$\text{UO}_2$	Flat plates	0.030 in. 0.069 cm	0.005 in. 0.012 cm	2.5 in. 5.8 cm	23 in. 53.0 cm	720
Th	U	Cylinder	0.75 in. 1.9 cm	See SS clad NaK bonded U			

\* Conditions calculated.

indicated in Table II. Their life is beyond that permitted by reactivity changes for a reactor and may very well be equivalent to complete burn-up of the fissile material. Environmental conditions permitted will be those for aluminum.

The principle of the aluminum-uranium elements may quite obviously be extended to a variety of systems in which uranium or a uranium compound is dispersed in a solid matrix, the latter chosen for its desired properties which include structural service, corrosion resistance, formability and neutron absorption cross section. These other elements are also listed in Table I.

Aluminum-UO<sub>2</sub> dispersions have been developed recently by Cunningham,<sup>18</sup> and are used in the pool-type research reactor set up at Geneva, Switzerland. Other inert uranium compounds also may be dispersed in aluminum. Performance comparable to the aluminum-uranium elements may be expected.

Austenitic steel-UO<sub>2</sub> dispersions have similarly been developed for small water cooled and moderated power plants. Again performance limits are probably beyond those required by practicable reactor systems. In a high power, high temperature system, thermal fatigue probably places a limit on the number of times a reactor may be started and stopped. S. R. Vandenberg and L. R. Coffin<sup>11</sup> show that at 400°C stainless steel will fail after a few hundred cycles at bending or thermal stresses corresponding to a heat flux of 300 watts/cm<sup>2</sup> through a thickness of 0.01 inch (0.025 cm).

Thorium-uranium cylinders contained in NaK or Na filled steel tubes may serve in power reactors such as the sodium-cooled graphite<sup>12</sup> moderated re-

#### MATERIALS IN WELL-BEHAVED MATRICES

Method of Assembly	Reactor	Maximum Temperature		Maximum Heat Flux	Maximum Specific Power
		Surface	Center		
Sides brazed into slotted Al plates	Materials Testing Reactor	240°F 116°C	— —	$6.1 \times 10^5$ BTU/hr/ft <sup>2</sup> 195 watts/cm <sup>2</sup>	$1.5 \times 10^7$ BTU/hr/lb U-235 9400 watts/gm U-235
Similar	ORNL Research Reactor pool type	200°F 93°C	— —	$1.0 \times 10^5$ BTU/hr/ft <sup>2</sup> 32 watts/cm <sup>2</sup>	$3.1 \times 10^6$ BTU/hr/lb U-235 2000 watts/gm U-235
	Pool Type Reactor Geneva, Switz.				
Brazed into SS assembly	Pool Type Research* Water Cooled Power Reactor*	554°F 290°C	566°F 297°C	$2.2 \times 10^5$ BTU/hr/ft <sup>2</sup> 70 watts/cm <sup>2</sup>	$3.1 \times 10^6$ BTU/hr/lb U-235 2000 watts/gm U-235
	Sodium Graphite Reactor*	960°F 516°C	1600°F 871°C	$8.5 \times 10^5$ BTU/hr/ft <sup>2</sup> 274 watts/cm <sup>2</sup>	$1.08 \times 10^6$ BTU/hr/lb U-235 694 watts/gm U-235

actor. Details of the optimum degree and method of dispersion of the approximately 4 w/o U-235 required are not solved but estimated performance of such elements is good. Central temperatures at least as high as 1400°C, the  $\alpha$ - $\beta$  transition temperature, should be permitted thus allowing the maximum specific power to be 720 watts/cm<sup>2</sup> if the cooling sodium is at 500°C and the rod diameter is 0.75 inch (1.90 cm). By making the rod diameter 0.25 inch (0.64 cm) the specific power can be increased to 6480 watts/cm<sup>2</sup>. Life corresponding to the burn-up permissible in the aluminum-uranium system at corresponding temperatures relative to the melting points of the two metals should be obtainable.

Zirconium-uranium alloys clad with zirconium have been studied in some detail and have suitable properties. Here uranium may be put in solution at elevated temperatures and precipitated upon cooling in standard metallurgical fashion. Excellent specific power and life may be obtained. However, the cost of the zirconium in such elements weighs against their use in power reactors.

*c. Plutonium.* Plutonium cylinders in steel cans served as elements described in Table III in a fast reactor cooled with mercury operated for re-

TABLE III. PLUTONIUM FUEL ELEMENT

Slug Dimensions	Jacket	Method of Closure	Application
5.5 in. (14.0 cm) length 0.65 in. (1.6 cm) diam.	0.010 in. (0.025 cm) wall mild steel can	Shielded arc	Fast Hg cooled research reactor

search purposes at the Los Alamos Scientific Laboratory.<sup>13</sup> No information exists on such elements. The specific power permitted by the low thermal conductivity and transition temperatures make this element undesirable as a fuel base material. It is likely that plutonium-uranium alloys will be used in fast breeder power reactors. However, here the metallurgical structure will be governed largely by the uranium and hence may be considered as related to that family of elements.

*d. Ceramic systems.* BeO-UO<sub>2</sub> systems were studied extensively at ANL and ORNL, and BMI during the years 1945 to 1947. A high-temperature, helium-cooled, BeO-moderated power reactor proposed by F. Daniels was the objective of these studies. The size and shape of the elements considered are indicated in Table IV. The methods of fabrication of a variety of shapes were developed at BMI and at the Norton Company. Radiation stability was established for cylindrical shapes. Volatilization of BeO was observed during

TABLE IV. CERAMIC FUEL ELEMENTS

Matrix	Dispersed Material	Shape and Dimensions	Remarks on Application
BeO	UO <sub>2</sub>	BeO tubes impregnated with UO <sub>2</sub> ; 0.25 in. (0.63 cm) thick × 1.5 in. (3.8 cm) OD × 1 in. (2.5 cm) ID × 4.5 in. (11.5 cm) long. Suspended inside BeO moderator bricks	Proposed for high-temperature power reactor by ORNL and ANL
Graphite	UO <sub>2</sub>	Hexagonal graphite block impregnated with UO <sub>2</sub> ; 8.37 in. (21.3 cm) diam. × 4 in. (10.2 cm) high	Low power research reactor proposed by NAA
SiC	UC <sub>2</sub>	Ceramic blocks of SiC plus UC <sub>2</sub>	Proposed for high-temperature gas turbine power plant
ThO <sub>2</sub>	UO <sub>2</sub>	—	Proposed fuel for thermal breeder reactors

exposure to a very low partial pressure of water vapor at temperatures of 1000°C,<sup>14</sup> thus prescribing requirements on the dryness of any cooling gas. At operating temperatures the specific power of such elements is probably limited by the heat flux to the gas coolant. However, on shutdown, thermal stresses and brittle behavior will limit either the life or the permissible thermal strain at operating temperatures. Thus, such elements provide examples of limitation b2 and 3 above.

Graphite elements in which the UO<sub>2</sub> or UC<sub>2</sub> is dispersed in graphite (1) by impregnation of the normally porous artificial graphite or (2) by mixing and graphitizing, were developed at North American Aviation and Battelle Memorial Institute respectively. The former development was for a low-power research reactor for which operating hazards were minimized. Although satisfactory under conditions customarily employed for graphite, these elements have not been used in any reactor.

Thorium and urania bodies have been developed by Johnson and Curtis.<sup>15</sup> Since thorium is nearly as dense as thorium metal, its use as the fertile material in a reactor for conversion or breeding and power is indicated. Performance and life have not been investigated.

## B. FLUID FUELS

Fluid fuels for nuclear reactors as compared to solid fuels discussed above offer the following advantages to the materials technologist: (1) freedom

from radiation damage, (2) freedom from the internal limitations of heat transfer discussed above, (3) simple preparation, and (4) less complicated and hence cheaper reprocessing. In place of the problems listed above for solid fuels there are those associated with pumping radioactive fluids, compact heat exchanger design, and corrosion of the whole reactor system. Thus one may replace a long-lived reactor assembly which contains short-lived troublesome fuel elements by a relatively short-lived reactor system. For a quantitative comparison of the two systems, more dependable data are needed on corrosion and expense of maintenance of fluid systems and fuel life and the expense of handling for solid fuel systems.

**1. Fundamentals.** The specific power of a fluid system may be estimated very approximately without recourse to a detailed design in the following two ways:

- (1) If the limiting heat flux and the surface-to-volume ratio in the exchanger are known approximately; for example, if the tube radius  $r_0$  is known, then just as in the case of solid fuels above,

$$P_s = \frac{2w}{r_0 \rho p} \quad (1)$$

- (2) An alternate method may be based on the time for a round trip by the fuel through the reactor circulation system, the heat capacity, and the permissible decrease in temperature. The approximate relation

$$P_s = \frac{c_p \Delta T}{t p} \quad (5)$$

where  $c_p$  is the specific heat (joules/g/°C),  $\Delta T$  is the temperature rise, and  $t$  is time for round trip in seconds. With commonly feasible fluid velocities and system dimensions, the time for a round trip falls between 1 and 10 seconds.

In ways analogous to the case of solid fuels, materials may place some of the limitations on performance of the fluid system, for example:

- (1) Limiting upper temperature of container and heat exchanger materials due to:
  - (a) Loss of strength.
  - (b) Excessive corrosion.
- (2) Limiting fluid velocities due to erosion.
- (3) Limiting thermal stresses in heat exchanger tubes.

Several examples of fluid systems are given in Table V.

TABLE V. FLUID FUEL SYSTEMS

Reactor	Fluid	Solute or Dispersed Material	Concentration Range	Temperature Range	Container Material	Precautions
Homogeneous Reactor Experiment	H <sub>2</sub> O	UO <sub>2</sub> SO <sub>4</sub>	30-40 grams U-235/liter	242-250°C 467-482°F	Stainless Steel	
NAA Water Boiler Neutron Source	H <sub>2</sub> O	UO <sub>2</sub> (NO <sub>3</sub> ) <sub>2</sub>	45-50 grams U-235/liter	20-87°C 60-189°F	Stainless Steel	
Los Alamos Power Reactor Experiment	H <sub>2</sub> O	(UO <sub>2</sub> ) <sub>3</sub> (PO <sub>4</sub> ) <sub>2</sub>	100-150 grams U-235/liter	20-455°C 60-851°F	Stainless Steel	Gold plating on all surfaces exposed to hot solution
Intermediate Scale Homogeneous Reactor Experiment	D <sub>2</sub> O	UO <sub>2</sub> SO <sub>4</sub>	4-5 grams U-235/liter	242-250°C 467-482°F	Stainless Steel	
	Bi	U	0.05-0.10 w/o U in Bi	400-550°C 752-1022°F	Low Cr, Mo-steel	Mg to getter O; Zr to inhibit mass transfer
	Bi	UBi <sub>2</sub> (slurry)	Max. suspension of 10 w/o U	Max. temp. of 950°F, 510°C	Low Cr, Mo-steel	
	Na	UO <sub>2</sub>	Max. suspension of 30 w/o U	Max. temp. of 1600°F, 870°C	Austenitic steels	

## 2. Fuel types

a. *Aqueous systems.* The first nuclear reactor to use an aqueous solution was put in operation at the Los Alamos Scientific Laboratory in the year 1944. It used a solution of uranyl sulfate in light water in a Type-347 stainless steel container. Subsequent designs used uranyl nitrate solutions. "Supo," now in use, dissipates up to 35 kw. Since that time five solution-type reactors have been put into operation including the Homogeneous Reactor Experiment (HRE) at ORNL.<sup>16</sup> Research reactors of this type avoid corrosion problems and have long life, because they operate in the fractional megawatt range, using uranyl sulfate or nitrate solutions at approximately atmospheric pressure and hence below 100°C. The HRE requires higher temperatures and fluid velocities both of which promote corrosion of stainless steel and limit operating conditions and life.

Uranyl phosphate solutions investigated at Los Alamos have the interesting property that there is no discontinuity in solubility across the critical point of water, thus permitting high temperature operation. Only the corrosion rate of the metals gold and platinum are sufficiently low to serve in contact

with this solution. Thus corrosion of container materials is a major problem for this system.

*b. Liquid metal fuels.* Bismuth, primarily because of its low absorption cross section for thermal neutrons, received attention as a reactor coolant during the year 1942, particularly by L. Szilard. The interaction with uranium was studied by R. Hoxing at Iowa State College and found to be too severe to permit direct contact. In a preliminary study of the binary system, stable intermetallic compounds were found. Exploratory studies at BMI indicated that the corrosion of iron by bismuth might be tolerable below 500°C. During the year 1943, E. P. Wigner proposed the use of a liquid bismuth-uranium alloy for a reactor but the above mentioned work indicated an unfavorably low solubility at reasonable temperatures for systems based on natural uranium. However, more careful determinations of solubilities of uranium in liquid metals by Hayes and Gordon at MIT during the years 1945 and 1946 and by Teitel at BNL led to the careful study of the system Bi-U at BNL.<sup>17</sup> These studies show that a bismuth solution containing about 800 ppm U-235 together with a few hundred ppm Mg and Zr may be contained in ferritic steel alloys or in graphite. Thus such a solution may serve as a circulating fuel in reactor systems capable of producing electric power at competitive commercial costs or better. The specific power of this fuel system should fall in the range 5000 to 10,000 watts per gram as indicated by use of the above expressions for the limits. The metallurgical problems are simply

TABLE VI. TENTATIVE FLUID FUEL SYSTEMS (STUDIED ONLY)

Fluid	Solute or Dispersed Solid	Obvious Material Problems
H <sub>2</sub> O } D <sub>2</sub> O }	U oxides	Stability of suspension: (a) colloidal properties, (b) redox properties in water subject to ionizing radiation, (c) stirring, rheological properties <i>vs</i> settling. Erosion of system.
NaK	UO <sub>2</sub>	(1) Erosion of system, (2) settling <i>vs</i> stirring.
He	UO <sub>2</sub>	None, outside of possible erosion and handling.
Bi	UBi <sub>2</sub>	Similar to solution, plus erosion. Maintenance of proper particle size, preparation and make-up.
Fused fluorides	UF <sub>4</sub> *	Corrosion due to the solubility of metals in molten salts.

\* Or a complex uranium fluorine ion.

the extension of the work referred to above and include determination of the properties and nature of the liquid metal solutions and the corrosion and its inhibition of container materials for the solutions.

A summary of other fluid fuel systems which have been suggested and studied in varying degrees but not used as yet is given in Table VI.

#### REFERENCES FOR CHAPTER X

1. F. Seitz, *Radiation Effects in Solids*, Physics Today 5(6):6-9 (1952); see also Geneva Papers:  
559—J. R. Johnson and C. E. Curtis, "The Technology of  $\text{UO}_2$  and  $\text{ThO}_2$ ."  
885—K. Carlsen, P. Lovland and S. Aas, "Notes on the Stability of Uranium Fuel Elements."  
961—M. Ristić, M. Novakovic, P. Anastasywic and N. Kovelić, "Thermal Strains and Deformations in the Rod and Canning in the Heterogeneous High Flux Reactor."
- See Part II of this book.
2. M. E. Ramsey and C. C. Cagle, "Ten Years' Operating Experience of the ORNL Graphite-Moderator Normal-Uranium Reactor," *Nuclear Engineering—Part I, Chemical Engineering Progress Symposium Series*, Vol. 50, No. 11, pp. 149-154 (1954).
3. W. H. Zinn, *The Argonne Heavy Water Reactor (CP-3 Prime)*, ANL-WHZ-311, August 10, 1951.
4. D. H. Gurinsky, "The Fabrication of the Fuel Elements of the BNL Reactor," Geneva Paper 828.
5. See, for example, Geneva Paper No. 486—M. E. Ramsey, "Research Program and Operating Experience on ORNL Reactors."
6. J. E. Draley and W. E. Ruther, "Aqueous Corrosion of Aluminum Alloys at Elevated Temperatures," Geneva Paper No. 535.
7. H. V. Lichtenberger, "The Experimental Breeder Reactor," *Nuclear Engineering—Part III, Chemical Engineering Progress Symposium Series*, Vol. 50, No. 13, pp. 139-146 (1954).
8. As described in Geneva Paper No. 815.
9. J. R. Huffman, *The Materials Testing Reactor*, Nucleonics 12(4):20-26 (1954).
10. *Compilation of U.S. and U.K. Uranium and Thorium Constitution Diagram*, H. A. Saller, F. A. Rough, Editors (1955), BMI-1000.
11. L. R. Coffin, Jr., *The Problem of Thermal Stress Fatigue in Austenitic Steels at Elevated Temperatures*, ASTM Special Technical Publication No. 165, pp. 31-50 (1954).
12. C. Starr, "A Sodium Graphite Reactor 75,000 Electrical Kilowatt Power Plant," Geneva Paper No. 493.
13. E. T. Jurney, "The Failure and Disassembly of Los Alamos Fast Reactor," *Nuclear Engineering—Part III, Chemical Engineering Progress Symposium Series*, Vol. 50, No. 13, pp. 191-199 (1954).
14. C. A. Hutchison, Jr. and J. G. Maln, *The Volatilization of Beryllium Oxide in the Presence of Water*, Amer. Chem. Soc. J. 71(4):1338-1339 (1949).
15. R. J. Johnson and C. E. Curtis, "The Technology of  $\text{UO}_2$  and  $\text{ThO}_2$ ," Geneva Paper No. 559.

16. A. M. Weinberg, *Power Reactors*, Scien. Amer. 191(6):33-39 (1954).
17. R. J. Teitel, D. H. Gurinsky, and J. S. Bryner, "Liquid-Metal Fuels and Liquid-Metal Breeder Blankets," *Nuclear Engineering—Part III, Chemical Engineering Progress Symposium Series*, Vol. 50, No. 13, pp. 11-13 (1954); J. E. Atherton et al., "Studies in the Uranium-Bismuth Fuel System," *Nuclear Engineering—Part II, Chemical Engineering Progress Symposium Series*, Vol. 50, No. 12, pp. 23-27 (1954).
18. As described in Geneva Paper No. 953.

## *Chapter XI*

---

### A URANIUM BASE FUEL ELEMENT \*<sup>1</sup> (Details of the fabrication of the Brookhaven fuel element)

---

The next three chapters will present detailed information of the fabrication procedures of solid fuel elements and specific studies of the metallurgical and chemical variables for fluid fuels. In this way it will be shown how the basic information presented in the first ten chapters has been applied to the solution of the specific problems which arise whenever a fuel system must be devised for the specific needs of a given reactor.

The Brookhaven pile is an air-cooled natural-uranium graphite-moderated reactor. Design studies indicated that the rate of heat dissipation from the uranium required a heat surface area which could be obtained only by using a finned casing. Since the reactor was built on a site which was relatively near to populated areas, the hazards resulting from a rupture of a fuel element had to be reduced to a minimum. The decision was made that the fuel elements should consist of long finned aluminum tubes in which the slugs would be encased. In order to monitor each element for leakage, a tube (called the helium tube) was attached to one end of each element. By monitoring the gas pressure in each element it is possible to determine the onset of a break in the fuel element. Since a large volume of inert gas at low pressure is used to maintain the atmosphere within the element, the issuance of gas from a small leak prevents the entrance of oxygen and nitrogen which would result in the oxidation of the uranium. It should also be noted that the He atmosphere in the tube aids in the heat transfer from the uranium slug to the casing.

For a flux of approximately  $4-5 \times 10^{12}$  neutrons/cm<sup>2</sup>/sec (design flux) calculations indicate that the interface temperature between the uranium and aluminum would be of the order of 350°C. Experiments<sup>1</sup> in which 2S aluminum was held in contact with uranium showed that a reaction takes place between the uranium and aluminum at this temperature and as low as 250°C. This fact also had to be taken into account in the design of a fuel element.

\* This chapter is based entirely on the following Geneva Paper: 828—D. H. Gurinsky, "The Fabrication of Fuel Elements for the BNL Reactor."

One other factor which had to be considered in setting up the canning or cladding procedure involved the operation of the helium system. On raising the power level, the gas pressure in the helium system would either increase or decrease depending on the gas volume in the cartridge element. It was decided that an attempt should be made to prevent the so-called "breathing" of the element by selecting the proper gas volume at room temperature such that on attaining the expected power level the resultant change in pressure in the fuel element would be small. This requires an assumption as to the average temperature of the fuel element assembly which was taken as 350°C.

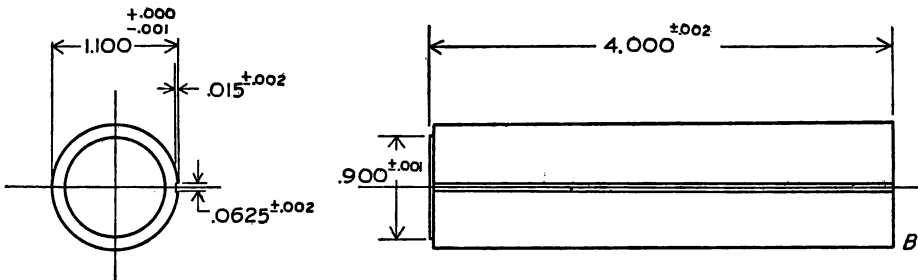
#### A. THE BASIC MATERIALS

The selection of the type of uranium, that is its method of fabrication, was based on the following considerations:

- (1) Uranium rods prepared by extrusion in the gamma phase do not elongate on temperature cycling as much as rolled material.
- (2) The necessary tonnage of gamma extruded stock could be obtained readily from commercial sources.
- (3) Gamma extruded material was cheaper than the rolled material.

The operations required to convert the gamma extruded rod to slugs were performed by an outside company under the supervision of the H. K. Ferguson Company. The operations performed at this contractor's plant consisted of the following. The 1.20-inch diameter rods were first straightened in a medart straightener. They were then rough-machined to rods 1.130 inches in diameter by 4 inches long. The rough-machined slugs were annealed and degassed at a temperature of 600°C for 12 hours in an atmosphere of argon gas. This step was included to decrease the hydrogen content of the metal and to relieve the machining and bending stresses. The slugs were then machined to finished dimensions indicated in Fig. 1. The finished and deburred slugs were then degreased in a vapor phase degreaser and then degassed by heating to 400°C for 4 hours in an atmosphere of argon gas. The slugs were then examined and packed in hermetically sealed containers and shipped to BNL.

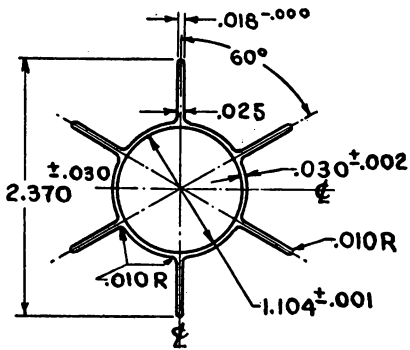
The finned aluminum tubing was fabricated by the Aluminum Company of America. The specifications of the tubing are given in Fig. 2. Figure 3 is a photograph of the as extruded and as drawn tubing. The tubing was formed by extruding the billets of 2S aluminum through a web type (or port hole) die. The metal is forced through 6 openings beyond which there is a mixing chamber and a stationary mandrel. After passing through the mixing chamber the metal sees a continuation of the mandrel which faces the portion of the die where the fins and walls of the tubing are formed. The extruded shape was



#### NOTES

1. END FACES MUST BE PARALLEL WITHIN  $\pm .001$ , IN REF. TO SLUG AXIS.
2. CYLINDRICAL SEC. TO BE GR'D FIN.
3. TOOL MARKS NOT TO EXCEED  $.003^{\circ}$  ON ENDS.
4. REMOVE ALL BURRS.

FIG. 1. Uranium slug.



#### SPECIFICATIONS

##### Purity:

Standard Specifications for 2S Aluminum. Impurities not to exceed 1%.

##### Dimensions:

1. Wall thickness  $0.030^{\circ} \pm 0.002^{\circ}$ .
2. Internal diameter  $1.104^{\circ} \pm 0.001^{\circ}$ —subject to specification #11.
3. Distance from tip of one fin to tip of opposite fin  $2.370^{\circ} \pm 0.030^{\circ}$ .
4. Fin dimensions at tip  $0.018^{\circ} - 0.000^{\circ} + .010R$ .
5. Spiral of fin  $1^{\circ}/\text{ft}$ .

##### Special Specifications:

6. Weight per foot not to exceed  $0.230 \text{ lb/ft}$ .
7. Bowing of tube—not greater than  $0.100^{\circ}$  in 10 ft.
8. Plug Test. The tube is acceptable

if it shows no sign of rupture after a tapered steel plug has been driven into both ends so as to expand the inside diameter by  $\frac{1}{8}^{\circ}$ .

9. Pressure Test. A pressure of  $90 \text{ lb/in.}^2$  of air shall be applied to the inside of each tube for a period of not less than five seconds. Any tube which leaks, as indicated by the formation of air bubbles in the testing fluid, shall be rejected.
10. Surface Inspection. The tubing and fins shall be clean, smooth, and free from seams, slivers, laminations, grooves, cracks, blisters, and other injurious defects.
11. Clearance. A  $4.500^{\circ} \times 1.101^{\circ}$  O.D. Micarta rod with chamfered ends shall readily pass through each tube. This will be considered the "Go" Gage. The "No Go" Gage shall be  $4.5^{\circ}$  long by  $1.105^{\circ}$  O.D. and should not pass through the tube.
12. Finished length  $12' - 6'' \pm 0.5''$ .
13. Packaging. Each tube should be encased in a  $\frac{3}{16}^{\circ}$  wall mailing tube for its full length and then shipped in a substantial wooden crate, the latter to be so constructed that the material can be repacked in the same container, i.e., closure can be effected by means of screws or straps of metal.

FIG. 2. Finned tube specifications.

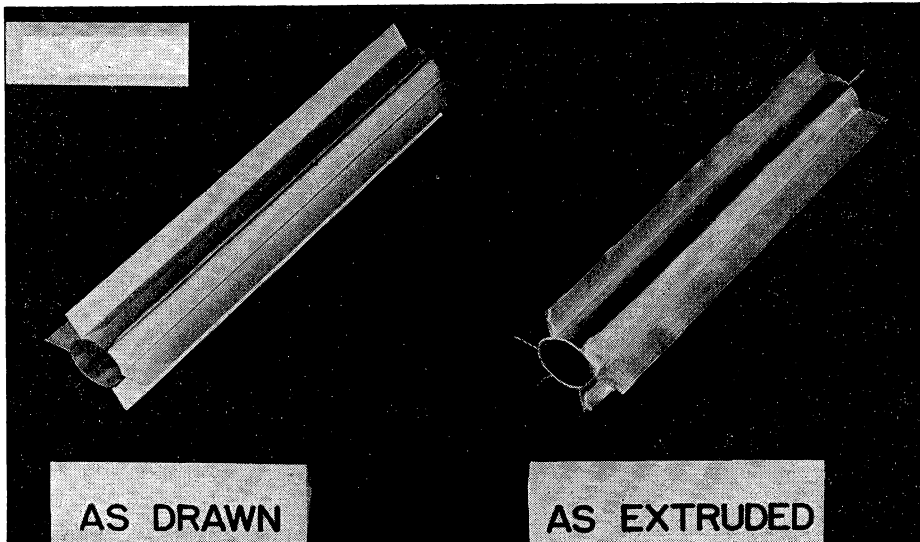


FIG. 3. Finned tubing.

slightly oversize so as to permit a drawing operation which, as seen from the photograph, resulted in a straightening of the fins and sizing of the tube. The total amount of cold work involved in this process was of the order of 15%.

As pointed out in the introduction, the high temperature at the interface between the aluminum and uranium posed the problem of how to prevent the reaction of uranium with aluminum at the operating temperature. Experimentation had demonstrated that aluminum which had been anodized to give a thickness of aluminum oxide of the order of 1 mil prevented the reaction of aluminum and uranium at temperatures of the order of 550°C. The interior of the 11½-foot tubes was, therefore, anodized in a sulfuric acid medium at the proper voltage and current conditions for a sufficient length of time to yield a layer which was measured at  $\frac{1}{10}$  of a mil. Further, the caps which were subsequently used to seal both ends of the fuel element were anodized on the surface which was to contact the uranium slug. Figure 4 is a drawing of the completed fuel element. Figure 5 gives the dimensions of the two caps used to close the ends of the finned tube.

#### B. THE PRODUCTION OPERATIONS

The production process was divided into 13 operations. These are:

- (1) Stripping the anodized film.
- (2) Trimming the finned tube.

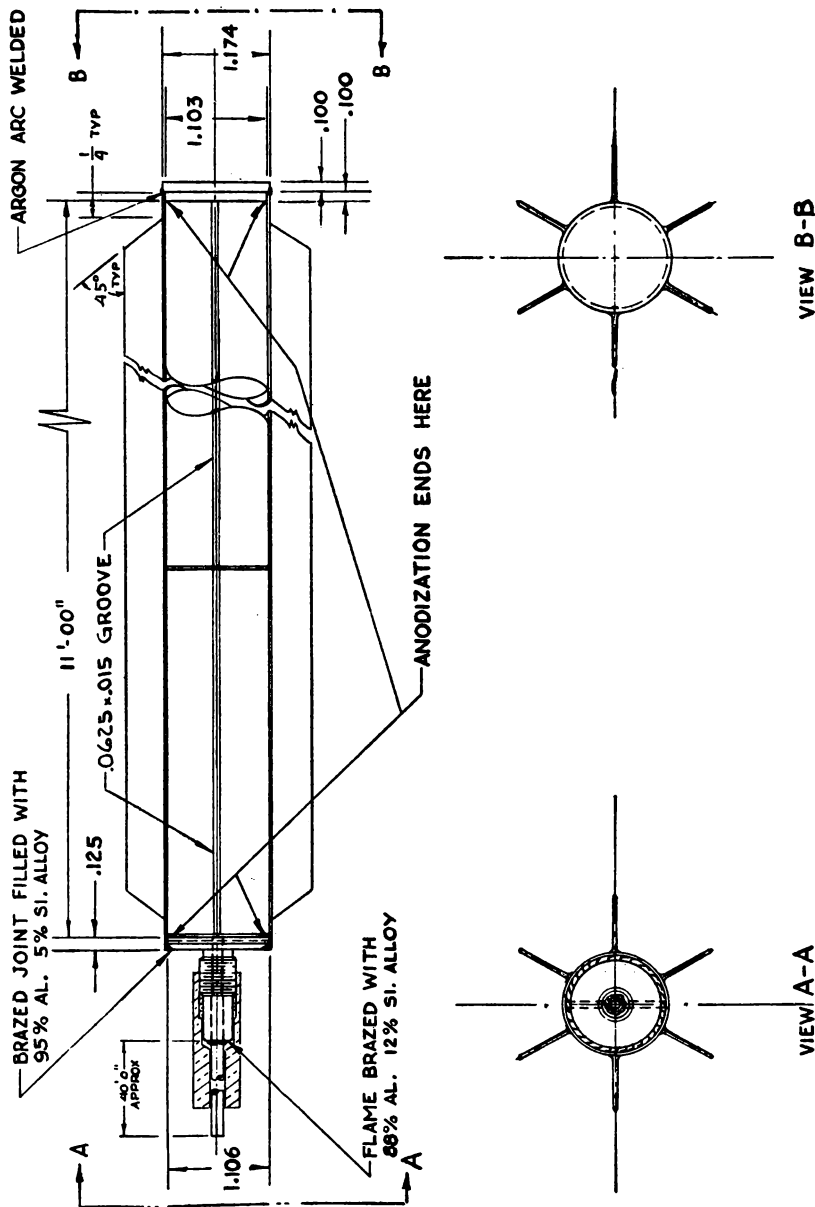
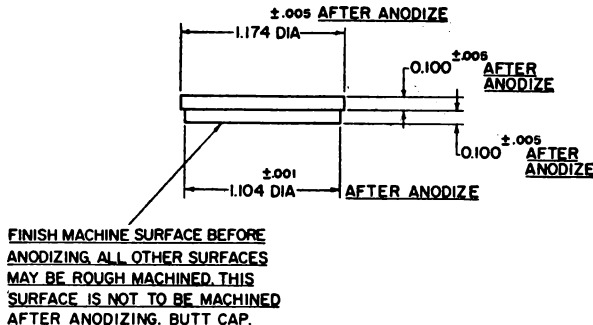
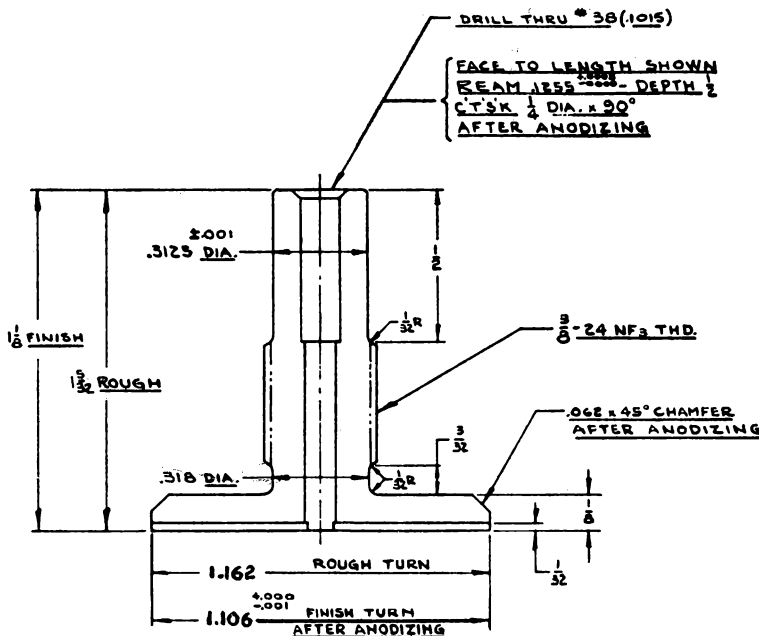


FIG. 4. BNL fuel element.



Butt Cap.



Helium Cap.

FIG. 5. End caps for finned tube.

- (3) Welding the butt closure.
- (4) Dehydrating the anodized film.
- (5) Leak test No. 1.
- (6) Loading the welded tube.
- (7) Trimming the loaded tube.
- (8) Induction brazing the helium cap.
- (9) Leak test No. 2.
- (10) Hydrostatic collapsing the finned tubing.
- (11) Flame brazing the anchor.
- (12) Flame brazing the helium tube to the fuel element.
- (13) Continuity and final leak test.

#### C. DESCRIPTION OF THE OPERATIONS

**1. Stripping the anodized film.** The anodized film was stripped from an area extending  $\frac{1}{4}$  inch from one end of each tube. It had been shown by experimentation that, although the anodized tube could be welded, these welds are porous unless the anodized layer is removed. The solution used for removal of the anodized layer from the region to be welded is a chromic and phosphoric acid solution formulated with 35 cc of 85% phosphoric acid and 20 grams of chromium trioxide added to 1 liter of water. The solution was contained in an aluminum vessel and was maintained at 90–95°C. The liquid level was maintained by a simple constant level device. A sieve-like platform permitted the use of a large volume of solution and prevented the submersion of the tube beyond the prescribed distance. The tubes were held in a vertical position by a device with a suspended movable plunger. The tubes were taken from the shipping boxes, bundled in units of 7, and were placed in the stripping bath for 10 minutes. A thorough rinse in hot water followed. After this, the bundle was placed, stripped end down, into an improvised drier made from a can with a heating element in the bottom. Each tube was carefully inspected to determine whether the line of demarcation of the anodized layer was sharp.

**2. Trimming the finned tube.** The stripped end was machined to leave a bare section of tube  $\frac{1}{10}$  of an inch long. Also in this operation the fins were cut back so that the leading edge made an angle of 45 degrees with the body of the tube. A rotary cutter was employed to trim the tube ends square and flat. A spindle-mounted clipper was used to cut back the fins. The tube was centered by a collet which was in turn locked into position to a sliding platform. The latter was moved so that the trimming cutter engaged the tube wall to remove the excess metal. The movable platform was moved back, the finned ends clipped with tin snips and the clipper was turned on. A pre-set stop provided the correct cut back on the fins as the platform was moved into the clipper.

**3. Welding the butt closure.** The operation consisted of insertion of the butt cap into the de-anodized end of the tube after the tube had been inserted into a collet which in turn was inserted into the collet of the welding machine. The welding machine was housed in a 9-foot stand to conserve space in the fabrication area. Figure 6 is a close-up of the welding arrangement. The

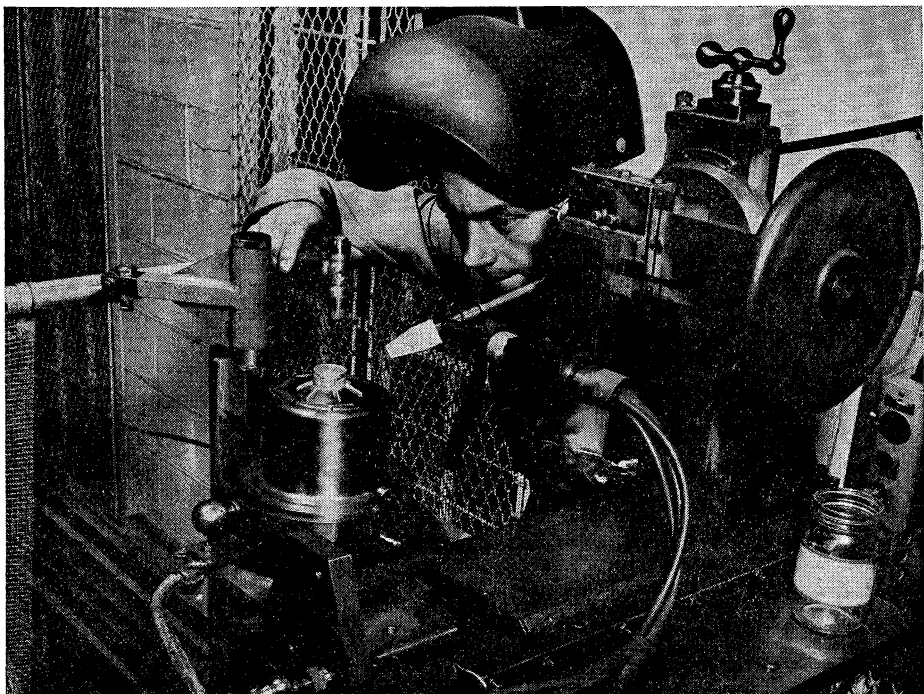


FIG. 6. Close up of welding arrangement.

weld was executed using an ac inert arc bathed in argon gas. The G.E. transformer had an open circuit voltage of 100 or 150 volts and was set to deliver 95 amperes. It was found that good welds could not be made with a high degree of reproducibility unless a heat sink ("chill") was inserted in the tube. The chill used was a uranium slug. The details of the operation consisted of the following.

The trimmed tube was inserted in the collet with care to prevent torn fins, and was clamped with the end extending  $\frac{1}{4}$  inch above the collet fingers. The uranium slug chill was placed in position; a cardboard tube was slipped over the tube to engage the collet; and the assembly was lifted vertically and inserted into the welding machine turntable. Two independent indexing points in the welding head assured proper line-up. The cap was placed and

adjusted for height by the welder (tapping with a plastic hammer) while the operator below adjusted the chill indexing rod. When the cap was seated firmly against the slug, the torch was moved into the proper position to form an arc gap of 0.030 inch from the tip of the tungsten electrode to the edge of the welding cap, against which the arc is struck.

The electrode was aimed directly at the upper edge of the cap. Looking at the torch in the vertical plane, i.e., facing the welding jig with the bearing in front, the torch made an angle of 35 degrees with the horizontal. Viewing the torch in the vertical plane at 90 degrees, with the welding jig bearing to the left, the torch made an angle of approximately 55 degrees with the horizontal. Looking down upon the torch, the torch was placed so that an imaginary line drawn through the axis of the electrode, through the arc point and through the center of the welding cap, would be a straight line. The cap diameter was 0.010 inch larger than the diameter of the tube to protect the thin tube wall from "burning down" when the arc was struck. The arc was initiated by depressing the start button at which time the high frequency, high voltage, ionizing pilot spark jumped the gap. The operator observed the arc and waited for a molten pool to form, at which time the rotating mechanism previously set at 4 rpm was set into motion. After the tube had rotated through 400 degrees, the start button on the control board was again depressed to begin operation of the "crater-filling." A stop switch was installed for emergency stop of the arc without "crater-filling." "Crater-filling" is an operation in which the primary of the transformer is moved away from the secondary of the transformer by actuating an air cylinder, thus the current in the arc is gradually reduced. When the primary has moved to a pre-set position the circuit is opened, turning off the power completely.

**4. Dehydrating the anodized film.** Preliminary heating tests had shown that when the anodized tube was heated to the neighborhood of 200°C, approximately 1 cc of water was released per 11½ feet of cartridge. Since this water would react with the uranium to form loosely held hydride and oxide, the water in the aluminum oxide film was removed. Further, this operation aided greatly in the subsequent leak test procedures by decreasing the pump down time. Fifteen tubes were processed at one time with a thermocouple placed at the center of the charge and the open ends of the tube facing towards the vacuum outlet. The furnace consisted of a 10-inch diameter tube wound with heating coils and was maintained at 350°C for 1 hour under vacuum.

**5. Leak test number 1.** This test was designed to determine whether the tube as a whole and the first weld were free of leaks. The finned tube was handled in a paper shipping tube. It was first rough-pumped and then, by closing and opening the proper valves, it was connected to the high vacuum system which in turn could be connected to a helium leak detector. By introducing helium gas between the shipping tube and the finned tube, the "leak tightness" of the

finned tube was determined. By turning a valve which was in turn connected to a metal cup into which the welded end of the tube protruded, the weld soundness could be determined. The basic pumping system used in this test and subsequent other two tests is illustrated in the dotted portion of Fig. 7.

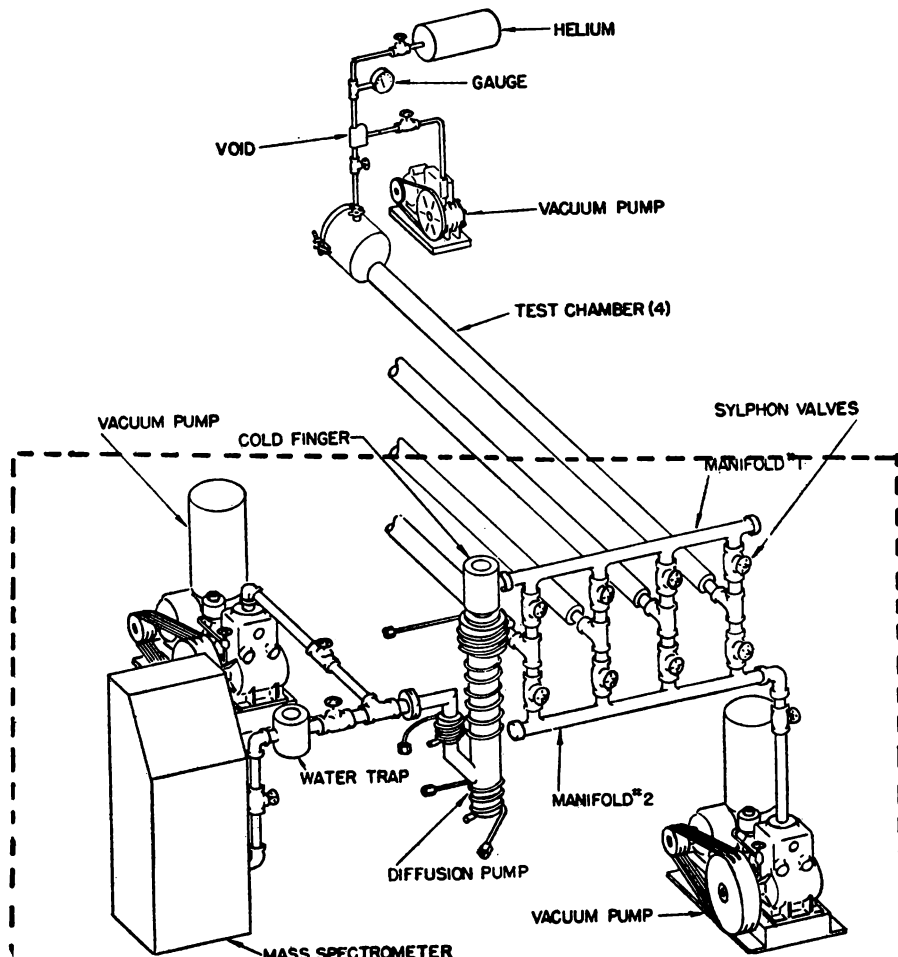


FIG. 7. Equipment for final leak test.

**6. Loading of the welded tube.** This operation consisted of the loading of the uranium slugs into the aluminum tube. Since the length of the cartridge as used in the reactor is 11 feet, and the length of the slug is 4 inches, 33 slugs were inserted into the tube. The anodized layer aided in this operation in that it was a hard surface which prevented galling. All tubes were tested with

respect to their abrasion resistance after they were anodized to determine whether the anodic film would be removed as a result of the rubbing which they would receive in the loading. The close tolerances for the uranium slugs and the finned tubing were required by this operation.

Prior to the start of the loading operation, the finned tubing was inserted into a process tube so that the element could be handled in subsequent operations. The process tube consisted of an aluminum tube which had on its ends collets which held the finned tube rigidly. Each slug was seated firmly on the previous slug using a calibrated ramrod. After the slugs had been loaded, the cartridge was adjusted in the process tube so that the welded end protruded  $\frac{1}{4}$  inch beyond the collet and then the collets were tightened.

**7. Trimming of the loaded tube.** This operation was performed on the same machine that was used in trimming the finned tube in step 2. The loaded tube was cut to size by gaging against the last slug, leaving  $\frac{1}{8}$  of an inch to receive the brazing cap.

**8. Induction brazing of the helium cap.** The final closure was made by induction brazing using Alcoa #43S filler rod (95% aluminum-5% silicon) and Alcoa #53 flux. The decision to braze the end cap to which the helium tube was to be attached was based on the fact that it was not possible to pre-determine the final position of the end slug since the cumulative error in the slugs might result in the slugs protruding beyond a predetermined, de-anodized section, thus permitting contact between slug and aluminum. It was found that hand scraping and the use of flux permitted an effective braze to be executed. Further, leaks which were found in the brazed joint could be repaired much more readily than leaks found in an inert arc weld.

In order to achieve easier alignment, the cartridges were brazed in a vertical position. A platform 6 feet square by 9 feet high was erected to provide working space and support for the main column assembly which received the loaded process tube. The main column assembly, fixed to a semipermanent foundation and set within a 14 inch wide by 36 inch deep recess cut into the platform, consisted of a rigid I-beam and a swinging column with a counter-balancing mechanism operated by a pneumatic cylinder. A standard 4 inch by 7.7 inch I-beam, 10 feet long, was used for the swinging column. Two ears and a transverse shaft were welded on the bottom of the column to provide a pivot within 2 bearings mounted in the frame assembly. The ears were connected to shock absorbers incorporated in the unit. The column was connected through springs and a toggle mechanism in such a way that when the column was in the downward position, i.e., about 3 feet from the floor at an inclined angle above the horizontal (supported by a swinging leg mounted on the back of the column), the springs were not under compression. The mechanism was actuated by air cylinders operated from a hand valve, which in turn put the springs under compression and brought the toggle mechanism over center.

This made it easy to swing the column plus load into the vertical. Just before the column reached the vertical, the toggle mechanism would go back over the center again, pull down the air cylinders, and release the springs. On the downward stroke, the column was restrained by the shock absorbers, as well as the friction in the air cylinders, and came down slowly to the inclined horizontal position. The turntable was operated by a dc variable speed motor connected to a G.E. Thymotrol. A long rod connected the turntable to a geared wheel at the top of the platform, made it possible to either raise or lower the turntable by turning a handwheel. An annular bearing was used to index accurately the workpiece.

Because of the size and weight of the radio-frequency generator and water economizer, they were placed on the floor at one side of the platform. Copper tubing was run from the generator through stand-off insulators up the side of the platform into a step-down transformer, which was mounted on a pedestal on top of the platform. Copper leads connected the transformer to the hinged work coil. All leads and tubing up to the primary of the transformer were contained in an enclosure to prevent injury to personnel.

The loaded cartridge, contained in a process tube, was carried from the trimming table and placed on the extended pivoted column. The pneumatic valve was pressed, after which the column was raised to the vertical position to rest within latch bars built into the upper plate. The annular bearing was slipped over the collet and set into the plate recess, whereupon the operator raised the process tube so that the finned tube was above the plate.

A hand scraper was inserted into the finned tube and rotated until the anodic film was removed. The brazing cap was inserted and tapped into position against the slug button with a plastic mallet. Alcoa #53 flux, mixed with 4 parts of alcohol, was applied to the joint with a camel hair brush. The induction coil was swung into position. After the process tube was adjusted so that the finned tube was  $\frac{1}{16}$  inch away from the coil, as shown in Fig. 8, by one operator, the other operator maintained the correct distance from coil to work. The work was rotated at 6-9 rpm. After the braze was completed, the coil was de-energized and swung back to the vertical position. The turntable was stopped to remove the flux with a bottle brush and hot water.

At this point in the production, the cartridge was removed from the process tube and handled in a carrier tube. (Preceding operations on the fuel rod required a process tube for indexing, whereas the production steps following brazing did not require that the cartridge be indexed.) After removal of the annular bearing, the process tube was lowered on the column to floor level, the collets were loosened, and the assembly was raised to a point just outside the latch position. A clamp was lowered and fixed to the process tube, then it was raised up, leaving the cartridge bare. The process tube was lowered over the

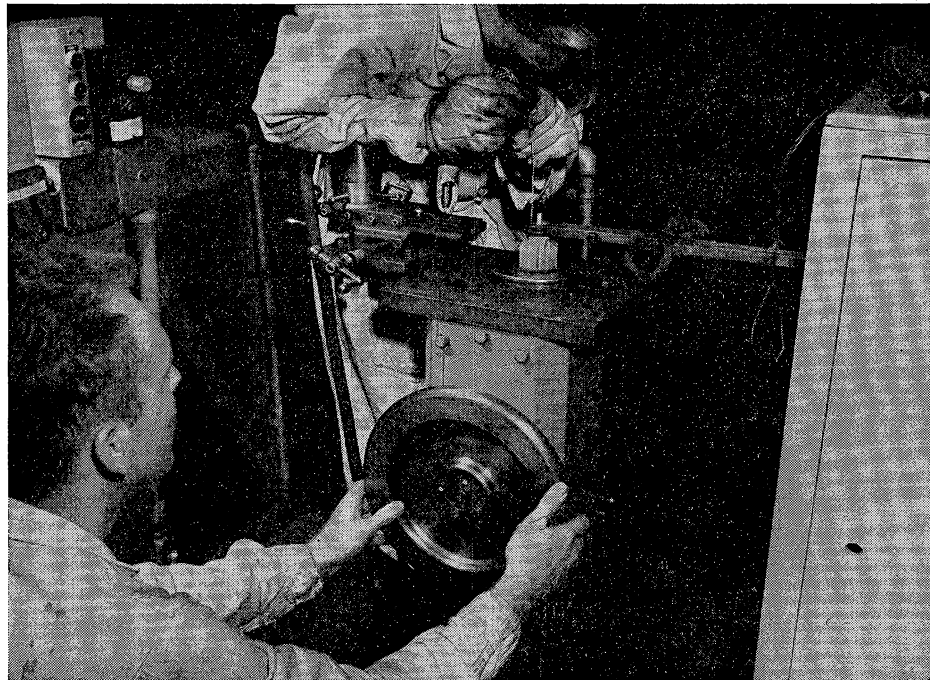


FIG. 8. Feeding of brazing rod to cap-tube interface.

cartridge, after which the swinging column was lowered. The assembly was removed and placed on a rolling table for delivery to leak test number 2.

**9. Leak test number 2.** The second leak test was necessary to check the brazed end and to re-check the weld and tube wall prior to compression (step No. 10), since, if a nonrepairable leak were present, the cartridge could be more readily decanned before compression.

The slot on the slug was included to aid in this leak test and the subsequent leak test. The apparatus used for testing was similar to that employed for the first leak test, except that the operation was done in the horizontal position. A rubber seal engaged the back (weld) end of the carrier tube, which was utilized as a helium envelope.

Each cartridge, encased in a carrier tube, was placed on the test table with the weld end engaged in the seal. A  $\frac{1}{4}$ -inch i.d. rubber vacuum tube was slipped over the brazed cap to connect the interior of the cartridge to the manifold pump.

Since the system was pumping on the equivalent of a  $\frac{1}{8}$ -inch tube  $11\frac{1}{2}$  feet to 15 feet long, the sensitivity was inherently low, and the time interval required to observe a leak in the far (welded) end of the tube was fairly long

(30 seconds). It was also found that the sensitivity at the braze was quite poor. Although the sensitivity of this test was low in comparison with later tests, it nevertheless served the purpose of sorting out tubes with leaks large enough to pass a detectable quantity of water during the next operation, hydrostatic collapsing.

The finally accepted general procedure in the test was to flood the tube length and weld with helium, wait for 2 minutes to insure ample time for a leak to appear, and then probe the braze for leaks. In case of a leak other than in the braze, the tube was rejected and decanned. A leaky braze was returned to the induction brazing operation for repair, if possible. A visual inspection of the braze was made at this leak test to insure a smooth clean braze metal deposit. If the braze was found faulty in this respect, the cartridge was immediately rejected and decanned. Tubes which showed excessive damage to the fins, braze, or weld caps due to mechanical injury were also separated here.

**10. Hydrostatic collapsing of the finned tubing.** The purpose of this operation was to bring the tube wall into more intimate contact with the slug to improve the heat transfer from the slug to the finned wall. The heat transfer calculations demonstrated the desirability of this operation. If it had been possible to maintain closer tolerances between slug and finned tube this step might have been eliminated. Another reason for including this step involves considerations of the helium system. As discussed previously, one of the objectives was to obtain a predetermined gas volume in the cartridge so as to minimize the breathing or surging of the detecting gas. The only way it was found possible to attain this objective was by the use of slugs of fixed dimensions in combination with the compression operation. Extensive tests were performed in which it was demonstrated that at pressures of the order of 2500 psi, the diameter and, further, the volume of a tube could be reduced quite reproducibly.

The compression chamber was constructed using a  $3\frac{1}{2}$ -inch stainless steel pipe, flanged and fitted to receive a plug containing O-ring seals. A simple valving arrangement permitted rapid pressurizing with a Blackhawk model No. 60 hydraulic pump.

Upon receipt of a cartridge from leak test number 2, a strip of absorbent paper was inserted in the brazed cap opening, and a rubber seal was screwed over the cap. The cartridge, in a carrier tube, was then loaded into the compression chamber. The plug was inserted, the gate dropped into position, and the water valve and air relief valves were opened. The air relief valve was closed when water drained into an indicator that was just beyond the air relief valve, thus showing that the chamber was filled with water. The water valve was closed and the system was hand pumped to 2500 psi.

The air relief valve was then opened permitting the pressure to drop to

atmospheric and the gate was lifted. The plug was removed to aid in the drainage of water. When sufficient water was drained out of the chamber, a pair of tongs was inserted into the steel storage tube; the operator pulled the assembly out of the chamber far enough for the hands to grasp it and complete its removal. The tube and cartridge were carried to supports. The cartridge was slid, welded end first, through an air drying ring into a dry tube. The sliding and drying action were stopped after all but a few inches of the cartridge was in the dry storage tube.

The rubber stopper was removed and the brazed end inspected for leaks by examining the absorbent paper from the cap. A volume check was made after inspection of the paper. This was accomplished by connecting the cartridge to a known volume of gas at a known pressure and noting the pressure drop when the systems were joined. If the cartridge showed neither the presence of water nor volume irregularities, a rubber bumper and a spring clip were placed over the brazed cap. The cartridge was pushed completely into the carrier tube, and the assembly was placed in a storage vault.

**11. Flame brazing of the anchor.** The purpose served by the anchor was to locate the fuel element relative to the graphite structure. On going from zero power to full power the fuel element expands approximately 1 inch. On cooling down, the element can move in either direction. To prevent this, the graphite of the pile was provided with a slot 20 inches from the central gap into which the anchor would drop when the fuel element was inserted into the pile.

An "anchor" is an arc of 2S aluminum,  $\frac{3}{4}$  inch wide. Its external face is convex. Each end is machined, leaving a ridge which is used to position the anchor on the fins of the cartridge (Fig. 9). A gage 20.70 inches long was designed to position the anchor accurately from the welded end of the cartridge. Alcoa #33 flux, mixed with two parts of alcohol, was used with filler rod composed of 88% aluminum and 12% silicon.

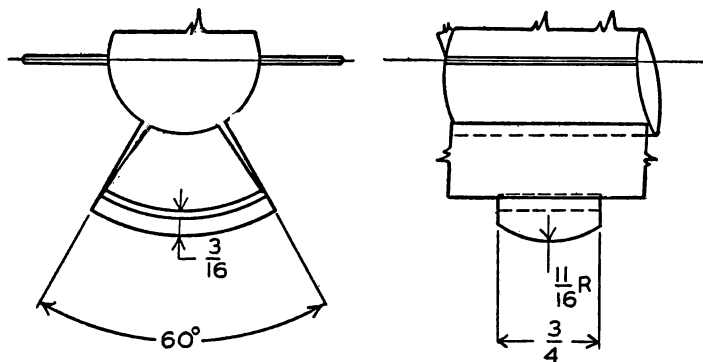


FIG. 9. Anchor detail.

The end of each cartridge was pushed out of the storage tube onto a supporting table, exposing some 25 inches of the welded end. A small amount of flux was spread uniformly on the surfaces to be brazed. The anchor was clamped in place, using the gage to locate it, and turned a quarter turn to place the joint to be brazed in a horizontal position. An oxygen acetylene flame was used. The brazing rod, coated with flux, was applied at the proper temperature. The anchor and fins were cleaned, while still hot, with water and a fiber bristle brush to crack the flux and remove it from the surfaces. The cartridges were then dried with compressed air, pushed back into the steel storage tubes, and moved to the next operation.

**12. Flame brazing of the helium tube to the fuel element.** The helium tube was a  $\frac{1}{8}$  inch o.d., .032 inch wall, 40 feet long coil of 2S aluminum contained in a cardboard cylinder of approximately 2 inch i.d. The end of the coil was straightened for about 4 inches and the aluminum protector was slipped on. The aluminum protector tube 2 inches long was used to prevent bending of the brazed joint in subsequent handling operations. The coil of tubing was placed in a vertical holder. The end of the helium tube was cleaned and brought to size with swaging pliers. A hydrogen gas flame and a brazing rod consisting of 88% aluminum-12% silicon were used to form the fillet weld about the tube. On completing this operation, water was sprayed on the hot surface to crack the flux. The joint was then cleaned and dried. Since it was felt that the cleaning operations in both brazing procedures were not stringent enough to remove the last traces of flux which might either result in corrosion of the aluminum in storage or might actually effect a temporary seal in the brazed joints, the completed assembly was given a more thorough cleaning in which a solution of 10% nitric acid and 10% sodium dichromate was dripped over both brazed joints. The total amount of solution used was 500 cc. The joints were then scrubbed using a monel brush to assure the removal of flux particles. This cleaning operation was followed by a rinse in hot running water. The wet areas were then dried thoroughly using compressed air. The completed assembly was then put into a storage tube and the helium coil was supported by inserting its cardboard container within the storage tube.

**13. Continuity and final leak test.** Since this test was the last to be performed to determine the soundness of the element and, therefore, its acceptance as a fuel element for insertion in the pile, this inspection was as stringent as could be devised. This test was used to determine:

- (1) Whether the helium tube and cartridge were interconnected.
- (2) Whether any leaks existed in any part of the helium tubing, the joints, or the finned tubing.

To accomplish the first of these objectives the assembly, which had been placed in the test chamber (see Fig. 7), was so oriented that the helium tube end rested in the large cylindrical section of the test chamber. The end of the helium tube was pushed through a compression seal and connected to a reservoir gas system. The reservoir gas system was pressurized to 80 pounds. The valve connecting it to the helium tube was then opened. Since the volume of the helium tube and the fuel element were known, the reservoir volume was chosen so that it was roughly equal to that of the sum of the volume of the helium tube and fuel element. If there was continuity between the helium tube and the fuel element on opening the valve the pressure gage would drop to  $\frac{1}{2}$  its initial value. The "leak tightness" of the total assembly was established by a helium leak test; the vacuum door of the large cylindrical section was closed. The system was first rough pumped to 100 microns and then by closing and opening the proper valves the pressure was further reduced to about 25 microns using the diffusion pump and the other large mechanical pump. When the vacuum gage indicated that the system had been brought to 25 microns, the pressure on the interior of the assembly was raised to 80 pounds. The valve to the backing pump for the diffusion pump was turned off and the valve to the mass spectrometer was opened. A leak in the assembly could be readily noted by the characteristic change in the current in the mass spectrometer. On completion of this test the pressure within the cartridge was reduced and the unit was transferred to the storage vault ready for insertion into the reactor.

#### D. DISCUSSION—RECENT CHANGES

The experience gained in operating the reactor indicated that the occasional failure that was noted in the fuel element was primarily due to the development of a leak in the helium tube, usually in the region of the brazed joint. This joint, i.e., the connection between the helium tube and the end cap was changed and also the method of joining the helium end cap to the tube was changed. Figure 10 shows the cap which is now being used in the new cartridge. In order to use this cap and an inert arc weld similar to the one that was discussed in step No. 3, the end of the finned tube which is to receive this cap has to be cleaned by the same procedure as was used in step No. 1. To accomplish this, the finned tube is cut longer than the summed length of 33 slugs plus the accumulated error. The two ends are chemically stripped of their anodic film. All of the operations up to No. 8 are performed in the same manner as indicated in the preceding description. Step No. 8 consists of the insertion of one end of the helium tube to the base of the cap shown in Fig. 10. The helium tube is flame brazed to the cap using flux and 88 per cent aluminum and 12 per cent silicon rod. This assembly, cap plus helium

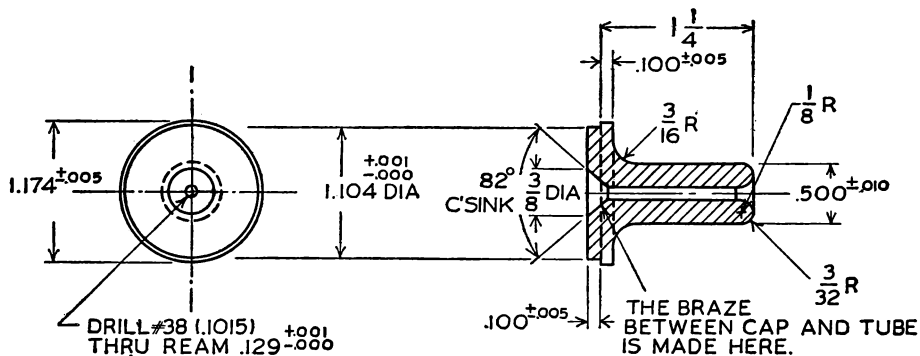


FIG. 10. New helium cap.

tube, after cleaning is seated in the cartridge. The void space, which resulted because the tube was cut too long, is filled with discs of various thicknesses of anodized aluminum so that the cap, on insertion, just makes contact with these filler discs. An inert arc weld is used to effect the closure using the same welding machine as was used in effecting step No. 3. These operations are then followed by steps Nos. 10, 11, and 13 as in the previous procedure.

In preparation for insertion of the fuel element into the reactor, the helium tube is straightened and a sleeve, shown in Fig. 11, is slipped along the helium tube until it meets with the helium tube cap. It is then fastened to this cap by two set screws. Attached to this latter cap is a tight coil of stainless steel wire 22 inches long which has been swaged tight in the smaller section of the cap of Fig. 11. The purpose of the coil of wire is to prevent sharp bends from being formed in the handling operations subsequent to insertion into the pile.

The evaluation of the relative merits of the two He cap designs which is

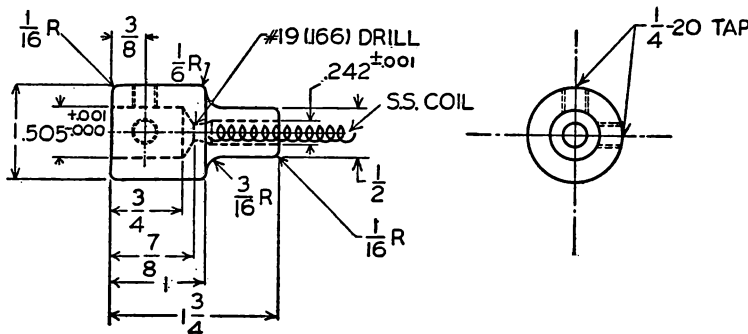


FIG. 11. Helium tube cap and stainless coil.

being made by R. W. Powell, head of BNL pile operations, has not been completed since the failure rate of either design requires long time tests for good statistics.

#### REFERENCES FOR CHAPTER XI

See Geneva Papers:

786—R. Kiessling, "The Solid State Reaction between Aluminum and Uranium."

860—M. Fox, "The Brookhaven Reactor."

762—R. F. Jackson, "Experience with B.E.P.O."

and

*Reactor Handbook*, Vol. 2, Engineering AECD-3646, Sect. 3, 5, p. 451.

## *Chapter XII*

---

### DISPERSION TYPE FUEL ELEMENTS \*<sup>1</sup>

---

In the first part of this chapter the dispersion type fuel elements, their features and methods of fabrication, will be discussed in detail. In the later portion of the chapter the procedure employed in the fabrication of the Materials Testing Reactor element, which has given excellent results in operation, is presented.

Dispersion type fuel elements are herein defined as elements in which the fuel is heterogeneous, consisting of a fissile phase dispersed in a continuous matrix of non-fissile material. For the purposes of this discussion, the non-fissile material will be limited to a pure metal or alloy. To minimize radiation damage and provide metallic properties, the diluent must predominate in volume and exist as a continuous matrix surrounding the fissile phase. The matrix metal in effect acts as the structural material in the fuel element.

#### A. THE DISPERSION TYPE FUEL ELEMENT

**1. Design objectives.** To discuss more effectively fuel elements, the general functions of a solid fuel element for a nuclear reactor are arbitrarily defined as:

- (1) Permanent space location of the fissile material in the reactor core.
- (2) Retention of fission products and fissile material.
- (3) Resistance to external and internal stresses without fracture or dimensional change.
- (4) Minimum parasitic capture of neutrons.
- (5) Transfer of heat with minimum thermal gradients.

The ability of a fuel element continuously to meet these requirements during operation is a measure of its merit relative to other types. The dispersion

\* This chapter is based on the following Geneva Papers:

561—C. E. Weber and H. H. Hirsch, "Dispersion Type Fuel Elements."  
953—J. E. Cunningham and E. J. Boyle, "MTR Type Fuel Elements."

type fuel element offers two unique advantages over elements having a homogeneous fissile core:

- (1) Increased operating life through localization of the fission product \* damage in and immediately adjacent to the dispersed phase, minimizing damage to the structural matrix metal.
- (2) Increased choice of fuel systems to permit use of normally metallurgically incompatible fuel and diluent metals and attainment of physical and mechanical properties not attainable in homogeneous fuel systems.

The specific dispersed phase and matrix metal used depends on the particular reactor design under consideration with factors such as operating temperature, type of coolant, and neutron energy spectrum limiting the materials choice. In general, however, to attain maximum endurance life, the volume fraction of the diluent metal should be large, the density of uranium in the dispersed phase should be high, and the parasitic neutron absorption cross section of the fissile phase and matrix materials should be low.

**2. Systems flexibility through dispersion techniques.** An important advantage of a dispersion system is the flexibility this technique offers in choice of fuel element materials and properties. Binary alloys of uranium and other metals vary widely in properties from those of either of the pure metals. Uranium is a reactive metal forming complicated systems with many intermetallic compounds and low melting eutectics. The thermal conductivity of alloy systems may be poor, diffusion of uranium as well as troublesome phase changes may occur during operation, and the mechanical properties and chemical reactivity of the binary system are often poor compared to the unalloyed metals. The dispersion approach allows the fuel element designer to incorporate the fissile material in a metal matrix without metallurgical interaction and thereby retain the desirable properties of the pure matrix metal. Uranium or other fissile elements can be pre-reacted to form a stable compound, in effect metallurgically deactivated, which can be incorporated into the matrix metal without further reaction. The ideal uranium dispersion would be elemental uranium since the metal obviously offers the highest density of uranium per unit volume. Magnesium is one of the few metals that can be mixed with uranium without reaction. Relatively high-density, chemically stable compounds such as  $\text{UO}_2$  can be employed with other metals. Intermetallic compounds may also be considered for a specific application. A number of fissile compounds of potential interest are given in Table I. The uranium content per unit volume of dispersed phase relative to the density of uranium is given as  $V_r$ .

\* The advantages obtained from the use of dispersion type elements with respect to radiation damage have already been discussed in Chapter IX.

## SOLID AND FLUID FUELS

TABLE I. FISSILE DISPERSANTS

Compound	Density, g/cc	$V_r$	Melting Point, °C
U	18.9	1.0	1133
UAl <sub>2</sub>	8.1	0.35	1590
UAl <sub>3</sub>	6.7	0.26	1320
UAl <sub>4</sub>	6.0 <sup>a</sup>	0.22	730
UBe <sub>13</sub>	4.37	0.15	2000
UC	13.6	0.69	2270
UC <sub>2</sub>	11.7	0.56	2400
UO <sub>2</sub>	10.96	0.53	2500
U <sub>6</sub> Fe	17.7	0.91	815
UFe <sub>2</sub>	13.2	0.48	1235
UN	14.3	0.71	2630
UPb	14.5 <sup>b</sup>	0.41	1280
U <sub>3</sub> Si	15.6	0.77	930 (d)
U <sub>3</sub> Si <sub>2</sub>	12.2	0.59	1665
U <sub>5</sub> Sn <sub>4</sub>	13.0 <sup>b</sup>	0.49	1500

The densities and melting points were taken from a paper by Katz and Rabinowitch<sup>2</sup> except for UBe<sub>13</sub> data taken from a paper by Buzzard.<sup>3</sup>

<sup>a</sup> Calculated assuming non-ideal mixing with a deviation equal to that observed with the other U-Al compounds.

<sup>b</sup> Calculated assuming ideal mixing.

The melting point of the compounds has been included to provide a relative indication of chemical stability. The list is not exhaustive, but uranium dioxide stands out because it contains a relatively high density of uranium, is quite chemically stable, and its technology of manufacture and handling is well understood.

Other dispersants may be better for specific applications. Metals which may be of interest as diluents are given in Table II.

The general criterion used in choosing these metals as diluents was their thermal neutron absorption cross section. The cross section per unit volume is of interest in design and has been included. It should be pointed out that the cross section of these and other metals is quite different in non-thermal reactors.

Many of the suggested dispersants are reactive and their reaction with the diluents in Table II has not been considered. Incorporation of a specific dispersant in a particular diluent is again so direct a function of reactor design, operating temperature and fabrication temperature, that fruitful generalization is not possible.

TABLE II. POTENTIAL MATRIX METALS

Matrix Metal	Melting Point, °C	Microscopic Absorption Cross Section, barns	Macroscopic Cross Section, cm <sup>2</sup> /cm <sup>3</sup>
Al	660	0.22	0.013
Be	1282 <sup>a</sup>	0.010	0.0013
Fe	1539	2.4	0.20
Mg	651	0.059	0.0025
Mo	2625	2.4	0.15
Nb	2415	1.1	0.061
Ni	1455	4.5	0.41
Ti	1670 <sup>b</sup>	5.8	0.33
V	1900 <sup>c</sup>	4.7	0.33
Zr	1852 <sup>d</sup>	0.18	0.008

The melting points were taken from the *Metals Handbook*,<sup>4</sup> except as noted. The microscopic cross sections were taken from the *General Electric Chart of the Nuclides*, Fourth Edition.

<sup>a</sup> See reference 3.

<sup>b</sup> See reference 5.

<sup>c</sup> See reference 6.

<sup>d</sup> See reference 7.

**3. Fabrication.** There are two general fabrication techniques available for producing dense dispersion type fuel elements: (1) melting and casting and (2) powder metallurgy. The material produced by either one of these methods must nearly always be mechanically reduced or worked to final size and shape. Such metal working generally improves mechanical properties and promotes bonding between the cladding and the core material. However, it can alter the structure and dispersion uniformity so that all of the potentially realizable advantages of the dispersion system are not attained. Fuel elements have, however, been prepared by both methods by applying the following principles and techniques.

*a. Melting and casting.* Although restricted in applicability, dispersion type fuel systems can be prepared by melting and casting. A binary alloy system can be used if the uranium-rich phase can be dispersed as islands throughout the non-fissile phase. The solid solubility for uranium must be negligible in the non-fissile or matrix phase. In addition, it is important that the uranium phase be a stable compound of reasonably high melting point and contain a high percentage of uranium. It is also desirable that the compound islands be large in size for reasons previously explained, and be more or less spherical in shape.

In practice, it has been difficult to find acceptable uranium systems with which all of these specifications can be met. The desired composition must fall within a phase range bordered by a high uranium compound and the pure alloying element. If a eutectic or eutectoid is formed in this phase region, the uranium phase must be susceptible to spheroidization by heat treatment, mechanical working, or a combination of these two. Obviously only a minimum of control can be maintained over the final particle size of the uranium phase. The application of this technique, then, to the production of acceptable dispersion type fuel systems has been the exception rather than the rule. A notable exception is the uranium-aluminum fuel plates used in the Materials Testing Reactor.

*b. Powder metallurgy techniques.* While melting and casting may be economically advantageous for a few specific fuel systems, the flexibility and versatility of a variety of powder metallurgy techniques offer one the possibility of producing high-quality fuel elements from many combinations of materials. Because it is possible to form and work elements below the melting point of either constituent, many systems, heretofore rejected upon the basis of extensive reaction, can now be considered. Also, systems composed of two or more components possessing widely different densities can be homogeneously intermixed and subsequently alloyed if desired. Another major advantage of the method is the opportunity of incorporating the fissile phase into the matrix in its optimum shape and size.

The method does possess several disadvantages, however. Both the matrix and fissile phases have to be obtained as properly sized and shaped powders, generally of high purity. The maintenance of this high purity may require the use of special inert atmosphere boxes for some materials which are highly reactive with the normal atmosphere. Finely divided Zr, Ti, U, UC, fall in this category. In order to produce dense bodies and develop the full strength and ductility of the matrix phase, the composite structure has to be mechanically worked. As we shall see later, this operation can destroy the shape and homogeneous distribution of the fuel phase which cannot be corrected by heat treatment as in the case of the U-Al castings.

There are several methods available for combining the components of the fuel system to produce a starting billet. The materials can be cold molded in a hardened die, sintered at a non-reacting temperature, jacketed, and hot or cold worked to final size and shape. The sintering step can be eliminated in many systems. The higher billet densities possible through the use of a hot pressing operation often warrants the use of this more time-consuming operation. This is particularly true where subsequent working operations are to be kept to a minimum. Round elements can be prepared in a similar fashion. Pressed round slugs are loaded into metal tubes which serve the dual purpose of retaining the slugs during mechanical reduction and serving as the cladding

of the final elements. The reduction to size may be carried out by groove rolling, swaging, or drawing. There are other methods of producing dense cladded elements from powder mixtures, but one in particular uses a somewhat unique approach and deserves special mention here. This process is best described as a hot co-extrusion technique. Referring to Fig. 1, the powder billet

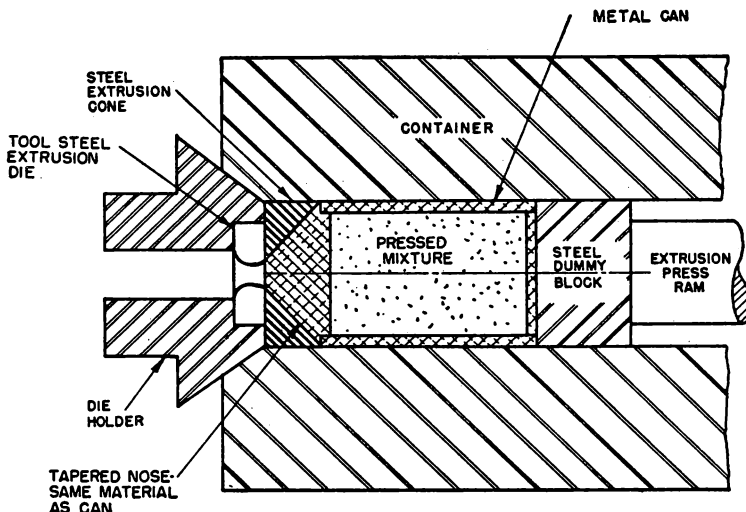


FIG. 1. Arrangement for co-extruding clad rods from pressed metal powder billets.

is placed or pressed inside a metal can or jacket fitted with a tapered nose and flat back plate. This billet is then heated to the extrusion temperature in a separate furnace, inserted into the preheated container of the extrusion press and ejected through the die by applying pressure to the relatively cold back dummy plug. The extrusion cone fitted over the die matches that on the end of the billet and causes the walls of the can to move and be reduced with the billet inside the can. Allowing for the porosity of the billet, both core and wall are reduced proportionate amounts. Upon establishing the proper extrusion parameters, most matrixes in Table I can be extruded into smooth concentric rods. Figure 2 shows the transverse cross section of an iron-UO<sub>2</sub> core clad in iron after being extruded from a 2½-inch diameter billet to ½ inch. Note the excellent uniformity of clad thickness around the whole perimeter of the core. This clad is so intimately bonded to the core that in bond strength tests the core will fail before the bond. The strength of the matrix in the core, adjusting for the volume of the fuel, is generally equal to the strength of the matrix in its solid wrought form.

Since all of the methods described for producing dispersion type elements

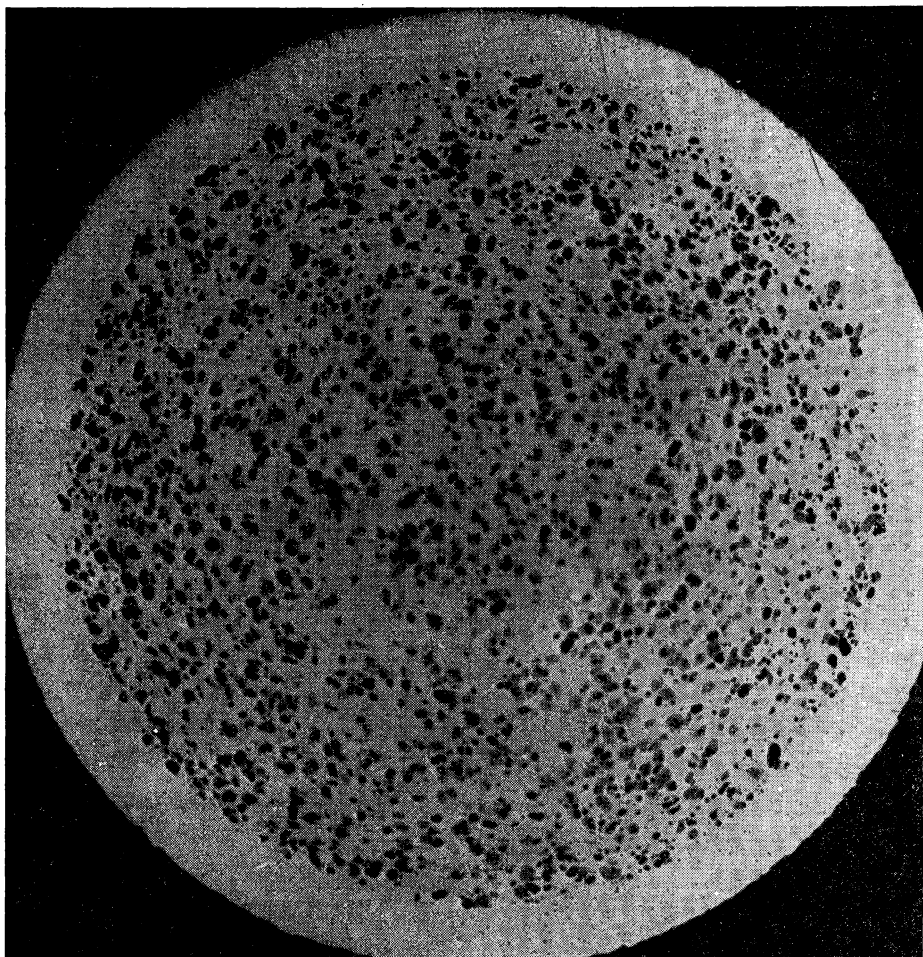


FIG. 2. Transverse cross section of iron clad, iron- $\text{UO}_2$  core co-extruded from  $2\frac{1}{2}$ " diameter to  $\frac{1}{2}$ " diameter (5X).

usually call for some mechanical working to bring the elements to final size and shape, it is necessary to examine the effect of such working on the structure that has been so painstakingly created. In Fig. 3, a longitudinal cross section of an iron clad core of iron- $\text{UO}_2$  is shown after approximately 50% cold reduction. The  $\text{UO}_2$  particles started out at approximately 150 microns in diameter. The fragmentation and longitudinal alignment of the  $\text{UO}_2$  particles (most of them have been pulled out in polishing) creates a structure which could not be expected to sustain high burn-ups. Hot rolling this material at  $1050^\circ\text{C}$  produced the much more favorable structure shown in Fig. 4. These

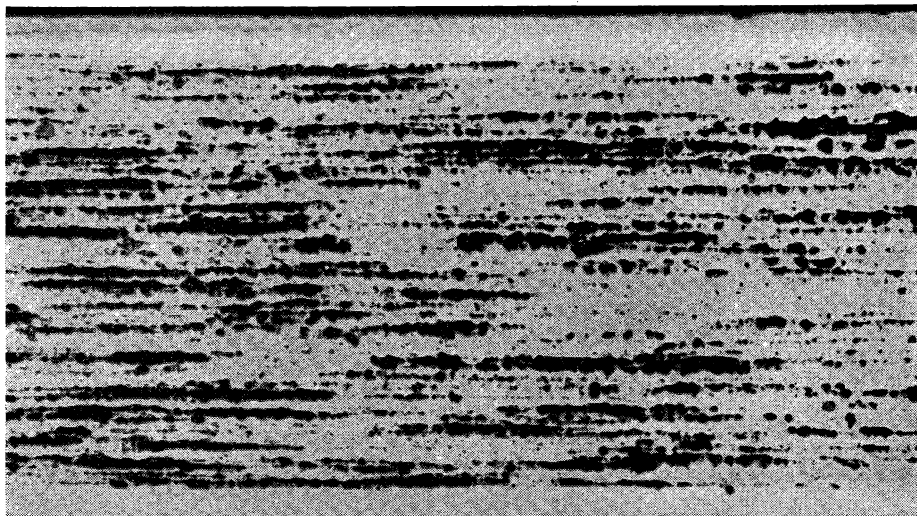


FIG. 3. Longitudinal cross section of cold rolled iron clad, iron- $\text{UO}_2$  core. Reduction in area 50% (20X).

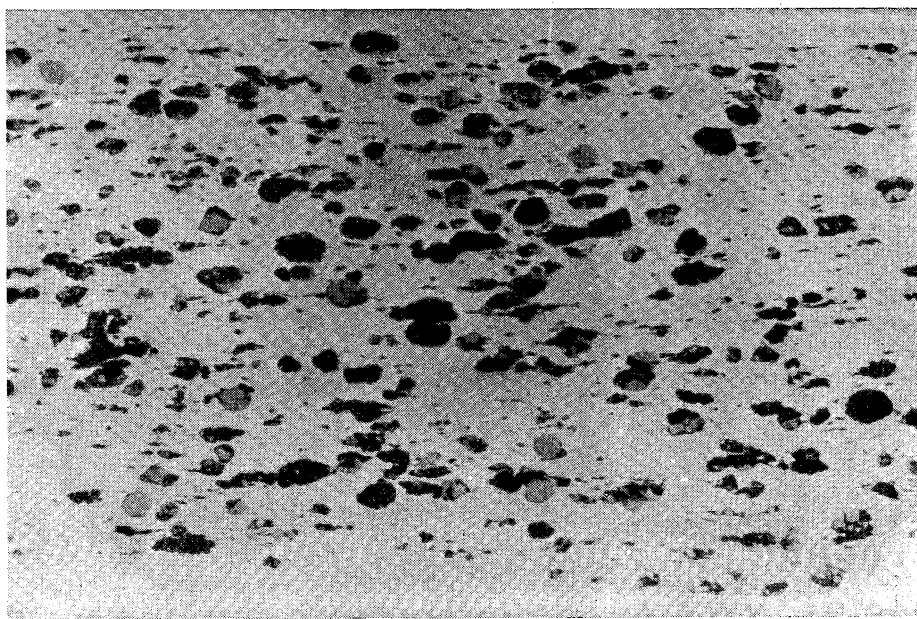


FIG. 4. Longitudinal cross section of iron clad, iron- $\text{UO}_2$  core hot rolled at 1050°C. Reduction in area 50% (20X).

and similar results with a variety of metals and alloys clearly illustrate the need of maintaining the matrix phase in a highly plastic state during any mechanical reduction. The strength, hardness, and density of the fissile phase are also important. High firing of the  $\text{UO}_2$  particles will, for example, greatly reduce its tendency to fragment during rolling.

In actual practice, the choice of particle size of the fissile phase is limited by the dimensions of the final element. A good rule of thumb sets the maximum particle size at one-quarter to one-third the minimum cross section of the fuel-bearing portion of the fuel element, the range reflecting the ductility of the matrix, and the relative clad and core thickness.

There is also a limitation imposed upon the maximum concentration of the fissile phase by the fabricability of the element and its ultimate mechanical properties. This limitation will vary with the size of the fissile particles and the ductility of the matrix, but for most materials there will be a sharp drop in mechanical properties at about 35 volume per cent of the fissile phase. If concentrations above this amount are desired, it may be necessary to select higher uranium concentration compounds. This latter concept was put to application in preparing the fuel plates for the United States reactor displayed at the International Conference on Peaceful Uses of Atomic Energy. The alloy core was to contain over 40 w/o uranium-aluminum alloy. In such an alloy an excessive amount of the aluminum would be tied up as the compound  $\text{UAl}_4$ . The resultant alloy cannot be rolled or otherwise worked into final shape. By substituting  $\text{UO}_2$  for the uranium, the weight concentration of uranium was increased to 54%, but the resultant volume concentration of the  $\text{UO}_2$  was only 22%.

#### B. THE MTR FUEL ELEMENT

Prior to the termination of World War II, as already indicated in Chapter X, work was initiated at Oak Ridge National Laboratory to develop and produce a cheap, reliable thin-plate fuel component for service in a high neutron flux reactor. This effort culminated in the successful start-up and sustained operation of the Materials Testing Reactor at the designed 30 megawatt power level on March 31, 1952. This date was a milestone in reactor development for it not only clearly demonstrated the feasibility of constructing a high-flux research reactor, but also proved that the basic principles employed in the design and manufacture of an aluminum plate-type element were sound.

The fuel elements are made of an assembly of plates, each of which contains an enriched uranium-aluminum alloy core clad on both sides with aluminum, as shown in Fig. 5. The plates are spaced to allow water to flow between them, the water thus serving as coolant and moderator.

Since the construction of the Materials Testing Reactor at the National

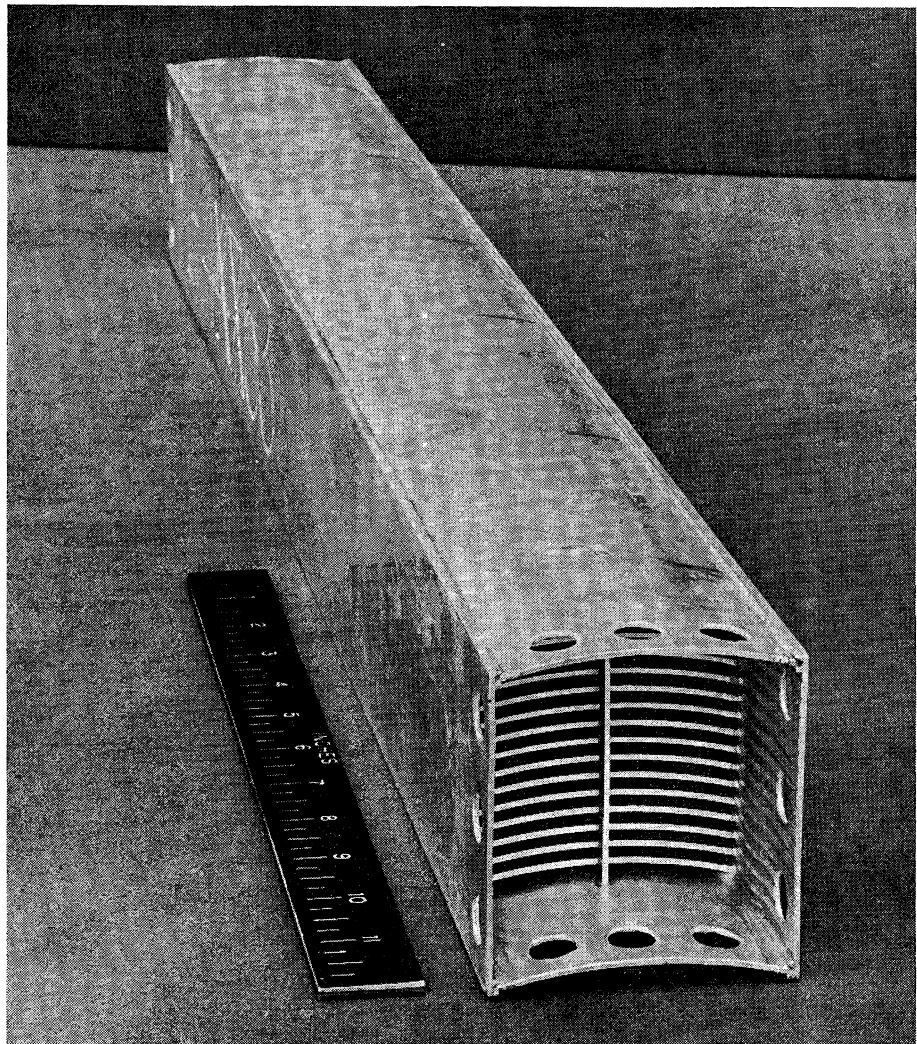


FIG. 5. Braze MTR fuel element.

Reactor Testing Station, Idaho Falls, Idaho, many research reactors in the United States have employed the aluminum plate fuel element. These include the Low Intensity Test Reactor, the Bulk Shielding Reactor and the Oak Ridge Research Reactor in Oak Ridge, the CP-5 Reactor at Argonne National Laboratory, the research reactors at Pennsylvania State University and the University of Michigan, and a number of others at various industrial and governmental research centers.

**1. Materials choice.** Aluminum was chosen for the cladding and structural material for research reactor fuel elements because of its low nuclear cross section, availability, low cost, fabricability and adequate mechanical, physical and chemical properties. The strength and thermal conductivity of aluminum are adequate for the thermal stresses and thermal gradients encountered; and its corrosion resistance is sufficient for the maximum temperatures, i.e., less than 100°C, encountered in the exit cooling water.

Fortunately, the aluminum-uranium alloy system is such that homogeneous alloys can be prepared with uranium contents up to 25 weight percentage. The aluminum-uranium phase diagram is shown in Chapter VII. It will be noted that in the composition range of interest, i.e., 14 to 25 w/o uranium, the structure consists of primary compounds of  $\text{UAl}_4$  surrounded by a matrix of eutectic between aluminum and  $\text{UAl}_4$ . The techniques for preparing such alloys and insuring a homogeneous distribution of uranium will be described in a later section of this chapter.

When it is necessary to prepare alloys with uranium contents greater than 25 weight percentage, difficulties with segregation and resultant non-uniform distribution of uranium are encountered. These difficulties can be obviated by the use of fuel plate cores with a powder metallurgy mixture of uranium oxide ( $\text{UO}_2$ ) and aluminum powder. Fuel plates, with uranium weight percentages up to 60, have been prepared with a uniform distribution of uranium.

**2. Description of fuel component.** Design and construction of aluminum plate-type elements were based on the following criteria: (1) loading the reactor with enriched uranium-235 fuel; (2) cladding to hermetically seal the fuel material from exposure to the reactor cooling water and retain the products of fission; and (3) use of plate-type construction to give a higher surface-to-volume ratio for heat transfer purposes.

The main ingredient of the fuel element is fissionable uranium-235. The fuel is incorporated into the fuel plates of the element in the form of either aluminum-uranium alloy or as a dispersion of  $\text{UO}_2$  in an aluminum powder matrix. The fuel plates, therefore, consist of a fuel-bearing or core section which is clad on all sides with wrought aluminum to form a three-ply composite fuel plate. The hot rolling operation employed results in a good metallurgical bond between clad and core material.

In the case of the Materials Testing Reactor, nineteen fuel plates are assembled into a single unit which is designated as a fuel element or assembly. The fuel plates, with a nominal 0.115-inch water gap between them, are brazed into a pair of aluminum side or spacer plates.

A cross sectional view of a Mark XI, MTR fuel element with dimensional specifications is given in Fig. 6. The spacer, or side plate, is 0.188 inch in thickness, while the 17 internal fuel-bearing plates are 0.050 inch in thickness. The external fuel plates are somewhat thicker, i.e., 0.065 inch, in order to give

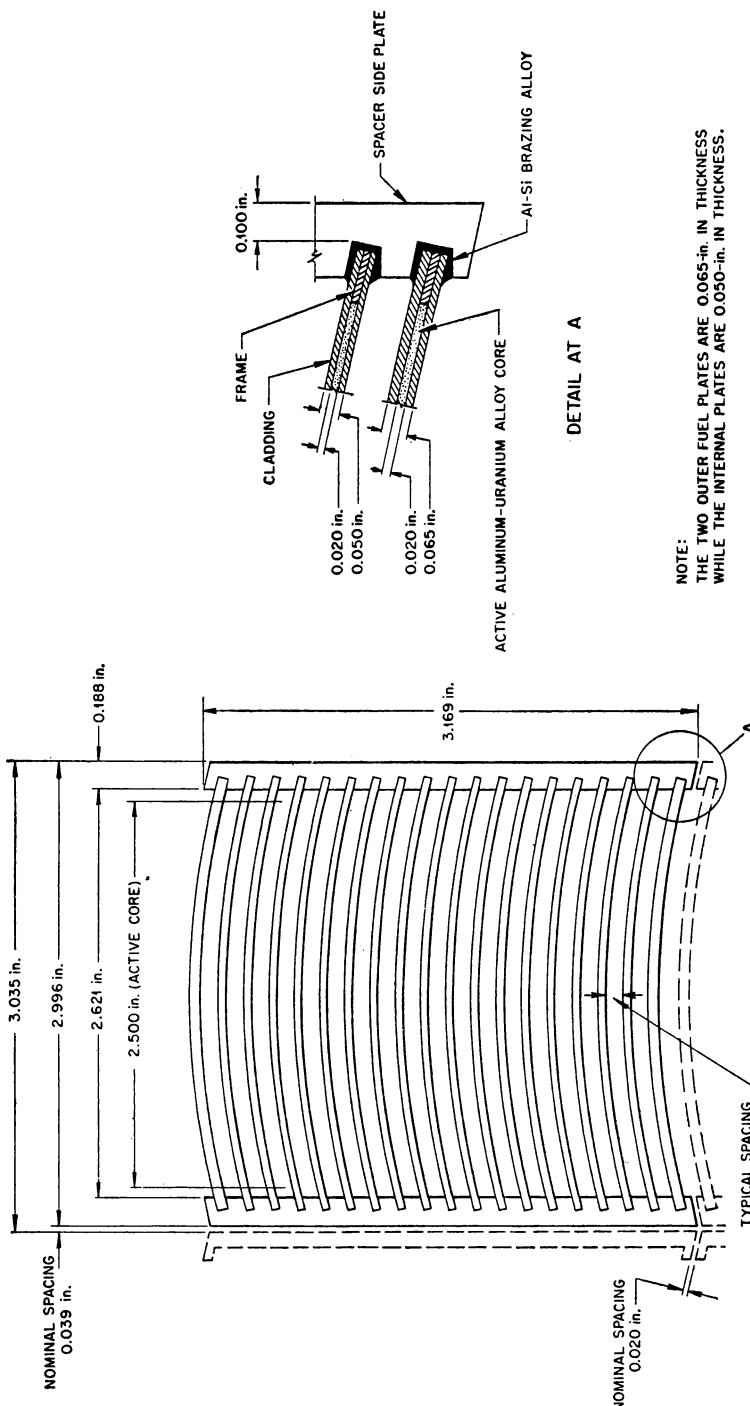


FIG. 6. Dimensional drawing of MTR fuel element cross section.

added cladding thickness and structural rigidity to the fuel component. The center-to-center dimension in the grid for positioning the fuel component is 3.035 inches, while the over-all assembly width is 2.996 inches. This difference allows for a nominal spacing between units in this direction of 0.039 inch. The spacing in the other direction is 0.117 inch, or the same as the water gap between adjacent fuel plates in the assembly.

The water, or heat-transfer medium, flows through the water passages at a velocity of 30 feet per second. The primary coolant system is not pressurized, since film boiling at the water-fuel plate surface interface does not occur under normal operation.

The unit is equipped with cast 356 aluminum alloy end boxes by plug welding. The purpose of the end fitting is to adapt the unit to the supporting grids which in turn firmly fix the position of the element in the reactor core. A spring is provided on the upper casting to allow for thermal expansion and tolerance limitations. These adapters also serve as transition pieces which convert the rectangular cross section of the fuel element to the smaller-sized holes in the grid. The fittings, of course, are hollow to permit free passage of the water through the fuel element. An over-all view of the finished fuel element with end adapters attached is illustrated in Fig. 7.

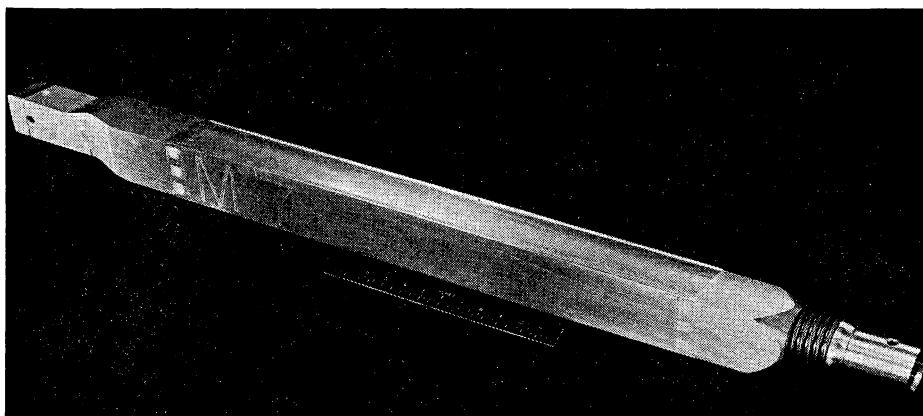


FIG. 7. Over-all view of finished MTR fuel element.

Additional specifications on the MTR Mark XI fuel element are given in Table III. Included for comparison are data on similar plate-type elements employed in the operation of several other research reactors in the United States.

**3. Fabrication of aluminum fuel plates.** Aluminum-clad fuel plates containing uranium-235 are currently fabricated by two methods. These methods, referred to as the alloy and powder method, differ only in the initial prepara-

TABLE III. DESIGN DATA ON SEVERAL ALUMINUM FUEL COMPONENTS IN SERVICE

Reactor Designation	LITR and MTR	CP-5	BSR	GCR
Number of fuel bearing plates	19	10	18	18
Spacer or side plate thickness, inches	0.188	0.125	0.188	0.110
Water gap spacing, inches	0.115	0.154	0.117	0.117
Core composition, w/o	10-20 U-Al Alloy	10-20 U-Al Alloy	10-20 U-Al Alloy	54 UO <sub>2</sub> -46 Al Powder
Metal-to-water volume ratio	0.69	0.39	0.74	0.63

tion of the fuel-bearing core section of the composite plate. The fabrication procedure employed in the manufacture of fuel plates by both methods is described below:

In the alloy method, high purity (99.7%) aluminum and uranium metal, enriched in the U-235 isotope, are alloyed directly to form uranium-aluminum alloy. The melt is prepared in a graphite crucible in the open atmosphere by induction heating. The melt size is fixed by critical mass considerations.

After solution of the uranium and degassing of the melt are complete, the molten alloy is poured into graphite molds to produce cast-alloy slabs for rolling. Because of the large density difference in the melt constituents, careful control of casting conditions is necessary to avoid segregation. Pouring temperature varies as a function of the uranium concentration between 700–1000°C (1292–1832°F). The total uranium and U-235 isotopic composition of the melt are verified by analyzing dip samples taken from the melt.

The cast-alloy slab is heated for one hour at 590°C (1094°F), and hot worked by rolling to produce strip stock of 0.25 inch in thickness. Alloy blanks or fuel plate cores, 2 × 2.25 by 0.25 inches in thickness, are punched from strip stock with a conventional punch and die set.

Similar fuel-bearing cores can be prepared by powder metallurgy techniques. The starting ingredients are (−325 mesh) aluminum powder and enriched UO<sub>2</sub> powder in the selected 44–105 micron size. After proportioning and blending, the amount of powder mixture required for each core compact is loaded into a die cavity and hydraulically pressed under a pressure of 33 tons per square inch.

Each alloy or pressed powder core is completely jacketed by the picture frame technique. The wrought aluminum encasing jacket consists of a frame piece for enclosing the four lateral sides and cover sheets. An exploded view illustrating the component parts, which make up the assembled composite plate for rolling, is shown in Fig. 8.

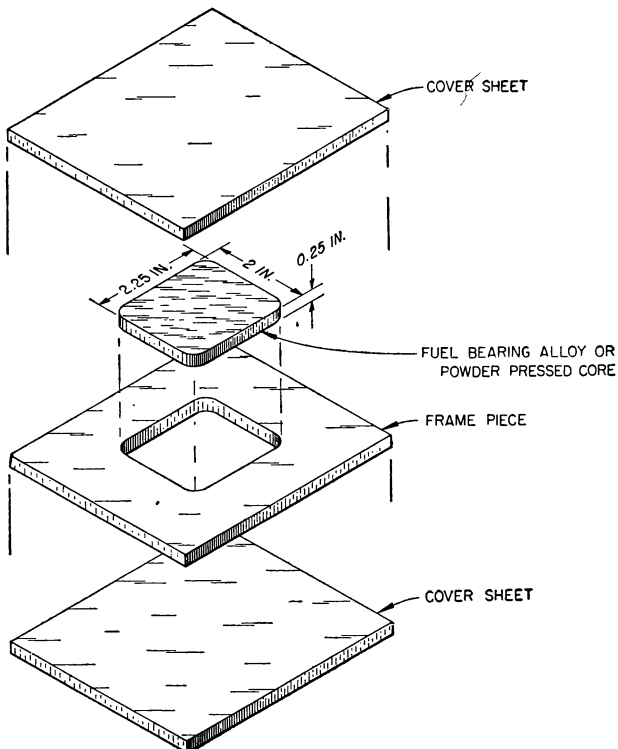


FIG. 8. Exploded view showing makeup of composite fuel plate prior to rolling.

The composite fuel plate assembly is thoroughly heated at 590°C (1094°F) and hot rolled from the starting thickness to 0.070 inch in order to achieve a sound metallurgical bond between clad and core material. The rolling schedule employed consists of six separate hot passes to yield a total reduction in thickness of 84%.

At this stage, the composite fuel plates are flux-annealed to prevent the formation of objectionable blisters which may occur on subsequent processing or during reactor service. Blisters are caused by hydrogen gas which is present in the alloy or mixture.

The flux-annealing treatment consists of coating the surface of the fuel plates with a slurry mixture of alcohol and brazing flux and annealing for one hour at 610°C (1130°F). After treatment, the water-soluble flux, which consists of a eutectic mixture of sodium, lithium, potassium fluorides and chlorides, is removed by a scrub wash. The plates are then dipped in an acid bath of 10 HNO<sub>3</sub>-2HF-80 volume per cent water solution, rinsed in hot water and dried.

The composite fuel plates are reduced cold in several passes to a final thickness of  $0.60 \pm 0.001$  and annealed for one hour at  $590^{\circ}\text{C}$  ( $1094^{\circ}\text{F}$ ). All acceptable plates are examined under a fluoroscopic x-ray screen to locate internal defects, determine straightness and delineate the fuel-bearing core section of the composite fuel plate. After rough shearing, the fuel plates are stacked and batch machined to final width and thickness.

The appearance of a transverse section cut from a finished fuel plate is illustrated in Fig. 9. Prior to assembly, the composite fuel plates are curved in a forming die to the desired 5.5-inch radius of curvature.

**4. Component assembly by brazing.** The curved fuel-bearing plates are joined into a single fuel assembly by brazing. In the case of the Geneva Conference Reactor, eighteen fuel-bearing plates were spaced at 0.177 inch apart and braze into a pair of  $\frac{1}{8}$ -inch thick side or spacer plates to form an integral fuel assembly or element.

The grooved side plates of the fuel element are prepared from braze-clad sheet stock. This material is a duplex sheet consisting of wrought aluminum sheet, clad on one side only with 12% silicon-aluminum brazing alloy. After batch machining the stock to final length and width, the grooves are cut through the braze-clad side of the plates by gang milling. The cutter is designed in a manner to permit cutting all grooves simultaneously with a minimum of chatter.

Prior to brazing, all component parts of the fuel element are thoroughly cleaned and the parts handled thereafter with white, cotton gloves. The side plate grooves are coated with a slurry of brazing flux and alcohol, and positioned upright in the drying jig. The fuel plates are inserted into the proper grooves, aligned and tightened in the jig.

The assembled fuel component is taken through the following sequence of operations which constitute the brazing cycle:

- (1) Dry in an oven at  $150^{\circ}\text{C}$  ( $302^{\circ}\text{F}$ ) for 3 to 4 hours to drive off the water and alcohol from the brazing flux.
- (2) Transfer from the metal drying jig to a ceramic brazing jig.
- (3) Preheat for one hour at  $500^{\circ}\text{C}$  ( $932^{\circ}\text{F}$ ) to thoroughly preheat the components and brazing jig.
- (4) Braze at  $610^{\circ}\text{C}$  ( $1130^{\circ}\text{F}$ ) in a forced-circulation furnace for 25 minutes.
- (5) Cool to room temperature and wash to remove the water-soluble brazing flux.
- (6) Clean in an acid bath followed by hot water rinsing and drying.

The assembly proper is equipped with a lower end box fitting to adapt the unit to the supporting grid, and firmly fix the position of the element in the reactor core. A horizontal handling bar is added to the upper end to facilitate loading and unloading the element in the reactor pool.

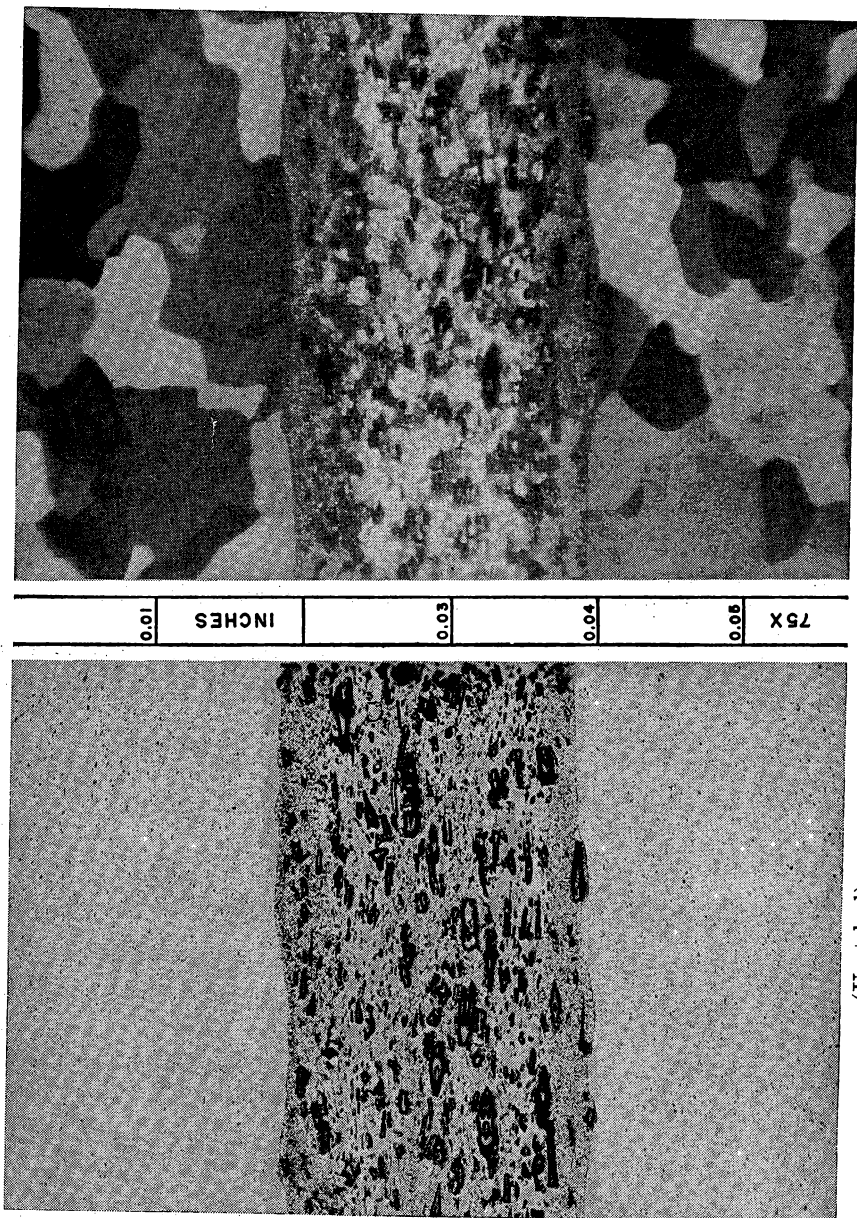


FIG. 9. Transverse section from composite fuel plate.  
(Etched)  
(Unetched)

**5. Reactor performance.** Aluminum fuel elements, described, have performed satisfactorily in reactor exposure to quite high burn-ups. There are only slight dimensional changes accompanied by slight decreases in density in such elements after long-term reactor exposure. With respect to mechanical and physical properties, it has been noted that the yield strength and hardness of an 18 weight percentage uranium-aluminum alloy were doubled after reactor exposure; and there was a marked decrease in ductility. Reductions of 20 to 30% in thermal conductivity have been recorded. However, under the operating conditions encountered in research reactors, the changes described above have not resulted in any fuel element failures or loss of operating efficiency.

## REFERENCES FOR CHAPTER XII

1. See also the following Geneva Papers:  
825—J. P. Howe, "The Metallurgy of Reactor Fuels."  
562—H. A. Saller, "Preparation, Properties and Cladding of Aluminum-Uranium Alloys."
2. J. K. Katz and E. I. Rabinowitch, *The Chemistry of Uranium*, McGraw-Hill Book Co., Inc., New York (1951).
3. R. W. Buzzard, Journal of Research of the National Bureau of Standards 50: No. 2, 63-67 (1953).
4. *Metals Handbook*, 1948 Edition, The American Society of Metals, Cleveland, Ohio (1948).
5. *Metals Handbook*, 1954 Supplement, The American Society of Metals, Cleveland, Ohio (1954).
6. H. K. Adenstedt, J. R. Pequignot, and J. M. Raymer, *The Titanium-Vanadium System*, Transactions of American Society for Metals 44:990-1003 (1952).
7. J. H. Keeler, Unpublished, as described in Geneva Paper No. 561.

# *Chapter XIII*

---

## **FLUID FUEL SYSTEMS \***

---

### **A. INTRODUCTION**

In this, the final chapter in the volume, the properties, problems and advantages of the most advanced type of fuel are discussed. Two types of fluid fuels are presented: the aqueous, which is under development at the Oak Ridge National Laboratory; and the liquid metal fuel, which is under investigation at the Brookhaven National Laboratory. The work on the aqueous system has advanced through a reactor experiment and shows sufficient promise so that a Homogeneous Reactor Test is in progress. The liquid metal fuel system work has progressed to the stage where a reactor experiment is now being considered.

The principal advantages of fluid fuel systems are:

**(1) All fluid fuel systems**

*(a) High specific power*

Since there is no heat-transfer barrier between fuel and coolant, the power density in a liquid-fuel reactor is limited only by the pumping rate and by the temperature rise of the fuel solution itself.

*(b) High burn-up of fuel*

In heterogeneous reactors, burn-up is limited by radiation damage to fuel elements or loss of reactivity. In liquid-fuel reactors, continual removal of poisons is possible as well as continual addition of new fuel, thereby permitting unlimited burn-up.

*(c) Simple fuel preparation and reprocessing*

The use of fluid fuel solutions eliminates the expensive fuel-element fabrication step and simplifies the reprocessing of depleted fuel.

\* This chapter is based on Sections 4 and 5, *Reactor Handbook*, Vol. 2, Engineering AECD-3646; Geneva Paper :821—C. H. Secoy, “Survey of Homogeneous Reactor Chemical Problems”; 118—Weeks, Klamut, and Gurinsky, “Corrosion Problems with Bismuth Uranium Fuels.”

(d) *Easy fuel handling*

Charging and discharging fuel can be accomplished without shutting down the reactor or providing extensive fuel handling facilities.

(e) *High neutron economy*

Neutron economy is improved by eliminating absorption of neutrons by cladding material and structural material within the reactor core.

(f) *Simple control system*

Density changes in the moderator fuel system create a sensitive, negative, temperature coefficient of reactivity which makes this system self-stabilizing. This eliminates the need for mechanically driven regulating rods. In addition, shim control can be achieved by changing the fuel concentration.

**(2) Aqueous systems**

(a) *Neutron economy*

An aqueous fuel system lends itself more readily to spherical geometry which minimizes neutron leakage.

(b) *Wide range of core sizes*

Depending on concentration and enrichment, critical H<sub>2</sub>O and D<sub>2</sub>O homogeneous reactors range from 1½ feet to more than 30 feet in diameter. There is, therefore, a wide range of application for these reactor systems.

**(3) Liquid metal fuel systems**

(a) *High thermal efficiency*

Since it should be possible to operate a liquid metal fuel at high temperatures at low pressures, the thermal efficiency obtainable should be high.

(b) *Absence of radiation effect on the fuel system*

A liquid metal system should be immune to radiation since the chemical bonding is very simple.

The problems encountered in fluid fuel systems are:

**(1) All fluid fuels**

(a) *Corrosion or erosion of equipment*

Circulation of fuel solutions at high rates creates corrosion and erosion problems in the reactor and its associated heat-removal equipment. Special provisions must, therefore, be made for decontaminating and maintaining equipment.

(b) *External circulation of fuel solution*

To achieve the high specific powers mentioned previously, heat is removed by circulating the fuel solutions through external heat exchangers. This increases the inventory of fuel and gives rise to a loss of delayed neutrons, and causes induced activity in the external

equipment which results in additional shielding and maintenance problems.

(c) *Limited uranium concentration*

In solution reactors the uranium is limited by solubility or by corrosion effects.

**(2) Aqueous systems**

(a) *Nuclear stability*

The nuclear stability of the reactor depends on both bubble formation and the hydrodynamics of the system. In aqueous reactors, excessive gas formation resulting from decomposition may occur at higher power densities and give rise to serious fluctuations in reactivity. Solution of these problems may require an extensive development effort for each reactor modification.

(b) *Limited operating temperature*

Either excessive pressure or the phase stability of aqueous systems limits the operating temperature range to 250 to 300°C. This results in lower thermal efficiencies.

(c) *Explosive decomposition product*

Radiation induced decomposition of the moderator can produce an explosive mixture of hydrogen and oxygen in the reactor system. This hazard means that special precautionary design measures must be taken.

**(3) Liquid metal systems**

(a) *Polonium hazard*

In the solution fuel, uranium dissolved in bismuth, the polonium formed by neutron capture of bismuth gives rise to an additional radioactive hazard.

(b) *High melting point*

The high melting point of bismuth makes start-up of a reactor more difficult.

(c) *High density*

The use of a high density fluid such as bismuth should result in an increased pumping cost.

## B. PROPERTIES OF $\text{UO}_2\text{SO}_4\text{-H}_2\text{O}$ FUEL SYSTEM

### 1. Chemical properties

a. *Solubility.* The utility of an aqueous solution in a homogeneous reactor depends on its physical and chemical stability over the range of desired reactor conditions. Of prime importance is the preservation of homogeneity over the desired concentration and temperature range.

The solubility of uranyl sulfate in  $H_2O$  has been determined by Secoy<sup>2</sup> from the ice— $UO_2SO_4 \cdot 3H_2O$  eutectic at  $-38.5$  to  $370^\circ C$ . Figure 1 shows the phase diagram for the system. From Fig. 1 it is apparent that, insofar as solid-liquid equilibria are involved, the solubility of uranyl sulfate in  $H_2O$  is higher at all temperatures from room temperature to  $370^\circ C$  than that required for any proposed homogeneous reactor.

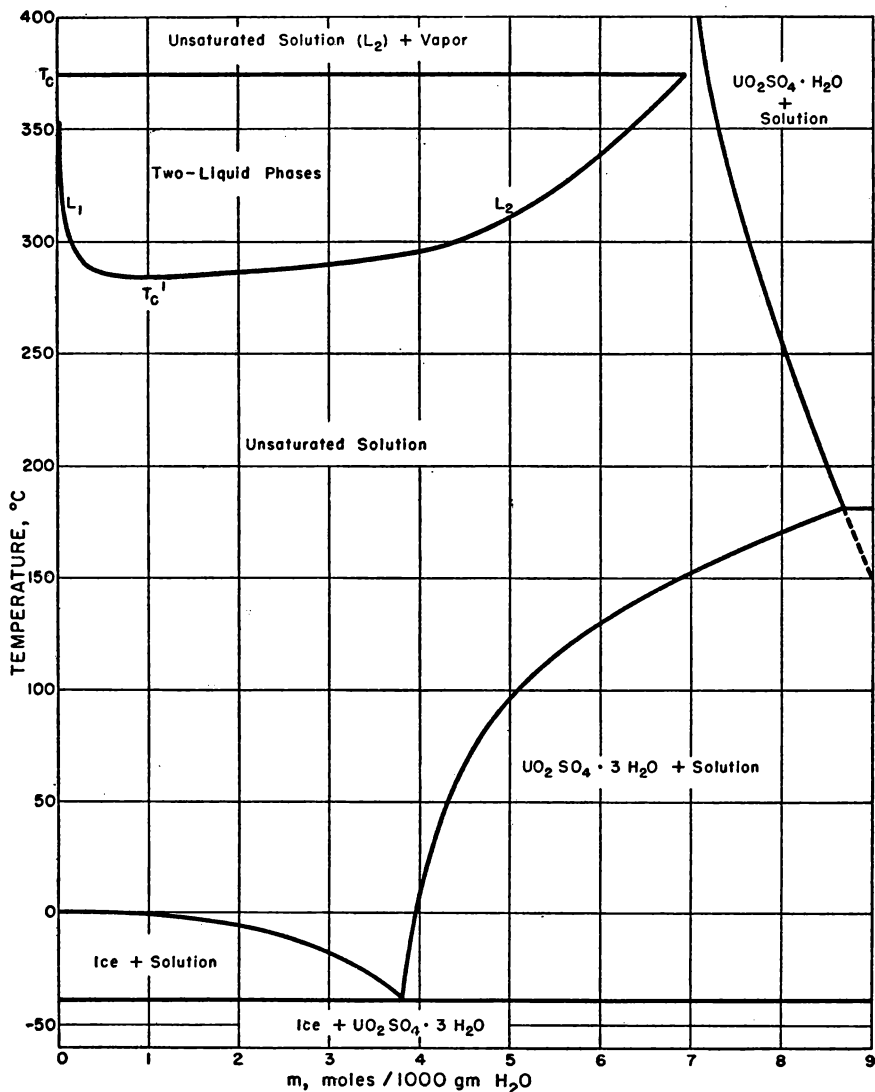


FIG. 1. Phase diagram for the system  $UO_2SO_4 \cdot H_2O$ .

Solutions of uranyl sulfate in  $H_2O$  not saturated with respect to the solid display a two-liquid phase region (miscibility gap) with a minimum critical solution temperature of  $284.5^\circ C$ . The upper limit of the region is the critical temperature of  $H_2O$  ( $374.0^\circ C$ ), at which temperature the water-rich liquid phase and the vapor phase become identical. This region has been studied extensively by Secoy<sup>2</sup> and by Jones and Marshall.<sup>3</sup> A graph of the region plotted from the data of Jones and Marshall is shown in Fig. 2. The data of

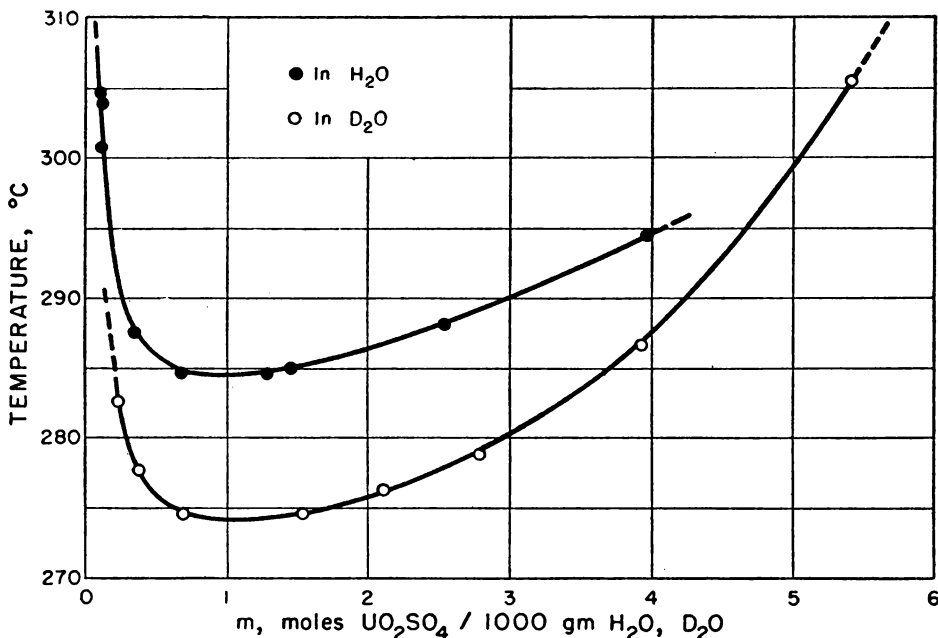
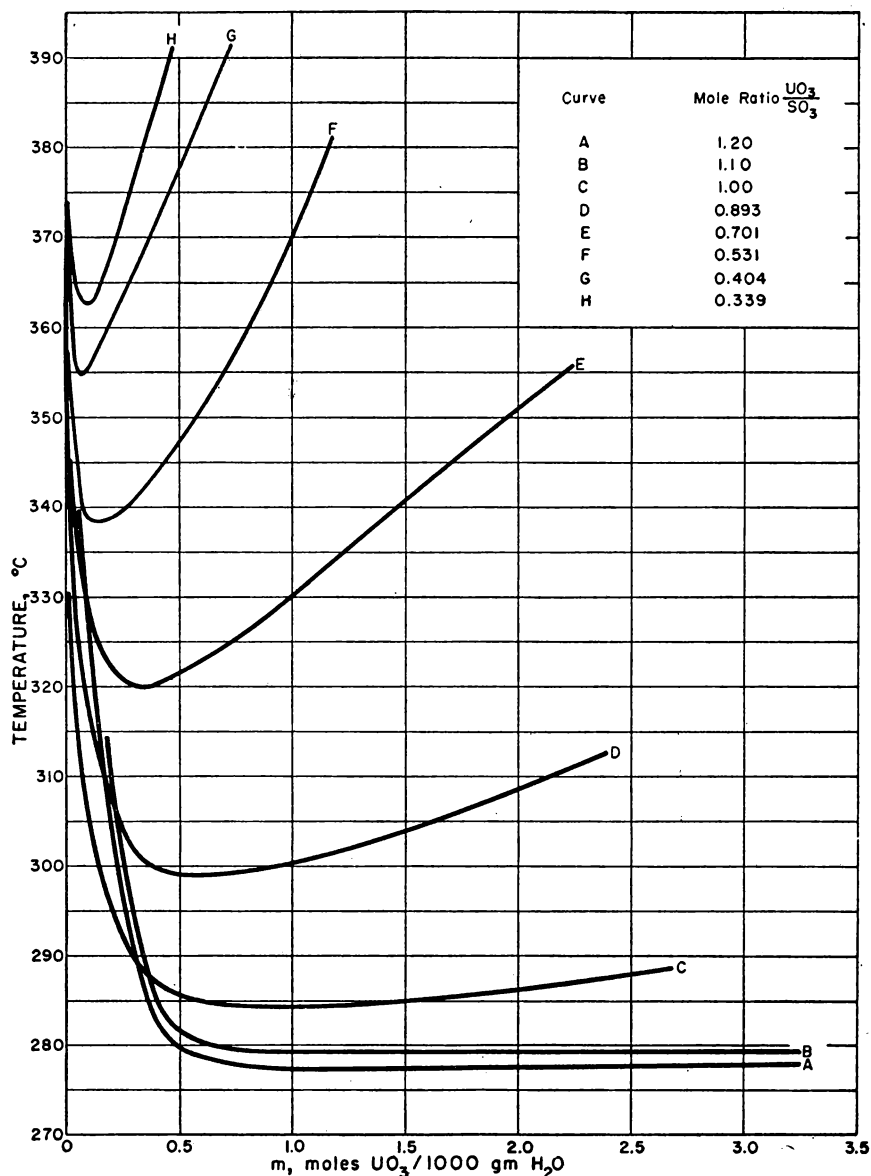


FIG. 2. Two-liquid phase region of uranyl sulfate in ordinary and heavy water.

the latter are believed more nearly correct than the earlier values in that there was a likelihood that the salt used by Secoy was contaminated with traces of acid. Figure 2 gives analogous data for the  $UO_2SO_4-D_2O$  system as determined by Jones and Marshall.<sup>3</sup> The upper temperature limit of homogeneous reactor operation is determined by these curves.

Since it is conceivable to operate a homogeneous reactor with a solution in which the mole ratio of  $UO_3$  to  $SO_3$  is other than unity, studies of the miscibility gap in the three-component system  $UO_3-SO_3-H_2O$  have been made by Secoy and co-workers.<sup>4</sup> Their data are presented graphically in Fig. 3. The marked elevation of the miscibility gap by the addition of sulfuric acid makes possible much higher temperatures of operation, provided a suitable container

FIG. 3. Two-liquid phase region in the system,  $\text{UO}_3\text{-SO}_3\text{-H}_2\text{O}$ .

material for the more acid solution is available and provided the increased pressure which accompanies the increase in temperature is not excessive.

*b. Hydrolysis.* Uranyl sulfate solutions are quite acidic because of hydrolysis. No extensive study of the hydrolytic equilibrium and its temperature dependence has been made, but the pH as a function of concentration has been measured by McInnes and Longsworth,<sup>5</sup> Helmholtz and Friedlander,<sup>6</sup> and Lietzke, Wright, and Marshall.<sup>7</sup> Their data are shown graphically in Fig. 4.

Also of interest in connection with the hydrolytic stability is the solubility of  $\text{UO}_3$  in uranyl sulfate solutions as a function of temperature and concentration. Although a complete study has not been made, some data are available. The general trends indicated by the data are (1) that the solubility of  $\text{UO}_3$  in uranyl sulfate solutions decreases markedly with increasing temperature and (2) that the solubility is nearly independent of the uranium concentration except in very dilute solutions where it also decreases sharply.

*c. Reduction of the uranyl ion.* At elevated temperatures, the uranyl ion is subject to reduction if reducing species are present either in the solution or as constituents of the containing vessel. The products are either black insoluble  $\text{UO}_2$  or  $\text{U}_3\text{O}_8$  or both.

*d. Radiation stability.* When fissioning takes place in aqueous fuel solutions of uranyl sulfate, the observable effects are those which follow upon the decomposition of water to hydrogen, oxygen, and peroxide. Except for the precipitation of uranyl peroxide as discussed below, it has not been possible to demonstrate any radiation instability of the uranyl sulfate. The leading reference<sup>8</sup> for the decomposition of water by fissioning solutions presents initial yields of hydrogen gas production for aqueous solutions of uranyl sulfate, fluoride, nitrate, and uranous sulfate, determined as functions of uranium concentration, isotopic enrichment, temperature, hydrogen ion concentration, and the presence or absence of various anions and added solutes. Values for  $G_{\text{H}_2}$  (molecules of hydrogen produced per 100 electron volts of energy absorbed by the solution) are presented in Fig. 5. For calculations in connection with aqueous reactor systems, it may sometimes be convenient to use the derived formula relating reactor power density to gas production:

$$K = 0.0052 \times G \times PD \text{ moles hydrogen/(liter)(min)} \quad (1)$$

where  $PD$  = the reactor power density in kw/liter, and  $G$  = value appropriate for the solution being considered. This formula assumes that all the fission energy is absorbed by the solution, whereas actually some gamma and some fast-neutron energy will escape. These reported yields all relate to solutions in light water. No yields for heavy-water solutions have been published. Research on this problem is presently under way at ORNL.

A secondary effect of radiation upon uranyl solutions is the formation and

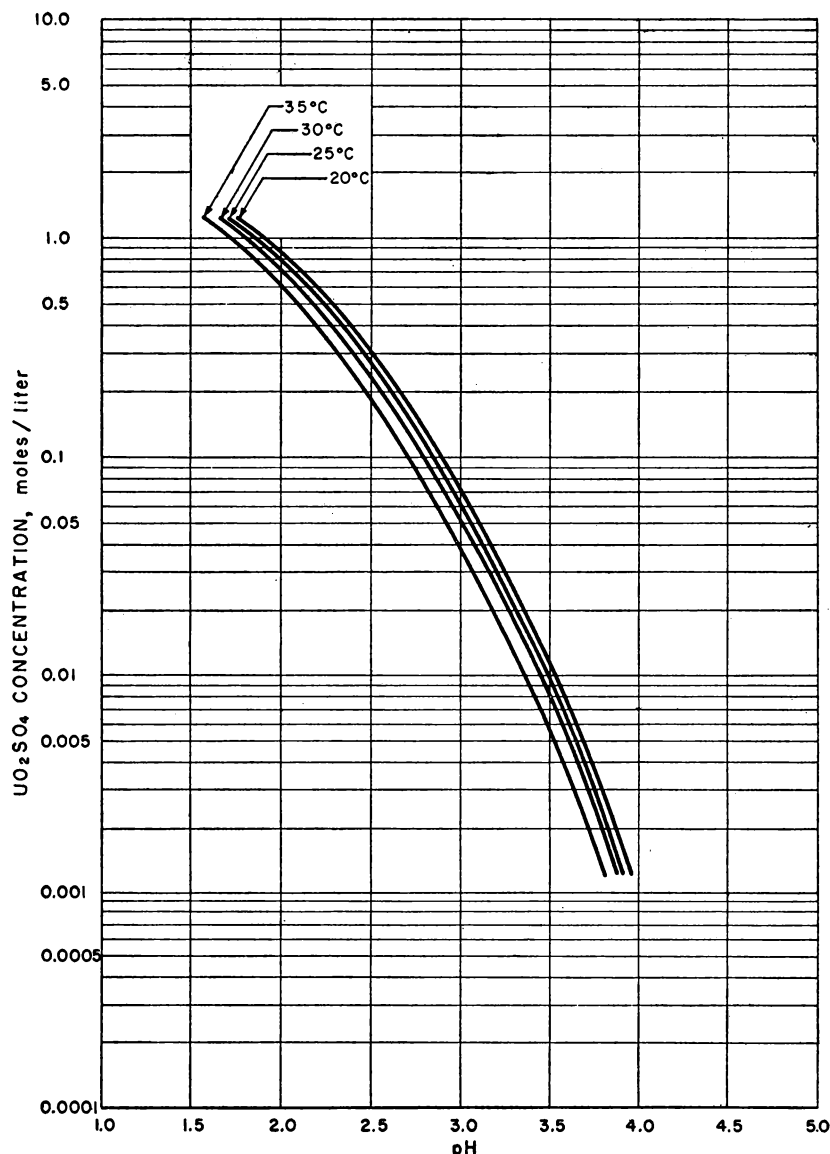


FIG. 4. The relationship of concentration to the pH in aqueous uranyl sulfate solutions at various temperatures.

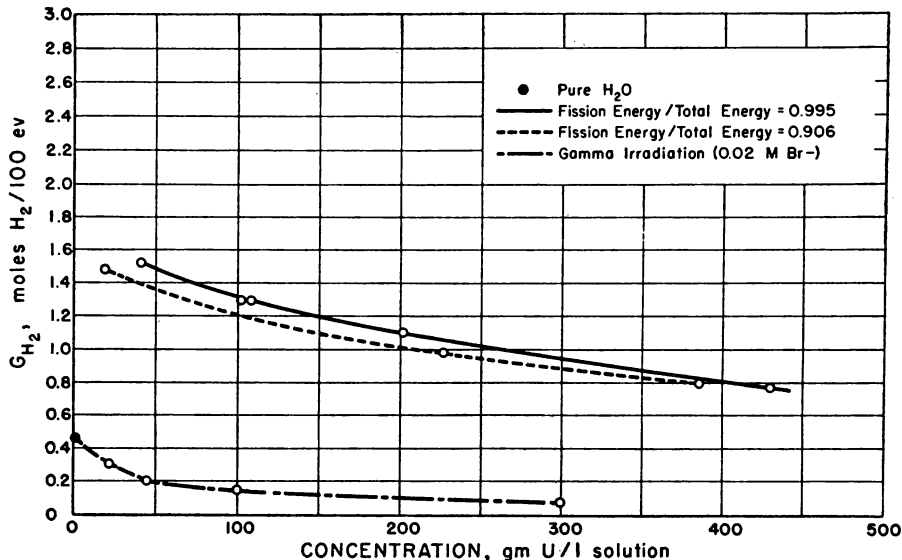


FIG. 5. Effect of uranium concentration on hydrogen gas yields from irradiated uranyl sulfate solutions.

precipitation of uranium peroxide. In discussing the products of irradiation, Boyle et al.<sup>8</sup> present considerable additional support for the assumption that peroxide is an intermediate in the formation of oxygen. Thus, for every molecule of hydrogen formed by radiation decomposition of water, one may assume that one molecule of peroxide is also formed; i.e.,  $G_{H_2} = G_{H_2O_2}$ . If environmental conditions are such that this peroxide is not destroyed, its concentration will rise until the associated equilibrium concentration of uranium peroxide exceeds its solubility limits. Studies of the kinetics of the decomposition of hydrogen peroxide in uranyl sulfate solutions at temperatures up to 100°C have been carried out by McDuffie et al.<sup>9</sup> The tolerable peroxide concentration, if precipitation is to be avoided, is related to a reactor power level, in the case of fissioning solution, by the expression:

$$PD = \frac{C_{ss}}{0.0052 \times G} K_1 \quad (2)$$

where  $C_{ss}$  = the allowable steady-state molar concentration of peroxide

$PD$  = reactor power density, kw/liter

$K_1$  = first-order rate constant for peroxide decomposition in the solution under consideration,  $\text{min}^{-1}$

A brief study<sup>10</sup> of the thermal decomposition of hydrated uranium peroxide in the presence of excess liquid water was made by sealing water slurries of

this compound into Pyrex glass capsules which were then heated for measured lengths of time at various temperatures. Subsequent analyses for total uranium and peroxide uranium were used to measure the extent of decomposition. The half-life for decomposition at 100°C was reported as about 400 hr, whereas the reaction was said to be essentially complete in one hour at 185°C.

Recent experiments at ORNL<sup>11</sup> have raised the possibility of the existence of precipitated uranium peroxide in uranyl sulfate solutions undergoing fission at high temperatures. From this work, it appears that the temperature dependence of the decomposition of peroxide, the tolerable concentration of peroxide to avoid precipitation, and/or the rates of decomposition of crystalline uranium peroxide once formed must be more carefully evaluated at elevated temperatures.

## 2. Physical properties

*a. Density.* Several investigators have measured the density of  $\text{UO}_2\text{SO}_4 \cdot \text{H}_2\text{O}$  solutions at temperatures between 0 and 100°C. Data have been obtained by Orban at the Mound Laboratory for 0.174 to 2.473 molar solutions at temperatures of 20 and 30°C.<sup>12</sup> Densities were measured at 30°C for solutions containing 25 to 60 w/o of anhydrous uranyl sulfate and at temperatures from 0 to 93°C for 51, 39.9, and 29.9% solutions by Helmholtz and Friedlander at Los Alamos.<sup>6</sup> Lietzke, Wright, and Marshall<sup>13</sup> measured the density of 0- to 3.33-molar solutions at 25°C.

Two series of measurements of solution densities at temperatures above 100°C have been reported by ORNL. Secoy determined the volume expansion of a 34.9% uranyl sulfate solution at temperatures from 22 to 372°C. W. H. Davenport and R. H. Powell obtained data for several concentrations at 50°C and for 4.6% solution at 184 to 232°C. These data are reported in convenient form by Marshall.<sup>14</sup>

Marshall has derived equations based on these data which relate the density of uranyl solution to that of water at the same temperature:

$$d_{\text{soln}} = \frac{1}{\frac{78.65}{U} - 1.046} + d_{\text{H}_2\text{O}} \quad (3)$$

$$= \frac{1}{\frac{120.9}{S} - 1.046} + d_{\text{H}_2\text{O}} \quad (4)$$

where  $d_{\text{soln}}$  and  $d_{\text{H}_2\text{O}}$  = densities of solution and pure water, respectively, at the saturated vapor pressure and the temperature of interest

$U$  = concentration of uranium in w/o

$S$  = concentration of sulfate in w/o

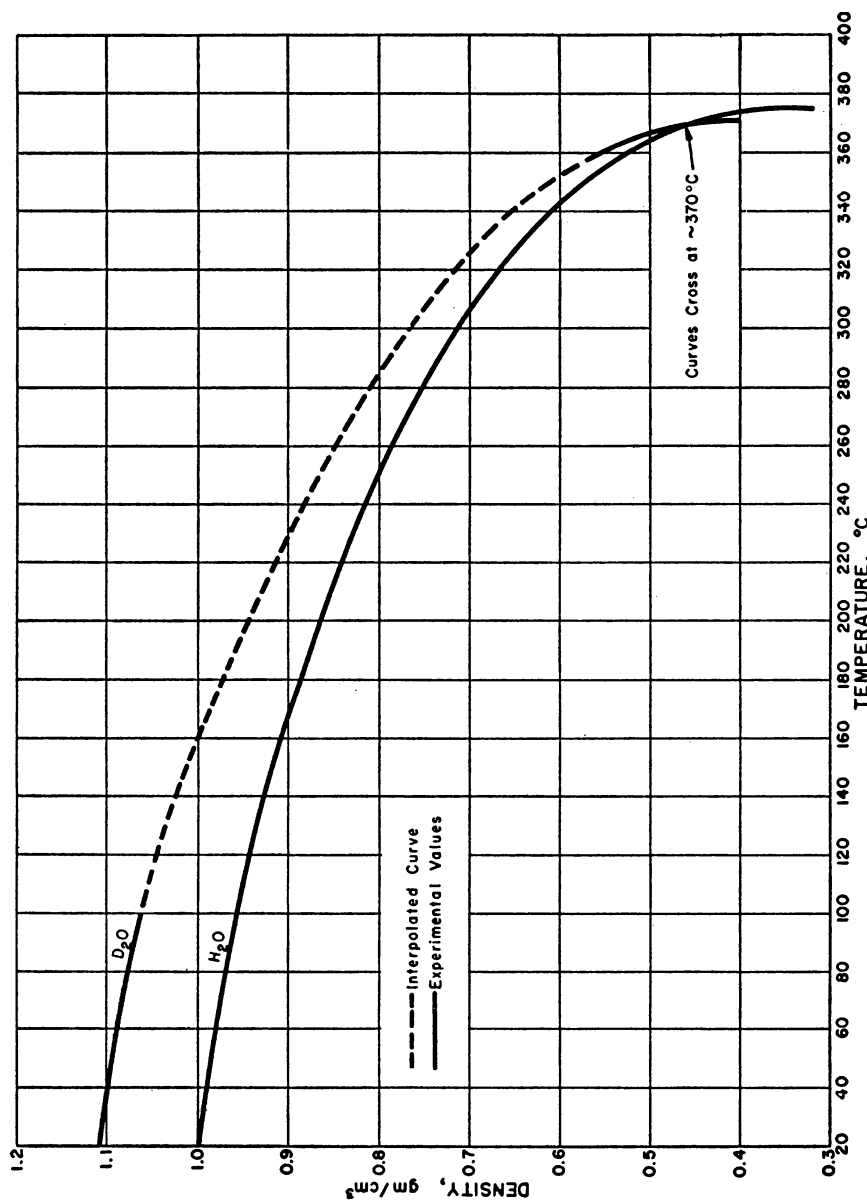


FIG. 6. Density-temperature relation for ordinary and heavy water. Pressure: one atmosphere to boiling point; saturation above boiling point.

The equations agree with the experimental data to  $\pm 0.5\%$  at temperatures from 25 to 300°C with solutions containing less than 10 w/o uranyl sulfate. Agreement to  $\pm 1.0\%$  in the temperature range 120 to 250°C and to  $\pm 2.0\%$  in the ranges 25 to 120°C and 250 to 280°C are obtained with concentrations from 10 to 50%.

A curve of the density of water at the saturation pressure as a function of temperature is plotted in Fig. 6 for use with Eqs. (3) and (4).

*b. Viscosity.* Van Winkle<sup>15</sup> has compared the data of Roarty et al. with published data for H<sub>2</sub>O and D<sub>2</sub>O to obtain the curves shown in Fig. 7. These curves are based upon extrapolation of low-temperature data to high temperatures and are not expected to be accurate.

*c. Heat capacity.* Van Winkle<sup>15</sup> has estimated the heat capacity of dehydrated uranyl sulfate by comparison with uranyl nitrate and with salts of other metals and has estimated the heat capacity of solutions of uranyl sulfate in D<sub>2</sub>O. His estimated heat capacities of solutions at 25 and 250°C are plotted in Fig. 8.

The formula:

$$(C_p)_T = (C_p)_{25} \frac{[C_p(\text{H}_2\text{O})]_T}{[C_p(\text{H}_2\text{O})]_{25}} \quad (5)$$

(where the symbols subscript *T* and 25 refer to temperatures on the centigrade scale at which the respective values for *C<sub>p</sub>* are to be obtained) may be used to estimate the heat capacities of UO<sub>2</sub>SO<sub>4</sub>·H<sub>2</sub>O solutions at elevated temperatures.

**3. Corrosion behavior and materials of construction.** Beall and Swartout<sup>1</sup> have stated that type 347 stainless steel was designated as the material of construction for the homogeneous reactor, except for the Zircaloy-2 core vessel and titanium at points of high turbulence such as pump impellers and the gas separator because previous corrosion and welding experience with this grade of stainless steel had been excellent. Further the homogeneous reactor experiment also had been constructed of this material.

### C. PROPERTIES OF THE U-Bi FUEL SYSTEM<sup>16</sup>

The studies of the U-Bi system as conducted at Brookhaven were aimed at determining the stability and corrosiveness of the fuel system in contact with the reactor construction materials, that is, the moderator graphite and the materials for containing and conduiting the fuel.

**1. The uranium-graphite reaction.** Experiments by Miller<sup>16</sup> in which uranium in bismuth was contacted with graphite for 60 hours (550°C) showed no detectable reaction. A series of small Graph-i-tite\* crucibles were therefore

\* Trade name for grade of graphite impervious to liquid metals produced by Graphite Specialties Corp., Niagara Falls, New York, U.S.A.

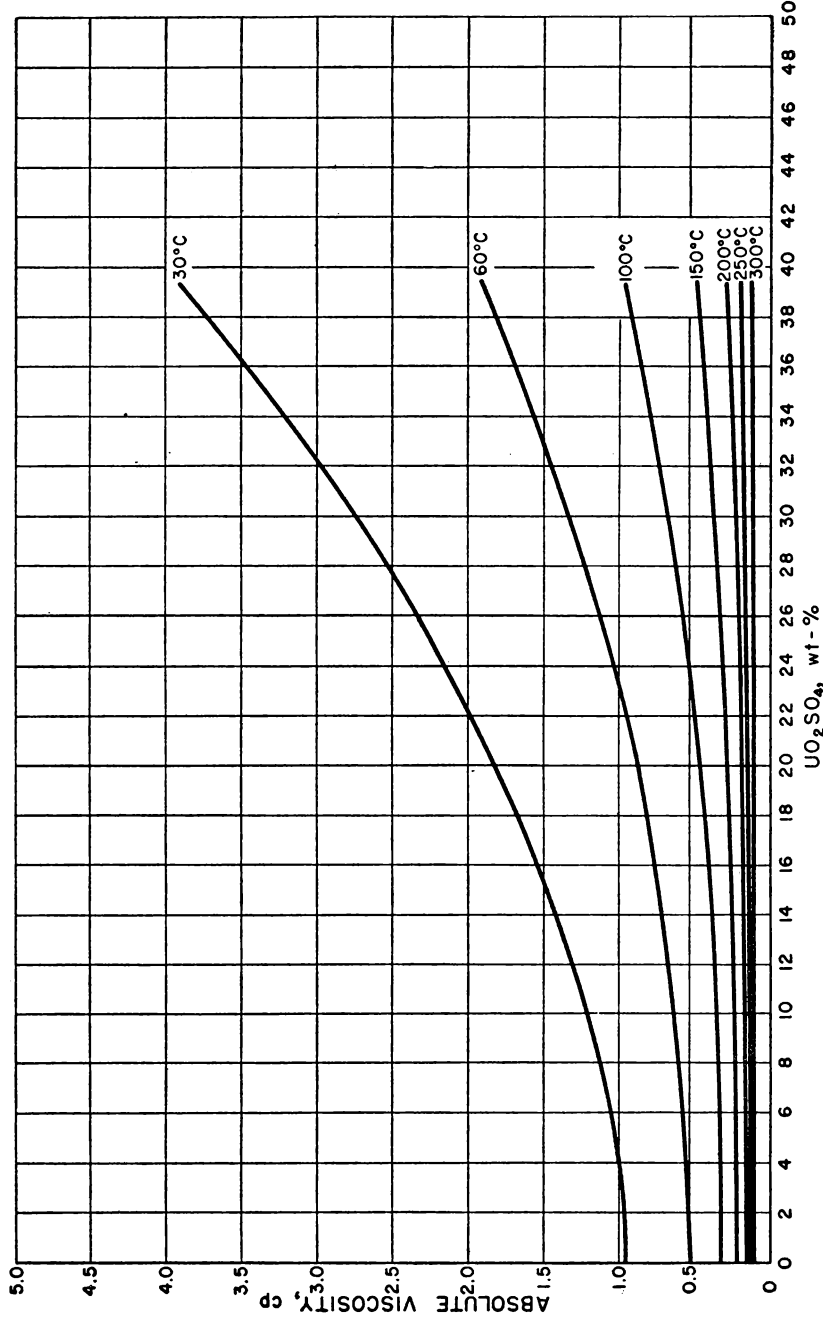


FIG. 7. Viscosity vs concentration for uranyl sulfate solutions at various temperatures.

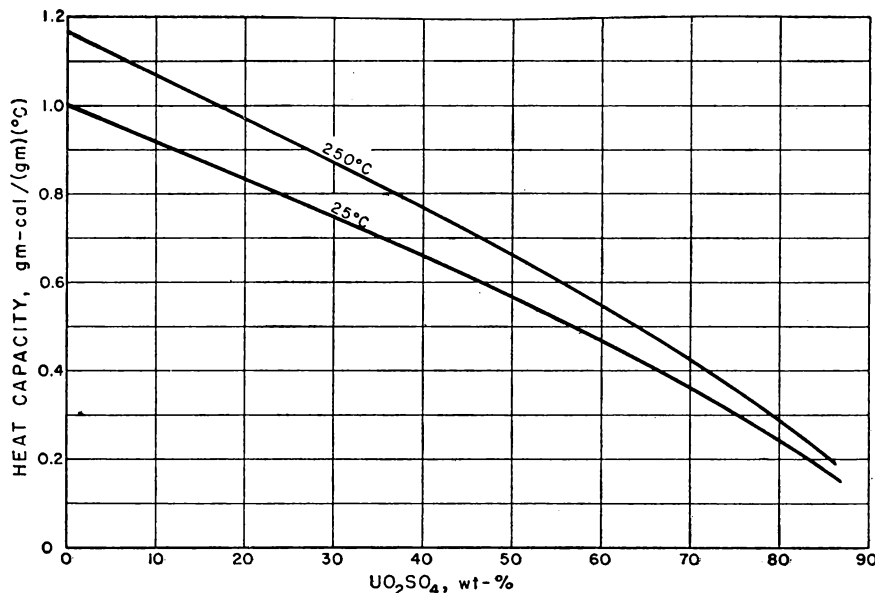


FIG. 8. Heat capacity of aqueous uranyl sulfate solutions.

equilibrated with bismuth and lead-bismuth solutions containing uranium and uranium + zirconium under an He atmosphere at 1000–1200°C for approximately 100 hours. After cooling in the furnace, each crucible was removed and sectioned into slices. One cross-sectional slice was polished and examined microscopically for carbide layer formation at the interface of the Graph-i-tite and the metal. The containing graphite wall of one of the slices was machined to leave a thickness of about 0.010 inch. X-ray reflection patterns were taken through the remaining Graph-i-tite to identify any surface deposits that might have formed at the carbon-bismuth interface.

The results obtained are summarized in Table I. It can be seen that when uranium was added to bismuth in concentrations of 1% or less, no UC was detected at temperatures up to 1200°C (Samples C<sub>2</sub>, C<sub>6</sub>, C<sub>8</sub>). However, when the uranium addition was increased to 4.7% (Sample H<sub>2</sub>), surface deposits of carbide were noted at 1100°C. The addition of zirconium to the liquid bismuth in all samples at temperatures of 1000°C or higher produced surface deposits of a solid solution of ZrC + ZrN identifiable by x-ray diffraction, but invisible at 250× except at 1200°C (Samples C<sub>5</sub>, C<sub>7</sub>, C<sub>9</sub>). Only sample H<sub>1</sub>, where the ratio of uranium to zirconium added was nearly 50 to 1, appears to be an exception to this observation. In all cases, formation of the ZrC-ZrN layer was accompanied by a marked increase in the apparent “wetting” observed between the liquid metal and the crucible wall.

## SOLID AND FLUID FUELS

TABLE I. REACTION BETWEEN GRAPH-I-TITE CRUCIBLES AND U-Bi SOLUTIONS AT ELEVATED TEMPERATURES

Sample	Liquid Metal	Additives, w/o	Reacted at		Surface Deposits	
			Temp., °C	Time, hr	Identified by X-ray Diffraction	Visible at 250X
C <sub>2</sub>	Bi	U 0.05	850	28	UN	None
C <sub>3</sub>	Bi	U 0.32 Mg 0.19 Zr 0.11	850	42	MgO	None
C <sub>5</sub>	Bi	U 0.42 Mg 0.18 Zr 0.18	1000	96	MgO ZrC + ZrN	None
C <sub>6</sub>	Bi	U 1.0	1000	100	None	None
C <sub>7</sub>	Bi	U 1.0 Zr 0.3	1000	100	ZrC + ZrN	None
C <sub>8</sub>	Bi	U 1.0	1200	120	None	None
C <sub>9</sub>	Bi	U 1.0 Zr 0.3	1200	120	ZrC + ZrN	Yes
H <sub>2</sub>	Bi	U 4.7	1100	96	UC	Yes—est. 120 μ
H <sub>1</sub>	Bi	U 4.2 Zr 0.09	1100	96	UC	Not examined
C <sub>10</sub>	Pb-Bi eut.	U 1.0	1000	96	UC	Yes
C <sub>11</sub>	Pb-Bi eut.	U 1.0 Zr 0.3	1000	96	ZrC + ZrN	None
T <sub>1</sub>	Pb-Bi eut.	U 2.0	1000	100	UC	Yes—20 μ
T <sub>2</sub>	Pb-Bi	U 2.0	900	100	UC	Yes—4 μ
H <sub>6</sub>	Pb-Bi	U 4.2 Zr 0.36	1100	96	ZrC + ZrN	None
C <sub>14</sub>	Pb-Bi	U 1.0	1000	96	Not examined	Yes
M <sub>3</sub>	Pb-Bi	Zr 0.54	1000	100	ZrC	None
M <sub>6</sub>	Pb-Bi	Zr 0.51	1100	96	ZrC	Yes—1.5 μ
M <sub>16</sub>	Pb-Bi	Zr 0.52	1200	100	ZrC	Yes—3.5 μ
M <sub>17</sub>	Pb-Bi	Zr 1.0	1200	100	ZrC	Yes—3.5 μ

The use of lead-bismuth eutectic rather than bismuth as a solvent produced a marked increase in the amount of the UC but not of the ZrC formed. Sadofsky<sup>16</sup> showed that microscopically visible deposits of UC were produced from 1% uranium alloys at 1000°C (Sample C<sub>10</sub>) and from 2% alloys at 900°C (Sample T<sub>2</sub>). However, the addition of 0.3% zirconium to this same alloy prevented formation of UC and produced a thin deposit of ZrC-ZrN solid solution not visible under magnification up to 500 $\times$  (Sample C<sub>11</sub>). The addition of 0.36% zirconium to 4.2% uranium alloy in lead-bismuth prevented formation of UC in 100 hours at 1100°C (Sample H<sub>6</sub>). This corresponds to an added uranium to zirconium weight ratio of 11.7 to 1, or atom ratio of 4.5 to 1.

The thickness of the UC deposit produced in 100 hours as a function of temperature was measured by Teitel<sup>18</sup> on samples H<sub>2</sub>, T<sub>1</sub>, and T<sub>2</sub> in order to obtain a 1/T plot. As these three results did not come from identical experiments with respect to concentration of uranium or nature of the solvent (both of which factors are suspected to influence the reaction), and as the deposits of UC on graphite were not adherent or uniform, the use of these data is questionable. However, the measurements did yield a nearly straight line when plotted as the logarithm of the thickness vs 1/T. From the slope, an activation energy of 55,000 calories can be calculated. Extrapolated to 550°C, the thickness of film is of the order of 1 Å. This extrapolation is substantiated by the observations made at 550°C, i.e., no layer detectable microscopically or by x-rays.

The thickness of the tightly adherent ZrC-ZrN deposits as a function of temperature and concentration has also been investigated in lead-bismuth solutions (Samples M<sub>3</sub>, M<sub>6</sub>, M<sub>16</sub>, M<sub>17</sub>). Samples M<sub>16</sub> and M<sub>17</sub> indicated little effect on the film thickness if the w/o of zirconium was varied from 0.5 to 1.0.

A striking demonstration of the ability of zirconium additions of approximately equal atomic per cent to prevent reaction of uranium with carbon at the liquid metal-graphite interface was obtained when autoradiographs of cross sections of crucibles C<sub>14</sub> and C<sub>11</sub> are compared, as in Fig. 9. Here the concentration of uranium at the surfaces of the crucible and the graphite inserts is seen as the radiation halos outlining these surfaces. The addition of 0.3% zirconium completely eliminated these halos. Since a much longer exposure was used in making the zirconium containing autoradiograph, the distribution of uranium throughout the lead-bismuth matrix is visible.

In another test to determine the relative stability of UC and ZrC, samples of a solid solution of ZrC-ZrN,\* which analyzed 78.5% ZrC and 21.5% ZrN were activated in the BNL pile to a Zr<sup>95</sup> activity of approximately 10<sup>5</sup> counts per minute per milligram. One-half gram of this sample was held at the bot-

\* Obtained from the American Electrometal Company, Yonkers, New York, U.S.A.

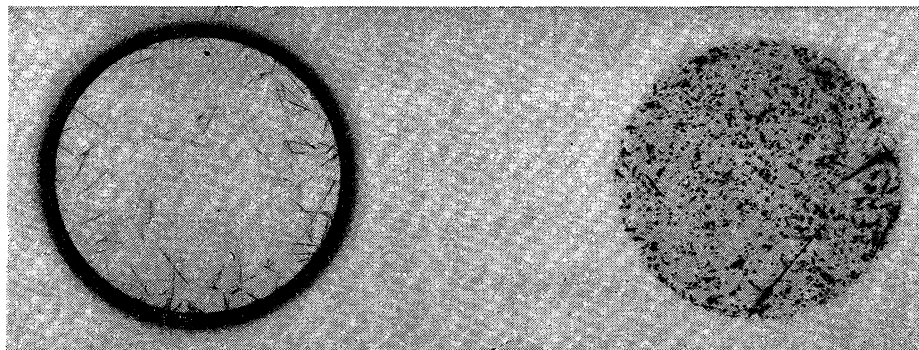


FIG. 9. Autoradiograph of crucibles C-14 and C-11.

tom of a graphite crucible, 350 grams of molten bismuth were vacuum filtered into the crucible, and the temperature raised to 550°C. A filtered liquid metal sample was taken after 24 hours equilibration time; no activity was observed in this sample. The subsequent operations performed on this experiment are outlined in Table II. The slight activity in samples 3-10 is definitely at-

TABLE II. LOG OF EXPERIMENT TO MEASURE REACTION BETWEEN RADIOACTIVE ZrC AND LIQUID BISMUTH SOLUTIONS .

Step	Added	Equili-bration Time, hr	Temp., °C	Activity in 10 Gram Sample
1	350 grams Bi—½ gram radioactive ZrC	24	550	None
2	500 ppm Mg to above	24	550	None
3	500 ppm U to above	72	550	26 c/m
4	—	96	550	19 c/m
5	1000 ppm more U added to above	48	550	90 c/m
6	61 grams Pb to above	24	550	66 c/m
7	500 ppm Zr to above	72	550	70 c/m
8	Raised temp. to 725°C	24	725	50 c/m
9	Raised temp. to 825°C	24	825	40 c/m
10	—	48	825	40 c/m

tributable to the uranium. When 0.0006 gram of the Zr<sup>95</sup>C was placed in the center of the 10 gram slug of bismuth (so as to have maximum self-adsorption) the counts per minute were found to be 1000 under this geometry. This corresponds to 60 ppm zirconium in the bismuth. It was concluded that ZrC does

not react with lead-bismuth containing 1500 ppm uranium and 500 ppm zirconium in 48 hours at 825°C.

The UC reactions were also studied by Klamut and Silberberg<sup>16</sup> in an engineering type test. Steel \* (2½ Chrome) and graphite were contacted with bismuth containing zirconium + magnesium. The concentration of these elements in the bismuth was determined as function of time. When no further drop in concentration of zirconium and magnesium was observed, a fixed quantity of uranium was added to the liquid alloy. The concentration of the uranium was then followed as a function of time. Two experiments which ran over 7000 hours showed that after an initial loss of the order of 15%, the concentration of uranium remained constant for the entire period of the test.

From the experiments on uranium, zirconium and carbides, it was concluded that zirconium prevents the formation of UC under conditions that normally would result in the formation of UC. The zirconium reacts to form a thin, adherent layer of ZrC-ZrN on the graphite surface. The amount of zirconium required is less than ¼ of the uranium atom concentrations in the liquid metal. The initial uranium loss noted in the composite tests (steel-graphite-uranium-zirconium-magnesium-bismuth) may be due to a reaction of the uranium with the surface impurities of the steel or the impurities in bismuth.

**2. Stability of the uranium bismuth fuel with respect to materials other than graphite.** The primary requisite of a material for a liquid metal fuel reactor must be its inertness to the fuel solution. In order to determine the stability of the uranium-bismuth fuel with respect to steel, a number of experiments were performed. These include a measurement of the effect of additives and steel corrosion products on the solubility of uranium in bismuth, a study of losses incurred on adding uranium to bismuth in steel, and the effect of several deoxidants added to bismuth on these losses.

*a. The effect of Fe, Cr, Ni, Mg, and Zr on the solubility of uranium in bismuth.* The solubility of uranium in pure bismuth was determined by Bareis,<sup>16</sup> using both a filtering and a settling method. The results obtained are shown in Fig. 10. This solubility curve can be approximated by the equation:

$$\log_{10} (\text{w/o U}) = 3.13 - \frac{2550}{T(\text{°K})} \quad (1)$$

The accuracy of this curve to within normal analytical error ( $\pm 10\%$ ) has been substantiated by subsequent work by Teitel.<sup>17</sup>

The effect of Fe and Cr on the solubility of uranium in bismuth was investigated by Bryner<sup>16</sup> at 450°C using a filtration technique. The chemical analysis of the filtrates from the Fe crucibles in which the experiments were performed indicate that the solubility of uranium in bismuth is not affected by

\* Nominal compositions of the steels used in this work are given in Table V.

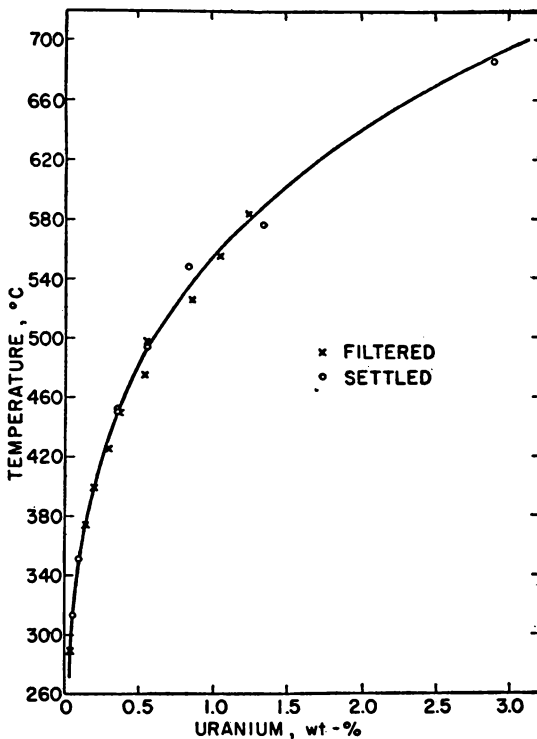


FIG. 10. Solubility of U in Bi.

the dissolved Fe. Two additional experiments were conducted to determine the stability of U-Fe intermetallic compounds in liquid bismuth. Microexamination of the residue obtained from equilibration of  $\text{UFe}_2$  with bismuth at 800°C followed by filtration at 450°C showed that the  $\text{UFe}_2$  had decomposed completely, forming  $\text{U}_3\text{Bi}_5$  and small particles of Fe in the bismuth. A specimen of  $\text{UFe}_2$  and  $\text{U}_6\text{Fe}$  eutectic decomposed partially, forming  $\text{U}_3\text{Bi}_5$ , and leaving lumps of what was presumed to be  $\text{UFe}_2 +$  eutectic. The filtrate from both experiments showed the normal uranium solubility. The results on Cr are not as conclusive, due to inadequate temperature control. They do suggest that Cr, like Fe, has little or no effect upon the solubility of uranium in bismuth.

The effect of Ni on the solubility of uranium in bismuth was first determined at 450°C by Bryner,<sup>16</sup> using a graphite crucible lined with approximately 3 grams of Ni sheet. In duplicate tests, the Ni sheet dissolved completely; the filtrate contained 0.012 w/o uranium and approximately 1.8 w/o Ni. This corresponds to approximately a 30 to 1 reduction in the uranium solubility. Two intermetallic compounds found in the residue were identified by metallographic and chemical analysis to be  $\text{UNi}_2$  and  $\text{UNi}_5$ . No  $\text{U}_3\text{Bi}_5$  was

observed in the residue. The compound  $\text{NiBi}_3$  precipitated in both filtrates upon cooling from 450°C.

The effect of several Ni concentrations on the solubility of uranium in bismuth was measured by Weisman.<sup>18</sup> Small, predetermined amounts of Ni foil were added to a uranium-bismuth alloy, and the alloy equilibrated before filtering. The results obtained at 500°C and at 350°C are shown in Fig. 11.

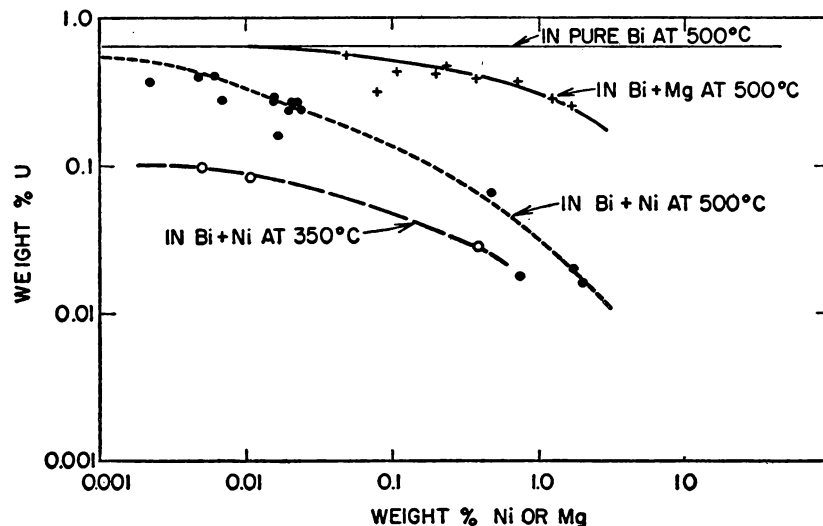


FIG. 11. The effect of Ni and Mg on the solubility of U in Bi.

It can be seen that the presence of Ni causes a large decrease in the solubility of uranium in bismuth.

The effect of magnesium on the solubility of uranium in bismuth was also investigated by Weisman at 500°C. These results are also shown in Fig. 11. It can be seen that, while magnesium has some effect on the uranium solubility, this is slight at 500°C at low magnesium concentrations.

The solubility of uranium in bismuth containing magnesium was determined as a function of temperature in a 5 chrome steel crucible by Weeks.<sup>16</sup> Filtered liquid metal samples were taken over the temperature range 300–635°C. Next, zirconium was added to the melt to make approximately 500 ppm and another series of liquid metal samples were taken. The samples were analyzed chemically for uranium, Fe, and Cr, and spectrographically for magnesium and zirconium. The results obtained are shown in Fig. 12. The data for the solubility of uranium in pure bismuth are also shown for comparison. The magnesium concentration averaged 1275 ppm and remained essentially constant throughout the experiment. When zirconium was present, it averaged 400 ppm, except at temperatures below 400°C where 400 ppm is greater than

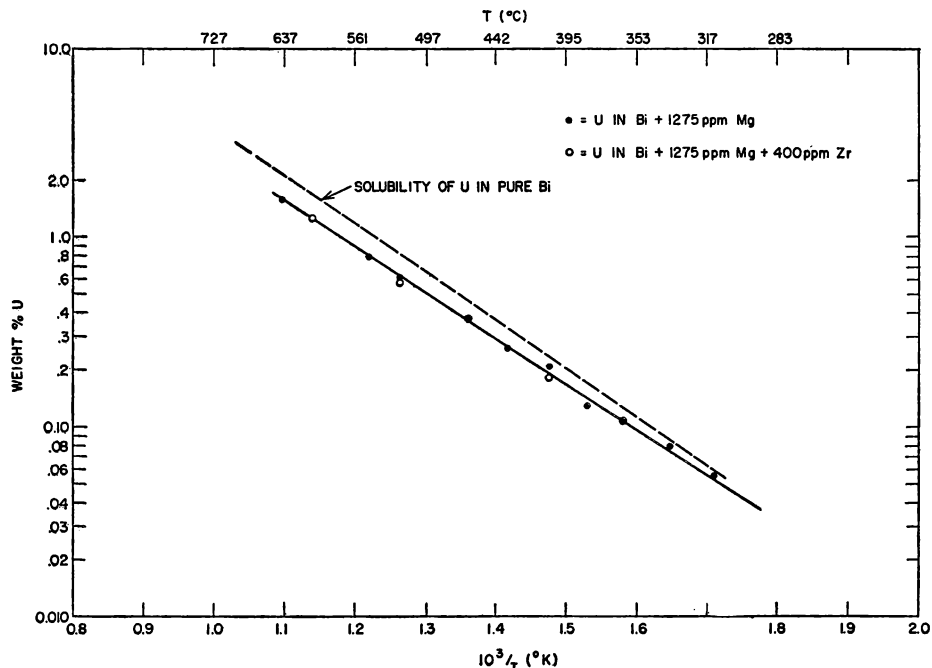


FIG. 12. The solubility of U in Bi and in 1275 ppm Mg + 400 ppm Zr in 5 chrome steel crucible.

saturation. Iron was present in all samples at approximately its normal saturation and Cr was less than 10 ppm in all samples. The results indicate that the effect of magnesium on the uranium solubility becomes greater as the temperature is increased, and that 400 ppm zirconium has no additional effect.

*b. The recovery \* of uranium upon addition to bismuth in steel systems.* Considerable difficulty was encountered by Klamut and Silberberg<sup>16</sup> in making quantitative uranium additions to liquid bismuth in steel containers. Attempts to add the uranium, magnesium and zirconium simultaneously to the system nearly always resulted in large (50% or greater) initial losses of uranium. However, after this initial loss, the concentration of uranium in one steel container remained constant at 450 ppm for over 20,000 hours.

Pre-conditioning the steel convection loops with bismuth containing magnesium and zirconium for periods from 43 to 660 hours before adding the uranium improved the recovery of uranium in the liquid metal to 80–87% in 5 tests. The concentrations of uranium in these pre-conditioned steel containers remained constant for the 2500 hours of operation.

\* The losses are probably due to reaction of uranium with oxides or nitrides on the surfaces of the steel.

A series of 2½ chrome steel "test-tube" experiments were performed to compare the relative abilities of various additions to bismuth to pre-condition the steel bismuth system in an effort at obtaining a higher recovery of uranium in the bismuth solution. One inch IPS 2½ chrome steel pipes were pre-treated with bismuth containing Mg + Zr, Th + Zr, and Ca + Zr until the concentration of these additives remained constant with time. Sufficient uranium was then added to each tube to make 1000 ppm and its concentration in the liquid metal was measured as a function of time. Pre-conditioning with 350 ppm magnesium and 250 ppm zirconium yielded a uranium recovery of 98% for 72 hours; the uranium concentration then dropped to 75% of its initial value and remained constant for 2500 hours. Increasing the magnesium concentration at this time to 1000 ppm had no effect on the amount of uranium in solution.

Pre-treatment with 1000 ppm magnesium and 250 ppm zirconium in the liquid bismuth gave a uranium recovery of 97% for the first 160 hours; this subsequently dropped to 84% and then remained constant for 800 hours.

Pre-conditioning with 200 ppm thorium and 250 ppm zirconium in the liquid metal gave a 100% recovery of uranium for over 800 hours. However, it was difficult to maintain thorium concentrations in the alloy; additional amounts had to be added twice during the experiment, and the concentration of thorium never stabilized. Pre-conditioning with 500 ppm Ca and 250 ppm Zr resulted in a 100% recovery for over 1200 hours (duration of test).

These data indicate that the best recoveries of uranium are obtained when very strong deoxidants such as Ca and Th are used.

**3. Corrosion and mass transfer of Fe and Fe + Cr by liquid bismuth.** If liquid bismuth is convectively circulated through a closed loop by maintaining a temperature gradient on opposite sides of the loop, the temperature differential of the solubility of the container metal in liquid bismuth will require the container metal continuously to dissolve in the hotter portion of the loop (or hot leg) and to precipitate from the supersaturated solution in the colder portion of the loop (or cold leg). This phenomenon was noted in the development of the mercury boiler. Reid<sup>19</sup> has reported that a marked reduction in transfer is achieved if titanium is added to the circulating mercury.

The early work on the corrosion resistance of materials to liquid bismuth is reviewed in the *Liquid Metal Handbook* (1952). It was found that ferritic iron, low carbon steel, and the low-alloy steels have good resistance to bismuth at temperatures below their transformation temperatures, whereas the austenitic (Ni-bearing) stainless steels suffer pronounced attack in the temperature range 480–1200°C.

Elgert and Egan<sup>20</sup> have also investigated the resistance of steels to dynamic corrosion and mass transfer by liquid bismuth. They attempted to control the process by using small amounts of Ti + Mg as inhibitors or by covering the metal with a protective coating such as an oxide or ceramic

layer. They found a greater than 100 fold reduction in the corrosion rate of 5 chrome steel by adding more than 50 ppm Ti and 350 ppm Mg to a thermal convection loop with a temperature differential 700–615°C. Deoxidation of the system by adding Ca or Mg to the liquid metal had little effect on the corrosion rate. Pre-coating the steel with a heavy oxide film reduced the corrosion rate. Little correlation was observed between the corrosion rate and the Cr content of the steels; all runs testing only chrome alloyed steels, without additives to the liquid metal, gave excessive corrosion rates.

Work by Cygan<sup>21</sup> on mass transfer of low carbon and chromium steels by lead-bismuth eutectic demonstrated that, when a steel surface is not completely deoxidized, considerable difficulty may be encountered due to formation of a  $\text{Bi}_2\text{O}_3$  plug in the cold leg. This difficulty was largely overcome by placing an Alnico magnet in a quartz capsule inside an enlarged chamber at the exit of the cold leg, the life of one loop being increased more than thirty-fold by this unique device.

Terry and Skeats<sup>27</sup> have published an extensive bibliography on the available information on corrosion and handling of liquid bismuth.

Based largely upon the experience gained in the development of the Hg boiler, the low chromium steels were investigated by Gurinsky et al.<sup>16</sup> as container materials for uranium-bismuth solutions, using metallic additives as inhibitors.

Of the two inhibitors, titanium and zirconium, discovered in the development of the Hg boiler, zirconium was selected over titanium for use in a reactor fuel because (1) it has a low capture cross section to thermal neutrons, and (2) it is a fission product, and thus will be continuously generated within the liquid metal stream. Further, the demonstration that zirconium will protect the uranium in the liquid bismuth from reaction with the graphite moderator strengthened the hope that zirconium could also be used successfully as an inhibitor to mass transfer of the container material by the liquid metal fuel. The test program consisted of engineering tests and fundamental work.

#### *a. Engineering tests*

(1) *Static tests.* Static testing first used by M. A. Cordovi<sup>22</sup> was extended by Atherton<sup>23</sup> to study corrosion of materials by liquid bismuth. All static testing was done at 550°C. Graphite was used to contain the test material because when uranium and zirconium are added to the bismuth, Pyrex or quartz is attacked by these materials, thus depleting them from the solution, and because graphite is very slightly soluble in bismuth and should not affect the test materials. Separate tests by Kammerer<sup>16</sup> to verify this showed that no carburization of the steel specimen was observed when zirconium was present in the bismuth even if the test was run at 750°C.

Two methods were used to purify the bismuth metal prior to feeding it into

the graphite crucible. One was to bubble purified H<sub>2</sub> through the molten bismuth and then filter it into the crucible. The other was just to filter into the crucible. The oxygen content of the bismuth thus treated was 2 and 4 ppm respectively. At the end of the test, i.e., 1000 hours at 550°C, the sample was removed from the furnace and the assembly immediately inverted. This operation decanted the bismuth from the graphite crucible into the Pyrex reservoir. After cooling, the sample and graphite container were visually inspected for wetting. A transverse section was then cut from the specimen and chrome plated. It was then mounted in bakelite and prepared for metallographic examination in the usual manner. Table III shows some of the

TABLE III. SAMPLE RESULTS OF STATIC CORROSION TESTS ON VARIOUS MATERIALS IN LIQUID BISMUTH 1000 HOURS AT 550°C

	Bismuth Media Chemical Composition				$1 \times 10^{-3}$ in. Maximum Penetration
	Bi	U	Mg	Zr	
Armco Iron *	100	—	—	—	0.71
Armco Iron	99.9	0.1	—	—	0.55
Armco Iron	99.9	—	0.1	—	0.78
Armco Iron	99.9	—	—	0.1	0
Armco Iron	99.8	—	0.1	0.1	0
2½ Chrome	100	—	—	—	0.59
2½ Chrome	99.6	0.4	—	—	0.78
2½ Chrome	99.8	0.1	0.05	0.05	0
5 Chrome	100	—	—	—	1.36
5 Chrome	99.4	0.4	0.1	0.1	0.34
304 Stainless Steel	99.6	0.4	—	—	2.1
Molybdenum	100	—	—	—	0

\* Analyses of these and other steels used in test work are given in Table V.

results obtained from these tests. The effect of zirconium and other metals added to the bismuth is evident.

(2) *Loop tests.* A thermal convection loop is probably the simplest method to study the corrosion and mass transfer by a circulating fluid. A typical loop of the type used by Silberberg<sup>16</sup> is shown in Fig. 13. Flow was established by applying heat to the well-insulated hot leg and removing it from the cold leg. For high gradient runs, fans were used to help remove heat from the cold leg. The calculated velocity through the loops (0.622 inch i.d.) was 0.1

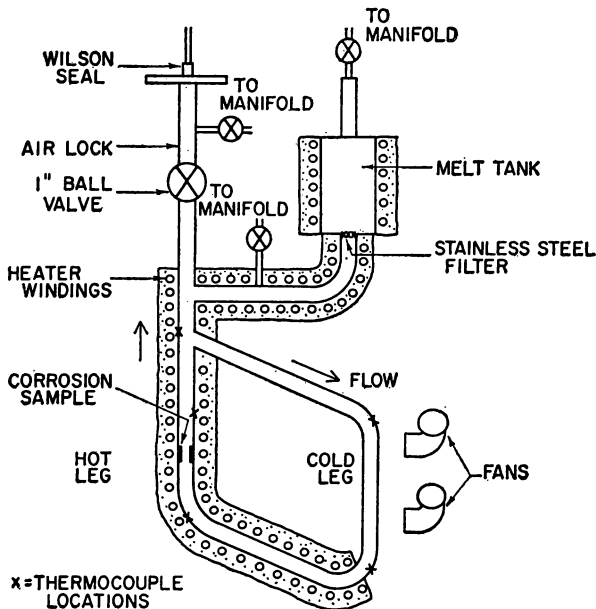


FIG. 13. Small bore thermal convection loop.

ft/sec. All loops were run with a 550°C maximum temperature. Minimum temperatures were either 520, 470, or 415°C, depending on the particular experiment. Temperatures were measured by thermocouples welded to the loop walls at various points. The actual bulk bismuth temperature was measured with a long, thin, flexible thermocouple  $\frac{1}{8}$  of an inch in diameter. The thermocouple was inserted into the operating loop through a Wilson seal and pushed through the loop to obtain the hottest and coldest bulk temperatures. The loop gas outlets were connected to a suitable manifold so that the various operations such as H<sub>2</sub> treating of the bismuth and pipe walls, filtering the bismuth, and taking liquid metal samples could be accomplished without exposing the loop interior or the liquid bismuth to air once the run was started. The air lock facilitated inserting additives, temperature probes, and liquid metal extractors into the loop while it was in operation. All loops had a machined and polished corrosion sample which was fitted into the hot leg. This sample was examined metallographically for maximum penetration and mode of attack.

The general procedure for running a loop was as follows: (1) the entire system was leak tested; (2) the bismuth and loop interior was dry H<sub>2</sub> treated at 500°C for 4 hours; (3) the bismuth was filtered into the loop through a 35 micron type 410 steel filter; (4) the additives were inserted into liquid bismuth and allowed to dissolve while the loop was operating isothermally; and

(5) the gradient was applied and the test was run for the duration selected, or until flow stopped. To detect build-up of plug material, gammagraphs were taken periodically.

The results of running some 25 loops indicated that the time required to plug completely a  $\frac{1}{2}$ -inch IPS- $2\frac{1}{4}$  chrome loop is approximately 300 hours when the circulating liquid is uranium-bismuth and the temperature gradient is  $40^{\circ}\text{C}$ . A loop 1.7 inches i.d. made of 5 chrome silicon steel running under the above conditions (except 60 ppm Mg was added to the U-Bi) took 2441 hours to plug.

Several loops operating under the above conditions ( $550^{\circ}\text{C}$  maximum temperature,  $510^{\circ}\text{C}$  minimum temperature) to which 250 ppm zirconium was added showed no signs of plugging. A  $\frac{1}{2}$ -inch IPS- $2\frac{1}{4}$  chrome loop and a 1.68 i.d. 5 chrome silicon loop have been circulating for 13,000 and 19,000 hours respectively. A third loop containing 1000 ppm zirconium and 1000 ppm magnesium added to the uranium-bismuth was shut down after 3000 hours of operation for metallographic examination. No transferred material was found in the cold leg and no corrosion of the standard sample in the hot leg was observed.

When the temperature gradient was increased to  $130^{\circ}\text{C}$  in loops containing 250 ppm zirconium, 300 ppm magnesium + 1000 ppm uranium in the bismuth, the radiographs of three of these loops showed transferred material in the cold leg soon after the gradient was applied. Two of these loops ( $2\frac{1}{4}$  chrome, one 0.622 i.d. and the other 0.5 i.d.) have operated for over 1800 hours. The third loop, 5 chrome-silicon, was shut down after 1060 hours for examination. Metallographic examination showed the corrosion rate on the hot leg sample to be 2 mils/year. The transferred material in the cold leg weighed 500 mg.

To determine the effect of velocity on corrosion and mass transfer, the pumped loop shown schematically in Fig. 14 was constructed by Turovlin, Wills, Silberberg, and Klamut.<sup>16</sup> Most of the loop was made of  $\frac{3}{4}$  IPS pipe. A high velocity section  $\frac{1}{4}$ -inch i.d.  $\times$  6 inches long located at the coldest point in the loop permitted a velocity of 8 ft/sec in the precipitation zone. A General Electric G3 electromagnetic pump circulated the bismuth. Flow measurements were made with a submerged orifice located in the sampling tank. Three standard corrosion samples were located at various portions of the loop. This loop was operated 1000 hours at a maximum bulk bismuth temperature of  $500^{\circ}\text{C}$  and a temperature gradient of  $125^{\circ}\text{C}$ . Flow was 1.2 gpm. In this time, no corrosion was noted on the standard samples, and very little deposition was found in the high velocity cold section. The test material was  $2\frac{1}{4}$  chrome steel.

*b. Corrosion fundamentals.* Recently, Shepard et al.<sup>24</sup> have made a detailed investigation of the effect of titanium, added as titanium metal or as  $\text{TiH}_2$ , upon the solution process of type 410 steel in liquid bismuth and lead bismuth

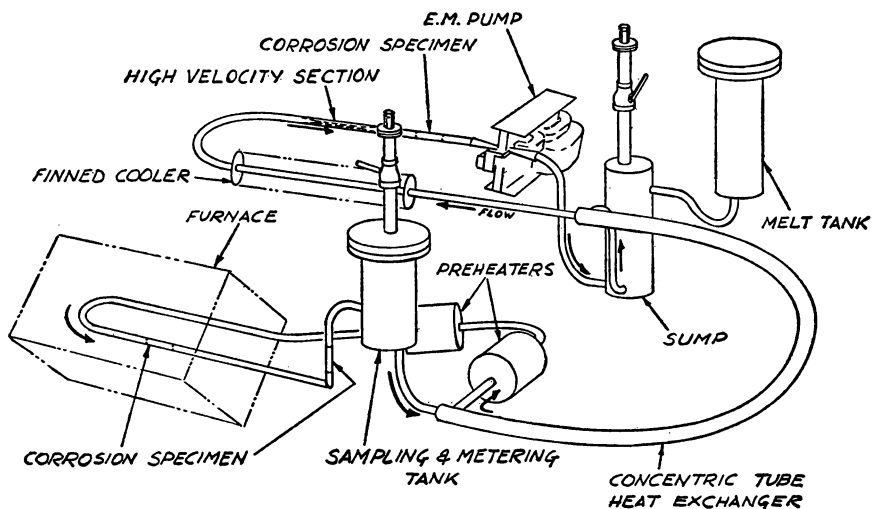


FIG. 14. High velocity loop layout and components.

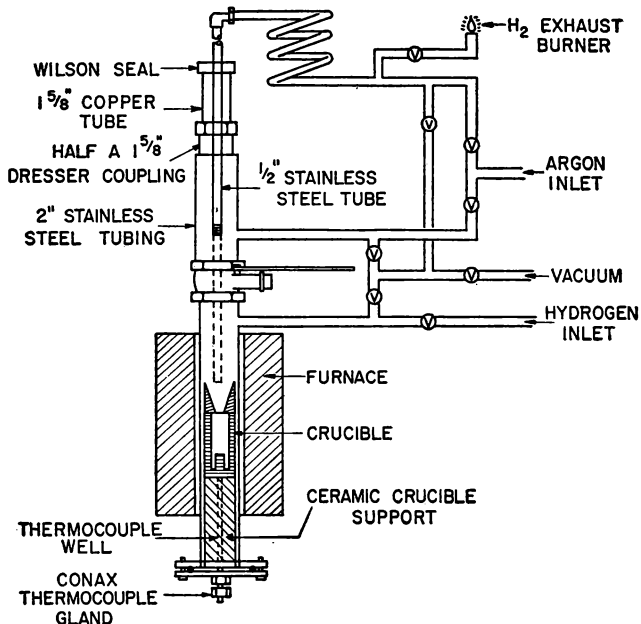


FIG. 15. Apparatus for measuring metal solubilities.

eutectic contained in a Vycor capsule. They observed a slight inhibition in the solution of Fe, and a marked inhibition in the solution of Cr in the presence of titanium additions. The inhibiting effect increased with repeated reuse of the capsules. Subjecting a capsule previously contacted with titanium-bismuth solution to fresh bismuth without titanium showed a rapid recovery in the Fe solution rate, but much more persistence in Cr inhibition. They suggested tentatively that at least part of the inhibition involves a selective affinity of titanium for oxygen, and pointed out that titanium was a powerful promoter for wetting of the steel by the bismuth. They also suggested that a barrier forms.

(1) *The solubility of Fe, Cr, Zr, and Mo in liquid bismuth.* Possible effects of the zirconium inhibitor upon the thermodynamics of the mass transfer process were investigated by Weeks.<sup>16</sup> The solubility of Fe in liquid bismuth was measured as a function of temperature in the presence of additives in the liquid metal. The solubilities of Cr and Mo in liquid bismuth were also measured using the apparatus of Fig. 15. By means of this apparatus, a series of filtered samples could be taken from the same batch of liquid metal without introduction of oxygen or nitrogen.

The solubility of iron in bismuth, in bismuth + 0.1% magnesium, in bismuth + 0.1% magnesium + 0.2% uranium, and in bismuth + 0.1% magnesium + saturation zirconium was measured using a pure iron crucible to which these additions were made. Similarly, the solubility of zirconium in bismuth + 0.1% magnesium was measured using a pure zirconium crucible. The results are shown in Figs. 16 and 17. Uranium + magnesium, in the quantities added, are seen to have no effect on the iron solubility. This solubility can be represented approximately by the equation:

$$\log_{10} (\text{ppm Fe}) = 6.41 - \frac{4110}{T}$$

to within  $\pm 15\%$  of the experimental data over the temperature range 450–650°C.

Zirconium is seen to increase slightly the iron solubility; this increase was reproducible and was measured during both cooling and heating cycles. The experimental data on the solubility of zirconium in bismuth can be approximated by the equation:

$$\log_{10} (\text{ppm Zr}) = 6.66 - \frac{2760}{T}$$

to within  $\pm 15\%$  over the temperature range 300–625°C. Iron has no effect upon this solubility.

The solubility of chromium in liquid bismuth was measured in a Cr-plated

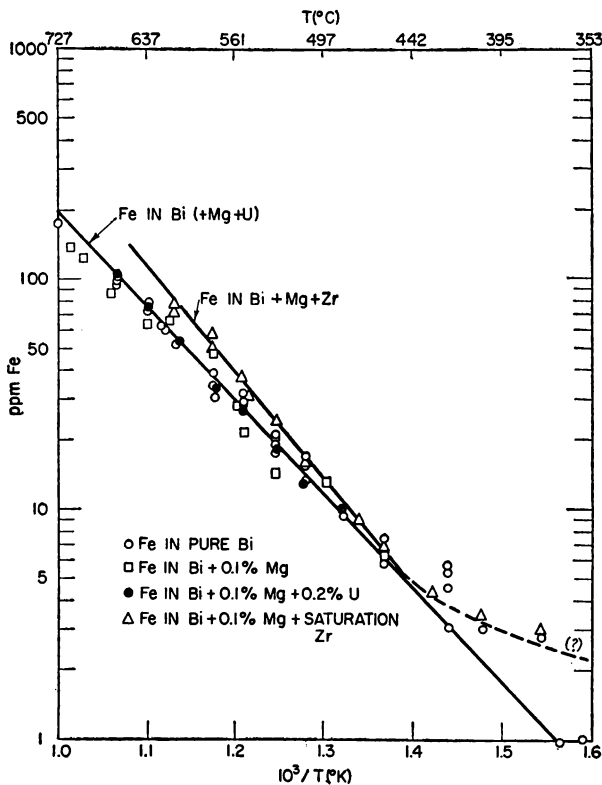


FIG. 16. The solubility of Fe in Bi.

mild steel crucible in which was wedged an irregularly shaped lump of Cr metal. Some data on the Cr solubility were also obtained using a Mo crucible into which was wedged a lump of metallic Cr. The results, using either method, were identical within experimental error. The solubility of Cr in bismuth is shown in Fig. 18. This curve can be approximated to within  $\pm 15\%$  of the experimental data between 400–635°C by the equation:

$$\log_{10} (\text{ppm Cr}) = 6.26 - \frac{3580}{T}$$

Zirconium was found to have no effect on the Cr solubility in this temperature range.

Two attempts have been made to measure the solubility of Mo in bismuth, using an Mo crucible: in one experiment Cr + Mg were present; in the other, the Mo crucible contained pure bismuth. In neither case was Mo detected

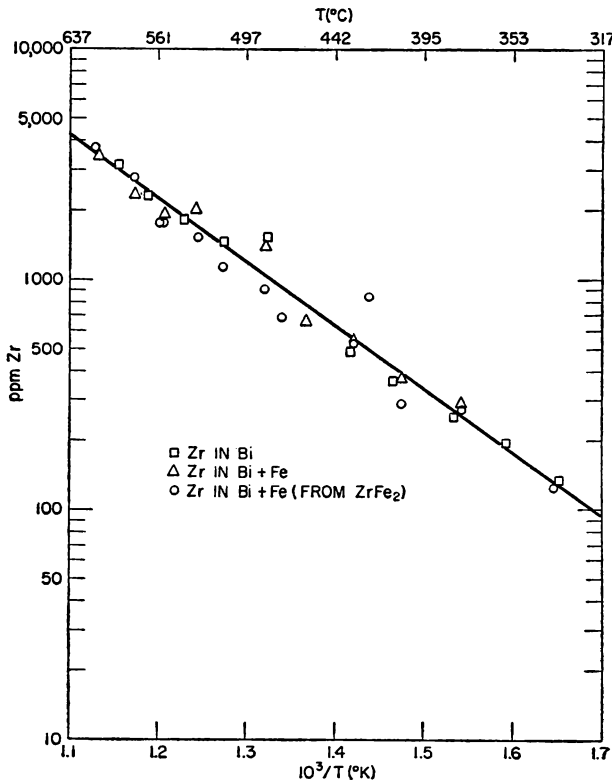


FIG. 17. The solubility of Zr in Bi.

spectrographically (detection limit: 1 ppm) in any of the samples taken, at temperature between 350–750°C.

Since it has been speculated (Nerad<sup>25</sup> and Reid<sup>19</sup>) that intermetallic compounds between iron and the titanium or zirconium might play an important role in the inhibition mechanism, an investigation of the behavior of Fe<sub>2</sub>Zr intermetallic compound in contact with bismuth was made. A 10-gram button of this alloy was wedged in the groove in the bottom of the pure iron crucible, and the solubility measured as a function of temperature in the usual manner. It was found that the zirconium and iron dissolved each to its normal solubility limit in the presence of the other. A mass of particulate iron was found in the residue upon cooling; some Fe<sub>2</sub>Zr was also identified in the residue, although the original lump had completely disintegrated.

(2) *Reaction of zirconium dissolved in bismuth with an iron crucible.* Experimental evidence has been obtained by Weeks<sup>16</sup> for deposition of zirconium on the surface of an iron crucible, using a radioactive zirconium tracer tech-

## SOLID AND FLUID FUELS

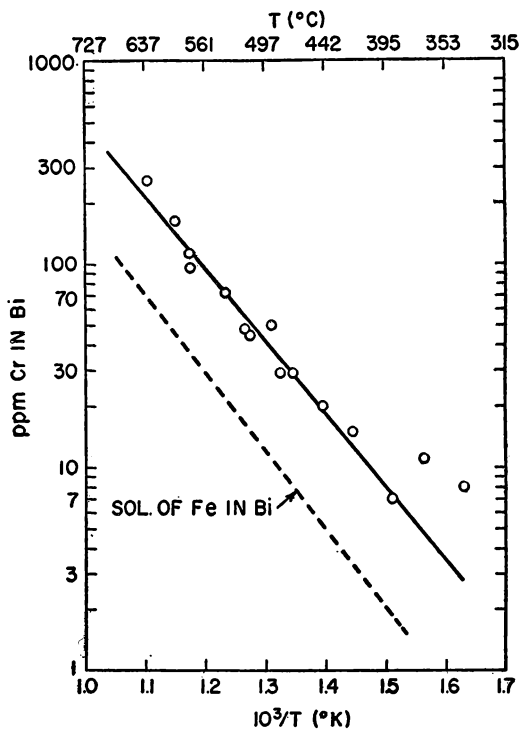


FIG. 18. Solubility of chromium in bismuth + 500 ppm magnesium.

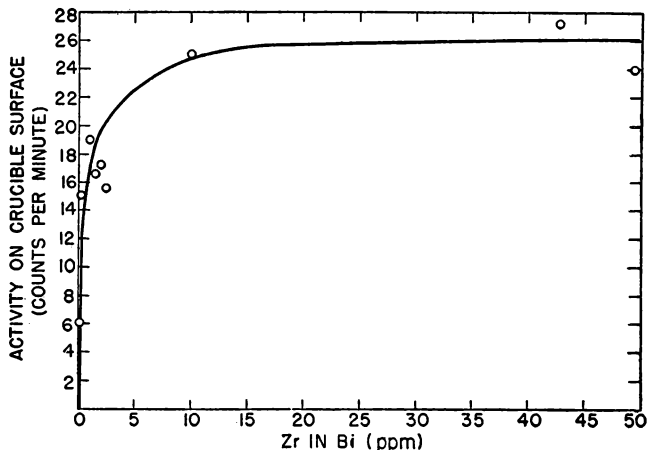


FIG. 19. Deposition of Zr on Fe from liquid Bi at 450°C.

nique. The results of equilibrating a solution of bismuth containing radioactive zirconium in a pure iron crucible for 1 hour at 450°C are shown in Fig. 19. The measured activity on the crucible surface is plotted against ppm zirconium in the bismuth. This curve resembles a Langmuir adsorption isotherm; "saturation" of the surface appears to be nearly complete at about 10 ppm zirconium in the bismuth. The amount of deposited activity at "saturation" corresponds to approximately 1 zirconium atom to every 8 iron atoms on the crucible surface, if the surface roughness factor of the crucible is taken to be 5. An adsorption energy of 17,000 calories per gram atom zirconium can be calculated from this curve, if it is assumed that this represents 450°C equilibrium.

Increasing the reaction temperature to 520°C and the equilibration time to 3 and 24 hours produced marked changes in the results obtained, as shown in Fig. 20. (The data obtained in 1 hour at 450°C are also shown here for comparison.) That the process occurring at 520°C is primarily film growth rather than adsorption is clearly demonstrated by the effect of time upon the amount of deposition. It should be noted also that this time effect is less important at higher concentrations of zirconium in bismuth; the 3- and 24-hour curves appear to be approaching one another when the zirconium concentration increases above 75 ppm.

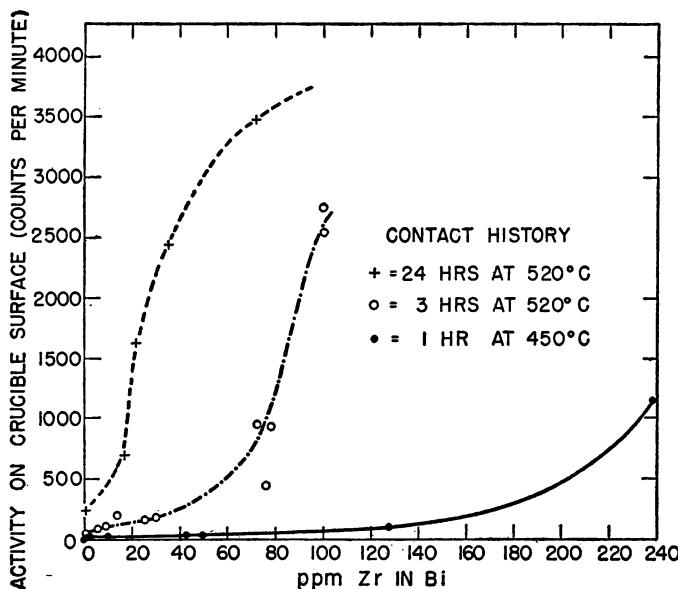


FIG. 20. Deposition of Zr on Fe from liquid Bi.

(3) *The effect of zirconium in bismuth on the solution and precipitation rates of iron from bismuth.* Since zirconium has been observed to deposit upon the surface of an iron crucible from zirconium-bismuth solutions, an attempt was made by Weeks<sup>16</sup> to measure the effect of this deposit upon the solution and precipitation rates of iron from bismuth in order to investigate the effect of the zirconium upon the mass transfer process.

The equipment and sampling method used were the same as for the measurement of the solubility of iron in bismuth. Experimentally, after filtering the bismuth into the crucible at 350°C, the crucible, liquid metal, and additives (if present) were equilibrated 24 hours (72 hours with zirconium + magnesium present) at some predetermined temperature, usually 400–450°C. The liquid metal was then sampled and the temperature raised to another predetermined value, usually 550 or 615°C. The liquid metal was sampled at  $\frac{1}{2}$  to 1 hour intervals during equilibration. Metal additives were either present in the crucible under investigation at the time the bismuth was filtered in, or were added during the original equilibration period.

In this manner, the amount of iron dissolved as a function of time was measured at 615°C in a high purity iron and in a 5 chrome crucible. The effect of zirconium + magnesium and of uranium + magnesium on the solution process was also measured. The results obtained are shown in Fig. 21. The temperature cycle of the apparatus in terms of the solubility of iron in bismuth is

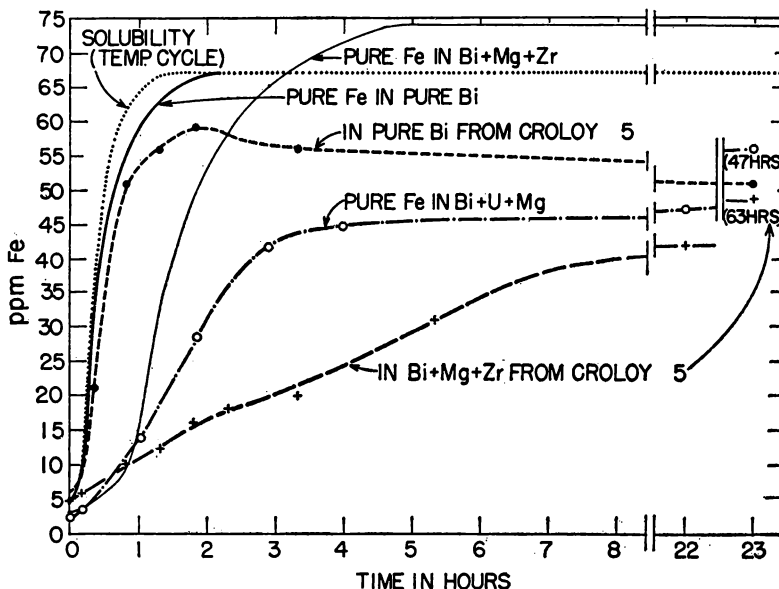


FIG. 21. The rate of solution of Fe in Bi temperature cycle 425–615°C.

also shown for reference. It can be seen that in pure bismuth, iron dissolved from both crucibles nearly as rapidly as the temperature was raised. The addition of zirconium + magnesium to the liquid bismuth retarded the rate of solution of pure iron considerably; the previously noted increase in the iron solubility in the presence of zirconium can also be observed in this curve. The addition of uranium + magnesium to the liquid metal had an even greater effect than zirconium + magnesium upon the solution rate of pure iron when measured in this manner. The retarding effect of zirconium + magnesium was much greater in the 5 chrome steel crucible than in the iron crucible. The apparent maximum in the amount of iron dissolved in pure bismuth at approximately 2 hours is possibly due to subsequent dissolution of Cr displacing the iron from solution, and was reported by Grassi, Bainbridge, and Harman<sup>26</sup> during dissolution of type 430 steel in lead-bismuth eutectic alloy. These samples unfortunately were not analyzed for Cr.

The effect of the additives upon the precipitation process was measured in a similar manner. After the crucible and liquid metal had equilibrated at the top temperature of the rate of solution run, the system was cooled to the original equilibration temperature (400 or 450°C) and the liquid metal again sampled at intervals during equilibration. Iron precipitated from pure bismuth nearly as rapidly as the temperature was lowered. Zirconium and magnesium caused a slight initial delay, followed by rapid precipitation of most of the excess dissolved iron; however, precipitation of the last few ppm above saturation was very slow in the presence of zirconium + magnesium. In the presence of uranium + magnesium, iron precipitated more slowly than from pure bismuth, but more rapidly than in the presence of zirconium + magnesium.

These effects become apparent when the data are plotted as the degree of supersaturation in the liquid metal (ppm in solution/equilibrium solubility) as a function of time (Fig. 22). It can be seen that zirconium + magnesium stabilize the solution at a supersaturation of 2 for a period of time greater than 7 hours at this temperature. Uranium + magnesium retard precipitation, but do not appear to stabilize the supersaturated solutions.

Precipitation data obtained in the 5 chrome crucible are shown in Fig. 23. In duplicate runs it was observed that the zirconium + magnesium stabilized the supersaturation of the solution at nearly 3 for periods greater than 24 hours. This degree of supersaturation suggests that mass transfer might be prevented in a circulating system in which the maximum supersaturation resulting from the temperature gradient does not exceed 3/1.

(4) *Mass transfer measurements with radioactive iron.* In order to obtain mass-transfer data on a qualitative basis in a much shorter time than by running thermal convection loops a "liquid metal convection pot" was constructed by Klamut.<sup>16</sup> A small radioactive sample was placed in the hottest

## SOLID AND FLUID FUELS

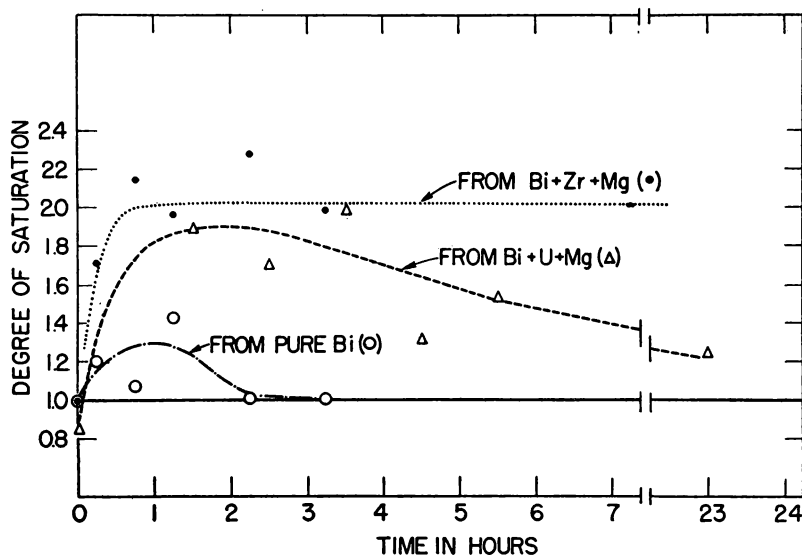


FIG. 22. Precipitation of Fe from Bi in pure iron crucible-temperature cycle: 615–425°C.

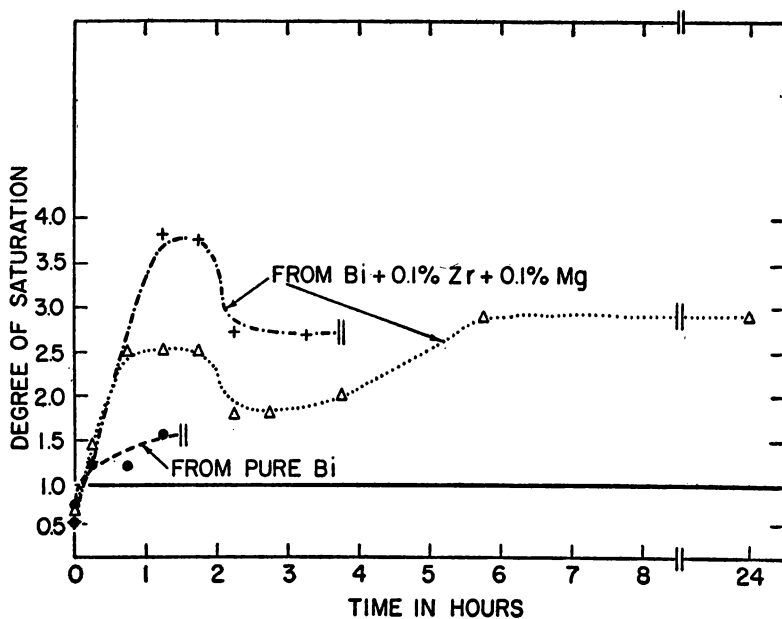


FIG. 23. Precipitation of Fe from Bi in Croloy 5 crucible-temperature cycle: 615–425°C.

portion of the pot and a similar nonradioactive sample in the coldest section. The normal temperature differential between the hot and cold samples, obtained during thermal convection in this apparatus, was 25–35°C, with a hot sample temperature of 470–485°C.

Using pure iron samples, mass transfer rates were measured in bismuth, bismuth + magnesium, bismuth + uranium + magnesium, bismuth + uranium + magnesium + zirconium, and bismuth + magnesium + zirconium. The effect of varying the zirconium concentration in this last system was also investigated. The results are given in Table IV. It can be seen that the change

TABLE IV. RELATIVE RATES OF MASS TRANSFER OF PURE Fe IN Bi IN GRAPHITE THERMAL CONVECTION POT

Run No.	Additives, ppm			$T_{\max}$ °C	$\Delta T$ °C	Transfer Rate, mg/hr $\times 10^{-5}$
	Mg	U	Zr			
3 *	—	—	—	467	32	430
4 *	—	—	—	475	31	645
18	—	—	—	438	23	13
17	100	—	—	466	25	2
8 *	130	800	—	484	48	1.2
12	400	2000	—	484	20	4.6
5 *	100	700	200	472	28	0.8
6 *	100	400	140	468	22	0.06
7 *	100	600	200	457	31	0.2
9 *	—	500	175	476	32	0.15
13	100	—	150	495	35	0.1
14	125	—	75	501	32	0.07
15	100	—	35	477	22	0.2
16	100	—	5	466	30	0.2

\* Tank argon atmosphere. Other runs in purified helium atmosphere.

from an argon atmosphere of questionable purity (runs 3 and 4) to a purified helium atmosphere (run 18) produced a considerable drop in the amount of activity transferred. The addition of magnesium (run 17) and magnesium + uranium (runs 8 and 12) further reduced the mass transfer rate. The addition of zirconium + magnesium, or zirconium + uranium + magnesium all but eliminated transfer under these conditions. With or without uranium, additions of zirconium in all concentrations from 5 to 250 ppm appeared to be equally effective in reducing mass transfer, within the accuracy of the counting technique. The observation that as little as 5 ppm zirconium prevented mass

transfer under these conditions correlates with the nearly complete "saturation" of the iron surface with zirconium at 450°C from bismuth containing 5 ppm zirconium.

(5) *The inhibition mechanism.* The experimental data obtained suggest that the action of zirconium as an inhibitor lies in its ability to form a deposit upon the iron or steel surface. This deposit affects both the solution and precipitation processes: by acting as a diffusion barrier, it decreases the rate of solution of the container metal; by changing the nature of the iron surface, it decreases the effectiveness of that surface as a nucleation site and decreases the tendency of the crystallites, once nucleated, to sinter together and to the container wall to form a compact mass or plug.

The exact manner in which zirconium produces these effects is not yet conclusively demonstrated. However, a possible mechanism can be proposed that is in agreement with the experimental data obtained to date.

Zirconium reacts with the pure iron to form an adherent surface deposit of zirconium-iron intermetallic compound. Two intermetallic compounds, ZrFe<sub>2</sub> and ZrFe<sub>3</sub>, exist in this system; both are stable, congruently melting at 1610 and 1520°C respectively. A stable monolayer of either of these compounds at the iron surface is a distinct possibility. Zirconium forms one of the most stable carbides and nitrides known. It is likely, therefore, that a zirconium deposit on a steel surface subsequently reacts with the C or N always present in commercial steels to form a surface layer of ZrC or ZrN, and that this layer is the inhibitor effective in steel systems. Attempts to identify the surface deposit by electron diffraction are presently planned. ZrN deposits have been identified by Sadofsky and Kammerer<sup>16</sup> using x-ray diffraction on steel surfaces contacted with bismuth containing zirconium at 750 and 550°C.

TABLE V. APPROXIMATE ANALYSES OF THE IRONS AND STEELS USED IN U-Bi STUDIES

Material	C	Mn	Si	Cr	Mo	Ni	Fe	Cu	O <sub>2</sub>	N <sub>2</sub>
Pure Fe	0.003	Trace	Faint trace	0	Faint trace	0	—	Trace	0.012	0.00018
Armco	0.015	0.028	0.025	—	—	—	99+	—	—	—
2 1/4 chrome	0.15	0.30–0.60	0.50	2.00–2.50	0.90–1.10	—	Bal.	—	—	—
5 chrome (Croloy 5)	0.15	0.30–0.60	0.50	4.00–6.00	0.45–0.65	—	Bal.	—	—	—
5 chrome silicon	0.15	0.30–0.60	1.00–2.00	4.00–6.00	0.45–0.65	—	Bal.	—	—	—
Type 410 steel	0.15	1.00	1.00	11.50–13.00	—	0.50	Bal.	—	—	—

The effect of the zirconium upon the cold leg precipitation processes probably lies in the ability of the surface deposit to satisfy the free bonds at the iron or steel surface. This action might greatly retard growth of the wall crystals or any of the crystallites nucleated in the solution phase, as zirconium might be expected to react with this surface also. Likewise, the presence of a surface deposit might effectively poison the ability of that surface to act as a nucleation site, thus requiring a higher degree of supersaturation for precipitation to occur.

## REFERENCES FOR CHAPTER XIII

1. See also the following Geneva Papers:  
498—S. E. Beall and J. A. Swartout, "The Homogeneous Reactor Test."  
496—R. B. Briggs and J. A. Swartout, "Aqueous Homogeneous Power Reactors."  
811—A. S. Kitzes and R. N. Lyon, "Aqueous Uranium and Thorium Slurries."  
936—H. deBryn, M. A. Hermons, Th. V. d. Plas, B. L. A. vd. Schee, and J. J. Went, "The Design of a Small Prototype of a Homogeneous Power Reactor Welded with Uranium Oxide Suspension."  
637—N. P. Sajin and P. Y. Duckina, "Production of High Purity Metallic Bismuth."
- 1a. *Reactor Handbook*, Vol. 2, Engineering Sec. 4, 5, AECD-3646, 1955.
2. C. H. Secoy, J. Am. Chem. Soc. 70:1948, p. 3450; 72:1950, p. 3343.
3. J. A. Swartout et al., ORNL-1280, 1952 (see ref. 1a).
4. J. A. Swartout et al., ORNL-1424, 1942 (see ref. 1a).  
J. S. Gill, E. V. Jones, and W. L. Marshall, ORNL-1318, 1952 (see ref. 1a).  
R. E. Leeds and C. H. Secoy, ORNL-870, 1950 (see ref. 1a).  
C. H. Secoy, ORNL-607, 1949 (see ref. 1a).
5. D. A. McInnes and L. G. Longsworth, "The Measurement and Interpretation of pH and Conductance Values of Aqueous Solutions of Uranyl Salts," Rockefeller Institute for Medical Research, University of Chicago, MDDC-911, Nov. 24, 1942.
6. I. Helmholtz and G. Friedlander, "Physical Properties of Uranyl Sulfate Solutions," Los Alamos Scientific Lab., MDDC-808, 1943.
7. M. H. Lietzke, H. W. Wright, and W. L. Marshall, ORNL-1121, 1951 (see ref. 1a).
8. J. W. Boyle, J. A. Ghormley, C. J. Hochanadel, W. F. Kieffer, and T. J. Sworski, ORNL-52-8-103, 3, No. 1, 1953 (see ref. 1a).
9. H. F. McDuffie et al., ORNL-1318 (see ref. 1a).
10. D. M. Gillies, "Some Studies of the Reactions of Uranium Oxides with Hydrogen, Oxygen, and Water," Columbia University, MDDC-647, June 1946.
11. H. F. McDuffie and J. W. Boyle, ORNL, 1952 (see ref. 1a).
12. E. Orban, Mound Lab., MLM-659, 1952 (see ref. 1a).
13. J. A. Swartout et al., ORNL-1121, 1951 (see ref. 1a).
14. W. L. Marshall, ORNL-CF-52-1-93, 1952 (see ref. 1a).
15. R. Van Winkle, ORNL-CF-52-1-124, 1952 (see ref. 1a).
16. Geneva Paper No. 118—Weeks, Klamut, Gurinsky, "Corrosion Problems with Bismuth Uranium Fuels"; see also the following Geneva Papers:  
No. 494—F. T. Miles and C. Williams, "Liquid Metal Fuel Reactor."  
No. 550—O. E. Dwyer, R. J. Teitel, and R. Wiswall, "High Temperature Processing Systems for Liquid Metal Fuel and Breeder Blankets."

## SOLID AND FLUID FUELS

17. R. J. Teitel, "The U-Bi System," to be published in *J. of Metals*.
18. J. Weisman, unpublished work, 1953.
19. R. C. Reid, A.S.M.E. Tech. Paper 51-5-13, 1951.
20. O. J. Elgert and C. J. Egan, USAEC Report MTA-12, 1953.
21. R. Cygan, USAEC Report NAA-SR-1060, 1954.
22. M. A. Cordovi, unpublished work, 1951.
23. J. E. Atherton, D. H. Gurinsky, O. F. Kammerer, C. J. Klamut, M. Silberberg, B. Turovlin, and J. Weeks, *Chem. Eng. Prog. Symposium Series 50*, No. 12, p. 23, 1954, *Nucleonics 12*:(7), p. 41, 1954.
24. O. C. Shepard, J. R. Morgan, R. Parkman, and R. D. Seibel, USAEC Report Nos. AECU-2794, 2915, 1953.
25. J. A. Nerad—private communication to R. J. Teitel, 1951.
26. R. C. Grassi, D. W. Bainbridge, and J. W. Harman, USAEC Report No. AECU-2201, 1952.
27. J. E. Terry and N. B. Skeats, *Liquid Metal Coolants. A Bibliography*. Report No. AERE Inf./Bib. 94, July 1954.

## ADDITIONAL CHAPTER REFERENCES

---

---

(Papers Presented at the Nuclear Engineering and Science Congress, Cleveland, Ohio, December, 1955)

These papers are included because they indicate the extension of the declassification. The reader is advised to look to the journals for their availability.

<i>Paper No.</i>	<i>Chapter</i>
123 "Powder Metallurgy of Uranium"—H. H. Hausner and J. L. Zambrow—Sylvania.	I
113 "Production of Uranium Metal"—D. S. Arnold, E. E. Polson, and E. S. Noe, National Lead Company.	I
92 "Diffusion of Fission Gases in Metallic Uranium"—M. B. Reynolds—G.E.	II
101 "Uranium-Zirconium System"—A. N. Holden and W. E. Seymour—G.E.	III
115 "Mechanical Properties of Uranium-Molybdenum Alloys"—M. B. Waldron, R. C. Burnett, and S. F. Pugh—Harwell.	III
333 "Hydrogen-Uranium Phase Diagrams"—M. W. Mallett and M. J. Trzeciak—BMI.	III
334 "Review and Redetermination of Hydrogen-Uranium Relationships"—M. W. Mallett, M. J. Trzeciak, and C. B. Griffith—BMI.	III
99 "Fabrication and Properties of Thorium"—H. A. Saller and J. A. Keeler—BMI.	VI
102 "Effects of Some Impurities on Mechanical Properties of Thorium Metal"—D. T. Peterson, R. F. Russi, and R. L. Mickelson—Iowa State College.	VI
103 "Strengthening of Thorium by Alloying, Heat Treatment and Cold Work"—H. R. Ogden, R. M. Goldhoff, and R. I. Jaffee—BMI.	VI
222 "Decomposition of Water by Fission Recoil Particles"—J. W. Boyle, W. F. Kieffer, C. J. Hockanadel, T. J. Sworski, and J. A. Ghormley—ORNL.	VII
89 "Effect of Nuclear Reactor Radiation on Structural Materials"—Ira F. Zartman—USAEC.	VIII
90 "Variations in Radiation Damage to Metals"—C. A. Bruch, W. E. McHugh, and R. W. Hockenbury—G.E.	VIII
91 "Effect of Nuclear Radiation on Structural Materials"—J. C. Wilson and D. S. Billington—ORNL.	VIII
93 "Some Effects Produced in Graphite by Neutron Irradiation in BNL Reactor"—W. L. Kosiba, G. J. Dienes, and D. H. Gurinsky—BNL.	VIII
94 "Irradiation Effects in Uranium and Its Alloys"—J. H. Paine and J. H. Kittel—ANL.	IX
107 "Fuel Element Economics in Sodium-graphite Power Reactors"—Woolsey and Hayward—North American.	X

<i>Paper No.</i>	<i>Chapter</i>
110 "Ceramic Fuel Materials for Nuclear Reactors"—J. R. Johnson—ORNL.	X
116 "Fuel Element Design"—C. E. Weber—G.E.	X
125 "Diffusion of Uranium through Graphite"—L. D. Loch, J. R. Gambino, and W. H. Duckworth—BMI.	X
130 "Non-destructive Testing of Reactor Fuel Elements"—W. J. McGonagle—ANL.	X
215 "Fuel Element Metallurgy, Corrosion and Coolant Problems"—Stuart McLain and Frank G. Foote—ANL.	X
78 "Fuel Elements for Nuclear Reactors"—John B. Anderson—Combustion Engineering.	X
50 "Liquid Bismuth as a Fuel Solvent and Heat Transport Medium for Nuclear Reactors"—O. E. Dwyer, D. H. Gurinsky, and J. R. Weeks—BNL.	XIII
71 " $\text{UO}_2\text{-NaK}$ Slurry as a Possible Reactor Fuel"—B. M. Abraham and H. E. Flotoro—ANL.	XIII
63 "Survey of Homogeneous Reactor Chemical Problems"—C. H. Secoy—ORNL.	XIII
104 "Properties of Zircaloy-2"—D. E. Thomas and F. Forscher—WAPD.	General
352 "Review of Solid Hydrides"—H. McCullough and B. Kopelman—Sylvania.	General
160 "Use of Radioisotopes in Materials Testing"—John L. Kuranz—Nuclear Instrument & Chemical Corporation.	General
7 "Essential Differences Among Basic Types of Reactors and Comparison of Different Significant Considerations Peculiar to Each"—Stuart McLain and Raymond O. Brittan—ANL.	General
108 "Oxidation Behavior of Reactor Materials"—R. A. U. Huddle—Harwell.	General
319 "Evolution of Gas from Graphite Moderator Material"—R. L. Carter and W. J. Greening—North American.	General
267 "Recent Results of Computation of Fission Product Levels in Reactor Fuels"—J. O. Blomeke—ORNL.	General
74 "Comparison of Na, Li and Pb as a Heat Transfer Medium"—W. D. Manly—ORNL.	General

## GENERAL BIBLIOGRAPHY

---

---

(Papers Presented at International Conference on the Peaceful Uses of Atomic Energy,  
Geneva, Switzerland, June, 1955)

*Paper No.*

- 118 "Corrosion problems with bismuth uranium fuels"—J. R. Weeks, J. Klamut, and D. H. Gurinsky et al.  
119 "Corrosion by liquid metals"—L. F. Epstein.  
122 "Mass transfer in molten metal and molten salt systems"—C. F. Bonilla.  
123 "Sodium and sodium-potassium alloy for reactor cooling and steam generation"—F. E. Crever et al.  
124 "The solubility of structural materials in sodium"—R. A. Baus et al.  
341 "Preparation of pure uranium metal"—B. Goldschmidt and P. Vertes.  
351 "Extrusion of uranium in the gamma phase"—J. A. Stohr and R. Chevigny.  
352 "Uranium-aluminium alloys"—G. Cabane and M. Englander.  
407 "Production of uranium metal"—L. Grainger.  
411 "Fundamental aspects of the corrosion of aluminium and their application to nuclear reactors"—R. A. U. Huddle.  
416 "Alloys of uranium and thorium"—P. C. L. Pfeil.  
417 "Heat transfer experiments with sodium and sodium-potassium alloy"—W. B. Hall.  
426 "Neutron capture in some coolant and canning materials in the intermediate energy range"—E. R. Rae.  
435 "Emission of active rare gases from fissile material during irradiation with slow neutrons"—F. J. Stubbs and G. N. Walton.  
436 "The condition of fission product iodine in irradiated uranium metal"—G. N. Walton et al.  
443 "Damage occurring in uranium during burn-up"—S. F. Pugh.  
444 "Radiation damage in non-fissile materials"—J. H. O. Varley.  
445 "Effect of radiation on heterogeneous systems of air or nitrogen and water"—J. Wright et al.  
485 "The materials testing reactor—Experimental program and operating experience"—R. L. Doan and J. R. Huffman.  
488 "Design and description of water boiler reactors"—L. D. P. King.  
489 "The 'Swimming Pool'—A low cost reactor for research and medicine"—W. M. Breazeale et al.  
490 "The materials testing reactor and related research reactors"—A. M. Weinberg and T. E. Cole.  
491 "A developmental fast neutron breeder reactor"—A. Amorosi et al.  
492 "A graphite-moderated nuclear power plant design"—A. B. Carson.  
493 "A sodium graphite reactor 75,000 electrical kilowatt power plant"—C. Starr.  
494 "Liquid metal fuel reactor"—F. T. Miles and C. Williams.  
495 "Boiling water reactors for industrial power"—H. P. Iskenderian et al.

*Paper No.*

- 496 "Aqueous homogeneous power reactor"—R. B. Briggs and J. A. Swartout.  
497 "The engineering design of a prototype boiling water reactor power plant"—J. M. Harrer et al.  
498 "The homogeneous reactor test"—S. E. Beall and J. A. Swartout.  
499 "The sodium reactor experiment"—W. E. Parkins.  
500 "Los Alamos power reactor experiments"—D. K. Froman et al.  
501 "The engineering design of a prototype fast neutron reactor power plant"—A. H. Barnes et al.  
531 "Fundamental considerations in the reduction processes of uranium and thorium"—B. Kopelman.  
533 "Zirconium metal production"—S. M. Shelton et al.  
534 "The production and properties of graphite for reactors"—L. M. Currie et al.  
535 "Aqueous corrosion of aluminium alloys at elevated temperatures"—J. E. Draley and W. E. Ruther.  
536 "Pressurized water reactor (PWR) water chemistry"—T. Rockwell, III, and P. Cohen.  
537 "Aqueous corrosion of zirconium and its alloys at elevated temperatures"—D. E. Thomas and I. H. Mandil.  
542 "High temperature fuel processing methods"—E. E. Motta.  
544 "Pyrometallurgical processing of nuclear materials"—H. M. Feder.  
545 "The purification of uranium reactor fuel by liquid-metal extraction"—A. F. Voigt.  
547 "Nuclear reactor fuel dissolution"—D. L. Foster et al.  
548 "The removal of fission products from stainless steel"—D. O. Campbell.  
550 "High temperature processing systems for liquid-metal fuels and breeder blankets"—O. E. Dwyer et al.  
555 "Physical metallurgy of uranium and its alloys"—F. G. Foote.  
556 "The metallurgy of thorium and its alloys"—O. N. Carlson et al.  
557 "Thermal cycling effects in uranium"—H. H. Chiswik.  
558 "The alloys of uranium"—H. A. Saller and F. A. Rough.  
559 "The technology of  $\text{UO}_2$  and  $\text{ThO}_2$ "—R. J. Johnson and C. E. Curtis.  
561 "Dispersion type fuel elements"—C. E. Weber and Hirsh.  
562 "Preparation, properties, and cladding of aluminum-uranium alloys"—H. A. Saller.  
615 "The first atomic power station in the USSR and the prospects of atomic power development"—N. A. Nikolayev.  
621 "The experimental nuclear reactor with ordinary water and enriched uranium"—Y. G. Nikolaev.  
622 "A 2,000 kilowatt thermal power nuclear reactor for research purposes"—Y. G. Nikolaev.  
623 "Experimental heavy water physical reactor"—A. I. Alichanow et al.  
624 "A boiling homogeneous nuclear reactor for power"—A. I. Alichanow et al.  
635 "Powder metallurgy of thorium"—G. A. Meyerson.  
636 "Metallurgy of thorium"—G. E. Kaplan.  
637 "Production of high purity metallic bismuth"—N. P. Sajin and P. Y. Dulkina.  
638 "Behaviour of the stainless steel IXI8H9T in contact with liquid lead and bismuth and their eutectic alloy at a temperature of 500 to 600°C"—L. I. Tzuprun and M. I. Tarytina.  
639 "Thermal conductivity of molten metals"—M. A. Miheyev et al.  
673 "Metal research 'hot' laboratory"—N. F. Pravdruk.  
679 "Radiolysis of water in the presence of  $\text{H}_2$  and  $\text{O}_2$  under the action of reactor irradiations, fission fragments and X-rays"—P. I. Dolin and B. W. Ershler.

*Paper No.*

- 680 "The effect of irradiation on the structure and properties of fissionable materials"—S. T. Konobeevsky et al.
- 681 "Effect of irradiation on structure and properties of fissionable materials"—S. T. Konobeevsky et al.
- 726 "Thermodynamics of the heavy elements"—B. B. Cunningham.
- 730 "The chemistry and the X-ray crystal structure of heavy-element compounds"—S. Fried and W. H. Zachariasen.
- 731 "Hydrolytic behaviour of the heavy elements"—K. A. Kraus.
- 735 "Vapor pressure of liquid plutonium"—T. E. Phipps et al.
- 737 "Recent developments in the chemistry of the uranium oxides"—H. R. Hoekstra and S. Siegel.
- 738 "The radiation chemistry of aqueous solutions"—A. O. Allen.
- 739 "The radiation-induced reaction of hydrogen and oxygen in water at 25°C to 250°C"—C. J. Hochanadel.
- 740 "The effects of reactor radiation upon high temperature static water systems"—J. R. Humphreys.
- 741 "The decomposition of water by fission recoil particles"—J. W. Boyle et al.
- 742 "Organics as reactor moderator-coolants: Some aspects of their thermal and radiation stabilities"—R. O. Bolt.
- 744 "Radiation damage in reactor materials"—D. S. Billington.
- 745 "Irradiation effects in uranium and its alloys"—F. G. Foote et al.
- 746 "Irradiation damage to carbon moderator materials"—W. K. Woods.
- 747 "The effects of irradiation on structural materials"—F. E. Faris.
- 748 "Radiation effects in alkali halides produced by high-energy protons and gamma rays"—K. Kobayashi et al.
- 749 "Radiation damage in the primary solid types"—F. Seitz and J. S. Koehler.
- 750 "Theoretical aspects of radiation damage in metals"—G. J. Dienes.
- 751 "Interpretation of radiation damage to graphite"—G. R. Hennig and J. E. Hove.
- 752 "Problems of the irradiation physics of semiconductors"—K. Lark-Horovitz.
- 753 "A review of investigations of radiation effects in ionic and covalent crystals"—J. H. Crawford, Jr.
- 762 "Experience with B.E.P.O."—R. F. Jackson.
- 786 "The solid state reaction between uranium and aluminium"—R. Kiessling.
- 787 "Observations on the corrosion of uranium in liquid sodium"—H. Mogard.
- 791 "Characteristics of the Swedish heavy water reactor"—E. Hellstrand et al.
- 809 "The formation of higher isotopes and higher elements by reactor irradiation of Pu-239; some nuclear properties of the heavier isotopes"—W. C. Bentley et al.
- 811 "Aqueous uranium and thorium slurries"—A. S. Kitzes and R. N. Lyon.
- 812 "The use of high temperature sodium in manufacture of Na-K alloy"—C. B. Jackson and R. C. Werner.
- 813 "Operating experience and experimental results obtained from a NaK cooled fast reactor"—B. C. Cerutti et al.
- 815 "Description of the pressurized water reactor (PWR) reactor power plant"—J. W. Simpson et al.
- 817 "The preparation of uranium metal by the reduction of uranium tetrafluoride with magnesium"—H. A. Wilhelm.
- 821 "Survey of homogeneous reactor chemical problems"—C. H. Secoy.
- 825 "The metallurgy of reactor fuels"—J. P. Howe.
- 826 "The intermetallic compounds of plutonium"—A. S. Coffinberry.
- 827 "Fabrication of alloyed uranium"—A. R. Kaufman.

*Paper No.*

- 828 "The fabrication of the fuel elements of the Brookhaven reactor"—D. H. Gurinsky.  
829 "Basic technology of the sodium graphite reactor"—S. Siegel et al.  
861 "Design and description of Argonne National Laboratory's Research Reactors (CP-3, CP-3', CP-5)"—W. H. Zinn.  
862 "Fuel cycles and reactor types"—A. M. Weinberg.  
866 "Liquid metal handling"—S. G. Bauer.  
867 "Possible role of thorium in nuclear energy"—J. V. Dunworth.  
880 "Corrosion of aluminium and aluminium alloys in aqueous solutions at high temperatures"—K. Carlsen.  
885 "Notes on stability of fuel elements"—K. Carlsen et al.  
888 "Practical experiences with the J.E.E.P."—T. J. Barendregt et al.  
936 "A 'wet' suspension of uranium oxide for a homogeneous power reactor"—H. de Bruyn et al.  
938 "A 'dry' suspension of uranium oxide for a heterogeneous power reactor"—H. de Bruyn et al.  
943 "Some experiments concerning pile materials"—B. Buras.  
947 "On the possibility to improve the heat transfer of uranium and aluminium surfaces in contact"—F. Boeschoten.  
953 "MTR-type fuel elements"—E. J. Boyle and J. E. Cunningham.  
961 "Thermal strains and deformations of the rod and the protective canning in the heterogeneous high flux reactor"—M. Ristić et al.

## SOME ABBREVIATIONS USED IN THE TEXT

---

w/o	Weight per cent
a/o	Atomic per cent
TTT	Time-temperature transformation (curves)
DPN (DPH)	Diamond Pyramid Number (Diamond Pyramid Hardness)
<i>nvt</i>	Integrated flux = flux times time $nv = \text{no. of neutrons/cm}^2/\text{sec}$ with velocity $v$ ; $t = \text{times}$
AERE	Atomic Energy Research Establishment (Harwell, England)
ANL	Argonne National Laboratory (Chicago, Illinois)
BNL	Brookhaven National Laboratory (Upton, New York)
HEW	Hanford Engineering Works (Richland, Washington)
ISC	Iowa State College (Ames, Iowa)
KAPL	Knolls Atomic Power Laboratory (Schenectady, New York)
LASL	Los Alamos Scientific Laboratory (Los Alamos, New Mexico)
NAA	North American Aviation (now Atomics International) Canoza Park, California
NMI	Nuclear Metals, Inc. (formerly MIT) (Cambridge, Massachusetts)
ORNL	Oak Ridge National Laboratory (Oak Ridge, Tennessee)
WAPD	Westinghouse Atomic Power Laboratory (Pittsburgh, Pennsylvania)
BEPO	British Experimental Pile (O)
BSR	Bulk Shielding Reactor
CP5	Chicago Pile #5
EBR	Experimental Breeder Reactor
GCR	Geneva Conference Reactor
HRE	Homogeneous Reactor Experiment
LITR	Low Intensity Test Reactor
LMFR	Liquid Metal Fuel Reactor
MTR	Materials Testing Reactor
PWR	Pressurized Water Reactor
SRE	Sodium Reactor Experiment



## SUBJECT INDEX

---

---

- Air**, thorium corrosion by, 135, 136  
**Air** and water, radiation effects on, 238  
**Alloys**, of thorium, 139  
    of uranium, 69-98  
**Aluminum**  
    cladding for uranium fuel elements, 246, 247, 260, 288  
    fission fragments in, range of, 225  
    matrix, for fuel components, 291, 295  
    for uranium-aluminum alloy dispersions, 250, 252  
    for uranium dioxide dispersions, 250, 251, 252, 288  
    melting point of, 281  
    neutron cross section of, 281  
    radiation effects in, 161, 164, 165, 200  
    reaction of, with uranium, 262  
    -uranium interface, diffusion across, 211, 248  
**Aluminum**, alloys of  
    with copper, radiation effects on, 165  
    with thorium, 121, 129  
    with uranium, 70, 72, 86, 219, 282, 286  
        aluminum clad, 288  
        densities and melting points of, 280  
        fuel element, 288, 291  
        phase diagram for, 71  
        radiation effects on, 184, 201  
    with uranium and silicon, 72  
**Aluminum oxide**, crucible of, 118  
    radiation effects on, 167  
**Ammonium diuranate**, preparation from uranyl nitrate, 19  
**Ammonium ion**, from radiolysis of water and nitrogen, 238  
**Anode**, graphite, 3  
**Antimony**, alloys of  
    with thorium, 129, 139  
    with uranium, 72  
**Area**, reduction of, *see* element and tensile data  
**Argon**, thorium corrosion by, 135, 136  
**Arsenic**, alloys of, with uranium, 72  
**Atoms**, displaced, number of, calculation of, 151  
    impurity, in solids, 160  
    interstitial, in solids, 150  
**Barium** nitrate, radium sulfate precipitation by, 18  
**Beryllia**, crucible of, 4, 99, 116, 118  
**Beryllium**  
    alloys of, with copper, 162  
        with thorium, 121, 129  
        with uranium, 72, 205, 280  
        with uranium and carbon, 72  
    melting point of, 281  
    neutron cross section of, 281  
    radiation effects on, 200  
**Beryllium oxide**, matrix for uranium dioxide dispersions, 253  
    uranium dioxide dispersion in, 228  
    -uranium dioxide system, 252  
**Biscuit**, of uranium, 6  
    of thorium, 116  
**Bismuth**  
    dispersant for nuclear fuels, 256  
    purification of, 318  
    reaction of, with graphite, 318  
        with zirconium carbide, 312  
    solubilities of metals in, apparatus for measuring, 322  
    solvent for nuclear fuels, 256  
**Bismuth**, alloys  
    with chromium, 323, 324  
    with chromium and magnesium, 326  
    corrosion by, 318, 319  
    with iron, 323, 324, 330  
    with iron and lead, 329  
    with iron and magnesium, 328, 329  
    with iron and zirconium, 325, 326, 327, 328, 329

**Bismuth alloys (Cont.)**

- with lead, corrosion of steel by, 318
  - with lead and titanium, corrosion of steel by, 323
  - with lead and zirconium, 310
  - with molybdenum, 323, 324
  - reactions of, with graphite, 310
  - stability of, 313
  - with thorium, 129, 139
  - with uranium, 72, 256, 314
    - corrosion of iron by, 321
    - fluid fuel, 256
    - fuel system, 255, 307
    - reaction of, with graphite, 310
    - stability of, 313
    - uranium carbide in, 310
    - uranium nitride in, 310
  - with uranium and calcium, 317
  - with uranium and chromium, 313, 323, 324
  - with uranium and iron, 313, 316, 328, 329
  - with uranium and lead, 72, 310
  - with uranium, lead and zirconium, 310
  - with uranium and magnesium, 256, 313, 315, 316, 317
  - with uranium, magnesium and zirconium, 310
  - with uranium and nickel, 313, 314, 315
  - with uranium and thorium, 317
  - with uranium and zirconium, 256, 310, 313, 316, 317
  - with zirconium, 313, 323, 324, 325
  - with zirconium and iron, 325, 326, 327
- Bismuth, corrosion by**
- of iron, 256, 317
    - effect of graphite, 331
    - effect of magnesium, 321, 331
    - effect of uranium, 331
    - effect of velocity, 321
    - effect of zirconium, 321, 331, 332
  - of steels, 317
    - effect of calcium, 318
    - effect of magnesium, 317, 318
    - effect of titanium, 317, 318, 321
    - effect of titanium hydride, 321
      - effect of zirconium, 318
  - of thorium, 137
- Boiling point, of thorium, 120**
- of uranium, 22**
- Bomb, direct-pour, 17**
- firing time of, 7, 15**

**Bomb (Cont.)**

- furnace for, 7, 8, 14
  - ignition of, time required for, 7
  - iron, 6
  - linings for, 6, 10, 11, 13
  - unloading, 8
  - uranium dioxide layer in, 11
- Bomb charge, 7, 14**
- density of, 10**
- effect of water in, 9**
- Booster, potassium chloride, for uranium tetrafluoride reduction, 5**
- thermal, for uranium tetrafluoride reduction, 5**
- Boric acid, in water, effect on radiolysis, 234, 235**
- Boron, alloys of, with uranium, 72**
- $\alpha$ -Brass, radiation effects in, 165**
- Bromine, thorium corrosion by, 136, 137**
- Bulk modulus, see element: elastic constants**
- tri-Butyl phosphate, thorium extraction by, 111, 112**
- uranium extraction by, 19, 111, 112**
- Cable, coaxial, radiation effects on, 176**
- Calcium**
- alloys of, with uranium, 72
  - thorium halide reduction by, 113
  - thorium oxide reduction by, 113, 114, 132
  - thorium tetrachloride reduction by, 114, 115
  - thorium tetrafluoride reduction by, 115
  - thorium oxychloride reduction by, 115
  - uranium tetrafluoride reduction by, 3, 4, 5, 8, 19
- Calcium fluoride, bomb liner of, 13**
- mould lining of, 20**
- slag, 4, 5, 20**
- Calcium hydride, uranium dioxide reduction by, 3**
- Calcium oxide, bomb lining of, 10, 116**
- crucible of, 118**
- Carbon, alloys of**
- with beryllium, 72
  - with thorium, 117, 121, 132, 139
    - fabrication of, 129
    - hardness of, 124
    - impact strength of, 126
    - phase diagram for, 140
    - tensile properties, 125

- Carbon alloys (*Cont.*)  
 with uranium, 72, 99, 219  
   grain size of, 37, 38, 45  
   recrystallization of, 41  
   structure of, 45
- Carbon, solubility in uranium, 99
- Casting, of uranium, 16, 99–103  
   of uranium alloys, 103–108
- Cathode, molybdenum, 4
- Cerium  
   alloys of, with thorium, 139  
     with uranium, 72, 73  
   in monazite sands, 110
- Chromium, alloys of  
   with bismuth, 323, 324  
   with bismuth and magnesium, 326  
   with uranium, 70, 71, 72, 73, 79, 80, 81,  
     86, 219  
     extrusion constants of, 105  
     fabrication of, 104  
     radiation effects on, 200, 205  
     tensile properties, 87  
   with  $\beta$ -uranium, density of, 23  
     lattice constants of, 23  
     thermal expansion of, 56  
   with  $\gamma$ -uranium, thermal expansion of, 23  
   with uranium and iron, 72
- Chromium, in water, effect on radiolysis, 234, 237
- Cobalt, alloys of, radiation effects on, 163  
   with thorium, 129  
   with uranium, 72  
     with uranium and iron, 72  
     with uranium and nickel, 72
- Collisions, replacement, in solids, 151
- Conductivity, electrical, of thorium, 120  
 thermal, radiation effects on, 210  
   of thorium, 120  
   of uranium, 22
- Copper  
   alloys of, with aluminum, 165  
     with beryllium, 162  
     with gallium, 165  
     with germanium, 165  
     with gold, 162  
     with manganese, 165  
     with thorium, pyrophoric, 129  
     with uranium, 70, 72, 104  
     with zinc, 165  
   cladding, for thorium, 128  
     for uranium, for  $\alpha$  extrusion, 101
- Copper (*Cont.*)  
   –copper oxide rectifier, 176  
   crucible of, 118  
   lubricant, for drawing thorium, 130  
     for thorium extrusion, 128  
   radiation effects on, 152, 153, 154, 161,  
     162, 165, 166  
     shear stress of, 161
- Corrosion tests, with a thermal convection loop, 319
- of thorium, 134  
   of thorium alloys, 134  
   of uranium, 91  
   of uranium alloys, 91  
   by water, 211
- Creep, of thorium, 127  
   of uranium, 66  
   of uranium alloys, 90
- Cross sections, neutron, 281
- Crucibles, aluminum oxide, 118  
   beryllia, 4, 99, 116, 118  
   calcium oxide, 118  
   copper, 118  
   graphite, 3, 99, 118, 307, 310  
   magnesium oxide, 118  
   steel, 114  
   tantalum, 118  
   thorium oxide, 118  
   zirconia, 118
- Crystals, ionic, 173  
   of  $\beta$ -uranium, 80
- Density, of bomb charge, 10  
   of thorium, 120  
   of uranium, 22, 23, 24  
   of  $\gamma$ -uranium–molybdenum alloy, 23  
   of uranium tetrafluoride, 9
- Diamond, 167
- Dielectrics, 176
- Diffusion couples, 211
- Diodes, 175, 176
- Dispersants, fissile, densities and melting points of, 280
- Dolomitic oxide, liner, for thorium tetrafluoride reduction, 116  
 lining for bombs, 10  
 sieve analysis of, 11
- Drawing, lubricant for, 101, 130  
   of thorium, 130  
   of uranium, 101
- Dryway plant, 19

Dust explosion, of thorium or thorium hydride, 144

**Elasticity**, modulus of, *see element: elastic constants*

Elastomers, ionization effects on, 150  
radiation effects on, 176

Electrical equipment, 175

Electronic equipment, 175

Electropolishing thorium, 138

Elongation, *see element: tensile properties*

Endurance limit of thorium, 127

Enthalpy, of thorium, 120  
of uranium, 22

Entropy, of uranium, 22

Ether, solvent for uranyl nitrate, 19

Expansion, thermal, of thorium, 120  
of uranium, 49, 53, 54, 55  
of  $\alpha$ -uranium, 22, 49, 50, 51, 52, 53  
of  $\beta$ -uranium, 56  
of  $\gamma$ -uranium, 23, 56

Explosion, of thorium dust, 144  
of thorium hydride dust, 144

Explosive gas mixtures, from water radiolysis, 229, 233

Extrusion constants, for  $\alpha$ -uranium, 102  
for uranium alloys, 105

Extrusion dies, 101

Extrusion liners, 101

Extrusion, of thorium, 128  
of uranium, 101

**Fabrication**, of thorium, 128  
of uranium, 33, 99–103  
of uranium alloys, 103–108

Filter, Nutsch, 19

Fissile dispersants, 280

Fission fragments, effects of, 149  
escape of, from uranium dioxide, 226  
range of, in fuels, 225

Fissionable materials, radiation effects on, 187–240

Forging, thorium, 129  
uranium, 103

Fuel element, Brookhaven, fabrication of, 259–277  
ceramic, radiation effects on, 227  
dispersion type, 278–295  
radiation effects on, 223  
fabrication of, 262, 265, 281, 282  
iron clad, 283, 284, 285

Fuel element (*Cont.*)  
for the Materials Testing Reactor, 286  
uranium, aluminum-clad, 246, 247, 248, 288  
uranium base, 259–277

Fuels, fluid, 242 ff.  
solid, 242 ff.  
coolant for, 245  
temperature gradient in, 245

Fuel system, containers, 255  
fluid, 296–334

Fuel technology, 243–258

Furnace, for bomb, 7, 14, 15, 16

Fusion, heat of, of thorium, 120  
of uranium, 22

**Gallium**  
alloys of, with copper, 165  
with thorium, 129  
with uranium, 72  
thorium corrosion by, 137

Gas blanket, 238, 239

**Germanium**  
alloys of, with copper, 165  
with thorium, 129  
with uranium, 70, 72  
radiation effects on, 153, 154, 175, 176

Glass, silica, 169, 171, 172

**Gold**, alloys of  
with copper, 162  
with thorium, 129  
with uranium, 70, 72

Graphite, anode of, 3  
crucibles of, 3, 99, 118  
container for bismuth solutions, 256, 313  
matrix, for uranium carbide dispersions, 253  
for uranium dioxide dispersions, 253  
mould, for thorium, 116  
radiation effects on, 156, 176  
reaction of, with bismuth, effect of zirconium, 318  
–uranium dispersion, 227  
–uranium dioxide dispersion, 227  
–uranium tritaectoxide dispersion, 227

Grain growth, in uranium, 33, 36, 37, 38

Grain size, in uranium, 37, 38, 42, 44, 45, 47, 63  
in  $\alpha$ -uranium, 46

Green salt, *see* Uranium tetrafluoride

Grinding thorium, 130, 138

- Hafnium**, alloys of  
with thorium, 139  
with uranium, 70, 71
- Hardening**, work, of thorium, 127
- Hardness**, effect of radiation on, 160, 210  
of thorium alloys, 124  
of uranium, 40, 62, 66
- Heat capacity** of thorium, 120  
of uranium, 22
- Heat of fusion**, of thorium, 120  
of uranium, 22
- Heat of sublimation**, of uranium, 22
- Heats of transformation**, of uranium, 22
- Heat of vaporization**, of thorium, 120  
of uranium, 22
- Heavy water**, density of, 306  
dispersion of uranium oxides, 256  
uranyl sulfate solution in, 255, 300
- Helium**, blanket gas, 238, 239  
dispersion of uranium dioxide in, 256
- Hydrazine**, from radiolysis of water and nitrogen, 238
- Hydrochloric acid**, in water, effect on radiolysis, 233
- Hydrofluoric acid**, thorium corrosion by, 136, 137
- Hydrogen**, migration of, through uranium oxide, 92  
thorium corrosion by, 136  
in thorium powder, 132  
in uranium, 17, 63, 64, 72  
in  $\alpha$ -uranium, 63  
from uranyl sulfate solutions, radiation effect, 304
- Hydrogen fluoride**, from uranium tetrafluoride and water, 10
- Hydrogen peroxide**, decomposition of, in uranyl sulfate solutions, 304  
from the radiolysis of water and nitrogen, 238  
uranium peroxide precipitation by, 18
- Hydrolysis**, of uranium tetrafluoride, 10
- Hydroxylamine**, from radiolysis of water and nitrogen, 238
- Impact strength** of thorium, 126, 128
- Inclusions**, in thorium, 139
- Inconel**, radiation effects on, 164
- Indium**, alloys of  
with thorium, 126  
with uranium, 72
- Insulation**, electrical, 176
- Intermediate compounds**, *see element: alloys*
- Interstitial atoms**, 150, 154, 155, 161, 162, 167, 174
- Ionization effects**, 150
- Iridium**, alloys of, with uranium, 72
- Iron**  
alloys of, with bismuth, 323, 324, 328, 329, 330  
radiation effects on, 163  
with thorium, 121, 129  
with uranium, 37, 38, 41, 70, 72, 101, 280  
with uranium and chromium, 72  
with uranium and cobalt, 72  
with zirconium, 332
- analyses of**, 332
- Armco**, corrosion of by bismuth solutions, 319  
radiation effects on, 165
- bomb**, for uranium tetrafluoride reduction, 6
- cladding** for thorium, 128
- corrosion of**, by bismuth, 256, 317, 319, 321, 331, 332
- critical shear stress of**, effect of radiation on, 161
- fission fragments in**, range of, 225
- lubricant for thorium extrusion**, 128
- matrix for uranium dioxide**, 283, 284, 285
- melting point of**, 281
- neutron cross section of**, 281
- radiation effects on**, 161, 165, 166  
—uranium interface, diffusion across, 249  
in water, effect on radiolysis, 234, 237
- Iron sulfate**, in water, effect on radiolysis, 234, 235
- Krypton** in uranium alloys, removal of, 201
- Lactose** and potassium nitrate, igniting agent, 20
- Lanthanum**, alloys of  
with thorium, 139  
with uranium, 72, 73
- Lattice constants**, of thorium, 120  
of uranium, 22, 23
- Lead**, alloys of  
with bismuth, corrosion of steel by, 318, 323  
with bismuth, solubility of iron in, 329  
with bismuth and zirconium, 310

- Lead alloys (Cont.)**
- with thorium, 129, 139
  - with uranium, 70, 72, 137
    - densities and melting points of, 280
    - with uranium and bismuth, 72, 310
    - with uranium, bismuth; and zirconium, 310
- Lead**, corrosion of thorium by, 137
- Lining**, for bomb, 10
- Liquids**, radiation effects on, 228
- Lithium**, thorium corrosion by, 136, 137
- Loop**, thermal convection, for corrosion tests, 319
- Machining** thorium, 130
- Magnesium**
- alloys of, with thorium, 115, 139
    - with uranium, 17, 72, 73, 279
    - phase diagram for, 76
    - with uranium, bismuth, and zirconium, 310
  - bomb charge of, 7
  - carbothermic, 11
  - cutting to size, 12
  - electrolytic, 11
  - ferrosilicon process, 11, 12
  - melting point of, 281
  - neutron cross section of, 281
  - purity of, 11
  - redistilled, 11
  - size distribution of, 13
  - thorium halide reduction by, 113
  - thorium tetrachloride reduction by, 114, 115, 132
  - uranium tetrafluoride reduction by, 3, 4, 5, 9, 10, 13
- Magnesium fluoride**, bomb liner of, 13
- slag**, 5
- Magnesium oxide**, crucible of, 118
- formation of, in bismuth solution, 310
  - lining for bomb, 10
- Manganese**
- alloys of, with copper, radiation effects on, 165
    - with uranium, 72
  - radiation effects on, 184
  - in water, effect on radiolysis, 234, 237
- Mass transfer**, *see element: corrosion*
- Melting point** of thorium, 120
- of uranium, 22, 99
- Mercury**
- alloys of, with uranium, 70, 72
  - corrosion by, 317
- Metallography** of thorium, 138
- Metallurgy**, powder, of thorium, 130
- Metallurgy**, of thorium, 109–145
- of thorium alloys, 136–143
  - of uranium, 3–108
- Metals**, matrix, melting points and neutron cross sections of, 281
- precious, recovery from uranium ore, 18
- solubilities of, apparatus for determination of, 322
- structural, radiation effects on, 162
- Microstructure**, radiation effects on, 165
- Mill**, Sendzimer, 103
- Modulus**, bulk, *see element: elastic constants*
- Modulus of elasticity**, *see element: elastic constants*
- Modulus of resilience**, *see element: elastic constants*
- Modulus, shear**, *see element: elastic constants*
- Modulus, Young's**, *see element: elastic constants*
- Molybdenum**
- alloys of with uranium, 70, 71, 72, 73, 76, 80, 82, 83, 89, 104, 106, 108, 219
  - corrosion of, 95
    - by water, 212
  - creep of, 91
  - extrusion constants of, 105
  - fabrication of, 107
  - melting of, 106
  - phase diagram, 77
  - radiation effects on, 200, 201, 205
  - tensile data, 87, 88
  - alloys of with  $\gamma$ -uranium, density of, 23
  - lattice constants of, 23
  - oxide film on, 94
  - thermal expansion of, 57
- cathode of, 4
- corrosion of by bismuth solutions, 319
- crucible liner, 114
- melting point of, 281
- neutron cross section of, 281
- radiation effect on, 164
- solubility of, in bismuth, 323, 324

- Monazite sand, caustic digestion process for, 112  
 composition of, 110  
 processing costs of, 113  
 sulfuric acid process for, 110  
 thorium source, 109
- Monazite sulfate, fractional crystallization of, 111  
 thorium phosphate solubility in, 110
- Neodymium**, alloys of, with uranium, 72, 73
- Neutrons, cross sections for, 281  
 elastic collisions with, 149  
 reaction of with thorium, 109
- Nickel  
 alloys of, radiation effects on, 163  
 with thorium, 129  
 with uranium, 72  
 with uranium and cobalt, 72  
 melting point of, 281  
 neutron cross section of, 281  
 radiation effects on, 163, 164, 165, 166
- Niobium, alloys of  
 with thorium, 124, 129  
 with uranium, 70, 71, 72, 76, 83, 89, 95, 104  
 corrosion of, 95  
 by water, radiation effects on, 211, 212  
 hardness of, 84  
 radiation effects on, 200, 201  
 with  $\gamma$ -uranium, oxide film on, 94  
 with uranium and tin, corrosion of, 96  
 with uranium and zirconium, 84  
 corrosion of, 95, 96  
 by water, radiation effects on, 211, 212  
 extrusion constants of, 105
- Niobium, melting point of, 281  
 neutron cross section of, 281
- Nitrates, from radiolysis of water and nitrogen, 239
- Nitric acid, from radiolysis of water and nitrogen, 238, 239
- Nitrites, from radiolysis of water and nitrogen, 238
- Nitrogen, blanket gas, 238, 239  
 in thorium, 117, 121, 125, 129, 132  
 thorium corrosion by, 135, 136  
 in uranium, effect on grain size, 37, 38
- Nitrogen (*Cont.*)  
 -uranium system, 72  
 and water, radiation effects on, 238
- Non-metals, radiation effects on, 167
- Nutsch filter, 19
- Orientation** in  $\alpha$ -uranium, 28, 30, 31
- Oxygen, in thorium, 117, 121, 124, 125, 129, 132  
 thorium corrosion by, 135, 136  
 -uranium system, 72
- Palladium**, alloys of  
 with thorium, 129  
 with uranium, 72
- Particle size, and radiation effects, 184
- Phase diagrams, for thorium and carbon, 140  
 for thorium and zirconium, 142  
 for uranium and aluminum, 71  
 for uranium and magnesium, 76  
 for uranium and molybdenum, 77  
 for uranium and thorium, 141  
 for uranium and silicon, 73  
 for uranium and tungsten, 75  
 for uranium and vanadium, 74  
 for uranium and zirconium, 78  
 for uranyl sulfate and water, 299
- Phase transformations, of thorium, 139  
 of uranium, 45
- Phosphorus, in monazite sands, 110  
 radiation effects in, 162  
 -uranium system, 72
- Plasticity of thorium powder, 132
- Plastics, ionization effects on, 150
- Plastomers, radiation effects on, 176
- Platinum, alloys of  
 with thorium, 129  
 with uranium, 72
- Plutonium, alloys of with uranium, fuel elements, 252  
 fuel elements, steel clad, 252
- Poisson's ratio, *see element: elastic constants*
- Pole figures, for  $\alpha$ -uranium, 31, 32
- Potassium, alloy of with sodium, dispersion of uranium dioxide in, 256  
 thorium tetrachloride reduction by, 113
- Potassium chlorate, booster for uranium tetrafluoride reduction, 5

- Potassium chloride, 173  
 Potassium nitrate and lactose, igniting agent, 20  
 Potassium thorium fluoride, reduction of, electrolytic, 115, 132  
 Potassium uranium fluoride, reduction of, electrolytic, 115  
 Powder metallurgy, of thorium, 130  
 Praseodymium, alloys of, with uranium, 72, 73  
 Pressing, lubricant for, 130  
     of thorium powder, 132  
     of uranium, 103  
 Pressure, vapor, of uranium, 22, 24  
 Production of thorium, 109–119  
 Proportional limit, *see element: elastic constants*  
 Pyrex, corrosion of, by bismuth solutions, 318  
 Pyrophoric alloy, of thorium and copper, 129  
 Pyrophoric thorium, 130  
 Quartz, corrosion of, by bismuth solutions, 318  
     radiation effects on, 169, 170  
 Quenching of uranium, 79  
**Radiation** damage, *see elements, alloys, and compounds: radiation effects*  
 Radiation effects, 146 ff.  
     on aqueous corrosion, 211  
     control of, 183  
     on diffusion couples, 211  
     of fission fragments, 149  
     in fissionable materials, 187–240  
     on hardness, 160, 210  
     ionization by, 150  
     metallographic, 209  
     on strength, 160  
     in structural materials, 160–186  
     on surfaces, 208  
     on tensile properties, 210  
     on thermal conductivity, 211  
 Radiolysis of water, 228, 233  
 Radium, in uranium ore, 18  
 Radium sulfate, precipitation of, by barium nitrate, 18  
 Radon, in uranium ore, 18  
 Rare earths, precipitation of, 111, 112, 113  
 Rare earth orthophosphates, in monazite sands, 110  
 Rare earth sulfates, solubility of, in water, 111  
 Reactors, 247, 295  
 Reactor control systems, 173  
 Recrystallization, of thorium, 121, 122, 123, 124  
     of uranium, 33, 39, 41, 42, 43, 44  
 Rectifiers, 176  
 Resilience, modulus of, *see element: elastic constants*  
 Rolling, thorium, 129  
     uranium, 101  
**Selenium**, radiation effects on, 176  
     –uranium system, 72  
 Semiconductors, 175, 176  
 Sendzimer mill, 103  
 Shear modulus, *see element: elastic constants*  
 Silica, radiation effects on, 169  
 Silica glass, radiation effects on, 169, 171, 172  
 Silicon, alloys of  
     with thorium, 121  
     with uranium, 70, 72, 86, 107, 108, 219  
     corrosion of, 95, 96, 97  
     by water, radiation effects on, 211  
     densities and melting points of, 280  
     extrusion constants of, 105  
     fabrication of, 107  
     grain size, 37, 38  
     melting of, 107  
     phase diagram, 73  
     radiation effects on, 201  
     with uranium and aluminum, 72  
 Silicon, radiation effects on, 175, 176  
 Silicon carbide matrix, for uranium carbide dispersions, 253  
 Silver, alloys of  
     with thorium, 129  
     with uranium, 72, 73  
 Sintering thorium powder, 132  
 Slip, in  $\alpha$ -uranium, 25, 26, 27  
 Sodium  
     alloys of, with potassium, dispersion of uranium dioxide in, 256  
     thorium corrosion by, 136, 137  
     with uranium, 72  
     thorium corrosion by, 137

- Sodium (*Cont.*)  
 thorium halide reduction by, 113  
 thorium tetrachloride reduction by, 114  
 uranium dioxide solution in, fuel system, 255
- Solids, displacement spikes in, 150  
 impurity atoms in, 150  
 ionization effects in, 150  
 radiation effects on, 150  
 replacement collisions in, 151  
 thermal spikes in, 150  
 vacancies in, 150
- Solutions, solid, *see element: alloys*  
 Solutions, solid, radiation effects on, 162
- Space group, of  $\alpha$ -uranium, 22  
 of  $\beta$ -uranium, 23
- Spikes, displacement, in solids, 150  
 thermal, in solids, 150
- Steels, analyses of, 332  
 container, for bismuth solutions, 256, 313  
 for fluid fuels, 255  
 for thorium powder preparations, 131  
 for uranyl sulfate solutions, 307
- corrosion of, by bismuth, 317, 318, 321  
 by bismuth and lead alloy, 318, 323
- crucible of, 114
- radiation effects on, 162, 163, 164
- stainless, container for fluid fuels, 255  
 corrosion of, by bismuth, 317, 319  
 matrix, for uranium dioxide dispersions, 250, 251  
 radiation effects on, 163, 164, 167
- and uranium, radiation effects and inter-diffusion of, 211
- uranium dioxide dispersions, radiation effects on, 226
- Strength, impact, of uranium, 66  
 of metals, effect of radiation, 160
- tensile, *see element: tensile properties*  
 yield, *see element: tensile properties*
- Sublimation, heat of, of uranium, 22
- Sulfur-uranium system, 72
- Sulfuric acid, in water, effect on radiolysis, 234, 235
- Superconducting transition, in thorium, 120
- Surfaces, radiation effects on, 208
- Swaging, thorium, 130  
 uranium, 103
- Tantalum  
 alloys of, with thorium, 124
- Tantalum alloys (*Cont.*)  
 with uranium, 70, 71, 72, 73  
 crucible of, 118  
 in uranium, effect on grain size, 37, 38
- Tellurium-uranium system, 72
- Temperature, of bombardment, and radiation effects, 183  
 and firing time of bomb, 15  
 gradient, effect on grain size, 47  
 of recrystallization, of thorium, 121  
 of uranium, 40  
 of softening, of thorium, 121  
 transformation, of uranium, 22  
 and uranium yield, 15, 16
- Tempering, of uranium, 79
- Tensile properties, radiation effects on, 210
- Tensile strength, *see tensile properties under each element*
- Thallium, alloys of  
 with thorium, 129, 139  
 with uranium, 72
- Thermal conductivity, of thorium, 120  
 of uranium, 22
- Thermal expansion, of thorium, 120  
 of  $\alpha$ -uranium, 22
- Thorium fuel element, 253
- Thorium  
 atomic diameter of, 139  
 boiling point of, 120  
 casting of, 118  
 castings of, pyrophoric surfaces, 130  
 compressibility of, 120  
 conductivity of, electrical, 120  
 thermal, 120  
 constants, lattice, 120  
 copper-clad, 128  
 corrosion of, 134  
 by air, 135, 136  
 by argon, 135, 136  
 by bismuth, 137  
 by bromine, 136, 137  
 by gallium, 137  
 by hydrofluoric acid, 136, 137  
 by hydrogen, 136  
 by lead, 137  
 by lithium, 136, 137  
 by nitrogen, 135, 136  
 by oxygen, 135, 136  
 by sodium, 137  
 by sodium and potassium alloy, 136, 137

Thorium (*Cont.*)

by uranium and lead alloy, 137  
 by water, 134  
 creep of, 127  
 crucibles for, 118  
 density of, 120  
 disintegration of, 109  
 drawing, 130  
   lubricant for, 130  
 elastic constants of, 120, 125, 127  
 electrical resistivity of, 120  
 electronegativity of, 139  
 electropolishing of, 138  
 endurance limit of, 127  
 enthalpy of, 120  
 etching of, 138  
 expansion of, thermal, 120  
 extraction of, from monazite sulfate, by  
   selective solvents, 111  
   with tributyl phosphate, 111, 112  
 extrusion of, 128  
   lubricant for, 128  
 fabrication of, 128  
 fatigue of, 127  
 fluoride film on, 136  
 forging of, 129  
 forming of, 128  
 fusion, heat of, 120  
 grinding, 130, 138  
 hazards in handling, 143  
 heat capacity of, 120  
 heat of fusion of, 120  
 heat of vaporization of, 120  
 impact strength of, 126, 128  
 inclusions in, 139  
 iron-clad, 128  
 lattice constants of, 120  
 machining of, 130  
 matrix, for uranium dispersions, 250, 251  
 mechanical properties of, 125  
 melting of, 118  
 melting point of, 120  
 metallography of, 138  
 metallurgy of, 109–145  
 in monazite sands, 110  
 nitride film on, 136  
 nitrogen in, 117, 121, 125  
 occurrence of, in nature, 109  
 oxygen in, 117, 121, 124, 125, 129  
 phase transformation of, 139  
 powder, carbon in, 132

Thorium, powder (*Cont.*)

compacts of, 133, 134  
 explosibility of, 144  
 hydrogen in, 132  
 metallurgy of, 130  
 nitrogen in, 132  
 oxygen in, 132  
 particle size of, 132  
 plasticity of, 132  
 preparation of, 114, 115, 131  
 pressing, 132  
 sintering, 132  
 from thorium hydride, 130, 131  
 volume of, 133  
 precipitation of, from monazite sand, 112  
   from monazite sulfate, 111  
 production of, 109–119  
 proportional limit of, 127  
 purification of, iodide process for, 116  
 radiation effects on, 223  
 radiation from, 143  
 radioactive daughters of, 111  
 radioactivity of, 143  
 reaction with a neutron, 109  
 recovery of, from monazite sands, 110  
 recrystallization of, 121, 122, 123, 124  
 recrystallized, orientation of, 125  
 rolling, 129  
 softening temperature of, 121  
 sponge, preparation of, 114, 115  
 strain in, effect on tensile properties, 126  
 stress strain diagram for, 126  
 superconducting, transition temperature  
   of, 120  
 swaging, 130  
 tensile strength of, 125  
 thermal conductivity of, 120  
 thermal expansion of, 120  
 thorium tetraiodide preparation from,  
   117  
 transformation temperature of, 120  
 transition temperature, superconducting,  
   120  
 vaporization, heat of, 120  
 work function of, 120  
 work hardening of, 127  
 yield strength of, 125, 127

Thorium, alloys of, 129, 139  
 with aluminum, 121, 129  
 with antimony, 129, 139  
 with beryllium, 121, 129

- Thorium alloys (*Cont.*)  
 with bismuth, 129, 139  
 with carbon, 117, 121, 124, 125, 129, 139  
     phase diagram for, 140  
 with cerium, 139  
 with cobalt, 129  
 with copper, pyrophoric, 129  
 corrosion of, 134  
 with gallium, 129  
 with germanium, 129  
 with gold, 129  
 with hafnium, 139  
 hardness of, 124  
 with indium, 126  
 with iron, 121, 129  
 with lanthanum, 139  
 with lead, 129, 139  
 with magnesium, 115, 139  
 metallurgy of, 136–143  
 with nickel, 129  
 with niobium, 124, 129  
 with palladium, 129  
 with platinum, 129  
 radiation effects on, 223  
 with silver, 129  
 with tantalum, 124  
 with thallium, 129, 139  
 with tin, 129  
 with titanium, 124, 129  
 with uranium, 70, 72, 73, 140  
     phase diagram for, 141  
     radiation effects on, 223  
 with zinc, 141  
 with zirconium, 129, 139, 142  
     corrosion of, by water, 137  
     phase diagram for, 142
- Thorium halide reduction, 113
- Thorium hydrides, 136  
 conversion of, to thorium powder, 130, 131  
 density of, 131  
 dust, explosibility of, 144  
 lattice constants of, 131
- Thorium nitrate, thorium oxalate preparation from, 115
- Thorium nitride, inclusions in thorium, 139
- Thorium oxalate, preparation from thorium nitrate, 115  
 thorium oxide preparation from, 116
- Thorium oxide, crucible of, 118  
 inclusions in thorium, 139
- Thorium oxide (*Cont.*)  
 matrix for uranium dioxide dispersions, 253  
 preparation from thorium oxalate, 116  
 reduction of, by calcium, 113, 114, 132  
 thorium fluoride preparation from, 116
- Thorium phosphate, solubility in monazite sulfate, 110
- Thorium potassium fluoride, electrolytic reduction of, 115, 132
- Thorium tetrachloride, purification of, 114  
 reduction of, 113, 114, 115, 132
- Thorium tetrafluoride, reduction of, 115, 116
- Thorium tetraiodide, decomposition of, 117  
 preparation of, from thorium, 117  
     from thorium oxide, 116
- Thoron, 143
- Thoryl chloride, reduction of, 115
- Tin, alloys of  
 with thorium, 129  
 with uranium, 72, 280  
 with uranium and niobium, 96
- Tin, radiation effects on, 162
- Titanium  
 alloys of, with thorium, 124, 129  
 with uranium, 70, 71, 73, 76, 89, 90, 91, 104, 201, 219  
 container for uranyl sulfate solutions, 307  
 melting point of, 281  
 neutron cross section of, 281
- Transformation, entropy of, of uranium, 22  
 heat of, of uranium, 22  
 temperature, of thorium, 120  
     of uranium, 22  
 of uranium alloys, 76, 86  
 in uranium–niobium alloys, 95
- Transistors, 175, 176
- Transition, superconducting, of thorium, 120
- Tricresyl phosphate, *see* Cresyl phosphate
- Tungsten, alloys of, with uranium, 70, 71, 72, 73  
 phase diagram for, 75
- Twinning, of  $\alpha$ -uranium, 26, 27, 28
- Unit cells, of uranium, 22, 23, 24
- Urania fuel element, 253
- Uranium  
 allotropic modifications of, 49

Uranium (*Cont.*)

-aluminum interface, diffusion across, 211, 248  
 anisotropy of, 49  
 annealing temperature of, 40, 42  
 atomic distances of, 69  
 biscuit, 6  
 body-centered cubic, *see*  $\gamma$ -Uranium  
 boiling point of, 22  
 brittleness of, 66  
 casting of, 16, 99-103  
 complexion, dispersion in fused fluorides, 256  
 cooling, 79  
 copper-clad, for  $\alpha$  extrusion, 101  
 corrosion of, 91, 94  
 covalent bonding of, 69  
 creep of, 66  
 density of, 22, 280  
 dimensions, radiation effects on, 188, 194  
 dispersion of, in thorium, 250, 251  
 drawing of, 101  
 ductility of, 66  
 elastic constants of, 57, 58, 59, 60, 61, 63, 67  
 enthalpy of, 22  
 entropy of, 22  
 entropy of transformation of, 22  
 extraction of, by selective solvents, 111  
     with tributyl phosphate, 111, 112  
 extrusion of, 101  
 fabrication of, 99-103  
 fission fragments in, range of, 225  
 forging of, 103  
 fuels, dispersions of, 250  
 fuel elements, 246, 247, 248, 249, 259-277  
 grain growth in, 33  
 grain size in, 37, 38, 42, 44, 45, 47, 63  
 graphite dispersion of, radiation effects on, 227  
 growth in, mechanism of, 221  
 hardness of, 62, 66  
 heat capacity of, 22  
 heat of fusion of, 22  
 heat of sublimation of, 22  
 heats of transformation of, 22  
 heat of vaporization of, 22  
 impact strength of, 66  
 inclusions in, effect on grain growth, 36, 37, 38

Uranium (*Cont.*)

ingots, composition of, 17  
 -iron interface, diffusion across, 249  
 lattice constants of, 22  
 mechanical properties of, 57  
 melting point of, 22, 99, 280  
 metallurgy of, 3-108  
 in monazite sands, 110  
 orbital electrons in, 69  
 ore, crushing, 18  
     extraction of, 18  
 radium in, 18  
 radon in, 18  
     sampling, 18  
 orthorhombic, *see*  $\alpha$ -Uranium  
 -oxygen system, 72  
 phase transformations in, 45  
 -phosphorus system, 72  
 physical properties of, 21  
 precipitation of, from monazite sand, 112  
     from monazite sulfate, 111  
 preparation of, 3-20  
 pressing of, 103  
 proportional limit of, 57, 59  
 purification of, 18  
 purity of, 19  
 quenching of, 79  
 radiation effects on, 187  
 radioactive daughters of, 111  
 reaction of, with aluminum, 262  
 recrystallization of, 33, 34, 35, 39, 41, 42, 43, 44  
 rolling of, 101  
 slugs, preparation of, 260, 261  
 solid solutions of, *see* Uranium, alloys of  
 solubility of, in bismuth, 314  
 solubility of carbon in, 99  
 and steel, radiation effects and interdiffusion, 211  
 straightening of, 103  
 strain in, effect on ductility, 66  
 stress-strain of, in compression, 57, 58  
 structure of, effect of carbon, 45  
 swaging of, 103  
 tempering of, 79  
 tensile properties, 40, 61, 63, 64, 65, 67, 87  
 tetragonal, *see*  $\beta$ -Uranium  
 thermal conductivity of, 22  
 thermal cycles in, 212  
 thermal expansion of, 49, 53, 54, 55

*Uranium (Cont.)*

thermal properties of, 21  
 from thorium disintegration, 109  
 transformation temperatures of, 22  
 uranium dioxide preparation from, 91  
 uranium hydride preparation from, 91, 92  
 vapor pressure of, 22, 24  
 waste, recovery of, 20  
 in water, effect on radiolysis, 234  
 yield of, and furnace temperature, 14, 15,  
 16

 *$\alpha$ -Uranium*

alloys of, 70  
 oxide film on, 94  
 atomic volume of, 22, 24  
 cross-slip in, 25, 26, 27  
 deformation mechanisms in, 21, 25, 27  
 density of, 22, 24  
 ductile transition in, effect of hydrogen,  
 63  
 electronic configuration of, 69  
 elongation of, effect of heat treatment, 65  
 extrusion constant for, 102  
 grain size of, effect of heat treatments, 46  
 kinking in, 25, 27  
 lattice constants of, 22  
 orientation in, 28, 30, 31  
 pole figures for, 31, 32  
 reduction of, effect of heat treatment, 65  
 shear stress, 25  
 single crystals, preparation of, 48  
 slip in, 25, 26, 27  
 solubility of elements in, 36  
 space group of, 22  
 tensile properties, 65  
 thermal expansion of, 22, 49, 50, 51, 52,  
 53  
 twinning system of, 26, 27, 28  
 unit cell of, 22, 24  
 valence of, 70

 *$\beta$ -Uranium*

alloys of, 71, 72  
 with chromium, 23, 56  
 atomic volume of, 23, 24  
 crystals of, 80  
 density of, 23, 24  
 elongation of, effect of heat treatment, 65  
 lattice constants, 23  
 reduction of, effect of heat treatment, 65  
 space group of, 23  
 tensile properties, 65

 *$\beta$ -Uranium (Cont.)*

thermal expansion of, 56  
 unit cell of, 23, 24  
 valence of, 72

 *$\gamma$ -Uranium*

alloys of, 71  
 with molybdenum, 23, 57, 94  
 with niobium, 94  
 oxide film on, 94  
 atomic volume of, 23, 24  
 density of, 23, 24  
 elongation of, effect of heat treatment,  
 65

expansion, linear, 23

lattice constants of, 23

reduction of, effect of heat treatment, 65

solubility of elements in, 37

tensile strength of, effect of heat treat-  
 ment, 65

thermal expansion of, 56

unit cell of, 23, 24

valence of, 71

Uranium, alloys of, 69-98; *see also*  $\alpha$ -Ura-  
 nium,  $\beta$ -Uranium,  $\gamma$ -Uranium

with aluminum, 70, 72, 86, 219, 282, 286  
 aluminum-clad, 288

densities and melting points of, 280  
 dispersions of, in aluminum, 250, 252

fuel element, 291

phase diagram for, 71

radiation effects in, 184, 201

with aluminum and silicon, 72

with antimony, 72

with arsenic, 72

with beryllium, 72

densities and melting points of, 280

radiation effects on, 205

with beryllium and carbon, 72

with bismuth, 72, 256, 314

fuel system, 255, 256, 307

reactions of, with graphite, 310

stability of, 313

uranium carbide in, 310

uranium nitride in, 310

with bismuth and calcium, 317

with bismuth and chromium, 313

with bismuth and iron, 313

with bismuth and lead, 72, 310

with bismuth, lead and zirconium, 310

with bismuth and magnesium, 256, 313,  
 315, 316, 317

Uranium alloys (*Cont.*)  
 with bismuth, magnesium, and zirconium, 310  
 with bismuth and nickel, 313, 314, 315  
 with bismuth and thorium, 317  
 with bismuth and zirconium, 256, 310, 313, 316, 317  
 with boron, 72  
 with calcium, 72  
 with carbon, 45, 72, 219  
 with carbon and beryllium, 72  
 casting of, 103–108  
 with cerium, 72, 73  
 with chromium, 70, 71, 72, 73, 79, 80, 81, 86, 219  
 extrusion constants of, 105  
 fabrication of, 104  
 melting of, 104  
 radiation effects on, 200, 205  
 tensile data, 87  
 with chromium and iron, 72  
 with cobalt, 72  
 with cobalt and iron, 72  
 with cobalt and nickel, 72  
 with copper, 70, 72  
 corrosion of, by water, 91  
 creep of, 90  
 extrusion constants of, 105  
 fabrication of, 103–108  
 with gallium, 72  
 with germanium, 70, 72  
 with gold, 70, 72  
 with hafnium, 70, 71  
 with hydrogen, 17, 66, 72  
 with indium, 72  
 with iridium, 72  
 with iron, 70, 72, 101, 280  
 with iron and chromium, 72  
 with iron and cobalt, 72  
 krypton removal from, 201  
 with lanthanum, 72, 73  
 with lead, 70, 72  
 densities and melting points of, 280  
 thorium corrosion by, 137  
 with lead and bismuth, 72, 310  
 with magnesium, 17, 72, 73, 279  
 phase diagram for, 76  
 with manganese, 72  
 mechanical properties of, 86  
 with mercury, 70, 72

Uranium alloys (*Cont.*)  
 with molybdenum, 70, 71, 72, 73, 76, 80, 82, 83, 89, 104, 106, 108, 219  
 corrosion of, 95  
 by water, radiation effects on, 212  
 creep of, 91  
 extrusion constants of, 105  
 fabrication of, 107  
 melting of, 106  
 phase diagram for, 77  
 radiation effects on, 200, 201, 205  
 tensile properties, 87, 88  
 with neodymium, 72, 73  
 with nickel, 72  
 with nickel and cobalt, 72  
 with niobium, 70, 71, 72, 76, 83, 89, 104  
 corrosion of, 95  
 by water, radiation effects on, 211, 212  
 hardness of, 84  
 radiation effects on, 200, 201  
 with niobium and tin, 96  
 with niobium and zirconium, 84  
 corrosion of, 95, 96  
 by water, radiation effects on, 211, 212  
 extrusion constants of, 105  
 with nitrogen, 72  
 with palladium, 72  
 with platinum, 72  
 with plutonium, fuel elements, 252  
 with praseodymium, 72, 73  
 radiation effects on, 187, 200  
 with selenium, 72  
 with silicon, 70, 72, 86, 107, 108, 219  
 corrosion of, 95, 96, 97  
 by water, radiation effects on, 211  
 densities and melting points of, 280  
 extrusion constants of, 105  
 fabrication of, 107  
 melting of, 107  
 phase diagram for, 73  
 radiation effects on, 201  
 with silicon and aluminum, 72  
 with silver, 72, 73  
 with sodium, 72, 255  
 with sulfur, 72  
 with tantalum, 70, 71, 72, 73  
 with tellurium, 72  
 with thallium, 72  
 with thorium, 70, 72, 73, 140

- Uranium alloys, with thorium (*Cont.*)  
     phase diagram for, 141  
     radiation effects on, 223  
     with thorium and bismuth, 317  
     with tin, 72  
         densities and melting points of, 280  
     with tin and niobium, 96  
     with titanium, 70, 71, 73, 76, 89, 104, 219  
         creep of, 90, 91  
         radiation effects on, 201  
     transformation kinetics of, 76  
     with tungsten, 70, 71, 72, 73  
         phase diagram for, 75  
     with vanadium, 70, 71, 72, 73, 104, 219  
         phase diagram for, 74  
         radiation effects on, 210  
     with zinc, 72  
     with zirconium, 70, 71, 73, 76, 83, 86, 89,  
         104, 219  
         corrosion of, by water, radiation effects  
             on, 211, 212  
         creep of, 89, 90  
         extrusion constants of, 105  
         fabrication of, 106  
         fuel elements, zirconium-clad, 252  
         hardness of, 84, 87  
         melting of, 106  
         oxide film on, 94  
         phase diagram for, 78  
         radiation effects on, 201, 205  
         tensile properties, 87, 88, 89  
     with zirconium and niobium, corrosion  
         of, 95, 96  
         corrosion of, by water, 211, 212  
         extrusion constants of, 105  
         hardness of, 84
- Uranium carbides, densities and melting  
     points of, 280  
     dispersions of, 253  
     formation of, in bismuth solutions, 310,  
         311, 313
- Uranium dioxide–beryllium oxide system,  
     252
- Uranium dioxide, densities and melting  
     points of, 280  
     dispersions of, 279  
         in aluminum, 250, 251, 252, 288  
         in beryllium oxide, 253  
             radiation effects on, 228  
         in graphite, 253  
             radiation effects on, 227
- Uranium dioxide, dispersions of (*Cont.*)  
     in helium, 256  
     in iron, 283, 284, 285  
     in sodium and potassium alloy, 256  
     in steels, 226, 250, 251  
         in thorium oxide, 253  
     fission fragments from, escape of, 226  
     fission fragments in, range of, 225  
     layer of, in bomb, 11  
     preparation, from uranium, 91  
         from uranium hydride, 93  
         from uranium tetrafluoride, 10  
         from uranium trioxide, 19  
     radiation effects on, 228  
     reduction of, with calcium hydride, 3  
     uranium tetrafluoride preparation from,  
         9, 19
- Uranium hydrides, 95  
     preparation of, from uranium, 91, 92  
     uranium dioxide preparation from, 93
- Uranium nitrate, extraction of, with  
     tributyl phosphate, 19
- Uranium nitride, density and melting  
     point of, 280  
     formation of, in bismuth solution, 310
- Uranium oxide, dispersion of, in heavy  
     water, 256  
     in water, 256  
     films of, 91, 92
- Uranium peroxide, precipitation of, by  
     hydrogen peroxide, 18  
     preparation of, from uranyl nitrate, 20  
     thermal decomposition of, 304  
     uranyl nitrate preparation from, 19
- Uranium potassium fluoride, reduction of, 3
- Uranium tetrafluoride, bomb charge of, 6, 7  
     density of, 9, 10  
     dispersion of, in fused fluorides, 256  
     hydrolysis of, 19  
     particle size distribution of, 10  
     preparation from uranium dioxide, 9, 19  
     purity of, 8, 9  
     reaction of, with water, 10  
     reduction of, with calcium, 3, 4, 5, 8, 19  
         with magnesium, 3, 4, 5, 9, 10, 13  
         thermal booster for, 5
- Uranium trioxide, preparation from am-  
     monium diuranate, 19  
     solubility of, in uranyl sulfate solutions,  
         302  
     uranium dioxide preparation from, 19

Uranium tritaoctoxide, dispersion in graphite, radiation effects on, 227  
radiation effects on, 228  
Uranyl fluoride, in water, effect on radiolysis, 136, 237  
Uranyl ion, reduction of, 302  
Uranyl nitrate, ammonium diuranate preparation from, 19  
ether extraction of, 19  
hexahydrate, 19  
preparation of, from uranium peroxide, 19  
from uranium wastes, 20  
uranium peroxide preparation from, 20  
water solution of, 255  
Uranyl peroxide, precipitation from uranyl sulfate, radiation effect, 302, 304  
Uranyl phosphate, water solution of, 255  
Uranyl sulfate, heavy water solutions of, 255, 300  
solutions of, uranium trioxide solubility in, 302  
uranyl peroxide precipitation from, radiation effect, 302, 304  
water solutions of, 308, 309  
containers for, 307  
density of, 305  
effect on radiolysis, 234, 235, 236  
fuel system, 255, 298  
hydrogen from, radiation effect, 304  
hydrogen peroxide decomposition in, 304  
pH of, 303  
phase diagrams for, 299, 300, 301

**Vacancies**, in solids, 150  
**Valence**, of uranium, 70, 71, 72  
**Vanadium**,  
alloys of, with uranium, 70, 71, 72, 73, 104, 219  
phase diagram for, 74  
radiation effects on, 201  
melting point of, 281  
neutron cross section of, 281  
**Vapor pressure**, of uranium, 22, 24  
**Vaporization**, heat of, of thorium, 120  
of uranium, 22  
**Vitrosil**, radiation effects on, 169, 170  
**Volume**, atomic, of uranium, 22, 23, 24

**Water**, and air, radiation effects on, 238

**Water (Cont.)**  
in bomb charge, effect of, 9  
corrosion of thorium by, 134  
corrosion of thorium and zirconium alloy by, 137  
density of, 306  
dispersion of uranium oxides in, 256  
gases from, detonating mixture of, 229, 233  
heavy, density of, 306  
dispersion of uranium oxides in, 256  
uranyl sulfate solution in, 255, 300  
and nitrogen, ammonium ion formation, 238  
hydrazine formation, 238  
hydrogen peroxide formation, 238  
hydroxylamine formation, 238  
nitrate formation, 239  
nitric acid formation, 238, 239  
nitrite formation, 238  
radiolysis of, 238  
radiolysis of, 228, 233  
effect of boric acid, 234, 235  
effect of chromium, 234, 237  
effect of hydrogen chloride, 233  
effect of iron, 234, 237  
effect of iron sulfate, 234, 235  
effect of manganese, 234, 237  
effect of sulfuric acid, 234, 235  
effect of uranium, 234  
effect of uranyl fluoride, 236, 237  
effect of uranyl sulfate, 234, 235, 236  
uranyl nitrate solution in, 255  
uranyl phosphate solution in, 255  
uranyl sulfate solutions in, density of, 305  
fuel system, 255, 298  
phase diagrams for, 299, 300, 301  
**Work function** of thorium, 120  
**Work hardening** of thorium, 127

**Yield strength**, *see element: elastic constants*  
**Young's modulus**, *see element: elastic constants*

**Zinc**,  
alloys of, with copper, radiation effects on, 165  
with uranium, 72  
radiation effects on, 161  
**Zirconia** crucible, 118

**Zirconium**

fission fragments in, range of, 225  
melting point of, 281  
neutron cross section of, 281  
radiation effects on, 164, 166, 200

**Zirconium, alloys of**

- with bismuth, 323, 324, 325, 326, 327
- with bismuth and lead, 310
- with iron, 332
- with thorium, 129, 139, 141, 142
  - phase diagram for, 142
- with uranium, 70, 71, 73, 76, 83, 86, 89,  
104, 219
  - corrosion of, by water, radiation  
effects on, 211, 212
  - creep of, 89, 90
  - extrusion constants of, 105
  - fabrication of, 106
  - hardness of, 84, 87
  - melting of, 106
  - oxide film on, 94

**Zirconium alloys (*Cont.*)**

- phase diagram for, 78
- radiation effects in, 201, 205
- tensile data, 87, 88, 89
- zirconium-clad, 252
- with uranium and bismuth, 310
- with uranium, bismuth and lead, 310
- with uranium, bismuth and magnesium,  
310
- with uranium and niobium, corrosion of,  
95, 96
  - corrosion of, by water, radiation effects  
on, 211, 212
  - extrusion constants of, 105
  - hardness of, 84
- Zirconium carbide, 332**
  - formation of, in bismuth solution, 310,  
311, 312
- Zirconium nitride, 332**
  - formation of, in bismuth solution, 310,  
311



## NAME INDEX

---

- ADAMS, R. E., 223  
Albrecht, W. M., 91, 93  
Alexander, B. H., 191  
Antal, J. J., 155  
Arnold, S. U., 101  
Aronin, L. R., 151  
Atherton, J. E., 318  
Ayres, J. A., 92
- BACH, J. H., 28, 29  
Bainbridge, D. W., 329  
Ballentine, D. S., 176  
Baluffi, R. W., 191  
Bauer, A. A., 82  
Beall, S. E., 307  
Beck, P. A., 29, 30, 31  
Bensen, M., 92  
Berggren, R. G., 164, 223  
Berzelius, J. J., 113  
Bettman, M., 191, 222  
Billington, D. S., 149, 160, 165, 201  
Blatt, F. J., 154  
Blewitt, T. H., 161  
Blumenthal, B., 48  
Boas, W., 221  
Bopp, C. D., 176  
Borie, B. S., Jr., 28  
Boyle, 121, 124, 278  
Boyle, E. J., 278  
Boyle, J. W., 304  
Brinkman, J. A., 150  
Brooks, H., 150  
Brown, G. W., 222  
Bruch, C. A., 163, 164  
Brugmann, W. H., 136  
Bryner, J. S., 313  
Bupp, L. P., 160  
Burke, J. E., 191, 221, 222  
Burnham, J. B., Jr., 28, 29  
Burton, M., 149
- Buttner, F. H., 191  
Buzzard, R. W., 280
- CADWELL, J. J., 210  
Cahn, R. W., 21, 192  
Calkins, G. D., 211  
Cardinal, L. C., 59, 60  
Carlson, O. N., 83, 84, 109, 120, 138, 140, 142  
Carroll, R. M., 223  
Castleman, L. S., 205  
Charlesby, A., 176  
Chernock, W. P., 28, 29, 30, 31  
Chevigny, R., 101  
Chiotti, P., 109, 120, 131  
Chiswik, H. H., 21, 47, 57, 62, 84, 187  
Coffin, L. R., 164, 251  
Coltman, R. R., 161  
Cooper, H. G., 154  
Cordovi, M. A., 318  
Cottrell, A. H., 193  
Crawford, J. H., Jr., 160, 167  
Cummings, W. V., 209  
Cunningham, J. E., 251, 278  
Curtis, C. E., 253  
Cygan, R., 318
- DANIELS, F., 252  
Davenport, W. H., 305  
Davis, W. W., 164  
Deem, H. W., 211  
Dickerson, R. F., 138  
Dienes, G. J., 139, 155, 162, 165, 167  
Dillon, R., 92  
Dolin, P. I., 187, 228  
Doll, D. T., 80  
Draley, J. E., 91, 92, 93, 94, 134, 136, 248  
Driggs, F. H., 115  
Duffey, J., 29  
Duwez, P., 80  
Dwight, A. E., 83, 84

- |  |  |
|--|--|
| ECKERT, F. H., 121, 124                    | JACOBSON, M., 144                        |
| Egan, C. J., 317                           | Jetter, L. K., 28, 29, 30                |
| Elgert, O. J., 317                         | Johnson, J. R., 253                      |
| Ershler, B. V., 187, 228                   | Johnson, W. E., 205                      |
| Eshelby, J. R., 161                        | Jones, E. V., 300                        |
| FARIS, F. E., 160                          | Jones, R. T., 205                        |
| Ferguson, H. K., 260                       | Jones, T. I., 80                         |
| Field, F., 94                              | Jones, W. M., 205                        |
| Fischer, A., 28                            | Jongenburger, P., 154                    |
| Fisher, E. S., 33, 36, 41, 43, 47, 48, 188 | KAMMER, E. W., 59, 60                    |
| Fleeman, J., 162                           | Kammerer, O. F., 318, 332                |
| Fletcher, J. F., 160                       | Kaplan, G. E., 115                       |
| Foote, F. G., 21, 69                       | Katz, J. K., 280                         |
| Frankel, J. P., 222                        | Kaufmann, A. R., 97, 99, 101             |
| Friedlander, G., 302, 305                  | Kelman, L. R., 92, 187                   |
| GILBREATH, J. R., 227, 228                 | Kernohan, R. H., 164, 165, 223, 227      |
| Gordon, P., 256                            | Kierstead, 227                           |
| Grainger, L., 3                            | Kilpatrick, M. F., 59, 60                |
| Grassi, R. C., 329                         | Kinchin, G. H., 151, 153                 |
| Gray, R. J., 138                           | Kittel, J. H., 187, 199                  |
| Grenell, L. H., 135                        | Klamut, C. J., 296, 313, 316, 321, 329   |
| Grossman, N., 57, 58, 59                   | Kneppel, D., 97                          |
| Guon, J., 94                               | Knott, H. W., 29, 31                     |
| Gurinsky, D. H., 259, 296, 318, 333        | Koehler, J. S., 149, 154                 |
| HAMBY, D. E., 124, 125                     | Kohn, W., 154                            |
| Hanks, G., 63                              | Konobeevsky, S. T., 160, 165, 187, 205   |
| Harman, J. W., 329                         | Krishnan, R. S., 168                     |
| Harris, G. B., 29                          | Kunz, F. W., 161, 192                    |
| Harrison, W. A., 152                       | Kutaitsev, V. I., 160, 187, 205          |
| Hartmann, I., 144                          | LACY, C. E., 191, 221, 222               |
| Hayes, E. E., 41, 43, 256                  | Laquer, H. L., 59, 60                    |
| Helmholtz, I., 302, 305                    | Last, G. A., 191                         |
| Hennig, G. R., 157                         | Leeser, D. O., 163                       |
| Herring, C., 191                           | Levy, P. W., 167, 169                    |
| Hirsch, H. H., 187, 278                    | Lietzke, M. H., 302, 305                 |
| Hochanadel, C. J., 233                     | Lilliendahl, W. C., 115                  |
| Hockenbury, R. W., 163, 164                | Little, K., 176                          |
| Hoffman, C. G., 80                         | Lloyd, L. T., 21, 47, 50, 52, 55, 56, 57 |
| Holden, A. N., 28, 66, 161, 192            | Longsworth, L. G., 302                   |
| Honeycombe, R. W. K., 221                  | Low, J. R., 163                          |
| Hove, J. E., 157                           | Lustman, B., 94                          |
| Howe, J. P., 191, 221, 222, 243            | MA, C.-C., 132                           |
| Hoxing, R., 256                            | McDuffie, H. F., 304                     |
| Hueschen, R. E., 210                       | McGee, W. E., 59, 60                     |
| Hunter, L. P., 227                         | McHugh, W. E., 163, 164                  |
| Huntington, H. B., 153                     | McInnes, D. A., 302                      |
| Hurst, 209                                 | McLachlan, D., 191                       |
|  | McLennan, D. E., 175                     |

- McReynolds, A. W., 161  
 McWhirter, J. W., 94  
 Magel, T. T., 97  
 Makin, M. J., 161  
 Mallett, M. W., 91, 93  
 Manning, G. K., 63  
 Marden, J. W., 113  
 Marsh, L. L., 63  
 Marshall, W. L., 300, 302, 305  
 Marx, J. W., 154  
 Mayfield, R. M., 43, 52, 57, 62, 199  
 Meerson (Meyerson), G. A., 132, 133, 134  
 Mesrobian, R. B., 176  
 Miller, W. E., 307  
 Mitchell, E. W. J., 169  
 Morgan, J. G., 164  
 Morris, P. R., 29  
 Muehlenkamp, C. T., 63  
 Mueller, M. H., 28, 29, 30, 31, 51, 57, 199  
 Murphy, G., 109, 120  
 Murphy, W. F., 223  
 Murray, G. T., 162  
 NABARRO, F. R. N., 191  
 Nagy, J., 144  
 Negy, 227  
 Nelson, C. M., 169, 174  
 Nelson, H. R., 135  
 Nerad, J. A., 325  
 Neufeld, J., 152  
 Norton, J. T., 29  
 Nottorf, R. W., 131  
 Nowotny, H., 142  
 OPINSKY, A. J., 191  
 Orban, E., 305  
 PAIGE, E. G. S., 169  
 Paine, S. H., 187, 211, 223  
 Pease, R. S., 151, 153  
 Peterson, D., 109, 120  
 Platzman, R. L., 175  
 Pohl, M. S., 138  
 Powell, R. W., 305  
 Pravdyuk, N. F., 160, 187, 205  
 Priceman, S., 57, 58, 59  
 Primak, W., 167  
 Pugh, S. F., 187  
 RABINOWITCH, E. I., 280  
 Rauh, E. G., 24  
 Read, F., 193  
 Reid, R. C., 317, 325  
 Rentschler, H. C., 113  
 Reynolds, M. B., 59, 60, 163  
 Rideout, S. P., 43, 44  
 Roarty, J. D., 307  
 Rogers, B. A., 109, 120, 131  
 Rosenblatt, D. B., 165  
 Ross, M., 176  
 Roth, H. P., 138  
 Rothman, S., 211  
 Rough, F. A., 69, 82, 139, 142  
 Rundle, R. E., 57, 140  
 Russell, H. W., 135  
 SADOFSKY, J., 311, 332  
 Saller, H. A., 66, 69, 82, 139, 142  
 Sanderson, M. J., 29, 30  
 Schulz, L. G., 28  
 Schwartz, C. M., 49  
 Schweinler, H. C., 168  
 Schwope, A. D., 53, 66  
 Secoy, C. H., 296, 299, 300, 305  
 Seigle, L. L., 191  
 Seitz, F., 149, 150, 151, 152  
 Senio, P., 205, 209, 228  
 Seymour, W. E., 28, 29, 31, 219  
 Shaw, K. G., 111  
 Shepard, O. C., 321  
 Siegel, S., 201  
 Silberberg, M., 313, 316, 319, 321  
 Simpson, O. C., 227, 228  
 Sisman, O., 176  
 Skeats, N. B., 318  
 Sloman, H. A., 132  
 Smith, J. F., 109, 120  
 Smoluchowski, R., 165, 174  
 Smutz, M., 109, 120  
 Snyder, W. S., 152  
 Stevens, D. K., 169  
 Stohr, J. A., 101  
 Straetz, R. P., 91, 92, 93  
 Sullivan, L. O., 163  
 Sutton, C. R., 163  
 Swartout, J. A., 307  
 Szilard, L., 256  
 TAUB, J. M., 63, 80  
 Taylor, W. E., 162  
 Teitel, R. J., 256, 311, 313  
 Terry, J. E., 318

## NAME INDEX

- Thewlis, J., 23, 57  
Thomas, D. E., 94  
Thompson, D. O., 161  
Thorn, K. J., 24  
Treco, R. M., 101  
Tucker, C. W., Jr., 23, 80, 205, 209, 228  
Turkalo, A. M., 191  
Turovlin, B., 321
- VANDENBERG, S. R., 251  
Van Winkle, R., 307  
Varley, J. H. O., 160, 174  
Vaughan, D. A., 49  
Veigel, N. D., 116  
Vigness, I., 59, 60  
Voss, M., 109, 120
- WABER, J. T., 63  
Wagener, S., 132
- Watten, B. E., 162  
Weber, C. E., 187, 278  
Weeks, J. R., 296, 323, 325, 328  
Weil, R., 211  
Weisman, J., 315  
Weiss, R. J., 155  
Wigner, E. P., 149, 151, 250, 256  
Wilhelm, H. A., 3, 99, 109, 120, 131  
Wills, F., 321
- Wilson, A. S., 57  
Wilson, J. C., 164, 165, 201, 223  
Wittels, M. C., 160, 167  
Witzig, W., 164  
Wohlberg, C., 227  
Woods, W. K., 160  
Wright, H. W., 302, 305  
Wright, J., 238, 239
- ZUKAS, J. C., 164











